NASA SP-38

ADVANCED BEARING TECHNOLOGY

NATIONAL AERONAUTICS AND SPACE ADMINISTRATION

ADVANCED BEARING TECHNOLOGY

First printing, 1964
Second printing, 1965
Third printing, 1966
Fourth printing, 1972

Library of Congress Catalog Card Number 64–60712

NASA SP-38

ADVANCED BEARING TECHNOLOGY

By
EDMOND E. BISSON
AND
WILLIAM J. ANDERSON
Lewis Research Center, Cleveland, Ohio

Scientific and Technical Information Division 1965
NATIONAL AERONAUTICS AND SPACE ADMINISTRATION
Washington, D.C.

PREFACE

THIS BOOK is an outgrowth of a set of lecture notes originally published for an advanced course on bearing technology at the University of California at Los Angeles. Its objectives are twofold:

(1) To present an exposition of the fundamentals of (a) friction and wear, (b) fluid film bearings, and (c) rolling-element bearings

(2) To demonstrate, through discussion of selected research results, how fundamental principles can be applied to the solution of unique and advanced bearing problems involving environmental factors such as extreme temperature, radiation, high vacuum, and corrosive fluids

The book is devoted primarily, in the examples and the discussion of research results, to advanced bearing problems; for example, the current and anticipated bearing problems in aircraft, in missiles, and in spacecraft are covered in some detail. The principles established and enunciated herein are, however, not limited in their application to advanced bearing problems. On the contrary, these principles apply equally well to mundane and ordinary bearing problems.

Many of the research investigations described herein were a part of the exploratory research program being conducted at the laboratories of the NASA Lewis Research Center by the authors and their colleagues. This research program was designed to explore the fundamentals in advanced problem areas and to establish basic principles, where possible, in these advanced areas. Application of these basic principles is possible not only within the advanced areas but under ordinary conditions as well.

The two chapters of this book written by guest authors are natural outgrowths of the lectures that they originally gave as part of the advanced course on bearing technology.

The authors are indebted to the members of the Lubrication and Wear and Editorial Branches of the Lewis Research Center for their assistance in reviewing and editing the manuscript. In particular, the assistance of Robert L. Johnson in technical matters and Margaret C. Appleby in editorial matters is appreciated.

Edmond E. Bisson
William J. Anderson

CONTENTS

CHAPTER 1

Introduction and Definition of Newer Problem Areas

By EDMOND E. BISSON

IT IS THE PURPOSE OF THIS BOOK to discuss some of the fundamentals of bearing technology and to examine closely current and anticipated problems in the field of bearings. After a general examination of problem areas, there will be some discourse on the possible approaches to these various problems.

Many of the subjects considered are not new. There are, however, many new applications in which the state of the art is not well defined, and further information is required before successful operation under extremely severe conditions is possible. Therefore, this book is divided generally into two principal parts: (1) a discussion of fundamentals, and (2) a review of current and anticipated bearing problems. The discussion of fundamentals should be applicable to many of the applications provided that the conditions can be well defined.

Some applications that impose extremely severe operating conditions on bearings and other surfaces to be lubricated include three general types, aircraft, missiles, and spacecraft. Each one of these applications will be discussed in turn—very generally at this point and in more detail later on. There are, of course, many other sources of bearing problems. These other bearing problems may be equally as severe as those discussed; the particular situations discussed in this book are for illustration only.

In aircraft applications, the operating conditions as applied to bearings and other lubricated surfaces have become quite severe, particularly with the advent of large, high-speed aircraft. Supersonic speeds, as well as high subsonic speeds, result in high operating temperatures over the entire aircraft but particularly within the engine. The stagnation temperature at high speeds is such as to cause a very high compressor-inlet temperature in the standard turbojet engine;

further compression of the air within the compressor (even though this may be a low-pressure-ratio compressor) results in a considerable temperature increase. Temperatures, as a function of Mach number, are shown in figure 1–1. The proposed Mach 3 transport would have a compressor-inlet temperature higher than 600° F and an estimated compressor-discharge temperature higher than 1200° F. As a general rule, the entire temperature level of the bearings within the turbojet engine for supersonic speeds (as well as for high subsonic speeds) is quite elevated. At the same time, many of the design features of the engine such as high rotative speeds and large size (resulting in large bearing sizes) further impose severe operating conditions on the bearings. The control surface bearings will also be required to operate at high ambient temperatures, since at supersonic speeds the entire aircraft structure will be exposed to high stagnation temperatures.

In missiles, the principal bearing problems occur in the turbopump. For high-performance missiles, the rocket engine usually incorporates a turbopump in order that high pressures may be available to the combustion chamber. Also, for high-performance missiles, high-energy propellants (e.g., liquid hydrogen and liquid oxygen) are utilized. Because most missiles are weight limited and must show a high degree of reliability, turbopump weight and complexity must be minimum. Thus, a complex lubrication system incorporating a separate lubricant may not be tolerated. Hence, for high-performance engines utilizing high-energy propellants, one thinks in terms of cooling and lubricating the bearings with the fluid being pumped, that is, with liquid hydrogen or liquid oxygen.

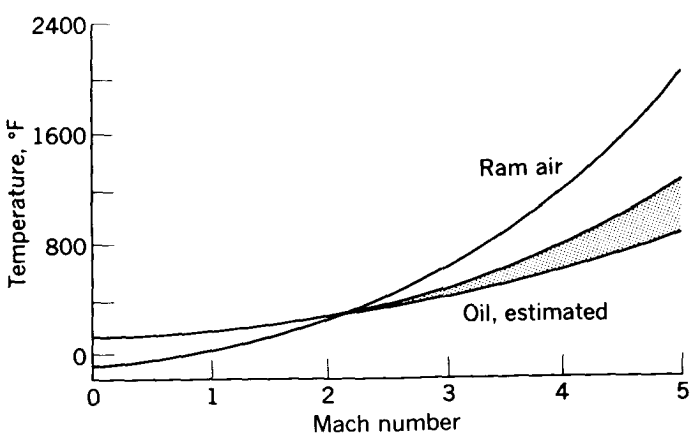

FIGURE 1–1.—Effect of Mach number on operating temperatures. (From ref. 3.)

Some of the properties of liquid hydrogen and liquid oxygen and other cryogenic liquids are shown in table 1–I. These fluids are not noted for their ability to lubricate effectively, particularly under boundary lubrication conditions; for example, liquid hydrogen is a poor lubricant for two significant reasons. First, it is a reducing medium; that is, it tends to reduce the surface oxide layers, which help appreciably in lubrication of surfaces under boundary conditions. Second, liquid hydrogen has an extremely low viscosity, and hence the possibility of building a hydrodynamic film is extremely remote. For example, the viscosity of liquid hydrogen at its boiling point (−423° F) is 2×10^{-9} reyn. This value is approximately equal to the viscosity of air at room temperature. (For comparison, the viscosity of SAE 30 oil at 100° F is 10^{-5} reyn.) Hydrogen is, however, an excellent coolant provided that the lubrication function can be supplied in some other manner. Similarly with the other fluids, such as oxygen and fluorine, problems occur because of chemical reactivity. This is particularly so with fluorine but is also true with liquid oxygen. Since both of these fluids are strong oxidizers, one can conceive of operating conditions within a bearing (particularly at the surfaces in pure sliding) under which the amount of heat generated at the sliding surface is great enough that chemical reaction occurs between the oxygen, or fluorine, and the bearing surface. Of particular importance is the fact that the reaction rate can reach disastrous levels; in other words, the surfaces can "burn." Under such conditions, one does not anticipate long life for such bearings.

TABLE 1–I.—PROPERTIES OF CRYOGENIC LIQUIDS

Liquid	Freezing point, °F	Boiling point, °F	Liquid density, lb/cu ft, at—		Liquid viscosity,[a] reyn, at—	
			Boiling point	−320° F	Boiling point	−320° F
Helium	[b]−458	−452	7.6	----	7×10^{-10}	----------
Hydrogen	−434	−423	4.4	----	19	----------
Nitrogen	−346	−320	50.1	50.1	230	230×10^{-10}
Fluorine	−360	−306	94.0	96.5	372	489
Argon	−309	−303	87.4	----	----------	----------
Oxygen	−361	−297	71.2	75.5	274	333
Methane	−299	−258	25.8	----	----------	----------

[a] Viscosity of SAE 30 oil at 100° F is approximately 10^{-5} reyn.
[b] At a pressure of 26 atm.

In spacecraft, the problem with bearings lies particularly in the pumps required to handle the working fluids. Again, if there are rocket engines, the turbopump for these engines will of necessity incorporate bearings cooled and lubricated by the fluid being pumped. Also, for spacecraft that are propelled by electric propulsion (ion propulsion, plasma propulsion, etc.), electric power for such propulsion may be generated by a turbine utilizing, as the working fluid, liquid metals such as mercury, rubidium, potassium, and sodium. As was the case for the bearings operating in turbopumps handling high-energy propellants, here again the fluids being pumped are not noted for their lubricating ability. Some of the properties of these materials are shown in table 1–II. These fluids are not only corrosive, but they have a strong reducing effect on surfaces. Thus, oxides on the bearing surfaces, which might normally help in the lubrication process, are quickly removed by the reducing action of the liquid metals. Also, at the very high temperatures under which the systems will be forced to operate in order to generate electric power in the megawatt range, the viscosity of these liquid metals will be quite low. Hence, we have a problem of using a fluid for lubrication which has low viscosity and is very corrosive.

Other problems in spacecraft involve the operation of mechanisms in a vacuum, for example, such components as horizon seekers, sun or star finders, or radar antennas. These components must normally operate in the vacuum of outer space, unless an attempt is made to solve the problem by using hermetically sealed systems, which are very complex and heavy. Since minimizing weight and complexity

TABLE 1–II.—PROPERTIES OF LIQUID METALS

Metal	Melting point, °F	Boiling point, °F	Liquid density, lb/cu ft at—		Liquid viscosity,[a] reyn, at—		Vapor pressure at 2200° R, lb/sq in. abs
			Boiling point	1200° F	Boiling point	1200° F	
Mercury	−38	674	794	752	13×10^{-8}	[b] 10×10^{-8}	3044
Rubidium	102	1295	81.9	82.7	2.2	2.2	91
Potassium	146	1395	41.4	43	1.9	2.0	64
Sodium	208	1630	46.3	49.3	2.2	2.9	25
Lithium	357	2430	26.2	29.2	[b] 2.0	[b] 2.7	0.5
NaK-78	12	1456	42.6	44.7	2.0	2.16	51

[a] Viscosity of SAE 30 oil at 100° F is approximately 10^{-5} reyn.
[b] Extrapolated.

is desirable, finding solutions for design and lubrication of bearings to be operated in vacuum is necessary. Figure 1–2 shows pressure as a function of altitude. Outside the Earth's atmosphere, the pressures involved are in the order of 10^{-13} millimeter of mercury in the solar system and in the order of 10^{-16} millimeter of mercury in interstellar space.

As can be seen from the quick description of some of the applications, which will be discussed later in more detail, there are many unique problems that will face the bearings of the immediate or distant future. Hence, of necessity, the fundamental principles that may be applied to bearing designs and lubrication techniques must be discussed in this book.

At this point, the mechanism of bearing failures under the severe conditions of operation previously described should be examined with some care. The examination should be concerned particularly with a search for some distinguishing feature common to all failures. If there *is* some distinguishing feature common to failures in most bearing types, the solution to prevention of these failures becomes appreciably simpler. Therefore, the failure modes of the three types of bearings are discussed individually.

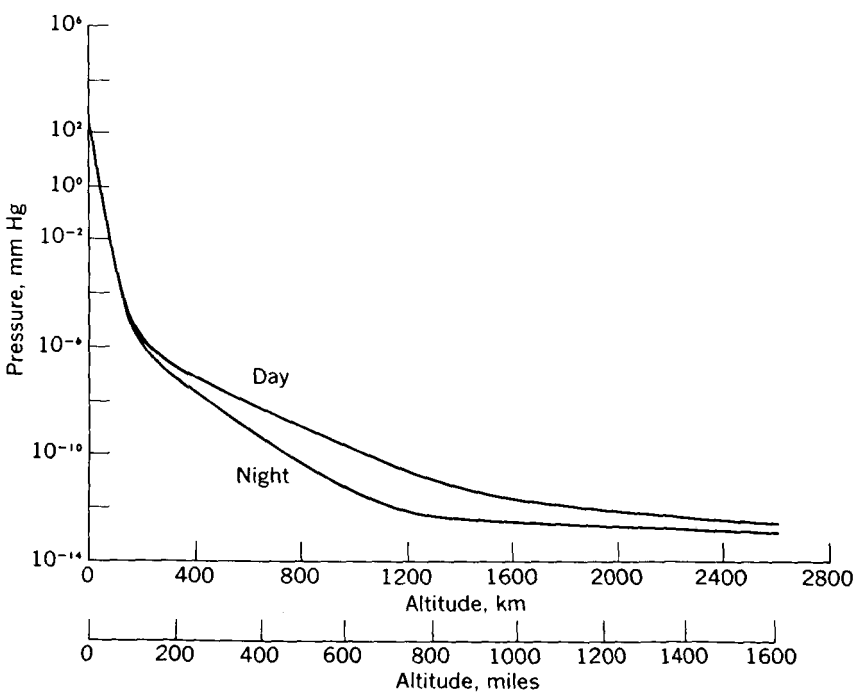

FIGURE 1–2.—Pressure as a function of altitude. (From ref. 4.)

In the rolling-element bearing, the most common type of failure involves a lubrication failure of the cage, usually at the cage locating surface. Figure 1–3 shows the various components of a rolling-element bearing. The cage is essentially a free-floating body and hence must be located at some rubbing surface, usually the inner or outer race. In figure 1–3, the cage is located by the inner race, as shown by the small clearance between cage and inner race. Thus, the cage-locating surface becomes essentially a plain bearing (i.e., a sleeve or hydrodynamic bearing) of small length-to-diameter ratio. Such a hydrodynamic bearing possesses very low load-carrying capacity, because it is difficult for pressure to build up between the surfaces since the end leakage is very high. Hence, boundary or thin-film lubrication exists at the cage-locating surface, and severe wear and metal transfer can occur because of the metal-to-metal contact.

By way of definition, figure 1–4 illustrates the regions of boundary lubrication and fluid lubrication. The curves are for a plain journal

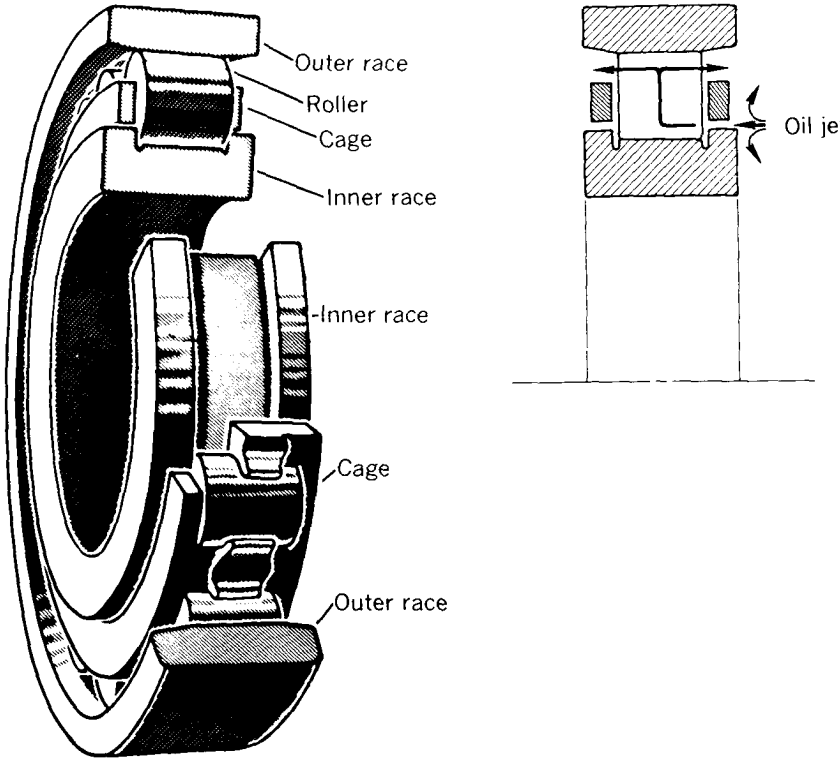

FIGURE 1–3.—Typical high-speed roller bearing.

bearing and show friction coefficient and film thickness plotted against the well-known parameter ZN/P, where Z is viscosity, N is rotational speed, and P is load per unit projected area or bearing pressure. To the right of the dashed vertical line is the region of fluid or thick-film lubrication where the surface asperities are completely separated by an oil film of such thickness that no metal-to-metal contact can occur. To the left of the dashed vertical line is the region of boundary or thin-film lubrication. As noted in the upper right sketch, the film thickness in boundary lubrication is so small that asperities can, and do, contact through the oil film (fig. 1–4).

In the case of fluid or thick-film lubrication, only the properties of the lubricant are of importance since the asperities do not contact. In the case of boundary or thin-film lubrication, the properties of the metals are of primary importance since there is true metal-to-metal contact at the asperities. While the properties of the lubricant under these conditions are of secondary importance, they are not to be

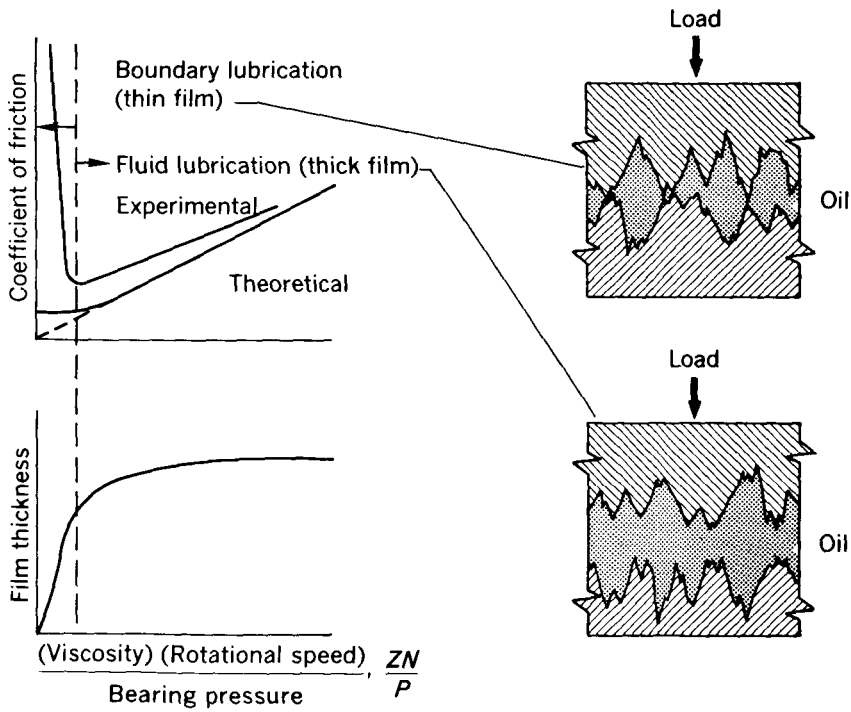

FIGURE 1–4.—Boundary and fluid lubrication.

neglected because they can strongly influence the type of damage that will occur. The lubricant in this case is serving as a contaminant. This contaminating function of the lubricant is discussed in more detail herein.

A second mode of failure in rolling-element bearings is that of wear; this failure is again a result of the existence of boundary lubrication permitting metal-to-metal contact.

A third mode of failure involves overheating and possible lockup. Overheating usually results from a combination of (1) boundary lubrication, (2) inadequate flow of the coolant-lubricant through the bearing, and (3) excessive heat generation in the bearing.

A fourth mode of failure involves fatigue under rolling-contact conditions. If the bearing has been properly designed to eliminate other failure modes (cage failure, wear, and overheating), the failure is expected to be caused by fatigue. Fatigue is one failure mode which is not dependent on boundary lubrication.

In hydrodynamic bearings, one of the common modes of failure is that of wear and/or seizure. This failure is usually caused by the existence of boundary lubrication or thin-film conditions at the bearing. The metal-to-metal contact under these conditions can result in excessive wear or, if extreme boundary lubrication occurs, can result in severe welding, adhesion, or total seizure. Boundary-lubrication conditions in this type of bearing are the result of a decrease in the value of the ZN/P parameter. As shown in figure 1–4, as this parameter decreases, film thickness decreases to a point where metal-to-metal contact takes place. The decrease in the parameter ZN/P may result from (1) a decrease in viscosity Z, possibly because of a marked increase in temperature of the lubricant film; (2) a decrease in speed N, usually during startup or shutdown, or (3) an increase in load P, possibly because of a dynamic load condition.

A second mode of failure in the hydrodynamic bearing is that of instability or oil-film whirl. This problem will be discussed more fully. A third mode of failure in hydrodynamic bearings is that of overheating, which can ultimately lead to boundary lubrication and, hence, to failure. Overheating can result from boundary lubrication or inadequate flow of lubricant-coolant through the bearing. A fourth mode of failure in hydrodynamic bearings is that of fatigue of the bearing materials. Fatigue is the direct result of application of cyclic stress to the bearing materials. While boundary lubrication is not a distinguishing feature of instability and fatigue, it is a distinguishing feature of the other modes of failure in hydrodynamic bearings.

In hydrostatic bearings, the chief mode of failure is that of instability, which may permit metal-to-metal contact and thus excessive wear and seizure.

From a discussion of the different failure modes of all bearing types, it is noted that a distinguishing feature common to many of these failure modes is the existence of boundary-lubrication conditions. Hence, it becomes important to know the mechanism involved when two surfaces slide together in the absence of enough lubricant to permit establishment of fluid or thick-film lubrication. When the mechanism of failure under these conditions of metal-to-metal contact is known, solutions can be devised to prevent severe adhesion and often complete seizure of the surfaces to each other.

Discussed herein are the principles of boundary lubrication and, in particular, the adhesion theory of friction. The strong adhesion and welding of surface to surface under adverse conditions are explored in detail and the principles involved in reducing friction, surface welding, and wear are explained.

The principles of hydrodynamic theory are also described. Since this discussion of hydrodynamic theory is concerned with the formation of thick films in order to achieve hydrodynamic lubrication, the discussions will cover the development of the Reynolds equation and show how such a film is produced and the pressure pattern within this film. The solutions for journal bearings and for slider bearings under these conditions will be discussed as well as solutions for some of the hydrodynamic bearing failure modes previously mentioned.

Also discussed are the principles of operation of hydrostatic bearings. Since the very low viscosities of some of the working fluids mentioned earlier may not permit development of a hydrodynamic or thick film, it may be necessary to design the bearings to operate under externally pressurized conditions. These are the so-called "hydrostatic bearings."

One chapter of this book is devoted to discussion of gas-lubricated bearings. The very high temperature levels expected in many applications may preclude the use of conventional liquid lubricants; under these conditions, gases may be used as the lubricant either in hydrodynamic or hydrostatic (externally pressurized) bearings.

The fundamentals of rolling-element bearings are described, and such items as bearing types and designs, the kinematics involved, the contact stresses, and the resulting fatigue problem as well as special problems of materials are explored.

Another chapter is devoted to the subject of modern developments in liquid lubricants. Liquid lubricants are still of considerable interest because of their anticipated use for many years and their versatility. One problem with the liquids is that of fluidity range;

this problem is illustrated very roughly in figure 1–5, which is a plot of viscosity against temperature for four different liquid lubricants. Also shown in figure 1–5 are the Mil–L–7808 specification limits. These specifications are for the lubricants presently used in many turbojet engines. The four different curves are representative of different classes. The polyglycols would have curves roughly between the extremes shown, while the fluorocarbons (which are quite stable fluids) generally have a steeper viscosity-temperature curve than does the petroleum. All the curves of figure 1–5, however, illustrate the fluidity problem to a certain degree, particularly as applied to high-temperature lubrication of bearings. Liquid lubricants, in general, show a very marked decrease in viscosity as temperature increases. At the low end of the temperature range, one quickly approaches the freezing point of most liquids. This fact (as well as high-temperature stability problems to be discussed later) places rather stringent requirements on the lubrication system designer, since it makes it mandatory for him to keep the lubricant temperature within certain well-defined limits.

A major problem with present liquid lubricants lies in their degradation at high temperatures. The degradation takes the form primarily

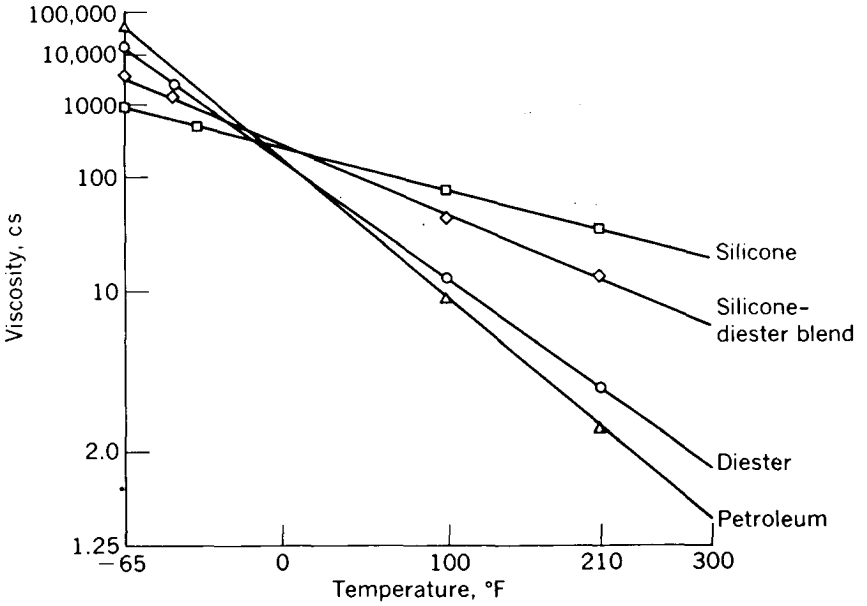

FIGURE 1–5.—Viscosity-temperature properties of various liquids. Mil–L–7808 specification limits: Maximum viscosity at −65° F, 13,000 centistokes; minimum viscosity at 210° F, 3.0 centistokes. (From ref. 5.)

of oxidation and also of decomposition because of thermal instability. Both of these mechanisms usually result in deposits on bearings and other parts from insolubles formed in the oil. Since the temperature limitation with liquids is established primarily by oxidation, one technique used to increase the temperature limitation involves the exclusion of oxygen. This exclusion can be achieved by use of a "closed" lubrication system or by use of an inert-gas blanket in the lubricating system. The closed lubrication system excludes oxygen by preventing the continual venting ("breathing") of the lubrication system. Experiments reported in reference 1 indicate that, with mineral oils, use of nitrogen as a blanketing medium increased the allowable bearing operating temperature as much as 150° F.

The next step beyond the present mineral oil and synthetic diester lubricants involves new classes of lubricants. These include such lubricants as polyphenyl ethers, hydrogenated petroleum fractions, or organometallics. Reference 2 shows that the hydrogenated petroleum fractions have the advantage at high temperature of showing clean "burn-off." That is, the oxidation products at high temperature are volatiles rather than insolubles. Since there is a relatively small amount of insolubles, the problem of deposition of the insolubles within the bearings during operation at high temperature is considerably reduced.

Because liquid lubricants are in many instances temperature limited to relatively low levels, it is necessary to consider the use of nonconventional lubricants such as solids and reactive gases. The solids include materials such as molybdenum disulfide and graphite as well as some newer materials (such as lead monoxide, calcium fluoride, and others). These solids may be utilized as loose powders to lubricate bearings or the bearing surfaces may be precoated with a thin film of lubricant. Reactive gases, that is, gases containing active atoms in the molecule, are discussed as possible lubricants under boundary-lubrication conditions. Here a distinction is made between the activity of the gases for this use and that of those used for externally pressurized bearings. In general, the gases for externally pressurized (hydrostatic) bearings would be relatively inert compared with the "reactive gases."

The commentary on liquid-metal-lubricated bearings is divided into two parts: First, a general discussion of the properties of the liquid metals, the general type of cycle, and the power-generation equipment which will use the liquid metals, and finally a discussion of the problems (such as high vapor pressure, corrosion, containment, low viscosity, etc.) to be expected with these materials at high temperature. Next

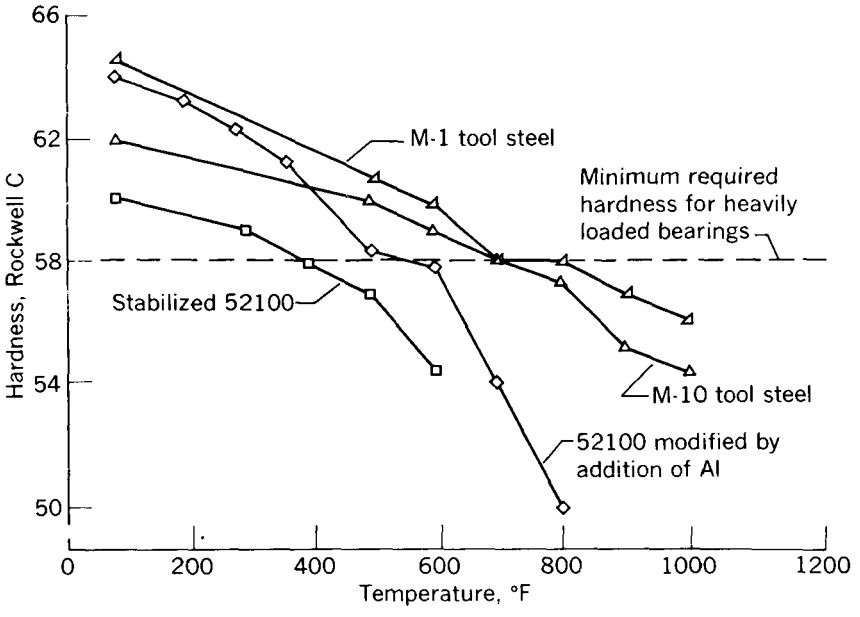

FIGURE 1–6.—Hardness of bearing materials at various temperatures. (From ref. 5.)

the hydrodynamics of bearings utilizing liquid metals as the working fluids will be covered.

The first part of the review of extreme-temperature bearing problems is concerned with the temperature limitation of conventional bearing materials and indicates the possible classes of materials for use at higher temperatures. As an example, figure 1–6 shows that the conventional material SAE 52100 for rolling-element bearings is limited by loss of hardness to temperatures lower than about 350° F. Other materials do, however, have promise of maintaining adequate hardness at high temperatures (fig. 1–6). The second part is devoted to the use of special lubrication techniques that permit bearing operation at very high temperatures. This includes discussion of such techniques as the "once-through" technique, which uses liquid lubricants at an extremely low flow rate. The discussion will also cover the operation of completely dry bearings.

Fatigue in rolling-element bearings is explored since it may become one of the very serious limitations on use of rolling-element bearings in mechanisms which have an *absolute* requirement of high reliability. This material will cover the effects of processing variables (such as material hardness, inclusions, classes of materials, etc.) as well as the

influence of operating variables (such as lubricant viscosity, viscosity-pressure coefficient of the lubricant, load, speed, etc.).

The problems of operation of bearings and other surfaces to be lubricated (such as shaft seals) under extremely low temperature conditions are examined. Here reference is to the operation of bearings and seals in the presence of cryogenic liquids, such as liquid hydrogen, liquid oxygen, etc. Results from fundamental friction studies in the presence of cryogenic liquids such as liquid hydrogen, liquid oxygen, and liquid nitrogen are presented. These results are used in a selection of materials for bearings to be operated in cryogenic liquids. There is also a discussion of studies of full-scale rolling element bearings in liquid hydrogen.

The effects of vacuum and radiation on operation of bearings or other lubricated surfaces are described. Since some of the applications involve spacecraft and particularly operation of components in the vacuum of outer space, it is necessary to understand the mechanisms by which surfaces can fail in vacuum. For example, we know that under pressures in the order of 10^{-6} to 10^{-16} millimeter of mercury, contaminating films on the surfaces will gradually disappear if these films are organic in nature. If they are inorganic in nature, the films may disappear only if the temperature of the surface is relatively high. The surfaces may, therefore, be denuded of their protective films and may thus fail from a lubrication standpoint. The use of a nuclear reactor as a source of heat for an electric-power-generation system to operate in space imposes a radiation hazard on all mechanisms operating on the spacecraft. Shielding will, of course, be utilized to some extent; however, it is possible that some mechanisms will be exposed to fairly high radiation dosages of gamma rays and neutrons. These mechanisms must operate over long periods of time with a high degree of reliability; hence the effects of radiation on lubricants and on surface films are important.

REFERENCES

1. Nemeth, Z. N., and Anderson, W. J.: Effect of Air and Nitrogen Atmospheres on the Temperature Limitations of Liquid and Solid Lubricants in Ball Bearings. Lubrication Eng., vol. 11, no. 4, July–Aug. 1955, pp. 267–273.
2. Klaus, E. Erwin, and Fenske, Merrell: Fluids, Lubricants, Fuels and Related Materials. TR 55-30, pt. 6, WADC, Feb. 1958.
3. Anon: Space Age Lubrication. Chem. Eng. News, vol. 39, no. 17, Apr. 24, 1961, pp. 117–124.
4. Jastrow, Robert: Lunar and Terrestrial Atmospheres. Advances in Aero. Sci. vol. 5. Plenum Press, Inc., 1960, pp. 338–345.
5. Johnson, R. L., and Bisson, Edmond E.: Bearings and Lubricants for Aircraft Turbine Engines. SAE Jour., vol. 63, no. 6, June 1955, pp. 60; 63–64.

CHAPTER 2

Boundary Lubrication

By EDMOND E. BISSON

I. THEORIES OF FRICTION AND WEAR

SINCE THIS BOOK is concerned with bearing technology, particularly under extreme conditions of operation, it is well to examine the conditions under which bearing failures are attained. It will be recalled that the distinguishing feature of practically all bearing failures (regardless of type) involves boundary lubrication to some degree. Thus, cage failures and excessive wear of rolling-element bearings are the direct result of boundary lubrication. With hydrodynamic bearings also, wear and seizure are the direct result of boundary lubrication. Instability in hydrodynamic or hydrostatic bearings is not an effect of boundary lubrication, yet it *causes* boundary lubrication, that is, metal-to-metal contact through the film, which eventually results in bearing failure.

Since boundary lubrication is such a distinguishing feature of bearing failures, this chapter examines boundary lubrication in considerable detail. A strong distinction is made here between boundary lubrication and fluid lubrication. Figure 2-1 shows these two regions. The curves for a plain journal bearing are of friction coefficient and film thickness plotted against the well-known parameter ZN/P, where Z is viscosity, N is rotational speed, and P is bearing pressure, all in consistent units. To the right of the dashed vertical line is the region of fluid lubrication: that is, thick film lubrication, where the surface asperities are completely separated by an oil film of such thickness that no metal-to-metal contact can occur. To the left of the dashed vertical line is the region of boundary or thin-film lubrication. As noted in the upper right-hand sketch, the film thickness in boundary lubrication is so small that asperities contact through the oil film.

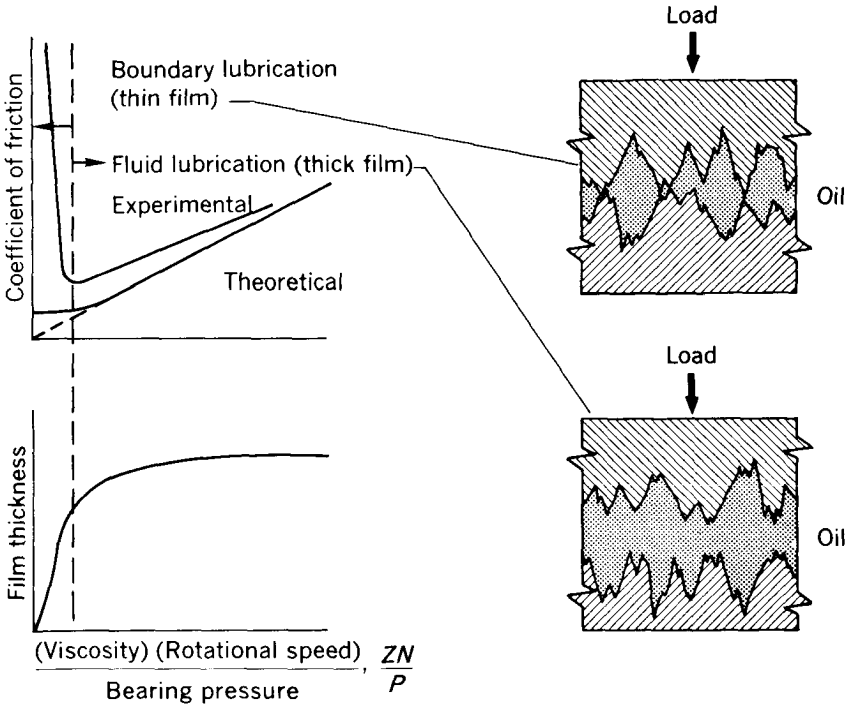

FIGURE 2–1.—Boundary and fluid lubrication.

In the case of fluid or thick-film lubrication, only the properties of the lubricant are of importance since the surface asperities do not contact. In the case of boundary or thin-film lubrication, the properties of the metals are of primary importance since there is true metal-to-metal contact by asperities. While the properties of the lubricant under these conditions may be of secondary importance, they are not to be neglected since they can strongly influence the type of damage which will occur. The lubricant in this case is serving as a contaminant. (This will be discussed in more detail later.)

As is well known, the presence of a contaminating film between sliding surfaces can have a marked effect on friction, wear, and surface damage. (A contaminant is defined as any material other than those comprising the sliding surfaces.) Some contaminants are beneficial (lubricants) while others are detrimental (abrasives). Considerable evidence (refs. 1 to 8) indicates the importance of solid surface films to the friction, wear, and surface failure properties of sliding surfaces. Physical and chemical surface changes have been associated with either satisfactory or unsatisfactory operation of metallic sliding surfaces (ref. 2). As an example, "run-in" has long been known to be

effective in improving the performance and the load-carrying capacity of surfaces. Among the factors that lead to satisfactory performance are the formation and maintenance of certain beneficial solid surface films. Some solid films can be formed on sliding surfaces by use of extreme pressure additives in lubricants. Theories for the mechanism of extreme pressure lubrication are discussed in references 3 and 8. Other solid films may be formed naturally such as by reaction of metallic surfaces with the ambient atmosphere under sliding conditions. Again, other solid films may be preformed and thereafter maintained by proper supply of the lubricating component.

The purposes of this first part of the discussion of boundary lubrication are (1) to present the fundamental principles involved in friction, (2) to discuss the various mechanisms of wear, and (3) to show the effect on friction, wear, and surface damage of factors (e.g., adsorbed gases, liquid monolayers, and adsorbed and chemisorbed films as well as solid solubility of the material combination).

SYMBOLS

A	real area of contact
A_o	apparent area of contact
E	modulus of elasticity
f	coefficient of friction
H	hardness (flow pressure)
h	average depth of wear
k	adhesive wear coefficient
k'	adhesive wear coefficient for a given material, h/PL
L	distance of travel; latent heat of fusion
N	rotational speed, rpm
P	average pressure or design stress, bearing pressure
p	flow pressure
S	shear force
s	shear strength
T	temperature, °K
T_m	melting temperature, °K
V	volume of wear material
W	load
Z	viscosity
ϵ	resistance to wear
ρ	density

ADHESION THEORY OF FRICTION

Analysis of the effects of solid surface films is based on the adhesion theory of friction. This adhesion theory of friction was advanced by Merchant in the United States (ref. 9) and by Bowden and Tabor in

England (ref. 8). This theory of friction is based on strong adhesive forces between contacting asperities. As the load is applied (see upper right-hand sketch of fig. 2–1), the asperities contact with resulting high stresses at the true contact area. This high stress forces out some of the lubricant and other contaminants. The true area of contact is so small that, following elastic deformation, the stress quickly reaches the yield stress of one of the two materials. Hence, plastic flow occurs and a "cleaning" action is obtained at the contact area. Because local areas are now somewhat clean and the stress is relatively high, "cold welding" can occur at the junction. Moving one surface relative to the other now requires shear at this welded junction.

The following equations represent some of the important concepts of the adhesion theory of friction:

Friction:

$$F=S+P=\text{Shear}+\text{Ploughing}=As+A'p$$

Contact area:

$$A=\frac{\text{Load}}{\text{Flow pressure}}=\frac{W}{p}$$

Friction coefficient:

$$f=\frac{\text{Friction}}{\text{Load}}=\frac{As}{W}+\frac{A'p}{W}=\frac{s}{p}+\frac{A'p}{W}$$

When the ploughing term is negligible,

$$f=\frac{s}{p}=\frac{\text{Shear strength}}{\text{Flow pressure}}$$

This friction theory states that the friction force is equal to the sum of two terms: the first a shear term, the second a ploughing or roughness term. The shear term is that force required to shear at the welded junction. (Note that shear may take place in the junction itself or adjacent to it on either side.) The ploughing term is that force which results from displacement of the softer of the two metals by an asperity of the hard metal. In many instances, the ploughing or roughness term is negligible in comparison with the shear term.

Each of the two terms comprising the friction force can be represented as the product of an area and a strength—either the shear strength or the flow pressure (compressive yield strength). The contact area is a function only of load and flow pressure and is not a function of the apparent area of contact. After the appropriate substitutions are made and the ploughing term is neglected, the friction coefficient is equal to the ratio of shear strength to flow pressure, s/p.

The last equation shows that reduction in friction coefficient (and, as will be developed later, reduction in wear) can be obtained if the ratio s/p can be reduced. Reduction of the ratio is obtained with low shear strength or high flow pressure, or both. It is extremely unlikely that both low shear strength and high flow pressure can be obtained in any one material. However, by the use of low shear strength films (with thicknesses as small as millionths of an inch) on hard base materials, both desirable conditions may be obtained (ref. 8, p. 112). Thus, low shear strength is obtained without appreciable decrease of the yield strength of the combination. The load will, therefore, be supported through the film by the hard base material while shear occurs within the soft thin film. These low-shear-strength films can be of the following types: oxides, chemical reaction films (chlorides, sulfides, etc.), metals, fluid lubricants, solid lubricants, etc.

Lead and indium, both of which have very low shear strengths, can be considered to illustrate the beneficial effect of metallic-plated films. Figure 2–2 shows some friction results obtained by Bowden and Tabor (ref. 8) for lead and indium films on various materials. The solid points are for either solid lead or solid indium. It should be noted that, for equal track widths (which means, in this case, equal shear areas), the friction force is the same whether the films are deposited on metals of various hardnesses or whether the friction force is measured for the solid material.

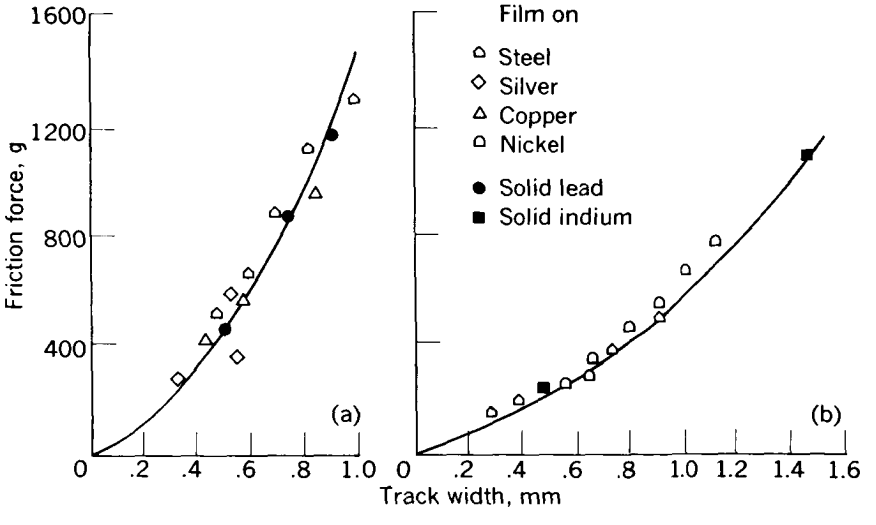

(a) Lead films. (b) Indium films.

FIGURE 2–2.—Friction of surfaces coated with lead and indium films as a function of track width. (Shear area $=f(W_i)$.) (From Bowden and Tabor, ref. 8.)

The importance of shear strength to the friction process is illustrated by figure 2–3. The curves show friction force, as a function of track width, for steel sliders on solids of copper, lead, or indium. The results show that, for equal track widths (i.e., equal shear areas), the three different materials aline themselves in accordance with their measured shear strengths. For purposes of comparison, the shear strengths (as measured by normal means employed to establish strength of materials) are given in figure 2–3. It will be noted that the ratio of friction forces is of the same order of magnitude as the ratio of measured shear strengths. In fact, since the friction forces can be converted to shear strengths by use of calculated contact areas, a comparison of calculated and measured shear strengths was made (ref. 8) as follows:

Material	Shear strength, g/sq mm	
	As normally measured	Calculated from friction force
Steel	90, 000	140, 000
Copper	16, 000	28, 000
Lead	750	1, 800
Indium	220	225

While there is no direct correlation between friction and wear, the adhesion theory of friction implies that the wear should be considerably decreased if the adhesion between the surfaces can be effectively reduced. The influence of contaminants has, up to this time been discussed on the basis of reducing shear strength only. However, another important manner in which a contaminant can be beneficial is its action to reduce the amount of welding by preventing metal-to-metal contact of the "clean" surfaces. It is well known that, for effective welding, fluxes must be used to remove contaminants and permit contact of clean surfaces. The reverse of this process is, of course, also true. Thus, introduction of a contaminant to prevent contact of clean surfaces should be detrimental to the welding process and should result in less adhesion between the surfaces. This reduced adhesion should, consequently, result in less wear and less metal transfer. The mechanisms of wear are discussed in greater detail later.

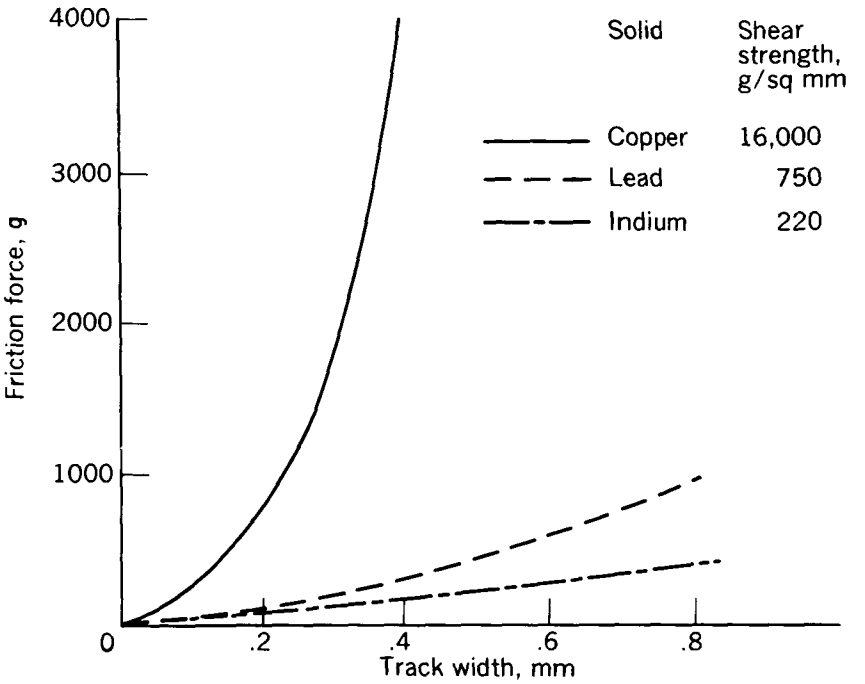

FIGURE 2–3.—Friction of steel sliding on various solids as a function of track width. (Shear area $=f(W_t)$.) (From Bowden and Tabor, ref. 8.)

FORMATION AND EFFECT OF SURFACE FILMS

Clean Surfaces

Most metals are covered by contaminating films of one type or other. Even metals freshly cleaned by lapping, grinding, etc., oxidize in a very short period of time. In fact, most metals acquire a layer of oxide between 10 and 100 angstroms (0.04 to 0.4×10^{-6} in.) thick in about 5 minutes or less. This is true for metals such as iron, nickel, and zinc. The oxidation of metals takes place even though only limited concentrations of oxygen are present, that is, even at very low oxygen partial pressures. One very effective means of removing the oxide layer is to heat the surfaces to relatively high temperatures in vacuum. This heating removes most organic films and, if the temperature is high enough, causes a removal of the oxide film. After removal of such a film, extremely high friction coefficients result if surfaces are bought together and an attempt is made to slide the surfaces. In fact, friction coefficients rise, from the general range of 0.2 to 0.5 to the general range of 6 to 10 (or even 100) if the heating in vacuum is done at sufficiently high temperatures. Outgassing of

metals results in high friction coefficients because it can produce surfaces so clean that adhesion between two such surfaces is greatly increased. Under these conditions, diffusion across the interface can occur with relative ease. Thus, nascent surfaces are to be avoided if these surfaces must be rubbed together. In other words, a contaminating film is required on surfaces in order to prevent severe surface damage and to avoid high friction.

Mechanism of Formation of Surface Films

Surface films may be formed in a variety of ways, among which the more important are (1) physical adsorption, (2) chemisorption, and (3) chemical reaction. It is necessary at this point to distinguish among these various processes. Such a distinction has previously been made by Uhlig (ref. 10) from whom the following is cited:

> *Physical adsorption* is characterized by reversibility. This means that increased concentration of adsorbent leads to increased adsorption on the metal surface; subsequent reduction in concentration removes a proportionate amount of adsorbed substance. The heat of physical adsorption is relatively low, falling in the range of 1000 to 2000 calories per gram-mole (typical of van der Waal's interaction). Physical adsorption is not specific, adsorption being possible in some range of temperature for all substances and surfaces. The amount of adsorption decreases with increase in temperature. [As temperature increases, the oriented adsorbed film will gradually show disorientation and finally be removed from the surface; such disorientation can be studied by electron or X-ray diffraction.]
>
> *Chemisorption* on the other hand is not reversible [generally] so that a chemisorbed substance may not necessarily wash off with a dilute solution of the adsorbent or any solvent. The heat of adsorption corresponds to [that for] chemical bonding and is correspondingly high, being in the neighborhood of 10,000 to 100,000 [200,000] calories per gram-mole. Chemisorption is specific and not general (as is physical adsorption). Only those substances chemisorb that have relatively high affinity for the substrate. Oxygen for example is physically adsorbed on glass but is chemisorbed on tungsten. Finally, chemisorption (within certain ranges of temperature) *increases* with increase in temperature, opposite to the behavior of physically adsorbed substances. In chemisorption, chemical bonding occurs but without metal atoms leaving their lattice. Electron diffraction, therefore, usually does not reveal a new structure.

Research on chemisorption has continued (refs. 11 and 12). Ehrlich (ref. 11) reviews much of the work on chemisorption and discusses the bonding in chemisorption and its relation to electronic structure. He states that the most popular theories hold that chemisorption involves a covalent bond (sharing of electrons between adsorbent and adsorbate). These theories suffer certain limitations and more information is required in this field. Criteria are available to identify both physical adsorption and chemisorption; it is sometimes extremely difficult to distinguish between them and, under some conditions, physical adsorption can occur over a primary chemisorbed film.

Uhlig continues (ref. 10):

Chemical reaction, in the usually accepted sense, differs from chemisorption in that a new structure forms—metal atoms leave their own lattice to enter a new lattice. It can be stated generally that chemisorption is possible only if an appreciable activation energy for reaction occurs. Should the activation energy be zero, as in some reactions, metal atoms immediately leave their lattice to form chemical compounds on the metal surface. Metallic calcium, for example, is immediately oxidized to CaO on exposure to air, and there is no chemisorption of oxygen.

An important distinction between chemisorption and chemical reaction is stated by Uhlig as follows:

Whereas chemisorbed films are monatomic or monomolecular, stoichiometric films formed by chemical reaction have unlimited thickness.

In general, the stability and durability of surface films is in the following order: (1) chemical reaction films, (2) chemisorbed films, and (3) physically adsorbed films.

Adsorbed Gases

As previously mentioned, the effect of contaminants on friction, wear, and surface damage can be quite appreciable. This result is true even though the contaminating film may be as thin and as poorly adherent as that obtained from adsorption of a gas. As an example of this sort of effect, figure 2–4 shows the reduction in friction coefficient which is obtained by adsorption of oxygen on outgassed iron surfaces. These surfaces have been outgassed in a vacuum (10^{-5} to 10^{-6} mm Hg) in order to clean the surfaces.

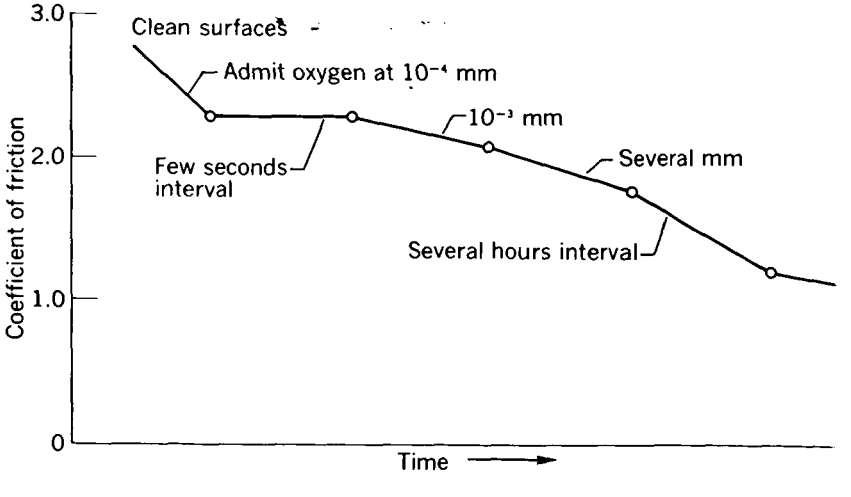

FIGURE 2–4.—Effect of oxygen on friction of outgassed iron surfaces. (From Bowden, ref. 38.)

We see from figure 2–4 that the friction coefficient is markedly reduced by admission of oxygen gas even though the oxygen pressure is very low (10^{-4} mm Hg). If the concentration of oxygen atoms is increased by increasing the pressure (in this case, 10^{-3}), the friction coefficient is reduced still more. As oxygen pressure is allowed to increase to several millimeters of mercury, the friction coefficient is reduced still further. Finally, figure 2–4 shows that, if the surfaces are allowed to stand for some period of time, the adsorbed oxygen film becomes more complete and the friction drops still further. It should be noted that the friction coefficient is still very high, that is, in the order of 1.0 rather than the 0.1 value normally encountered in effective lubrication. An important observation from these results, however, is that seizure of the clean metals is prevented by even a *trace* of oxygen, as obtained at 10^{-4} millimeters. It is possible that, with oxygen, chemical reaction took place with the clean iron surfaces to form one of the iron oxides. The oxide formed could be one of the lower oxides, FeO or Fe_3O_4; both of these oxides, as will be shown later, are effective in preventing seizure of the iron surfaces one to another. The higher iron oxide Fe_2O_3 (which is detrimental) would require a greater concentration of oxygen atoms.

The effect of chlorine on the friction of outgassed iron surfaces is shown in figure 2–5. As chlorine is admitted at a pressure of about 1 millimeter of mercury, the friction coefficient immediately drops to a relatively low value. In this case, the effect is nonreversible, as is shown in the figure at the point where the chlorine was frozen out and

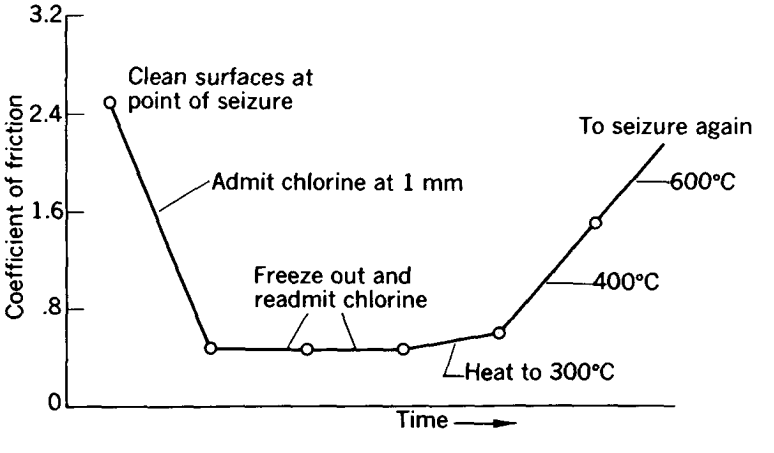

FIGURE 2–5.—Effect of chlorine on friction of outgassed iron surfaces. (From Bowden, ref. 38.)

then readmitted. No appreciable change in the friction coefficient occurred under these conditions. In fact, it was necessary to heat the surfaces to a temperature of about 400° C before the resulting film was broken up and the friction again rose appreciably. Quite probably, with chlorine and clean iron surfaces, chemical reaction took place at the surface to form an iron chloride film (probably $FeCl_2$). The indicated necessity to heat the surfaces to 400° C probably corresponds to the temperature required to obtain decomposition of this chemical reaction film.

The effect of addition of hydrogen sulfide on the friction of outgassed iron surfaces is shown in figure 2–6; the friction coefficient is reduced abruptly and appreciably. Seizure of the surfaces was prevented. The reduction in friction coefficient with hydrogen sulfide is not as great as it was with admission of chlorine to the chamber. Note, however, that this film is much more stable and may be heated to over 790° C before decomposition of the film takes place and friction rises. It is probable that with hydrogen sulfide reaction occurs with the clean iron surfaces to form the iron sulfide film FeS. The iron chloride film $FeCl_2$ has a lower shear strength than FeS (ref. 8); this difference in shear strength would explain the difference in friction coefficient. An important point to be noted here is that admission

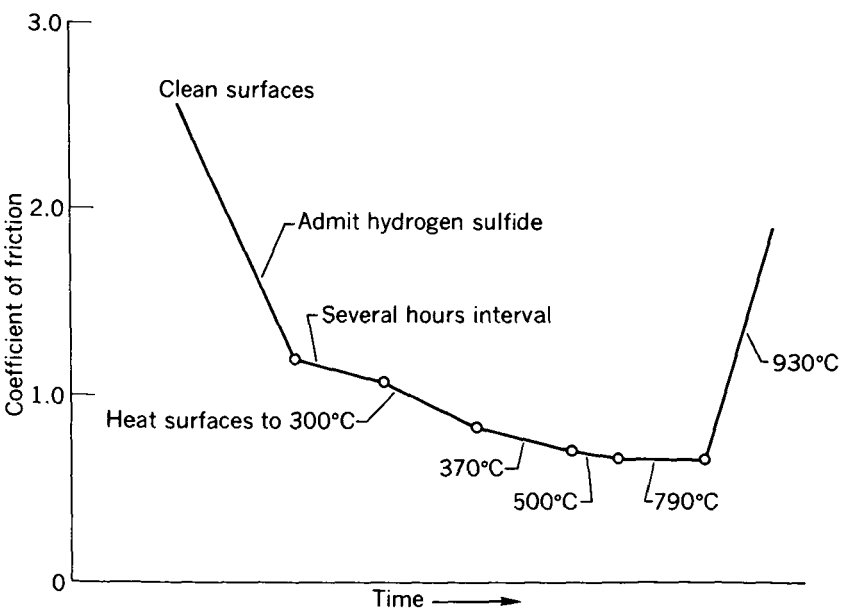

FIGURE 2–6.—Effect of hydrogen sulfide on friction of outgassed iron surfaces. (From Bowden, ref. 38.)

of *both* chlorine and hydrogen sulfide to the chamber resulted in prevention of seizure of the metal surfaces. Frequently, the prevention of seizure can be more important than reduction of friction coefficient per se.

Monolayers and Multilayers

It is possible to show, by use of monolayers and multilayers, that a very thin film of lubricant at the surface can be effective in reducing friction. In studying the effects of monolayers or multilayers, it is convenient to use the well-known Langmuir-Blodgett technique. This technique involves floating an insoluble monolayer on the surface of water and then transferring it from the surface of the water to the surface of the solid to which the monolayer or multilayer is to be applied. This transfer has been likened (ref. 13) to the laying of a carpet on the solid surface. This technique is therefore convenient for deposition of films of known and controllable thickness. Since the Langmuir-Blodgett technique enables one to study either monolayers or multilayers, it has frequently been used where a number of layers are to be applied to a surface in order to study the wear properties of lubricant layers. Data from reference 8 show that, with a long-chain fatty acid (stearic acid) deposited on stainless steel, friction coefficient (even with a single layer, i.e., a monolayer) is relatively low at about 0.1. The friction, however, rises rapidly as continued runs are made over the same track. These data are shown in figure 2–7. With either a monolayer or with multilayers of 3, 9, or 53 films, the friction coefficient starts at about the same value, 0.1. The greater the number of films, the longer it takes to wear off or displace this protective film and, consequently, the longer the time in which the film is an effective boundary lubricant. With stearic acid, the film is close packed and regularly oriented with the polar group at the solid surface.

Layers applied by use of the Langmuir-Blodgett technique are not, according to reference 13, entirely equivalent to the type of protective film developed from lubricants in practice; they are not equivalent with respect to either molecular packing or composition. Hence, other methods of applying monomolecular films have been explored. One such method has been used by Zisman (ref. 13). This method is based on a technique for adsorbing from solution a monomolecular film of any polar-nonpolar organic compound on a clean smooth solid surface and for completely separating the resulting film-coated solid from the solution. This procedure is sometimes referred to as the oleophobic film method. The procedure has also been referred to as

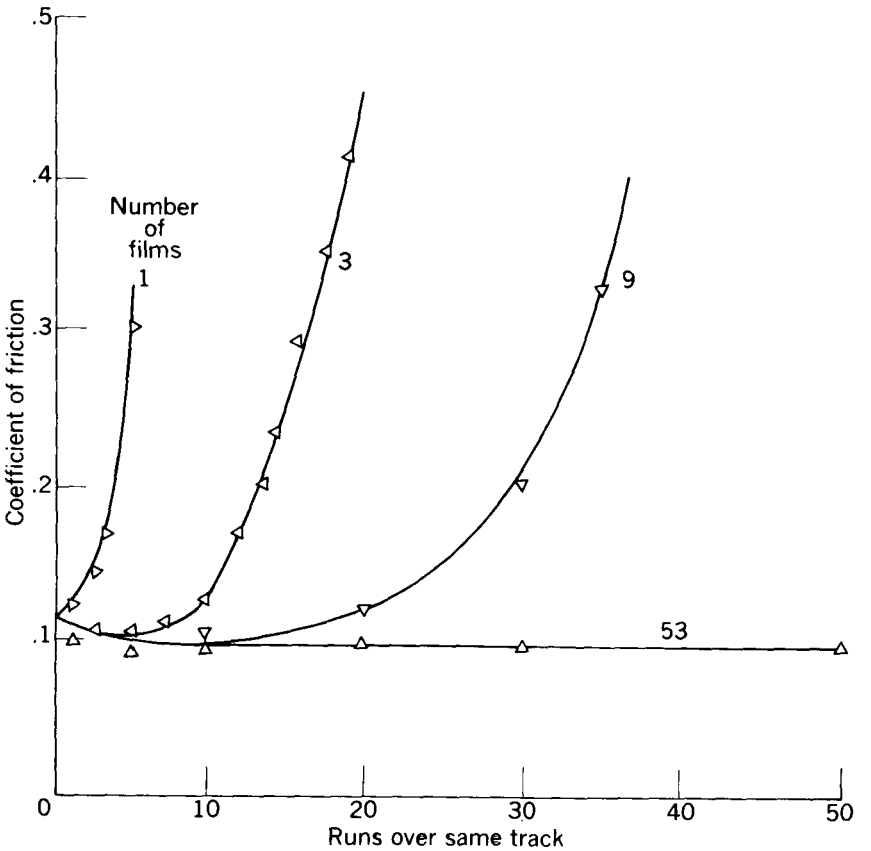

FIGURE 2-7.—Wear of stearic acid films on stainless steel. (From Bowden and Tabor, ref. 8.)

the withdrawal or the retraction method. As the names imply, the method involves application of a solution which wets the solid surface with the desired monomolecular film; the film then repels the remainder of the material. In the case of the data from reference 13, many of the experiments were conducted under conditions where no liquid phase was present; hence only a solid monolayer was present at the surface. It was shown that the condensed monolayer of many polar-nonpolar organic compounds lowered the friction coefficient as much as the bulk phase of the lubricant. These data also showed a greater durability of adsorbed monolayers than those applied by the Langmuir-Blodgett technique. The films of reference 13 were able to

withstand dozens of repeated traverses of the slider under high unit loads as compared with only a few traverses with films applied by the Langmuir-Blodgett technique (as shown in fig. 2–7). It is believed that this superior performance is explained by the fact that the oleophobic monolayers have more close-packed and strongly cohesive structures.

Chemical Films

The importance of chemical attack to the boundary lubrication process cannot be overemphasized. Some of the results already presented indicate the strong effects of films formed by chemical reaction on the friction, wear, and surface damage of metals. Experiments were carried out by Bowden, Tabor, et al. (ref. 8) using similar metals for their two friction specimens. They used as a lubricant a pure fatty acid (lauric acid) and applied it as a thin film. The results show that the lubricating properties depend markedly on the nature of the metal surfaces to be lubricated. With unreactive materials such as nickel, platinum, silver, and glass, the fatty acid is no more effective than a paraffin oil. In these experiments, the lauric acid was present as a 1 percent solution in paraffin oil. Other experiments (where the lauric acid was present as a relatively thick film) showed that effective lubrication was obtained and the friction coefficient was in the order of 0.1; this result is to be contrasted to friction coefficients of 0.3 to 0.7 for the unreactive materials previously mentioned. However, if the temperature of the surfaces was increased to a temperature just above the melting point of the lauric acid (approximately 40° C), pure lauric acid was no better as a lubricant than the 1 percent solution in paraffin oil or the paraffin oil itself.

In contrast, the results for lubrication of reactive metals show that very effective lubrication may be obtained with a 1 percent solution of lauric acid in paraffin oil.

The results obtained led to a study (ref. 8) of the chemical reactivity of various substances with fatty acids under standard conditions; the various metals were heated to 150° C in contact with the acid. The results showed that the metals fell into two distinct classes: (a) those for which chemical attack is absent or very slight (platinum, nickel, aluminum, chromium, glass, and silver), and (b) those for which chemical attack is marked (zinc, cadmium, copper, and magnesium). The friction results obtained with these materials show a strong

correlation between chemical reactivity and lubricating properties, as shown by the following results:

Metal	Coefficient of friction	Acid reacting, percent
Unreactive:		
Platinum	0. 25	0. 0
Nickel	. 28	. 0
Aluminum	. 30	. 0
Chromium	. 34	Trace
Glass	3–. 4	. 0
Silver	. 55	. 0
Reactive:		
Zinc	0. 24	10. 0
Cadmium	. 05	9. 3
Copper	. 08	4. 6
Magnesium	. 08	Trace

Experiments made with these same combinations of materials and with an increase in temperature in order to determine the temperature at which effective lubrication was no longer obtained show some interesting results. They show that the fatty acid film is effective as a lubricant at temperatures greater than the melting point of the acid, at which point disorientation of a physically adsorbed film would be expected. These results suggest that under certain conditions ". . . lubrication is effected not by the fatty acid itself, but by the metallic soap formed as a result of chemical reaction between the metal and the fatty acid" (ref. 8, p. 202). The data of figure 2–8 (ref. 8) tend to support this view. These data show that the temperature at which ineffective lubrication is obtained (the transition temperature) occurs at 50° to 70° C above the melting point of the acid. Other research results (ref. 8) show that the transition temperature corresponds approximately to the melting temperature of the metallic soap film formed by chemical reaction.

Further research done by Bowden and coworkers has shown that an oxide film on the metal surface may be necessary for formation of the metallic soap film which is effective in boundary lubrication. This necessity would explain the poor results obtained with materials like platinum and chromium.

Solid Solubility of Material Combinations

Solid solubility of metal combinations is a significant factor because of its effect on adhesion and, thus, on friction and wear. Ernst and

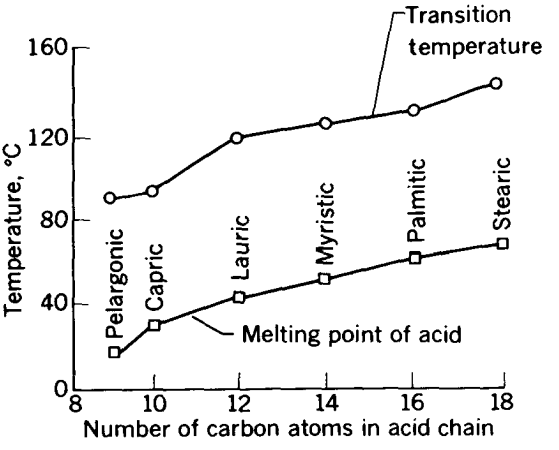

FIGURE 2–8.—Transition temperature of various fatty acids on steel surfaces. (From Bowden and Tabor, ref. 8.)

Merchant (ref. 14) have made a comparison of predicted and observed friction coefficients for various material combinations on the basis of calculated shear strength. These are presented in table 2–I. For the comparisons listed in the table, Ernst and Merchant have divided the material combinations into two groups: (a) pairs forming solid solutions at room temperature, and (b) pairs almost mutually insoluble at room temperature. The predicted (calculated) friction coefficients of table 2–I are based on the equation $f=s/H$. The value of s was calculated from the following equation:

$$s=0.427\ (L/3)\ \rho \ln\ (T_m/T)$$

In this equation, s is the static shear strength of the crystalline solid, T is the observation temperature in degrees absolute, T_m is the melting temperature of the crystalline solid form existing at T in degrees absolute, L is the latent heat of fusion of the solid crystalline form existing at temperature T, and ρ is the density of the solid crystalline form at temperature T.

In the case of "mixed pairs" such as shown in table 2–I, the value of hardness H is obviously the hardness of the softer of the two materials. The corresponding value of s is the shear strength of the weaker member of the pair. In the comparison of table 2–I, it will be noted that the predictions given by the equation are fully confirmed for the pairs forming solid solutions. Only in the case of mutually insoluble pairs do the observed values differ appreciably from the predicted values.

TABLE 2–I.—COMPARISON OF PREDICTED[a] AND OBSERVED FRICTION COEFFICIENTS [b]

Pair	Coefficient of friction, f	
	Predicted	Observed
Pairs forming solid solutions at room temperature		
Al-Fe	1. 05	1. 05
Al-Zn	. 85	. 82
Co-Fe	----------	[c] . 54
Co-Cu	. 90	. 89
Co-Al	1. 05	1. 01
Cu-Cd	. 83	. 85
Cu-Zn	. 85	. 86
Zn-Fe	. 85	. 85
Zn-Sb	. 85	. 85
Pairs almost mutually insoluble at room temperature		
Cd-Al	$<$0. 83	0. 57
Cd-Bi	$<$. 83	. 79
Cd-Fe	$<$. 83	. 64
Cd-Zn	$<$. 83	. 62
Cu-Fe	$<$1. 35	1. 05
Zn-Bi	$<$. 86	. 70

[a] Based on $f=s/H$, where $s=0.427L/3\rho \log_e (T_m/T)$.
[b] From ref. 14.
[c] This value used to calculate s for Co.

Solid solubility is also important to wear of metals. From the standpoint of wear, a reduction can be obtained provided that (a) adhesion is reduced to a minimum, or (b) if welds are formed, they must be weaker than either of the two slider materials. When the welds are weaker than either of the metals forming the pair, shearing takes place in the weld and no metal is transferred from one specimen to the other. If, on the other hand, the weld is stronger, shearing will take place in one of the slider materials and thus metal will be transferred from one to the other.

Roach, Goodzeit, and Hunnicutt (ref. 15) and, later, Goodzeit (ref. 16) investigated criteria for minimum scoring of metal pairs. The following discussion is based on their investigation.

In order to resist scoring, the metal pair must thus form a weld weaker than either of the metals. If the metals are mutually soluble, the weld is stronger. However, a strong weld may occur even when

the metals are insoluble. In a true metal represented by the elements in the left-hand columns of the periodic table (table 2–II), the bonds that hold the atoms and the crystal lattice are mobile and the electrons from the outer shell are free to move about inside the crystal. The mobility of "metallic bonding" gives metals their strength and ductility. As one moves toward the right-hand side of the periodic table the bonds become more "covalent" and atoms tend to share the electron pairs which are no longer free to move about within the crystal lattice. Covalent crystals are brittle and friable. When two metals are welded together and when one tends to covalent bonding (that is, when it is in the B-Subgroup), the weld seems to have covalent bonding and it is brittle and friable. For such pairs of metals, scoring is minimized because of this weak weld.

If the two metals form a chemical compound, the bond in the compound is generally covalent so that the weld is weak and scoring is minimized. At least one metal in an intermetallic compound is almost always from the B-Subgroup.

Roach, Goodzeit, and Hunnicutt (refs. 15 and 16) advanced criteria to permit prediction of which pairs of metallic elements can slide with minimum scoring. The criteria are stated as follows: "Two metals can slide on each other with relatively little scoring if *both* the following conditions are met: (1) the two metals are insoluble in each other and (2) at least one of the metals is from the B-Subgroup of the periodic table." These investigators studied extensively a large number of metal pairs in order to check the criteria. They concluded that there are 114 pairs of metals which seem to support the criteria and only 9 which do not support the criteria. Therefore, the results are predictable in 93 percent of the cases.

WEAR

Burwell (ref. 17) has published an excellent survey of possible wear mechanisms; much of the discussion in this section is from this reference. He points out that wear can be classified in at least four principal distinct and independent phenomena, as follows:

(1) Adhesive or galling wear
(2) Abrasive and cutting wear
(3) Corrosive wear
(4) Surface fatigue
(5) Minor types

TABLE 2-II.—PERIODIC TABLE

IA	IIA	IIIB	IVB	VB	VIB	VIIB	VIII			IB	IIB	IIIA	IVA	VA	VIA	VIIA	Inert gases
H																H	He
Li	Be											B	C	N	O	F	Ne
Na	Mg											Al	Si	P	S	Cl	Ar
K	Ca	Sc	Ti	V	Cr	Mn	Fe	Co	Ni	Cu	Zn	Ga	Ge	As	Se	Br	Kr
Rb	Sr	Y	Zr	Nb	Mo	Tc	Ru	Rh	Pd	Ag	Cd	In	Sn	Sb	Te	I	Xe
Cs	Ba	La	Hf	Ta	W	Re	Os	Ir	Pt	Au	Hg	Tl	Pb	Bi	Po	At	Rn
Fr	Ra	Ac															

Adhesive Wear

In the discussion of adhesive wear, Burwell notes that one can write an equation for wear as follows:

$$V=kAL \tag{2-1}$$

where

V volume of wear material
k wear coefficient
A real area of contact
L distance of travel

Since the real area of contact is equal to the ratio of load W to hardness (flow pressure) H, this ratio can be substituted in equation (2-1). If we make the substitution, we obtain the following equation:

$$V=k\frac{WL}{H}$$

or, for a given material,

$$V=k'WL \tag{2-2}$$

If we divide both sides of equation (2-2) by the apparent contact area A_o, the equation becomes

$$h=k\frac{PL}{H}=k'PL \text{ (for a given material)} \tag{2-3}$$

where the average depth of wear $h=V/A_o$ and the average pressure or design stress $P=W/A_o$. In other words, for a given material, the adhesive wear coefficient k' is given by the ratio

$$k'=\frac{h}{PL} \tag{2-4}$$

Figure 2-9 shows the results of some wear experiments for two loads as conducted by Burwell. We see first that wear is a linear function of distance and, second, that it is a function of load. Figure 2-10 presents the results obtained at the NASA laboratories, which show that wear is a linear function of load and is *completely* independent of apparent area of contact (over the range studied). Results of NASA wear experiments are also given in figure 2-11; these data also show that wear is *not* influenced by apparent area of contact. Even though apparent area of contact varied over a range great enough to change nominal contact stress from 41 to 273 psi, all points fall on the same wear-time curve.

The results of figures 2-9 to 2-11 tend to show that equation (2-2) is applicable. Burwell's results at variable loads confirm the results shown in figure 2-10: that is, wear is directly proportional to load.

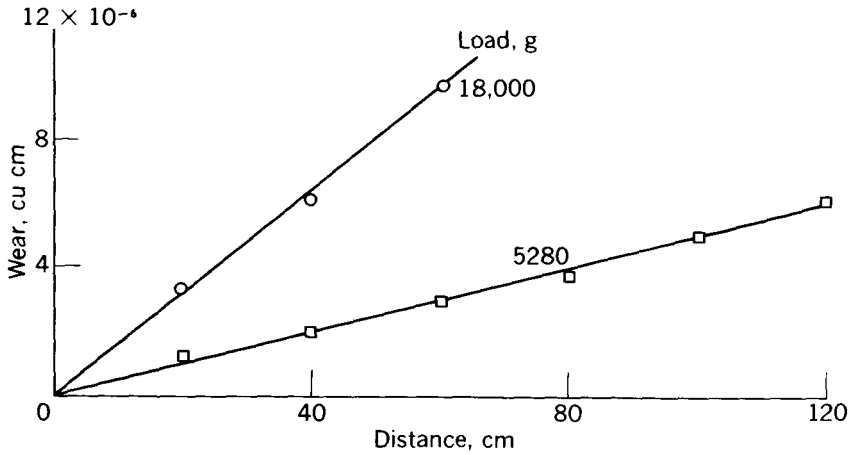

FIGURE 2–9.—Volume of wear as a function of the distance of travel. (From Burwell, ref. 17.)

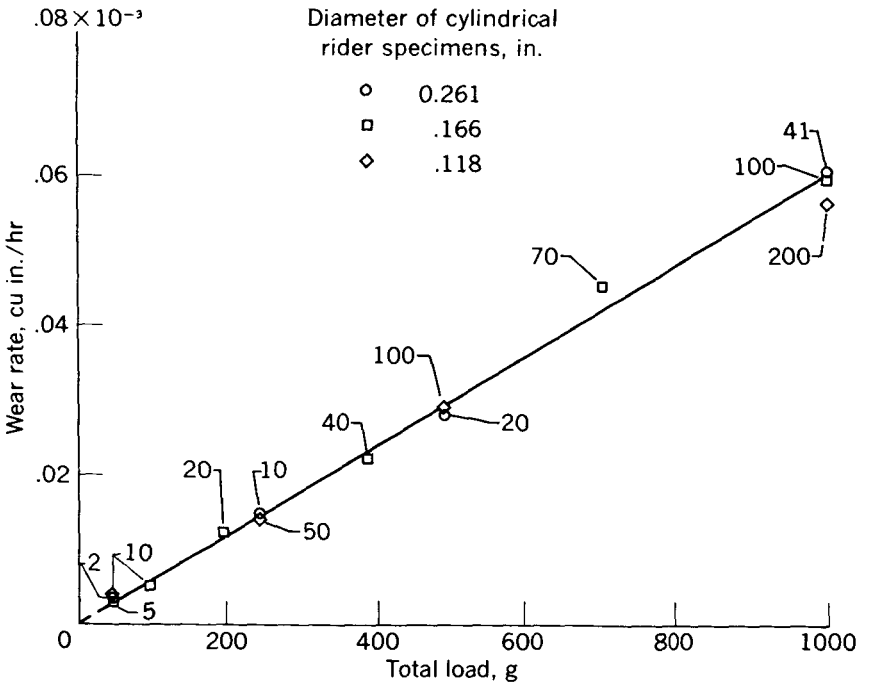

FIGURE 2–10.—Effect of total load and unit load on wear of carbon against chromium plate. Sliding velocity, 10,000 feet per minute; temperature, 360° F; atmosphere, dry air. (Numbers beside data points indicate apparent contact stress in psi.) (From ref. 41.)

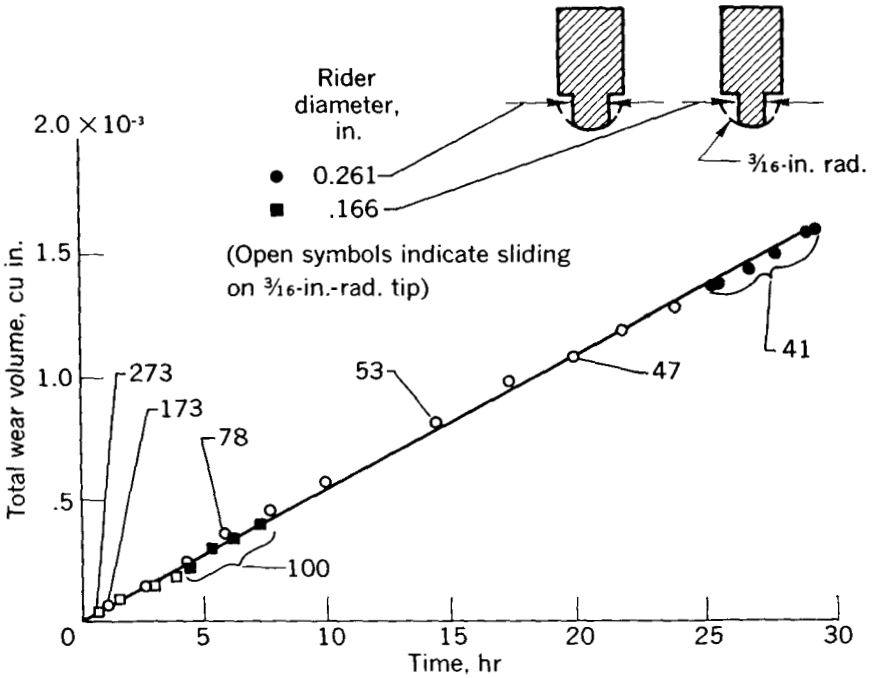

FIGURE 2–11.—Wear of typical carbon against chromium plate. Sliding velocity, 10,000 feet per minute; load, 1000 grams; temperature, 360° F; atmosphere, dry air. (Numbers beside data points indicate apparent contact stress in psi.) (From ref. 41.)

In other words, k' is a constant characteristic of the material over a range of speeds and loads.

Burwell continued his experiments at higher loads and found some peculiar results. As the load was increased to a point generally exceeding the range of accepted engineering design, it was found that the adhesive wear coefficient k' was no longer constant but increased rapidly with load (average compressive stress). These results are shown in figure 2–12, which is a plot of the adhesive wear coefficient k' against pressure. These curves show that the value of wear coefficient is constant up to a value of average pressure, which is approximately one-third of the indentation hardness. Above this pressure, the wear coefficient rises sharply and the curve is finally terminated by the onset of large scale welding and seizure. The curve of figure 2–12(b) is for the same steel as that for figure 2–12(a) except that the steel has been hardened to about twice the Brinell hardness. The curve for the hard steel again shows that the wear coefficient is constant up to a value of approximately one-third of the indentation

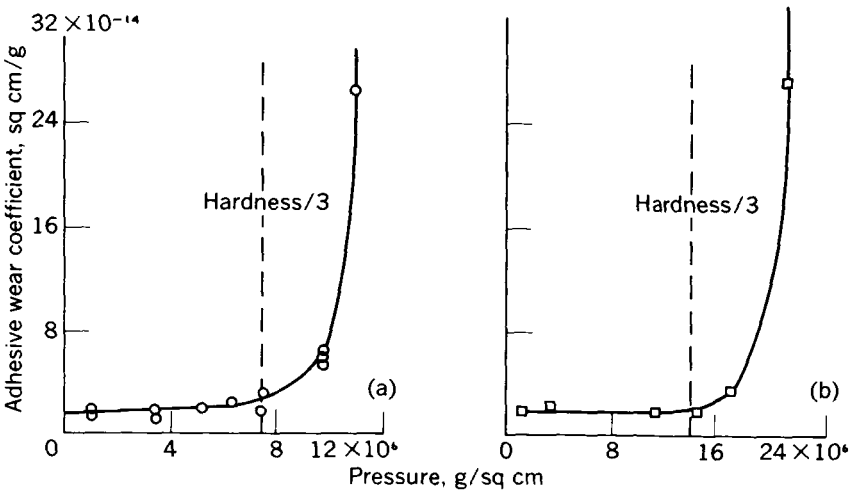

(a) Brinell hardness, 223. (b) Brinell hardness, 430.

FIGURE 2–12.—Wear coefficient as a function of average stress for two steels. (From Burwell, ref. 17.)

hardness. It will be noted in this case, however, that the average pressure is appreciably higher because of the higher hardness.

Abrasive and Cutting Wear

Burwell points out that abrasive and cutting wear are, in general the same type of damage to the surface. In one case, damage is accomplished by a hard surface plowing or gouging out a softer surface. There are two general situations for this type of wear: (1) the hard surface in question is the harder of the two rubbing surfaces (cutting wear); (2) the hard surface is a third body, generally a small particle of grit or abrasive caught between the two surfaces and sufficiently harder than these surfaces that it abrades either one or both of them (abrasive wear). Cutting wear is strongly influenced by the choice of the combination of materials while abrasive wear is strongly influenced by the type of foreign object (abrasive) which may form and be present between the surfaces. Frequently the foreign objects are formed by chemical reaction with the surrounding atmosphere.

Kruschov (ref. 18) correlates resistance to wear with hardness of various "technically pure metals." His results are shown in figure 2–13. Kruschov states also that prework hardening did not change results; he explains this result by saying that wear resistance, as measured in abrasive wear tests, is a function of the materials in their *maximum* work-hardness state. The points labeled "40" and "y12"

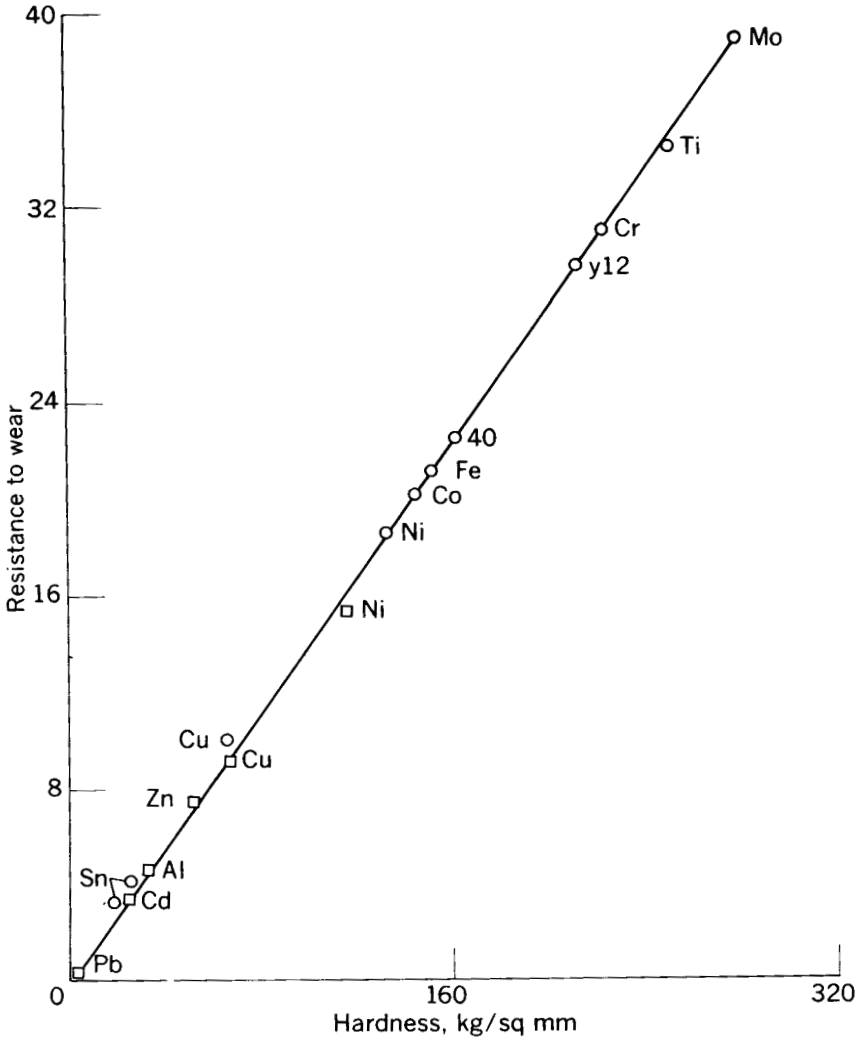

FIGURE 2–13.—Resistance to wear as a function of hardness. (From Kruschov, ref. 18.)

are for carbon steel specimens of 0.40 and 1.2 percent carbon, respectively; these specimens are in the annealed state. As noted in figure 2–13, these points fall on the same curve as for the technically pure metals.

Spurr and Newcomb (ref. 19) conducted wear experiments sliding various metals against hard, abraded "silver-steel" rods; their results (fig. 2–14) correlated wear with elastic modulus and with hardness.

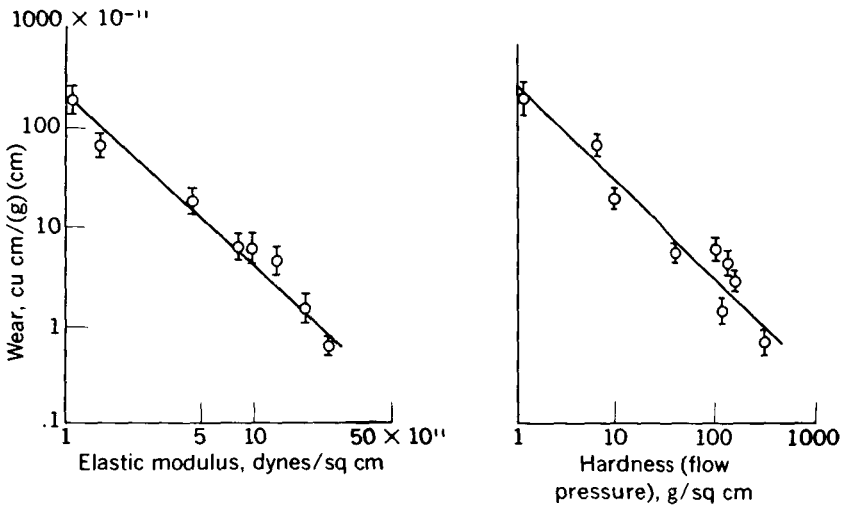

FIGURE 2–14.—Effect of elastic modulus and hardness on wear. (From Spurr and Newcomb, ref. 19.)

The effect of hardness on wear shows good agreement with Kruschov. In spite of Spurr and Newcomb's strong statement that "wear of metals is determined by their elastic modulus rather than by their hardness," the data of figure 2–14 show similar wear trends for both elastic modulus and hardness. This similarity does not seem totally unexpected since comparison of various metals indicates that hardness and elastic modulus are somewhat related.

Burwell notes that, until recently, the above comments represented the extent of the knowledge of the effect of various factors on abrasive wear. However, a rationalization of both abrasive and cutting wear in terms of the mechanical properties of the material is now beginning to evolve. The effect of hardness has been mentioned. Oberle (ref. 20) points out that a measure of abrasive wear resistance may be in the amount of elastic deformation that the surface can sustain. In other words, if in the presence of a hard abrasive particle, the surface in question can deform elastically to get out of the way, little damage will be done to the surface by the abrasive particle. The larger the elastic limit of strain, therefore, the better the surface should be able to resist damage by an abrasive or other hard surface. Rubber is an example of a type of material that can resist abrasion through elastic deformation. Water-lubricated rubber bearings for propeller shafts of ships operating in sandy water, as in harbors or shallow bottoms, have proven much more effective with respect to wear than have bronze or lignum vitae bearings, which wore excessively.

The elastic limit of strain is defined as the elastic limit of stress divided by the elastic modulus E. The elastic limit of stress, in turn, is proportional to the indentation hardness H. In other words (from ref. 17), E_{lim} is proportional to H/E. Since a large elastic limit of strain is desired for wear resistance, the value of H/E should be high. Table 2–III indicates the values of H/E for various materials; materials are listed in descending order of H/E. An interesting observation is that general experience on resistance to wear would arrange these materials in much the same order as the calculated value of H/E.

TABLE 2–III.—RATIO OF HARDNESS TO MODULUS OF ELASTICITY FOR VARIOUS MATERIALS

Material	Condition	Modulus of elasticity, E, psi	Brinell hardness number, H	Hardness/elastic modulus, H/E [a]
Alundum (Al_2O_3)	Bonded	14×10^6	2000	143×10^{-6}
Chromium plate	Bright	12	1000	83
Gray iron	Hard	15	500	33
Tungsten carbide	9% Cobalt	81	1800	22
Steel	Hard	29	600	21
Titanium	Hard	17. 5	300	17
Aluminum alloy	Hard	10. 5	120	11
Gray iron	As cast	15	150	10
Structural steel	Soft	30	150	5
Malleable iron	Soft	25	125	5
Wrought iron	Soft	29	100	3. 5
Chromium metal	As cast	36	125	3. 5
Copper	Soft	16	40	2. 5
Silver	Pure	11	25	2. 3
Aluminum	Pure	10	20	2. 0
Lead	Pure	2	4	2. 0
Tin	Pure	6	4	. 7

[a] From Oberle, ref. 20.

The elastic modulus is known to depend on certain fundamental properties of the material and of its crystal structure. In single crystals, it may be significantly different in different crystal directions. For instance, in alpha iron (ref. 17),

Crystallographic direction	Elastic modulus, E, psi
100	19, 200, 000
111	41, 240, 000

This is why chromium plate, which has an oriented crystal structure, is considerably higher in the table than cast chromium metal.

Corrosive Wear

The third important wear mechanism under sliding conditions, according to Burwell (ref. 17), is corrosive wear. Here corrosive wear is distinguished from abrasive wear in that corrosion is assumed to take place at the surfaces first, after which rubbing of the sliding surfaces removes the surface compound(s). A combination of corrosive and abrasive wear can, of course, be obtained if the corrosion compound is abrasive and acts as an abrasive wear particle. Corrosion is very much dependent on (1) the nature of the atmosphere, (2) the nature of the materials which are rubbing in the presence of this atmosphere, and (3) the presence or absence of a lubricant film. The lubricant film may act in two ways: (1) to reduce the severity of the rubbing process, and (2) to act as a blanketing film between the atmosphere and the materials and thus to prevent reaction. As previously implied, corrosion may purposely be employed in order to form a low shear strength lubricant film at the surfaces. In this case, lubrication would be done with a process known as controlled corrosion.

Surface Fatigue

The final major category of wear is that of surface fatigue, in which damage to the surface takes place by local pitting or flaking. Normally surface fatigue is a function of the number of stress cycles to which a given unit volume of the surface is subjected. The fatigue phenomenon will be discussed in more detail in chapter 12.

SUMMARY

Under extreme boundary-lubrication conditions where metal-to-metal contact occurs, the adhesion theory of friction predicts that friction and tendency to surface failure (by welding) of rubbing metals can be reduced; this reduction can be accomplished by a reduction of the ratio s/p. In this ratio, s is the shear strength of the softer of the two contacting materials, and p is the flow (yield) pressure of the softer of the two contacting materials. The most practical means of reducing the ratio s/p is to reduce the value of s. The use of thin, low shear strength films on hard base materials results in a reduction of s with negligible reduction of p. Thus, any low shear strength material (e.g., certain oxides, sulfides, plated films, liquid lubricants, etc.) that acts as a contaminant between sliding surfaces should be effective in reducing friction and surface failure.

Experimental investigations from the literature and from the NASA

laboratories produced the following results, which are consistent with the views expressed in the preceding paragraph on low shear strength contaminating films:

Formation of a contaminating film by physical adsorption of gases, liquids, or solids is beneficial. Film formation by chemisorption or chemical reaction between the surroundings and the surface is even more beneficial than with physical adsorption, primarily because of greater stability of the film so produced. Thickness of the surface film is extremely important to continued surface protection; even a monomolecular film could, however, provide initial surface protection and reduction of friction.

Solid solubility is extremely important in its effect on welding and particularly on the strength of the weld. For minimum adhesive wear, the combination of rubbing metals should not be mutually soluble.

While no direct correlation between friction and wear has been established, the principles advanced in the adhesion theory of friction for reduction of friction are also equally applicable to reduction in wear. A contaminating film which can reduce the amount of welding will markedly reduce the amount of adhesive wear. Another factor of appreciable importance in adhesive wear is that the average pressure (design stress) must be below approximately one-third of the indentation hardness, in order that the adhesive wear coefficient remain low and independent of contact stress. In the case of abrasive and cutting wear, the elastic limit of strain (which is defined as the ratio of indentation hardness to elastic modulus) may be important; the larger the elastic limit of strain, the better the wear resistance. In general, this concept has been confirmed experimentally.

II. INFLUENCE OF SOLID SURFACE FILMS ON FRICTION AND WEAR

As noted in part I of this chapter, the adhesion theory of friction predicts that friction and welding between rubbing surfaces can be reduced by reduction of the ratio s/p; s is the shear strength and p is the flow (yield) pressure of the softer of the two contacting materials. The use of thin, low shear strength films on hard base materials results in a reduction of s with negligible reduction of p. Data presented in part I showed the beneficial effect of films formed by physical adsorption or chemisorption (and possible subsequent chemical reaction) of gases, liquids, and solids.

The purpose of this part of the chapter is to show the relation of surface films of various types to the friction, wear, and surface damage of sliding metals. Study of the role of surface films requires consideration of how the film is formed. The film may be (1) formed

naturally, (2) preformed, or (3) formed by physical adsorption, chemisorption, or chemical reaction. Much of the material on solid surface films presented herein is discussed in more detail in reference 21.

APPARATUS AND PROCEDURE

Most of the experimental friction and wear studies of this chapter were conducted with the kinetic friction apparatus shown in figure 2–15 or with modifications thereof. This apparatus is described in detail in reference 22. The principal elements of the apparatus are the specimens, which are an elastically restrained spherical rider and a rotating disk. The rider is loaded with weights applied along its vertical axis. Friction force between the rider and the disk is measured by four strain gages mounted on a beryllium-copper dynamometer ring. A radial-feed mechanism, when operating, causes the rider to traverse a spiral track on the rotating disk; the rider thus slides on the virgin surface of the disk. When solid surface films were investigated, they were usually applied to the disk specimen before testing.

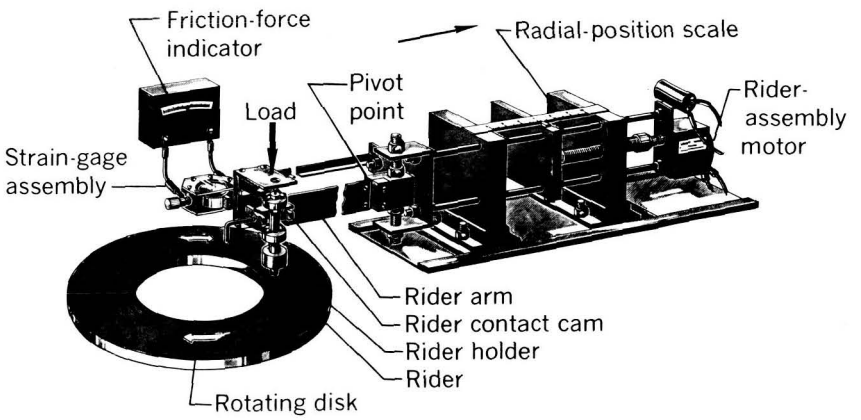

FIGURE 2–15.—Schematic diagram of apparatus. (From ref. 22.)

Most of the studies were made with specimens of steel sliding on steel. Some studies were made with nonferrous materials such as nickel or copper alloys. The solid films investigated included various oxides, sulfides, and chlorides of iron as well as solid lubricants such as molybdenum disulfide and graphite. Formation of the various preformed films is described in detail in reference 21. For comparative purposes, a load of 269 grams was used in obtaining most of the data presented. This load produces an initial Hertz surface stress of 126,000 psi. The friction data presented are typical of those obtained in many runs; for the sake of simplicity, therefore, only data from a typical run are plotted.

SOLID SURFACE FILMS

Clean Steel on Clean Steel

For comparison with results on various films, it is necessary first to establish a base line of results with uncoated surfaces. For steel-on-steel surfaces cleaned by outgassing at 1000° C in vacuum, friction coefficients as high as 3.5 have been measured (ref. 23). These surfaces were considered to be free of ordinary contaminants and much of the oxides. For steel-on-steel surfaces cleaned in air by the method used in the experiments described in this chapter, the maximum friction coefficient in air is 0.54 (fig. 2–16). The surfaces operating with a friction coefficient of 0.54 were known (refs. 24 and 25) to have a film predominantly Fe_3O_4 approximately 25 A thick (about 10^{-7} in.). At the higher sliding velocities, figure 2–16 shows that a downward trend of friction coefficient is obtained. For steel-on-steel surfaces lubricated with very thin films of either SAE 10 lubricant (or oleic acid), the friction coefficient was approximately 0.10 at minimum sliding velocity and decreased to 0.06 at 6600 feet per minute (fig. 2–16).

Surface appearance of the wear area of the rider specimens for both the dry and lubricated runs is shown in figure 2–17. The photomicrographs show that surface failure by welding occurred with the dry specimen; no welding is evident for the lubricated specimens, but ploughing is apparent. The welding for dry steel was extensive and resulted in appreciable "tearing-out" and metal transfer.

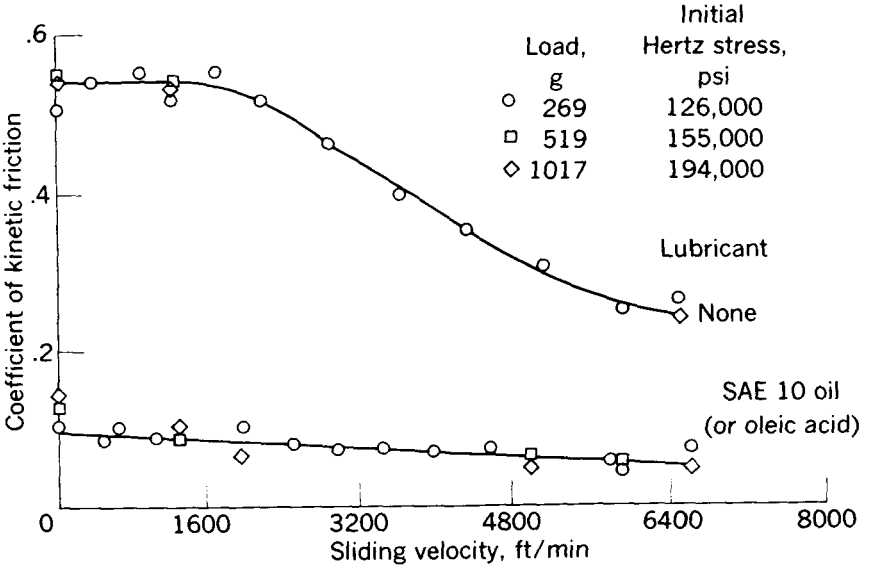

FIGURE 2–16.—Friction of dry and boundary lubricated steel surfaces. (From ref. 21.)

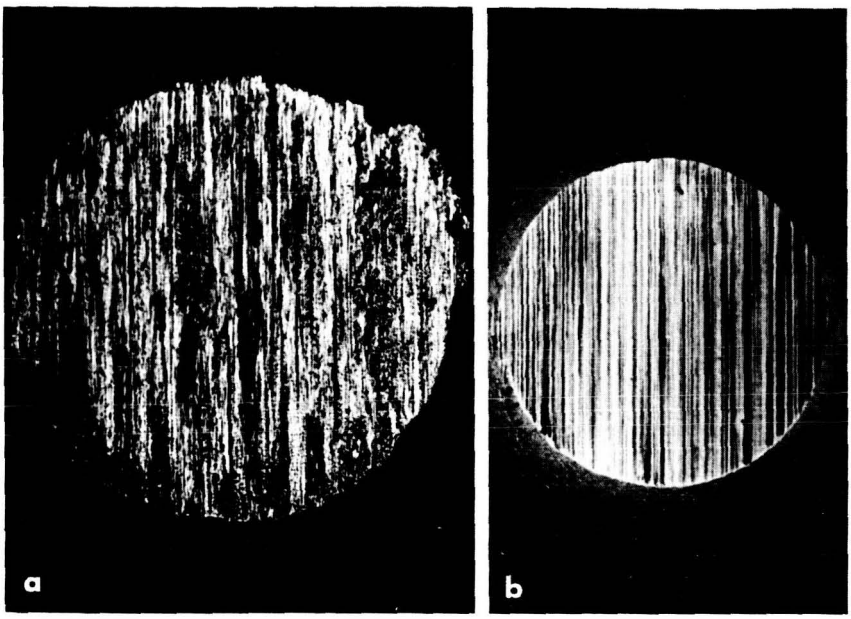

(a) Clean dry steel; diameter, 0. 038 inch.

(b) Effectively boundary lubricated steel; diameter, 0. 028 inch.

FIGURE 2–17.—Photomicrographs of rider wear areas. (From ref. 21.)

Naturally Formed Surface Films

Iron oxides.—The downward trend of friction coefficient with increase in sliding velocity for the dry steel specimens of figure 2–16 is considered a result of formation of beneficial iron oxide films of appreciable thickness. Formation of oxide films would be accelerated at higher sliding velocities because of a higher rate of heat generation at the sliding surfaces resulting from the increased release of frictional energy. Partially confirming this concept is the fact that, when the steel slider was permitted to traverse the same wear track on the disk (fig. 2–18), FeO was identified (by X-ray diffraction) as the chief constituent in the wear debris; there was a coincident reduction in friction coefficient from 0.38 to 0.24. It is reasonable to assume that the FeO film was being formed at all times and that the film thickness was built up with continued traversals of the same track.

It is hypothesized that under sliding conditions of variable severity for specimens of steel on steel surface oxides form in the following order: FeO to Fe_3O_4 to Fe_2O_3. Considerable evidence (refs. 2, 4, 5, 24, 26, and 27) confirms the importance of oxides in the reduction of friction, wear, and surface damage of sliding surfaces. On most run-in surfaces, oxides have been identified. Figure 2–19, which is based on references

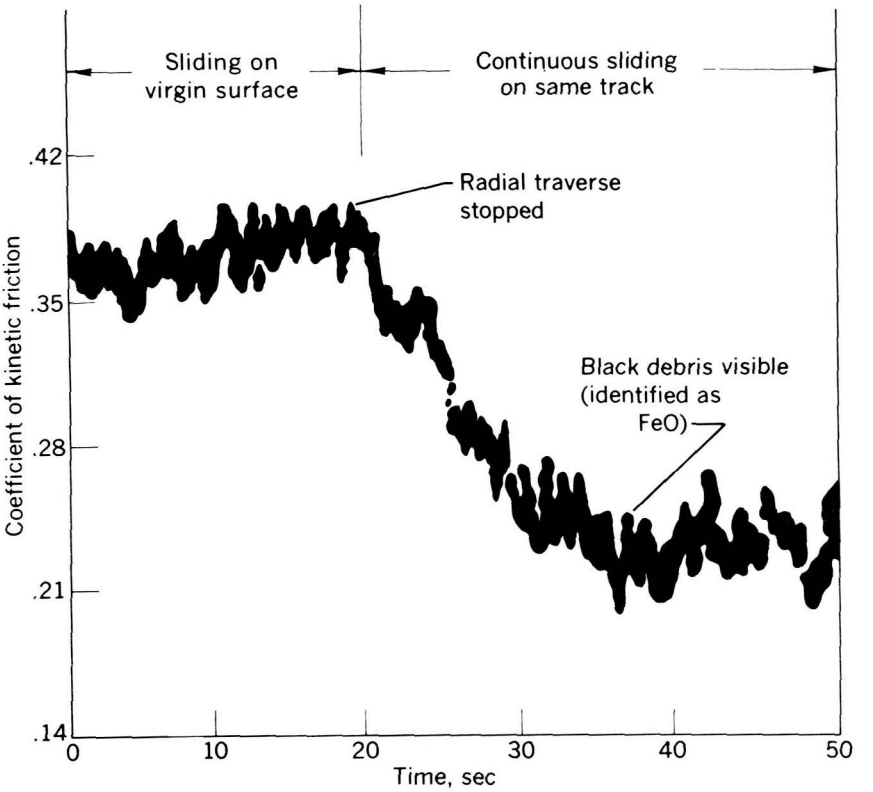

FIGURE 2–18.—Recording potentiometer trace showing effect of high-velocity sliding over a continuous path (without radial traverse) on coefficient of kinetic friction. Black wear debris (ferrous oxide, FeO) visible at beginning of lower stable friction value. Unlubricated steel; load, 269 grams; sliding velocity, 4000 feet per minute; radius of spherical rider specimen, ⅛ inch. (From ref. 22.)

2 and 26, shows, in a qualitative manner, the estimated amounts of Fe_3O_4 and Fe_2O_3 present after various degrees of run-in. As shown, the amount of Fe_3O_4 increases to a maximum for the fully run-in condition; after surface failure, less Fe_3O_4 is present. On the other hand, Fe_2O_3 shows a slight increase with degree of run-in to the fully run-in point, after which a marked increase in Fe_2O_3 is observed with failure of the surfaces. The surface films were identified by electron and X-ray diffraction.

In agreement with the implications of figure 2–19, Finch (ref. 27) states that iron oxide layers are detected on most run-in surfaces. He indicates (as does Campbell, ref. 6) that oxides play a part in the

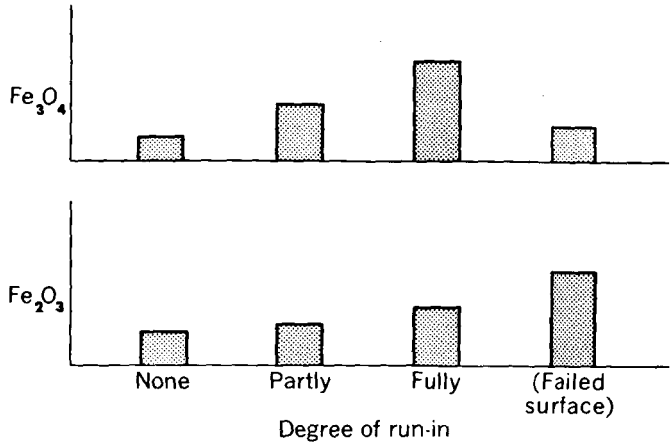

FIGURE 2–19.—Effect of run-in on formation of films of Fe_3O_4 and Fe_2O_3. (Based on refs. 2 and 26.)

mechanism of friction by affecting the ratio of welded to unwelded area. He also indicates that injurious oxides can be formed by excessive loading. This point is confirmed in figure 2–19, which shows that the oxide film Fe_2O_3 appears on the surface under surface failure conditions.

Since the data of figure 2–18 show the effect of a naturally formed iron oxide film, it is interesting to study surfaces which are rubbed together under conditions less conducive to formation of naturally formed films. Such a study was made and reported in reference 39.

Data of reference 39 show that prevention of oxide formation by exclusion of oxygen from clean specimens produces a high friction coefficient. Figure 2–20 shows that the use of highly purified cetane as a "blanketing" medium produces a friction coefficient greater than 1.0 at high sliding velocities. Similar results on the action of benzene as a "blanketing" medium in metal cutting experiments are reported by Ernst and Merchant (ref. 14); they found that friction coefficient was increased in the presence of benzene and decreased in its absence.

Miscellaneous films.—In some practical applications also, surface films have a marked effect on friction, wear, and damage of sliding surfaces (refs. 28, 29, and 30). Most of the bearings employed in the turbine-type aircraft engines are rolling-contact bearings (ref. 28). One of the principal sources of failure in such bearings has been the cage (separator, retainer). Most cage failures are, in turn, caused by faulty lubrication at the cage locating surface (because of boundary lubrication conditions). One means of reducing the severity of this problem is to use a cage material that has less tendency to adhere to

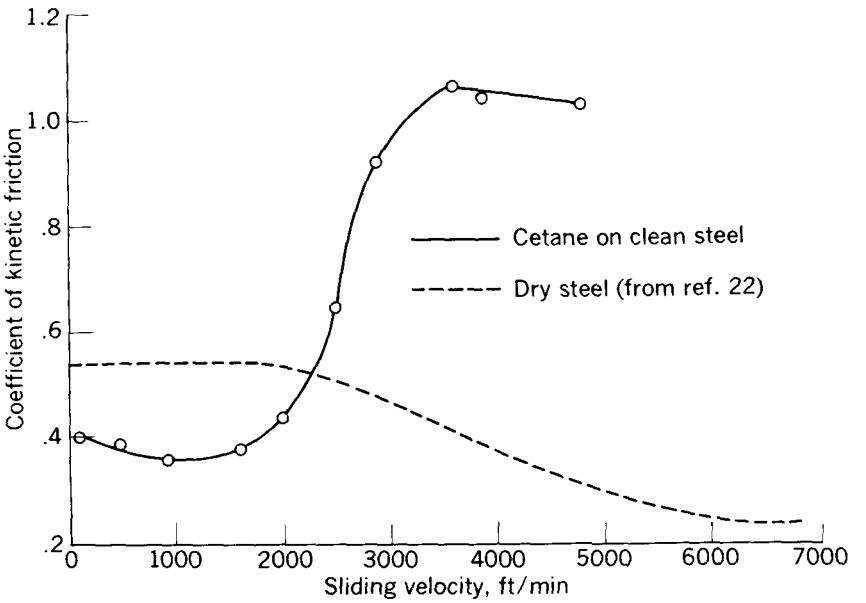

FIGURE 2–20.—Data showing effect of cetane as blanketing medium (to restrict availability of oxygen to specimen surfaces) on friction of steel against steel. Load, 269 grams; radius of spherical rider specimen, ⅛ inch. (From ref. 39.)

steel (under marginal conditions of lubrication) than the materials in current use. One experimental approach was to study the friction and wear properties of various materials, both dry and lubricated; the results were analyzed to determine the film-forming properties of the several materials. Results of this study are described in detail in reference 28. The study covered the sliding, against SAE 52100, of materials such as bronze (containing 7.5 percent lead), beryllium copper, Nichrome V, nodular iron, and gray cast iron. Figure 2–21 presents some of the wear and friction data obtained for these materials.

From the investigation of reference 28 it was determined that the ability of materials to form surface films that prevent welding is a most important factor in both dry friction and boundary lubrication. The surface films formed were derived from within the structure of the various materials (e.g., graphitic carbon in cast iron and lead in bronze). Under both dry and lubricated conditions, the nickel-base alloys form films believed to be nickel oxide (NiO). When present, the films reduced wear and friction of these materials. In this investigation, the films apparently had a greater effect on reduction of surface

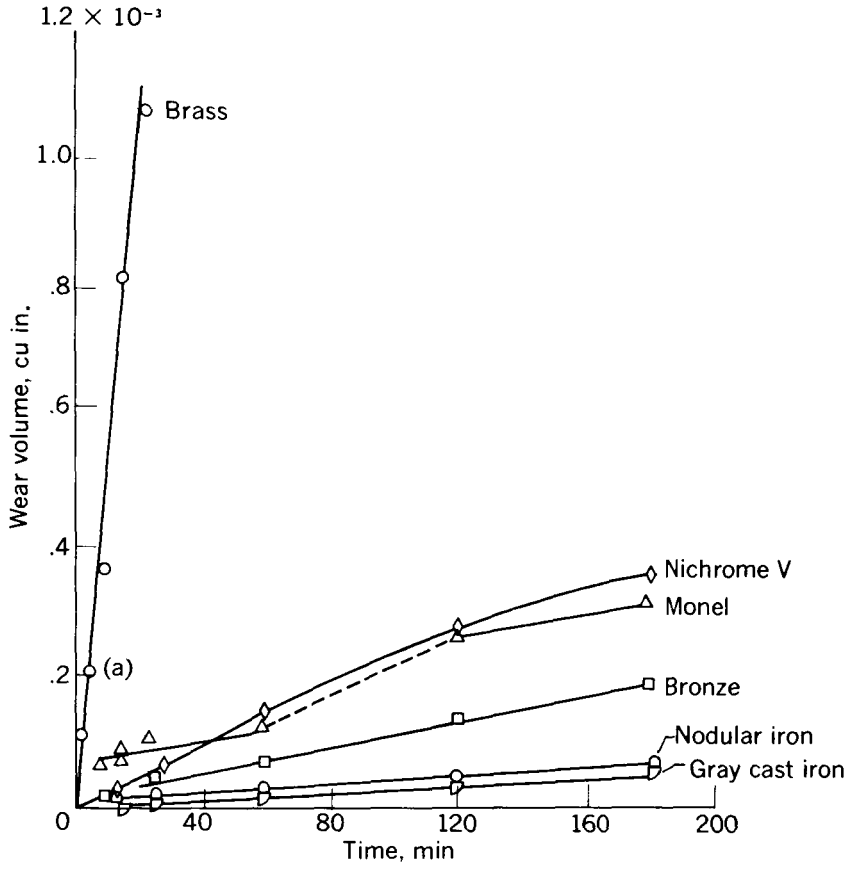

(a) Wear as a function of time; load, 50 grams.

FIGURE 2–21.—Wear and friction of various materials sliding against 52100 steel; unlubricated. (From ref. 28.)

damage and of wear than on reduction of friction (fig. 2–21). The friction coefficient with the material showing least wear (nodular iron) was relatively high (i.e., approximately 0.5). These results illustrate the lack of a direct correlation of wear and friction.

Nickel oxide.—It was observed (refs. 29, 30, and 40) that good performance (low wear and prevention of surface damage) of nickel alloys was obtained when a surface film of nickel oxide was present. Research by the NACA (ref. 31) also showed that, with increase in temperature, wear of Inconel sliding against steel decreases. This result would be expected, since an oxide film could form more readily at the higher temperatures. The reduction in both wear and friction with increase in temperature is shown in figure 2–22. The data show

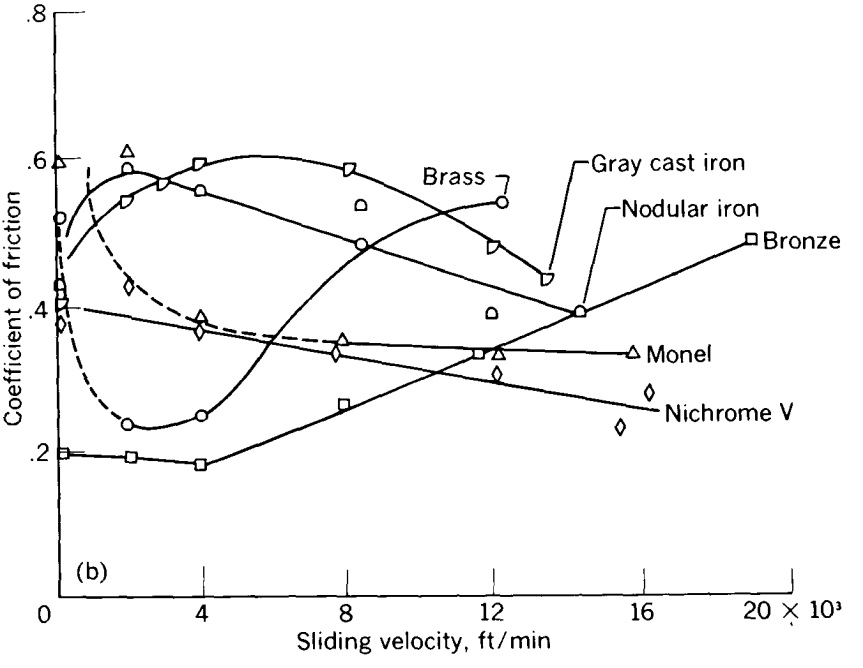

(b) Friction as a function of sliding velocity; load, 100 grams.

FIGURE 2–21.—Concluded. Wear and friction of various materials sliding against 52100 steel. (From ref. 28.)

that wear at temperatures between 600° and 1000° F is approximately one-twentieth that at 80° F. Analysis of these data would lead to the following hypothesis: Wear is presumed to be that of nickel oxide at temperatures greater than 600° F and is presumed to be that of Inconel at lower temperatures. The dashed line of figure 2–22 is an extrapolation of the wear curve for nickel oxide to the lower temperatures.

The effect of the film on wear was checked with two types of experiments: in the first, specimens with preformed nickel oxide films were tested; in the second, an attempt was made to prevent the natural formation and repair of the oxide film by limiting the availability of oxygen to the specimens. Films were preformed by two methods. One film was preformed on a cast Inconel specimen by making a wear run in air at 1000° F; a room-temperature wear run was then made with this same specimen. As indicated in figure 2–22, the wear rate was approximately one-tenth of that obtained with an untreated specimen. The second method of preforming the film on cast Inconel was heating it in molten caustic, sodium hydroxide. The specimen

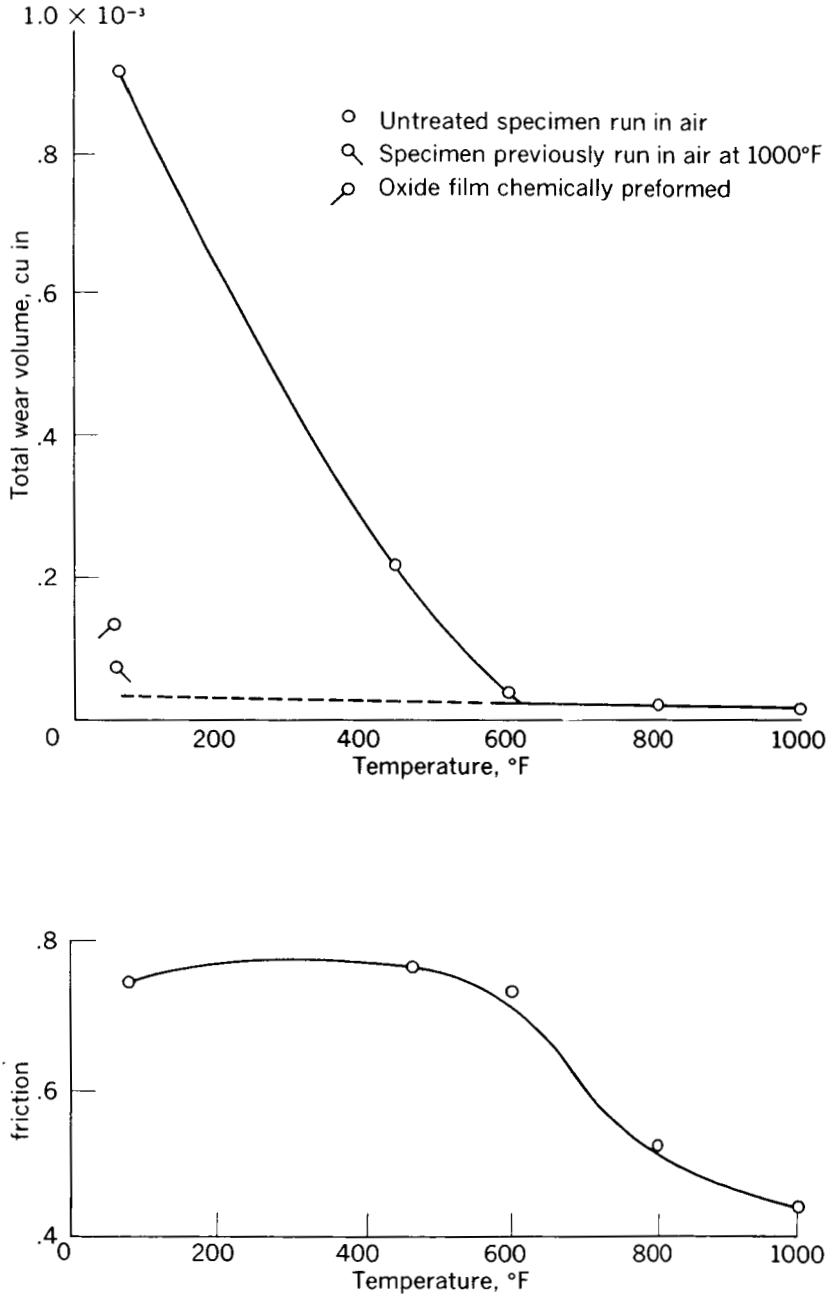

FIGURE 2–22.—Wear and friction of cast Inconel (rider) sliding against M–10 tool steel (disk); unlubricated. Sliding velocity, 120 feet per minute; load, 1200 grams; radius of spherical rider specimen, 3/16 inch. (From ref. 31.)

was then run at room temperature; wear was again approximately one-tenth of that obtained under similar conditions with an untreated specimen of the same material.

The experiment involving oxygen availability was made with cast Inconel at 1000° F in an atmosphere of argon. Although some oxide was undoubtedly formed (because air was present as a contaminant in the argon), wear was higher by a factor of 4. The wear results at 1000° F in both the air and argon atmospheres are shown in bar graph form (fig. 2–23(a)); also shown in bar graph form are the wear results at 80° F for Inconel specimens with and without the NiO film (fig. 2–23(b)). These results point to the beneficial effect of the nickel oxide film on both wear and prevention of surface damage.

Lacquer or varnish films.—In reciprocating engines, good wear performance has been associated with the formation of a very thin lacquer or varnish film on the surfaces of components such as cylinders or journal bearings. The aircraft turbine engine is generally characterized by high operating temperatures; these high temperatures accelerate the processes of oxidation, polymerization, and decomposition of the lubricants. These processes of degradation of lubricants result in formation of lacquer films on hot surfaces such as bearings. Because these films occur naturally, a fundamental evaluation of the

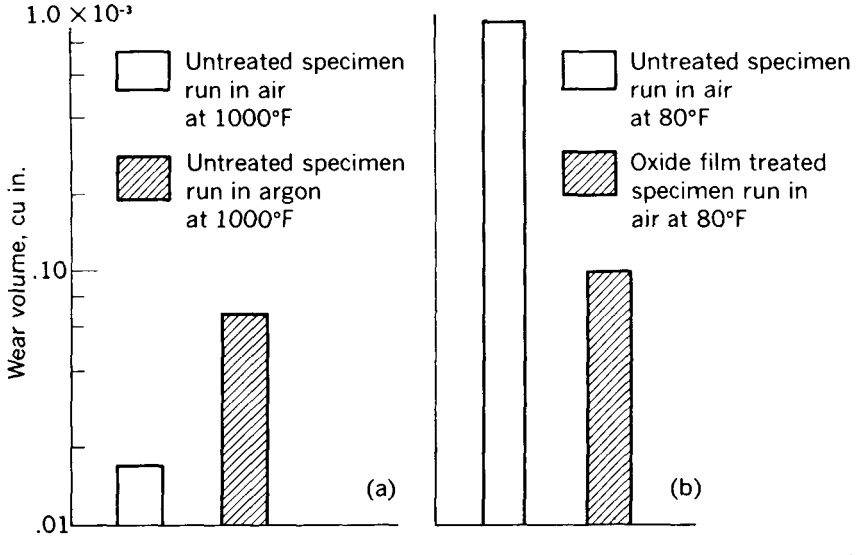

(a) Air and argon atmospheres.

(b) Oxide film and untreated specimens.

FIGURE 2–23.—Effect on wear of atmosphere (air or argon) and of surface treatment (oxide treated or untreated). (Data from ref. 40.)

role of such films in friction and surface damage was considered worthwhile. Their influence on surface damage was particularly important in the gas turbine engine, which has bearings that operate dry for a short time after startup of the engine. This condition is the result of the high-temperature "soak-back" of the turbine bearing after shutdown of the engine (refs. 32 and 33). Since the flow of coolant-lubricant stops with shutdown, the bearing temperature increases because of the large reservoir of heat in adjacent large metal masses, such as the turbine wheel. When the engine is restarted after a period of shutdown, the bearings operate without lubricant for a short time until lubricant flow is established. During this initial period the bearing parts, including the cage, operate dry. Because the cage has been a principal source of bearing failures and these cage failures have been established as the direct result of lubrication failures (ref. 33, discussion, p. 184), a study was made of the friction and damage characteristics of films formed on steel surfaces by decomposition of several types of lubricants. These lubricant types included ordinary petroleums and synthetic lubricants of the diester, glycol, and silicone types. Results of this investigation are reported in detail in reference 21.

In general, when the data of reference 21 are compared with those from dry, clean, steel surfaces, they show that the decomposition products reduced friction and surface damage of slider surfaces. The effect of surface films in reducing friction and protecting the surfaces is strikingly demonstrated in figure 2–24, which shows friction coefficient under three conditions: (1) with silicone (a poor lubricant) alone, (2) with a silicone decomposition film, and (3) with silicone fluid over a decomposition film. The marked reduction in friction with decom-

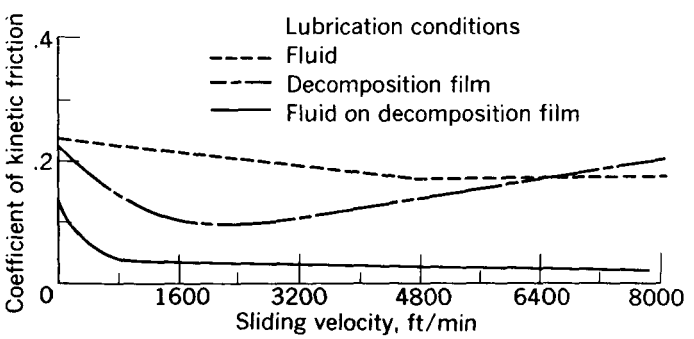

FIGURE 2–24.—Effect on friction of a silicone and its decomposition film. (From ref. 21.)

position films is apparent. Furthermore, with the fluid alone, surface damage was severe; appearance of the rider was similar to that shown in figure 2–17(a). With the decomposition film alone and with the fluid over its decomposition film, damage to the surfaces was very slight; rider appearance was similar to that of figure 2–17(b).

There will be more discussion of the lubrication effect, in rolling element bearings, of decomposition films in chapter 11.

Preformed Films

Studies were made of a number of preformed solid surface films of the type formed (1) naturally (as in the case of oxides), (2) by chemical reaction of surfaces with active additives, or (3) from solid lubricants (such as molybdenum disulfide and graphite) that function as supplemental lubricants (ref. 34).

Iron oxides.—Because of the indicated importance of iron oxides, data were obtained on films 1200 A (5×10^{-6} in.) thick of the specific oxides Fe_3O_4 and Fe_2O_3 (fig. 2–25). The friction coefficients, as well as the condition of the rider surfaces, show that Fe_3O_4 can be quite beneficial in decreasing friction and in preventing surface damage. In comparison, Fe_2O_3 showed high friction, excessive welding, and surface damage.

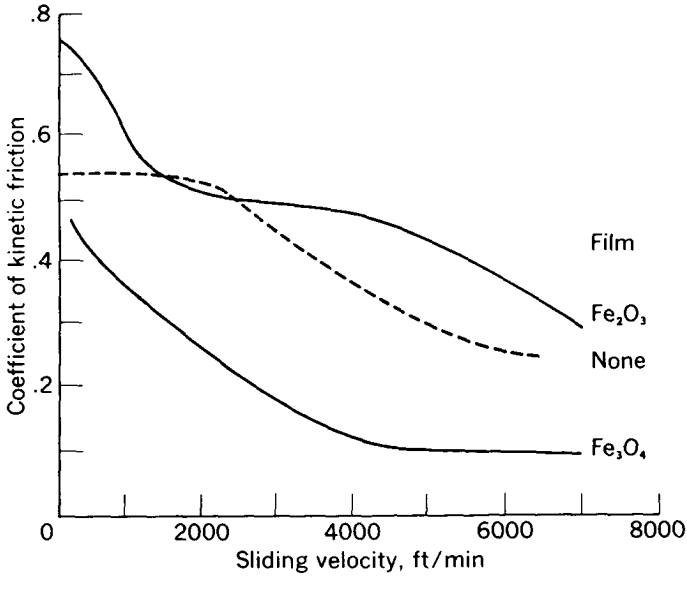

FIGURE 2–25.—Friction of preformed Fe_2O_3 and Fe_3O_4 films 1200 A thick. (From ref. 35.)

These data, as well as the data on naturally occurring iron oxide films previously discussed, emphasize the importance of iron oxide films to friction, wear, and surface damage.

Chlorides and sulfides.—The mechanism of extreme pressure lubricants is considered to be one of chemical reaction between active additives and the metal surfaces. With steel surfaces, iron compounds of chlorine, sulfur, or phosphorus are formed, depending upon the type of additive used. Results of an investigation (ref. 35) on preformed chloride and sulfide films approximately 1000 A (4×10^{-6} in.) thick are shown in figure 2–26. Visual examination of the surfaces showed that both FeS and $FeCl_2$ are effective in preventing excessive surface damage; $FeCl_2$ is much more effective than FeS, however, in reducing friction (fig. 2–26).

Metallic soaps.—At the present time, the theory is rather generally accepted that boundary lubrication by materials such as fatty acids is effected primarily by chemisorption rather than by physical adsorption alone. This point was discussed earlier. Lubrication is most effective, therefore, when there is some reaction of the fatty acids with the metals to form a metallic soap. Reference 8 shows that lubrication with fatty acids and the formation of metallic soaps is very markedly affected by the presence or absence of oxide films. There is a discussion in reference 21 which shows that the type of oxide film is also extremely important. Stearic acid was effective as a lubricant to sliding velocities of only 3000 feet per minute with Fe_2O_3; in contrast, effective lubrication was obtained to 7000 feet per minute with Fe_3O_4.

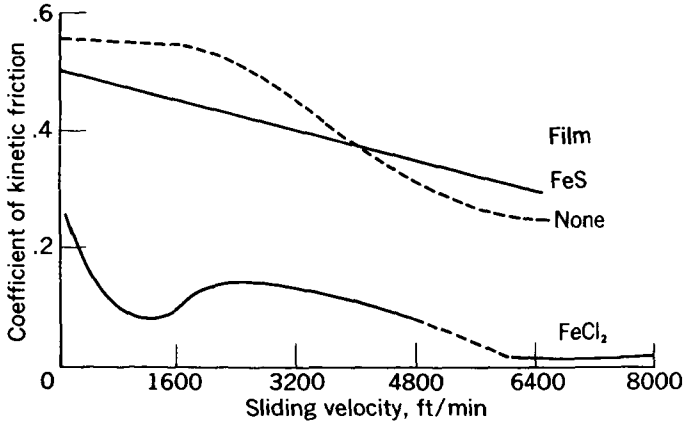

FIGURE 2–26.—Friction at high sliding velocities of steel against steel with no film and with preformed films of $FeCl_2$ and FeS approximately 1000 A thick. Radius of spherical rider specimen, ⅛ inch. (From ref. 35.)

Solid lubricants.—While solid lubricants is the subject of chapter 8 in which various solids are discussed in considerable detail, the results of some early experiments will be discussed here. The primary object of the discussion in this chapter is to indicate, in a general manner, the influence of solid lubricants on friction, wear, and surface damage of sliding metals.

As indicated in reference 36, a "self-repairing" film is the most effective means of maintaining a film at the surface. Other types of film are, however, effective for limited periods of time. Preliminary friction studies were conducted with molybdenum disulfide (MoS_2) and graphite because of their low shear strength and laminar structure.

Experimental friction results with preformed films of MoS_2 and graphite are shown in figure 2–27. These data are discussed in detail in reference 35. At low speeds, friction is approximately the same; at higher speeds, friction of MoS_2 is lower. Visual observation of the rider specimens indicated that some welding had occurred with the graphite film and none with the MoS_2 film. Occurrence of welding with the graphite film was probably the result of the manner of film formation. Important differences between the graphite and the MoS_2 films were the manner in which the two films were formed. The graphite film was a rubbed film (estimated thickness less than 0.0005 in.) and may not have adhered well or been completely continuous on the surface. The MoS_2 film was a continuous film (estimated thickness 0.005 in.) bonded to the surface by the resin bond method described in reference 37. As will be discussed in chapter 8, a resin-

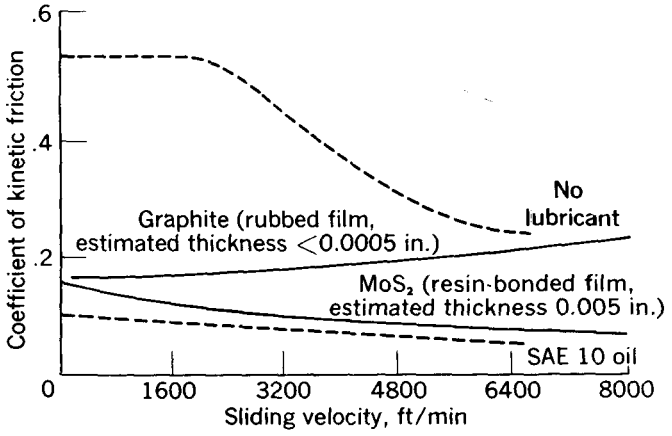

FIGURE 2–27.—Friction at high sliding velocities of steel against steel with preformed films of molybdenum disulfide and graphite. Radius of spherical rider specimen, ⅛ inch. (From ref. 35.)

bonded film of graphite shows friction results similar to those for a resin-bonded MoS_2 film.

Molybdenum disulfide as an inhibitor of fretting.—As indicated in reference 21, early studies of the mechanism of fretting (commonly called "fretting corrosion" or "friction oxidation") suggested that fretting damage is caused basically by high adhesive forces; the adhesion theory of friction should therefore apply equally to this problem as well as to normal friction problems. In consequence, a contaminating film of low shear strength should be effective in the mitigation of fretting. Because of the effectiveness of MoS_2 as a solid-film lubricant, it was checked for its effectiveness as an inhibitor of fretting. Data obtained that show MoS_2 to be an effective fretting inhibitor are presented in the following table. For comparison purposes, data for clean specimens and for specimens lubricated with mineral oil are included.

Fretting specimen	Surface film	Cycles to start of fretting
Steel ball on glass flat	None	1 to 30
	Mineral oil	1500
	MoS_2, dusted	72, 000
	MoS_2, bonded	28, 000, 000
Steel flat on steel flat	None	<100
	MoS_2, bonded	10, 000, 000

These results show that any contaminant (even mineral oil) delays the start of fretting; this effect is believed to result from reduction of the adhesive forces responsible for fretting. Of the various methods of applying MoS_2, bonding of the film was clearly superior, probably because of the strong adherence of the bonded film to the surface.

SUMMARY OF RESULTS

As predicted by the adhesion theory of friction, experiments showed that friction, wear, and surface damage of rubbing materials can be reduced by solid surface films. These films act in two ways: (1) they reduce shear strength, and (2) they act as contaminants to reduce welding by reducing contact of clean metal to clean metal. Reduction of surface failure and welding contributes markedly to lower wear.

Experimental investigations produced the following results, which are consistent with the views expressed in the preceding paragraph on low shear strength contaminating films.

Experiments with iron oxides show that FeO and Fe_3O_4 are generally beneficial, while Fe_2O_3 is harmful. With steel specimens in sliding,

exclusion of oxygen by use of a blanketing medium prevented the formation of the beneficial oxides and permitted extensive surface welding. In fact, the results of these and other investigations indicate that, with many metals and particularly ferrous alloys, effective lubrication is very often dependent on the presence of an oxide film, which serves to protect the surface.

Wear studies showed that prevention of surface damage and maintenance of low wear could be associated with the formation of naturally occurring surface films on one or both of the sliding specimens; for cast irons, the surface film consisted of graphitic carbon and, for various nickel alloys, the film consisted of the nickel oxide (NiO). In one investigation with cast Inconel sliding against hardened tool steel at temperatures ranging from 80° to 1000° F, a very marked downward trend of wear with increase in temperature was observed. This downward trend is the result of formation of beneficial nickel oxide(s) at the higher temperature. In this investigation, wear at 80° F was reduced by a factor of 10 through pretreatment of the Inconel specimen to form a nickel oxide surface film. In this same investigation, wear at 1000° F was increased by a factor of 4 by limiting formation of the oxide film; this was done by limiting the availability of oxygen by displacement of air with argon.

REFERENCES

1. Bowden, F. P., and Tabor, D.: The Lubrication by Thin Metallic Films and the Action of Bearing Metals. Jour. Appl. Phys., vol. 14, no. 3, Mar. 1943, pp. 141–151.
2. Good, J. N., and Godfrey, Douglas: Changes Found on Run-In and Scuffed Surfaces of Steel, Chrome Plate, and Cast Iron. NACA TN 1432, 1947.
3. Prutton, C. F., Turnbull, David, and Dlouhy, George: Mechanism of Action of Organic Chlorine and Sulfur Compounds in Extreme-Pressure Lubrication. Jour. Inst. Petroleum (London), vol. 32, no. 266, Feb. 1946, pp. 90–118.
4. Hughes, T. P., and Whittingham, G.: The Influence of Surface Films on the Dry and Lubricated Sliding of Metals. Trans. Faraday Soc., vol. XXXVIII, no. 249, pt. 1, Jan. 1942, pp. 9–27.
5. Webb, Wells A.: The Influence of Iron Oxide on Wear of Rubbing Surfaces. Science, vol. 99, no. 2575, May 5, 1944, pp. 369–371.
6. Campbell, W. E.: Solid Lubricants. Lubrication Eng., vol. 46, no. 4, Aug. 1953, pp. 195–200.
7. Tingle, E. D.: The Importance of Surface Oxide Films in the Friction and Lubrication of Metals. Trans. Faraday Soc., vol. 46, no. 326, pt. 2, Feb. 1950, pp. 93–102.
8. Bowden, F. P., and Tabor, D.: The Friction and Lubrication of Solids. Clarendon Press (Oxford), 1950.
9. Merchant, M. E.: The Mechanism of Static Friction. Jour. Appl. Phys., vol. 11, no. 3, Mar. 1940, p. 230.
10. Larsen, R. G., and Perry, G. L.: Chemical Aspects of Wear and Friction. Mechanical Wear, Proc. Conf. on Wear, M.I.T., John T. Burwell, Jr., ed., June 1948. (Discussion by H. H. Uhlig, pp. 90–92.)

11. EHRLICH, GERT: Adsorption on Clean Surfaces. Conf. on Clean Surfaces, Annals of New York Academy Sci., vol. 101, art. 3, Jan. 23, 1963, pp. 722–755.
12. TRAPNELL, B. M. W.: The Activities of Evaporated Metal Films in Gas Chemisorption. Proc. Roy. Soc. (London), ser. A, vol. 218, no. 1135, July 1953, pp. 566–577.
13. ZISMAN, W. A.: Friction, Durability and Wettability Properties of Monomolecular Films on Solids. Symposium on Friction and Wear, R. Davies, ed., Elsevier Pub. Co., 1959.
14. ERNST, HANS, and MERCHANT, M. EUGENE: Chip Formation, Friction and Finish. The Cincinnati Milling Machine Co., Aug. 24, 1940.
15. ROACH, A. E., GOODZEIT, C. L., and HUNNICUTT, R. P.: Scoring Characteristics of Thirty-eight Different Elemental Metals in High Speed Sliding Contact with Steel. Trans. ASME, vol. 78, no. 8, Nov. 1956, pp. 1659–1667.
16. GOODZEIT, C. L.: Compatability of Metals in Bearing Contact. Preprint 58–MD–9, ASME, 1958.
17. BURWELL, JOHN T., JR.: Survey of Possible Wear Mechanisms. Wear, vol. 1, no. 2, Oct. 1957, pp. 119–141.
18. KRUSCHOV, M. M.: Resistance of Metals to Wear by Abrasion, as Related to Hardness. Inst. Mech. Eng. Proc. Conf. on Lubrication and Wear (London), 1957, p. 655.
19. SPURR, R. T., and NEWCOMB, T. P.: The Friction and Wear of Various Materials Sliding Against Unlubricated Surfaces of Different Types and Degrees of Roughness. Inst. Mech. Eng. Proc. Conf. on Lubrication and Wear (London), 1957, p. 269.
20. OBERLE, T. L.: Properties Influencing Wear of Metals. Jour. Metals, vol. 3, no. 6, June 1951, pp. 438–439G.
21. BISSON, EDMOND E., JOHNSON, ROBERT L., SWIKERT, MAX A., and GODFREY, DOUGLAS: Friction, Wear, and Surface Damage of Metals as Affected by Solid Surface Films. NACA Rep. 1254, 1956. (Supersedes NACA TN 3444.)
22. JOHNSON, ROBERT L., SWIKERT, MAX A., and BISSON, EDMOND E.: Friction at High Sliding Velocities. NACA TN 1442, 1947.
23. BOWDEN, F. P., and YOUNG, J. E.: Friction of Clean Metals and the Influence of Adsorbed Films. Proc. Roy Soc. (London), ser. A, vol. 208, no. 1094, Sept. 7, 1951, pp. 311–325.
24. HARRIS, JAY C.: Films and Surface Cleanliness. Metal Finishing, vol. 44, nos. 8–9, Aug.–Sept. 1946, pp. 328–333; 386–388.
25. NELSON, H. R.: The Primary Oxide Film on Iron. Jour. Chem. Phys., vol. 5, no. 4, Apr. 1937, pp. 252–259.
26. POMEY, J.: Friction and Wear. NACA TM 1318, 1952. (Trans. of Le frottement et l'usure, Rapport Technique 36, Office Nat. d'Etudes et de Recherches Aéronautiques. Travaux du Groupement Francais pour le Developpement des Recherches Aéronautiques (G.R.A.), 1948.)
27. FINCH, G. T.: The Structure of Sliding Surfaces. Engineering (London), vol. CLIX, no. 4131, Mar. 16, 1945, p. 215.
28. JOHNSON, ROBERT L., SWIKERT, MAX A., and BISSON, EDMOND E.: Investigation of Wear and Friction Properties under Sliding Conditions of Some Materials Suitable for Cages of Rolling-Contact Bearings. NACA Rep. 1062, 1952. (Supersedes NACA TN 2384.)

29. JOHNSON, ROBERT L., SWIKERT, MAX A., and BISSON, EDMOND E.: Wear and Sliding Friction Properties of Nickel Alloys Suited for Cages of High-Temperature Rolling-Contact Bearings. I—Alloys Retaining Mechanical Properties to 600° F. NACA TN 2758, 1952.

30. JOHNSON, ROBERT L., SWIKERT, MAX A., and BISSON, EDMOND E.: Wear and Sliding Friction Properties of Nickel Alloys Suited for Cages of High-Temperature Rolling-Contact Bearings. II—Alloys Retaining Mechanical Properties Above 600° F. NACA TN 2759, 1952.

31. JOHNSON, R. L., and BISSON, EDMOND E.: Bearings and Lubricants for Aircraft Turbine Engines. SAE Jour., vol. 63, no. 6, June 1955, pp. 60; 63–64.

32. HUNT, KENNETH C.: Petroleum Requirements of British Gas Turbines. II—Lubricants. SAE Jour., vol. 59, no. 11, Nov. 1951, pp. 20–21.

33. WILCOCK, DONALD F., and JONES, FREDERICK C.: Improved High-Speed Roller-Bearings. Lubrication Eng., vol. 5, no. 3, June 1949, pp. 129–133. (Discussion by D. Gurney, vol. 5, no. 4, Aug. 1949, p. 184.)

34. BISSON, E. E., and JOHNSON, R. L.: NACA Friction Studies of Lubrication at High Sliding Velocities. Lubrication Eng., vol. 6, no. 1, Feb. 1950, pp. 16–20.

35. JOHNSON, ROBERT L., GODFREY, DOUGLAS, and BISSON, EDMOND E.: Friction of Solid Films on Steel at High Sliding Velocities. NACA TN 1578, 1948.

36. BISSON, EDMOND E.: The Influence of Solid Surface Films on the Friction and Surface Damage of Steel at High Sliding Velocities. Lubrication Eng., vol. 9, no. 2, Apr. 1953, pp. 75–77.

37. GODFREY, DOUGLAS, and BISSON, EDMOND E.: Bonding of Molybdenum Disulfide to Various Materials to Form a Solid Lubricating Film. I—The Bonding Mechanism. NACA TN 2628, 1952.

38. BOWDEN, F. P.: The Influence of Surface Films on the Friction, Adhesion and Surface Damage of Solids. The Fundamental Aspects of Lubrication, Annals of New York Academy Sci., vol. 53, art. 4, June 27, 1951, pp. 753–994.

39. JOHNSON, ROBERT L., SWIKERT, MAX A., and BISSON, EDMOND E.: Friction at High Sliding Velocities of Surfaces Lubricated with Sulfur as an Additive. NACA TN 1720, 1948.

40. BISSON, EDMOND E., JOHNSON, ROBERT L., and SWIKERT, MAX A.: Friction Wear and Surface Damage of Metals as Affected by Solid Surface Films: A Review of NACA Research. Inst. Mech. Eng. Proc. Conf. on Lubrication and Wear (London), 1957, pp. 384–391.

41. JOHNSON, ROBERT L., SWIKERT, MAX A., and BAILEY, JOHN M.: Wear of Typical Carbon-Base Sliding Seal Materials at Temperatures to 700° F. NACA TN 3595, 1956.

BIBLIOGRAPHY

FENG, I-MING: A New Theory of Metal Transfer and Wear. Lubrication Eng., vol. 10, no. 1, Feb. 1954, pp. 34–38.

GODFREY, DOUGLAS, and NELSON, ERVA C.: Oxidation Characteristics of Molybdenum Disulfide and Effect of Such Oxidation on Its Role as a Solid-Film Lubricant. NACA TN 1882, 1949.

JOHNSON, R. L., SWIKERT, M. A., and BISSON, E. E.: Effects of Sliding Velocity and Temperature on Wear and Friction of Several Materials. Lubrication Eng., vol. 11, no. 3, May–June, 1955, pp. 164–170.

JOHNSON, R. L., SWIKERT, M. A., and BISSON, E. E.: Friction and Wear of Hot-Pressed Bearing Materials Containing Molybdenum Disulfide. NACA TN 2027, 1950.

PETERSON, M. B., and JOHNSON, R. L.: Factors Influencing Friction and Wear with Solid Lubricants. Lubrication Eng., vol. 11, no. 5, Sept–Oct. 1955, pp. 325–331.

PETERSON, M. B., and JOHNSON, R. L.: Friction Studies of Graphite and Mixtures of Graphite with Several Metallic Oxides and Salts at Temperatures to 1000° F. NACA TN 3657, 1956.

PETERSON, M. B., and JOHNSON, R. L.: Solid Lubricants for Temperatures to 1000° F. Lubrication Eng., vol. 13, no. 4, Apr. 1957, pp. 203–207.

CHAPTER 3

Hydrodynamic Lubrication

By WILLIAM J. ANDERSON

HYDRODYNAMIC LUBRICATION implies a complete separation of the surfaces in relative motion through the creation of a load-carrying continuous fluid film. Discussion of the many thousand types of machinery, the operation of which is dependent on hydrodynamic bearings, would be superfluous. The wide range of hydrodynamic bearing applications shows that hydrodynamic theory is extensive.

Hydrodynamic bearings can be divided into two broad classifications: bearings that support radial loads and those that support thrust or axial loads. Journal bearings of several types carry radial loads while tilting shoe, tapered land, and other special types of flat bearings carry thrust loads. Basic hydrodynamic theory will be developed first, after which applications to the analysis of radial and thrust bearings will be discussed.

SYMBOLS

B	width parallel to direction of motion or normal to direction of flow, in.
$\overline{B}$	pivot location
C_n	capacity number, dimensionless
C_1,C_2,C_3,C_4	constants
c	bearing radial clearance, in.
c_d	bearing diametral clearance, in.
D,d	diameter, in.
e	bearing eccentricity, in.
F	friction force per unit length, lb/in.
F'	oil film force, lb
f	friction coefficient, dimensionless
h	film thickness, in.
K	fluid film radial spring constant, lb/in.
k	ratio of slider bearing inlet to outlet film thickness

k_1	rotor spring constant, lb/in.
L, l	length normal to direction of motion, in.
M	torque or moment, lb in.
m	rotor mass, lb sec^2/in.
m	slider-bearing slope, dimensionless
N	shaft speed, rpm
N'	shaft speed, rps
O	center
P	load pressure per unit projected bearing area, lb/sq in.
p	pressure, lb/sq in.
Q	oil flow, cu in./sec
q	oil flow per unit width, sq in./sec
R,r	radius, in.
S	Sommerfeld number, dimensionless
t	time, sec
U,u	velocity in x-direction, in./sec
V,v	velocity in y-direction, in./sec
W	load, lb; or load per unit length, lb/in.
w	velocity in z-direction, in./sec
x,y,z	coordinates
$\bar{x}$	location of center of pressure
α	angular displacement of journal
β	angular coordinate measured from maximum film thickness point
γ	weight density, lb/cu in.
ϵ	eccentricity ratio, dimensionless
θ	angle between a reference line and load vector
μ	viscosity, lb-sec/sq in.
τ	shear stress, lb/sq in.
φ	angle between load vector and minimum film thickness point
ψ	fictitious angle in Sommerfeld substitution
ω	angular velocity, rps

Subscripts:

a	atmospheric
b	bearing
c	capillary
j	journal
m	moving
P	load
s	supply
o	rotor critical
x	in direction of x-coordinate

z	in direction of z-coordinate
1	value at leading edge of film
2	value at trailing edge of film

MECHANISM OF PRESSURE DEVELOPMENT IN AN OIL FILM

Before the Reynolds equation, which is the differential equation relating viscosity, film thickness, pressure, and sliding velocity, is derived, it would be well to evolve a physical understanding of pressure development in an oil film. This can be done by examining the pressure conditions that must prevail to maintain flow continuity with various film configurations.

Consider two parallel plane surfaces separated by a lubricant film. As shown in figure 3–1, the lower surface is stationary and the upper surface is moving with a velocity U in a direction parallel with the surfaces. The local flow velocity in the film u varies uniformly from zero at the stationary surface to U at the moving surface. If the plates are very wide in the direction perpendicular to the direction of motion, the rate of flow that crosses the left boundary AB will be equal to the flow that crosses the right boundary CD. The flows that cross these two boundaries result only from velocity gradients, and, since they are equal, the continuity requirements are satisfied without any pressure buildup. Therefore, no pressure buildup will result when two parallel surfaces are moving relative to each other only in a direction parallel to the surface.

Next, consider the two plane surfaces inclined slightly with respect to each other, with one of the surfaces in motion in a direction parallel to its surface (fig. 3–2(a)). Again, as with parallel surfaces, the local flow velocity u in the film varies uniformly from zero at the stationary

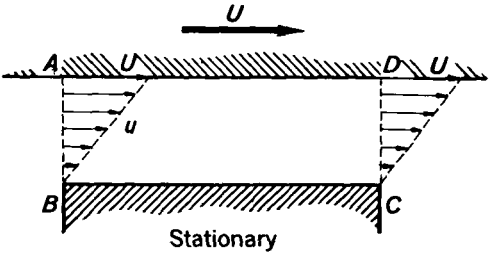

FIGURE 3–1.—Velocity distribution between two parallel surfaces in relative motion.

surface to U at the moving surface. Assume that the plates are wide in the direction perpendicular to the direction of motion so that no flow occurs except in the direction of motion. Then the velocity flow that crosses the boundary AB will be greater than the flow that crosses the boundary CD. The requirements of flow continuity thus are not satisfied since no sources or sinks exist between the two boundaries. It can be surmised that there will be a pressure buildup in the oil film until the continuity of flow is satisfied.

The flow, which results from the pressure buildup, is sketched schematically in figure 3–2(b). The local flow velocity that results from pressure gradients is zero at both surfaces since no interfacial slip is assumed. The velocity is a maximum at a point halfway between the two surfaces. The velocity profiles are parabolic. Because pressure flow is always from a region of higher to a region of lower pressure, the flow is out of the bearing at both boundaries.

The pressure flow at the boundary AB opposes the velocity flow, while the pressure flow at CD is in the same direction as the velocity flow. If the velocity and pressure flows are superimposed, the flow profiles that result are as shown in figure 3–2(c). The required equality of flow across AB and CD can now be maintained with the proper combination of velocity and pressure within the film. At some section EF within the film there is no pressure flow, and the velocity profile across the film is again linear. This is the point of maximum pressure or the point at which there is no pressure gradient.

It has been deduced previously that some inclination of two plane surfaces in relative motion is required in order to achieve a pressure buildup. This deduction can be qualified further by requiring that the film be convergent in the direction of motion. A divergent film will not produce a pressure buildup. A convergent film in a hydrodynamic bearing is called the wedge film. This wedge film is one of two ways in which pressure or, equivalently, load capacity can be generated in a hydrodynamic bearing.

The possibility of relative motion in a direction normal to the surfaces has not been mentioned previously. There is no reason to believe that this motion may not occur in bearings, and therefore it is of interest to determine what happens when it does occur. Figure 3–3 illustrates two parallel plane surfaces that are separated by a lubricant film with the upper surface moving toward the lower. Lubricant is being squeezed out of the volume between the surfaces. Since the surfaces have no velocity in the direction of flow, the only cause of this

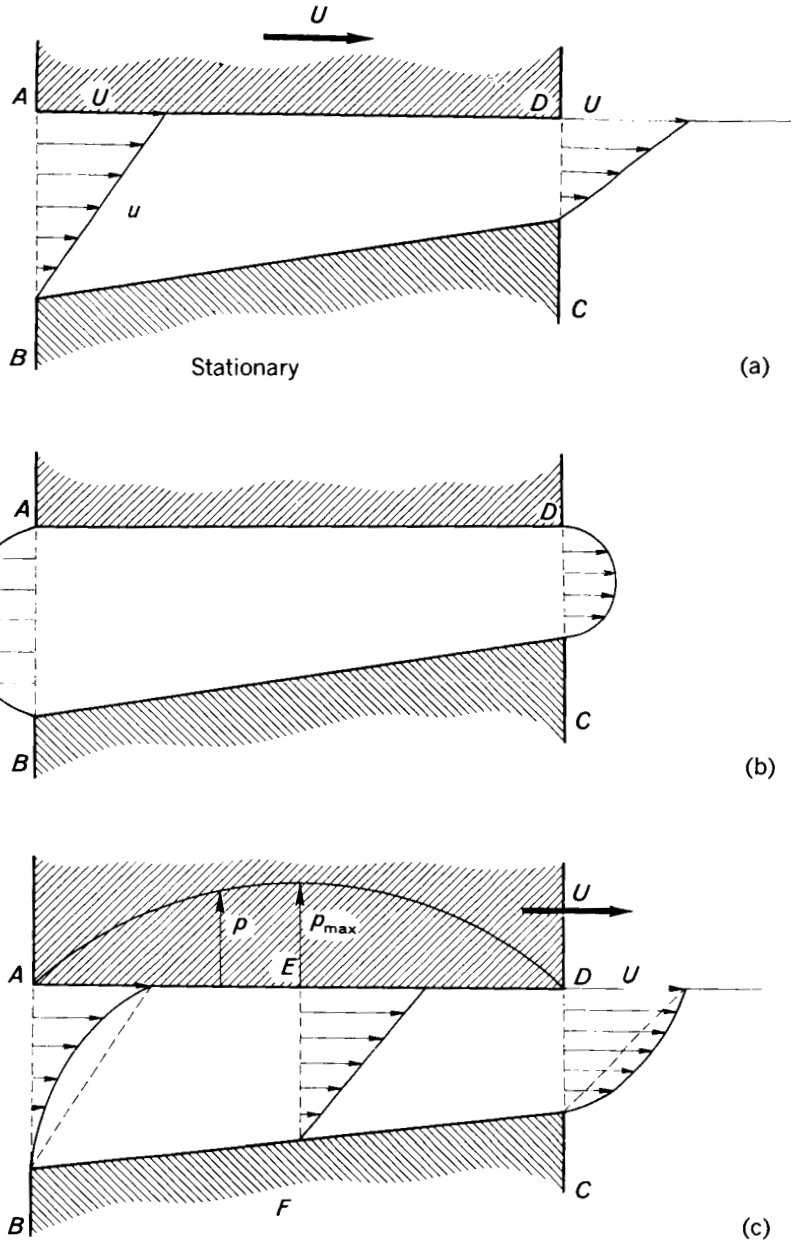

(a) Velocity distribution as a result of relative motion.
(b) Velocity distribution as a result of pressure buildup in lubricant film.
(c) Velocity distribution as a result of superimposed velocity and pressure flows.

FIGURE 3–2.—Flow between two inclined plane surfaces.

flow is a pressure gradient. Relative motion toward each other of two surfaces separated by a lubricant film will then result in a pressure buildup as shown in figure 3–3. In a hydrodynamic bearing this film is called the squeeze film. It can result in considerable additional load capacity in dynamically loaded bearings.

Load capacity can be built up in a hydrodynamic bearing from both the wedge-film and the squeeze-film actions. The next task is to establish the variables involved by deriving and solving the appropriate differential equations.

The differential equation that relates viscosity, film thickness, pressure, and sliding velocity was first developed by Osborne Reynolds and is named for him. In the derivation of the Reynolds equation, the following assumptions are made:

(1) The flow is laminar.

(2) The fluid is Newtonian (Newton's definition of viscosity holds: viscosity=shear stress/shear rate) and the viscosity is constant across the film.

(3) Inertia forces are small as compared with viscous shear forces and are neglected. (Reynolds number is low.)

(4) The weight of the fluid is negligible compared with other forces.

(5) No slip exists at the fluid-solid interface.

(6) The film thickness is small compared with any radii of curvature.

(7) The pressure across the film is constant.

(8) The inclination of one surface relative to the other is so small that the sine of the angle of inclination can be set equal to the angle and the cosine can be set equal to unity.

The following derivations are patterned after those of J. T. Burwell, which appeared in unpublished notes. Figure 3–4 shows that the moving member has a tangential velocity U and a normal velocity V.

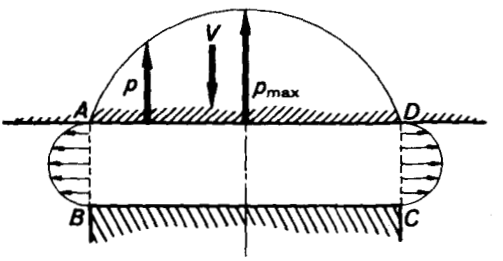

FIGURE 3–3.—Flow between parallel surfaces that approach each other.

The coordinate axes are directed as shown with the origin in the moving member. An infinitesimal volume of fluid with dimensions dx, dy, and dz in the film is shown. Pressure forces act on four faces and shear forces act on two faces. Note that there is no net pressure force in the y-direction (assumption (7)). Let the fluid particle have velocities u, v, and w in the x-, y-, and z-directions.

If the forces in the x-direction are equated with negligible fluid accelerations,

$$p\,dy\,dz+\left(\tau_x+\frac{\partial \tau_x}{\partial y}\,dy\right)dx\,dz-\left(p+\frac{\partial p}{\partial x}\,dx\right)dy\,dz-\tau_x\,dx\,dz=0 \quad (3\text{-}1)$$

$$\frac{\partial p}{\partial x}=\frac{\partial \tau_x}{\partial y} \quad (3\text{-}2)$$

From the definition of viscosity,

$$\mu=\frac{\tau_x}{\frac{\partial u}{\partial y}} \quad (3\text{-}3)$$

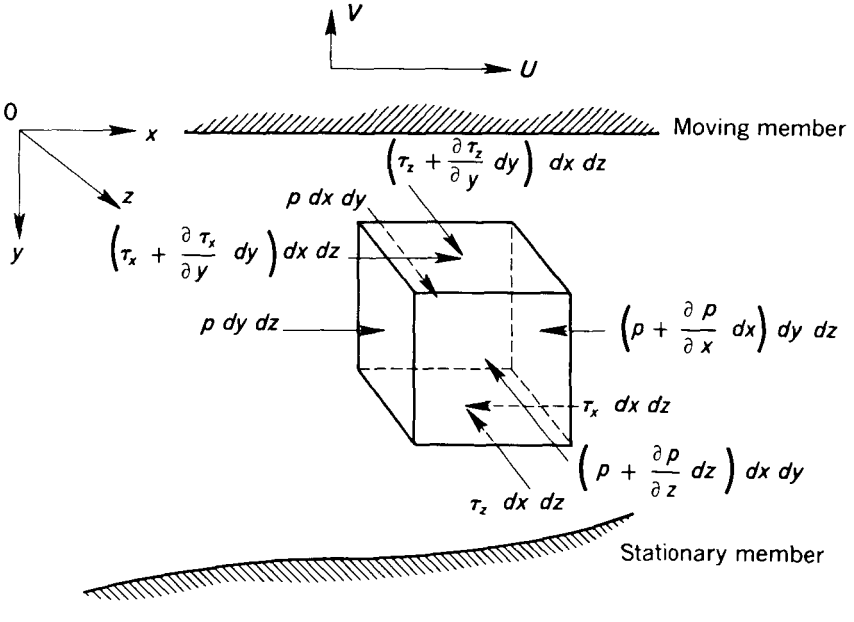

FIGURE 3–4.—Stressed element in fluid film.

$$\frac{\partial p}{\partial x}=\mu\frac{\partial^2 u}{\partial y^2} \tag{3-4}$$

Similarly, in the z-direction

$$\frac{\partial p}{\partial z}=\mu\frac{\partial^2 w}{\partial y^2} \tag{3-5}$$

Equations (3–4) and (3–5) can be integrated with respect to y since pressure p is independent of y. Integration twice yields

$$u=C_1+C_2y+\frac{1}{2\mu}y^2\frac{\partial p}{\partial x} \tag{3-6}$$

$$w=C_3+C_4y+\frac{1}{2\mu}y^2\frac{\partial p}{\partial z} \tag{3-7}$$

Specific boundary conditions are used to determine the constants C_1, C_2, C_3, and C_4:

In the x-direction C_1 and C_2 are determined by

$$\begin{array}{llll} u=U & \text{at} & y=0 \\ u=0 & \text{at} & y=h \end{array}$$

where h is the thickness of the film at any point.

Then

$$u(y)=\frac{(h-y)}{h}(U)-\frac{y(h-y)}{2\mu}\frac{\partial p}{\partial x} \tag{3-8}$$

The variation of the velocity u across the film as given in equation (3–8) is the sum of two terms. The first is the linear variation in velocity from the stationary surface at $y=h$ to the one moving with velocity U at $y=0$. It is independent of viscosity and is constant throughout the film.

The second term in the velocity distribution is that due to the pressure gradient in the x-direction. The distribution across the film is parabolic and is dependent on viscosity.

In the z-direction, C_3 and C_4 are determined by

$$\begin{array}{llll} w=0 & \text{at} & y=0 \\ w=0 & \text{at} & y=h \end{array}$$

Then

$$w(y)=-\frac{y(h-y)}{2\mu}\frac{\partial p}{\partial z} \tag{3-9}$$

In the z-direction, the velocity distribution is parabolic and results from the pressure gradient in the z-direction.

Because the Reynolds equation is essentially a continuity equation, the next step in its derivation is the calculation of flow rates in the film. When a unit width is considered, the flows in the x- and the z-directions q_x and q_z are obtained by integration of the velocities u and w over the film thickness:

$$q_x = \int_0^h u \, dy = \frac{Uh}{2} - \frac{h^3}{12\mu} \frac{\partial p}{\partial x} \tag{3-10}$$

$$q_z = \int_0^h w \, dy = -\frac{h^3}{12\mu} \frac{\partial p}{\partial z} \tag{3-11}$$

If a volume of fluid of cross section $dx \, dz$ extends across the film of thickness h and an expression is written for the net mass flow out of the volume in the x- and z-directions, this expression must equal the rate of change of mass in the volume (fig. 3–5):

$$\frac{\partial(\gamma q_x)}{\partial x} dx \, dz + \frac{\partial(\gamma q_z)}{\partial z} dx \, dz = -\frac{\partial(\gamma h)}{\partial t} dx \, dz \tag{3-12}$$

where $\partial h/\partial t = V$ is positive when away from the other surface.

Substituting for q_x and q_z from equations (3–10) and (3–11) gives

$$\frac{\partial}{\partial x}\left(\frac{\gamma h^3}{12\mu} \frac{\partial p}{\partial x}\right) + \frac{\partial}{\partial z}\left(\frac{\gamma h^3}{12\mu} \frac{\partial p}{\partial z}\right) = \frac{1}{2} \frac{\partial}{\partial x} (\gamma U h) + \frac{\partial(\gamma h)}{\partial t} \tag{3-13}$$

Equation (3–13) is a generalized form of the Reynolds equation. It applies for full film lubrication in any bearing configuration for both compressible and incompressible fluids when the assumptions made

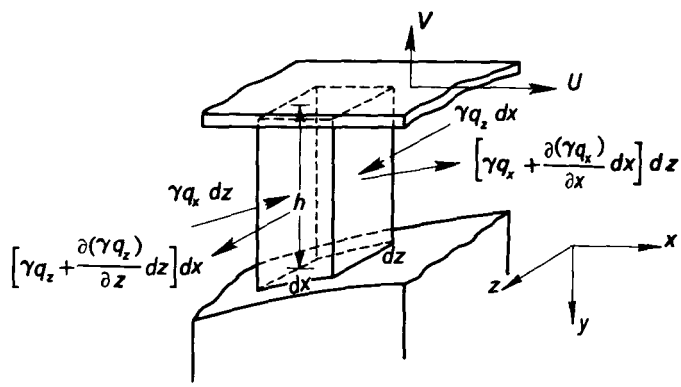

FIGURE 3–5.—Flow components into and out of fluid volume.

in its derivation are valid. Solution of the Reynolds equation for a particular bearing configuration results in an expression for the pressure throughout the film as a function of viscosity, film shape, and velocity. Integration of the pressure over the film area yields the total load supported by the film.

In addition to the load capacity obtained from the solution of the Reynolds equation, an expression for the power loss in a bearing must be developed to define completely the bearing characteristics.

The velocity distribution in the direction of motion, which is given by equation (3–8), can be used to obtain an expression for the shear stress in the x-direction exerted on the upper layer by the lower layer at any level y in the film:

$$\tau_x = \mu \frac{\partial u}{\partial y} = -\frac{\mu U}{h} - \left(\frac{h}{2} - y\right) \frac{\partial p}{\partial x} \tag{3–14}$$

At the moving surface ($y=0$), this expression becomes

$$(\tau_x)_m = -\frac{\mu U}{h} - \frac{h}{2} \frac{\partial p}{\partial x} \tag{3–15}$$

At the stationary surface ($y=h$), the force exerted by the film on the surface is

$$(\tau_x)_s = \frac{\mu U}{h} - \frac{h}{2} \frac{\partial p}{\partial x} \tag{3–16}$$

Through integration over the bearing area, the friction force becomes

$$F = \iint \tau_x \, dx \, dz = \pm \iint \frac{\mu U}{h} \, dx \, dz - \iint \frac{h}{2} \frac{\partial p}{\partial x} \, dx \, dz \tag{3–17}$$

The upper sign is used for the stationary surface, and the lower sign is used for the moving surface.

Equation (3–17) can be written in a more understandable form by integration of the second term on the right by parts:

$$\int_x \frac{h}{2} \frac{\partial p}{\partial x} \, dx = \frac{1}{2} \left\{ [h(p-p_a)]_{x_1}^{x_2} - \int_x \frac{\partial h}{\partial x} (p-p_a) \, dx \right\} \tag{3–18}$$

Generally $p=p_a$ at both edges of the film x_1 and x_2 so that the first term on the right vanishes. Then, when equation (3–18) is substituted into equation (3–17),

$$F=\pm\iint\frac{\mu U}{h}\,dx\,dz-\frac{1}{2}\iint(p-p_a)\,\frac{\partial h}{\partial x}\,dx\,dz \qquad (3\text{–}19)$$

The signs have been changed in equation (3–19) so that U may be taken as a positive quantity.

An examination of equations (3–17) or (3–19) shows that the friction forces on the moving and the stationary surfaces are not equal. The first term on the right arises from the viscous drag and is dependent on the viscosity and the velocity gradient. The second term on the right arises from pressure forces. Equations (3–17) and (3–19) show that, in order for this term not to vanish, there must exist both a pressure gradient and a varying film thickness.

No exact solution of the generalized form of the Reynolds equation given by equation (3–13) has been obtained. Approximate solutions for specific conditions have been obtained by the use of infinite series and relaxation techniques, and accurate numerical solutions have been obtained through the use of digital computers. While all these approximate solutions are valuable, the true value falls far short of that of a general solution.

The Reynolds equation is readily solvable if it is assumed that the bearing is wide relative to its length (the so-called infinite bearing), or that the bearing is short enough that the pressure-induced circumferential flow is negligible (the short bearing solution).

Sommerfeld (ref. 1) and Harrison (ref. 2) present a solution for the infinite bearing that assumes $\partial p/\partial z=0$. With this assumption and the assumption of constant density and zero normal velocity, equation (3–13) can be written

$$\frac{\partial}{\partial x}\left(\frac{h^3}{\mu}\,\frac{\partial p}{\partial x}\right)=6U\,\frac{\partial h}{\partial x} \qquad (3\text{–}20)$$

Infinite Tapered-Shoe Slider Bearing

Figure 3–6 shows the configuration and notation for an infinite tapered-shoe slider bearing. The equation to be solved is

$$\frac{d}{dx}\left(h^3\,\frac{dp}{dx}\right)=6\mu U\,\frac{dh}{dx} \qquad (3\text{–}21)$$

This equation can be integrated directly to obtain

$$\frac{dp}{dx}=\frac{6\mu U}{h^2}-\frac{C_1}{h^3} \qquad (3\text{–}22)$$

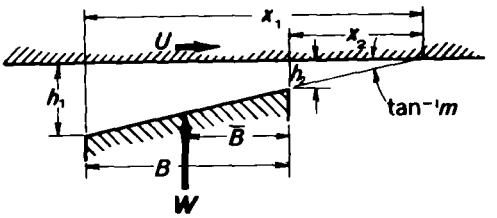

FIGURE 3–6.—Slider-bearing configuration.

Substitution of $h=mx$, where m is the slider-bearing slope, and integration yield

$$p-p_a=-\frac{6\mu U}{m^2x}+\frac{C_1}{2m^3x^2}+C_2 \tag{3-23}$$

The constants C_1 and C_2 are evaluated from the boundary conditions, which are $p=p_a$ at $x=x_1$ and x_2. Then

$$p-p_a=\frac{6\mu U}{m^2}\frac{(x_1-x)(x-x_2)}{(x_1+x_2)x^2} \tag{3-24}$$

Substituting the film thicknesses $h_1=mx_1$ and $h_2=mx_2$ yields

$$p-p_a=6\mu UB\frac{(h_1-h)(h-h_2)}{(h_1^2-h_2^2)h^2} \tag{3-25}$$

Since $h_1>h>h_2$, this expression is always positive, which indicates that the pressure in the oil film under the stator is everywhere greater than the ambient pressure. One of the important parameters in determining slider-bearing performance is the ratio of film thicknesses k. If $k=h_1/h_2=1+(mB/h_2)$, equation (3–24) can be written as

$$p-p_a=\frac{6\mu UB}{h_2^2}\frac{\left(\frac{k}{k-1}B-x\right)\left(x-\frac{1}{k-1}B\right)}{(k^2-1)x^2} \tag{3-26}$$

From the curves shown in figure 3–7, it can be seen that there is an optimum value of k. The maximum pressure point always lies downstream of the midpoint of the stator and moves farther downstream as k increases.

The load carried by the oil film is obtained by integration of the pressure over the bearing area. The load per unit length is

$$W=\int_{x_1}^{x_2}(p-p_a)\mathrm{d}x \tag{3-27}$$

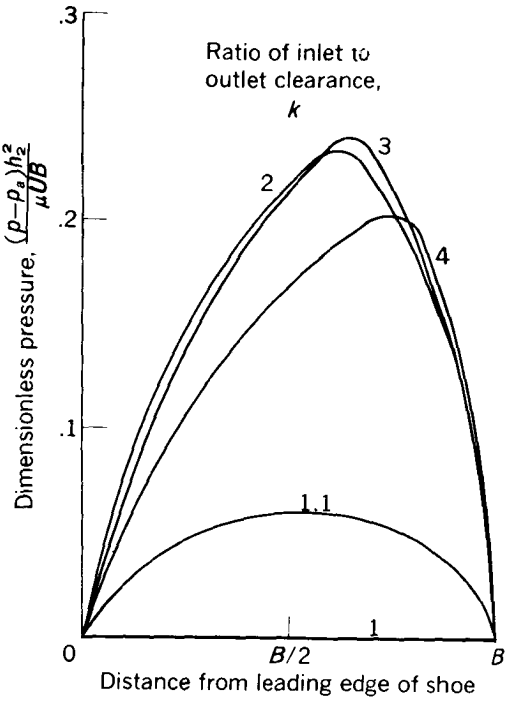

FIGURE 3-7.—Slider-bearing pressure profiles for various ratios of inlet to outlet clearance.

$$\frac{W}{\mu U}=\frac{6}{m^2}\left[\ln\left(\frac{m}{h_2/B}+1\right)-\frac{2m}{m+(2h_2/B)}\right] \tag{3-28}$$

In terms of k,

$$W=\frac{\mu U}{(h_2/B)^2}\,\frac{\ln k-\dfrac{2(k-1)}{k+1}}{(k-1)^2} \tag{3-29}$$

Infinite Kingsbury or Pivoted Slider Bearing

For the infinite fixed-angle slider bearing, m is fixed and only h_2 remains to be determined. For the pivoted slider or Kingsbury bearing, the location of the pivot ($\overline{B}$, fig. 3-6) can also be chosen at will. From figure 3-7, it is seen that the pressure pattern shifts with changes in k, which denote changes in h_2 and m. Thus, unless the resultant of the film pressure or the center of pressure passes through the pivot point, there will be a resulting moment that will act to change the tilt of the shoe as well as the minimum film thickness. In order,

then, to determine how a pivoted slider bearing behaves, an equation for the dependence of the center of pressure on other variables must be derived and solved.

The position of the center of pressure is given by

$$\bar{x}=\frac{1}{W}\int_{x_1}^{x_2} x(p-p_a)\,dx \tag{3-30}$$

Substituting for $p-p_a$ from equation (3–26) and integrating yield

$$\bar{x}=\frac{\mu U B^3}{W h_2^2}\,\frac{k\ln k-\frac{1}{2}(k^2-1)+(k-1)^2}{(k-1)^3(k+1)} \tag{3-31}$$

Substituting the expression for load W from equation (3–29) gives

$$\bar{x}=\frac{\frac{1}{2}(k^2-1)-k\ln k}{(k^2-1)\ln k-2(k-1)^2}\,B \tag{3-32}$$

From the definition of k

$$x_2=\frac{1}{k-1}\,B \tag{3-33}$$

Then in terms of k

$$\frac{\bar{B}}{B}=\frac{x-x_2}{B}=\frac{\frac{1}{2}(k-1)(k+5)-(2k+1)\ln k}{(k^2-1)\ln k-2(k-1)^2} \tag{3-34}$$

Some values of $\bar{B}/B$ for different values of k follow:

k	$\bar{B}/B$
1	0. 50
2	. 43
3	. 39
4	. 36
5	. 35

For a centrally pivoted shoe, $k=1$ and no pressure will be developed. This is unfortunate since using a centrally located pivot to allow operation in either direction would be desirable. Actually, centrally pivoted sliders have considerable load capacity because of several factors not considered in this simplified theory. During operation,

the surface of a plane shoe may deflect because of pressure forces and may distort because of thermal gradients to produce a curved surface. It can be shown analytically that a centrally pivoted curved slider bearing has a nonzero load capacity. In addition, the lubricant viscosity may change in flowing through the bearing, and this change can result in a nonzero load capacity for a centrally pivoted slider bearing.

Two equations (3–29) and (3–34) and the definition of k are used to design a tilting-pad slider bearing. These determine h_2, m, and k. Solution is accomplished most easily by plotting equations (3–29) and (3–34) against k and by eliminating k graphically.

Friction coefficients for plane slider bearings can be most conveniently calculated from the generalized friction equation (3–19). Substituting $h=mx$ gives

$$F=\pm\int_z\int_{x_1}^{x_2}\frac{\mu U}{mx}\,dx\,dz-\frac{m}{2}\int_z\int_{x_1}^{x_2}(p-p_a)\,dx\,dz \tag{3–35}$$

This equation can be integrated by noting that the second integral is the total load:

$$F=\pm\frac{\mu U}{m}\ln k-\frac{m}{2}W \tag{3–36}$$

where F is the friction force per unit length. The upper sign refers to the force on the stationary surface, and the lower sign refers to that on the slider.

A friction coefficient f, which is defined as the ratio of the friction force to the normal load, is

$$f=\frac{F}{W}=\pm\frac{\mu U}{W}\frac{\ln k}{m}-\frac{m}{2} \tag{3–37}$$

Equations (3–36) and (3–37) are convenient for use with a fixed-angle slider with m known. For a pivoted slider, the value of m in terms of k and the value of W from equation (3–29) are substituted into equations (3–36) and (3–37) to give

$$F=-\mu\frac{UB}{h_2}\frac{4\ln k-\dfrac{6(k-1)}{k+1}}{k-1} \tag{3–38}$$

on the slider and

$$F=\frac{\mu UB}{h_2}\frac{2\ln k-\frac{6(k-1)}{k+1}}{k-1} \tag{3-39}$$

on the stator.

The friction forces on the slider and the shoe are different because the drag produced by the pressure flow in the fluid film acts in the same direction on both surfaces while the viscous drag acts in opposite directions. The pressure-flow drag in equation (3-36) is $mW/2$ on each surface. The difference between the two total friction forces is twice this or mW. As a result, the tangential force on the slider is mW greater than the tangential force in the opposite direction on the shoe. The apparent anomaly in the static equilibrium of the oil film is resolved by noting that the hydrostatic pressure acts normal to the surface of the shoe so that it has a horizontal component $W \sin m \cong Wm$.

Infinite Journal Bearing

In a journal bearing (fig. 3-8) h can be expressed as

$$h=c+e\cos\beta \tag{3-40}$$

or

$$h=c(1+\epsilon\cos\beta) \tag{3-41}$$

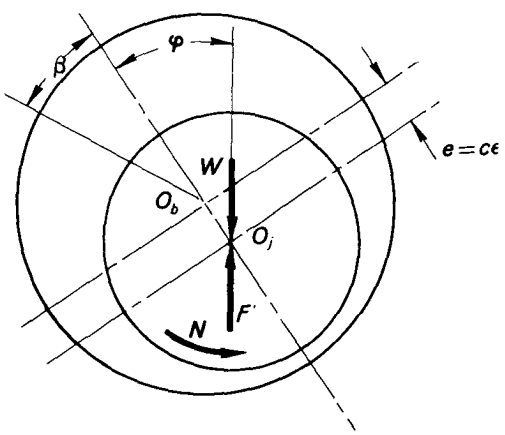

FIGURE 3-8.—Journal-bearing configuration.

If $x=R\beta$, $dx=R\,d\beta$, and $U=2\pi RN$, equation (3–20) becomes

$$\frac{1}{R^2}\frac{\partial}{\partial\beta}\left[\frac{1}{\mu}(1+\epsilon\cos\beta)^3\frac{\partial p}{\partial\beta}\right]=-\frac{12\pi N\epsilon\sin\beta}{c^2} \tag{3–42}$$

Equation (3–42) can be integrated twice to give an expression for the pressure distribution that will contain two integration constants. These constants are determined by the assumed boundary conditions. The correct boundary conditions, on the other hand, may depend on the conditions under which the journal bearing is operating. In contrast to the slider bearing in which the film converged throughout the bearing, the film in the journal bearing is convergent for $0<\beta<\pi$ and divergent for $\pi<\beta<2\pi$. Unless, then, oil is supplied from the bearing sides or in a quantity copious enough to keep the bearing cavity filled, the film cannot be continuous in the divergent portion. By use of glass sleeves it can be shown that the film in a journal bearing does, in effect, break up into streamers in the divergent portion. On the other hand, it may be possible to maintain a continuous film in a bearing that runs submerged in lubricant. Obviously then there are at least two sets of boundary conditions, the validity of which depends on the operating conditions.

For an incomplete oil film, Reynolds determined that the proper boundary conditions are

$$\left.\begin{aligned} p&=p_a\\ \frac{dp}{d\beta}&=0\end{aligned}\right\} \quad \text{at} \quad \beta=-\beta_m \tag{3–43a}$$

and

$$p=p_a=p_s \quad \text{at} \quad \beta=\beta_s \tag{3–43b}$$

The angle β_m is the angle at which the maximum pressure occurs in the film and the angle β_s locates the supply hole or groove.

The choice of boundary conditions given by equations (3–43a and b) can be better understood by integration of equation (3–42) once to obtain

$$(1+\epsilon\cos\beta)^3\frac{dp}{d\beta}=12\pi\mu\left(\frac{R}{c}\right)^2 N\epsilon\cos\beta+C_1' \tag{3–44}$$

where C_1' is a constant of integration. Then

$$C_1' = -12\pi\mu\left(\frac{R}{c}\right)^2 N\epsilon \cos \beta_m \tag{3-45}$$

where β_m is the angle at which $dp/d\beta = 0$ (the point of maximum pressure).

Then

$$\frac{dp}{d\beta} = 12\pi\left(\frac{R}{c}\right)^2 \mu N\epsilon\left[\frac{\cos\beta - \cos\beta_m}{(1+\epsilon\cos\beta)^3}\right] \tag{3-46}$$

From equation (3-46)

$$\frac{dp}{d\beta} = 0 \qquad \text{when} \qquad \beta = \pm\beta_m$$

For a continuous or unbroken film the proper boundary conditions are that the pressure shall be continuous in β with a period 2π and that

$$p - p_a = p_s \qquad \text{at} \qquad \beta = \beta_s \tag{3-47}$$

The boundary conditions for a continuous film are called the Sommerfeld conditions since they were proposed by him to obtain the first analytical solution for the pressure distribution in a journal-bearing oil film (ref. 1).

Integration of equation (3-42) yields

$$\frac{dp}{d\beta} = 12\pi\left(\frac{R}{c}\right)^2 \mu N\left[\frac{1}{(1+\epsilon\cos\beta)^2} - \frac{C_1}{(1+\epsilon\cos\beta)^3}\right] \tag{3-48}$$

Expressions for the two integrals to be evaluated in equation (3-48) can be found in a table of integrals, but the expressions can be simplified considerably by an ingenious transformation suggested by Sommerfeld wherein

$$1+\epsilon\cos\beta = \frac{1-\epsilon^2}{1-\epsilon\cos\psi} \tag{3-49}$$

Then

$$d\beta = \frac{(1-\epsilon^2)^{1/2}}{1-\epsilon\cos\psi}\, d\psi \tag{3-50}$$

The angle ψ is a fictitious angle.

The pressure distribution in a journal bearing with an interrupted film is complex and involves an undetermined constant, which physically represents the total circumferential flow per unit of axial width due to the rotation of the shaft.

For a continuous film, the Sommerfeld conditions given by equation (3–47) allow straightforward calculation of the integration constants. The resulting expression for pressure is

$$p-p_a=\frac{12\pi\left(\frac{R}{c}\right)^2\mu N\epsilon}{2+\epsilon^2}\frac{(2+\epsilon\cos\beta)\sin\beta}{(1+\epsilon\cos\beta)^2}+p_c \tag{3–51}$$

where p_c is the pressure at $\beta=0$.

The load capacity per unit length of the infinite journal is obtained by summation of forces parallel to the line of centers and normal thereto:

$$W\cos\varphi=-\int R(p-p_a)\cos\beta\,d\beta \tag{3–52}$$

$$W\sin\varphi=\int R(p-p_a)\sin\beta\,d\beta \tag{3–53}$$

$$W=[(W\cos\varphi)^2+(W\sin\varphi)^2]^{1/2} \tag{3–54}$$

For the continuous oil film the integration is carried on completely around the shaft from 0 to 2π and yields

$$W\cos\varphi=0 \tag{3–55}$$

$$W\sin\varphi=24\pi^2\left(\frac{R}{c}\right)^2\mu NR\frac{\epsilon}{(2+\epsilon^2)(1-\epsilon^2)^{1/2}} \tag{3–56}$$

From equation (3–55) $\varphi=\pm 90°$, and from equation (3–56) $\sin\varphi$ is always positive. Therefore, for the infinite journal $\varphi=90°$. Then

$$W=24\pi^2\left(\frac{R}{c}\right)^2\mu NR\frac{\epsilon}{(2+\epsilon^2)(1-\epsilon^2)^{1/2}} \tag{3–57}$$

If the Sommerfeld number S is defined as

$$S=\left(\frac{D}{c_d}\right)^2\mu\frac{N}{P} \tag{3–58}$$

where the load pressure P is

$$P=\frac{W}{LD} \tag{3-59}$$

then

$$\frac{1}{S}=\frac{12\pi^2\epsilon}{(2+\epsilon^2)(1-\epsilon^2)^{1/2}} \tag{3-60}$$

Equation (3-19) can be used to determine journal-bearing friction. Multiplying both sides by R and making the necessary substitutions result in the following expression for bearing torque per unit length:

$$M=\pm\frac{2\pi R^3\mu N}{c}\int_{\beta_1}^{\beta_2}\frac{d\beta}{1+\epsilon\cos\beta}-\frac{c\epsilon}{2}\int_0^1\int_{\beta_1}^{\beta_2}(p-p_a)\sin\beta R\,d\beta\,dz \tag{3-61}$$

The upper sign refers to the torque on the stationary bearing while the lower sign refers to the torque on the moving journal. In equation (3-61), the integral of the second term on the right is equal to $W\sin\varphi$. Therefore

$$M_b=-\frac{c\epsilon W\sin\varphi}{2}+\frac{2\pi R^3\mu N}{c}\int_{\beta_1}^{\beta_2}\frac{d\beta}{1+\epsilon\cos\beta} \tag{3-62a}$$

$$M_j=-\frac{c\epsilon W\sin\varphi}{2}-\frac{2\pi R^3\mu N}{c}\int_{\beta_1}^{\beta_2}\frac{d\beta}{1+\epsilon\cos\beta} \tag{3-62b}$$

For the friction coefficient M/RW

$$\frac{R}{c}f_j=\frac{\epsilon}{2}\sin\varphi+\pi S\int_{\beta_1}^{\beta_2}\frac{d\beta}{1+\epsilon\cos\beta} \tag{3-63}$$

$$\frac{R}{c}f_b=-\frac{\epsilon}{2}\sin\varphi+\pi S\int_{\beta_1}^{\beta_2}\frac{d\beta}{1+\epsilon\cos\beta} \tag{3-64}$$

These equations are applicable for bearings with any film extent. For an incomplete film β_1 and β_2 must be known.

The difference in torque on the journal and bearing always equals $Wc\epsilon\sin\varphi$. This difference arises because the resultants of the oil-film forces on the shaft and bearing must always pass through the centers. Since the bearing and journal centers are not coincident but are separated by the horizontal distance $c\epsilon\sin\varphi$, the couple $Wc\epsilon\sin\varphi$ is developed. This amount of excess torque must be applied to the journal.

Short Bearing Theory Applied to Journal Bearings

Michell (ref. 3) first suggested a solution to the Reynolds equation that neglects the first of the two left-hand terms. Cardullo (ref. 4) applied this solution to the pressure distribution in journal bearings of lengths

commonly found in engineering practice. DuBois and Ocvirk presented further refinements and much experimental data to demonstrate the validity of the short bearing theory (ref. 5). The following development follows that of reference 5. This solution assumes that the pressure-induced circumferential flow is small compared with velocity-induced flow in the circumferential direction, and that it includes axial flow.

The simplified version of the Reynolds equation is

$$\frac{\partial}{\partial z}\left(h^3 \frac{\partial p}{\partial z}\right)=6\mu U \frac{\partial h}{\partial x} \tag{3-65}$$

Since h is not a function of z, equation (3-65) may be written

$$\frac{\mathrm{d}^2 p}{\mathrm{d}z^2}=\frac{6\mu U}{3}\frac{\mathrm{d}h}{\mathrm{d}x} \tag{3-66}$$

Integrating equation (3-66) twice gives

$$p=\frac{6\mu U}{h^3}\frac{\mathrm{d}h}{\mathrm{d}x}\frac{z^2}{2}+C_1 z+C_2 \tag{3-67}$$

The constant C_1 can be evaluated if it is noted that $\mathrm{d}p/\mathrm{d}z=0$ at the axial centerline of the bearing because of symmetry. Likewise the condition that $p=p_a$ at $z=\pm\, l\,/2$ determines C_2. Then

$$p-p_a=\frac{3\mu U}{h^3}\frac{\mathrm{d}h}{\mathrm{d}x}\left(z^2-\frac{l^2}{4}\right) \tag{3-68}$$

In a journal bearing, as shown in figure 3-8, h is given by

$$h=c+e\cos\beta \tag{3-69}$$

$$h=c(1+\epsilon\cos\beta) \tag{3-70}$$

Then

$$\frac{\mathrm{d}h}{\mathrm{d}\beta}=-c\epsilon\sin\beta \tag{3-71}$$

Since $\mathrm{d}x=r\,\mathrm{d}\beta$,

$$p-p_a=\frac{3\mu U}{Rc^2}\left(\frac{l^2}{4}-z^2\right)\frac{\epsilon\sin\beta}{(1+\epsilon\cos\beta)^3} \tag{3-72}$$

Equation (3-72) shows that the pressure distribution is parabolic in the z-direction and sinusoidal in the circumferential direction. Because zero pressure is obtained when $\beta=0,\ \pi,\ 2\pi,\ \ldots,\ n\pi$, positive pressures exist only in the converging portion of the oil film.

The load capacity of the bearing can be obtained by integrating the pressure throughout the film:

$$W\cos\varphi=-2\int_0^{\pi}\int_0^{l/2}(p-p_a)R\cos\beta\,d\beta\,dz \tag{3-73}$$

$$W\sin\varphi=2\int_0^{\pi}\int_0^{l/2}(p-p_a)R\sin\beta\,d\beta\,dz \tag{3-74}$$

Substituting equation (3-72) for $p-p_a$ and integrating with respect to z give

$$W\cos\varphi=-\frac{\mu U l^3}{2c^2}\int_0^{\pi}\frac{\epsilon\sin\beta\cos\beta}{(1+\epsilon\cos\beta)^3}\,d\beta \tag{3-75}$$

$$W\sin\varphi=\frac{\mu U l^3}{2c^2}\int_0^{\pi}\frac{\epsilon\sin^2\beta}{(1+\epsilon\cos\beta)^3}\,d\beta \tag{3-76}$$

When integrations with respect to β are carried out with the aid of Sommerfeld's substitution (eqs. (3-49) and (3-50)), the results are

$$W\cos\varphi=\frac{\mu U l^3}{c^2}\frac{\epsilon^2}{(1-\epsilon^2)^2} \tag{3-77}$$

$$W\sin\varphi=\frac{\mu U l^3}{4c^2}\frac{\pi\epsilon}{(1-\epsilon^2)^{3/2}} \tag{3-78}$$

The applied load is given by

$$W=[(W\cos\varphi)^2+(W\sin\varphi)^2]^{1/2} \tag{3-79}$$

$$W=\frac{\mu U l^3}{4c^2}\frac{\epsilon}{(1-\epsilon^2)^2}[\pi^2(1-\epsilon^2)+16\epsilon^2]^{1/2} \tag{3-80}$$

If

$$W=2Pl R \tag{3-81}$$

and

$$U=\pi dN' \tag{3-82}$$

equation (3-80) can be rearranged to give

$$\frac{\mu N'}{P}\left(\frac{D}{c_d}\right)^2\left(\frac{l}{D}\right)^2=\frac{(1-\epsilon^2)^2}{\pi\epsilon}\left[\frac{1}{\pi^2(1-\epsilon^2)+16\epsilon^2}\right]^{1/2} \tag{3-83}$$

The quantity on the left is nondimensional and is dependent only on eccentricity ratio. It was first presented by DuBois and Ocvirk (ref. 5) and is termed the capacity number. The capacity number C_n is the Sommerfeld number multiplied by the square of the length-diameter ratio.

The attitude angle of a short journal bearing is

$$\tan \varphi = \frac{W \sin \varphi}{W \cos \varphi} \tag{3-84a}$$

$$\tan \varphi = \frac{\pi}{4} \frac{(1-\epsilon^2)^{1/2}}{\epsilon} \tag{3-84b}$$

As previously stated, the short bearing theory neglects the pressure flow in the circumferential direction and hence assumes a linear velocity profile in the oil film in the circumferential direction. In the calculation of bearing friction, therefore, the second term in both equations (3–15) and (3–16) vanishes so that the bearing and journal torques are equal. The shearing stress is therefore

$$(\tau_x)_m = -\frac{\mu U}{h} \tag{3-85a}$$

$$(\tau_x)_s = +\frac{\mu U}{h} \tag{3-85b}$$

The circumferential friction force F then becomes

$$F = 2\int_0^{l/2} \int_0^{2\pi} \frac{\mu U}{h} R \, d\beta \, dz \tag{3-86}$$

$$F = \frac{\mu U l R}{c} \int_0^{2\pi} \frac{d\beta}{1+\epsilon \cos \beta} \tag{3-87}$$

$$F = \frac{\mu U l R}{c} \frac{2\pi}{(1-\epsilon^2)^{1/2}} \tag{3-88}$$

The bearing or journal torque M becomes

$$M = \frac{\mu U l R^2}{c} \frac{2\pi}{(1-\epsilon^2)^{1/2}} \tag{3-89}$$

The coefficient of friction f is

$$f = \frac{F}{W} = \frac{\mu U l R}{W c} \frac{2\pi}{(1-\epsilon^2)^{1/2}} \tag{3-90}$$

$$f\left(\frac{R}{c}\right)\left(\frac{l}{D}\right)^2 = \frac{\mu N'}{P}\left(\frac{R}{c}\right)^2\left(\frac{l}{D}\right)^2 \frac{2\pi^2}{(1-\epsilon^2)^{1/2}} \tag{3-91}$$

$$f\left(\frac{R}{c}\right)\left(\frac{l}{D}\right)^2 = C_n \frac{2\pi^2}{(1-\epsilon^2)^{1/2}} \tag{3-92}$$

In addition to load capacity and friction, the oil flow from the bearing is an important parameter. Equation (3–11) can be used to calculate the total oil flow from the bearing if the proper substitutions are made for h and $\partial p/\partial z$. At any point in the film, the axial flow is

$$dQ=\frac{Uc\epsilon z}{2}\sin\beta\, d\beta \tag{3–93}$$

At the ends of the bearing, where $z=\pm l/2$

$$dQ_z=\frac{Uc\epsilon l}{4}\sin\beta\, d\beta \tag{3–94}$$

The flow will be outward from the bearing when $0<\beta<\pi$ where the pressures are positive. Then the total outward flow from the bearing will be

$$Q=2\int_0^{\pi}\frac{Uc\epsilon l}{4}\sin\beta\, d\beta \tag{3–95}$$

$$Q=Uc\epsilon l \tag{3–96}$$

$$Q=\pi Dlc_d\frac{N'}{2}\epsilon \tag{3–97}$$

Solutions for Finite Bearings

Previously only solutions of the Reynolds equation that neglect axial flow or neglect pressure flow in the circumferential direction have been discussed. The short bearing theory developed for journal bearings has considerable utility in the design of bearings with length-diameter ratios of 1 or less. The solutions for infinite bearings, however, are of academic interest in that they help to understand bearing behavior, but they are not in themselves useful for designing bearings.

A complete discussion of the available solutions to the complete Reynolds equation is beyond the scope of this book, but some brief remarks will be made and references to the literature given. For slider bearings, the Reynolds equation was first solved by A. G. M. Michell (ref. 6) and somewhat later by Muskat, Morgan, and Meres (ref. 7). Briefly, solutions were obtained for constant viscosity by assuming that the pressure was equal to that in the infinite bearing minus a pressure drop p' caused by side leakage in the finite bearing. Substitution of the expression for pressure into the Reynolds equation led to a differential equation for p' that could be solved in series form. The coefficients of the series terms were in turn solutions of the Bessel equation of the first order.

This solution, while exact when a sufficient number of series terms is employed, is unworkable for the design engineer. The advent of

high-speed digital computers has led to the compilation of a variety of solutions that provide design information for slider bearings of a variety of configurations. Reference 8 contains such solutions.

For journal bearings, Muskat and Morgan (refs. 9 to 13) obtained a solution by means of a series expansion for a complete film. This solution, however, is applicable only to eccentricity ratios up to 0.5. A solution that used relaxation techniques was obtained for a single example of an incomplete film by Cameron and Wood (ref. 14).

Digital-computer solutions for finite journal bearings of various length-diameter ratios and arc lengths with the assumption of constant viscosity are reported in references 15 and 16. These solutions are useful for the design of journal bearings.

This brief list of references does not begin to describe the literature available on hydrodynamic lubrication. There are literally hundreds of references available, all of which are useful to some degree in solving bearing problems. Contributions to the literature are being made continually with fewer and fewer simplifying assumptions.

DYNAMIC LOADS AND INSTABILITIES IN JOURNAL BEARINGS

In the discussion up to now, it has been assumed that there was no relative motion of the bearing and shaft centers during operation. In real machinery, however, the steady-state situation often does not prevail, as in starting, in stopping, or in changing the bearing load suddenly. Changes in bearing loads may result from meshing gears, engaging clutches, etc., or may be periodic as in all reciprocating machinery. In addition, rotating loads superimposed on unidirectional loads result from shaft unbalance.

It is extremely important, therefore, to acquire an understanding of the behavior of journal bearings under dynamic loading situations. Specifically, it is important to know the magnitude of the journal oscillations so that minimum film thicknesses can be determined; it is also important to know whether the journal motion is stable, that is, whether the amplitude will be bounded or whether it will be unstable and increase in amplitude until the bearing is destroyed.

The generalized Reynolds equation (eq. (3–13)) may be written for a journal bearing:

$$\frac{1}{R^2}\frac{\partial}{\partial\beta}\left[\frac{c^3}{\mu}(1+\epsilon\cos\beta)^3\frac{\partial p}{\partial\beta}\right]+\frac{\partial}{\partial z}\left[\frac{c^3}{\mu}(1+\epsilon\cos\beta)^3\frac{\partial p}{\partial z}\right]$$
$$=\frac{6}{R}\frac{\partial}{\partial\beta}[c(1+\epsilon\cos\beta)U]+12V \quad (3\text{–}98)$$

In this analysis, the direction of the load W is no longer fixed and hence will not be used as a reference. A vertical line drawn through the bearing center O_b (fig. 3–9) will be the reference direction.

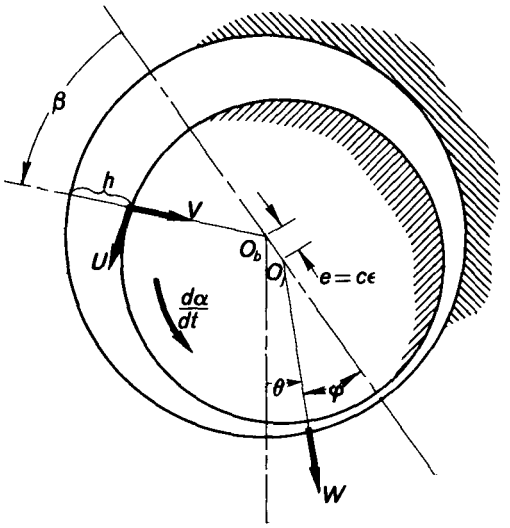

FIGURE 3-9.—Dynamically loaded journal-bearing configuration.

The angular velocity of the journal about its own center is represented by $d\alpha/dt$. The angle between the load vector W and the reference direction is θ. The angle between W and the minimum film-thickness point is φ. Angular displacements are assumed to be positive when in the direction of shaft rotation.

The velocities U and V of a point on the journal surface at angle β must be expressed in terms of the quantities c, ϵ, β, φ, θ, and $d\alpha/dt$. The velocity of the journal center O_j relative to the fixed bearing center O_b consists of the radial component $c(d\epsilon/dt)$ and the tangential component $c\epsilon(d/dt)(\theta+\varphi)$. Resolving these components parallel to U and V at position θ gives

$$U=c\frac{d\epsilon}{dt}\sin\beta-c\epsilon\frac{d}{dt}(\theta+\varphi)\cos\beta+R\frac{d\alpha}{dt} \tag{3-99}$$

$$V=c\frac{d\epsilon}{dt}\cos\beta+c\epsilon\frac{d}{dt}(\theta+\varphi)\sin\beta \tag{3-100}$$

The term $R(d\alpha/dt)$ was previously considered a constant $2\pi RN$, but it may now be considered variable. Substitution of expressions (3-

99) and (3–100) into (3–98) yields the general differential equation for a dynamically loaded journal bearing. As for the unidirectional load, however, the solution for the dynamically loaded three-dimensional bearing becomes too complex. Even though neglecting the variation of pressure in the z-direction represents a fictitious bearing, much knowledge can be gained from this type of investigation. With this assumption, equation (3–98) becomes

$$\frac{\mathrm{d}}{\mathrm{d}\beta}\left[\frac{1}{\mu}(1+\epsilon\cos\beta)^3\frac{\mathrm{d}p}{\mathrm{d}\beta}\right]=\frac{6R}{c^2}\frac{\mathrm{d}}{\mathrm{d}\beta}\left\{(1+\epsilon\cos\beta)\left[R\frac{\mathrm{d}\alpha}{\mathrm{d}t}+c\frac{\mathrm{d}\epsilon}{\mathrm{d}t}\sin\beta\right.\right.$$

$$\left.\left.-c\epsilon\cos\beta\frac{\mathrm{d}}{\mathrm{d}t}(\theta+\varphi)\right]\right\}+12\left(\frac{R}{c}\right)^2\left\{\frac{d\epsilon}{\mathrm{d}t}\cos\beta+\epsilon\sin\beta\left[\frac{\mathrm{d}}{\mathrm{d}t}(\theta+\varphi)\right]\right\} \tag{3–101}$$

Integrating with respect to β gives

$$(1+\epsilon\cos\beta)^3\frac{\mathrm{d}p}{\mathrm{d}\beta}=6\left(\frac{R}{c}\right)^2\mu(1+\epsilon\cos\beta)\frac{\mathrm{d}\alpha}{\mathrm{d}t}$$

$$+\left[12\left(\frac{R}{c}\right)^2+6\frac{R}{c}(1+\epsilon\cos\beta)\right]\mu\frac{\mathrm{d}\epsilon}{\mathrm{d}t}\sin\beta$$

$$-\left[12\left(\frac{R}{c}\right)^2+6\frac{R}{c}(1+\epsilon\cos\beta)\right]\mu\epsilon\frac{\mathrm{d}}{\mathrm{d}t}(\theta+\varphi)\cos\beta+C_1 \tag{3–102}$$

where C_1 is a constant of integration. Since R/c is large, the terms $6(R/c)(1+\epsilon\cos\beta)$ are small compared with $12(R/c)^2$ and thus may be neglected. When these terms are dropped, equation (3–102) becomes

$$\frac{\mathrm{d}p}{\mathrm{d}\beta}=\frac{6\left(\frac{R}{c}\right)^2\mu}{(1+\epsilon\cos\beta)^2}\frac{\mathrm{d}}{\mathrm{d}t}[\alpha-2(\theta+\varphi)]$$

$$+12\left(\frac{R}{c}\right)^2\frac{\mu\sin\beta}{(1+\epsilon\cos\beta)^3}\frac{\mathrm{d}\epsilon}{\mathrm{d}t}+\frac{C_1}{(1+\epsilon\cos\beta)^3} \tag{3–103}$$

Equation (3–103) is most easily integrated by use of the Sommerfeld substitution given by equations (3–49) and (3–50). A continuous

film and constant viscosity are assumed. Then

$$p-p_a=6\left(\frac{R}{c}\right)^2\mu\left\{\frac{\epsilon(2+\epsilon\cos\beta)\sin\beta}{(2+\epsilon^2)(1+\epsilon\cos\beta)^2}\frac{\mathrm{d}}{\mathrm{d}t}(\alpha-2\theta-2\varphi)+\frac{1}{\epsilon}\left[\frac{1}{(1+\epsilon\cos\beta)^2}-\frac{1}{(1+\epsilon)^2}\right]\frac{\mathrm{d}\epsilon}{\mathrm{d}t}\right\} \quad (3\text{–}104)$$

Equation (3–104) was first obtained by Harrison (ref. 17) and by Swift (ref. 18). Its derivation is also given in reference 19.

The first term on the right side of equation (3–104) represents the pressure developed by the tangential motion of the surface of the journal relative to the surface of the bearing and is commonly called the wedge film. The second term on the right represents the pressure developed by the motion of the journal and bearing toward or away from each other and is commonly called the squeeze film.

The load capacity results from integration of the pressure around the bearing:

$$W\sin\varphi=6\left(\frac{R}{c}\right)^2\mu R\frac{\mathrm{d}}{\mathrm{d}t}(\alpha-2\theta-2\varphi)\frac{2\pi\epsilon}{(2+\epsilon^2)(1-\epsilon^2)^{1/2}} \quad (3\text{–}105)$$

$$W\cos\varphi=6\left(\frac{R}{c}\right)^2\mu R\frac{\mathrm{d}\epsilon}{\mathrm{d}t}\frac{2\pi}{(1-\epsilon^2)^{3/2}} \quad (3\text{–}106)$$

The Sommerfeld number is defined as $S=(R/c)^2(\mu N_j/P)$ where N_j is the speed of the journal; then, equations (3–105) and (3–106) become

$$\frac{\epsilon}{(2+\epsilon^2)(1-\epsilon^2)^{1/2}}\frac{1}{2\pi N_j}\frac{\mathrm{d}}{\mathrm{d}t}(\alpha-2\theta-2\varphi)=\frac{1}{12\pi^2S}\sin\varphi \quad (3\text{–}107)$$

$$\frac{1}{(1-\epsilon^2)^{3/2}}\frac{1}{2\pi N_j}\frac{\mathrm{d}\epsilon}{\mathrm{d}t}=\frac{1}{12\pi^2S}\cos\varphi \quad (3\text{–}108)$$

For the case of a constant load that rotates at constant speed, S is constant and $\mathrm{d}\theta/\mathrm{d}t=2\pi N_P$, where N_P is the angular speed of the load vector. If the shaft speed is constant, $\mathrm{d}\alpha/\mathrm{d}t=2\pi N_j$. Equations (3–107) and (3–108) then become

$$\frac{\epsilon}{(2+\epsilon^2)(1-\epsilon^2)^{1/2}}\left(1-2\frac{N_P}{N_j}-\frac{2}{2\pi N_j}\frac{\mathrm{d}\varphi}{\mathrm{d}t}\right)=\frac{1}{12\pi^2S}\sin\varphi \quad (3\text{–}109)$$

$$\frac{1}{(1-\epsilon^2)^{3/2}}\frac{1}{2\pi N_j}\frac{\mathrm{d}\epsilon}{\mathrm{d}t}=\frac{1}{12\pi^2S}\cos\varphi \quad (3\text{–}110)$$

If the journal center is assumed to be in equilibrium,

$$\frac{d\epsilon}{dt}=0$$

and

$$\frac{d\varphi}{dt}=0$$

Then

$$\frac{\epsilon}{(2+\epsilon^2)(1-\epsilon^2)^{1/2}}\left(1-2\frac{N_P}{N_j}\right)=\pm\frac{1}{12\pi^2 S} \tag{3-111}$$

and

$$\varphi=\pm\frac{\pi}{2} \tag{3-112}$$

From equation (3-111), when N_P is zero, the original Sommerfeld equation for a constant, unidirectional load, equation (3-57) results. For the rotating load, the load capacity becomes zero when

$$1-2\frac{N_P}{N_j}=0 \tag{3-113}$$

or

$$N_P=\frac{N_j}{2} \tag{3-114}$$

When the load vector rotates in the same direction as the journal at one-half the angular speed of the journal, the load capacity vanishes. The physical explanation for this is quite simple. The load capacity of a journal bearing depends on its ability to pump fluid into the converging wedge. If the flow is laminar, the average lubricant velocity is approximately one-half the peripheral speed in the direction of shaft rotation. If $N_P=N_j/2$, the minimum film-thickness point is moving at one-half the peripheral velocity of the journal and the net fluid pumped is zero. Under these conditions the load capacity vanishes.

Newkirk (ref. 20) discusses two typical cases of rotor vibration, one for a heavy rotor on a flexible shaft and one for a short, very stiff shaft. The flexible rotor whirled at its first critical frequency when the shaft speed was greater than twice the critical frequency. Whirl frequency was approximately constant with varying shaft speed. The stiff shaft whirled at low speeds, and the whirl frequency was somewhat less than one-half the running speed. Whirling of the stiff shaft ceased at high speed.

Harrison (ref. 17), in an analytical investigation for infinite bearings, found that a change in load or in speed did not result in the journal seeking a new position but in revolution of the journal in a closed orbit. In the case of the flexible shaft, the mass of the rotor and the shaft flexibility determine the natural frequency of the rotor. Jarring

of the rotor results in a vibration of the shaft at its critical frequency and in displacements of the journal at the same frequency. Harrison's analysis explains the tendency of the oil film to convert vibration of the shaft into a circular motion of the shaft center or shaft whirl. If the natural frequency of the rotor is greater than one-half the journal speed, the oil forces will retard and damp out the whirl because the maximum whirl speed is the speed at which the bearing can pump the lubricant around in the bearing clearance or one-half the journal speed.

If the natural frequency of the rotor is equal to or less than one-half the journal speed, the oil forces will aid in building up the whirl. To understand this reaction, first consider a loaded bearing as in figure 3–8. The oil film force F' will be equal and opposite to the load W. If the bearing is running at essentially no load and the journal is jarred to displace it within the bearing clearance, a force F' will be generated in the oil film. As before, it will pass through O_j. Since the attitude angle φ is not zero, F' will exert a moment about O_b that can accelerate O_j into an orbit about O_b. When the angular velocity of O_j reaches $(1/2)N_j$, the bearing has theoretically zero load capacity and negligible ability to resist whirl. The whirl frequency remains constant over a range of journal speeds because the rotor forces are dominant. Any tendency of the oil-film forces to build up a whirl at the frequency of whirl of the bearing (about one-half the journal speed) would not receive much response except at the natural frequency of the rotor. This phenomenon is frequently called resonant whirl.

For the short, stiff shaft, running speeds are far below the shaft critical speed, and shaft flexing due to shocks is negligible. The frequency of shaft whirl is then determined by the frequency of journal whirl, which is equal to or slightly less than one-half the journal speed. With the stiff shaft, then, the whirl frequency varies with and remains slightly less than one-half the journal speed. This phenomenon is sometimes called half-frequency whirl.

The prediction of the onset of whirl in a journal bearing is difficult because of the many factors upon which the whirl impending frequency depends. Some of these factors are the rotor stiffness, the oil-film stiffness, the rotor polar moment of inertia, the rotor transverse moment of inertia, and external loads, both rotating and unidirectional.

Two types of half-frequency whirl are commonly encountered with rigidly supported bearings:

(1) Translatory whirl, during which the shaft and bearing axes remain essentially parallel

(2) Conical whirl, during which the shaft and bearing axes are inclined with the shaft axis tracing out cones in space

In any system the whirl that will occur first will be the one with the lowest threshold speed. Generally it has been shown (refs. 21 and 22) that the threshold of instability may be represented by

$$\mathcal{M}\omega^2\left(\frac{1}{k_1}+\frac{1}{K}\right)<4 \tag{3-115}$$

where $\mathcal{M}$ is the mass of the rotor, k_1 is the rotor stiffness, and K is the radial fluid film stiffness. The difficulty in using such a relation is in calculating the fluid-film stiffness. Calculations of fluid-film forces for both incompressible and compressible fluids are given in reference 23. Typical results for an incompressible fluid are shown in figure 3–10 for a wide range of the parameter E where

$$\mathrm{E}=\frac{k_1 c^3 \pi}{2\mu l R^3 \omega_o} \tag{3-116}$$

The ratio of angular speed to the critical angular speed based on radial

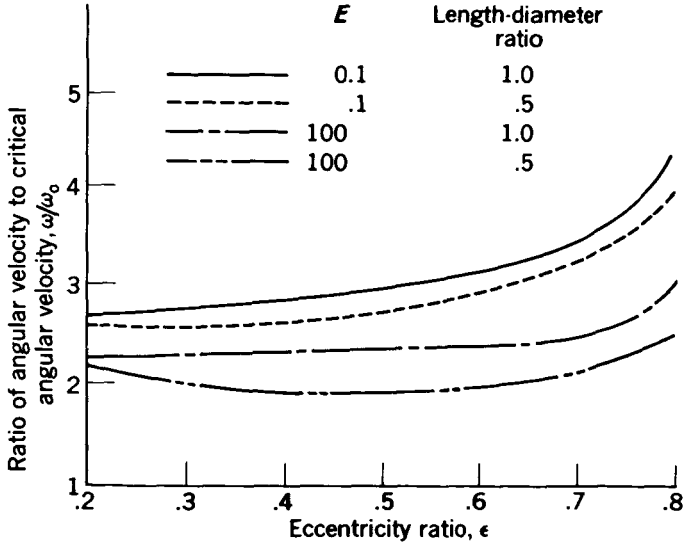

FIGURE 3–10.—Ratio of angular velocity to critical angular velocity as function of eccentricity ratio for incompressible fluids. Radius, 1 inch; ratio of bearing radial clearance to radius, 10^{-3}; rotor spring constant, 1.25×10^6 pounds per inch; rotor mass, 0.1 pound second squared per inch; $E=k_1c^3\pi/2\mu l R^3\omega_o$. (From ref. 23.)

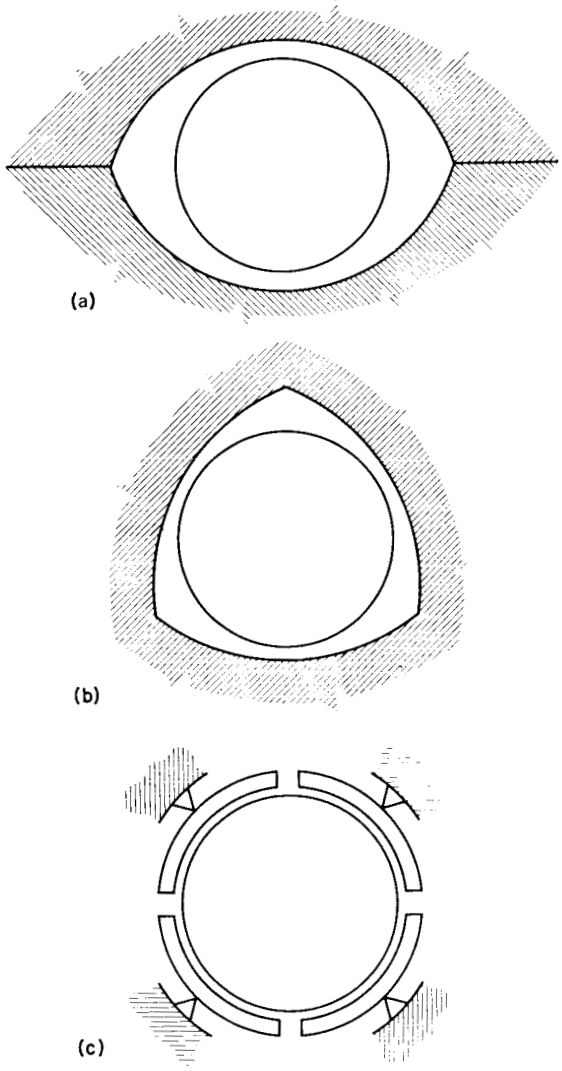

(a) Elliptical bearing.
(b) Three-lobe bearing.
(c) Pivoted-pad bearing.

FIGURE 3–11.—Three types of whirl-resistant journal bearings.

film forces increases with increasing eccentricity ratio (load). The effect of other variables in the parameter E can easily be determined.

Journal-bearing instabilities occur most frequently in vertically mounted shafts and, in general, in lightly loaded bearings. Efforts to

inhibit whirl usually involve creating artificial loads in the bearing to supplement the external load or reducing the load capacity of the bearing. As an example of the latter, a journal with three axial grooves inhibits whirl better than does a journal without grooves because the grooves essentially make the bearing a 120° partial bearing with a lower load capacity. Still more effective in inhibiting whirl are the elliptical bearing, the three-lobe bearing, and the pivoted-pad journal bearing (fig. 3–11). All these bearings provide built-in oil wedges even when there is no external load. A discussion of these bearings and their ability to inhibit whirl is given in reference 24.

CONCLUDING REMARKS

This brief discussion of hydrodynamic bearings has included the two principal analytic solutions plus reference to computer solutions. In the design of any bearing, however, a heat balance must be considered if the bearing behavior is to be predicted with any accuracy. Techniques for estimation of bearing-temperature rise are outlined in reference 25. In calculation of load capacity, the proper choice of oil viscosity depends on a good estimate of bearing-temperature rise. Bearing-temperature rise, however, depends to a great extent on the particular installation so that overall rules cannot be established.

REFERENCES

1. Sommerfeld, A.: The Hydrodynamic Theory of Lubrication Friction. Math. and Phys., vol. 50, nos. 1–2, 1904, pp. 97–155.
2. Harrison, W. J.: The Hydrodynamical Theory of Lubrication with Special Reference to Air as a Lubricant. Proc. Cambridge Phil. Soc., vol. 22, no. 3, 1913, pp. 39–54.
3. Michell, A. G. M.: Progress in Fluid-Film Lubrication. ASME Trans., MSP–51–21, vol. 51, 1929, pp. 153–163.
4. Cardullo, F. E.: Some Practical Deductions from Theory of Lubrication of Short Cylindrical Bearings. ASME Trans., MSP–52–12, vol. 52, 1930, pp. 143–153.
5. DuBois, G. B., and Ocvirk, F. W.: Analytical Derivation and Experimental Evaluation of Short-Bearing Approximation for Full Journal Bearings. NACA Rep. 1157, 1953.
6. Michell, A. G. M.: The Lubrication of Plane Surfaces. Zs. Math. Phys., vol. 52, 1905, pp. 123–137.
7. Muskat, M., Morgan, F., and Meres, M. W.: Studies in Lubrication. VII. The Lubrication of Plane Sliders of Finite Width. Jour. Appl. Phys., vol. 11, no. 3, 1940, pp. 208–219.

8. RAIMONDI, A. A., and BOYD, J.: Applying Bearing Theory to the Analysis and Design of Pad-Type Bearings. Pt. I—Fixed Pad Bearings. Pt. II—Pivoted Pad Bearings. ASME Trans., vol. 77, no. 3, Apr. 1955, pp. 287–309.
9. MUSKAT, M., and MORGAN, F.: The Thick-Film Lubrication of Journal Bearings of Finite Width. Jour. Appl. Mech., vol. 5, no. 3, Sept. 1938, pp. A–117—A–118.
10. MUSKAT, M., and MORGAN, F.: Studies in Lubrication. V. The Theory of the Thick Film Lubrication of Flooded Journal Bearings and Bearings with Circumferential Grooves. Jour. Appl. Phys., vol. 10, no. 6, June 1939, pp. 398–407.
11. MUSKAT, M., and MORGAN, F.: Studies in Lubrication. III. The Theory of the Thick Film Lubrication of a Complete Journal Bearing of Finite Length with Arbitrary Positions of the Lubricant Source. Jour. Appl. Phys., vol. 10, no. 1, Jan. 1939, pp. 46–61.
12. MORGAN, F., and MUSKAT, M.: Studies in Lubrication. II. Experimental Friction Coefficients for Thick Film Lubrication of Complete Journal Bearings. Jour. Appl. Phys., vol. 9, no. 8, Aug. 1938, pp. 539–546.
13. MORGAN, F., and MUSKAT, M.: Studies in Lubrication. IV. The Experimental Variation of the Coefficient of Friction with the Strength of the Lubricant Source for a Complete Journal Bearing. Jour. Appl. Phys., vol. 10, no. 5, May 1939, pp. 327–334.
14. CAMERON, A., and WOOD, W. L.: The Full Journal Bearing. Proc. Inst. Mech. Eng., vol. 161, 1949, pp. 59–72.
15. RAIMONDI, A., and BOYD, J.: A Solution for the Finite Journal Bearing and Its Application to Analysis and Design, pts. I, II, and III. ASLE Trans., vol. 1, no. 1, 1958, pp. 159–209.
16. PINKUS, O.: Solution of Reynolds' Equation for Finite Journal Bearings. ASME Trans., vol. 80, no. 4, May 1958, pp. 858–864.
17. HARRISON, W. J.: The Hydrodynamical Theory of the Lubrication of a Cylindrical Bearing Under Variable Load, and of a Pivot Bearing. Trans. Cambridge Phil. Soc., vol. 22, 1920, pp. 373–388.
18. SWIFT, H. W.: Fluctuating Loads in Sleeve Bearings. Jour. Inst. Civil Eng., vol. 5, no. 4, Feb. 1937, pp. 161–195.
19. BURWELL, J. T.: Hydrodynamic Lubrication of Sleeve Bearings Subject to Varying Loads. Lubrication Eng., vol. 4, no. 2, Apr. 1948, pp. 67–71; 74.
20. NEWKIRK, B. L.: Varieties of Shaft Disturbances Due to Fluid Films in Journal Bearings. ASME Trans., vol. 78, no. 5, July 1956, pp. 985–988.
21. PORITSKY, H.: Contribution to the Theory of Oil Whip. Trans. ASME, vol. 75, no. 6, Aug. 1953, pp. 1153–1161.
22. BOEKER, G. F., and STERNLICHT, B.: Investigation of Translatory Fluid Whirl in Vertical Machines. ASME Trans., vol. 78, no. 1, Jan. 1956, pp. 13–20.
23. STERNLICHT, B., PORITSKY, H., and ARWAS, E.: Dynamic Stability Aspects of Cylindrical Journal Bearings Using Compressible and Incompressible Fluids. General Electric Co., 1959.
24. PINKUS, O.: Sleeve Bearing Design. Product Eng., vol. 26, no. 8, Aug. 1955 pp. 134–139.
25. WILCOCK, D. F., and BOOSER, R.: Bearing Design and Application. McGraw-Hill Book Co., Inc., 1957.

CHAPTER 4

Hydrostatic Lubrication

By WILLIAM J. ANDERSON

IN CONTRAST TO HYDRODYNAMIC BEARINGS, in which the load-carrying capacity depends on pressures built up within the film, hydrostatic bearings derive load capacity from an external pressure source. This external pressurization ultimately supplies the force that supports the load. Hydrostatic bearings have been designed for use with both incompressible and compressible fluids. Behavior of hydrostatic bearings depends on whether or not the fluid is incompressible. As would be expected, bearings using incompressible fluids are far less troublesome than are those that use compressible fluids. This discussion is confined to incompressible fluid bearings Compressible fluid bearings are discussed with gas-lubricated bearings.

SYMBOLS

A	area, sq in.
b	width parallel to direction of motion or normal to direction of flow, in.
C_D	orifice discharge coefficient
d	diameter, in.
g	acceleration due to gravity, in./sec^2
H	pumping power, lb-in./sec
h	film thickness, in.
K	fluid film radial spring constant, lb/in.
L	length of flow element in direction of flow, in.
M,M'	torque or moment, lb-in.
p	pressure, lb/sq in.
Δp	pressure drop, lb/sq in.
p_1	pressure on pad 1, lb/sq in.
Q	oil flow, cu in./sec
R,r	radius, in.
R_1	pad radius, in.

R_2	bearing radius, in.
u	velocity in x-direction, in./sec
W	load, lb
x	coordinate
γ	weight density, lb/cu in.
μ	viscosity, lb-sec/sq in.
τ	shear stress, lb/sq in.

Subscripts:

a	atmospheric
c	capillary
o	orifice
r	pad
s	supply
v	flow control valve
x	in direction of x-coordinate

CHARACTERISTICS OF HYDROSTATIC BEARINGS

Hydrodynamic bearings require relative motion of the bearing surfaces in order to build up the load-supporting pressures. Therefore, when a bearing is required to support a load with little or no relative motion between the surfaces, a hydrostatic bearing must be used. A hydrodynamic bearing has no load capacity with little or no relative motion between the surfaces. Hydrostatic bearings may also be required in applications where, for one reason or another, touching or rubbing of the bearing surfaces cannot be permitted at startup and shutdown. Under extreme conditions of temperature or corrosivity, it may be necessary to use bearing materials with poor sliding friction properties. In such instances, surface contact may result in galling and surface welding, which would make the bearing inoperative. In circumstances such as these, a hydrostatic or a combination hydrostatic-hydrodynamic bearing is required to prevent surface contact at starting and stopping. Hydrostatic bearings are used frequently where low-friction supports are required for stationary assemblies. In addition to low friction, hydrostatic bearings offer the advantages of high load capacity independent of rotation and of high stiffness. Hydrostatic bearings, however, offer the disadvantage of requiring high-pressure pumps and high oil flows.

SIMPLE THRUST BEARING ANALYSIS

The simplest type of a hydrostatic bearing is a circular, flat-plate thrust bearing with a single lubricant feed line. A typical bearing is sketched in figure 4–1. It is desired to know the flow and the load capacity.

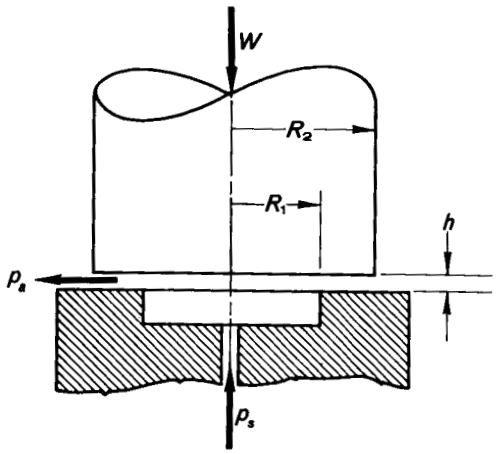

FIGURE 4–1.—Hydrostatic thrust bearing.

The formula for flow in a narrow slot is

$$Q=-\frac{bh^3}{12\mu}\frac{\mathrm{d}p}{\mathrm{d}x} \tag{4–1}$$

and for a circular bearing,

$$\left.\begin{aligned} b&=2\pi R\\ \mathrm{d}x&=\mathrm{d}R \end{aligned}\right\} \tag{4–2}$$

Then

$$Q=-\frac{2\pi h^3 R}{12\mu}\frac{\mathrm{d}p}{\mathrm{d}R} \tag{4–3}$$

$$\int_{R_1}^{R_2}\frac{\mathrm{d}R}{R}=-\frac{2\pi h^3}{12\mu Q}\int_{p_s}^{p_a}\mathrm{d}p \tag{4–4}$$

$$\ln\frac{R_2}{R_1}=\frac{\pi h^3}{6\mu Q}(p_s-p_a) \tag{4–5}$$

$$Q=\frac{\pi h^3(p_s-p_a)}{6\mu\ln\dfrac{R_2}{R_1}} \tag{4–6}$$

Because the load capacity of the bearing is equal to the integral of the pressure over the bearing area,

$$W=\pi R_1^2(p_s-p_a)+\int_{R_1}^{R_2} 2\pi R(p-p_a)\mathrm{d}R \tag{4-7}$$

The pressure p at any radius R can be obtained by integration of equation (4–3) from R_1 to R:

$$p-p_a=-\frac{6\mu Q \ln \frac{R}{R_2}}{\pi h^3} \tag{4-8}$$

or

$$p-p_a=\frac{6\mu Q \ln \frac{R_2}{R}}{\pi h^3} \tag{4-9}$$

Then

$$W=\pi R_1^2(p_s-p_a)-\frac{12\mu Q}{h^3}\int_{R_1}^{R_2} R \ln \frac{R}{R_2}\,\mathrm{d}R \tag{4-10}$$

When equation (4–10) is integrated,

$$W=\pi R_1^2(p_s-p_a)-\frac{12\mu Q}{h^3}\left(\frac{R^2}{2}\ln R-\frac{R^2}{4}-\ln R_2\,\frac{R^2}{2}\right)_{R_1}^{R_2} \tag{4-11}$$

Evaluation and substitution for Q gives

$$W=\frac{\pi(p_s-p_a)}{2}\left(\frac{R_2^2-R_1^2}{\ln \frac{R_2}{R_1}}\right) \tag{4-12}$$

It is seen that the load capacity is directly proportional to the supply pressure above ambient.

COMPENSATION

The simple single-pad thrust bearing illustrated in figure 4–1 is satisfactory only for supporting pure thrust load. It cannot cope with misalinements or moment loading that may result from misalinement of the bearing parts. A multipad bearing with built-in regulation of pad pressures must be used. Regulation of pad pressures is accomplished by use of a flow resistance between the pressure source and the pad. Commonly used types of resistances include capillary tubes, orifices, and flow-control valves. The pressure drop

across capillaries and orifices varies with the flow. Flow-control valves maintain constant flow regardless of the pressure drop.

Consider a circular four-pad compensated thrust bearing (fig. 4–2) and what happens when the bearing is misalined, as shown in figure 4–3. If the bearing is misalined because of a moment M, the clearance in pad 1 momentarily decreases while that in pad 2 momentarily increases. This clearance decrease reduces the flow from pad 1 and the flow through the resistance to pad 1 and vice versa from pad 2 and through resistance 2. The decreased flow through resistance 1 reduces the pressure drop $(p_s - p_1)$ and thereby increases pressure in pad 1 p_1 since the supply pressure p_s is constant. The opposite occurs in pad 2, and the alining moment M' is created. The principle of compensation is necessary for the proper functioning of journal bearings. When the load is applied, the journal becomes eccentric. The pressure in the pad with the reduced clearance increases and decreases in the pad with the increased clearance. This difference in pressures supports the load.

FLOW THROUGH COMPENSATING RESISTANCES

The flow through a capillary tube may be derived from consideration of a cylindrical slug of fluid as shown in figure 4–4. When forces on the thin slug are equated,

$$\Delta p \pi r^2 = 2\pi r L \tau_z \tag{4–13}$$

Since

$$\tau_z = -\mu \frac{du}{dr} \qquad (du/dr \text{ is negative}) \tag{4–14}$$

$$\Delta p \pi r^2 = -2\pi r L \mu \frac{du}{dr} \tag{4–15}$$

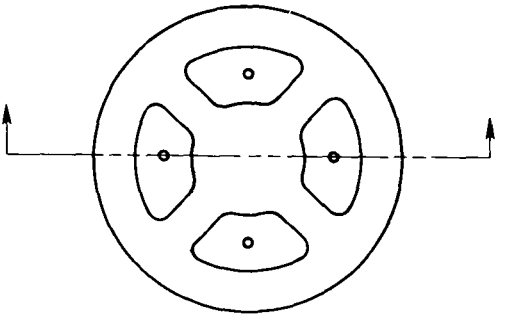

FIGURE 4–2.—Four-pad thrust bearing.

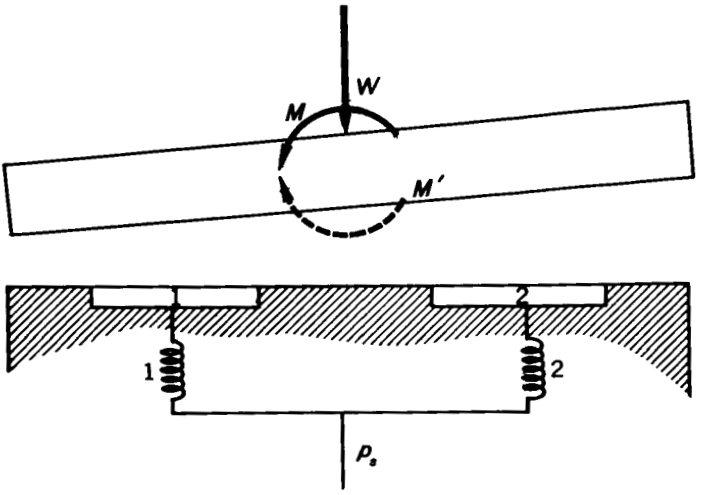

FIGURE 4–3.—Section through four-pad compensated thrust bearing.

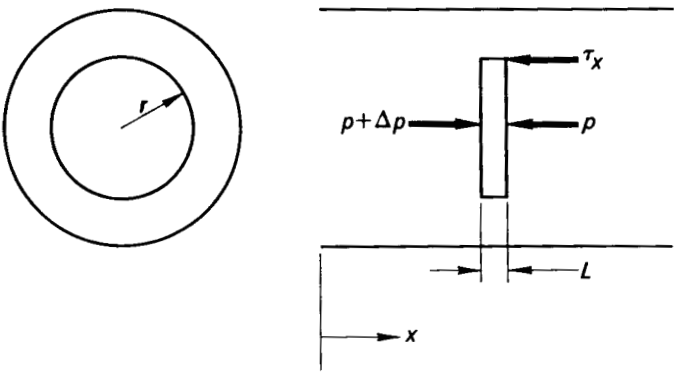

FIGURE 4–4.—Flow elements in a capillary tube.

so that

$$du = -\frac{\Delta p}{2L\mu} r\, dr \tag{4–16}$$

Noting that $u=0$ at the wall ($r=R$),

$$\int_u^o du = -\frac{\Delta p}{2L\mu} \int_r^R r\, dr \tag{4–17}$$

$$u=\frac{\Delta p}{4L\mu}(R^2-r^2) \tag{4-18}$$

$$dQ_c=2\pi ru\,dr \tag{4-19}$$

$$Q_c=2\pi\int_o^R \frac{\Delta p}{4L\mu}(R^2-r^2)r\,dr \tag{4-20}$$

Then

$$Q_c=\frac{\pi\Delta pR^4}{8L\mu} \tag{4-21}$$

Equation (4–21) is sometimes called the Hagen-Poiseuille law.

The velocity of discharge from a sharp-edged orifice is obtained from Bernoulli's equation

$$V=\sqrt{\frac{2\Delta pg}{\gamma}} \tag{4-22}$$

The volume flow is

$$Q_o=C_DAV \tag{4-23}$$

The orifice discharge coefficient C_D is ordinarily taken as 0.6 so that, in cubic inches per second

$$Q_o=13d_o^2\sqrt{\frac{\Delta p}{\gamma}} \tag{4-24}$$

A flow-control valve maintains a constant flow rate regardless of the pressure drop across it, so that

$$Q_v=\text{const.} \tag{4-25}$$

DETERMINATION OF BEARING OPERATING CONDITIONS

With the type of compensating element and the bearing geometry known, the operating film thickness under load can be determined. For the simple bearing (fig. 4–1) with capillary compensation, the flow into the pad (eq. (4–21)) is equated with the flow out of the pad (eq. 4–6)):

$$\frac{\pi(p_s-p_r)d^4}{128L\mu}=\frac{\pi h^3(p_r-p_a)}{6\mu\ln\left(\frac{R_2}{R_1}\right)} \tag{4-26}$$

The required pad pressure to support a given load W is obtained from equation (4–12). With the pad pressure determined, the manifold pressure is then a known function of the film thickness h and the dimensions of the capillary. These variables can be adjusted to suit the particular installation.

In a journal bearing, the zero-load film thickness is fixed at one-half the total bearing clearance. The external resistances will determine the zero-load pad pressures in terms of the supply pressure p_s. The resistances are usually so designed that the pressure drop through the resistance is approximately the same as that through the bearing at zero load.

In addition to the pressure and the flow, knowing the pumping power requirements for a hydrostatic bearing is important. The power required H is

$$H=(p_s-p_a)Q \tag{4-27}$$

Design equations and charts for several different bearing configurations, which include a full cylindrical bearing, are given in reference 1. Design charts and equations for orifice and capillary compensated journal bearings are given in reference 2. Methods for determination of flow, film thickness, and load capacity of thrust bearings are given in reference 3.

DETERMINATION OF OPTIMUM BEARING PROPORTIONS

It is a relatively simple matter to choose a particular bearing configuration that will satisfactorily support a given load. The particular design chosen, however, may be far from the optimum one with regard to the required pumping power. If the bearing is large, it may be of considerable economic importance to design for minimum pumping power.

If the bearing size is consiered to be fixed by available space or other factors, the recess size can be optimized in a straightforward way. Consider, for example, the simple bearing without compensation shown in figure 4–1. The load capacity from equation (4–12) is

$$W=\frac{\pi(p_r-p_a)}{2}\left(\frac{R_2^2-R_1^2}{\ln\frac{R_2}{R_1}}\right) \tag{4-12}$$

Solving for p_r-p_a yields

$$p_r-p_a=\frac{2W\ln\left(\frac{R_2}{R_1}\right)}{\pi(R_2^2-R_1^2)} \tag{4-28}$$

The flow from the bearing given by equation (4–6) is

$$Q=\frac{\pi h^3(p_r-p_a)}{6\mu \ln\left(\frac{R_2}{R_1}\right)} \tag{4–6}$$

From equation (4–27), with substitutions for Q and p_r-p_a (the external resistance is neglected so that $p_r=p_s$),

$$H=K\frac{\ln\left(\frac{R_2}{R_1}\right)}{(R_2^2-R_1^2)^2} \tag{4–29}$$

Differentiating with respect to R_1 yields

$$\frac{\partial H}{\partial R_1}=K\frac{-\frac{(R_2^2-R_1^2)}{R_1}+4R_1\ln\left(\frac{R_2}{R_1}\right)}{(R_2^2-R_1^2)^3} \tag{4–30}$$

Then, for minimum power loss, with $\partial H/\partial R_1$ equated to zero,

$$\ln\frac{R_2}{R_1}=\frac{R_2^2-R_1^2}{4R_1^2} \tag{4–31}$$

or

$$\frac{R_1}{R_2}=0.53 \tag{4–32}$$

Optimization of power loss by differentiation ordinarily cannot be accomplished for more complex bearings. Loeb and Ripple (ref. 4) have optimized the dimensions of several configurations of more complex thrust bearings by using an electric analog field plotter.

BEARING STIFFNESS

In many installations, the bearing deflection under load is important. The rate of change of load with film thickness is called the bearing stiffness. The general procedure for obtaining the stiffness of a bearing is as follows:

(1) Obtain an equation for flow from the bearing in terms of p_r, h^3, μ, and bearing geometry:

$$Q_1=Q_1(p_r,\ h^3,\ \mu,\ \text{bearing geometry}) \tag{4–33}$$

(2) Obtain an equation for load capacity in terms of p_r and bearing geometry:

$$W=W_1(p_r,\ \text{bearing geometry}) \tag{4–34}$$

(3) Obtain an equation for flow through the restrictor or restrictors in terms of p_s, p_r, and restrictor geometry:

$$Q_2 = Q_2(p_s,\ p_r,\ \text{restrictor geometry}) \tag{4-35}$$

(4) Solve for p_r in terms of W from equation (4-34) and substitute into equations (4-33) and (4-35) to obtain

$$Q_1 = Q_3(p_s,\ h^3,\ \mu,\ W,\ \text{bearing geometry}) \tag{4-33a}$$

and

$$Q_2 = Q_4(p_s,\ W,\ \text{restrictor geometry, bearing geometry}) \tag{4-35a}$$

(5) Equate equations (4-33a) and (4-35a) and solve for W in terms of p_s, h, μ, and bearing and restrictor geometry:

$$W = W_2(p_s,\ h,\ \mu,\ \text{bearing and restrictor geometry}) \tag{4-36}$$

Differentiation of equation (4-36) with respect to h yields an expression for bearing stiffness. Elwell and Sternlicht (ref. 5) determined expressions for the stiffness of circular hydrostatic bearings with

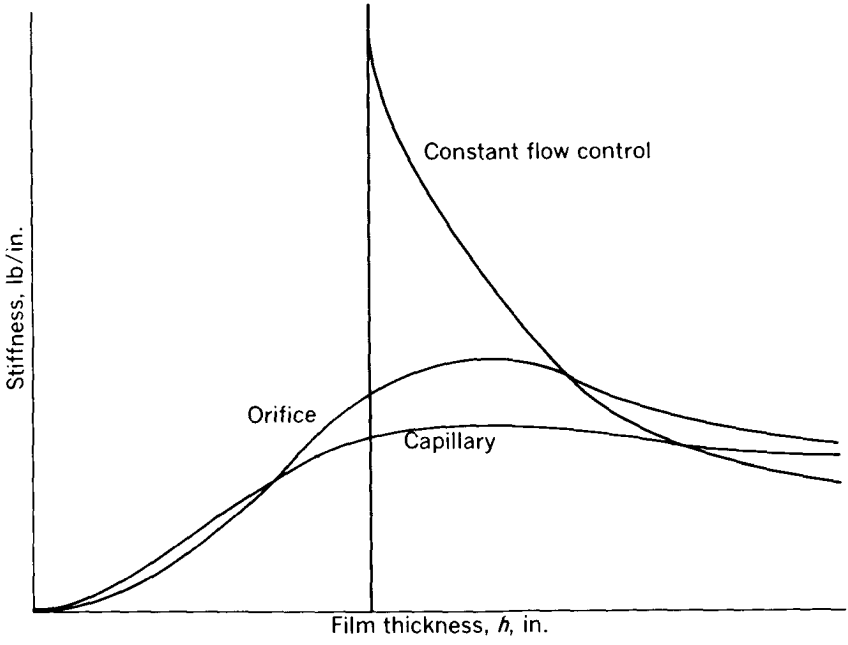

FIGURE 4-5.—Hydrostatic bearing stiffness as a function of film thickness for three types of compensation. (From ref. 5.)

capillary, orifice, and constant-flow valve compensation. They found that the constant-flow control valve bearing was stiffer than either the orifice or capillary bearings over a range of film thicknesses as shown in figure 4–5. The stiffness of this bearing, however, fell to zero when the film thickness reached a specific nonzero value, which corresponded to the maximum supply pressure. Orifice compensation generally produced a slightly stiffer bearing than capillary compensation except at low film thicknesses. Experimental data of pressure and flow as functions of load and of load as a function of film thickness are given in reference 5 in support of the analyses.

Malanoski and Loeb (ref. 6) have worked out "stiffness factors" for orifice, capillary, and constant-flow control compensation. This comparison was based on operation of the bearing at a given load and film thickness. Under these conditions, the constant-flow control-valve compensated bearing was always stiffer than the orifice compensated bearing, which was always stiffer than the capillary compensated bearing. With the load and film thickness held constant,

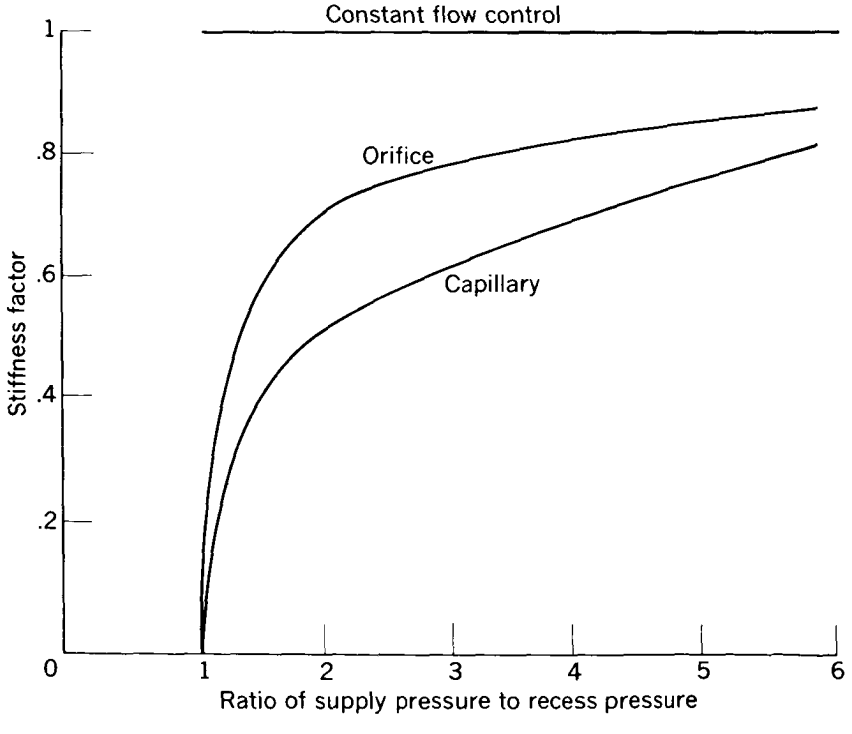

FIGURE 4–6.—Hydrostatic bearing stiffness at constant load and film thickness for three types of compensation. (From ref. 6.)

the variable of importance became the pressure ratio p_s/p_r. The results of the analysis of reference 6 are given in figure 4–6.

Note that, for orifice or capillary compensation, maximum stiffness is obtained at high pressure ratios. If stiffness is of prime importance and either of these two methods of compensation must be used, it is important to bear this in mind.

REFERENCES

1. Wilcock, D. F., and Booser, E. R.: Bearing Design and Application. McGraw-Hill Book Co., Inc., 1957.
2. Raimondi, A. A., and Boyd, J.: An Analysis of Orifice- and Capillary-Compensated Hydrostatic Journal Bearings. Lubrication Eng., vol. 13, no. 1, Jan. 1957, pp. 28–37.
3. Loeb, A. M.: The Determination of Hydrostatic Bearing Characteristics Through the Use of the Electric Analog Field Plotter. ASLE Trans., vol. 1, no. 1, 1958, pp. 217–224.
4. Loeb, A. M., and Rippel, H. C.: Determination of Optimum Proportions for Hydrostatic Bearings. ASLE Trans., vol. 1, no. 2, Oct. 1958, pp. 241–247.
5. Elwell, R. C., and Sternlicht, B.: Theoretical and Experimental Analysis of Hydrostatic Thrust Bearings. Jour. Basic Eng. (Trans. ASME), ser. D, vol. 82, no. 3, Sept. 1960, pp. 505–512.
6. Malanoski, S. B., and Loeb, A. M.: The Effect of the Method of Compensation on Hydrostatic Bearing Stiffness. Paper 60-LUB-12, ASME, 1960.

CHAPTER 5

Gas-Lubricated Bearings

By J. S. AUSMAN*

GAS-LUBRICATED BEARINGS are analogous to liquid-lubricated bearings in many respects. Gases are viscous and can act as lubricants although the bearing generally must have much closer clearances on account of the relative smallness of gas viscosity compared with liquid viscosity. The compressibility of gases complicates the analysis by making the Reynolds equation nonlinear. On the other hand certain aspects of gas bearings tend to simplify their analysis as compared with the analysis of liquid bearings. Perhaps the most significant simplification is that the gas film is continuous or complete throughout the bearing. That is, there is no film breakdown due to cavitation or ventilation as occurs in the low-pressure region of liquid-lubricated bearings. Further simplifications are that the gas lubricating film remains more nearly isothermal and more nearly laminar than does a liquid lubricating film.

The validity of the isothermal assumption can be verified as follows. Suppose that in a bearing of clearance h and relative surface velocity U, the gas somehow achieved a uniform temperature ΔT greater than that of the walls. How fast is the heat represented by this excess temperature dissipated to the walls? The solution to the transient heat conduction problem of a slab of material initially at a temperature ΔT above that of its two surfaces tells us that the temperature difference at the center of the "slab of gas" will decrease to $\Delta T/3$ in a time t

$$t=0.13\,\frac{c_p\rho h^2}{K} \tag{5-1}$$

where

c_p heat capacity of lubricating gas

h thickness of lubricating gas film (bearing clearance)

*Litton Industries, Inc., Guidance and Control Systems Division, Woodland Hills, Calif.

K heat conductivity of lubricating gas
ρ density of lubricating gas

This time will be very short compared with the average time required for the gas midway between the two bearing walls to traverse the bearing provided

$$t << \frac{B}{U/2}$$

where B is the characteristic length of the bearing in the direction of motion. Some typical numerical values are checked as follows.

For an air bearing with a clearance of 10^{-3} inch,

$$t = 0.13 \frac{0.24 \frac{\text{Btu}}{(\text{lb})(^\circ\text{F})} \times 0.0662 \frac{\text{lb}}{\text{cu ft}} \times 10^{-6} \text{ sq in.} \times 3600 \frac{\text{sec}}{\text{hr}}}{0.0162 \frac{\text{Btu}}{(\text{hr})(\text{ft})(^\circ\text{F})} \times 144 \frac{\text{sq in.}}{\text{sq ft}}} = 3.2 \ \mu\text{sec}$$

By comparison, the centerline transit time in a 1-inch-long bearing with a relative surface velocity of 5×10^3 inches per second (about 50,000 rpm on a 1 in. radius) is

$$\frac{B}{U/2} = \frac{1 \text{ in.} \times 2}{5 \times 10^3 \text{ in./sec}} = 400 \ \mu\text{sec}$$

Comparison of the above figures shows that for all practical purposes the gas temperature will remain the same as the temperature of the bearing walls. As most bearing surfaces are made of good heat conductive materials, the isothermal assumption is a good one. Effectively, the gas lubricant is in intimate contact with a constant-temperature, infinite heat sink.

Transition from laminar to turbulent flow is largely dependent upon Reynolds number $Re = Uh/\nu$ where ν is the kinematic viscosity of the lubricating gas. The critical value for the Reynolds number above which turbulence occurs is somewhat vague but it is generally believed to be somewhere in the range

$$500 < Re_{crit} < 2000$$

For comparison, a typical 1-inch-diameter, air-lubricated journal bearing operating with a radial clearance of 10^{-3} inch at a speed of 50,000 rpm would have a Reynolds number of less than 100. Clearly most gas-lubricated bearings will operate in the laminar flow region unless their size and speed are extraordinarily large.

The laminar flow condition means that the basic Reynolds equation (which neglects fluid inertia terms) is valid. As derived in chapter 3,

this basic equation is

$$\frac{\partial}{\partial x}\left(\rho h^3 \frac{\partial p}{\partial x}\right)+\frac{\partial}{\partial y}\left(\rho h^3 \frac{\partial p}{\partial y}\right)=6\mu U \frac{\partial}{\partial x}(\rho h)+12\mu \frac{\partial(\rho h)}{\partial t} \qquad (5\text{–}2)$$

The gas density ρ must now be replaced by a function of the pressure p, whereas for a liquid lubricant the density is, of course, presumed constant. The perfect gas law,

$$p=\rho \mathcal{R} T \qquad (5\text{–}3)$$

together with the condition of constant temperature provides the required compressibility relation between ρ and p. Substitution of equation (5–3) into equation (5–2) yields

$$\frac{\partial}{\partial x}\left(ph^3 \frac{\partial p}{\partial x}\right)+\frac{\partial}{\partial y}\left(ph^3 \frac{\partial p}{\partial y}\right)=6\mu U \frac{\partial}{\partial x}(ph)+12\mu \frac{\partial(ph)}{\partial t} \qquad (5\text{–}4)$$

Note that, in contrast to equation (3–13) for liquid lubrication, the left side of equation (5–4) is nonlinear in the variable p.

Because of this nonlinearity, no general analytical solution to this equation has been found. Approximate methods of solution invariably rely on some means of linearizing the equation. Another approach is to replace the differential equation with a finite-difference equation which can be solved by trial-and-error iterative procedures with the aid of a high-speed digital computer (refs. 1 and 2).

The first simplification to equation (5–4) is to consider only time-invariant lubrication and thereby to drop the $\partial(ph)/\partial t$ term. The remaining equation is often reduced further by ignoring either the side flow terms $\frac{\partial}{\partial y}\left[ph^3\,(\partial p/\partial y)\right]$ or the so-called "parabolic portion" $\frac{\partial}{\partial x}\left[ph^3\,(\partial p/\partial x)\right]$ of the main bearing flow. The first of these approximations is the "infinitely long bearing" approximation (ref. 3); the second is the "short bearing" approximation (ref. 4). If there is no relative motion, as in an externally pressurized bearing, $U=0$ and the term in equation (5–4) containing U vanishes. Further simplifications result if the clearance h is a constant.

The following sections discuss some of these methods of obtaining approximate solutions. Results are presented in forms intended to illustrate the fundamental nature and behavior of gas lubrication. Typical design curves are also given for guides, but it should be emphasized that a good basic understanding of the physical phenomenon is still one of the best design tools. The design of gas bearings is still far from routine, and significant contributions can be made by clever design engineers.

SELF-ACTING BEARINGS

General

Considerable insight can be gained into the behavior of self-acting gas-lubricated bearings without completely solving equation (5–4). For example, consider Harrison's equation (ref. 3), obtained by neglecting the $\partial/\partial y$ term as well as the $\partial/\partial t$ term:

$$\frac{\partial}{\partial x}\left(ph^3\frac{\partial p}{\partial x}\right)=6\mu U\frac{\partial}{\partial x}(ph) \tag{5–5}$$

This equation integrates immediately into

$$\frac{\partial p}{\partial x}=\frac{6\mu U}{ph^3}(ph-K_1) \tag{5–6}$$

where K_1 is a constant of integration.

Let us now consider the behavior of the gas pressure at very high speeds as $U\to\infty$. When on physical grounds $\partial p/\partial x$ is assumed to remain finite, the only way in which equation (5–6) can be satisfied as $U\to\infty$ is to have $ph\to K_1$. This gives the high-speed asymptote for gas-lubricated bearings:

$$\lim_{U\to\infty} ph=\text{constant}=p_0h_0 \tag{5–7}$$

where p_0 is the ambient pressure at the inlet clearance h_0. A fundamental difference exists in equation (5–7) between liquid lubrication and gas lubrication. In liquid lubrication the pressure and load (integrated pressure) are directly proportional to speed and viscosity and independent of ambient pressure. In self-acting gas-lubricated bearings at very high speeds the pressure and load (integrated pressure) become independent of speed and viscosity but directly proportional to ambient pressure.

Next let us consider gas lubrication at very small velocities as $U\to 0$. Equation (5–6) shows that as $U\to 0$, $\partial p/\partial x\to 0$ as the first power of U. In other words, for small U, $\partial p/\partial x$ is of order U.

Expanding equation (5–5) yields

$$p\frac{\partial}{\partial x}\left(h^3\frac{\partial p}{\partial x}\right)-6\mu Up\frac{\partial h}{\partial x}=-h^3\left(\frac{\partial p}{\partial x}\right)^2+6\mu Uh\frac{\partial p}{\partial x} \tag{5–8}$$

Note that the two terms on the right side of equation (5–8) are of order U^2: that is, as $U\to 0$ they will become negligible with respect to the two terms on the left side. At low speeds, then, the gas lubrica-

tion equation reduces to

$$\frac{\partial}{\partial x}\left(h^3 \frac{\partial p}{\partial x}\right)=6\mu U \frac{\partial h}{\partial x} \qquad (\text{as } U \to 0) \qquad (5\text{–}9)$$

This equation is the same as the liquid-lubrication equation, and brings us to a second important principle: At low speeds self-acting gas lubrication can be considered incompressible, and the same results derived for complete film lubrication by liquids apply directly to low-speed gas lubrication.

These same arguments can be applied to the more general two-dimensional equation (eq. (5–4)) with the $\partial/\partial t$ term omitted to reach the same conclusion (ref. 5). In addition, it is worthwhile noting from equation (5–5) that the high-speed asymptote

$$\lim_{U \to \infty} \frac{\partial}{\partial x}(ph)=0$$

is determined solely from the right side of the equation independently of the terms appearing on the left side. This means that the high-speed asymptote for finite length bearings is the same as that for infinite length bearings. In other words, side flow can be neglected even on short bearings if the speed is sufficiently high.

These three fundamental characteristics of self-acting gas lubrication are presented pictorially in figure 5–1. To repeat the important points for emphasis,

(1) At very low speeds gas bearing behavior is closely approximated by incompressible or liquid lubrication solutions of the same bearing geometry.

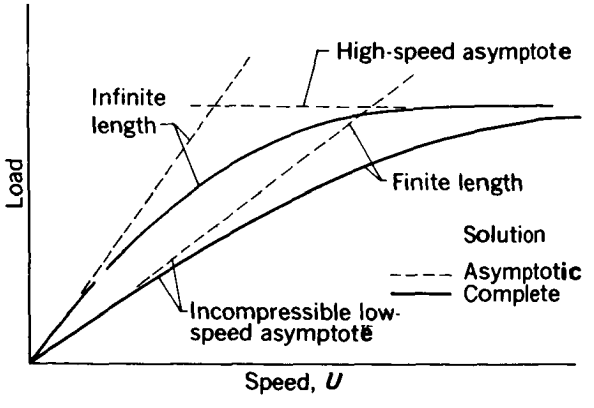

FIGURE 5–1.—Variation of load as a function of speed on self-acting gas-lubricated bearings.

(2) At very high speeds, ph=constant, and load becomes independent of speed.

(3) At very high speeds side flow effects are negligible and finite and infinite length bearing solutions both approach ph=constant.

Journal Bearings

For journal bearings it is convenient to change the variables in equation (5–4) by the substitutions

$$\partial x = R\partial\theta$$
$$\partial y = R\partial\eta$$
$$U = R\omega$$

The resulting equation (with the time-dependent term omitted) is

$$\frac{\partial}{\partial\theta}\left(ph^3\frac{\partial p}{\partial\theta}\right)+\frac{\partial}{\partial\eta}\left(ph^3\frac{\partial p}{\partial\eta}\right)=6\mu\omega R^2\frac{\partial}{\partial\theta}(ph) \tag{5–10}$$

Assuming a purely translational displacement ϵc of the journal shaft relative to the bearing sleeve, we can write the following equation for the film thickness h:

$$h=c(1+\epsilon\cos\theta) \tag{5–11}$$

where

c average radial clearance
ϵ eccentricity ratio

The perturbation method (ref. 6) is one technique employed to linearize equation (5–10) in order to obtain an approximate solution. The general concept is to substitute equation (5–11) and

$$p=p_0+\Delta p \tag{5–12}$$

into equation (5–10) and neglect all terms of order ϵ^2 or higher. In this procedure Δp is assumed to be of order ϵ. It is also noted that $d(\Delta p)=dp$, so that the first-order (in ϵ) perturbation equation becomes

$$\frac{\partial^2 p}{\partial\theta^2}+\frac{\partial^2 p}{\partial\eta^2}=\frac{6\mu\omega R^2}{p_0c^2}\left(\frac{\partial p}{\partial\theta}-\epsilon p_0\sin\theta\right) \tag{5–13}$$

The dimensionless group $6\mu\omega R^2/p_0c^2$ is usually designated as Λ and called the "compressibility bearing number," "compressibility number," or "bearing number." It or some similar dimensionless number is a fundamental parameter in self-acting gas lubrication.

Equation (5–13) can be solved (ref. 6) for the first-order perturbation pressure, which in turn can be integrated in the usual fashion to obtain load components W_1' and W_2' parallel to and perpendicular to the line of centers. The results are

$$\frac{W_1'}{p_0 LD}=\frac{\pi}{2}\frac{\epsilon\Lambda}{1+\Lambda^2}\left[\Lambda+f_1\left(\Lambda,\frac{L}{D}\right)\right] \tag{5-14}$$

and

$$\frac{W_2'}{p_0 LD}=\frac{\pi}{2}\frac{\epsilon\Lambda}{1+\Lambda^2}\left[1-f_2\left(\Lambda,\frac{L}{D}\right)\right] \tag{5-15}$$

where

$$f_1\left(\Lambda,\frac{L}{D}\right)=\frac{(\sigma-\xi\Lambda)\sin 2\xi\frac{L}{D}-(\sigma\Lambda+\xi)\sinh 2\sigma\frac{L}{D}}{\frac{L}{D}\sqrt{1+\Lambda^2}\left(\cosh 2\sigma\frac{L}{D}+\cos 2\xi\frac{L}{D}\right)}$$

$$f_2\left(\Lambda,\frac{L}{D}\right)=\frac{(\sigma-\xi\Lambda)\sinh 2\sigma\frac{L}{D}+(\sigma\Lambda+\xi)\sin 2\xi\frac{L}{D}}{\frac{L}{D}\sqrt{1+\Lambda^2}\left(\cosh 2\sigma\frac{L}{D}+\cos 2\xi\frac{L}{D}\right)}$$

where

$$\Lambda=\frac{6\mu\omega R^2}{p_0 c^2}$$

$$\sigma=\sqrt{\frac{(1+\Lambda^2)^{1/2}+1}{2}} \qquad \text{(Positive roots)}$$

$$\xi=\sqrt{\frac{(1+\Lambda^2)^{1/2}-1}{2}} \qquad \text{(Positive roots)}$$

Figure 5–2 is a graph of equations (5–14) and (5–15) in terms of total load $W'=\sqrt{(W_1')^2+(W_2')^2}$ and attitude angle $\varphi=\tan^{-1}(W_2'/W_1')$ for several L/D ratios. Note from equations (5–14) and (5–15) that the first-order perturbation solution yields a load linearly related to eccentricity ratio ϵ. This is a consequence of the linearization and is valid only for small ϵ, say $\epsilon<0.3$, although as a conservative engineering approximation it may be used for higher values. Actually, the load increases much more sharply at high values of ϵ as indicated in figure 5–3.

The so-called "linearized ph" solution (ref. 7) was developed to correct this deficiency of the first-order perturbation solution at high eccentricity ratios. The general method of linearization is essentially the same as the perturbation method except that the product ph is considered to be the dependent variable. To do this, we arrange equation (5–10) so that p always appears multiplied by h. Into this equation in ph equation (5–11) and

$$ph=p_0 c+\Delta(ph) \tag{5-16}$$

are then substituted and only first-order terms in the eccentricity ratio ϵ retained. It is assumed that $\Delta(ph)$ is of order ϵ. The resulting

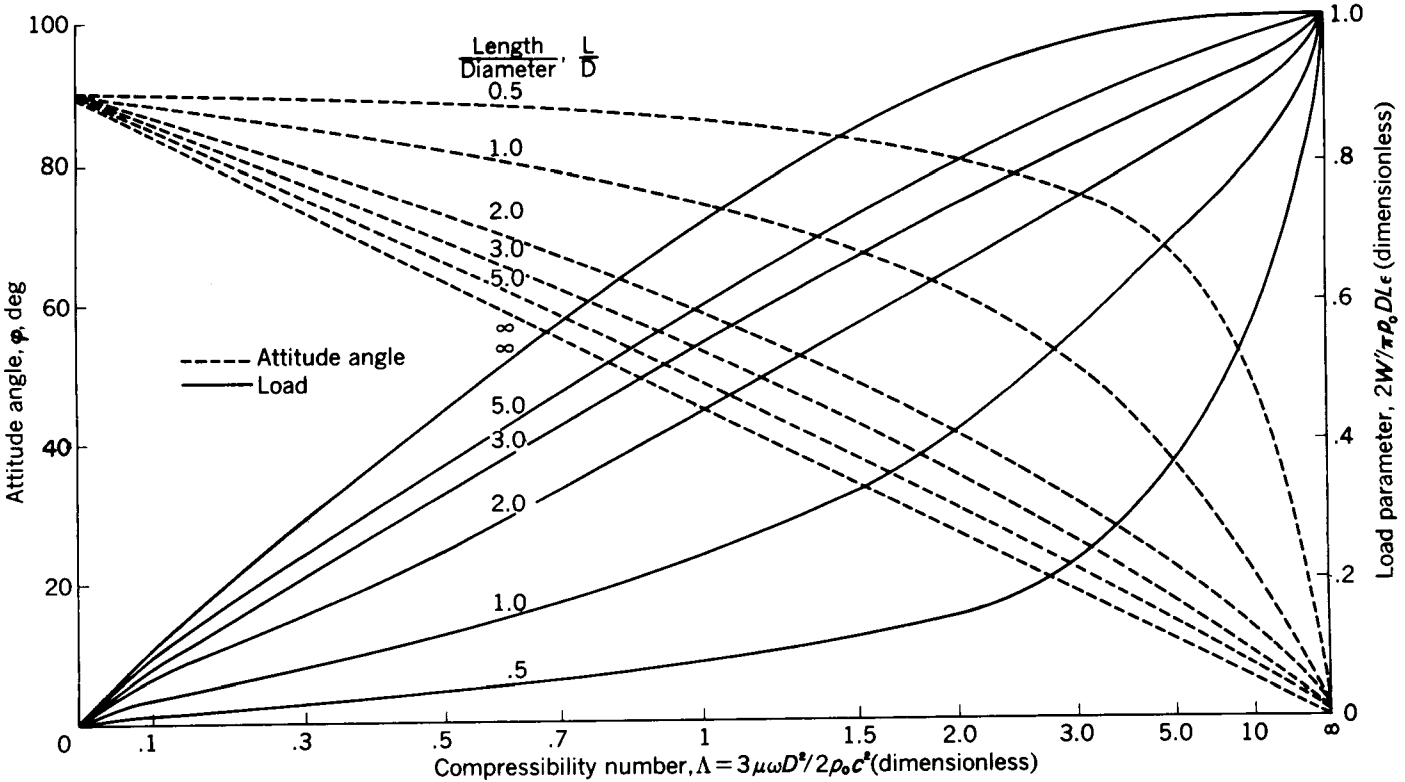

FIGURE 5–2.—Design chart for radially loaded self-acting gas-lubricated journal bearings (isothermal first-order perturbation solution).

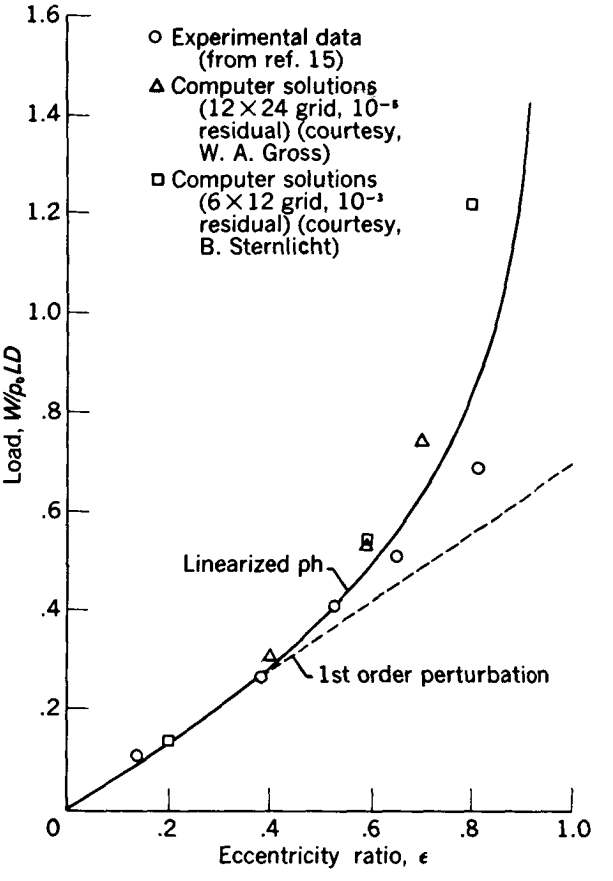

FIGURE 5–3.—Load plotted against eccentricity-ratio comparisons for a finite-length, self-acting, gas-lubricated journal bearing. $\Lambda = 1.3$; $L/D = 1.5$. (From ref 7.)

"linearized ph" equation is

$$\frac{\partial^2(ph)}{\partial\theta^2} + \frac{\partial^2(ph)}{\partial\eta^2} = \Lambda\left[\frac{\partial(ph)}{\partial\theta} - \epsilon p_0 c \cos\theta\right] \tag{5–17}$$

Equation (5–17) is essentially the same form as the first-order perturbation equation (5–13) and can be solved in the same manner for ph. Once ph is found, the pressure p can, of course, be obtained by dividing by h as given in equation (5–11). The resulting expression for p is then put into the load component integrals to obtain W_1 and W_2. The results are

$$W_1 = \frac{2}{\epsilon^2}\left[\frac{1-(1-\epsilon^2)^{1/2}}{(1-\epsilon^2)^{1/2}}\right] W_1' \tag{5–18}$$

$$W_2=\frac{2}{\epsilon^2}\left[1-(1-\epsilon^2)^{1/2}\right]W_2' \tag{5-19}$$

In total load W and attitude angle φ form

$$W=\sqrt{W_1^2+W_2^2}=W'\frac{2}{\epsilon^2}\left[\frac{1-(1-\epsilon^2)^{1/2}}{(1-\epsilon^2)^{1/2}}\right](1-\epsilon^2\sin^2\varphi')^{1/2} \tag{5-20}$$

and

$$\tan\varphi=\tan\frac{W_2}{W_1}=(1-\epsilon^2)^{1/2}\tan\varphi' \tag{5-21}$$

where W_1', W_2', W', and φ' are the values given by the first-order perturbation solution. Equations (5–18) to (5–21) express the linearized *ph* solution as corrections to the first-order perturbation solution. This is a very convenient form for the designer. A "rough cut" design can be made first by using the perturbation solution. This design can later be improved by applying the linearized *ph* corrections. Figure 5–3 shows the effectiveness of this method in estimating the load versus eccentricity characteristic for a particular bearing.

The bearing friction torque and power dissipated in a journal bearing are easily estimated by the simple but fairly accurate formulas

$$Q=\frac{\pi}{4}\frac{\mu\omega LD^3}{c\sqrt{1-\epsilon^2}} \qquad \text{(Torque)} \tag{5-22}$$

$$H=\frac{\pi}{4}\frac{\mu\omega^2 LD^3}{c\sqrt{1-\epsilon^2}} \qquad \text{(Power)} \tag{5-23}$$

Numerical example:

Estimate the maximum load which can be carried by a 1-inch-diameter by 1-inch-long self-acting gas-lubricated journal bearing operating at 1500 radians per second (14,400 rpm) with 300-microinch average radial clearance and a minimum clearance of 60 microinches. Assume an ambient pressure of 15 pounds per square inch and a lubricant viscosity of 3×10^{-9} pound-second per square inch.

(1) Compute $\Lambda=\dfrac{6\mu\omega R^2}{p_0c^2}$ and $\dfrac{L}{D}$:

$$\Lambda=\frac{6\times3\times10^{-9}\,\dfrac{\text{(lb) (sec)}}{\text{sq in.}}\times1.5\times10^3\,\dfrac{1}{\text{sec}}\times0.25\text{ sq in.}}{15\,\dfrac{\text{lb}}{\text{sq in.}}\times9\times10^{-8}\text{ sq in.}}$$

$$\Lambda=5$$

$$\frac{L}{D}=\frac{1\text{ in.}}{1\text{ in.}}=1$$

(2) Enter figure 5–2 with Λ and L/D to obtain W' and φ'

$$W'=0.66\frac{\pi}{2}p_0LD\epsilon$$

$$W'=15\ \epsilon\ \text{lb}$$

$$\varphi'=35°$$

(3) Compute ϵ and W:

$$\epsilon=\frac{300-60}{300}=0.80$$

$$W=15\ \text{lb}\left\{\frac{2[1-(1-0.64)^{1/2}]}{0.80(1-0.64)^{1/2}}\right\}(1-0.64\times0.33)^{1/2}=22\ \text{lb}$$

Note that the unit load capacity on this bearing $W/LD=22$ pounds per square inch actually exceeds the ambient pressure.

Thrust Bearings

Self-acting gas-lubricated thrust bearings usually are made by permanently etching a contoured surface into one of two opposing disks. Various contoured shapes may be used as indicated in figure 5–4. Either the fixed disk or the rotating disk may be contoured. Conceivably both could be contoured, but manufacturing simplicity usually dictates that one surface be made flat. Of these types of thrust bearings, the spiral groove is probably the best. Analysis of this configuration (ref. 8) is difficult, however.

The stepped bearing is perhaps the easiest to analyze, and for this reason it will be considered here even though it may not be as effective a thrust bearing as some of the others. One design approach is

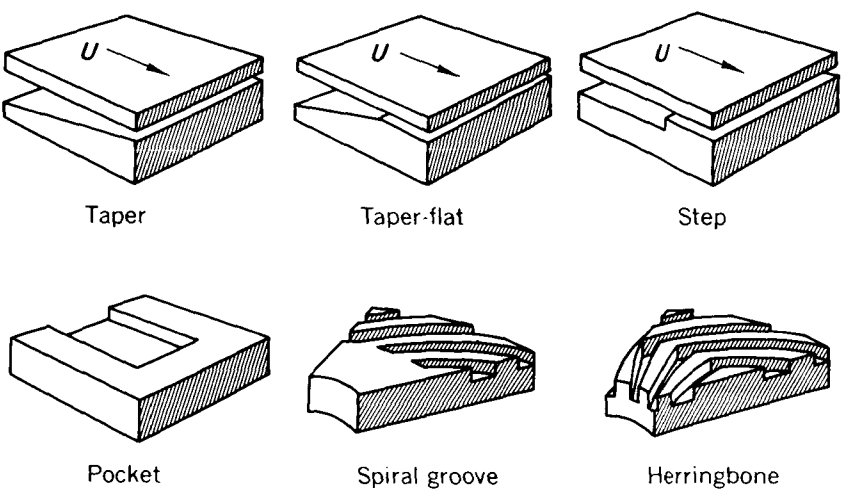

FIGURE 5–4.—Examples of thrust bearings.

to use the step-bearing results to estimate the overall size of bearing required and then to build something a little different. For example, the pocket bearing should be somewhat better than a step bearing because it actually is a step bearing with ridges along the sides to restrict side leakage. Because of its relative simplicity, step bearing analysis might well be used to make a conservative design for a pocket bearing.

The big advantage in analyzing step bearings is that the bearing clearance h is constant throughout each of two regions. The Reynolds equation can be linearized by a simple perturbation method and solved in each of the two regions separately. The two solutions are then matched at the step by requiring the pressure to be continuous across the step and by matching the mass flow crossing the step. One other reason in favor of using the step bearing for design purposes is that a solution also exists for the case of incompressible lubrication (ref. 9). This provides a convenient check on the compressible solution at low speeds.

For a constant bearing clearance, as in the step bearing, equation (5–4) with the $\partial/\partial t$ term omitted reduces to

$$\frac{\partial}{\partial x}\left(p\frac{\partial p}{\partial x}\right)+\frac{\partial}{\partial y}\left(p\frac{\partial p}{\partial y}\right)=\frac{6\mu U}{h^2}\frac{\partial p}{\partial x} \tag{5–24}$$

The linearized form of the equation can be written directly by substituting

$$\left.\begin{aligned} p&=p_0+\Delta p\\ \partial(\Delta p)&=\partial p\end{aligned}\right\} \tag{5–25}$$

and neglecting all but first-order terms in Δp to obtain

$$\frac{\partial^2 p}{\partial\left(\frac{x}{R}\right)^2}+\frac{\partial^2 p}{\partial\left(\frac{y}{R}\right)^2}=\Lambda_h\frac{\partial p}{\partial\left(\frac{x}{R}\right)} \tag{5–26}$$

where

$$\Lambda_h=\frac{6\mu UR}{p_0h^2}$$

Note that the bearing compressibility characteristic Λ_h differs from one region to the other and also changes as the clearance changes under varying loads. This makes Λ_h a somewhat inconvenient design parameter. For this reason, a more convenient but at the same time more artificial bearing characteristic $\Lambda_\Delta=6\mu UR/p_o\Delta^2$ is introduced, where Δ is the depth of the recess, or step, separating the two regions. The usefulness of Λ_Δ stems from the fact that it remains constant for a particular bearing regardless of load variations.

Equation (5–26) can also be written and solved (ref. 10) in polar coordinates (r,θ); this solution is of most interest. The details of the solution are too lengthy to be given here. The results are best summarized in table 5–I and figure 5–5. Table 5–I gives the optimum number of pads and step location for a given value of Λ_Δ or $(\Lambda_\Delta)_1$ as listed in table 5–I and inner- to outer-radius ratio b or $(b)_1$. From table 5–I can be calculated the unit load (load per unit area) $(P)_1$ for the given values of $(\Lambda_\Delta)_1$ when the minimum clearance s is equal to the depth of the step Δ. This value $(P)_1$ determines one point and hence the entire ordinate scale for figure 5–5. The corresponding $(\Lambda_\Delta)_1$ value also determines the scale for labeling the solid and dashed parameter lines in figure 5–5.

A typical procedure for estimating the load against minimum clearance characteristics of a bearing under design is as follows:

(1) Compute the radius ratio b=inner radius/outer radius and the bearing characteristic $\Lambda_\Delta=6\mu\omega R^2/p_0\Delta^2$.

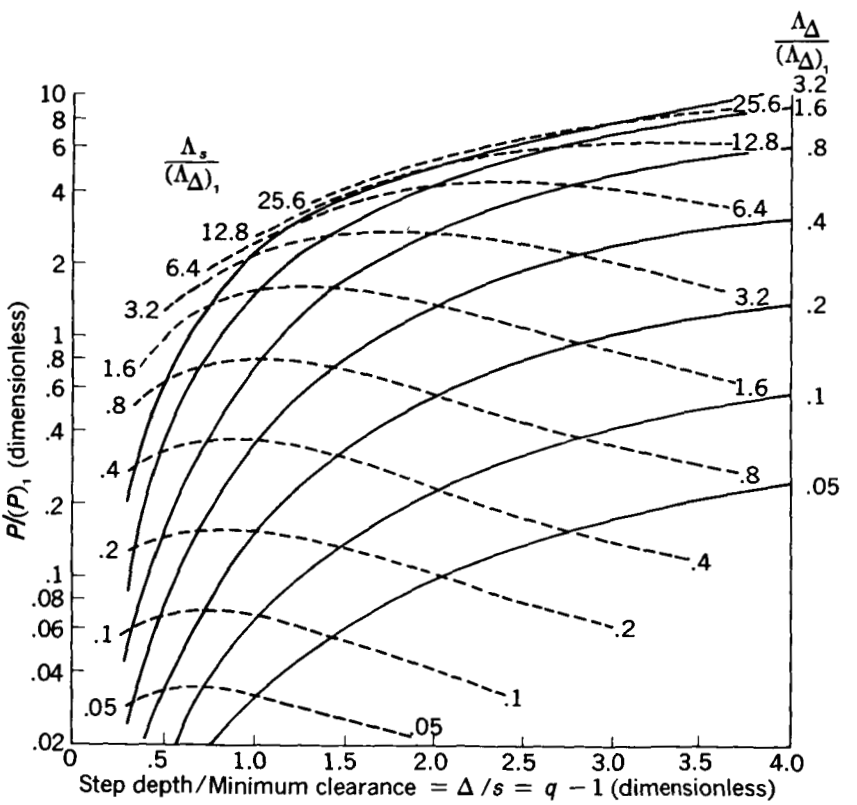

FIGURE 5–5.—Stepped sector thrust pad design chart.

(2) Enter table 5–I at the nearest values of $(b_1 \approx b$ and $(\Lambda_\Delta)_1 \approx \Lambda_\Delta$ to obtain optimum number of pads N, optimum step location τ/γ, and the unit load $(P)_1$ when the minimum clearance s is equal to the step depth Δ.

(3) Use $(P)_1$ in the ordinate scale of figure 5–5 and the $\Lambda_\Delta/(\Lambda_\Delta)_1$ curve to obtain unit load P (or actual load NW) as a function of s. If necessary, a new $\Lambda_\Delta/(\Lambda_\Delta)_1$ curve can be sketched in quite accurately with the aid of the $\Lambda_s/(\Lambda_\Delta)_1$ curves and the relation $\Lambda_\Delta=(s/\Delta)^2\Lambda_s$.

(4) If two opposing thrust bearings are employed, the P (or W) against s curve for the second bearing can be sketched as a mirror image of the first about the line s=constant which intersects the load curve at the desired preload. The net load at any value of s is then the difference between the two mirror image curves of load against minimum clearance.

Numerical example:

Estimate the net load carried by an opposing pair of identical, near optimum design, stepped, thrust bearings when the minimum clearances are 60 microinches on one and 300 microinches on the other bearing. The thrust bearings have a 0.25-inch inner radius, a 1-inch outer radius, and a 180-microinch step depth, and are operating at an angular velocity of 865 radians per second (8250 rpm). Assume the lubricant gas viscosity is 3×10^{-9} pound-second per square inch and ambient pressure is 15 pounds per square inch absolute.

(1) Compute b and Λ_Δ.

$$b=\frac{0.25}{1}=0.25$$

$$\Lambda_\Delta=\frac{6\mu\omega R^2}{p_0\Delta^2}=\frac{6\times3\times10^{-9}\times865\times1}{15\times3.24\times10^{-8}}=32$$

(2) Enter table 5–I for $(b)_1=0.3$ and $(\Lambda_\Delta)_1=40$. (Close to $b=0.25$ $\Lambda_\Delta=32$.)

Optimum number of pads $N=4$
Optimum step location $=\tau/\gamma=0.29$
$(P)_1=0.270p_0=4.05$ lb/sq in.

(3) Enter figure 5–5 on $\Lambda_\Delta/(\Lambda_\Delta)_1=32/40=0.8$ curve

(a) at $\frac{\Delta}{s}=\frac{180}{60}=3$ to read off $\frac{P}{(P)_1}=4.5$ or $P=18.2$ lb/sq in.

(b) at $\frac{\Delta}{s}=\frac{180}{300}=0.6$ to read off $\frac{P}{(P)_1}=0.24$ or $P=0.97$ lb/sq in.

TABLE 5–I.—OPTIMUM NUMBER OF PADS AND LOCATION OF STEP FOR MAXIMUM LOAD AT A COMPRESSION RATIO OF 2

[Ratio of maximum clearance (leading sector) to minimum clearance (trailing sector), $(s+\Delta)/s$, 2; angular width of groove between pads, δ, 2°]

Inner radius/ outer radius, b	$\Lambda_\Delta=\Lambda_s$	Number of pads, N	Leading sector angle/ total pad angle per pad, τ/γ	Unit load/ ambient pressure, P/p_0
0. 20	10	4	0. 45	0. 064
	20	4	. 39	. 141
	40	3	. 26	. 286
	80	3	. 16	. 470
	160	3	. 10	. 638
0. 30	10	5	0. 45	0. 059
	20	5	. 39	. 131
	40	4	. 29	. 270
	80	4	. 20	. 457
	160	4	. 12	. 622
0. 40	10	6	0. 46	0. 053
	20	6	. 39	. 119
	40	5	. 31	. 248
	80	5	. 23	. 431
	160	5	. 14	. 602
0. 50	10	8	0. 48	0. 046
	20	7	. 39	. 103
	40	7	. 33	. 219
	80	6	. 23	. 397
	160	6	. 14	. 572
0. 60	10	11	0. 49	0. 038
	20	10	. 42	. 084
	40	9	. 36	. 184
	80	8	. 25	. 349
	160	7	. 17	. 530
0. 70	10	15	0. 50	0. 029
	20	14	. 45	. 063
	40	12	. 36	. 141
	80	11	. 28	. 284
	160	9	. 17	. 466
0. 75	10	18	0. 51	0. 024
	20	17	. 46	. 052
	40	15	. 37	. 116
	80	13	. 28	. 243
	160	11	. 19	. 421
0. 80	10	23	0. 53	0. 019
	20	21	. 48	. 041
	40	19	. 40	. 091
	80	17	. 31	. 194
	160	14	. 22	. 363

(4) The net load is

$$NW=\pi R^2(1-b^2)(P_3-P_{0.6})$$
$$=\pi\times 1 \text{ sq in. } (1-0.062)\ (18.2-0.97) \text{ lb/sq in.}$$

or

$$NW=50.8 \text{ lb}$$

Note once again that the net unit load capacity of 17 pounds per square inch actually exceeds the ambient pressure.

EXTERNALLY PRESSURIZED BEARINGS

Step Bearing

When there is little or no viscous pumping action of the bearing surfaces to self-lubricate the bearing, the lubricant must be forced between the surfaces by external pressurization. The basic principles involved in this type of lubrication are exemplified in the step outlet restrictor bearing shown in figure 5–6. Figure 5–6 could represent the cross section of a circular thrust bearing, the cross section of a rectangular thrust bearing, or the cross section of half a journal bearing. Here figure 5–6 will be considered to represent a cross section through the short dimension of a long, narrow rectangular bearing so that the flow is essentially one dimensional and perpendicular to the long axis of the rectangle.

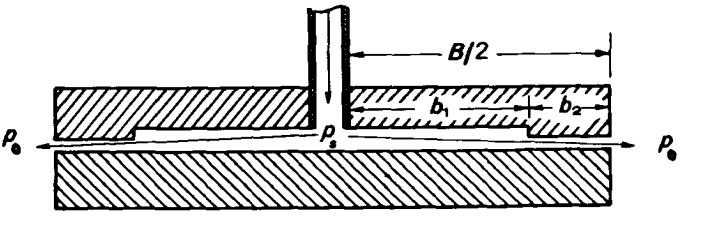

FIGURE 5–6.—Externally pressurized step outlet restrictor bearing.

As there is no relative motion of the surfaces, U equals zero. Dropping the time-dependent term, as previously, and neglecting the $\partial/\partial y$ term by virtue of the one-dimensional flow assumption reduce equation

(5–4) for each of the two sections of constant film thickness h to

$$\frac{\partial^2 p^2}{\partial x^2}=0 \tag{5–27}$$

The solution to equation (5–27) is simply

$$p^2=\begin{cases} p_s^2-C_1 x & \text{In region 1} \\ p_0^2+C_2\left(\frac{B}{2}-x\right) & \text{In region 2} \end{cases} \tag{5–28}$$

where region 1 is the recessed region of clearance h_1 next to the supply pressure p_s and region 2 is the restricting land region of clearance h_2 next to the exhaust at ambient pressure p_0. The two constants C_1 and C_2 are determined by matching the pressure and mass-flow rate across the step:

$$\left.\begin{aligned} C_1&=\frac{1}{h_1^3}\left[\frac{p_s^2-p_0^2}{(b_1/h_1^3)+(b_2/h_2^3)}\right] \\ C_2&=\frac{1}{h_2^3}\left[\frac{p_s^2-p_0^2}{(b_1/h_1^3)+(b_2/h_2^3)}\right] \end{aligned}\right\} \tag{5–29}$$

Figure 5–7 is a typical plot of p^2 and the resulting pressure p obtained from the square root. The straight-line pressure distribution which would be obtained by assuming incompressible flow is also shown. Note in figure 5–7 that the difference is relatively small between the actual compressible lubricant pressure distribution and the distribution for an incompressible lubricant. In fact, the loads given by the area between the pressure distribution curves and the line for constant $p_0=1$ atmosphere differ by less than 10 percent even though the supply pressure is 5 atmospheres.

In externally pressurized bearings the lubricant mass-flow rate is an important design quantity. For a bearing of clearance h and length L, the mass-flow rate is given by

$$M=-\frac{Lh^3}{12\mu\mathcal{R}T}\frac{\partial p^2}{\partial x} \tag{5–30}$$

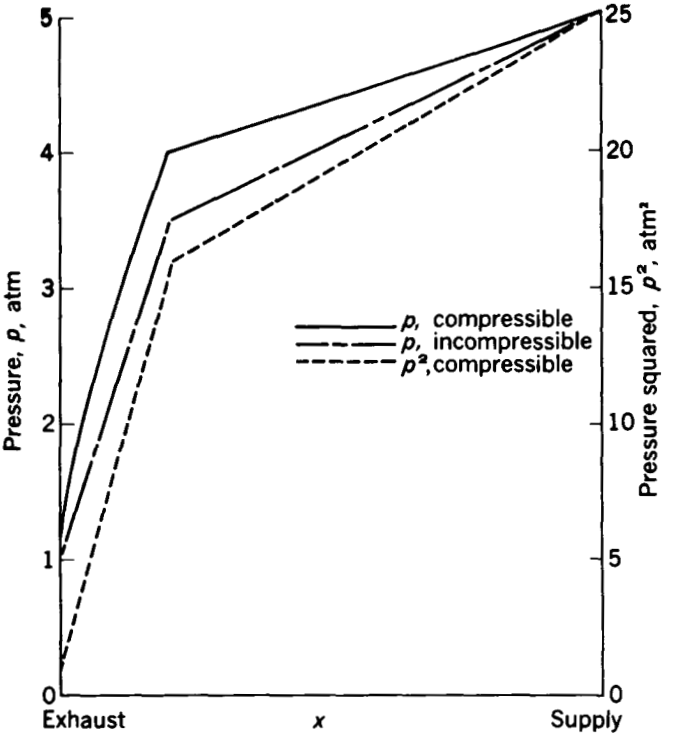

FIGURE 5-7.—Comparison of pressure distribution in an externally pressurized step bearing for compressible and for incompressible lubrication.

Obtaining $\partial p^2/\partial x$ from (5–28) and (5–29), we have for the mass-flow rate

$$M=\frac{L(p_s^2-p_0^2)}{12\mu\mathcal{R}T\left(\frac{b_1}{h_1^3}+\frac{b_2}{h_2^3}\right)} \tag{5-31}$$

Employing the incompressible approximations to estimate load on a bearing whose step is midway along the bearing ($b_1=B/4$) and neglecting the inlet area at p_s, we compute the load W to be

$$\frac{W}{(p_s-p_o)LB}=\frac{1}{2}+\frac{1}{4}\left(\frac{q^3-1}{q^3+1}\right) \tag{5-32}$$

where $q=h_2/h_1$ is the compression ratio.

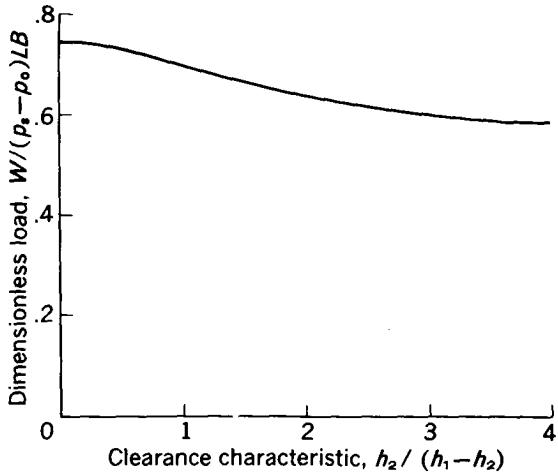

FIGURE 5–8.—Dimensionless load plotted against clearance characteristic for a step outlet restrictor bearing. $b_1=B/4$.

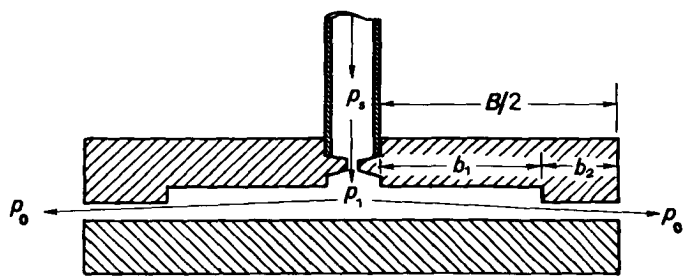

FIGURE 5–9.—Recessed bearing with orifice inlet restrictor.

Equation (5–32) is plotted in figure 5–8 as a function of $h_2/(h_1-h_2)=(q-1)^{-1}$. Note that the maximum possible variation in load from large values of $h_2/(h_1-h_2)$ to very small values of $h_2/(h_1-h_2)$ is only $0.25(p_s-p_0)LB$. This variation could be increased somewhat (to a maximum limiting value of $0.5(p_s-p_0)LB$) by placing the step closer to the outlet but the fact remains that the maximum load variation is going to be between $0.25(p_s-p_0)LB$ and $0.50(p_s-p_0)LB$. Also, as the minimum clearance h_2 increases, the mass-flow rate increases very rapidly, approximately as h_2^3.

One means of increasing the load range and at the same time limiting mass flow at large clearances is to put an orifice restriction on the inlet as indicated in figure 5–9. This effectively reduces the supply pressure as the clearance and mass flow increase. The maximum load capacity for a single thrust bearing is no greater, but the

minimum load is made smaller. This means that the stiffness of the orifice-compensated bearing will be increased over that of the step bearing, and also that the net load capacity of two opposing bearings will be increased. For these reasons, most externally pressurized bearings are the orifice-inlet-restrictor type discussed in the next section.

Orifice-Restrictor Bearing

An orifice inlet restrictor (fig. 5–9) limits the maximum mass-flow rate and reduces the effective supply pressure from p_s to p_1. Analysis of the flow from pressure p_1 to the exhaust pressure p_0 proceeds exactly as before. The only new problem is to compute the pressure drop $p_s - p_1$ across the orifice.

Orifice flow within the orifice itself is nearly always adiabatic so that the unchoked mass-flow rate through the orifice can be written as

$$M = C_D A p_s \left\{ \frac{2k}{(k-1)\mathcal{R}T} \left[\left(\frac{p_1}{p_s}\right)^{2/k} - \left(\frac{p_1}{p_s}\right)^{\frac{k+1}{k}} \right] \right\}^{1/2} \tag{5–33}$$

where T is the absolute temperature of the inlet gas at pressure p_s.

If p_1/p_s is less than the critical pressure ratio below which sonic velocity occurs at the orifice, the flow is said to be choked and

$$M = C_D A p_s \left\{ \frac{2k}{(k-1)\mathcal{R}T} [R_c^{2/k} - R_c^{(k+1)/k}] \right\}^{1/2} \tag{5–34}$$

for

$$\frac{p_1}{p_s} \leqq R_c$$

where $R_c = \left(\frac{2}{1+k}\right)^{k/(k-1)}$ is the critical pressure ratio. The mass-flow rate through the orifice must be the same as that through the rest of the bearing. By analogy with equation (5–31) the mass-flow rate through the bearing can be written

$$M = \frac{L(p_1^2 - p_0^2)}{12\mu\mathcal{R}T\left(\frac{b_1}{h_1^3} + \frac{b_2}{h_2^3}\right)} \tag{5–35}$$

Equating equation (5–33) or (5–34) to equation (5–35) yields an expression for determining the pressure p_1:

$$p_1 = p_0 \left\{ 1 + \Lambda_0 \frac{p_s}{p_0} \left[\left(\frac{p_1}{p_s}\right)^{2/k} - \left(\frac{p_1}{p_s}\right)^{(1+k)/k} \right]^{1/2} \right\}^{1/2} \quad \text{for } \frac{p_1}{p_s} > R_c \tag{5–36}$$

$$p_1 = p_0 \left\{ 1 + \Lambda_0 \frac{p_s}{p_0} [R_c^{2/k} - R_c^{(k+1)/k}]^{1/2} \right\}^{1/2} \quad \text{for } \frac{p_1}{p_s} \leqq R_c \tag{5–37}$$

The orifice restrictor bearing parameter Λ_0 is defined as

$$\Lambda_0=\frac{12\mu C_D A}{Lp_0}\left(\frac{b_1}{h_1^3}+\frac{b_2}{h_2^3}\right)\left(\frac{2k\mathcal{R}T}{k-1}\right)^{1/2} \tag{5-38}$$

Equation (36) cannot be solved explicitly for p_1. It can be solved graphically by the following technique. First rewrite equation (36) in the following form:

$$\Lambda_0=\frac{\frac{p_s}{p_0}\left[\left(\frac{p_1}{p_s}\right)^2-\left(\frac{p_0}{p_s}\right)^2\right]}{\left[\left(\frac{p_1}{p_s}\right)^{2/k}-\left(\frac{p_1}{p_s}\right)^{\frac{1+k}{k}}\right]^{1/2}} \tag{5-39}$$

For a given ratio p_s/p_0, Λ_0 can be plotted as a function of p_1/p_s from equation (39) as the example shows in figure 5-10. The parameter Λ_0 can also be plotted as a function of minimum clearance h_2 from equation (38) as shown, for example, by the dotted line in figure 5-10. These two curves can now be compared at equivalent values of Λ_0 to obtain p_1/p_s as a function of minimum clearance h_2. This graphical technique is useful for obtaining p_1/p_s when $p_1/p_s>R_c$. When $p_1/p_s<R_c$, the flow is choked and equations (37) and (38) can be used directly to determine p_1 as a function of minimum clearance.

Once p_1 is determined, the bearing load can be computed as in the preceding section. Again using the incompressible approximation to compute the load W on a bearing whose recess takes up half the bearing surface ($b_1=b_2$), we have by analogy with equation (5-32):

$$\frac{W}{(p_s-p_0)LB}=\frac{p_1-p_0}{p_s-p_0}\left(\frac{1}{2}+\frac{1}{4}\frac{q^3-1}{q^3+1}\right) \tag{5-40}$$

where LB is the bearing surface area and $q=h_1/h_2$.

From equations (5-37), (5-39), and (5-40), the load has been computed and plotted in figure 5-11 as a function of $h_2/(h_1-h_2)$ for comparison with figure 5-8. Note the wider load range and greater bearing stiffness achievable with the orifice restrictor.

Actually, it is not necessary to have a recess or step in the bearing surface when an inlet restrictor is employed. In fact, many bearings consist simply of parallel surfaces with high-pressure gas entering through several small holes in one of the surfaces. Such a bearing is sometimes called an "inherently compensated" orifice bearing. For a discussion of this as well as several other types of inlet restrictors, the reader is referred to a paper by Tang and Gross (ref. 11), which summarizes the equations and includes complete sets of design curves as well as numerical examples.

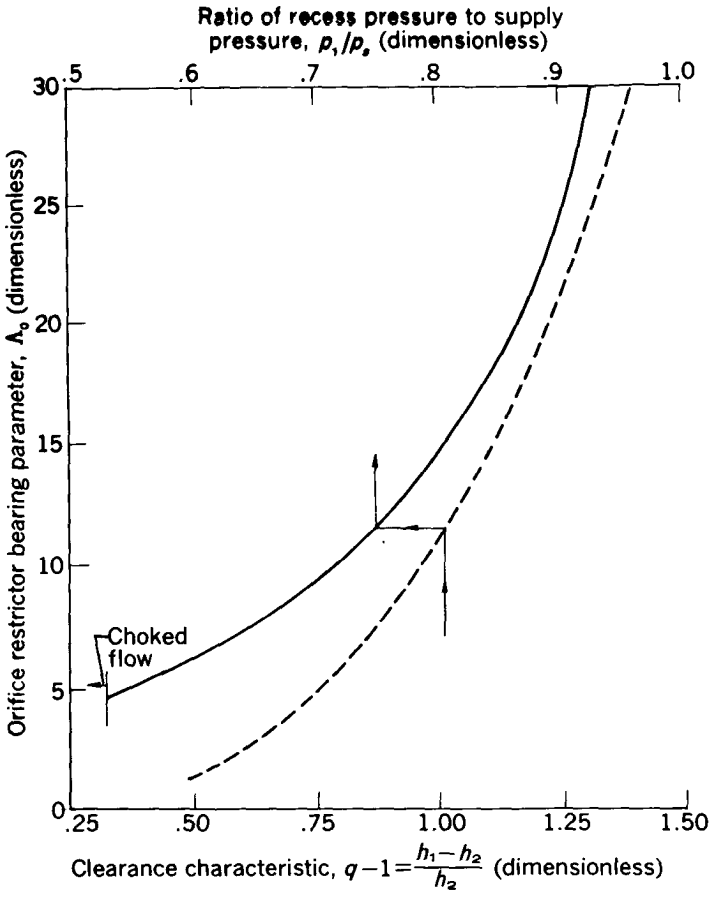

FIGURE 5–10.—Graphical determination of pressure ratio, p_1/p_s. $k=1.4$;

$$p_s/p_0=5;\ \Lambda_0=\frac{10(1+q^3)(q-1)^3}{q^3}.$$

STABILITY

Throughout the preceding discussion, the time-dependent term $\frac{\partial}{\partial_t}(ph)$ was omitted from the Reynolds equation. The resulting solutions therefore are for steady-state conditions only. There is no guarantee, however, that steady-state conditions will ever be achieved. In other words, some of the preceding steady-state solutions may be unstable and therefore physically unrealizable.

The field of stability of gas-lubricated bearings has received considerable attention in recent years, so that understanding of this

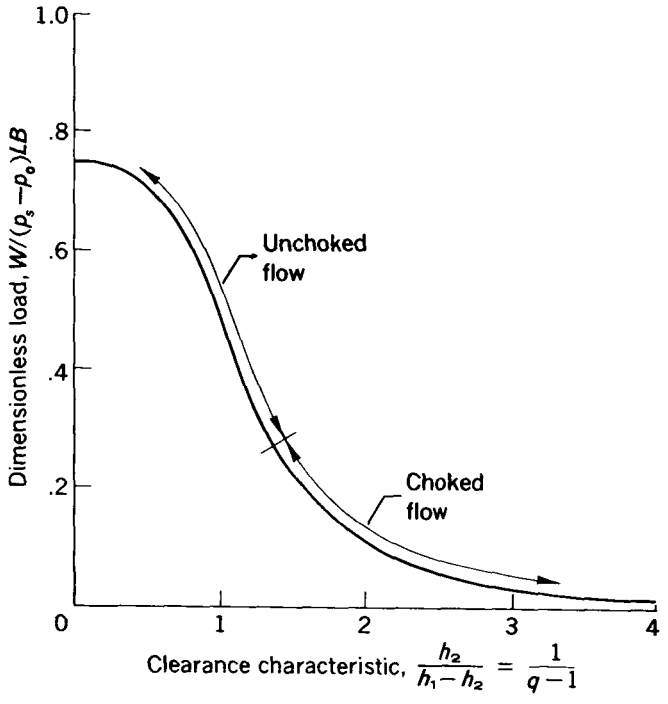

FIGURE 5–11.—Dimensionless load plotted against clearance characteristics for step bearing with inlet orifice restrictor. $k=1.4$; $p_s/p_0=5$;

$$\Lambda_0=\frac{10(1+q^3)(q-1)^3}{q^3}.$$

subject is increasing rapidly. In actual design and development today, the stability problem is still unresolved to such an extent that it is usually attacked experimentally by trial and error. From such experimental data, some general empirical conclusions can be drawn. First, let us define certain terms commonly used in discussions of bearing stability.

The most serious and least understood type of instability in gas-lubricated bearings is the phenomenon known as "half-frequency whirl" or "half-speed whirl." It occurs on rotating journal bearings and manifests itself as either or both an orbiting of the journal center of mass (translatory whirl) or a coning of the journal axis (conical whirl) at a frequency very nearly one-half the rotor speed. If the bearing sleeves are resiliently mounted, they may also exhibit half-frequency whirl. Half-frequency whirl is a self-excited oscillation.

The origin of half-speed whirl arises from a complicated intercoupling between the Reynolds equation and the equations of journal motion. To demonstrate this intercoupling phenomenon, let us consider the simplified problem of an infinitely long, self-acting journal bearing. The first-order perturbation approximation for the Reynolds equation is

$$\frac{\partial^2 p}{\partial^2 \theta}-\Lambda\frac{\partial p}{\partial \theta}-\frac{2\Lambda}{\omega}\frac{\partial p}{\partial t}=\frac{\Lambda p_0}{c}\frac{\partial h}{\partial \theta}+\frac{2\Lambda p_0}{\omega c}\frac{\partial h}{\partial t} \tag{5–41}$$

where

$$\frac{h}{c}=1-\epsilon_X\cos\theta-\epsilon_Y\sin\theta$$

and ϵ_X and ϵ_Y are the X- and Y-components of eccentricity ratio; X and Y are fixed rectangular coordinate directions in the plane normal to the bearing axis.

Multiplying equation (5–41) by $\cos\theta$ and integrating with respect to θ from 0 to 2π give

$$\frac{W_X}{RL}+\Lambda\frac{W_Y}{RL}+\frac{2\Lambda}{\omega}\frac{\dot{W}_X}{RL}=-\pi\Lambda p_0\epsilon_Y-\frac{2\pi\Lambda p_0}{\omega}\dot{\epsilon}_X \tag{5–42}$$

where W_X and W_Y are the pressure forces in the X- and Y-directions, respectively:

$$W_Y=-RL\int_0^{2\pi} p\cos\theta\,d\theta \tag{5–43}$$

$$W_Y=-RL\int_0^{2\pi} p\sin\theta\,d\theta \tag{5–44}$$

Similarly, multiplying equation (5–41) by $\sin\theta$ and integrating over θ from 0 to 2π yield

$$\frac{W_Y}{RL}-\Lambda\frac{W_X}{RL}+\frac{2\Lambda}{\omega}\frac{\dot{W}_Y}{RL}=\pi\Lambda p_0\epsilon_X-\frac{2\pi\Lambda p_0}{\omega}\dot{\epsilon}_Y \tag{5–45}$$

Equations (5–42) and (5–45) represent the integrated form of the Reynolds equation. To these must be coupled the equations of journal motion,

$$mc\ddot{\epsilon}_X=W_X+V_X \tag{5–46}$$

$$mc\ddot{\epsilon}_Y=W_Y+V_Y \tag{5–47}$$

where m is the mass of the journal and V_X and V_Y are the X- and Y-components of externally applied load. For the purposes of the present discussion, let us take $V_X=V_Y=0$, which corresponds to an unloaded bearing. Substituting equations (5–46) and (5–47) into equations (5–42) and (5–45) yields

$$\left[2\Omega\Lambda\left(\frac{s}{\omega}\right)^3+\Omega\left(\frac{s}{\omega}\right)^2+2\Lambda\frac{s}{\omega}\right]\epsilon_X+\left[\Omega\Lambda\left(\frac{s}{\omega}\right)^2+\Lambda\right]\epsilon_Y=0 \quad (5\text{–}48)$$

$$-\left[\Omega\Lambda\left(\frac{s}{\omega}\right)^2+\Lambda\right]\epsilon_X+\left[2\Omega\Lambda\left(\frac{s}{\omega}\right)^3+\Omega\left(\frac{s}{\omega}\right)^2+2\Lambda\frac{s}{\omega}\right]\epsilon_Y=0 \quad (5\text{–}49)$$

where

$$\Omega=\frac{mc\omega^2}{\pi p_0 RL}$$

and s is an operator representing differentiation with respect to time.

The characteristic equation resulting from the determinant of the coefficients of ϵ_X and ϵ_Y in equations (5–48) and (5–49) is

$$4\Omega^2\Lambda^2\left(\frac{s}{\omega}\right)^6+4\Omega^2\Lambda\left(\frac{s}{\omega}\right)^5+[\Omega^2(1+\Lambda^2)+8\Omega\Lambda^2]\left(\frac{s}{\omega}\right)^4+4\Omega\Lambda\left(\frac{s}{\omega}\right)^3$$
$$+(4\Omega\Lambda^2+4\Lambda^2)\left(\frac{s}{\omega}\right)^2+\Lambda^2=0 \quad (5\text{–}50)$$

This characteristic equation is immediately recognized as representing an unstable system because it contains no first-power term in s. A little insight into the nature of this instability can be attained by examining the special case where Ω is sufficiently small to be negligible. Neglecting all terms containing Ω in equation (5–50), we have simply

$$\left[4\left(\frac{s}{\omega}\right)^2+1\right]\Lambda^2=0 \quad (5\text{–}51)$$

for which

$$s=\pm j\frac{\omega}{2} \quad (5\text{–}52)$$

where

$$j=\sqrt{-1}$$

Equation (5–52) shows that (for negligible values of Ω) there is one pair of purely imaginary roots at a frequency of $\omega/2$. This means that the system is capable of supporting self-sustained oscillations at a frequency of $\omega/2$, half rotor frequency.

The foregoing simplified treatment provides a qualitative picture of half-speed whirl. It shows that the unloaded journal bearing is unstable, that it has a pronounced tendency toward self-sustained oscillations at a frequency of $\omega/2$, and that the new parameter $\Omega = mc\omega^2/\pi p_0 RL$ is important in determining stability behavior.

A more quantitative treatment of stability that utilizes equation (5–41) fails because equation (5–41), the first-order perturbation approximation to the Reynolds equation, does not include the important stabilizing effect of increasing bearing stiffness at increasing eccentricity ratios (see fig. 5–3). Several methods are available for treating this nonlinear effect (refs. 12, 13, and 14) and all show that journal bearings can be made stable by operating at a sufficiently high eccentricity ratio.

Another type of dynamic behavior due to forced vibrations is sometimes discussed with bearing instability and whirl although it is not really an instability in the true sense of the word. This is the natural tendency of any resilient mechanical system to respond to vibratory inputs. Rotor unbalance is the most common source of vibration input and, of course, causes the bearing system to respond at the same frequency as that of the input, namely 1 cycle per revolution. For this reason, the resulting whirl is called synchronous whirl. It may also occur in the translatory mode, in the conical mode, or in a combination of the two.

When synchronous whirl excites a resonance in the bearing system, severe amplification can occur. The frequency of such a resonance is referred to as a critical speed. As a large rotating piece suspended between two journal bearings can have many normal modes of vibration, it has many critical speeds, and each one should be specifically defined. It is not sufficient to refer to first critical, second critical, third critical, etc., unless they are first defined. In some usages, for example, the first critical speed does not necessarily mean the lowest frequency resonance, but rather refers to a particular mode of vibration.

Another source of excitation for mechanical resonances, is half-frequency whirl. The resulting amplification is frequently catastrophic to the bearing. The fact that half-frequency whirl is the excitation means that such a resonant amplification can be expected at almost exactly twice a critical speed. This combination of instability phenomena is referred to as resonant whip or resonant fluid film whirl.

A pneumatic instability similar to water hammer can occur in externally pressurized bearings. Also there is a phenomenon known as lockup which can occur in inherently compensated orifice bearings. This results when the gas-supported member bottoms out and closes off the orifices on one side so that they give less repelling force than the orifices on the large clearance side of the bearing. Under such conditions the bearing will not lift off or float freely but will remain bottomed when the gas supply is turned on.

As implied earlier, there is as yet no generally valid quantitative procedure for predicting regions of stability in all gas-lubricated bearings. However, some qualitative remarks based on experimental observations can be made. For example, it is known that journal bearings are most susceptable to half-frequency whirl when the eccentricity ratio is small. Also, self-acting thrust bearings are apparently completely free of stability problems. Consequently the usual methods of avoiding half-frequency whirl are to avoid small eccentricity ratios or to add steps or grooves to the journal surface similar to those used on thrust bearings. Some methods of avoiding small eccentricity ratios are to operate at high static or dynamic (unbalance) loads, to misaline the bearing, to build an eccentric or elliptical bearing sleeve, to pressure load the bearing eccentrically either by pressurizing the high-pressure side or by venting the low-pressure side, and to decrease the ambient pressure and thereby decrease the stiffness of the bearing. Small clearance bearings ($c/R<0.0004$) tend to be stable for some reason as yet unclear. Perhaps at these small clearances the natural surface asperities and machining imperfections become such a significant portion of the total clearance that the bearing appears to be grooved as a thrust bearing.

Pneumatic instability is never observed or, at least, is unreported on simple step restrictor bearings. Of the inlet orifice restrictor type bearings, the ones with the least amount of recessed volume appear to be the most stable. For this reason, the inherently compensated type with no recess depth at all is the most stable of the inlet orifice restrictor bearings. One technique sometimes employed to distribute high pressure over a large area with a low recess volume is to use a manifold system of narrow distribution grooves radiating from the inlet orifice to another peripheral groove encompassing the distribution system.

NOMENCLATURE

A	area of orifice
B	width of a rectangular bearing
b	ratio of inner to outer radius
b_1	value of b used in table 5–I

b_1 distance from inlet to step
b_2 distance from step to outlet or exhaust
C_D orifice discharge coefficient
C_1, C_2 constant of integration
c_p specific heat of gas at constant pressure
c average radial clearance in a journal bearing
D diameter of journal bearing
f_1, f_2 functions of Λ and L/D in journal-bearing perturbation solution
H power
h local clearance in bearing
h_1, h_2 clearance in b_1 and b_2 regions, respectively
K heat conductivity
K_1 constant of integration
k ratio of specific heats
L length of bearing
M mass flow rate
m mass of journal
N number of pads, $2\pi/(\gamma+\delta)$
P unit load or load per bearing area, $\frac{NW}{\pi R^2(1-b^2)}$
$(P)_1$ value of P used in table 5–I
p pressure
p_s supply pressure
p_0 ambient pressure
p_1 recess pressure or pressure at outlet of orifice
Q torque
q compression ratio, h_1/h_2 or $(s+\Delta)/s$
R radius of bearing
$\mathcal{R}$ gas constant
R_c critical pressure ratio, $\left(\frac{2}{1+k}\right)^{k/(k-1)}$
s minimum clearance region in step bearing
T temperature
t time
U velocity of moving bearing surface
V load applied to journal
W pressure force acting on bearing pad
x, y coordinate system in plane of bearing with x in direction of bearing motion or main gas flow
Δ step or recess depth
δ groove width between pads
θ, η x/R and y/R, respectively
ϵ eccentricity ratio

Λ compressibility bearing number, $6\mu\omega R^2/p_0c^2$

Λ_h $6\mu UR/p_0h^2$

Λ_Δ $6\mu UR/p_0\Delta^2$; $6\mu\omega R^2/p_0\Delta^2$

$(\Lambda_\Delta)_1$ value of Λ_Δ used in table 5–I

Λ_s $6\mu\omega R^2/p_0s^2$

Λ_0 $\dfrac{12\mu C_D A}{Lp_0}\left(\dfrac{b_1}{h_1^3}+\dfrac{b_2}{h_2^3}\right)\sqrt{\dfrac{2k\mathcal{R}T}{k-1}}$

γ total pad angle per pad

τ leading sector angle

μ viscosity of gas lubricant

φ attitude angle

ρ density of gas lubricant

Ω bearing stability parameter, $mc\omega^2/\pi p_0RL$

ω bearing angular velocity, U/R

Subscripts:

X,Y fixed coordinate system in plane normal to bearing spin axis

REFERENCES

1. Gross, W. A.: Numerical Analysis or Gas-Lubricating Films. First Int. Symposium on Gas-Lubricated Bearings. ACR–49, Office Naval Res., Oct. 1959, pp. 193–222.
2. Raimondi, A. A.: A Numerical Solution for the Gas Lubricated Full Journal Bearing of Finite Length. Trans. ASLE, vol. 4, no. 1, Apr. 1961, pp. 131–155.
3. Harrison, W. J.: The Hydrodynamical Theory of Lubrication with Special Reference to Air as a Lubricant. Trans. Cambridge Phil. Soc., vol. 22, 1913, pp. 39–54.
4. Ocvirk, F. W.: Short-Bearing Approximation for Full Journal Bearings. NACA TN 2808, 1952.
5. Scheinberg, S. A.: Gas Lubrication of Sliding Bearings (Theory and Calculations), Friction and Wear in Machines. Inst. Machine Sci., Academy Sci., USSR, vol. 8, 1953, pp. 107–204.
6. Ausman, J. S.: Theory and Design of Self-Acting Gas-Lubricated Journal Bearings Including Misalignment Effects. First Int. Symposium on Gas-Lubricated Bearings, ACR–49, Office Naval Res., Oct. 1959, pp. 161–192.
7. Ausman, J. S.: An Improved Analytical Solution for Self-Acting, Gas-Lubricated Journal Bearings of Finite Length. Jour. Basic Eng. (ASME Trans.), ser. D, vol. 83, no. 2, June 1961, pp. 188–194.
8. Whipple, R. T. P.: Theory of the Spiral Grooved Thrust Bearing with Liquid or Gas Lubricant. T/R 622, British AERE, 1951.
9. Archibald, F. R.: A Simple Hydrodynamic Thrust Bearing. Trans. ASME, vol. 72, no. 4, May 1950, pp. 393–400.
10. Ausman, J. S.: An Approximate Solution for Self-Acting Gas Lubrication of Stepped Sector Thrust Bearings. Trans. ASLE, vol. 4, no. 2, Nov. 1961, pp. 304–313.

11. TANG, I. C., and GROSS W. A.: Analysis and Design of Externally Pressurized Gas Bearings. Trans. ASLE, vol. 5, no. 1, Apr. 1962, pp. 261–284.
12. AUSMAN, J. S.: Linearized pH Stability Theory for Translatary Half-Speed Whirl of Long, Self-Acting Gas-Lubricated Journal Bearings. Paper 62–WA–185, ASME, 1962.
13. CHENG, H. S., and TRUMPLER, P. R.: Stability of the High-Speed Journal Bearing Under Steady Load. Paper 62–WA–101, ASME, 1962.
14. CASTELLI, V., and ELROD, H. G.: Two Approaches to the Solution of the Stability Problem for 360° Gas Lubricated Journal Bearings. Interim Rep. I–A2049–20, Franklin Inst., June 1962.
15. STERNLICHT, B., and ELWELL, R. C.: Theoretical and Experimental Analysis of Hydrodynamic Gas Lubricated Journal Bearings. Trans. ASME, vol. 80, 1959, pp. 865–878.

CHAPTER 6

Rolling-Element Bearings

By WILLIAM J. ANDERSON

IN CONTRAST TO HYDRODYNAMIC BEARINGS, which depend for low-friction characteristics on a fluid film between the journal and the bearing surfaces, rolling-element bearings employ a number of balls or rollers that roll in an annular space. To some extent, these rollers help to avoid gross sliding and the high coefficients of friction that are associated with sliding. The term rolling element is used to describe this class of bearing because the contact between the rolling elements and the races or rings consists more of sliding than of actual rolling. A rolling contact implies no interfacial slip; this condition is seldom maintained because of material elasticity and geometric factors. Rolling-element bearings ordinarily consist of two races or rings (the inner race and the outer race), a set of rolling elements (either balls or rollers), and a separator (sometimes called a cage or retainer) for keeping the set of rolling elements approximately equally spaced.

Rolling-element bearings offer the following advantages when they are compared with hydrodynamic bearings: (1) low starting friction, (2) low operating friction, which is comparable to hydrodynamic bearings at low speeds and somewhat less at high speeds, (3) less sensitivity to interruptions in lubrication than hydrodynamic bearings, and (4) a capability of supporting combined loads with several types of bearings. In this latter respect, rolling-element bearings are more versatile than hydrodynamic bearings, which usually can support only radial or thrust loads.

Rolling-element bearings also have the following disadvantages: (1) They occupy more space in the radial direction than do hydrodynamic bearings and (2) they have a finite fatigue life because of repeated stresses at the ball-race contacts, which is in contrast to hydrodynamic bearings that usually offer an almost infinite fatigue life.

SYMBOLS

a	semimajor axis of contact ellipse, in.
b	semiminor axis of contact ellipse, in.
C	specific dynamic capacity, lb
C_o	specific static capacity, lb
CF	centrifugal force
D,d	ball or rolling-element diameter, in.
E	Young's modulus of elasticity, lb/sq in., or pitch diameter, in.
$E(\epsilon)$	complete elliptic integral of the second order
F	sliding friction force, lb
f	coefficient of sliding friction
g,ϵ,μ,ν,τ	functions used in calculation of Hertz stresses
H	heat generated, in.-lb/sec
I	moment of inertia, (in.-lb)(sec^2)
$K(\epsilon)$	complete elliptic integral of the first order
L	life, millions of revolutions
l	length of line contact or rolling element, in.
M	moment, in.-lb
n	load-life exponent
P	normal ball load, lb
Q	load distribution factor
R	radius, in.
S	normal stress, lb/sq in.
V	linear velocity, in./sec
W	bearing load, lb
x,y,z	coordinates
x_0	location of rolling band
Z	number of balls
α	contact angle, deg
β	angle between load vector and bearing radial plane, deg, or angle between rolling elements, deg
γ	angle between rolling axis and tangent plane at outer-race contact, deg
δ	normal approach or deflection, in.
θ	elastic constant
ξ	coefficient of rolling resistance
σ	Poisson's ratio
ω	angular velocity, radians/sec
Subscripts:	
a	axial, body a
B	ball
b	body b
c	cage or separator

f	frictional
G	gyroscopic
IR,i	inner race
m	mean
max	maximum
OR,o	outer race
r	radial, rolling
s	spin
x	in direction of x-axis
y	in direction of y-axis
z	in direction of z-axis

BEARING TYPES

The various types of rolling-element bearings may be placed in two broad categories; the first of these is ball bearings. The most common types of ball bearings are as follows:

(1) Deep groove or Conrad
(2) Angular contact
(3) Self-alining
(4) Duplex
(5) Ball thrust

A typical deep-groove ball bearing is shown in figure 6–1. This bearing has moderately high radial-load capacity and moderate thrust-load capacity. Figure 6–2 shows an angular-contact bearing. This bearing has a higher thrust-load capacity than a deep-groove bearing, but it can carry thrust load in only one direction. A self-alining ball bearing with the outer-race groove ground to a spherical shape is illustrated in figure 6–3(a). This bearing has a relatively low load capacity but is insensitive to shaft and to housing misalinements.

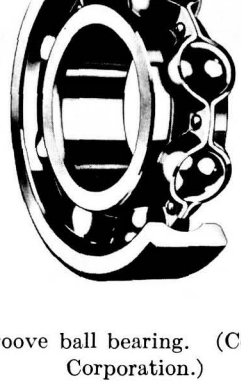

FIGURE 6–1.—Deep-groove ball bearing. (Courtesy Marlin Rockwell Corporation.)

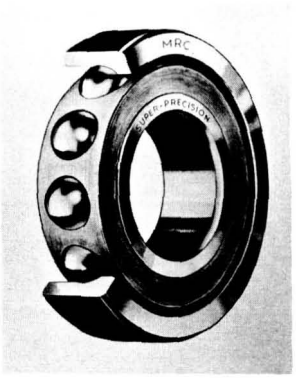

FIGURE 6–2.—Angular-contact ball bearing. (Courtesy Marlin Rockwell Corporation.)

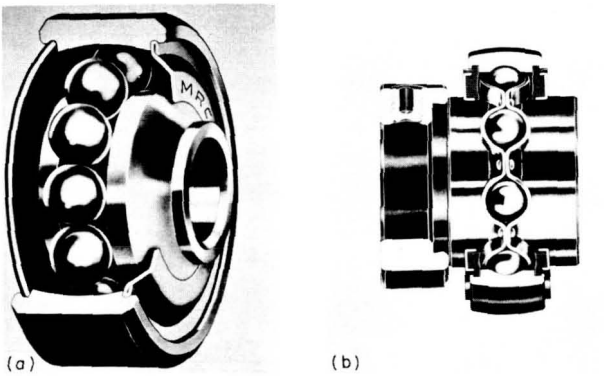

(a) Groove of outer race ground to spherical shape.
(b) Outside diameter of outer race ground to fit spherical housing.

FIGURE 6–3.—Self-alining ball bearing. (Courtesy Marlin Rockwell Corporation.)

Figure 6–3(b) shows a second type of self-alining ball bearing with the self-alining feature obtained by grinding the outer-race outside diameter in a spherical shape to fit a spherical housing. This bearing has a higher load capacity than the bearing in figure 6–3(a), but care must be taken to maintain freedom of movement between the outer race and the housing.

Angular-contact bearings are usually used in pairs in duplex mounts. Different types of duplex mounts are shown in figure 6–4(a) (back to back) and in figure 6–4(b) (face to face). These two arrangements make it possible to carry thrust load in either direction. Bearings are so manufactured as matched pairs that, when they are mated and the races made flush, each bearing is preloaded slightly. This pre-

loading provides greater stiffness and helps to prevent ball skidding with acceleration at light load. When a high unidirectional thrust load must be carried, a duplex tandem mount (fig. 6–4(c)) is used. With careful manufacture and installation, a tandem bearing pair may have a thrust capacity as high as 1.8 times the capacity of a single bearing. A thrust ball bearing is shown in figure 6–5. This bearing has a high thrust capacity but is limited to low speeds because of the high degree of sliding in the ball-race contacts.

The second broad category is that of roller bearings. Common types are

(1) Cylindrical
(2) Tapered
(3) Spherical
(4) Needle

Cylindrical-roller bearings (fig. 6–6) are best suited of all roller-bearing types for high-speed operation. These bearings carry only radial load, and they are frequently used where freedom of movement of the shaft in the axial direction must be provided because of differential expansion. Tapered-roller bearings (fig. 6–7) and spherical-roller bearings (fig. 6–8) are high-load-capacity low-speed roller bearings with combined radial-load and thrust-load capability. Needle bearings (fig. 6–9) are capable of carrying high loads and are useful in applications where limited radial space is available.

While rolling-element bearings are usually equipped with a separator, in some instances they are not. Bearings without separators are

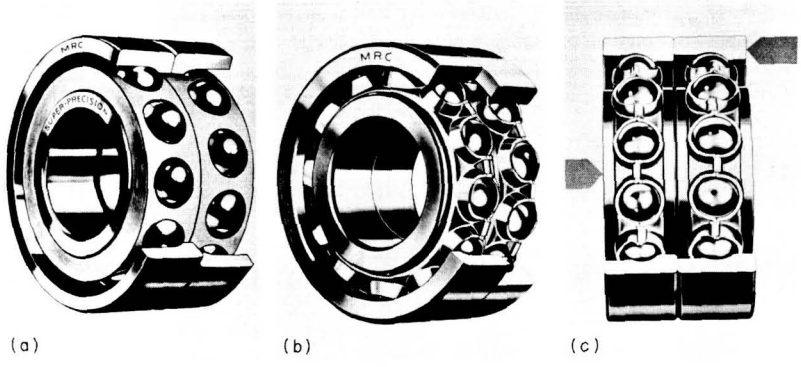

(a) Mounted back to back.
(b) Mounted face to face.
(c) Mounted in tandem.

FIGURE 6–4.—Duplex angular-contact ball bearing. (Courtesy Marlin Rockwell Corporation.)

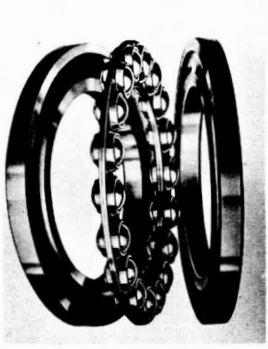

FIGURE 6–5.—Thrust ball bearing. (Courtesy Marlin Rockwell Corporation.)

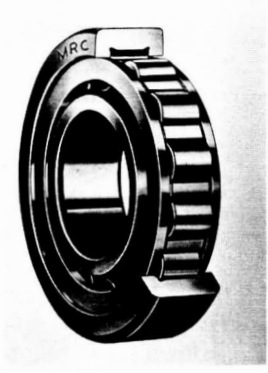

FIGURE 6–6.—Cylindrical-roller bearing. (Courtesy Marlin Rockwell Corporation.)

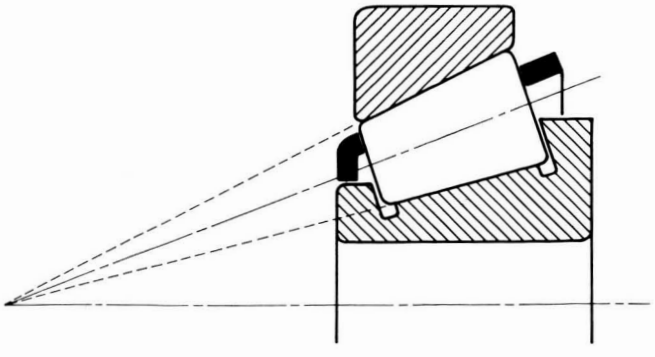

FIGURE 6–7.—Tapered-roller bearing.

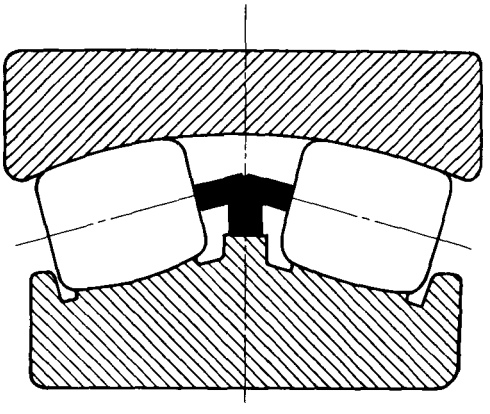

FIGURE 6–8.—Spherical-roller bearing.

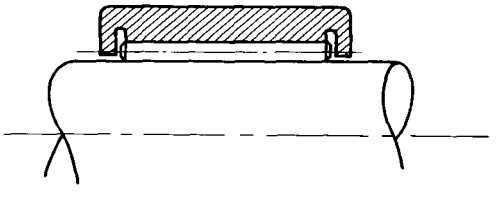

FIGURE 6–9.—Needle bearing with shaft as inner race.

usually termed full-complement bearings. A common type of full-complement roller bearing is the needle bearing. In some low-speed applications where load capacity is of primary importance, full-complement ball bearings are used. In this type of bearing, the annular space between the races is packed with the maximum number of balls.

ROLLING FRICTION

The concepts of rolling friction are important as the characteristics and behavior of rolling-element bearings depend on rolling friction. The theories of Reynolds (ref. 1) and of Heathcote (ref. 2) were previously well accepted as correctly explaining the origin of rolling friction for a ball in a groove. The energy lost in rolling was believed to be that required to overcome the interfacial slip which occurs because of the curved shape of the contact area. As shown in figure 6–10, the ball rolls about the x-axis and makes contact with the groove from a to b. If the groove is fixed, then for zero slip over the contact

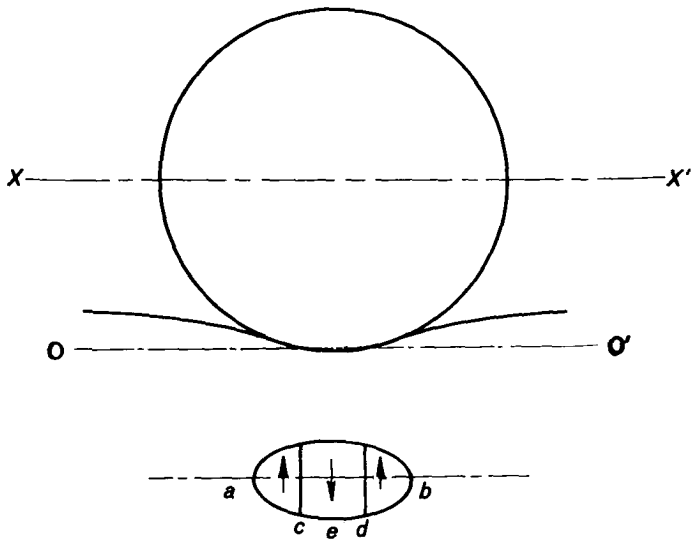

FIGURE 6–10.—Differential slip due to curvature of contact ellipse.

area no point within the area should have a velocity in the direction of rolling. The surface of the contact area is curved, however, so that points a and b are at different radii from the x-axis than are points c and d. For an inelastic ball, points a and b must have different velocities with respect to the x-axis than do points c and d because the velocity of any point on the ball relative to the x-axis equals the angular velocity ω times the radius from the x-axis. Slip must occur at various points over the contact area unless the body is so elastic that yielding can take place in the contact area to prevent this interfacial slip. The theory of Reynolds and later of Heathcote assumed that this interfacial slip took place, and that the forces required to make a ball roll were those forces required to overcome the friction due to this interfacial slip. In the contact area, rolling without slip will occur at a specific radius from the x-axis. Where the radius is greater than this radius to the rolling point, slip will occur in one direction, and, where it is less than the radius to this rolling point, slip will occur in the other direction. In figure 6–10 the lines to points c and d represent the approximate location of the rolling bands, and the arrows shown in the three portions of the contact area represent the directions of interfacial slip when the ball is rolling into the paper.

The location of the two rolling bands relative to the axis of the contact ellipse can be obtained by means of a summation of the forces acting on the ball in the direction of rolling. With reference to figure 6–11, these forces are

$$2F_2 - F_1 = \xi P \tag{6-1}$$

The forces F_1 and F_2 represent sliding friction forces. From the Hertz theory of contact stresses, which will be discussed more fully later, the pressure pattern over the contact area is ellipsoidal so that the pressure variation along any axis is elliptical. When this assump-

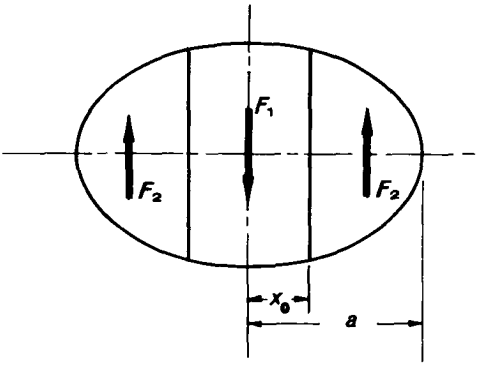

Figure 6–11.—Friction forces in contact ellipse.

tion of the pressure variation is used, F_1 and F_2 are obtained by integrating the pressure times the coefficient of friction over the particular area on which these forces act. These integrals are

$$F_1 = 2\left(\frac{3Pf}{2\pi ab}\right)\int_0^{x_0}\int_{-b\left(1-\frac{x^2}{a^2}\right)^{1/2}}^{b\left(1-\frac{x^2}{a^2}\right)^{1/2}}\left(1-\frac{x^2}{a^2}-\frac{y^2}{b^2}\right)^{1/2} dy\,dx \tag{6-2}$$

$$F_2 = \frac{3Pf}{2\pi ab}\int_{x_0}^{a}\int_{-b\left(1-\frac{x^2}{a^2}\right)^{1/2}}^{b\left(1-\frac{x^2}{a^2}\right)^{1/2}}\left(1-\frac{x^2}{a^2}-\frac{y^2}{b^2}\right)^{1/2} dy\,dx \tag{6-3}$$

Equations (6–2) and (6–3) can be integrated with standard integrals:

$$F_1=\frac{3Pf}{2a}\left(x_0-\frac{x_0^3}{3a^2}\right) \tag{6–4}$$

$$F_2=\frac{3Pf}{4a}\left(\frac{2a}{3}+\frac{x_0^3}{3a^2}-x_0\right) \tag{6–5}$$

Substituting equations (6–4) and (6–5) into equation (6–1) and simplifying yield

$$3\left(\frac{x_0}{a}\right)-\left(\frac{x_0}{a}\right)^3=1-\frac{\xi}{f} \tag{6–6}$$

For bearing steels, the ratio of ξ/f is so small that

$$\frac{x_0}{a}\cong 0.347 \tag{6–7}$$

Eldredge (ref. 3) determined the following expression for the force required to overcome the friction due to interfacial slip:

$$F=\frac{fP}{12}\left(\frac{2a}{D}\right)^2 \tag{6–8}$$

Recent work done by Eldredge and Tabor (refs. 4 to 6) and by Drutowski (ref. 7) indicates that the greater portion of rolling resistance results from elastic hysteresis losses in the metal rather than from friction due to interfacial slip.

Palmgren, in reference 8 and in a discussion to reference 6, states that loss of energy due to interfacial slip constitutes a large portion of the rolling resistance. Thus, Palmgren and Tabor appeared to disagree; however, a closer examination of the experimental data on which Palmgren based his conclusions reveals that Palmgren's work was done with full bearings and that a great deal of slippage occurs in practically all bearings, as shown in the discussion of kinematics of roller bearings. This slippage accounts for the greater portion of the

energy lost in a rolling bearing. The gross sliding in the contact areas between the rolling elements and the races in a rolling bearing, however, is differentiated from the interfacial slip that was first discussed by Heathcote and which is discussed by Tabor in his basic work on rolling resistance. Actually, both Tabor and Palmgren appear to be correct; the controversy arises because they are talking about different things. Tabor discussed basic rolling resistance, which is a factor in the total energy lost in a rolling bearing, and Palmgren discussed the friction that arises from gross sliding in the contact areas, which is far greater than the loss due to hysteresis effects.

FRICTION LOSSES IN ROLLING BEARINGS

Some of the factors that affect the magnitude of friction losses in rolling bearings are

(1) Bearing size
(2) Bearing type
(3) Bearing design
(4) Load (magnitude and type, either thrust or radial)
(5) Speed
(6) Oil viscosity
(7) Oil flow

In a specific bearing, friction losses consist of

(1) Sliding friction losses in the contacts between the rolling elements and the raceways
(2) Hysteresis losses due to the damping capacity of the raceway and the ball material
(3) Sliding friction losses between the separator and its locating race surface and between the separator pockets and the rolling elements
(4) Shearing of oil films between the bearing parts and oil churning losses caused by excess lubricant within the bearing

The relative magnitude of each of these friction losses depends on the bearing type and design, the lubricant, and the type of lubrication.

Palmgren (ref. 8) presents friction coefficients for various types of bearings that may be used for rough calculations of bearing torque. These values were computed at a bearing load that will give a life of 1×10^9 revolutions for the respective bearings. As the bearing load approaches zero, the friction coefficient becomes infinite because the

bearing torque remains finite. Friction coefficients given by Palmgren in reference 8 are given in the following table:

Bearing	Friction coefficient
Self-alining ball	0.0010
Cylindrical roller, with flange-guided short rollers	.0011
Thrust ball	.0013
Single-row deep-groove ball	.0015
Tapered and spherical roller, with flange-guided rollers	.0018
Needle	.0045

All these friction coefficients are referenced to the bearing bore.

Palmgren (ref. 8) and Muzzoli (ref. 9) attempted to relate all the factors that influence rolling-bearing torque. Palmgren outlined a method for computing the torque of several types of bearings by calculating the zero-load torque and the sliding and the hysteresis losses due to the load. Muzzoli's equation for bearing torque is discussed in reference 10, page 84. A number of factors in these equations must be known in order to make them useful. The validity depends on the accuracy with which some of these factors are determined.

CONTACT STRESSES

The contact of two solid, curved elastic bodies at a point or along a line results in elastic and sometimes plastic deformation of the bodies at the contact. The contact areas become finite in extent as a result of this deformation and consist of circular, elliptical, or rectangular areas. Hertz (ref. 11) investigated mathematically the shape and size of the pressure area and the distribution of stress over the contact area. The relations that were developed by Hertz agree with experimental results for bodies in static contact where the dimensions of the projected contact area are small in comparison with the radii of the bodies.

The derivations of the Hertz equations are complex and only a brief summary of the results will be given herein. The various equations obtained by Hertz together with charts of the various functions that appear in the Hertz equations are given in references 8, 12, and 13.

For point contact under a load P, a pressure area with semiaxes a and b results. Hertz gives the dimensions of the pressure area in terms of the transcendental functions μ and ν as

$$a=\mu g \tag{6-9}$$

$$b=\nu g \tag{6-10}$$

where

$$g=\left[\frac{3P(\theta_a+\theta_b)}{8\left(\frac{1}{R_{a,1}}+\frac{1}{R_{a,2}}+\frac{1}{R_{b,1}}+\frac{1}{R_{b,2}}\right)}\right]^{1/3} \tag{6-11}$$

The subscripts 1 and 2 refer to planes that are orthogonal to the tangent plane and contain the major and minor axes of the contact ellipse. The sign of each radius is positive if the center of curvature is in the body and is negative if the center of curvature is outside the body.

The elastic constants θ_a and θ_b for the two bodies are functions of the modulus of elasticity E and of Poisson's ratio σ:

$$\theta_a=\frac{4(1-\sigma_a^2)}{E_a} \tag{6-12}$$

$$\theta_b=\frac{4(1-\sigma_b^2)}{E_b} \tag{6-13}$$

For point contact of steel ($E=29\times10^6$; Poisson's ratio $\sigma=1/4$), the mean compressive stress $S_m\equiv P/\pi ab$ is

$$S_m=\frac{15079\left(\frac{1}{R_{a,1}}+\frac{1}{R_{a,2}}+\frac{1}{R_{b,1}}+\frac{1}{R_{b,2}}\right)^{2/3}P^{1/3}}{\mu\nu} \tag{6-14}$$

The stress in point contact varies as the cube root of the normal force. Functions μ and ν are related through the auxiliary angle ϵ as

$$\cos\epsilon=\frac{\nu}{\mu} \tag{6-15}$$

and

$$\nu=\left[\frac{2E(\epsilon)\cos\epsilon}{\pi}\right]^{1/3} \tag{6-16}$$

The angle ϵ is found from the relation

$$\cos\tau=1-\frac{2[K(\epsilon)-E(\epsilon)]\cot^2\epsilon}{E(\epsilon)} \tag{6-17}$$

where

$$\cos\tau=\frac{\frac{1}{R_{a,1}}-\frac{1}{R_{a,2}}+\frac{1}{R_{b,1}}-\frac{1}{R_{b,2}}}{\frac{1}{R_{a,1}}+\frac{1}{R_{a,2}}+\frac{1}{R_{b,1}}+\frac{1}{R_{b,2}}} \tag{6-18}$$

Complete elliptic integrals of the first and second orders $K(\epsilon)$ and $E(\epsilon)$ have the modulus sin ϵ:

$$K(\epsilon)=\int_0^{\pi/2}\frac{d\varphi}{(1-\sin^2\epsilon\sin^2\varphi)^{1/2}} \tag{6-19}$$

$$E(\epsilon)=\int_0^{\pi/2}(1-\sin^2\epsilon\sin^2\varphi)^{1/2}\,d\varphi \tag{6-20}$$

The functions μ and ν are usually plotted with cos τ for easy calculation.

The compressive stress at any point on the contact area (fig. 6–12) is equal to the ordinate of a semiellipsoid of revolution erected on the contact area as a base. At any point x, the stress y is

$$S=\frac{3P}{2\pi ab}\left(1-\frac{x^2}{a^2}-\frac{y^2}{b^2}\right)^{1/2} \tag{6-21}$$

The maximum compressive stress that acts at the center of the contact area is

$$S_{max}=\frac{3P}{2\pi ab}=\frac{3}{2}S_m \tag{6-22}$$

For line contact if the total load is distributed evenly along the length l, the semiwidth of the pressure rectangle is

$$b=\left[\frac{P(\theta_a+\theta_b)}{\pi l\left(\frac{1}{R_a}+\frac{1}{R_b}\right)}\right]^{1/2} \tag{6-23}$$

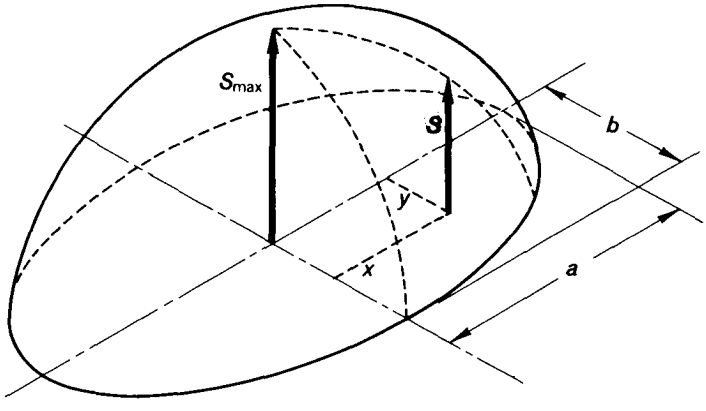

FIGURE 6–12.—Stress ellipsoid.

and the mean compressive stress is

$$S_m=\frac{P}{2b\ell} \tag{6-24}$$

For steel, the semiwidth of the pressure rectangle is

$$b=0.00028692\left[\frac{P}{\ell\left(\frac{1}{R_a}+\frac{1}{R_b}\right)}\right]^{1/2} \tag{6-25}$$

and the mean stress is

$$S_m=1742.6\left[\frac{P}{\ell}\left(\frac{1}{R_a}+\frac{1}{R_b}\right)\right]^{1/2} \tag{6-26}$$

The compressive stress at a distance y from the center of the contact line to the edge is equal to the ordinate of a cylinder erected with the contact line as a base. Then

$$S=\frac{2P}{\pi\ell b}\left[1-\left(\frac{y}{b}\right)^2\right]^{1/2} \tag{6-27}$$

The maximum stress is

$$S_{max}=\frac{2P}{\pi\ell b} \tag{6-28}$$

The maximum stress is $4/\pi$ or 1.273 times the mean stress.

Thus, for point contact, the stress varies as the cube root of the normal force, and the maximum stress is 1.5 times the mean stress. For line contact, the stress varies as the square root of the normal force, and the maximum stress is 1.273 times the mean stress.

In addition to the surface compressive stresses, the stresses that exist in the interior of each contacting body in the region near the contact area are of interest. Subsurface stresses for point contact have been determined by several investigators including Thomas and Hoersch (ref. 14). An outline of their derivation together with charts, which facilitate easy calculation, is given in reference 13.

Consider an elementary particle at a depth z below the pressure surface and located on the z-axis as shown in figure 6–13. There are three principal stresses S_x, S_y, and S_z that act on the particle.

As shown in figure 6–13, the z-axis is directed normal to the surface, and the x-axis is in the direction of the major axis. The three principal stresses are plotted against the depth from the surface in figure 6–14. The principal stresses are all compressive and diminish in intensity with greater depth from the surface. At a value of z/b

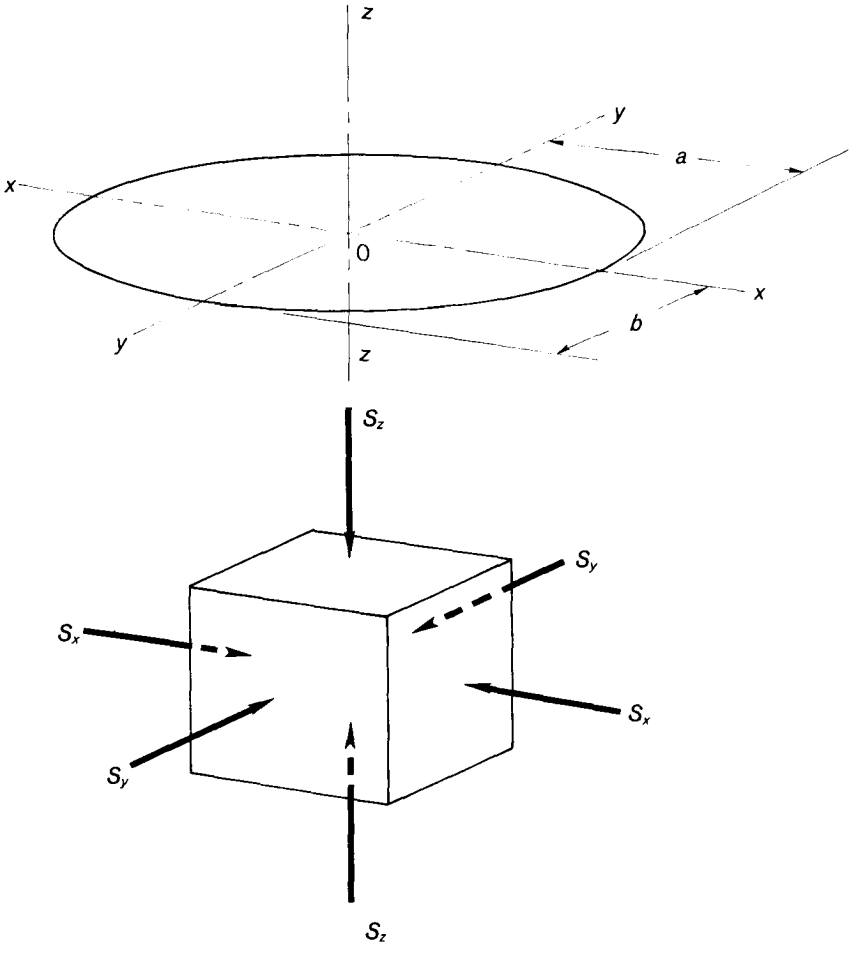

FIGURE 6–13.—Contact ellipse and coordinate axes.

of about 1.5, S_y becomes slightly tensile. The stress S_y diminishes more rapidly than does S_x, and the maximum shear stress, which is one-half the difference between any two principal stresses, is determined by the stresses S_z and S_y. The maximum value of τ occurs below the surface, as shown in figure 6–14. Since ductile materials fail in shear, material failures might originate below the surface. This failure has been observed and will be discussed fully in chapter 12.

DEFORMATIONS

In addition to knowing the stresses set up within the components of rolling bearings by the bearing loads, knowing the amount the bearing components will elastically deform under load is important.

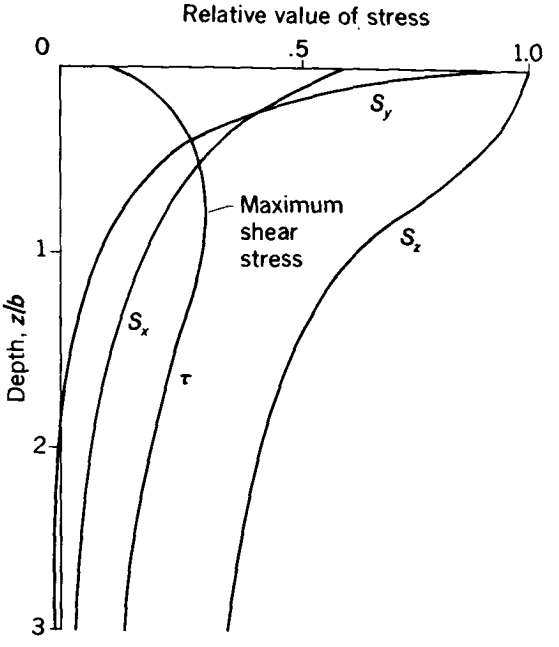

FIGURE 6–14.—Relative value of three principal stresses and of shear stress with depth from surface.

This problem was also solved by Hertz (ref. 15). The normal approach δ of two bodies in point contact (ref. 13) is

$$\delta=\frac{3P(\theta_a+\theta_b)}{8\pi a}K(\epsilon) \tag{6–29}$$

Substituting in equations (6–9), (6–10), (6–11), and (6–16) yields

$$\delta=\frac{0.192417(\theta_a+\theta_b)^{2/3}K(\epsilon)\cos^{2/3}\epsilon}{[E(\epsilon)]^{1/3}}\left[\sum\left(\frac{1}{R}\right)\right]^{1/3}P^{2/3} \tag{6–30}$$

Reference 13 contains charts that facilitate solving normal approach problems. For bodies of steel with a Poisson's ratio of ¼ and a Young's modulus of 29 million,

$$\delta=7.8107\times10^{-6}\frac{K(\epsilon)\cos^{2/3}\epsilon}{[E(\epsilon)]^{1/3}}\left(\frac{1}{R_{a,1}}+\frac{1}{R_{a,2}}+\frac{1}{R_{b,1}}+\frac{1}{R_{b,2}}\right)^{1/3}P^{2/3} \tag{6–31}$$

The compressive deformation in line contact cannot be simply expressed. Palmgren (ref. 8) gives an expression for the approach between the axis of a finite-length cylinder compressed between two infinite plane-surfaced bodies and a distant point in either of the support bodies:

$$\delta=0.39(\theta_a+\theta_b)^{0.9}\frac{P^{0.9}}{L^{0.8}} \tag{6-32}$$

Equation (6–32) may be applied to roller bearings. From equation (6–32), for line contact, the radius of curvature of the roller does not affect the deflection.

Equations (6–12), (6–13), (6–30), (6–31), and (6–32) show that the normal approach of two bodies in contact depends on the normal load, the geometry, and certain material constants. The calculation of deflections in a complete bearing requires a knowledge of its geometry, material, and the radial and the axial components of load. From the load components, the load on the most heavily loaded rolling element must be calculated. Exact calculations of deflection are complex and tedious.

In general, when both radial and axial loads are applied to a bearing inner ring, the ring will be displaced both axially and radially. The direction of the resultant displacement, however, may not coincide with the direction of the load vector. If α is the bearing contact angle defined as the angle between a line drawn through the ball contact points and the radial plane of the bearing (fig. 6–15), and β is the angle between the load vector and the radial plane, then the relation between the radial displacement δ_r and the axial displacement δ_a is given in figure 6–16 (ref. 8). With a thrust load, $\tan\alpha/\tan\beta=0$, and the resulting displacement is in the axial direction ($\delta_r=0$). For a radial displacement ($\delta_a=0$), $\tan\alpha/\tan\beta=0.823$ for point contact and 0.785 for line contact. A radial load can be applied to single-row bearings only when $\alpha=0$ in which case the displacement is also radial.

Palmgren (ref. 8) gives the deflection formuals, which are approximately true for standard bearings, under load conditions that give radial deflection. For self-alining ball bearings,

$$\delta_r=\frac{2.53\times10^{-5}}{\cos\alpha}\left(\frac{P^2}{d}\right)^{1/3} \tag{6-33}$$

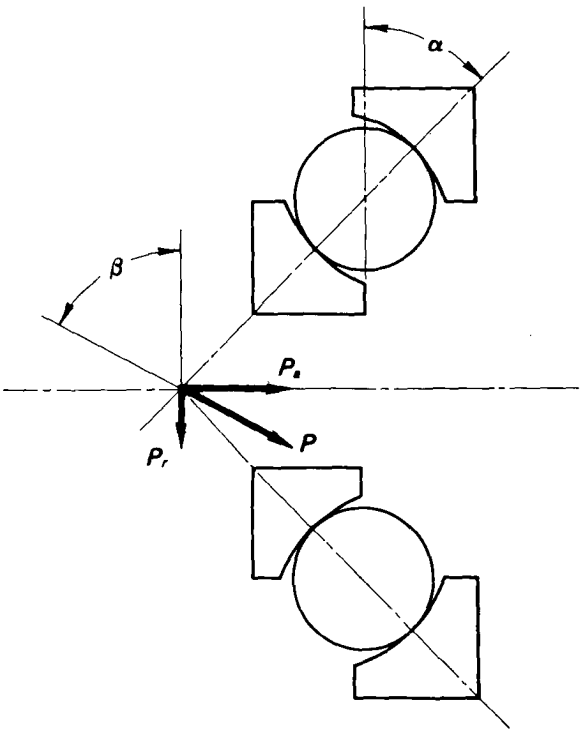

FIGURE 6–15.—Bearing-contact angle α and load-vector direction β.

For deep-groove and angular-contact bearings,

$$\delta_r = \frac{1.58 \times 10^{-5}}{\cos \alpha} \left(\frac{P^2}{d} \right)^{1/3} \tag{6-34}$$

For roller bearings with point contact at one race and line contact at the other,

$$\delta_r = \frac{4.31 \times 10^{-6}}{\cos \alpha} \frac{(P^3)^{1/4}}{l^{1/2}} \tag{6-35}$$

For roller bearings with line contact at both raceways,

$$\delta_r = \frac{8.73 \times 10^{-7}}{\cos \alpha} \frac{P^{0.9}}{l^{0.8}} \tag{6-36}$$

With axial load, the corresponding equations are

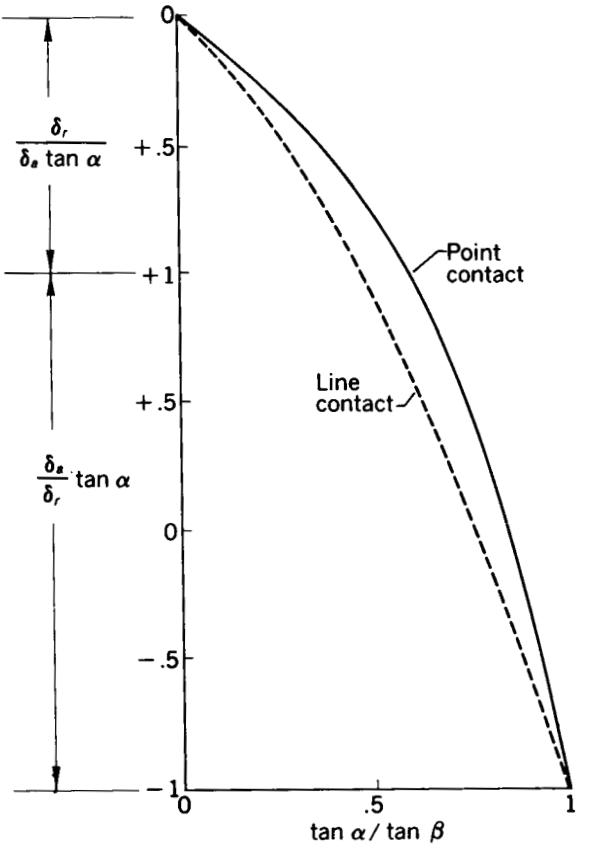

FIGURE 6–16.—Relation between contact angle α and load-vector direction β and axial and radial bearing deflections.

$$\delta_a = \frac{2.53 \times 10^{-5}}{\sin \alpha} \left(\frac{P^2}{d}\right)^{1/3} \tag{6–33a}$$

$$\delta_a = \frac{1.58 \times 10^{-5}}{\sin \alpha} \left(\frac{P^2}{d}\right)^{1/3} \tag{6–34a}$$

$$\delta_a = \frac{4.31 \times 10^{-6}}{\sin \alpha} \frac{(P^3)^{1/4}}{l^{1/2}} \tag{6–35a}$$

$$\delta_a = \frac{8.73 \times 10^{-7}}{\sin \alpha} \frac{P^{0.9}}{l^{0.8}} \tag{6–36a}$$

All deflections are in inches and are for zero clearance bearings. The load on the most heavily loaded rolling element P is in pounds, and the rolling-element diameter d is in inches.

KINEMATICS

Normal Speeds

The relative motion of the separator, the balls, and the races of a ball bearing is important to understand the performance of this type of bearing. If ω_i is the angular velocity of the inner race, then the velocity of point A (fig. 6–17) is

$$V_A=\omega_i\overline{AB} \tag{6–37}$$

Similarly, if ω_o is the angular velocity of the outer race, then the velocity of point C is

$$V_C=\omega_o\overline{CD} \tag{6–38}$$

From geometry,

$$\overline{AB}=\frac{E}{2}-\frac{d}{2}\cos\alpha \tag{6–39}$$

and

$$\overline{CD}=\frac{E}{2}+\frac{d}{2}\cos\alpha \tag{6–40}$$

The velocity of the ball center V_0 is

$$V_0=\frac{1}{2}(V_A+V_C) \tag{6–41}$$

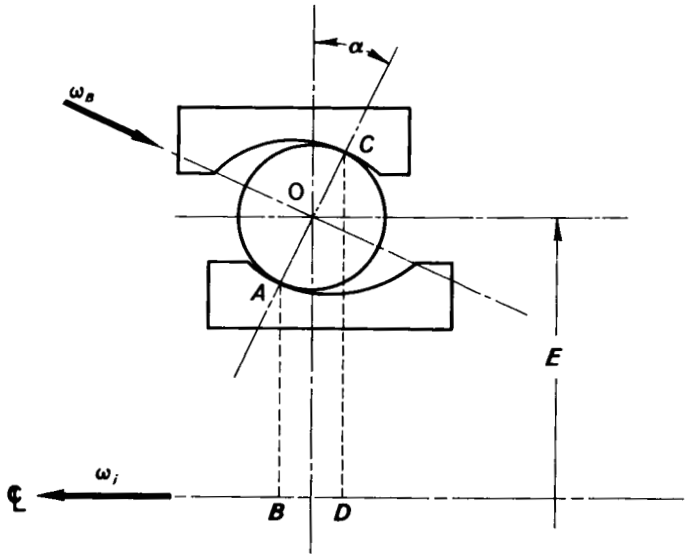

FIGURE 6–17.—Relation for derivation of retainer angular velocity.

Substituting equations (6–37) and (6–38) into equation (6–41) gives

$$V_0=\frac{1}{2}\left[\frac{\omega_i}{2}(E-d\cos\alpha)+\frac{\omega_o}{2}(E+d\cos\alpha)\right] \tag{6–42}$$

The angular velocity of the separator or ball set ω_c about the shaft axis is

$$\omega_c=\frac{V_0}{E/2} \tag{6–43}$$

Then

$$\omega_c=\frac{1}{2}\left[\omega_i\left(1-\frac{d\cos\alpha}{E}\right)+\omega_o\left(1+\frac{d\cos\alpha}{E}\right)\right] \tag{6–44}$$

The speed of the separator when the outer race is fixed is

$$\omega_c=\frac{\omega_i}{2}\left(1-\frac{d\cos\alpha}{E}\right) \tag{6–45}$$

For $\alpha<90°$, the separator speed is always less than half the shaft speed. When both races rotate, the speed of the inner race relative to the separator is

$$\omega_{i/c}=\omega_i-\omega_c=\frac{1}{2}(\omega_i-\omega_o)\left(1+\frac{d\cos\alpha}{E}\right) \tag{6–46}$$

The speed of the outer race relative to the separator is

$$\omega_{o/c}=\omega_o-\omega_c=\frac{1}{2}(\omega_o-\omega_i)\left(1-\frac{d\cos\alpha}{E}\right) \tag{6–47}$$

From equations (6–46) and (6–47), the speed of the inner race relative to the separator is always greater than that of the outer race relative to the separator. A point on the inner-race ball track will receive a greater number of stress cycles per unit time than will a point on the outer race.

For ball bearings that operate at nominal speeds, the centrifugal force on the balls is so negligible that the only forces that keep the ball in equilibrium are the two contact forces. For such conditions, the contact forces are equal and opposite, and the inner- and the outer-race contact angles are approximately equal. Even when the

two contact angles are equal, true rolling of the ball can occur only at one contact. As shown in figure 6–18, the ball is rolling about axis $0A$, and true rolling occurs at the inner-race contact B but not at the outer-race contact C.

If the ball has an angular velocity ω_B about the axis $0A$, then it has a rolling component ω_r and a spin component $\omega_{s,o}$ relative to the outer race as shown in figure 6–19. The frictional heat generated at the ball-race contact, where slip takes place, is

$$H_f=\omega_s M_s \tag{6–48}$$

where M_s is the twisting moment required to cause slip. Poritsky, Hewlett, and Coleman (ref. 16) integrated the friction force over the contact ellipse to obtain M_s as

$$M_s=\frac{3}{8}fPaE(\epsilon) \tag{6–49}$$

When $b/a=1$, $\epsilon=0°$ and $E=\pi/2$. When $b/a=0$, $\epsilon=90°$ and $E=1$. For the same P, M_s will be greater for the ellipse with the greater

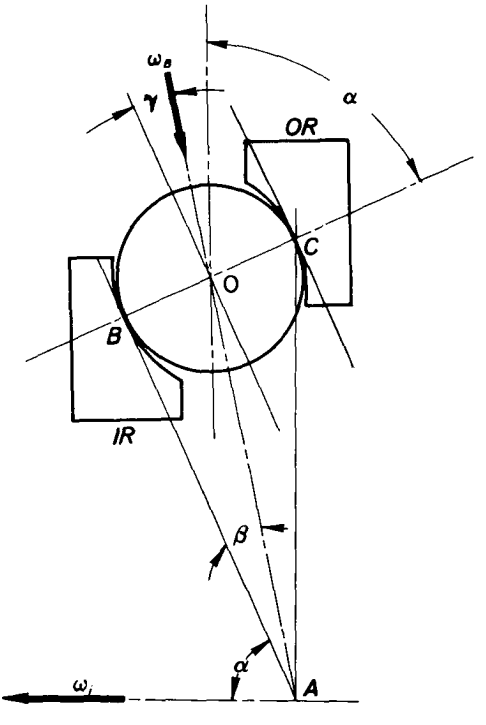

FIGURE 6–18.—Relation for derivation of ball-spin velocity with inner-race control.

eccentricity because the increase in a is greater than the decrease in E. In a given ball bearing that operates under a given speed and load, rolling will always take place at one race and spinning at the other. Rolling will take place at the race where M_s is greater because of the greater gripping action. This action is referred to as ball

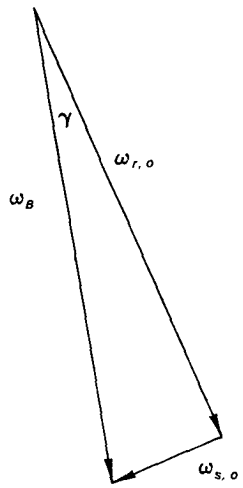

FIGURE 6–19.—Rolling and spinning components of ball velocity at outer race

control. If a bearing is designed with equal race curvatures (race curvature is defined as the ratio of the race-groove radius in a plane normal to the rolling direction to the ball diameter) and the operating speed is such that centrifugal forces are negligible, spinning will usually occur at the outer race (fig. 6–18). This spinning results from the fact that the inner-race contact ellipse has a greater eccentricity than the outer-race contact ellipse.

The frictional heat generated at the ball-race contact where spinning takes place accounts for a significant portion of the total bearing friction loss. The closer the race curvatures, the greater the frictional heat developed. On the other hand, open race curvatures, which reduce friction, also increase the maximum contact stresses and, consequently, reduce the bearing fatigue life. (See chapter 12.)

High Speeds

At high speeds, the centrifugal force developed on the balls becomes significant, and the contact angles at the inner and the outer races are no longer equal. Jones (ref. 17) presents a method for calculating inner- and outer-race contact angles in bearings that operate at high speed. This divergence of contact angles tends to increase the angular velocity of spin between the ball and the slipping race and

to aggravate the problem of heat generation. Figure 6–20 illustrates contact geometry at high speed in a ball bearing with ball control at the inner race. The velocity diagram of the ball relative to the outer race remains the same as in figure 6–19 except that γ has become greater and the magnitude of $\omega_{s,o}$ has increased.

Since the magnitude of P_o becomes greater with increasing centrifugal force, ball control probably will be shifted to the outer race unless the race curvatures are adjusted to prevent this. Figure 6–21 illustrates ball control at the outer race. The velocity of the ball relative to the inner race is shown in figure 6–22. The inner-race angular velocity ω_i must be subtracted from the angular velocity of the ball ω_B to obtain the velocity of the ball relative to the inner race $\omega_{B/i}$. The spin component of the ball relative to the inner race is then $\omega_{s,i}$. In most instances, $\omega_{s,i}$ will be greater than $\omega_{s,o}$ so that great care must be taken in designing a ball bearing for a high-speed application where heat generation is critical. Reference 17 can be used to calculate the two operating contact angles for various values of assumed race curvature. The spinning moments given by equation (6–49) can be calculated to determine which race will have ball control. The heat generated because of ball spin (eq. (6–48)) can

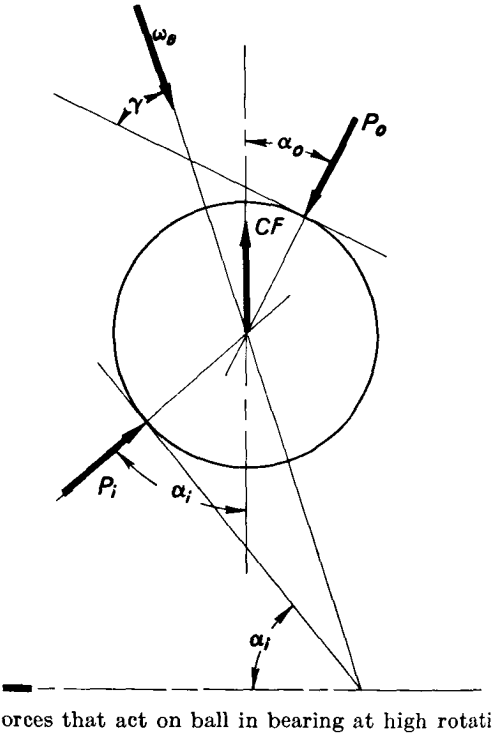

FIGURE 6–20.—Forces that act on ball in bearing at high rotative speeds. Ball control at inner race.

be calculated by solving for the value of ω_s in velocity diagrams similar to figure 6–19 or 6–22.

A further cause of possible ball skidding in lightly loaded ball bearings that operate at high speed is the gyroscopic moment that acts on each ball. If the contact angle α is other than zero, there will be a component of spin about the axis through 0 normal to the paper in figure 6–18, and a gyroscopic couple will develop. The magnitude of this moment M_G will be

$$M_G = I\omega_B\omega_c \sin(\alpha+\beta_1) \tag{6–50}$$

where I is the moment of inertia of a ball about the axis through 0 and ω_c is given by equation (6–45). For the ball shown in figure 6–18, the gyroscopic moment will tend to rotate the ball clockwise in the plane of the paper. Rotation will be resisted by the friction forces at the inner- and the outer-race contacts, which are fP_i and fP_o, respectively. Whether or not slip takes place depends on the magnitude of the bearing load. In lightly loaded bearings that operate at high speeds, slippage is a possibility.

LOAD DISTRIBUTION

When a ball bearing is subjected to a radial load, the balls are not equally loaded. At best, only half the balls are loaded at any given

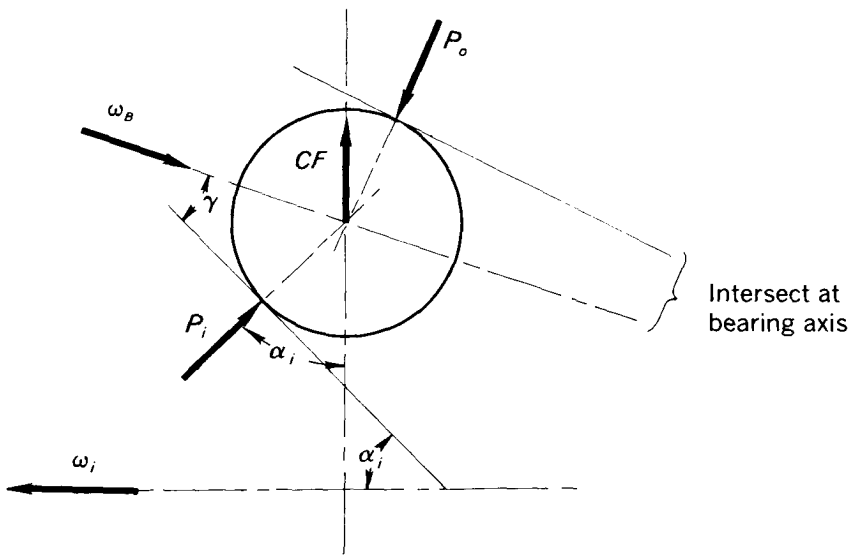

FIGURE 6–21.—Forces that act on ball in bearing at high rotative speeds. Ball control at outer race.

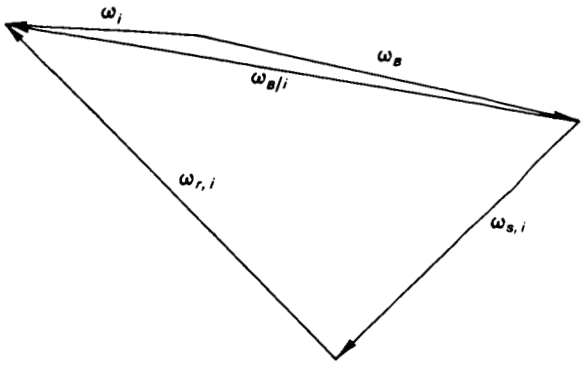

FIGURE 6–22.—Velocity diagram for computing ball-spin velocity for ball control at inner race.

time, and the actual load on each of the loaded balls depends on its position in the bearing relative to the load vector.

Stribeck (ref. 18) investigated the load distribution in radially loaded bearings and developed an expression for the most heavily loaded ball. For static equilibrium of the bearing in figure 6–23,

$$W_r = P_1 + 2P_2 \cos \beta + 2P_3 \cos 2\beta + \ldots \tag{6–51}$$

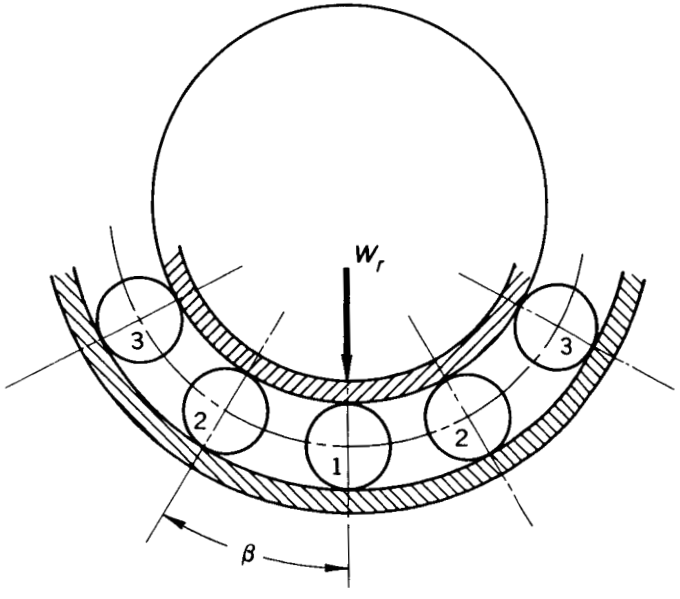

FIGURE 6–23.—Relation used to calculate distribution of ball load due to a radial load W_r.

The normal approach between two surfaces in point contact is proportional to $P^{2/3}$:

$$\frac{\delta_2}{\delta_1}=\left(\frac{P_2}{P_1}\right)^{2/3} \tag{6-52}$$

or

$$\frac{P_2}{P_1}=\left(\frac{\delta_2}{\delta_1}\right)^{3/2} \tag{6-53}$$

If the races remain circular,

$$\delta_2=\delta_1 \cos \beta \tag{6-54}$$

and

$$\delta_3=\delta_1 \cos 2\beta \tag{6-55}$$

Then

$$\frac{P_2}{P_1}=(\cos \beta)^{3/2} \tag{6-56}$$

and

$$\frac{P_3}{P_1}=(\cos 2\beta)^{3/2} \tag{6-57}$$

Substituting equations (6–56), (6–57), etc., into equation (6–51) gives

$$W_r=P_1[1+2(\cos \beta)^{5/2}+2(\cos 2\beta)^{5/2}+\ldots] \tag{6-58}$$

If Z equals the number of balls,

$$\beta=\frac{360}{Z} \tag{6-59}$$

The quantity in brackets in equation (6–58) is called the load-distribution factor Q, which depends only on Z. Stribeck found that the quantity Z/Q remained approximately constant at 4.37. To allow for possible uncircularity of the balls and the races and for bearing clearance, Stribeck took the value of Z/Q to be 5. Then

$$P_1=P_{max}=W_r \frac{5}{Z} \tag{6-60}$$

In an axially loaded bearing, all the balls are equally loaded so that

$$P_{max}=\frac{W_a}{Z \sin \alpha} \tag{6-61}$$

For combined load conditions, the maximum ball load depends on the initial contact angle and the magnitudes of W_r and W_a.

SPECIFIC DYNAMIC CAPACITY AND LIFE

In ordinary bearing applications where extreme speeds and temperatures are not present, a properly installed and lubricated bearing will fail because of material fatigue. The repeated stresses developed in the contact areas between the rolling elements and the races eventually result in failure of the material, which manifests itself as a fatigue crack. The fatigue crack propagates until a piece of the race or rolling-element material spalls out and produces the failure. Many bearings fail because of reasons other than fatigue, but in ordinary applications these failures are considered avoidable if the bearing is properly handled, installed, and lubricated and is not overloaded.

If a number of similar bearings are tested to fatigue at a specific load, there is a wide dispersion of life among the various bearings. For a group of 30 or more bearings, the ratio of the longset to the shortest life may be of the order of 20 or more. A curve of life as a function of the percent of bearings that failed can be drawn for any group of bearings. For a group of 30 or more bearings, the longest life would be of the order of four or five times the average life. The term life, as used in bearing catalogs, usually means the life that is exceeded by 90 percent of the bearings. This is the so-called B–10 or 10-percent life. The 10-percent life is one-fifth the average of 50-percent life for a normal life-dispersion curve.

If two groups of identical bearings are run to fatigue at two different loads, the life varies inversely as the nth power of the load:

$$\frac{L_2}{L_1}=\left(\frac{W_1}{W_2}\right)^n \tag{6–62}$$

For point contact $n=3$ and for line contact $n=4$. For point contact, then,

$$\frac{W_1}{W_2}=\left(\frac{L_2}{L_1}\right)^{1/3} \tag{6–63}$$

$$W_1L_1^{1/3}=W_2L_2^{1/3}=\text{constant} \tag{6–64}$$

If W in equation (6–64) is a radial load that acts on a radial bearing and L is a million revolutions with rotation of the inner race, then the constant in equation (6–64) is the specific dynamic capacity. The specific dynamic capacity for thrust bearings is determined if W is a thrust load.

In terms of the specific dynamic capacity C,

$$L=\left(\frac{C}{P}\right)^3 \tag{6–65}$$

where L is the life in millions of revolutions and P is the equivalent load. In general, ball bearings support both radial and thrust loads, and formulas for obtaining the equivalent load P in terms of radial and thrust loads are given for various bearing types in most bearing catalogs.

The bearing-design factors that affect the specific dynamic capacity are the race conformities, the rolling-element dimensions, and the number of rolling elements. Recent research has shown that the bearing material and both the lubricant viscosity and the base stock can have marked effects on fatigue. The original bearing-fatigue investigations, which include those of Palmgren (ref. 8), were made before the advent of the extreme temperatures and speeds to which rolling bearings are now subjected. As a result, the great majority of bearings were made of SAE 51100 or SAE 52100 alloys and wide variations in material-fatigue strength were not encountered. In addition, all rolling bearings were lubricated with a mineral oil such as SAE 30 or with a mineral-base soap grease so that the effect of the lubricant on fatigue was not important enough to be included among the parameters affecting fatigue life.

This problem will be discussed in chapter 12 along with formulas for calculating dynamic capacity.

SPECIFIC STATIC CAPACITY

From considerations of allowable permanent deformation, there is a limit to the load that a bearing can support while not rotating. The maximum load that a bearing can be permitted to support when not rotating is called the specific static capacity. It is arbitrarily defined as the load that will produce a permanent deformation of the race and the rolling element at a contact of 0.0001 times the rolling-element diameter. When permanent deformations exceed this value, bearing vibration and noise increase noticeably when the bearing is subsequently rotated under lesser loads. Specific static capacity is determined by the maximum rolling-element load and the race conformity at the contact.

As a result of this definition of the specific static capacity C_o, a bearing can be loaded above the specific static capacity as long as this load is applied only when the bearing is rotating. The permanent deformations that occur during rotation will be distributed evenly around the periphery of the races and will not be harmful until they become more extensive.

Static and dynamic load capacities are normally given for all bearings in bearing catalogs.

LUBRICATION

The term lubrication, in the broadest sense, means the effective reduction of friction between surfaces in relative motion. Some sort of lubrication must be provided to rolling-element bearings to ensure successful operation. In many rolling-element bearing applications, the externally applied lubricant serves both as a lubricant and as a coolant and, in a few extreme cases, strictly as a coolant. These applications include extreme speeds, elevated temperatures, and operation in fluids such as fuels or propellants that are not ordinarily considered to be lubricants. Unusual applications will be considered separately and conventional lubrication techniques will be discussed here. Conventional lubrication techniques can be divided into three broad categories:

(1) Grease lubrication
(2) Solid oil lubrication
(3) Oil-air-mist lubrication

Grease Lubrication

Lubricating greases consist of a lubricating oil and a thickener. Grease-lubricated bearings are generally used for moderate operating conditions and bearings that are required to operate for extended periods of time without relubrication. Conventional greases are limited in temperature to about 250° F and in DN value (product of bearing bore in mm and speed in rpm) to about 250,000, although recent research on synthetic greases has extended the temperature limit beyond 450° F and grease-lubricated bearings have been run successfully at DN values as high as 1 million. Grease-lubricated bearings with double seals are used advantageously with contaminating conditions. Since the bearing cavity is charged with the grease, torque values are not as low as with an oil-lubricated bearing. Greases cannot be used if heat flow to the bearing is significant enough to require a circulating flow of lubricant to remove the heat.

The thickeners used in conventional greases are usually sodium, calcium, or lithium soaps, although barium, strontium, and aluminum soaps are used if water resistance is important. In recent years, thickeners of inorganic materials such as bentonite clay have been used in synthetic greases.

Lime-base or calcium-soap greases are insoluble in water and are only suitable for use to about 130° F because of their low melting points. Their consistency is buttery and they have a tendency to channel or to separate from the part to be lubricated as a result of centrifugal forces. The calcium-soap greases, for this reason, are more satisfactory for use in sleeve bearings than in rolling bearings.

Soda-base or sodium-soap greases are more stable than calcium-

soap greases and are suitable for temperatures to about 200° F. They are water soluble in contrast to the lime-base greases, which are insoluble in water. The structure is spongelike so they do not tend to channel. They are widely used in rolling bearings. Aluminum-base greases are water insoluble and do not tend to channel. They are stable to fairly high temperatures but are somewhat more expensive than lime- and soda-base greases.

Lithium-soap greases have been used recently because of their desirable characteristics over a wide temperature range and their good oxidation resistance.

Common greases ordinarily use petroleum oils such as SAE 20 or 30. Low-temperature greases may use less viscous oils, and high-temperature greases may use more viscous oils. Synthetic greases that use silicones, diesters, polyglycols, and other synthetic oils are used for applications above 250° F.

Solid-Oil Lubrication

Solid-oil lubrication with a recirculating system is normally employed for high-speed applications especially when a considerable amount of heat must be removed from the bearing. An example is the lubrication system used in turbojet engines for the rotor bearings. The high power loss in the bearings plus the flow of heat to the bearings from hot engine parts makes it necessary to use high oil flows to maintain allowable bearing temperatures. While the oil acts as a coolant, the high flow rates frequently aggravate the problem by increasing the rate of heat generation due to oil churning.

Oil jets or nozzles are normally used to introduce the oil in the form of a high-velocity stream directed at the face of the bearing. The most efficient lubrication and cooling is obtained when the jet is directed at the space between the retainer and the inner race. Multiple jets spaced around the periphery are used to reduce circumferential temperature gradients in bearings that support high radial loads.

Oil is normally drained from both sides of the bearing to minimize oil churning losses. If bearing temperature is critical, the oil may be drained only from the side opposite the oil jet, which forces all the oil to flow through the bearing and increases the cooling efficiency. This method is sometimes referred to as puddling.

Oil-Air-Mist Lubrication

At extremely high speeds where any appreciable quantity of oil present in the bearings would cause an intolerable power loss due to oil churning, utilization of oil-mist lubrication is necessary. Small-bore bearings that operate in the speed range from 50,000 to above 100,000 rpm are usually lubricated with oil mist. The effect of oil

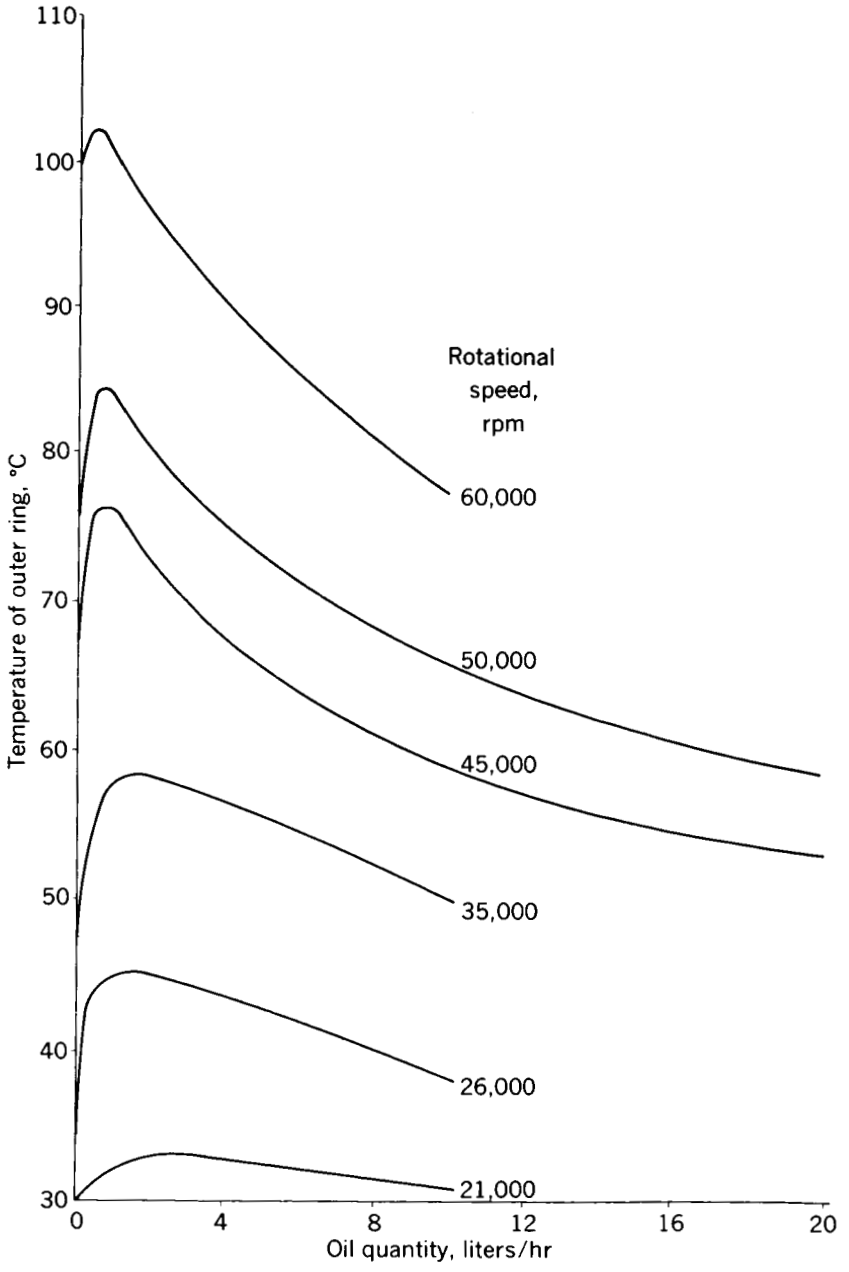

FIGURE 6-24.—Relation between bearing temperature and oil supplied for 6202-size deep-groove ball bearing (15-mm-diam. bore); radial clearance, approximately 20 microns; radial load, 0.4 kilogram; axial load, 4 kilograms. (From ref. 19.)

flow on bearing power loss for a wide range of oil flows can be surmised from the data reported in reference 19 and shown in figure 6–24. In the low oil-flow range, the bearing operating temperature increases with increasing oil flow, which indicates that churning losses increase faster than cooling effectiveness. In the high oil-flow range the cooling effectiveness increases faster than the churning losses, which results in a gradual decrease in the bearing operating temperature. The bearing power loss, however, continues to increase throughout the entire range of oil flows.

Oil-mist systems are noncirculating; the oil is passed through the bearing once and then discarded. Extremely low oil flows are required for the lubrication function exclusive of cooling. Commercial oil-mist generators are available for systems that contain one to many bearings. Since the required oil flows are low, a nominal capacity sump is adequate for supplying a multiple-bearing system for an extended period of time.

Data on the minimum oil-flow requirements of ball bearings are presented in reference 20. Ball bearings with 75-millimeter bore operated satisfactorily at 12,000 rpm, 400° F, and 1000-pound-thrust load with oil flows as low as 0.003 pound per minute.

REFERENCES

1. Reynolds, O.: On Rolling Friction. Phil. Trans. Roy. Soc. (London), vol. 166, 1876, pp. 155–174.
2. Heathcote, H. L.: The Ball Bearing in the Making, Under Test and in Service. Proc. Inst. Automotive Eng., vol. 15, 1921, pp. 569–702.
3. Eldredge, K. R.: Rolling Friction of Spheres on Surfaces. Ph. D. Thesis, Cambridge Univ., 1952.
4. Eldredge, K. R., and Tabor, D.: The Mechanism of Rolling Friction. I. The Plastic Range. Proc. Roy. Soc. (London), ser. A, vol. 229, no. 1177, Apr. 21, 1955, pp. 181–198.
5. Tabor, D.: The Mechanism of Rolling Friction. II. The Elastic Range. Proc. Roy. Soc. (London), ser. A, vol. 229, no. 1177, Apr. 21, 1955, pp. 198–220.
6. Tabor, D.: The Mechanism of "Free" Rolling Friction. Lubrication Eng., vol. 12, no. 6, Nov.–Dec. 1956, pp. 379–386.
7. Drutowski, Richard C.: Energy Losses of Balls Rolling on Plates. Record of Proc. Instr. Ball Bearing Conf., sponsored by New Departure, General Motors Corp., Cleveland (Ohio), Mar. 26–27, 1958, pp. 97–116.
8. Palmgren, A.: Ball and Roller Bearing Engineering, third ed., SKF Industries, Inc., 1959.
9. Muzzoli, M.: Ricerche di ingegneria, Sept.–Oct. 1934.
10. Wilcock, D. F., and Booser, E. R.: Bearing Design and Application. McGraw-Hill Book Co., Inc., 1957.
11. Hertz, H.: The Contact of Elastic Bodies. Gesammelte Werke, vol. 1, 1881.
12. Allan, R. K.: Rolling Bearings. Sir Isaac Pitman & Sons, Ltd., 1945.

13. JONES, A. B.: New Departure—Analysis of Stresses and Deflections. Vols. I–II. New Departure Div., Gen. Motors Corp., 1946.
14. THOMAS, HOWARD R., and HOERSCH, VICTOR A.: Stresses Due to the Pressure of One Elastic Solid Upon Another with Special Reference to Railroad Rails. Bull. 212, Eng. Exp. Station, Univ. Illinois, 1930.
15. LOVE, A. E. H.: Mathematical Theory of Elasticity. Fourth ed., Dover Pub., 1944, p. 197.
16. PORITSKY, H., HEWLETT, C. W., JR., and COLEMAN, R. E., JR.: Sliding Friction of Ball Bearings of the Pivot Type. Jour. Appl. Mech., vol. 14, no. 4, Dec. 1947, pp. 261–268.
17. JONES, A. B.: The Life of High-Speed Ball Bearings. Trans. ASME, vol. 74, no. 5, July 1952, pp. 695–699; discussion, pp. 699–703.
18. STRIBECK, R.: Ball Bearings for Various Loads. Trans. ASME, vol. 29, 1907, pp. 420–463; discussion, pp. 464–467.
19. GETZLAFF, G.: The Behavior of Rolling Bearings at Very High Running Speeds. Eng. Digest, vol. 13, no. 11, Sept. 1952, pp. 379–384.
20. SCHULLER, FREDRICK T., and ANDERSON, WILLIAM J.: Operating Characteristics of 75 Millimeter Bore Ball Bearings at Minimum Oil Flow Rates over a Temperature Range to 500° F. Lubrication Eng., vol. 17, no. 6, June 1961, pp. 291–298.

Page intentionally left blank

CHAPTER 7

Liquid Lubricants

By DOUGLAS H. MORETON*

MAN'S FIRST SIGNIFICANT USE OF LUBRICANTS involved natural fats and oils. The first recorded use of petroleum as a lubricant dates back to 4000 B.C., but the first commercial use for lubricant purposes began in the middle 1800's. Petroleum technology has satisfied the increasing requirements of conventional bearing operating conditions through two principal methods: first, the use of selected refining methods and, second, the use of chemical additives. More recently, the synthetic lubricants have emerged and, subsequent to the synthetics, the organometallics and the liquid metals. Hydrocarbon oils extracted from petroleum sources, however, still represent the largest production and bulk usage of lubricants in bearings.

The significant factors in the development of liquid lubricants have been the anticipated use and the resulting environment considerations. Home, industrial, and automotive uses have contributed much to the evolution and the development of lubricants. The more recent and perhaps the most demanding requirements for liquid lubricants are found in aircraft and in space projects. Such applications have reached levels of speed, temperature, pressure, and gaseous environment considerably beyond the previous limits.

These factors emphasize the necessity of selecting a lubricant for the use intended and of giving serious consideration to the anticipated environment and to possible effects on other systems and exposed materials.

PROPERTIES OF LUBRICANTS

There are literally hundreds of chemical and physical properties by which liquid lubricants may be categorized. Some important properties of bearing lubricants will be discussed in the following order: (1) oxidation, (2) viscosity, (3) thermal stability, (4) volatility, (5) lubricating properties, (6) flammability, and (7) hydrolytic stability.

*Synthetic Fluids Service, Inc., Pacific Palisades, California.

Oxidation

A review of the failures of liquid lubricants and bearings shows that the most prominent factor that contributes to lubricant failure has usually been oxidation. The results of oxidative deterioration are often easily confused with other factors, for instance, thermal deterioration. When a lubricant starts to fail through oxidation, the result is usually the formation of both soluble and insoluble compounds that may appear as resins, sludges, or acidic compounds. These effects in turn manifest themselves as follows:

(1) In a gradual rise in viscosity of the lubricant
(2) In the formation of adherent surface deposits that may interfere in small clearance spaces
(3) In corrosion or deterioration of metal parts
(4) In general dirtying of the system through sludges or other insoluble components

Certain metal surfaces and small metal wear particles exert a pronounced catalytic effect in promoting the oxidation rate of many lubricants. Iron may cause such an effect with one lubricant and copper alloys with another. Freshly exposed surfaces due to the wear process are the most active in this regard.

There are several methods by which oxidation can be controlled; the most popular method is the addition of oxidation inhibitors that retard the rate or the effects of oxidation. As is illustrated in figure 7–1, a time lag called the induction period exists before the oxidative effect becomes significant, after which a rapid rise in either acidity or viscosity of the lubricant is usually noted. The effect of the oxidation inhibitor is usually one of increasing the induction-period time after which the same symptoms appear. In so doing, the shape of the curve is sometimes altered, and, when the induction period is exceeded, the rise in acidity or viscosity is often more sharp than for an uninhibited fluid.

A second method of controlling oxidation is to limit temperature since oxidation rate is strongly influenced by heat. A third method of oxidation control is to blanket the lubricating system with an inert atmosphere such as nitrogen. This method is more effective if the fluid can be outgassed before the lubricant is introduced into the system. Oxygen carried in the fluid as entrained or dissolved gas can significantly influence the rate of oxidative deterioration of the fluid.

There are many complex relations between the type of lubricant and its resistance to oxidation. Controversy exists regarding the actual mechanism by which an oil is oxidized, but it is generally agreed that oxidation proceeds in a chain-like autocatalytic fashion that involves the formation of organic peroxides. The peroxides can, in turn, increase the rate of oxidation of the remaining oil. In hydrocarbon

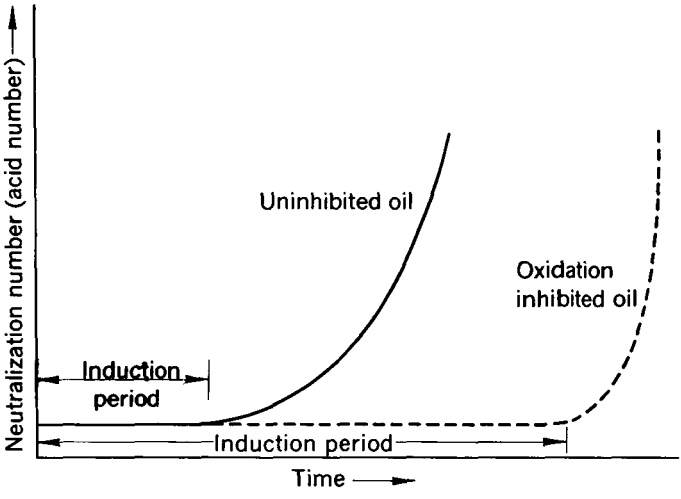

FIGURE 7–1.—Effect of oxidation inhibitor on induction period.

oils, the saturated straight-chain types are generally more resistant to oxidation than unsaturated compounds, ring compounds, and those easily capable of developing free radicals.

For synthetic oils, the oxidation phenomenon is peculiar to each type and may result in effects completely different from those expected of petroleum oils. For example, the oxidation products of silicone polymer oils are often gels that appear as rubbery compounds. While polyglycol ethers are more readily oxidized, they usually develop high-volatility oxidation products, which evolve as gases and therefore do not increase the viscosity of the remaining oil.

The inference should not be drawn that all the effects of oxidation are harmful. In many lubricants, small quantities of oxidation reaction products are beneficial and even necessary to the lubrication process. The structural aspects of oxidation in some synthetic types will be discussed subsequently in the section SYNTHETIC LUBRICANTS.

Viscosity

Probably the most important single property of liquid lubricants is viscosity, which is a fundamental characteristic of pure liquids. Viscosity is a measure of fluid friction and is defined as the ratio of the shearing stress to the rate of shear. Viscosity is related broadly to molecular weight; kinematic viscosity is expressed in centistokes

and absolute viscosity is expressed in centipoises or reyns. Absolute viscosity is the product of kinematic viscosity and density at the same temperature in consistent units. In figure 7–2, the viscosities of various lubricants are plotted against temperature. An important characteristic of each lubricant type is the rate at which viscosity decreases with temperature, which is often expressed as the viscosity index. Another method of describing this rate of change in viscosity is the ASTM slope. This numerical expression is the slope of the viscosity-temperature curve between two selected temperatures when plotted on the ASTM viscosity coordinates as in figure 7–2. High slopes represent low viscosity indexes and larger viscosity changes with temperature.

High molecular weight, long-chain polymeric additives that are sparingly soluble in the base lubricant can significantly alter viscosity index. They are usually referred to as V.I. improvers and are customarily used in quantities varying from 1 to 10 percent by weight. V.I. improvers raise the viscosity of the base oil to which they are added, but more important, their nonlinear solubility characteristics

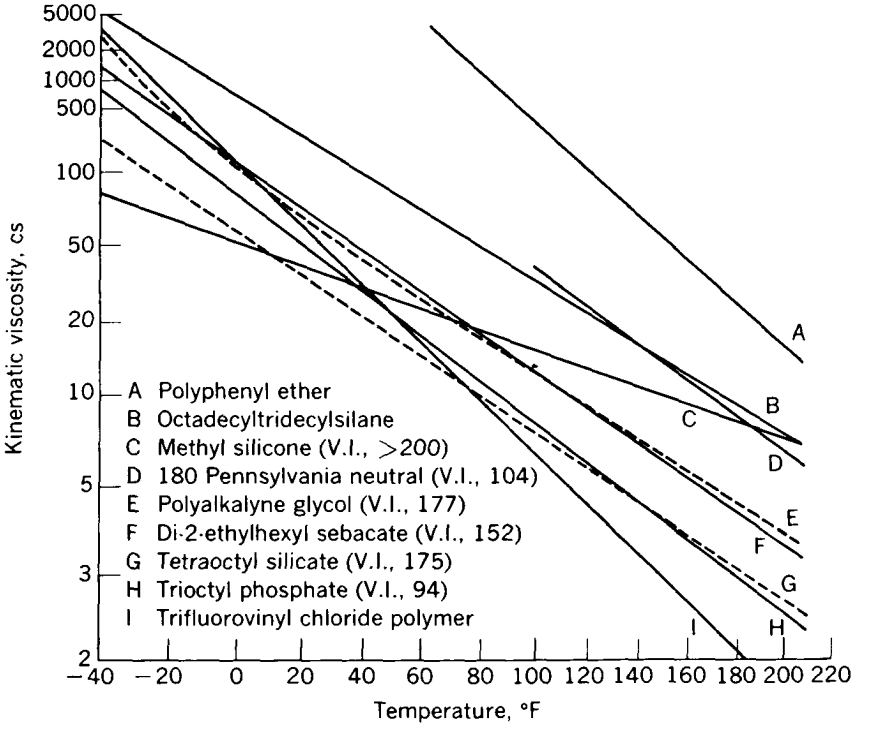

FIGURE 7–2.—Viscosity-temperature characteristics of various lubricants.

cause them to increase the viscosity to a greater degree at high temperatures than at low temperatures (fig. 7–3). As increments of polymer are added, the gain in V.I. is not proportional. The degree of this effect can be controlled through the molecular weight and the structure of the polymer. One disadvantage of V.I. improvers is a tendency to break down under high shear stresses and in turn to lower the molecular weight. The result is to lower the viscosity permanently and to degrade the viscosity index. Permanent loss of viscosity can also occur because of thermal or oxidative breakdown of the polymeric additives. At high shear rates, a temporary loss of viscosity can occur, as these same long-chain polymer additives tend to line up in the direction of flow in passing through capillary spaces. This effect is transient, and tests before and after passage of the lubricant through these spaces will not necessarily reflect the viscosity present during the actual flow.

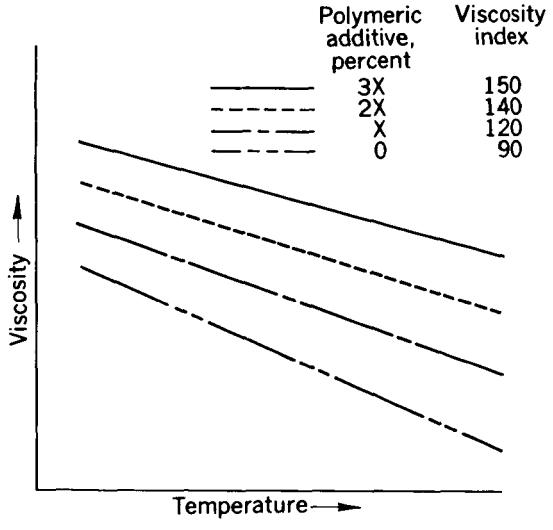

FIGURE 7–3.—Typical response of polymeric viscosity-index improvers for base oil with various additives.

Another viscosity characteristic is the change of viscosity with pressure. In general, the viscosity of liquids increases as pressure increases. Hydrocarbons with steep viscosity-temperature curves tend to exhibit steep viscosity-pressure curves. The viscosity-pressure characteristics of the synthetic lubricants cannot be generalized because of the varying elements and structures that may be present.

Thermal Stability

Thermal stability or pyrolytic stability is a fundamental characteristic of the pure lubricant type and to a lesser degree of the physical and chemical structural differences within a given class of lubricants. Thermal instability is difficult to distinguish from other high-temperature effects, such as oxidation. Evaporative loss of liquid from a system at high temperatures is often mistaken as thermal instability. Small concentrations of dissolved or entrained water can react at high temperatures with the lubricant or with contaminants in the lubricant to produce complicated hydrolytic instability reactions, which are often confused with thermal instability.

Care should be taken in examining the thermal stability of a compound that one or more of the following precautions are observed:

(1) The material is either in a sealed or evacuated ampule.
(2) Oxygen, air, or other entrained gases that may react are not present.
(3) An inert gaseous blanket is provided.

Certain fundamental rules exist by which the thermal stability of lubricants can be characterized generally. In straight-chain hydrocarbons, short alkyl chain lengths ordinarily produce the highest thermal stability. As chain length increases, thermal stability decreases. Simple aromatic structures are more thermally stable for a given molecular weight than straight-chain compounds.

In synthetic lubricants, the rules for thermal stability are far more complicated. Large differences exist in the thermal stability of the various types of synthetic lubricants. These differences usually result from the fact that new atoms have been introduced and new bonds are present in addition to carbon-hydrogen or carbon-carbon bonds. Thermal stability is related, basically, to the strength of the bond between any two atoms and to the forces or strains that exist on that bond.

There are few known additives that can increase the thermal stability of a lubricant. This property is usually fundamental to the pure compound and only in rare cases can it be changed by the addition of other chemical materials. The purity of the compound, however, is important. Small concentrations of thermally less-stable impurities (often in the form of related similar compounds to the one under study) can confuse the results of such tests.

Volatility

The volatility (vapor pressure at a specified temperature) of a lubricant is another characteristic that is fundamental to the molecular structure and the type of the lubricant. Volatility, in any homologous series of lubricants, is related basically to molecular weight: the higher the molecular weight, the lower the volatility. In general, the volatility of a mixture will initially reflect the volatility of the most volatile ingredient. If the vapors are unconfined, selective evaporation will ultimately yield the highest boiling compounds as a residue.

The evaporation rate is increased by reduction in ambient pressure. As temperature increases, molecular activity increases, and higher volatility results. In general, volatility cannot be controlled through the use of additives.

Lubricating Properties

The lubricating properties of a liquid lubricant are difficult to define. The principal duties of a lubricant are (1) to prevent metal-to-metal contact and (2) to minimize the damages that can occur in intermittent contact. This first duty is principally a function of viscosity; the second duty is a chemical function.

Before discussing the complicated problem of the addition of chemicals and additives to lubricating materials to improve lubricating properties, the lubricating properties of the pure materials should be examined. If lubricants are so refined that all natural contaminating chemicals are removed, the hydrocarbons differ in their ability to lubricate or separate metal surfaces primarily through differences in viscosity. Such is not the case for many of the synthetics that will be discussed subsequently. Many of the synthetics contain chemical materials that contribute to the reaction at the surfaces. In addition to viscosity, other ways in which metal surfaces can be protected from gross physical damage are by surface film formation or by alteration, such as (1) physical adsorption, (2) chemisorption, or (3) chemical reaction. The mechanism of film formation is discussed in chapter 2.

The most common materials used as chemical reaction additives are sulfur, phosphorous, halogen compounds, and some metals and metal salts. The principal mode of operation of these chemicals is the formation of a salt or metal eutectic of low melting point and low shear strength. In an ideal situation, the additive has little effect

where temperatures are moderate and the metal surfaces are separated by a continuous oil film. In the event of metal-to-metal contact, these chemicals react with the metal surface. The reaction film separates the two surfaces and prevents actual welding or galling from taking place.

The use of such extreme-pressure or antiwelding additives presents a problem, however, since almost all the materials previously named are reactive materials and are potentially corrosive to many metals and alloys. Hence, the process of preventing seizure or minimizing adhesive wear in either the boundary or the extreme-pressure mode of operation is a sacrificial process. The problem is to control the rate of reaction. Some of the chemical additive is used up each time it reacts, and a small amount of the metal surface is sacrificed in reacting with the chemical.

Flammability

Flammability represents a complex chemical relation of atmosphere, heat, and ignition sources. An essential relation also exists with some of the other properties of the lubricant such as its volatility, its oxidative and thermal stability, and, to a certain extent, its viscosity.

The most important factor that affects flammability is the chemical composition of the lubricant. Few differences exist in hydrocarbons in their bulk or spray flammability other than the variations exhibited by differences in volatility or viscosity. The combination of hydrogen and carbon in hydrocarbons renders them readily ignitable, at least from open flames and sparks.

With flameless hot surfaces as potential ignition sources, thermal stability becomes important. For example, benzene is readily ignitable from open flames or sparks, but it is very difficult to ignite from hot surfaces because of its thermal stability.

This same effect can be observed with some of the high thermal stability synthetics. Other synthetics exhibit good hot-surface resistance to flammability in addition to self-quenching properties if ignited by open flames or sparks. Still others are effective fire suppressants. The overall fire resistance of a liquid lubricant cannot necessarily be predicted readily by examining its chemical structure or its physical characteristics. A broad spectrum of appropriate test methods must be used to characterize the flammability properties of a lubricant. Chemical additives have rarely been effective in improving this property. Additive quantities necessary to produce distinguishable effects are usually prohibitively large.

Hydrolysis or Water Resistance

The hydrolytic stability (water resistance) of a lubricant can be a very important consideration. The prevention of moisture (in the form of condensate or entrainment) from entering most lubricating systems is difficult. Hydrocarbons, as lubricants, are relatively unaffected by water. Additives or contaminants in compounded hydrocarbon oils or other hydrolysis resistant lubricants can change this property radically, since such additives are rarely as insensitive to water as the hydrocarbon and many are easily hydrolyzed. Hydrolysis should be carefully differentiated from the mere presence of entrained or entrapped water, which can cause rusting or some other corrosive effects. In true hydrolysis, water actually reacts with the lubricant molecule and alters its basic chemical and physical properties or generates decomposition products.

If the basic type of lubricant involved is susceptible to hydrolytic attack, several general rules apply:

(1) As molecular weight increases, hydrolytic stability generally increases.

(2) At a given molecular weight, straight alkyl-chain compounds are generally more easily attacked by water than highly branched structures.

(3) Short substituents in the form of side chains closely packed near the point of possible attack often hinder the entry of the water molecule.

(4) As operating temperatures are increased, the presence of moisture becomes more important, since hydrolytic attack usually increases with increase in temperature.

(5) At sustained temperatures above the boiling point of water a material is not assumed to be free from the possibilities of hydrolytic attack. Often very small percentages of water retained in the molecule can be severe in their effects when combined with other chemical contaminants.

(6) Chemical additives are rarely effective in improving this property and are not ordinarily used.

The results of hydrolysis and water contamination can vary widely depending upon the source of the breakdown. Some common expected results are

(1) Change in physical properties of the fluid
(2) Generation of sludges and other insoluble compounds
(3) Development of insolubility of essential additives in compounded fluids
(4) Corrosive attack or stains on metal surfaces
(5) The release of alcohols and other volatile compounds that results from actual chemical breakdown

SYNTHETIC LUBRICANTS

The discussion of synthetic lubricants in this chapter will be limited to nonpetroleum types. Remarks are further confined to materials that have seen reasonable use in the past, are presently being used, or are anticipated for significant use as synthetic lubricants. The classes that will be considered are (1) dibasic-acid esters, (2) phosphate esters, (3) silicone polymers, (4) silicate esters, (5) polyglycol ethers and related compounds, (6) halogenated compounds, (7) polyphenyl ethers, (8) silanes, and (9) organometallic compounds.

The general properties of these classes of synthetic lubricants will be compared with petroleum lubricants intended for the same uses, and their availability and indicated fields of utility will be discussed. The principal reason for choosing a synthetic lubricant is usually the result of an increase in severity of operating conditions or a new design in which ordinary lubricants will not be satisfactory. *Synthetic lubricants should not be selected over readily available and invariably less expensive petroleum lubricants if the operating conditions do not provide clear and compelling reasons for the choice of the synthetic.* The introduction of synthetic lubricants into a new design is usually more easily accomplished than the conversion of an existing machine to their use.

The largest single reason for the increased use of synthetics has been a radical increase in the range of temperatures under which lubricants are expected to perform. In aerospace use, high speeds, high altitudes, and the proximity of cryogenic systems have all influenced the extension of temperature extremes. This demand for lubricants to serve a wide temperature range has clearly indicated that a petroleum product with a sufficiently low viscosity to be mobile at very low temperatures would be unusable because of extremely high volatility at high temperatures.

Most of the synthetic lubricants that have been used (or proposed) demonstrate appreciably lower viscosity for a given volatility than equivalent petroleum materials; conversely, they have lower volatility for a given viscosity. An example of the low volatility of some of the synthetics is shown in table 7–I. In this table, the weight losses by evaporation are shown for some of the dibasic-acid esters made from organic acids of 6, 9, and 10 carbon atoms esterified with hexyl (C_6) and octyl (C_8) alcohols. The lowest molecular weight (highest volatility) ester in this group lost less than 0.4 percent by weight in 168 hours at 150° F. Viscosities at −40° F for these same samples range from 219 to 1410 centistokes. Petroleum oils of comparable viscosity at −40° F could be expected to lose from 10 to 25 percent by weight in such a test.

TABLE 7–I.—EVAPORATION RATES OF SOME DIBASIC-ACID ESTERS

Ester	Molecular weight	Viscosity at −40° F, cs	Evaporation rate[a] (volatility), percent weight loss
Di(2-ethylbutyl)adipate	314. 5	219	0. 34
Di(2-ethylhexyl)adipate	370. 6	807	. 07
Di(2-ethylbutyl)azelate	356. 5	500	. 05
Di(2-ethylhexyl)azelate	412. 5	1190	<. 05
Di(2-ethylhexyl)sebacate	426. 7	1410	<. 05

[a] Percent weight loss in 168 hr at 150° F in a convection-type oven. For comparison, petroleum oils of comparable viscosity at −40° F would show weight losses of 10 to 25 percent.

There are other reasons for using synthetics. Some have extremely good chemical lubricating properties; others have extremely good thermal stability; and still others have better oxidation resistance than petroleum oils. Several of the classes of synthetics have excellent fire resistance. In the case of extreme fire hazard or in the possible presence of liquid oxygen or hydrogen peroxide, this factor alone can be a compelling reason for the selection of synthetics.

Most of the synthetics proposed or in use have much better viscosity-temperature characteristics than the best petroleum hydrocarbons; that is, they have higher viscosity indexes or lower ASTM slopes. Figure 7–2 illustrates the comparative viscosity-temperature properties of some of these classes of synthetics as compared to a petroleum hydrocarbon.

Some of the characteristic properties of synthetic lubricants require considerable caution in use, particularly in machines designed for petroleum products. For instance, many of the synthetic lubricants are strong chemical solvents. This property has the advantages of reducing the surface buildup of sludges and varnishes but often promotes strong swelling and degrading effects on many of the natural and synthetic rubbers, plastics, adhesives, and paints used in industry. By contrast, some of the synthetics (such as the silicones and silicates) are rather poor solvents; this can result in an equally undesirable hardening and shrinking effect on many elastomers. For most of the synthetics there are, however, satisfactory rubber-like, plastic, and related materials for engineering applications.

The majority of the synthetic lubricants, despite low volatility and generally good ability to wet metal surfaces, show poor rust prevention qualities as compared with petroleum products of equivalent viscosity. Most of the synthetic lubricants are readily improved by use of conventional polar-type rust-preventive additives.

TABLE 7–II.—GENERAL PROPERTIES [a] OF SOME CLASSES OF SYNTHETIC LUBRICANTS

Lubricant	Volatility	Viscosity-temperature characteristics	Oxidation resistance	Lubrication characteristics	Thermal stability	Resistance to hydrolysis	Flammability characteristics	Solvent effect on paints, rubber, etc.	Resistant materials available	Solubility in petroleum and other synthetics	Improvement additive compatibility	Price range per gallon	Typical applications
Dibasic-acid esters	Generally lower	Good to excellent	Fair to good	Fair to good	Fair to good	Fair to good	Poor to fair	Pronounced effect	Some	Good to excellent	Generally good	$3–$10	Instrument oils, low-volatility grease bases, special hydraulic fluids, jet-turbine lubricants.
Phosphate esters	Generally lower	Fair to good	Good	Good to excellent	Poor to fair	Poor to good	Good to excellent	Pronounced effect	Yes	Good to excellent	Generally good	$4–$12	Fire-resistant hydraulic fluids, low-volatility high-lubricity grease bases, lubrication additives in other synthetics, special low-temperature lubricants.
Silicones	Much lower	Excellent	Good to excellent	Poor to fair	Good to excellent	Excellent	Poor to good	Generally small effect	Yes	Poor	Poor	$20–$40	High-temperature bearings, condensation pump lubricant, low-volatility grease base for lightly loaded bearings, damping fluids, devices requiring minimum viscosity change with temperature
Silicate esters	Lower	Excellent	Poor to fair	Fair to good	Good	Poor to fair	Poor to fair	Some effect	Yes	Fair to good	Fair to good	$8–$20	Heat-transfer fluids, high-temperature hydraulic fluids, low-volatility, low-viscosity grease bases, components for low-viscosity hydraulic fluids

Polyglycol ethers	Approximately equal	Good to excellent	Poor to fair	Good	Fair to good	Fair to good	Fair to good	Pronounced effect on paint, small effect on rubber	Some	Fair to good	Generally good	$2–$6	Special hydraulic fluids, forming and drawing lubricants, low-temperature grease bases, vacuum-pump lubricants, component of other synthetic lubricant formulations
Halocarbons	Some lower, some higher	Poor	Excellent	Poor to excellent	Poor to excellent	Poor to excellent	Excellent	Widely variable	--------	Generally poor	Widely variable	$5–$200	Nonflammable, extreme oxidation-resistant lubricants for plant processes or devices handling reactive materials
Polyphenyl ethers	Much lower	Poor to fair, generally high pour points	Fair to good	Fair to good	Good to excellent	Fair to good	Poor to fair	Some effect	Yes	Fair	----------	Over $100	High-temperature fluid for reactor coolant, hydraulic applications at very high temperature, applications not yet fully developed
Silanes	Much lower	Fair to good	Poor to fair	Fair to good	Good to excellent	Good	Poor to fair	Generally small effect	Yes	Fair	Fair	----------	Base stocks for high-temperature greases, hydraulic fluids and engine lubricants, require extensive formulation

[a] Properties are for typical class members, comparing synthetics with well-refined petroleum products in equivalent service. For comparative purposes, the petroleum product would rate as fair to good. Exceptions are flammability where petroleum products would rate "poor" and hydrolysis where petroleum products would be rated "excellent."

The characteristics of several individual classes of synthetic lubricants are summarized in table 7–II. The broad descriptions used to characterize the functional properties of these materials are generalizations and should be used with caution. These general properties are for uncompounded typical lubricants as relatively pure materials. Properties that are indicated as deficient may or may not be improved by compounding. Since some standard of comparison must be used, the properties are described relative to high-quality petroleum hydrocarbon lubricants for an equivalent function. This table should not be used to compare the various classes of synthetics with each other.

Dibasic-Acid Esters

The dibasic-acid esters represent one of the most widely researched and commonly used classes of synthetic lubricants. These esters are a reaction product of a dicarboxylic acid and an alcohol. The result is an organic diester with the typical structure R—O—[R′]—O—R where R is the organic radical from the alcohol and R′ the carbon chain in the acid. Dibasic-acid esters, which are readily manufactured from a wide variety of organic acids and alcohols, are used in low-volatility greases, turbine lubricants, low-volatility instrument lubricants, and components in numerous synthetic lubricant formulations. Many members of the class are available from petroleum hydrocarbon synthesis; others are available from such sources as castor beans and animal tallow. As a general rule, dibasic-acid esters are characterized by very good viscosity-temperature properties, low volatilities, and low freezing points (table 7–II). Their chemical lubricating characteristics vary somewhat, depending upon their particular structure, but they are generally as good as or better than equiviscous petroleum hydrocarbons. Dibasic-acid esters are high in chemical solvency and readily accept additives such as lubricating additives, oxidation inhibitors, some rust inhibitors, and viscosity-index improvers. Similarly, they often exhibit high solvency for many elastomers. Their thermal stability, while not the equivalent of some pure saturated hydrocarbons, is good. The diesters are approximately equal in oxidation stability to petroleum oils. Most members of this class blend readily with many other synthetics and with petroleum oils. Their resistance to hydrolysis is generally good, particularly in the high-molecular-weight members of the family, but not equal to that of petroleum oils. Di(2-ethylhexyl)sebacate, which emerged as a commercial plastic and rubber plasticizer, is the principal liquid ingredient in many synthetic greases, jet-turbine lubricants, and low-volatility instrument oils.

Phosphate Esters

Another important class of synthetics is the phosphate esters, which are reaction products of orthophosphoric acid and various alcohols, although they are rarely made by direct combination. The typical structure is

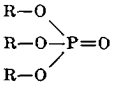

where R may be either aryl or alkyl hydrocarbons or a mixture of both. The phosphates are more properly described as organic-inorganic esters since the acid involved is an inorganic acid. Phosphate esters, such as tricresyl phosphate, have been widely used in small proportions as lubricating additives for petroleum lubricants and some other synthetics. Other members of this class possess sufficient chemical stability and other satisfactory properties to enable their use as a principal component of a synthetic lubricant.

Many phosphate esters have excellent fire-resistant properties and most of them are better than petroleum oils (table 7–II). The oxidative stability of most phosphate esters is good, and thermal stability, while generally inferior to hydrocarbons, varies significantly with structure. Most phosphate esters have peculiarly sharp limits of upper temperature stability and will sustain considerable thermal abuse if this limit is not exceeded. Few are usable above 300° F

Hydrolytic stability in the phosphate esters ranges from poor to good depending on structure and molecular weight. For example, the short-chain trialkyl esters (such as trimethyl phosphate and triethyl phosphate) are readily hydrolyzed. Most phosphate esters have strong chemical-solvency properties that result in ready admixture with other synthetics and with petroleum hydrocarbons. For the same reasons, they are strong solvents for paints and for many synthetic rubbers, but a number of elastomeric and plastic materials are compatible with these esters. Volatilities of phosphate esters are low and are in the same general order as those of the dibasic-acid esters. While a wide selection of viscosities is available, the viscosity-temperature characteristics of most phosphate esters can be classified only as fair to good and more or less equivalent to petroleum hydrocarbons. Significant volumes of the phosphate esters are used as fire-resistant lubricants or as components of fire-resistant hydraulic fluids in (1) the metals industries, (2) the aircraft industry, and (3) naval ships.

Silicone Polymers

The silicones are a diversified class of synthetics. Although research work on these materials dates back to the early 1900's, they did not come into significant use as synthetic lubricants until the

early 1940's. Many members of the silicone lubricant family exist, but the most common ones used as synthetic lubricants are probably the dimethylsilicones and the methylphenyl silicones. Unlike the synthetic classes previously discussed, the silicones are polymeric materials, and various viscosity grades are available as a result of increasing chain length in an otherwise similar molecule. They are chemically characterized by many repeating structures of silicon and oxygen with the alkyl or aromatic radicals as side chains. The typical silicone structure is

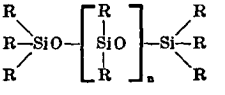

Some of these materials have the best viscosity-temperature characteristics of any of the synthetics now generally known (table 7–II). Their volatilities are exceptionally low when compared with other liquids of equivalent viscosity. Their oxidation resistance at temperatures up to perhaps 300° F is excellent, but their low volatilities have brought about use at significantly higher temperatures where their oxidation resistance fails rapidly and results in characteristic gel formations. The thermal stability of the class is good with many of the phenyl substitution types in the excellent class. Unfortunately, the silicones with such increased aromatic substitution become increasingly poor in viscosity-temperature properties and even approach those of the petroleum hydrocarbons. The chemical solvency properties of the silicones are distinctly different from most of the other synthetics. They do not readily accept additives, and only extremely low-viscosity members are soluble in petroleum products or in other synthetics. This low chemical solvency also results in minimal effects on most plastic, rubber, and paint-like materials. Sustained operation at elevated temperatures with many synthetic elastomers results in a gradual hardening of the rubber in contact with the silicones, which is apparently due to a preferential replacement of rubber plasticizer. The hydrolysis resistance of the silicones in neutral media is excellent.

The foregoing characteristics indicate that the silicones are ideal synthetic lubricants, but unfortunately their lubricating properties do not fall into this category. While the silicone polymers are excellent hydrodynamic lubricants, their chemical lubricating characteristics are poor except in special instances. Their chemical lubricating properties are also specific with regard to metal surfaces. On ferrous-base alloys, silicone polymers are extremely poor; on brasses and other copper-bearing alloys, they generally equal petroleum products. In more recent years, halogens have replaced

hydrogen on some of the hydrocarbon substituents in the molecule with a resulting improvement in lubricating properties that has permitted successful use in many machines. The silicones have been used as lubricants in high-temperature greases, in specialty high-temperature functional fluids, and as damping media where their excellent viscosity-temperature properties are utilized.

Silicate Esters

The silicate esters were mentioned in chemical literature as early as 1846, but their use as synthetic lubricants is relatively new. Since silicon is the central atom of the structure, they can be classed as inorganic-organic esters. A typical structure appears as follows:

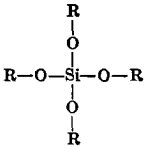

The central atom of silicon (or in the case of the dimer form two central silicon atoms) is ordinarily bonded through oxygen to four alkyl, aryl, or mixed hydrocarbon radicals. The orthosilicates, as they are often called, are obtained through the reaction of silicon tetrachloride with the desired alcohol or by the reaction of the proper alcohol with ethyl silicate. A high degree of purity is necessary with this class of compounds, since many of the less desirable characteristics of the silicates are emphasized by small traces of impurities.

The desirable feature of the silicate esters is the combination of high thermal stability, low viscosity, and relatively low volatility (table 7–II). With proper oxidation inhibitors, silicate esters have operated satisfactorily at temperatures in the range of 400° F and higher. Careful compounding is ordinarily required with these materials to maintain adequate control over other physical properties (such as viscosity) at these elevated temperatures. Silicate esters are rarely used as synthetic lubricants in the form of pure materials. The silicate esters are available in a number of different viscosities, depending on the chemical type and the structure. Most of the alkyl substituents have excellent viscosity-temperature characteristics with viscosity indexes in the 150 to 200 range. They have unusually low volatilities for given viscosities, and, unlike the closely related silicone polymers, they have fair to good lubricating properties. Again, unlike the silicones, they are compatible with many conventional lubrication improving agents and respond well to the addition of these materials. Chemical solvency effects of the silicates on other materials are variable but generally minimal.

The wide temperature range of the silicates would indicate a more extensive use, but their usefulness is limited by a deficiency in hydrolytic stability. This instability has, in some cases, been successfully inhibited with certain chemical additives and, in other cases, through appropriate control of structural configuration. The hydrolysis products are not particularly harmful since they are not high in corrosivity, but they do form gel-like materials that can clog filters and cause problems where small clearances are involved. The oxidation stability and rust-preventive properties of most of the silicates are not good, but they respond well to some additives. One of the principal uses of silicates is as a low-temperature ordnance lubricant and corrosion preventive. They have also been used as the base stocks in synthetic lubricants for high-temperature hydraulic fluids, as lubricants, and as heat-transfer materials for cooling electronic gear.

Polyglycol Ethers and Related Compounds

Many types of polyhydric alcohol compounds and glycol derivative compounds have been proposed as synthetic lubricants. Probably the most distinctive family group, however, is the group of polyglycol ethers, which are described as polyalkylene glycols and derivatives. They are manufactured as an addition product by (1) the reaction of an alcohol and a propylene oxide that results in a water-insoluble series or (2) the reaction of an alcohol and a mixture of propylene and ethylene oxide that produces a water-soluble series. Both series are available in a variety of viscosities and types. A typical structure of the propylene oxide type would be

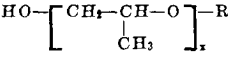

If the two basic types of structure and structural modification of the terminal endings of the chain are considered, widely variable viscosity-temperature characteristics can result, and no generalization of this property should be attempted. Many polyglycol ethers are equivalent to or superior to petroleum products in viscosity-temperature properties (table 7–II), with viscosity indexes as high as 150. Most of the polyglycol ethers have low pour points, low solvency effects on various types of natural and synthetic rubber, and good resistance to sludge and varnish formation at relatively elevated temperatures. They are compatible with many other types of synthetics; the oil-soluble types are compatible with some petroleum lubricants. The volatility characteristics of this class of synthetics are in the same general order as petroleum products, but some specific members show advantages over petroleum in this property. The oxidation resistance of the

glycol-type synthetics is somewhat lacking. They exhibit a unique property in that the decomposition products are often volatile compounds that are readily carried off in vented systems.

The water-soluble types are used in many places where a synthetic lubricant compatible with water and still not injurious to elastomeric products is needed. Both series are used in automotive brake fluids and in various other industrial lubricants.

Halogenated Compounds

The fluorinated and chlorinated compounds cannot be described properly as a chemical family. Extensive synthesis over many years has produced many types of organic compounds in which the hydrogen has been replaced either completely or in part by chlorine and fluorine (and in some instances, by other halogens). Minor amounts of halogen substitution in the production of certain synthetic lubricants to achieve better chemical lubricating properties do not ordinarily yield new materials with distinctly different properties. This discussion will be confined to compounds where a large percentage of the hydrogen in the organic radical has been replaced by either chlorine or fluorine and usually has yielded radically different properties. Many of the ester, polymer, and other synthetic lubricants previously described have been thus altered into new species.

Probably the most representative class of the fluorinated and chlorinated compounds is the halocarbons (table 7–II), where the hydrogen in a hydrocarbon compound has been replaced completely or in part by chlorine or fluorine. The older of these two classes is that of the chlorinated hydrocarbons since chlorination is more easily achieved than fluorination. The halocarbons and many other related materials have often been used as extreme-pressure additives since the presence of halogen in the molecule usually produces high chemical activity (from an antiwelding or extreme-pressure standpoint). This strong chemical activity of the halogens is one of the problems that deters their use as synthetic lubricants. In chlorinated aromatics, the chlorine is attached to an aromatic nucleus that is conducive to better chemical stability from the standpoint of heat and of hydrolytic effects. When chlorine is substituted for hydrogen in alkyl hydrocarbons, chemical stability is difficult to achieve. An example of a nonaromatic chlorinated hydrocarbon is hexachlorobutadiene, an effective lubricant that is difficult to inhibit against corrosion. The aim is to produce a molecule with sufficient stability to retain the halogen until actual or incipient metal contact. At this time, sufficient, but not excessive, halogen should be released to prevent seizure or galling. The liberation of excessive amounts of halogen results in the formation of highly corrosive and sometimes toxic end products.

Recently, much emphasis has been placed on the development of fluorinated hydrocarbons. Substitution of fluorine for hydrogen in the molecule is ordinarily more difficult than substitution of chlorine. When this fluorination is accomplished, a more stable material is usually achieved. The partially or fully fluorinated hydrocarbons have a high degree of nonflammability, have a high degree of chemical stability, and are almost completely inert. This inertness is responsible for their use in the processing of highly flammable materials such as hydrogen peroxide and liquid oxygen.

A typical structure for this type of compound is the chlorotrifluoroethylene polymer oil with the general formula

The R and R′ terminal groups are terminal groups of Cl, F, or CF_2Cl. The most stable fluorocarbons unfortunately show little compatability with other lubricants either synthetic or natural. Similarly, they are not particularly effective lubricants on many metal surfaces. Those with good low-temperature properties often have high volatility at elevated temperature as compared to petroleum lubricants, and, in general, the halocarbons have poor viscosity-temperature characteristics and narrower liquid range than equivalent hydrocarbon compounds. Despite these disadvantages and usually high densities (up to 2.0 g/ml at 100° F), the halocarbons have found limited use as synthetic lubricants.

Polyphenyl Ethers

One of the newest classes of synthetics is the polyphenyl ethers, which have been developed within the last several years because of the need for lubricants to perform at temperatures above 500° F and/or in the presence of high radiation levels. While much data has been accumulated on relatively few members of the species, too few individual compounds have been researched to characterize the species accurately. The properties subsequently discussed represent those members that have already been developed and researched intensively. The high-temperature stability and radiation resistance of the aromatic hydrocarbons plus the viscosity-temperature advantages inherent in the oxygen-ether linkage between hydrocarbons led to the development of this class of materials.

A typical family member of this class and one of the more promising candidates is m-bis(m-phenoxy-phenoxy)benzene; the structure for this compound would appear as follows:

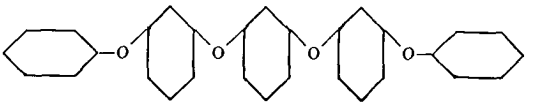

Numerous related compounds have been synthesized although insufficient quantities have been produced to evaluate their utility as synthetic lubricants. Properties of several of the polyphenyl ethers are given in table 7–III. Initial decomposition temperatures of these materials are often in excess of 750° to 800° F as compared with 500° to 600° F for some of the better silicone materials, which previously were our best high-temperature synthetics.

As might be expected from their highly aromatic structure, the viscosity properties are not outstanding (table 7–II). Notwithstanding the advantages of the oxygen-ether linkage, the highly aromatic structure of the polyphenyl ethers renders them viscous and in many cases also produces high freezing points. The metaisomers of this ether structure, however, have ASTM slopes at high temperatures that compare favorably with the diesters over their normal temperature range. Few have freezing points or pour points that permit their use much below the range of 0° to −20° F. Their volatility characteristics are good. Oxidation resistance compares favorably with petroleum hydrocarbons. Their chemical lubricating properties are roughly comparable to those of the diesters and the hydrocarbons. From the standpoint of resistance to hydrolysis, the polyphenyl ethers are stable. Their fire resistance is no more outstanding than their volatilities would suggest as they are largely composed of carbon and hydrogen. Here again, because of the predominance of the aromatic structure, their spontaneous ignition temperatures are high (approx. 1000° F and higher).

Insufficient data have been accumulated to describe properly the solvency properties of polyphenyl ethers; many additives are soluble in this class of materials. With extremely high-temperature materials such as the polyphenyl ethers, however, compounding must be approached with caution because of the difficulty of finding chemical additives with sufficiently high thermal stability in addition to required additive effectiveness. The greatest improvements, for instance, in oxidation stability have been achieved through emphasizing purity of the compound in original synthesis rather than by use of additives. The importance of organic elastomeric seals and related engineering materials is questionable with these liquids since very few elastomers will permit operation up to temperatures that are attainable by the polyphenyl ethers as lubricants.

Despite high cost, this class of materials is used experimentally as high-temperature fluids for reactor coolants, in high-temperature

TABLE 7–III.—PROPERTIES OF TYPICAL POLYPHENYL ETHERS

	mix-bis(mix-phenoxy phenyl)ether	mix-bis(mix-phenoxy phenoxy)benzene	m-bis(m-pnenoxy phenoxy)benzene
Abbreviated nomenclature	mix-mix-mix-4P3E	mix-mix-mix-5P4E	mmm-5P43
Structure	(a)	(b)	(c)
Molecular weight	354. 4	446. 5	446. 5
Boiling point, ° F (at 760 mm Hg)	900	982	948
Pour point, ° F	5	40	40
Viscosity, cs, at—			
100° F	70	363	332
210° F	6. 3	13. 1	12. 7
400° F	1. 4	2. 1	2. 04
700° F	. 47	. 65	. 63
Flash point, ° F	465	550	540
Evaporation loss, percent by weight at 500° F	33. 3	5. 1	3. 62
Spontaneous ignition temperature, ° F	1095	1135	1050
Initial decomposition temperature, ° F (isoteniscope)	835	847	870
Small-scale panel coking test, mg at 800° F	----------	. 8	. 2
0.5 Mole Dornte oxidation test, hr at 500° F	280	49	330

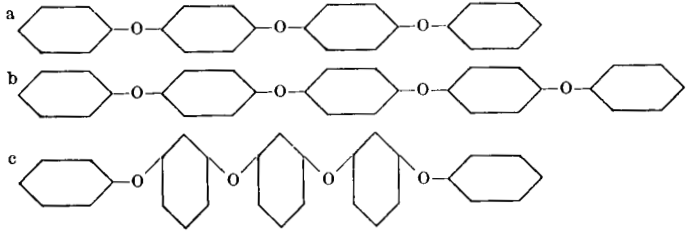

hydraulic fluid formulations, and for high-temperature aerospace applications.

Silanes

Silanes closely follow polyphenyl ethers in high-temperature stability. The silane differs from the silicone in that it (1) is not a polymer and (2) lacks the familiar silicon-oxygen linkage that provides the central backbone of the silicone polymer fluid type.

Numerous organosilanes have been prepared and evaluated for possible use as high-temperature fluids and lubricants. An organosilane has the following representative structure:

The substituent radicals can be either aromatic, alkyl, or mixed (usually two aromatics and two alkyls). Better viscometric properties result with alkyl substituents, and better thermal-stability properties are ordinarily obtained with aromatic substituents.

Silanes have low volatilities compared to equivalent hydrocarbons (table 7–II). They have viscosity-temperature characteristics that range from fair to good. Their oxidation resistance can be classified as poor to fair because of the characteristic desire of silicon to unite with oxygen and the lack of effective inhibitors. The lubricating properties of the silanes are generally better than the silicones and can be classified as fair to good. Thermal stability is their outstanding characteristic and is rated good to excellent. Hydrolysis resistance is apparently good and fire resistance is roughly equivalent to that of hydrocarbons. They have higher solvency properties than the silicones and accept conventional additives in much the same fashion as petroleum hydrocarbons. The presence of aromatic, as compared to aliphatic, substituents on the silicon leads to high swell in the presence of rubber-like compounds and, in general, high solvencies. Some of the silanes approach the polyphenyl ethers in resistance to moderate radiation dosage and are superior to petroleum hydrocarbons. Their use is anticipated as base stocks for high-temperature greases and hydraulic fluids and possibly as high-temperature engine lubricants.

Organometallic Compounds

The structural mobility and wide liquid ranges of most organic compounds plus the good thermal stability, generally good oxidation resistance, and other features present in many metallic compounds suggest the possibility of combining these materials as organometallics. Such chemistry is not new; lead tetraethyl, used for suppression of detonation in gasoline engines, is an example. Similarly alkyl

compounds of mercury, zinc, and other metals have long been known; they have, however, a particular reputation for being highly unstable, and the alkyls of aluminum and zinc often spontaneously ignite in air. More recently, in an effort to develop thermally stable additives for synthetic lubricants, materials such as tetraphenyl tin and bis(phenoxy phenyl tin) have been evaluated as stable high-temperature antioxidants. Triphenyl antimony sulfide has been synthesized and evaluated as a successful additive for improving antiwelding or lubricating properties. No typical structure can be shown for this class since the list of metals is large, and the number of organic compounds that may be attached to these metal elements is almost infinite (e.g., there are several hundred known organic compounds of tin alone). The organometallics, however, are by no means as unstable as some of the earlier members mentioned previously, and many possibilities exist in the creation of new compounds for possible use as additives or as base stocks for high-temperature fluids. This class could well become an intermediate between organic compounds and liquid metals as lubricants, which are discussed in chapter 14.

CONCLUDING REMARKS

No attempt has been made herein to assess the property of toxicity in various lubricants. There are numerous test methods used to characterize this property, and assuredly great differences may exist in the various classes of lubricants. Similarly, specific dosage limits can vary among individual members of the same class of materials. Real problems can develop from skin contact, vapor or mist inhalation, and oral ingestion. The problem belongs properly in the fields of toxicologists, industrial hygienists, and physicians. Most lubricant suppliers are thorough in the consideration of this property and in furnishing necessary data or suggestions for the handling of new products.

In selecting a lubricant for a machine or a machine component, the following suggestions are offered:

(1) Outline the known operating and environmental requirements of the machine (e.g., loads, speeds, temperatures, atmosphere, duty cycles, material exposure, etc.).

(2) Integrate the lubrication requirements as early in the design or development cycle as possible. In initial design stages, material changes necessary for lubricant compatibility are more readily accomplished; more time is available for testing, and changes are less costly.

(3) Consider the fluid cost in terms of the total probable usage (i.e., the original quantity needed, the makeup fluid or use rate, and the probable fluid life). Balance such factors against machine shutdown or the cost of replacement parts.

(4) Unless the machine is lubricated for life, consider the supply. Is worldwide availability a necessity; are competitive sources necessary or desirable; are specifications available (either proprietary, commercial, or government)?

(5) The properties of the lubricant selected should be known. More service failures of lubricants have probably resulted from improper selection of lubricants than from failure of lubricants to perform the service for which they were designed or were most suited.

BIBLIOGRAPHY

Dibasic-Acid Esters

ANON.: Development Work on Lubricants for Aircraft Turbine Engines. PRL Rep. 6.1, Penn. State College, Jan. 22, 1952.

ANON.: Dibasic Acid Esters and Ester Type Fluids and Lubricants. PRL Rep. 3.49, Penn. State College, Jan. 15, 1951.

ANON.: Esters as Synthetic Lubricants. PRL Rep. 1–50, Penn. State College, Jan. 1950.

ANON.: Physical Properties of Several Dibasic Acid Esters. PRL Rep. 1, Table 1B, Penn. State College, May 7, 1941.

ATKINS, D. C., et al.: Synthetic Lubricants from Branched Chain Diesters. Rep. P–2576, Naval Res. Lab., July 1945.

BRIED, E. M., KIDDER, H. F., MURPHY, C. M., and ZISMAN, W. A.: Synthetic Lubricant Fluids from Branched-Chain Diesters. Physical and Chemical Properties of Pure Diesters. Ind. and Eng. Chem., vol. 39, no. 4, 1947, pp. 484–491.

GLAVIS, F. J., and STRINGER, H. R.: Synthetic Lubricants from Diesters. Spec. Pub. 77, ASTM, June 1947, pp. 16–25.

MCTURK, W. E., MATUSZAK, A. H., and CARRIER, E. W.: Synthetic Lubricants. MX–1576, Standard Oil Dev. Co., Apr. 1951.

RAVNER, H., MURPHY, C. M., and SMITH, N. L.: Phenothiazine-Type Antioxidants and Their Mode of Action. Rep. 3546, Naval Res. Lab., Jan. 1950.

Phosphate Esters

ANON.: Some Preliminary Studies of the Suitability of Tri-N-Butyl Phosphate as a Base Stock for Hydraulic Fluids and Lubricants. PRL Rep. 3.12, Penn. State College, Jan. 1946.

ANON.: A Study of the Utilization of Tri-Alkyl Phosphate Esters as Base Stock for Hydraulic Fluids and Special Lubricants. PRL Rep. 3.26, Penn. State College, Nov. 1946.

HATTON, ROGER E.: Phosphate Esters. Synthetic Lubricants, Reigh C. Gunderson and Andrew W. Hart, eds., Reinhold Pub. Co., 1962, pp. 103–150.

MORETON, D. H.: Development and Testing of Fire Resistant Hydraulic Fluid. Paper Presented at SAE Meeting (Detroit), Jan. 10–14, 1949.

Silicone Polymers

BAUM, GEORGE, and ADAMS, HAROLD W.: Silicone Fluids as High Temperature Jet Engine Oils and Hydraulic Fluids. TR 58–213, WADC, Apr. 1959.

BROPHY, J. E., MILITZ, R. O., and ZISMAN, W. A.: Dimethyl-Silicone-Polymer Fluids and Their Performance Characteristics in Unilaterally Loaded Journal Bearings. Trans. ASME, vol. 68, no. 4, May 1946, pp. 355–360.

BROWN, E. D., JR.: Silicone Based Hydraulic Fluids. TR 57–93, WADC, 1957.
BROWN, EDGAR D., HOLDSTOCK, NORMAN G., and MCGUIRE, JOHN M.: Silicone Fluid Research for the Development of High Temperature Hydraulic Fluid and Engine Oils. TR 56–168, pt. III, WADC, Feb. 1957.
FITZSIMMONS, V. G., PICKETT, D. L., and ZISMAN, W. A.: Dimethyl-Silicone-Polymer Fluids and Their Performance Characteristics in Hydraulic Systems. Trans. ASME, vol. 68, no. 4, May 1946, pp. 361–369.
GADSBY, G. N.: Silicones—A Consideration of Some Factors Relative to Their Use as Lubricants. Sci. Lubrication, vol. 3, no. 10, Oct. 1951, pp. 15–19; 32. (See also Lubrication Eng., vol. 3, no. 11, Nov. 1951, pp. 15–17; 33.)
GRANT, G., and CURRIE, C. C.: Properties and Performance of Silicone Lubricants. Paper Presented at Annual Meeting ASME, Nov. 1950.
ROCHOW, EUGENE G.: An Introduction to the Chemistry of the Silicones. Second ed., John Wiley & Sons, Inc., 1946.

Silicate Esters

HATTON, ROGER E.: Silicate Esters. Synthetic Lubricants, Reigh C. Gunderson and Andrew W. Hart, eds., Reinhold Pub. Co., 1962, pp. 323–356.
POST, HOWARD W.: Chemistry of the Aliphatic Orthoesters. ACS Monograph, Reinhold Pub. Co., 1943.

Polyglycol Ether Compounds

MILLETT, W. H.: Industrial Uses of Some Polyether Synthetic Lubricants. Iron and Steel Eng., vol. 25, no. 8, Aug. 1948, pp. 51–58; discussion, pp. 58–60.
RUSS, J. M., JR.: Properties and Uses of Some New Synthetic Lubricants. Lubrication Eng., vol. 2, no. 4, Dec. 1946, pp. 151–157.
RUSS, J. M., JR.: Ucon. Synthetic Lubricants and Hydraulic Fluids. Paper Presented at ASTM Meeting, Philadelphia (Penn.), June 1947.
SULLIVAN, M. V., WOLFE, J. K., and ZISMAN, W. A.: Flammability of the Higher Boiling Liquids and Their Mists. Ind. and Eng. Chem., vol. 39, no. 12, Dec. 1947, pp. 1607–1614.
GUNDERSON, R. C., and MILLETT, W. H.: Polyglycols. Synthetic Lubricants, Reigh C. Gunderson and Andrew W. Hart, eds., Reinhold Pub. Co., 1962, pp. 61–102.

Halocarbons

ANON.: The Development of Less Inflammable Types of Hydraulic Fluids. PRL Rep. 3.41, Penn. State College, Apr. 1948.
ANON.: Polyhalo Organic Compounds as Less Flammable Aircraft Hydraulic Fluids. Air Force Tech. Rep. 5746, Materials Lab., Wright-Patterson Air Force Base, Jan. 1949.
ASHTON, W. E., and STRACK, C. A.: Chlorofluorocarbon Polymers. Synthetic Lubricants, Reigh C. Gunderson and Andrew W. Hart, eds., Reinhold Pub. Co., 1962, pp. 246–263.
HUDLICKY, MILOS: Chemistry of Organic Fluorine Compounds. Macmillan Co., 1962.
MCBEE, E. T., et al.: Chlorine and Fluorine Containing Organic Compounds for Non-Flammable Materials. Purdue Res. Foundation, Purdue Univ., May 1950.

Silanes

ADAMS, HAROLD W., and BAUM, GEORGE: Laboratory Evaluation of Silane Fluids as Potential Base Stocks for Hydraulic Fluids and Lubricants. TR 57–168, WADC, Mar. 1958.

SAWYER, A. W.: Formulation of Silane Base High Temperature Hydraulic Fluid. TR 58-407, pts. I-II, WADC, June 1959.

Polyphenyl Ethers

BLAKE, E. S., EDWARDS, J. W., HAMMAN, W. C., and REICHARD, T.: High Temperature Base Stock Fluids. TR 57-437, WADC, Dec. 1957.

KLAUS, E. E., FENSKE, M. R., and TEWKSBURY, E. J.: Fluids, Lubricants, Fuels and Related Materials. TR 55-30, pt. VIII, WADC, June 1960, pp. 97-98.

MAHONEY, C. L., BARNUM, E. R., SAARI, W. S., SAX, K. J., and KERLIN, W. W.: Nuclear Radiation Resistant High Tempreature Lubricants. TR 59-173, WADC, Sept. 1959.

RICE, WILLIAM L. R., Nuclear Radiation Resistant Lubricants. TR 57-299, pt. 1, WADD, May 1957.

Organometallics

GILMAN, H., and GORSICH, R. D.: Organo-Metallic and Organo-Metalloidal High Temperature Lubricants and Related Materials. TR 53-426, pt. 4, WADC, 1954.

General

DIVISION OF PETROLEUM CHEMISTRY, AMERICAN CHEMICAL SOCIETY: SYNTHETIC Lubricating Oils Symposium. Ind. and Eng. Chem., vol. 42, no. 12, Dec. 1950, pp. 2414-2462.

GUNDERSON, REIGH C., and HART, ANDREW W., eds.: Synthetic Lubricants. Reinhold Pub. Co., 1962.

JOHNSON, ROBERT L., and PETERSON, MARSHALL B.: Status Report—High Temperature Lubrication. Lubrication. Eng., vol. 17, no. 9, Sept. 1961, pp. 451-455.

KLAUS, E. E., TEWKSBURY, E. J., and FENSKE, M. R.: Critical Comparison of Several Fluids as High Temperature Lubricants. Jour. Chem. and Eng. Data, vol. 6, no. 1, Jan. 1961, pp. 99-106.

KLAUS, E. E., TEWKSBURY, E. J., and FENSKE, M. R.: Preparation, Properties, and Some Applications of Super-Refined Mineral Oils. Paper 61-LC-10, ASLE, 1961.

MACKS, FRED: Lubrication Reference Manual for Missile and Space Vehicle Propulsion at Temperatures Above 700° F. TR 58-638, WADC, vol. I, pt. I, Jan. 1959.

MCHUGH, KENNETH L., SMITH, JOHN O., STEMNISKI, JOHN R., and WILSON, GLENN R.: Research and Development on High-Temperature Additives for Lubricants and Hydraulic Fluids. TR 59-191, pt. II, WADC, June 1960.

RUBIN, BERNARD, and GLASS, EDWARD M.: The Air Force Looks at Synthetic Lubricants. SAE Jour., vol. 4, no. 2, Apr. 1950, pp. 287-296.

WILLIAMS, A. E.: Synthetic Lubricating Oils. Sci. Lubrication, vol. 2, no. 2, Feb. 1950, pp. 2-5.

Page intentionally left blank

CHAPTER 8

Nonconventional Lubricants

By EDMOND E. BISSON

I. SOLIDS

WHEN OPERATION OF MECHANISMS IS REQUIRED at high temperatures or at low pressures, normal liquid lubricants are not usually suitable. Normal liquids are temperature limited because of thermal or oxidative instability at high temperatures. (For liquids, thermal instability means instability in the absence of oxygen; oxidative instability means instability in the presence of oxygen.) Also, most liquids which are suitable for lubrication over the normal temperature range will have high volatility (i.e., high vapor pressure) at high temperatures. In accordance, for operation at high temperatures, lubricants other than the normal liquids must be considered. For operation at these temperatures, nonconventional lubricants, such as solids or gases, appear particularly promising.

Many solids have been investigated for their effectiveness as solid lubricants (ref.1). These include the common solids, graphite and molybdenum disulfide, as well as a number of additional solids some with and some without layer-lattice structures. For example, in reference 1, the solids with layer-lattice structures included $CoCl_2$, $NiCl_2$, $CdCl_2$, $Mg(OH)_2$, TiS_2, PbI_2, $Ca(OH)_2$, MoS_2, WS_2, HgI_2, $PbCl_2$, $HgCl_2$, $CuBr_2$, Ag_2SO_4, and Na_2SO_4. The low shear-strength solids without layer-lattice structures included AgCN, CuCl, and AgI. Other solids investigated included Fe_3O_4, NiO, mica, talc, and BN.

Examples of applications in which nonconventional lubricants are required include mechanisms in inaccessible locations, such as (1) control surface bearings embedded in the structure of aircraft, and (2) the bearings for satellites or space vehicles, which must of necessity operate in a vacuum environment, besides being completely inaccessible during their lifetimes.

This part of chapter 8 discusses solids as lubricants and encompasses (1) the requirements for solid lubricants, (2) the role of such lubricants in the reduction of friction and of wear in operating mechanisms, and (3) the method of application or use of such lubricants.

REQUIREMENTS

The principal requirements for solid lubricants may be listed as follows:

(1) Thermal (and oxidative) stability
(2) Low shear strength
(3) Surface protection
(4) Good bonding properties (surface adherence)
(5) Laminar structure (desirable, but not absolutely necessary)

Peterson, Murray, and Florek (ref. 2) review some of the general considerations behind the selection of solids for use as solid lubricants in considerable detail.

Since solid lubricants are considered for high-temperature use, it is obvious that they must have good thermal (and oxidative) stability. Thermal stability in the case of liquids is normally thought of as stability in the absence of oxygen. In the case of solids, however, thermal stability will be defined as stability, not only in the absence of, but in the presence of gases (such as oxygen, nitrogen, and others). Thermal stability thus includes normal decomposition of solids. The chemical thermal stability may be estimated from the heat of formation (or, more exactly, the free energy of formation) especially as used to calculate free energy of reaction of the solid with the surrounding atmosphere to produce various compounds. The physical thermal stability involves changes in the crystal structure as a result of temperature; change of crystal structure can often result in change of friction (by alteration of shear strength).

The second requirement for solid lubricants is that of low shear strength. It should be emphasized that this requirement is desirable but not absolutely necessary since prevention of surface welding is sometimes more important than the friction coefficient or friction torque per se.

Peterson, Murray, and Florek (ref. 2) list the properties of metals of interest from the standpoint of low shear strength (i.e., softness); these properties are shown in the following table from their paper:

Metal	Moh hardness	Melting point, °C
Indium	1	155
Thallium	1. 2	304
Lead	1. 5	328
Tin	1. 8	232
Cadmium	2	321
Gold	2. 5	1063
Silver	2. 5–3	961
Platinum	4. 3	1755
Rhodium	4. 5–5	1955

The metals with low values of Moh hardness (such as indium, lead, and tin) are those normally thought of as having low shear strength. These metals are frequently utilized in plain journal bearings where frequent "start-stop" service is a feature of the mechanism; the common silver-lead-indium bearing is an example of the use of these metals.

The third requirement is that of surface protection, which has been previously mentioned. It is absolutely necessary, particularly for a mechanism which is to operate for long periods of time unattended, that the surfaces in relative sliding be protected from gross welding and gross metal transfer. Otherwise, an exponential wear-rate curve is obtained and the surfaces will seize completely or be so badly worn as to be unusable.

A fourth requirement is that of good bonding properties. This requirement implies that the solids, if used in loose powder form, should have good adherence to the surfaces to be lubricated. If the solids are bonded with some other bonding agent, the important requirements will become compatibility with the bonding agent, the base metal, and the base metal oxide.

The fifth important requirement for selection of solid lubricants is that these solids have a laminar structure if possible. This requirement is desirable but not absolutely necessary since it has been shown many times that effective lubrication and surface protection can be obtained from solids which do not have a laminar structure. If the solids do have a laminar structure, however, and do have good surface adherence properties, it is probable that the lubricating effectiveness will be better than that of solids with other types of crystal structure (ref. 1). Graphite and molybdenum disulfide, which have been used extensively as solid lubricants, have a layer-lattice structure. In the case of metallic salts with the general formula AX_2, this layered structure may be represented as

X^-	X^-	X^-
A^{++}	A^{++}	A^{++}
X^-	X^-	X^-
X^-	X^-	X^-
A^{++}	A^{++}	A^{++}
X^-	X^-	X^-

where the forces within the layer are the strong covalent or ionic forces, while the forces between the successive layers are the relatively weak molecular or Van der Waals forces (ref. 3).

SOLIDS WITH VARIOUS CRYSTAL STRUCTURES

Peterson and Johnson (ref. 1) made a rather complete investigation of the friction and wear characteristics of solids with various crystal

structures. A résumé of their studies and some examples are presented in this section.

As discussed in reference 1, there are three general types of layer-lattice crystal structure in AX_2 compounds: the $CdCl_2$ type, the CdI_2 type, and the MoS_2 type. In the $CdCl_2$ and the CdI_2 type lattices, the forces within the layer are more ionic in character than they are with the MoS_2 type lattice; the difference between the $CdCl_2$ type and the CdI_2 type is in the position of one layer upon the other. Although only MoS_2 and WS_2 have the MoS_2 lattice type, there are numerous compounds that have the $CdCl_2$ and the CdI_2 type structure. A list of such AX_2 compounds formed by common divalent and quadrivalent cations and anions along with their crystal types is shown in table 8–I.

TABLE 8–I.—CRYSTAL TYPES OF AX_2 COMPOUNDS [a]

Metal	Type of compound					
	Fluoride	Chloride	Bromide	Iodide	Hydroxide	Sulfide
Mg	CaF_2	$CdCl_2$	CdI_2	CdI_2	CdI_2	-----
Ca	CaF_2	-----	-----	CdI_2	CdI_2	-----
Ti	TiO_2	-----	-----	-----	-----	CdI_2
Mn	TiO_2	$CdCl_2$	CdI_2	CdI_2	CdI_2	FeS_2
Fe	-----	$CdCl_2$	CdI_2	CdI_2	CdI_2	FeS_2
Co	-----	$CdCl_2$	CdI_2	CdI_2	CdI_2	FeS_2
Ni	-----	$CdCl_2$	$CdCl_2$	$CdCl_2$	$CdCl_2$	FeS_2
Zn	TiO_2	$CdCl_2$	CdI_2	CdI_2	CdI_2	-----
Sr	CaF_2	CaF_2	-----	-----	-----	-----
Mo	-----	-----	-----	-----	-----	MoS_2
Pd	-----	$CdCl_2$	-----	-----	-----	CdI_2
Co	-----	$CdCl_2$	$CdCl_2$	CdI_2	CdI_2	CdI_2
Sn	-----	-----	-----	-----	-----	CdI_2
Ba	CaF_2	-----	-----	-----	CdI_2	-----
W	-----	-----	-----	-----	-----	MoS_2
Pt	-----	$CdCl_2$	-----	-----	-----	CdI_2
Hg	-----	$HgCl_2$	$HgBr_2$	$HgBr_2$	-----	-----
Pb	-----	$PbBr_2$	$PbBr_2$	CdI_2	-----	CdI_2

[a] From ref. 4.

The investigation of reference 1 was made to determine the lubricating effectiveness of several layer-lattice solids and to understand the basis of their lubricating action. A secondary purpose was to indicate whether or not a layer-lattice structure was sufficient as the primary criterion for a good solid lubricant.

Layer-Lattice Structure

The results of an investigation made with three solids that have the $CdCl_2$ type lattice ($CoCl_2$, $NiCl_2$, and $CdCl_2$) are reported in table 8–II. The results show that $CoCl_2$ and $CdCl_2$ were effective lubricants and that $NiCl_2$ was rated as an ineffective lubricant because the friction-

TABLE 8-II.—FRICTION WITH VARIOUS POWDERED SOLIDS[a]

Material	Coefficient of friction after—		Wear area, sq in.	Observed effect of solid on specimens
	1 min	30 min		
Effective lubricants				
MoS_2	0.017	0.047	0.0016	None
CdI_2	.04	.06	.0023	None
$CdCl_2$	.03	.07	.0019	None
WS_2	.05	.08	.0018	None
Ag_2SO_4	.14	.14	[b]	None
PbI_2	.28	.28	.0018	None
Graphite	.06	.11	.0034	None
$Zn(C_{18}H_{35}O_2)_2$	.07	.11	.0032	None
$CoCl_2$	.04	.10	.0020	Slight rusting
HgI_2	.18	.18	.0021	Appreciable corrosion
$CuBr_2$	.04	.06	.0021	Considerable rusting
AgI	.19	.25	.0033	None
SAE 60	.13	.108	.0020	----------
Ineffective lubricants				
$NiCl_2$	0.03	0.10–0.15	0.0024	Rusting
$Ca(OH)_2$	.18	.2 – .25	.0026	None
$Mg(OH)_2$	.32	[c]	----	None
TiS_2	.20	[c]	----	----------
I_2	.15	.30	----	----------
$HgCl_2$	.32	.38	----	Appreciable corrosion
$PbCl_2$	.31	.45	.0029	None
AgCN	.02	-----	.0036	----------
CuCl	.38	.37	.0029	Slight rusting
Na_2SO_4	.36	[c]	----	None
Fe_3O_4	[c]	-----	----	None
BN	[c]	-----	----	None
NiO	[c]	-----	----	None
Mica	[c]	-----	----	None
Talc	[c]	-----	----	None

[a] From ref. 1.
[b] Negligible.
[c] Failed to lubricate.

time curve showed an upward trend in spite of a very low initial friction coefficient. An investigation was also made with compounds that have the CdI_2 structure ($Mg(OH)_2$, TiS_2, PbI_2, $Ca(OH)_2$, and CdI_2). Solid iodine was included for comparison purposes. In general, of this group, only CdI_2 and PbI_2 were effective lubricants (table 8–II). PbI_2, however, had a relatively high friction coefficient in spite of the fact that it afforded complete surface protection to the specimens. All other solids showed an upward trend in the friction-time curves and, hence, were rated ineffective. With both CdI_2 and

PbI_2, a continuous film was maintained on both the slider and the disk, as was confirmed by visual observation of the specimens after test.

An investigation of reference 1 included several layer-lattice solids (chosen from ref. 4) that were not of the $CdCl_2$, CdI_2, or MoS_2 type structure. These included HgI_2, $PbCl_2$, $CuBr_2$, Ag_2SO_4, and isomorphous Na_2SO_4. Results for these solids are also shown in table 8–II. HgI_2 was an effective lubricant in spite of the fact that the friction coefficient was relatively high (0.18). The results for $PbCl_2$ and $HgCl_2$ showed that these solids were not effective lubricants. Both of them showed friction-time curves which were high and erratic as well as having an upward trend. For the solid $CuBr_2$, whose structure consists of $CuBr_2$ chains arranged in such a way that a layer structure is produced (ref. 5), friction was low throughout the test and a continuous film was maintained on the slider and disk. This film, however, decomposed rapidly when exposed to moisture. The result indicates that other compounds with this chain structure may be effective solid lubricants. Because of its instability in the presence of moisture, however, $CuBr_2$ does not appear suitable for moist atmospheres. A comparison is made of the results of the lubricating effectiveness of the layer-lattice solids, Ag_2SO_4 and isomorphous Na_2SO_4. While the friction for Ag_2SO_4 was relatively high, it can be rated as an effective lubricant because it forms a continuous film. With Na_2SO_4, however, the friction was high and complete surface failure was obtained; thus Na_2SO_4 is rated as an ineffective lubricant.

Low-Shear-Strength Solids Without Layer-Lattice Structure

Several compounds with low-shear-strength, but without layer-lattice structure were investigated in reference 1; these compounds include AgCN, CuCl, and AgI. Of these three compounds, only AgI proved to be an effective lubricant; it showed results similar to those of many of the layer-lattice lubricants: namely, the formation of a continuous film on the two rubbing specimens.

Discussion of Results

When used in loose powder form, the ability of a solid to lubricate seems to be associated with its ability to form a film on the surface. Those materials that do not form a film show surface failure. If a thick film is built up on both the slider and the disk, the friction force reflects the shear strength of the solid lubricant. Those materials that adequately protect the surfaces from galling and wear are considered most effective as solid lubricants. In the experiments of reference 1, the materials that retained an effective film on the slider and disk and thus gave low friction and low wear were MoS_2, graphite (in moist air), $Zn(C_{18}H_{35}O_2)_2$ (zinc stearate), $CuBr_2$, $CoCl_2$, HgI_2, PbI_2, Ag_2SO_4, $CdCl_2$, AgI, CdI_2, and WS_2.

Type of structure can be a useful guide in the selection of low-shear-strength materials. For example, materials of the $CdCl_2$, CdI_2, and other layer-lattice types generally show promise, and although they were not as effective as MoS_2, they were at least as effective as zinc stearate or graphite in the tests of reference 1. An example of the inadequacy of type of structure as the sole guide is apparent when the results for the layer-lattice solids, Ag_2SO_4 and Na_2SO_4, are compared; Ag_2SO_4 was an effective lubricant and Na_2SO_4 failed to lubricate.

The ability of a loose powdered solid lubricant to form and maintain a continuous film is influenced by the materials being lubricated, the surface finish, the presence of other films, the environment, the method of application, and other factors. Use of solid lubricants in loose powder form must recognize these factors.

METALS, OXIDES, MOLYBDATES, AND TUNGSTATES

Peterson, et al. (ref. 2) made a study of metals, oxides, molybdates, and tungstates as loose, powdered lubricants. Their results are summarized in table 8–III, where the influence of test temperature and melting point are shown. In general, the results of experiments with the metals, silver, gold, and lead, at temperatures below their melting point showed high friction coefficients (greater than 0.3, generally). On the other hand, at a temperature above the melting point for lead, the friction coefficient was relatively low, 0.17. In this case, of course, the lead was present as a molten film and lubrication was quasi-hydrodynamic.

Peterson, et al. state that silver appears to be one of the best lubricants for use over the entire temperature range even though friction is higher at room temperature than desirable. Another limitation of silver is that oxidation of the underlying surface reduces the bonding of a silver film; the film then has a tendency to spall from the surface. Experiments with silver films over a temperature range from room temperature to 650° C (1200° F) showed that, as temperature was decreased from 650° C (1200° F) toward room temperature, friction coefficient rose considerably when the temperature approached 300° C (572° F). This rise in friction corresponds almost directly with changes in the tensile strength of silver (ref. 6).

Peterson, et al. also state ". . . of the oxides tested [at 704° C (1300° F)], PbO, MoO_3, WO_3, Co_2O_3, ZnO, CdO, Cu_2O, and SrO flowed into a continuous solid film and prevented surface damage even though the friction was high in many instances." The lowest friction obtained was with PbO. Although the friction was higher when the other oxides were used, there was no surface damage to the friction specimens in any case. With the harder oxides, the sliding action merely brushed the compound from the surface and considerable

TABLE 8-III.—FRICTION OF VARIOUS MATERIALS AS LUBRICANTS [a]

Material	Melting point, °C	Test temperature, °C	Coefficient of friction
Metals			
Ag	960.5	788	0.40
Ag	960.5	27	.40
Au	1063	788	.57
Al	660	427	1.00
Pb	327.5	260	.35
Pb	327.5	649	[b].17
Pb	327.5	27	.24
Oxides			
B_2O_3	577	650	[b]0.14
PbO	888	704	.12
MoO_3	795	704	.20
MoO_3	795	482	.59
Co_2O_3	[c]900	704	.28
WO_3	2130	704	.55
Cu_2O	1235	704	.44
ZnO	1800	704	.33
CdO	[c]900–1000	704	.48
NiO	Ni_2O_3 at 400	704	[d]
Fe_3O_4	[c]1528	740	[d]
Cr_2O_3	1900	740	[d]
Molybdates			
$PbMoO_4$	1065	704	0.32
$PbMoO_4$	1065	27	.50
Tungstates			
Na_2WO_4	700	704	0.17
Na_2WO_4	700	27	.55

[a] Data from ref. 2.
[b] Molten film.
[c] Decomposes.
[d] Failed.

surface damage took place. With these hard oxides, therefore, effective lubrication was not obtained. MoO_3 showed some promise at 704° C (1300° F) but poor results at 482° C (900° F).

At a test temperature of 704° C (1300° F), some of the molybdates and tungstates gave reasonably good results from the standpoint of low friction coefficient and protection from surface damage. Friction tests at lower temperatures, however, with even the most promising materials indicated that the oxides, molybdates, and the tungstates were relatively ineffective as loose powders. Each of the compounds

was brushed from the surface and considerable surface damage was obtained.

Excellent sliding characteristics were observed with molten B_2O_3 as shown in table 8–III. This might be expected since B_2O_3 is a "glass" and glasses have been used as metal working lubricants at high temperatures for a number of years (ref. 7). B_2O_3 has also been used as a component of a ceramic binder to bond solid lubricants such as CaF_2 to the surface of metals to be lubricated; the glass-forming tendency of B_2O_3 is very useful under these conditions (ref. 8).

As previously mentioned, the static shear strength of a crystalline solid should be theoretically predictable on the basis of the solid's latent heat of fusion, its density, its melting temperature, and the actual operating temperature. The theoretical equation for shear strength was derived by Merchant (ref. 9). Peterson, et al. (ref. 2) checked the correlation between melting point and friction coefficient for the molybdates and tungstates. They found that the correlation was reasonable for these materials at temperatures between 600° and 1400° C (1112° and 2552° F).

MOLYBDENUM DISULFIDE

Bonded Films

As is well known, molybdenum disulfide is a solid lubricant material which has found wide acceptance and is extremely useful in lubricating mechanisms that must operate under conditions where normal lubrication is not entirely adequate. Some experimental friction results with MoS_2 compared with graphite, SAE 10 oil, and operation of the friction specimens unlubricated are shown in figure 8–1. Approxi-

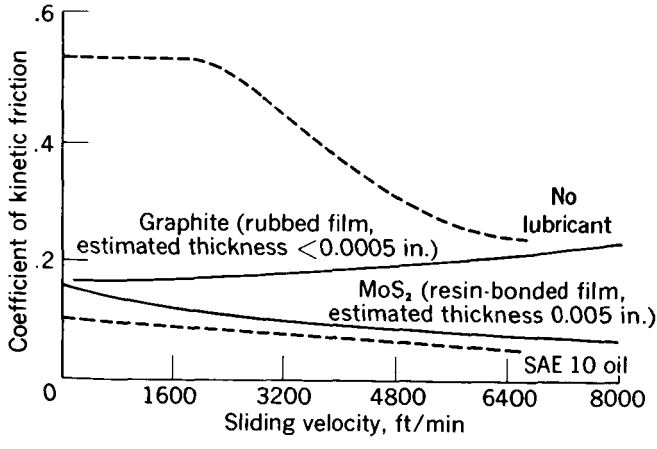

FIGURE 8–1.—Friction at high sliding velocities of steel against steel with preformed films of molybdenum disulfide and graphite. Radius of spherical rider specimen, ⅛ inch. (From ref. 42.)

mately equal friction coefficients are obtained at the lowest sliding velocity for the two solid lubricants, MoS_2 and graphite. At the higher sliding velocities, the divergence of the curves is caused by the manner of application of the two solid lubricants. The MoS_2 was resin-bonded to the surface (estimated thickness, 0.005 in.) while the graphite was simply rubbed on the surface (estimated thickness, less than 0.0005 in.). As a result, the graphite was not a continuous film as was the MoS_2 and, hence, could not withstand the severe conditions of operation (such as high sliding velocities) as well as MoS_2. A resin-bonded graphite film will give results similar to those with the resin-bonded MoS_2, as will be shown in a later figure. The friction coefficient for MoS_2 in all cases is higher than that reported by some other investigators. This probably results from the fact that the conditions, particularly the initial Hertz stress of 126,000 psi between the contacting surfaces, were very severe in these experiments.

Resin-bonded MoS_2 films are extremely effective in many lubricating applications. Early research at NASA on the bonding mechanisms between MoS_2 and various metallic surfaces, as well as glass, indicated that the MoS_2 particles were bound to each other and to the surface by the resin (ref. 10). It was also found in the studies of reference 10 that any resin-forming organic fluid would provide a reasonably good bond for MoS_2 (and other solid lubricants of this type) to the surface. Included among such resin-forming liquids are such things as corn syrup, glycerol, silicone varnish, and an asphalt-base resin. Each of these four liquids was shown (ref. 10) to form a resin which bonded quite effectively to the surface.

Unfortunately, resins such as those previously described are temperature limited themselves. In consequence, as the operating temperature of a mechanism with a bonded MoS_2 film is increased, a threshold temperature is reached at which the bond begins to break down and friction and wear both increase rapidly. This result is illustrated in figure 8–2. It will be noted that at temperatures above 600° F both friction coefficient and wear increase sharply. This result can be attributed to failure of the resin binder. (Time of exposure to temperature could influence the position of the curves of fig. 8–2; sufficient data to show this effect are not yet available.) These results indicate that a different class of binder is required for high-temperature operation. This new class of binder as applied to different solid lubricants will be discussed later.

MoS_2 bonded with a sodium silicate binder, as developed by Devine, Lamson, and Bowen (ref. 11), appears promising under various conditions such as at high temperatures (to 750° F) or under radiation (gamma-ray exposure to 5×10^9 r). A typical coating composition includes 66 percent MoS_2, 11 percent graphite, and 23 percent sodium

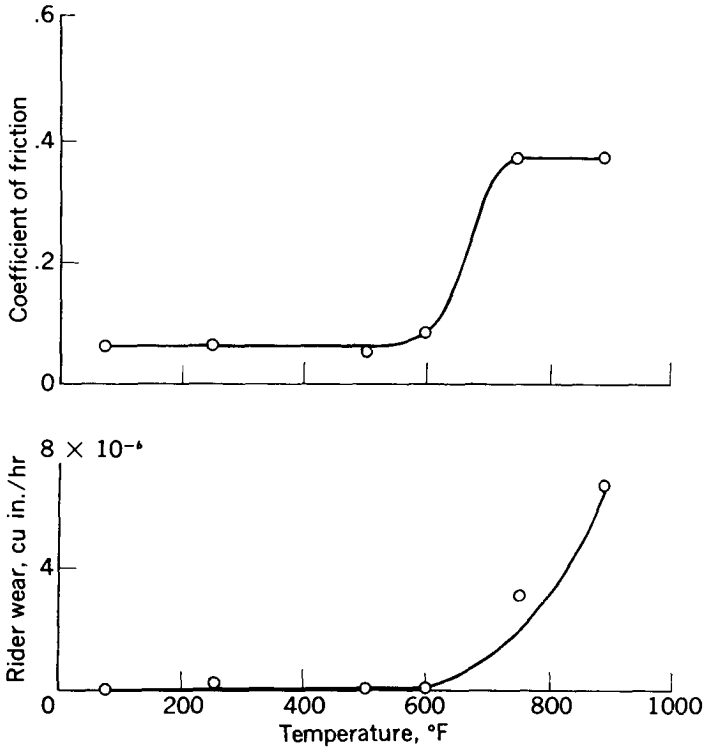

FIGURE 8–2.—Effect of temperature on lubricating properties of resin-bonded molybdenum disulfide. Coating thickness, 0.0003 inch; sliding velocity, 430 feet per minute; load, 1000 grams. (From ref. 43.)

silicate. There will be more discussion of the results of reference 11 in chapter 11.

Loose Powders

Loose powdered solids have been used for a number of years quite successfully for lubrication of ball bearings at temperatures to 1000° F. Figure 8–3 shows the results of one of these bearing investigations. As shown in the figure, lubrication with graphite in air was completely successful to and including 1000° F. The bearing was in excellent condition after the test. With molybdenum disulfide in air, failure took place at about 800° F. With MoS_2, oxidation begins to take place at a temperature of about 750° F, as is discussed later in this chapter. Since the oxidation products of MoS_2 are molybdenum trioxide, MoO_3, and a sulfur compound, there are problems with both abrasion and corrosion. Since the mechanism of failure with MoS_2 in air was known, the use of a nonoxidizing (inert) atmosphere should improve the situation. The point at 1000° F labeled MoS_2—nitrogen

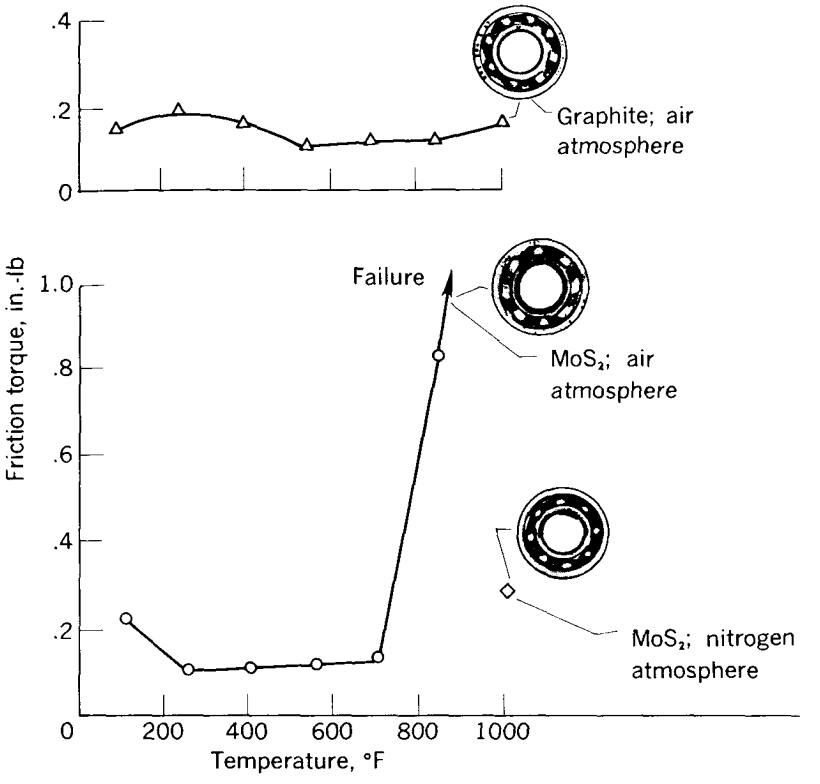

FIGURE 8–3.—Lubrication of ball bearing with powdered solids at temperatures from 100° to 1000° F. (From ref. 44.)

atmosphere showed that it was possible to operate a ball bearing lubricated with MoS_2 at 1000° F for 20 hours without failure provided that an inert atmosphere (nitrogen) was used.

Confirming evidence of the good bearing lubrication results of MoS_2 in nitrogen was obtained in the studies of reference 12. These studies showed promise for this combination as a lubricant for 20-millimeter-bore ball bearings at speeds to 30,000 rpm, thrust loads of 100 pounds, and temperatures from 80° to 1200° F for periods to 10 hours. Mixtures of MoS_2 and metal-free phthalocyanine in a nitrogen atmosphere also appeared promising under these conditions.

The friction characteristics of MoS_2 and WS_2 in oxidizing (air) and in inert (argon) atmospheres are shown in figure 8–4. Both solid lubricants were effective to higher temperatures in the nonoxidizing atmosphere (argon). In the oxidizing atmosphere (air), MoS_2 and WS_2 oxidized to MoO_3 and WO_3. The results of studies by Johnson and Sliney (ref. 13) indicate that between 500° and 1200° F, WO_3 has

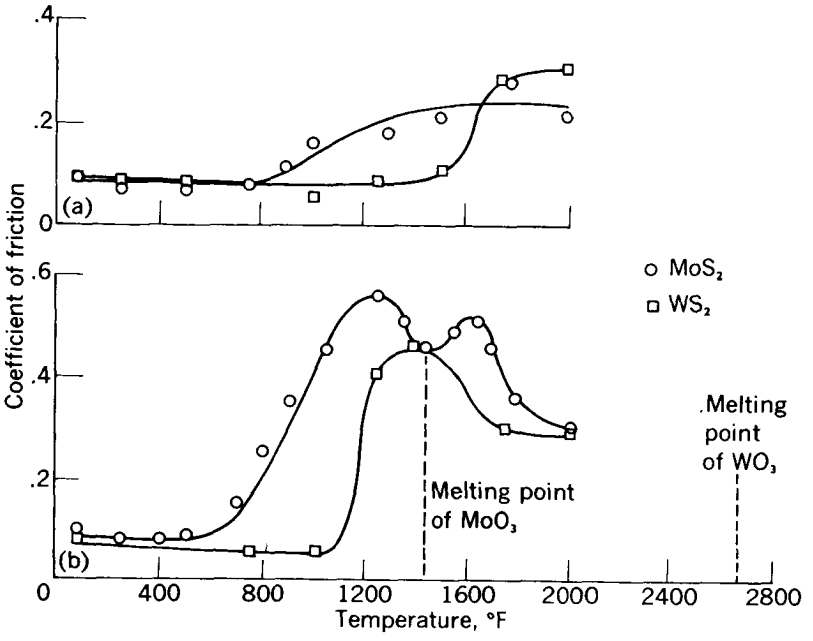

(a) Argon atmosphere.
(b) Air atmosphere.

FIGURE 8–4.—Friction of molybdenum disulfide and tungsten sulfide in air and argon. (From ref. 13.)

a friction coefficient considerably lower than that of MoO_3; friction coefficients with both oxides are, however, appreciably greater than those normally obtained with effective lubricants.

When solid lubricants are used, it is extremely important that the solid be highly purified. Small amounts of certain contaminants can result in extremely large increases in wear as is shown in figure 8–5. Wear was increased by a very large amount in changing from a silica content of 0 to 0.5 percent; further increases in silica content resulted in lesser increases in wear. The friction coefficient was influenced very little over the entire range of concentration of silica; these results illustrate, again, the lack of direct correlation between friction and wear.

Powdered Metal Mixes Containing Molybdenum Disulfide

One obvious means of utilizing a solid lubricant in part of a mechanism which is practically inaccessible involves the addition of the solid lubricants to powdered metal mixes to form the component of the mechanism. An investigation was made to check the feasibility of this method of lubrication (ref. 14). The results of this investiga-

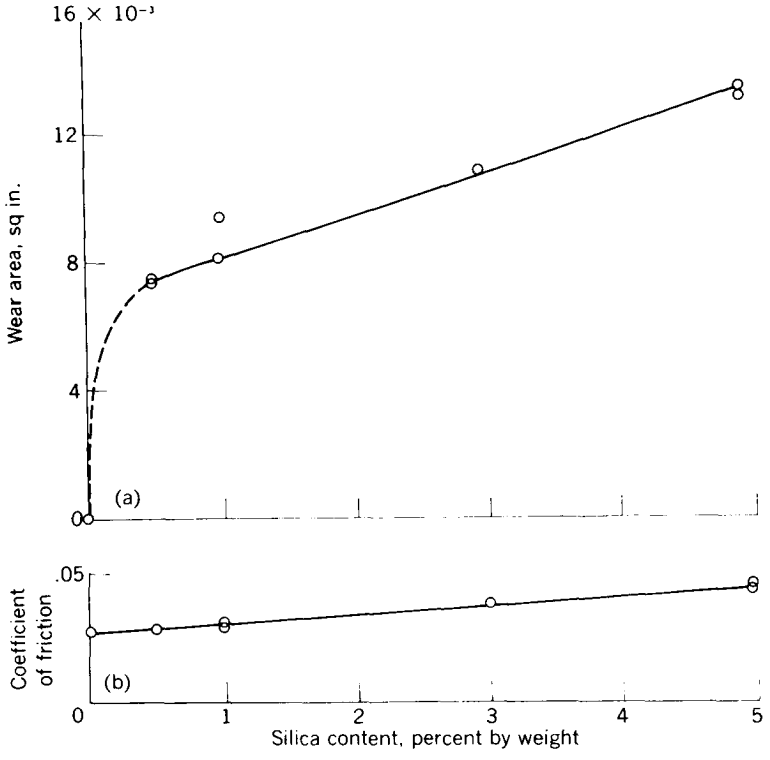

(a) Wear.
(b) Friction.

FIGURE 8-5.—Effect of additions of silica to a highly purified grade of molybdenum disulfide on wear and friction of steel specimens in dry air. Sliding velocity, 5.7 feet per minute; load, 40 pounds; duration of run, 6 hours. (From ref. 45.)

tion are shown in figure 8-6. The investigation consisted of adding various percentages of MoS_2 to a 5 percent copper, 95 percent silver mixture. As MoS_2 was added, the percentage of silver was decreased. The friction coefficient was little affected by increases in concentration of MoS_2 (fig. 8-6). On the other hand, wear was very strongly influenced by the concentration of MoS_2. High wear at low concentrations resulted from lack of effective lubrication; high wear at high concentrations probably resulted from lack of physical strength of the material. Since the specimens are operated without external lubrication, such materials show some promise for severe conditions of load, speed, and lack of lubrication. In these experiments, welding (as observed visually) was absent for all compacts that contained 5 percent or more MoS_2. The material apparently formed an effective lubricant film on the surface by transfer of solid lubricant from within the structure of the material.

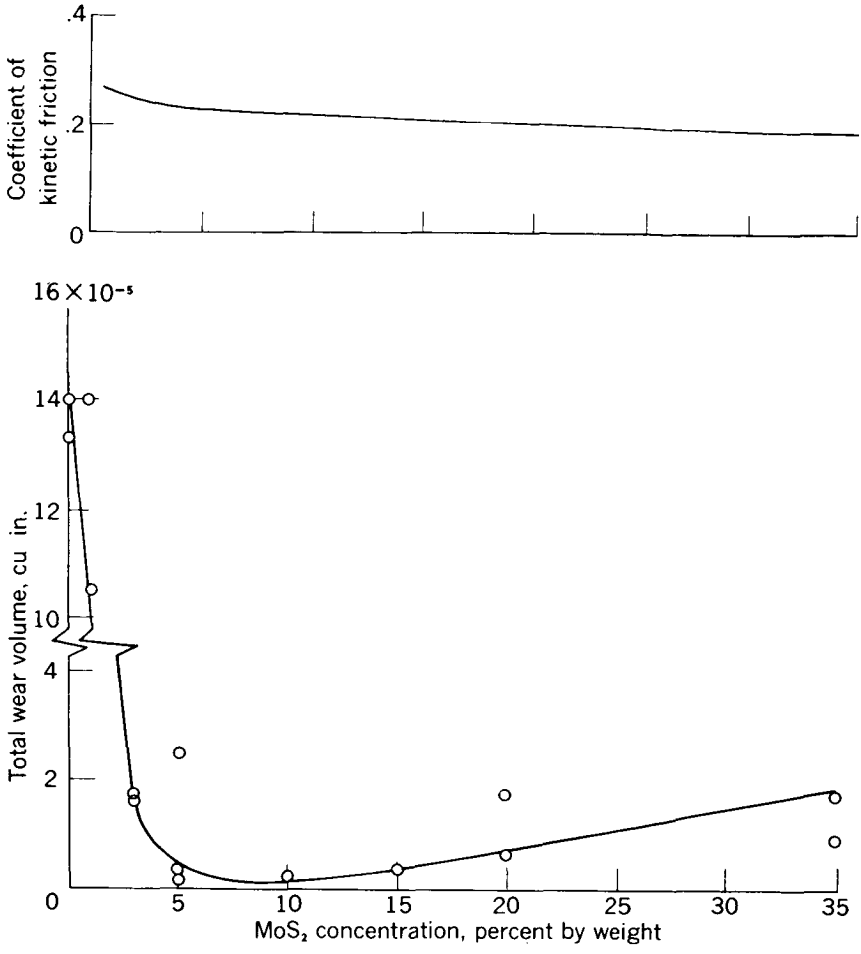

FIGURE 8–6.—Wear and friction of powder metallurgy specimens containing molybdenum disulfide. (From ref. 14.)

Oxidation of Molybdenum Disulfide

An X-ray diffraction investigation of the chemical stability at high temperatures of MoS_2 was made (ref. 15). This investigation showed that, in vacuum, there is no phase change of the MoS_2 at temperatures to 1000° F. In the presence of oxygen, however, MoS_2 oxidized to molybdenum trioxide (MoO_3) at a very low rate at 750° F; the rate of oxidation increased steadily with increase in temperature as shown in figure 8–7. (Time of exposure to temperature can influence oxidation; this time factor is not shown in fig. 8–7).

Friction studies were made (ref. 15) of a film of pure MoO_3 applied to a clean steel disk by an evaporation technique; the MoO_3 was con-

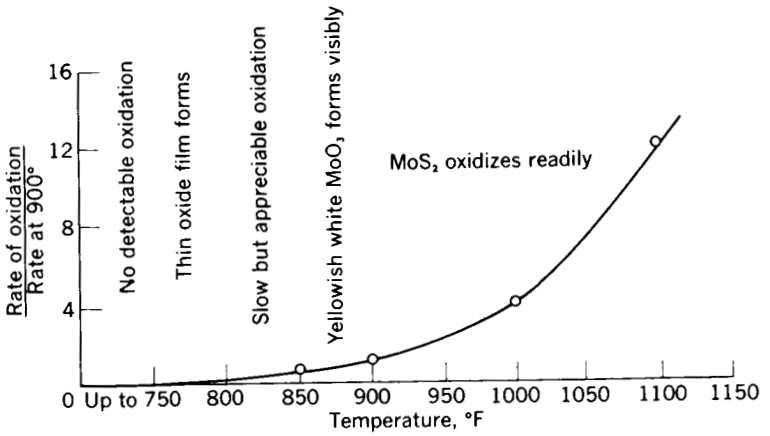

FIGURE 8–7.—Oxidation characteristics of molybdenum disulfide in air. (Data from ref. 15.)

densed from the vapor state on a steel disk until a film approximately 0.003 inch thick was present. Friction coefficients obtained with this film (upper curve of fig. 8–8) were higher than those for clean steel on clean steel at all sliding velocities. Studies were also made (ref. 15) of an evaporated MoO_3 film applied to a steel disk on which there

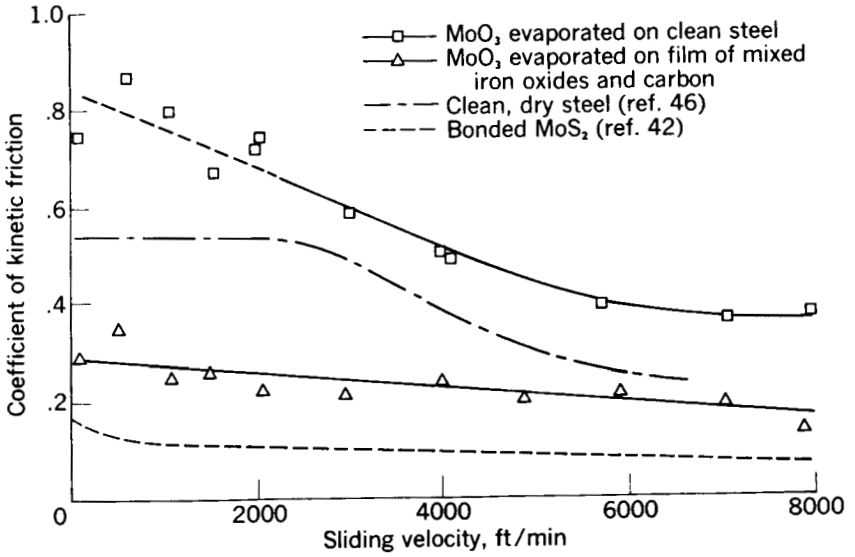

FIGURE 8–8.—Effect of evaporated molybdenum trioxide films on friction of steel against steel at high sliding velocities. Radius of spherical rider specimen, ⅛ inch. (From ref. 15.)

was a thin film of mixed iron oxides and carbon. (This base film was produced by painting the surface of the hot disk with corn syrup. As discussed in ref. 10, the corn syrup reduces Fe_2O_3 to Fe_3O_4 at high temperatures.) Friction with the evaporated MoO_3 film applied over the mixed iron oxides and carbon is shown in figure 8–8; friction coefficient for this film is higher than that for a bonded MoS_2 film, but lower than that with either MoO_3 on clean steel or for clean dry steel. These results illustrate the beneficial effect of the iron oxide (Fe_3O_4) on friction.

Further experiments with a film of MoO_3 were made (refs. 15 and 16); the results are shown in figure 8–9. The data show that a rubbed

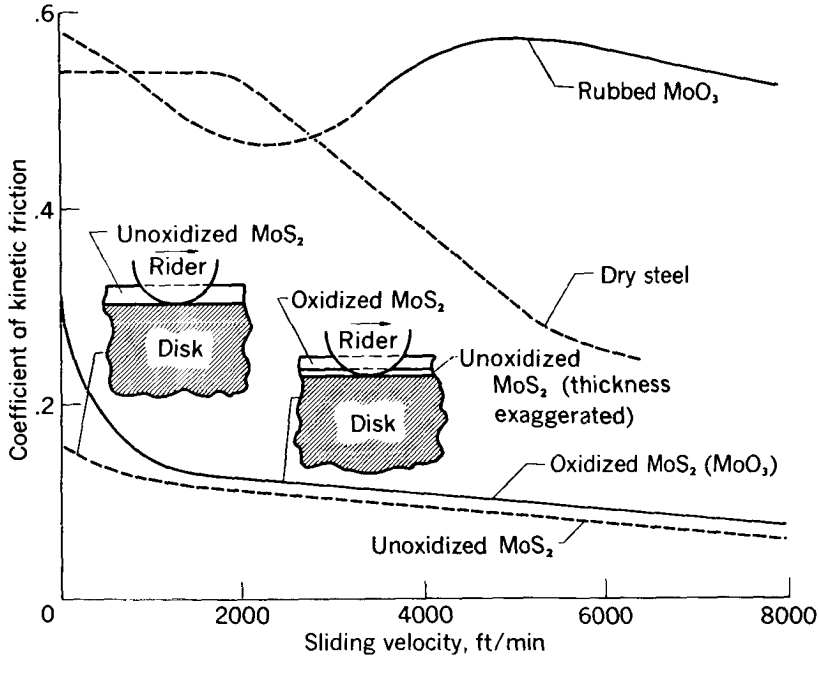

FIGURE 8–9.—Friction of unoxidized and oxidized molybdenum disulfide films. (From refs. 15 and 16.)

film of MoO_3 is a very poor lubricant, and its use resulted in high friction and excessive welding. The "oxidized" MoS_2 film, however, showed results remarkably similar to those for the unoxidized MoS_2 film. An explanation of the mechanism of the MoS_2 in the oxidized condition must consider the actual surface films in both oxidized and unoxidized conditions. Sketches of the two surface films based on an hypothesis that explains the mechanism are shown in the figure. While conditions in these experiments were intended to give as nearly

complete oxidation as possible, undoubtedly some fraction of the MoS_2 remained unoxidized. Even though this fraction was extremely small, it acts as an effective solid lubricant at the surface. The film immediately adjacent to the surface appears to be that part which produced the beneficial results.

Figures 8–8 and 8–9 show that MoO_3 is not an effective lubricant; these results are in direct contrast to those of reference 2, which reported good results with MoO_3. It should be noted, however, that the test temperature for the NASA (NACA) experiments was about 80° F, whereas the test temperature for the experiments of reference 2 was 1300° F.

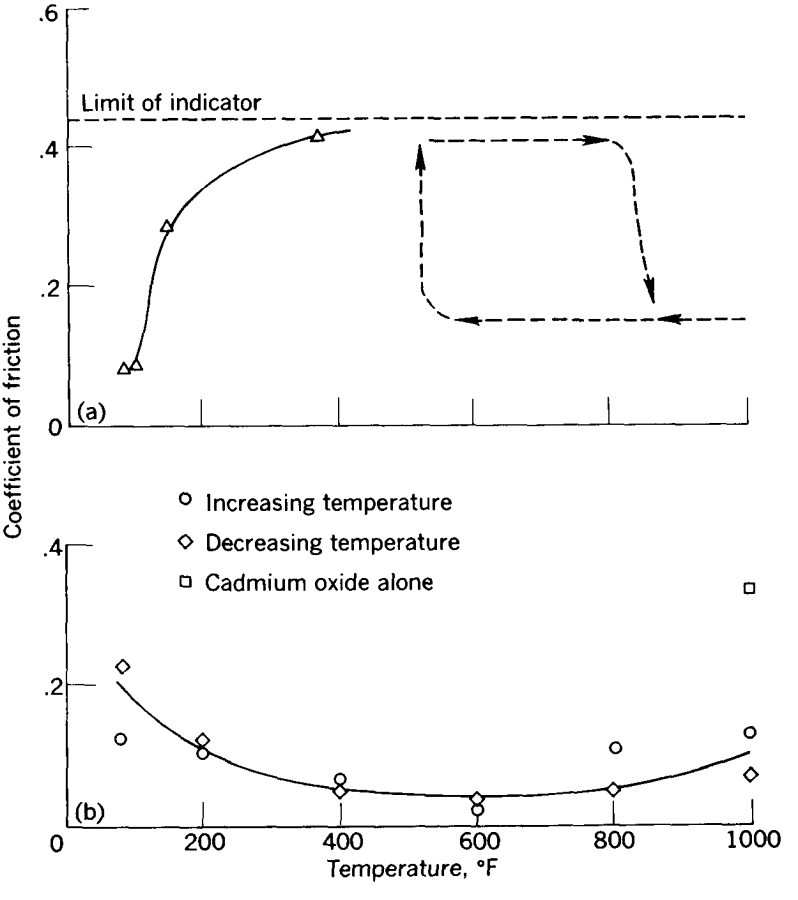

(a) Graphite alone.
(b) Cadmium oxide—graphite mixture.

FIGURE 8–10.—Lubrication with cadmium oxide—graphite mixture. Sliding velocity, 5.7 feet per minute; load, 40 pounds. (From ref. 47.)

GRAPHITE

High-Temperature Results

NASA–NACA has been working with graphite as a lubricant for quite a number of years, and the apparent inconsistency of results obtained with this material proved intriguing. Experiments indicated that graphite was a very effective lubricant at room temperature as well as at 1000° F, but was not always an effective lubricant at temperatures between these two extremes. As an example, the results of friction tests using powdered graphite as the solid lubricant for cast Inconel sliding against Inconel X are shown in figure 8–10(a). As will be noted in figure 8–10(a), the friction coefficient is quite low at room temperature, but increases rapidly as temperature rises to about 200° F; the friction coefficient is quite high at this temperature. Note, however, that as the temperature continues to increase the friction coefficient shows a marked reduction at temperatures above approximately 800° F and graphite is again an effective lubricant at 1000° F. The hysteresis loop shown on the right side of figure 8–10(a) between temperatures of 550° and 800° F could be reproduced many times. When the specimens were on the upper portion of the curve, the surfaces were severely galled and graphite was definitely *not* an effective lubricant. At 80° F, 1000° F, or on the lower portion of the hysteresis loop, graphite was a very effective lubricant. Remarkably similar results were obtained in the studies of reference 12. Low friction was obtained at low temperature and at high (to 1200° F) temperature; friction was high, however, in the temperature range from 300° to 800° F.

The obvious difference between the medium-temperature runs and the 1000° F runs is the amount of oxide which was formed on the metal surfaces. It was presumed, therefore, that the increase in the amount of oxide present at 1000° F aided the graphite lubrication by improving adherence of the graphite powder to the metal.

Confirming evidence of the peculiar results obtained with graphite as the lubricant over the temperature range from 75° to 1000° F was obtained in some bearing experiments. These results (fig. 8–11) show that for ordinary nondried graphite (the triangular points) the friction torque with a small bearing was relatively constant over the entire temperature range. With dry graphite and dry air, however, the friction torque at 700° F is considerably higher than that over the remainder of the run. This result partly confirms the results already discussed for the friction studies: that is, graphite is a good lubricant at room temperature and at 1000° F, but is not as effective at some intermediate temperature. This result again is considered to be an effect of the oxide formation on metal surfaces.

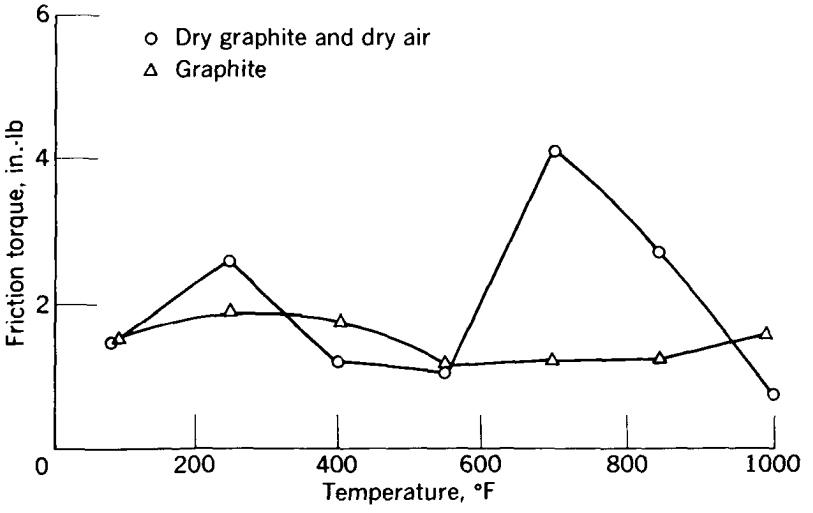

FIGURE 8–11.—Lubrication of bearings with graphite. Rotational speed, 2500 rpm; thrust load, 110 pounds; atmosphere, air; bearing cage, beryllium copper. (From ref. 44.)

Mechanism of Lubrication With Powdered Graphite

The data previously presented show that graphite effectively lubricates various metal combinations at low temperatures and at high temperatures but not at all intermediate temperatures. The generally accepted theory (that graphite lubricates because of adsorbed water or gaseous films) seems incapable of explaining these results. Therefore, a supplementary hypothesis is advanced.

It is hypothesized (ref. 17) that effective lubrication is possible with powdered graphite provided *either* of two conditions is met: (1) an adsorbed water or vapor film is present, or (2) an oxide film of the proper type is continuously present on one or both of the lubricated surfaces. The oxide film is believed to improve the adherence of graphite to the surface. In this hypothesis, it is presumed that graphite is a lubricant at all temperatures and that the indicated failures of graphite to lubricate under adverse conditions in the past have been due to the lack of proper adherence of the powdered graphite to the surfaces to be lubricated.

The severe wear of carbon brushes in World War II aircraft flying at high altitudes, which was attributed to the lack of moisture to provide an adsorbed film on the surface, can just as well be attributed to another reason. It must be appreciated that as altitude increases the availability of oxygen is decreased markedly; hence, the oxide-forming capabilities of the metal surface of the commutator are also sharply reduced. Reduction in amount of oxides on the commutator

could therefore result in increased carbon brush wear through lack of formation on the commutator of a beneficial mating graphite film.

In order to check the hypothesis, experiments were designed (ref. 17) to show the influence of atmosphere on the lubricating effectiveness of graphite. These experiments included friction studies with cast Inconel sliding on Inconel X in an atmosphere of

(1) Forming gas (7 percent hydrogen, 93 percent nitrogen)
(2) Dry air
(3) Moist air

Other experiments were made with ball bearings running in

(1) Ordinary air (includes moisture)
(2) Dry air
(3) Dry purified nitrogen
(4) Moist purified nitrogen
(5) Forming gas

With these experiments, the effects of oxidizing, reducing, inert, and moist atmospheres could be observed. The forming gas was considered to be an effective reducing medium at the temperature of these experiments, 1000° F.

The results of the friction experiments in these various atmospheres are shown in figure 8–12. In forming gas, graphite was not an effective

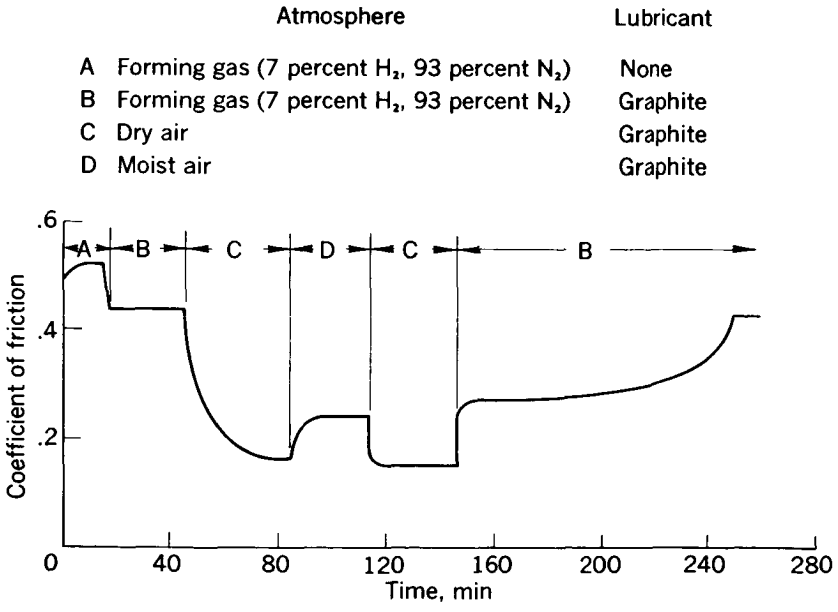

FIGURE 8–12.—Effect of atmosphere on lubrication with graphite. Temperature, 1000° F. (From ref. 17.)

lubricant. In either dry air or in moist air, graphite was an effective lubricant, and the friction coefficient was of the order of 0.2. During the period of time from about 150 to 250 minutes, after an oxide film had formed on the specimens and forming gas was subsequently introduced as the atmosphere, some time lapsed for the oxide film to wear off and, hence, for the friction coefficient to increase. However, friction coefficient did finally return to a value very nearly that obtained in the first run in forming gas.

The results of the bearing experiments show that at 1000° F in either dry air or moist air the bearings ran successfully for a number of hours (ref. 17). The bearing run in dry purified nitrogen failed after 5¼ hours. The bearing run in moist nitrogen ran successfully for 20 hours although the friction torque with this bearing was appreciably higher than that in dry air.

The bearings after experiments conducted in a reducing atmosphere or in air at 1000° F are shown in figure 8–13. In dry forming gas (a

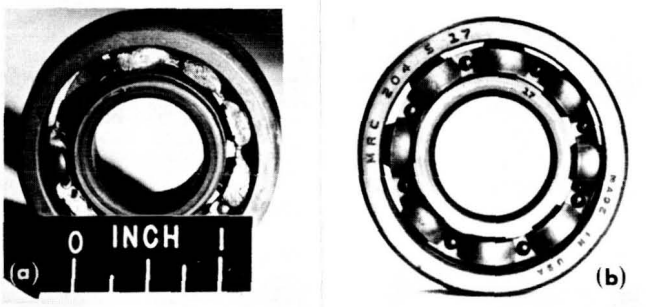

(a) Reducing atmosphere. (b) Air atmosphere.

FIGURE 8–13.—Bearings lubricated with graphite. Temperature, 1000° F. (From ref. 17.)

reducing atmosphere), the friction torque of the bearing increased fivefold over a period of 5½ hours and the bearing failed, as is shown in the photograph. For comparison, a bearing run in air for 20 hours at 1000° F is shown on the right side of figure 8–13; this bearing is in excellent condition.

Mixtures of Graphite With Soft Oxides and Salts

As previously shown in figure 8–10(b), mixtures of graphite and soft oxides can be appreciably effective over a broad temperature range from 100° to 1000° F, even though the graphite alone does not lubricate effectively over this entire temperature range and the soft oxide alone is not a particularly effective lubricant at the maximum temperature. A cadmium oxide—graphite mixture (fig. 8–10(b)) has friction coefficients in the order of 0.1 or less over most of the tem-

perature range from 100° to 1000° F. As shown in figure 8–10(a), graphite is not an effective lubricant over the entire temperature range; also, cadmium oxide is a relatively poor lubricant at a temperature of 1000° F, having a friction coefficient greater than 0.3 (fig. 8–10(b)). In spite of this, the mixture is, however, effective over the entire temperature range. The cadmium oxide is presumed to improve the adherence of graphite to the surface and, hence, to improve the lubricating effectiveness.

In studies of reference 12 a graphite—cadmium oxide mixture appeared very promising as a lubricant for 20-millimeter-bore ball bearings at speeds to 30,000 rpm, loads of 100 pounds, temperatures of 80° to 1200° F, and periods of time to 10 hours.

Figure 8–14 shows results with mixtures of sodium sulfate and graphite, as well as with a resin-bonded graphite film. The results of the mixture compare favorably with the results of a resin-bonded graphite film at 400° F. Interpretation of these results would imply that the metallic salt may be acting as a bonding agent for the graphite. The fact that the preheated mixture gave identical results shows that residual moisture present on the salts does not substantially influence the results.

The results of figure 8–14 illustrate the effectiveness of graphite when applied as a resin-bonded film. These results are in contrast to those of figure 8–1 which are for a *rubbed* graphite film. As shown in figure 8–14, friction coefficient is very low when the graphite is present as a continuous, bonded film.

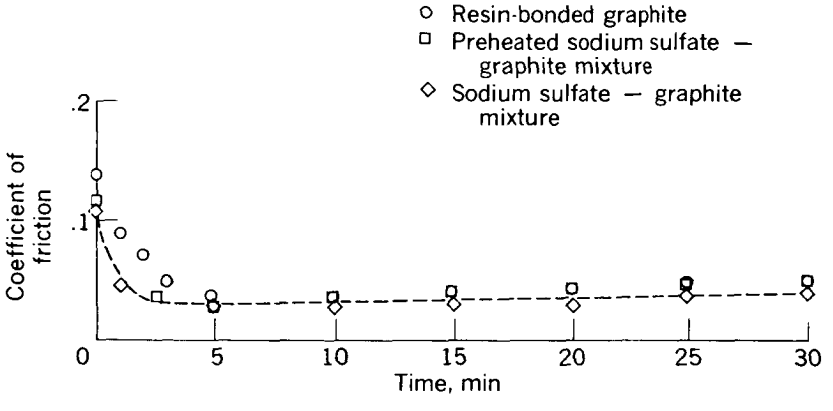

FIGURE 8–14.—Effect of sliding time on the friction coefficient of cast Inconel sliding against Inconel X with resin-bonded graphite, preheated sodium sulfate—graphite mixture, and sodium sulfate—graphite mixture as lubricants. Lubricant not returned to track; sliding velocity, 5.7 feet per minute; load, 40 pounds; temperature, 400° F. (From ref. 47.)

LEAD MONOXIDE

Loose Powders

Lead monoxide (PbO) was shown by Peterson and Johnson (ref. 18) to be an effective lubricant at 1000° F and possibly at higher temperatures. At lower temperatures, however, (700° to 900° F) PbO had poor oxidation resistance and was converted to red lead (Pb_3O_4), which is not a good lubricant. Fortunately, Pb_3O_4 will revert to PbO at temperatures of 1000° F or greater. These results are illustrated in figure 8–15; as shown, the friction coefficient is relatively low at 1000° F, but as temperature is decreased from 1000° F friction coefficient increases fairly rapidly.

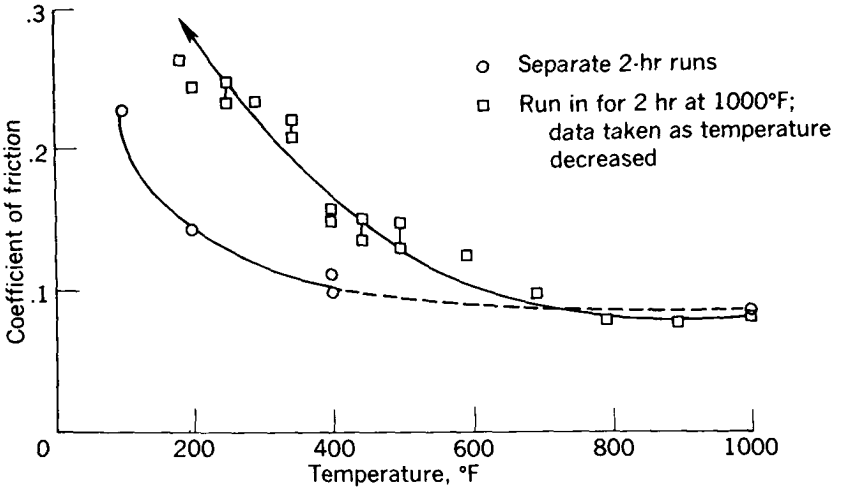

FIGURE 8–15.—Lead monoxide as a lubricant at varied temperatures. Cast Inconel sliding on Inconel X; sliding velocity, 5.7 feet per minute; load, 40 pounds. (From ref. 18.)

Thermochemical and chemical kinetics data are helpful in describing the oxidation characteristics of PbO. Thermochemical data from references 19 and 21 are presented in figure 8–16; here is plotted, as a function of temperature, the free-energy change (ΔF) involved in the formation of 1 mole of Pb_3O_4 by the oxidation of PbO. The curves intersect ΔF equals zero at 940° for oxygen ($p_{O_2}=1$ atm) and 850° F for air ($p_{O_2}=0.21$ atm). The negative values of ΔF at lower temperatures indicate that Pb_3O_4 is the more stable low-temperature oxide. Conversely, the temperature range over which ΔF is positive indicates that Pb_3O_4 will be reduced to PbO at these temperatures. Although thermodynamic data such as these indicate the direction in which a reaction tends, they give no indication as to *rate* of reaction.

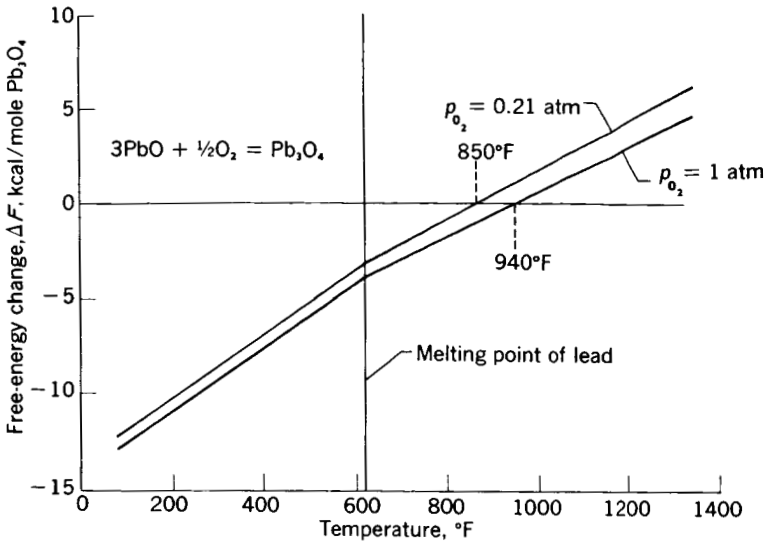

FIGURE 8–16.—Thermochemistry of lead monoxide at various temperatures. (From refs. 19 and 21.)

The oxidation rates of PbO at various temperatures are given in reference 20 and are plotted in figure 8–17. (This figure as well as the previous one and the discussion thereof are taken from ref. 21.) The

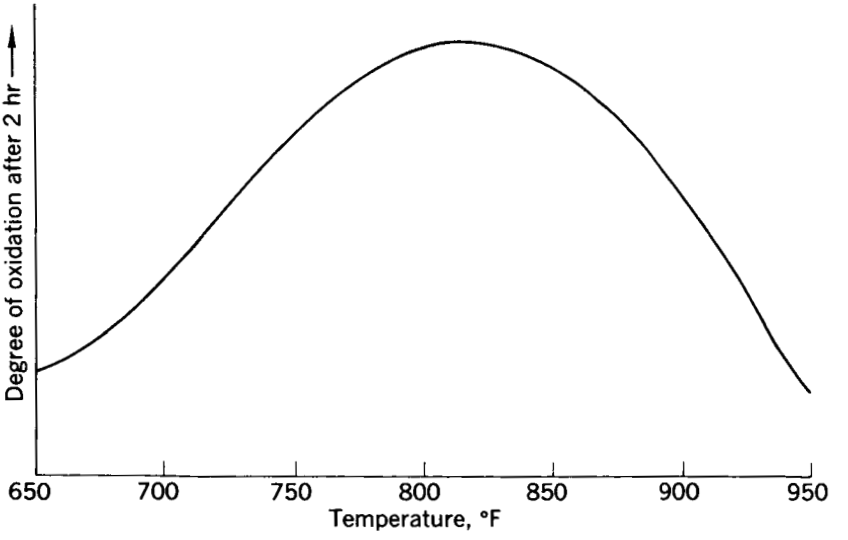

FIGURE 8–17.—Stability of lead monoxide at various temperatures. (From refs. 20 and 21.)

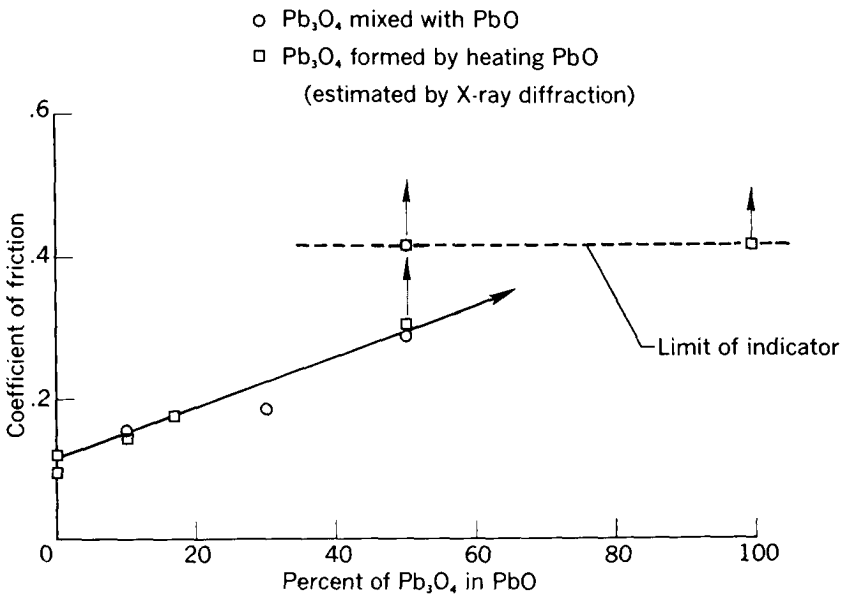

FIGURE 8–18.—Effect of red lead (Pb_3O_4) in lead monoxide on lubrication at 400° F. Cast Inconel sliding on Inconel X; sliding velocity, 5.7 feet per minute; load, 40 pounds. (From ref. 18.)

maximum oxidation rate occurs at 820° F and represents about 35 percent oxidation of PbO after 2 hours at temperature. The oxidation rate decreases to very low values below 650° F. Beyond the maximum, the oxidation rate extrapolates to 0 at 980° F in reasonable agreement with the thermodynamic data.

The presence of Pb_3O_4 in PbO at any time is undesirable because it reduces lubricating effectiveness as illustrated in figure 8–18. The data for figure 8–18 show that as the percentage of Pb_3O_4 in PbO is increased from 0 to 100 percent the friction coefficient increases fairly drastically, that is, from 0.1 at 0 percent Pb_3O_4 to greater than 0.4 at 100 percent Pb_3O_4.

There are a number of possible methods for inhibiting the oxidation of PbO. One of these methods is to combine it with other oxides capable of stabilizing the monoxide form of lead oxide. A second method is to disperse PbO particles throughout a second phase capable of physically shielding the particles from direct contact with the oxidizing atmosphere (ref. 21). Both methods for inhibiting oxidation of PbO can be achieved by fusing it with certain other oxides in order to form ceramic compositions having a duplex structure with PbO dispersed throughout a second phase.

Bonded Films

The desirable properties of ceramic-composition lubricant coatings are as follows:

(1) Low friction and wear under service conditions
(2) Duplex structure:
    (a) Low-shear-strength solid lubricant for lubrication under moderate sliding conditions
    (b) Relatively hard matrix with glaze-forming tendencies for high-temperature lubrication
(3) Expansion coefficient that matches that of the base metal
(4) Good oxidation resistance and chemical stability at high temperatures

A study of the binary phase diagrams for PbO indicated that a duplex structure might be obtained in a PbO-base ceramic containing small amounts of silica (SiO_2). The phase equilibrium diagram for the PbO-SiO_2 system is shown in figure 8–19. This phase diagram is taken from reference 48. The reason for choice of the PbO-SiO_2 system is discussed in detail by Sliney and Johnson (ref. 43). Some of their discussion is included in the following paragraphs.

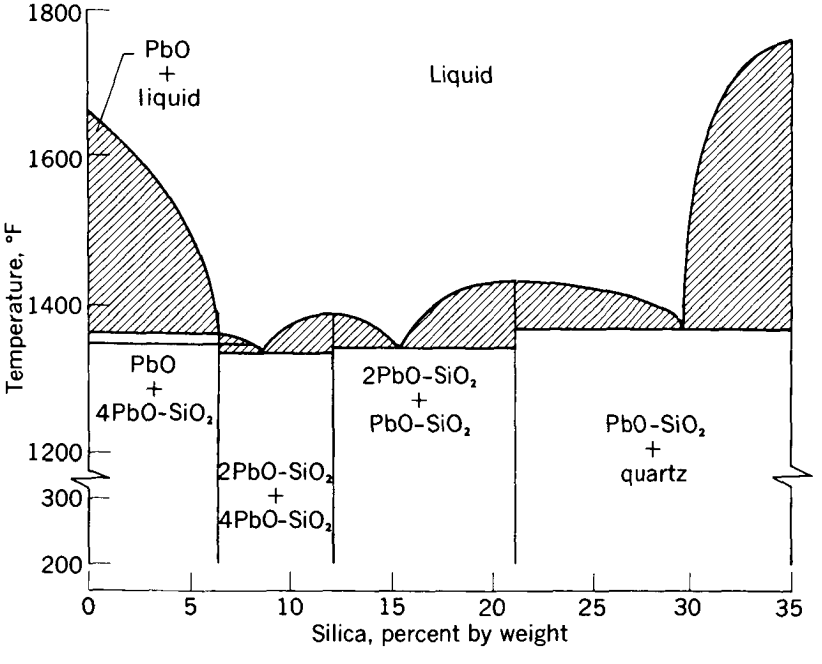

FIGURE 8–19.—Phase diagram for lead monoxide—silica system. (From ref. 48.)

Pure PbO melts at 1628° F; however, the phase diagram shows that a eutectic is formed with 8.22 percent by weight of SiO_2 and PbO. This eutectic melts at 1317° F and has a lower temperature range for softening than pure PbO. When melts containing less than 6.7 percent by weight SiO_2 are cooled, the first phase to solidify is PbO. After complete solidification, discrete particles of PbO are dispersed throughout a tetralead silicate ($4PbO\text{-}SiO_2$) phase. Several advantages may thereby be derived, for example:

(1) The silicate phase functions as a binder and increases the strength of the coating.

(2) The silicate phase surrounding the PbO particles protects them from oxidizing atmospheres and thus minimizes the conversion to higher oxides.

(3) The presence of silica increases the range of softening temperatures and the vitrification or glass-forming tendency of the coating.

A pronounced vitrification tendency promotes the formation of glazes on the ceramic wear tracks. It has been observed that the friction and wear of metals in sliding contact with ceramics generally decreases sharply when a glaze forms on the ceramic surface (refs 22 and 23). It is also interesting to note that molten glass has been successfully used as a die lubricant in the extrusion of metal (ref. 7). The presence of small amounts of SiO_2 also appreciably reduces the volatility of PbO at elevated temperatures (ref. 20).

An investigation was made of the friction and wear properties of a film of $PbO\text{-}SiO_2$ with a coating thickness of 0.001 inch. The results are shown in figure 8–20 along with results for a resin-bonded MoS_2 coating of 0.0003-inch thickness. The MoS_2 coating gave lower rider wear and friction than the PbO coatings at temperatures below 500° F. At temperatures above 600° F, however, the friction and wear with the MoS_2 coating increased significantly, whereas the PbO coatings provided more effective lubrication. It should be noted that 600° F is the limiting temperature for the resin binder of that particular MoS_2 formulation.

Some of the results of experiments made over a wide range of sliding velocities and temperatures with a $PbO\text{-}SiO_2$ coating (ref. 21) are shown in figure 8–21. As either sliding velocity or temperature increase, friction coefficient decreases. The increase in velocity apparently generates enough heat at the sliding interface to produce an effect somewhat similar to that imposed by operating at higher temperatures. This result shows that the best friction results are obtained under the most severe conditions.

One of the questions that must be asked with respect to any solid lubricant film which is applied as a preformed film relates to the endurance properties of such a film. Comparison of the cycles to

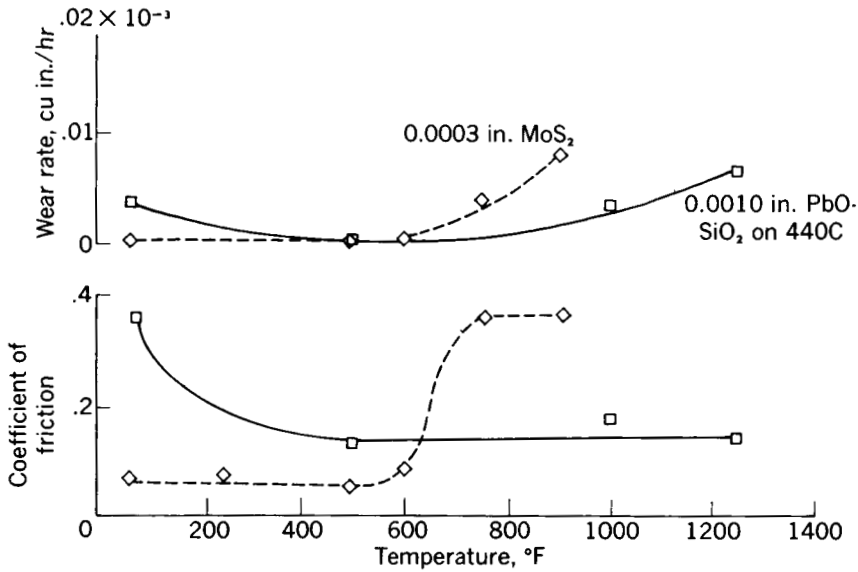

FIGURE 8–20.—Effect of temperature on friction properties of bonded lead monoxide. (Data from ref. 21.)

failure for a PbO film with those for a standard resin-bonded MoS_2 film showed that the PbO films at 500° and 1250° F had endurance

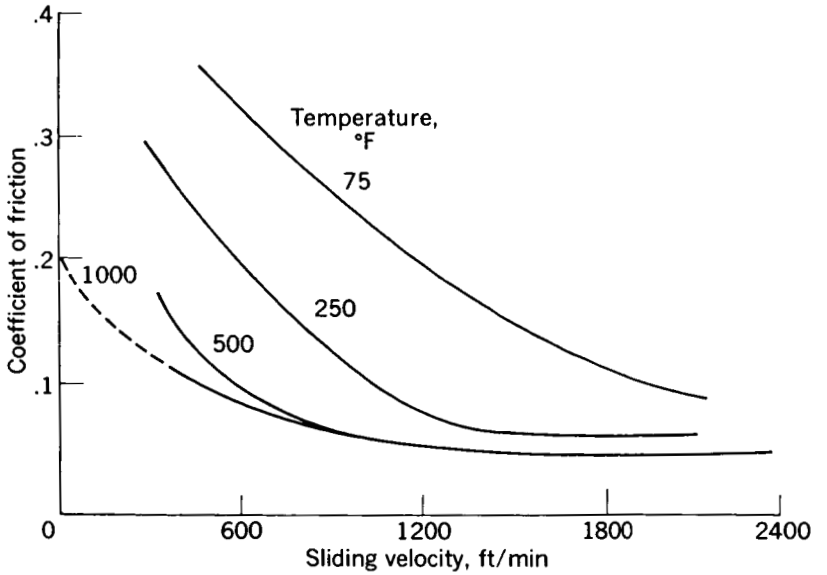

FIGURE 8–21.—Friction characteristics of bonded lead monoxide at various sliding velocities. (From ref. 21.)

lives of approximately the same order of magnitude as did an MoS_2 film at room temperature. (A resin-bonded MoS_2 film is very effective, particularly at room temperature.) As expected from the adverse effect of temperature on the resin binder previously discussed, the resin-bonded MoS_2 film had poorer endurance properties at 500° F than did the $PbO\text{-}SiO_2$ film. Some of these results will be presented later in a comparison with other solid lubricants.

A further question, which can be and is frequently asked, is whether the results of friction experiments (such as have been described) apply equally well to a "practical" application such as a full-scale rolling-contact bearing. Since the $PbO\text{-}SiO_2$ coating showed good performance in the friction tests, the $PbO\text{-}SiO_2$ coating was applied to retainers of 35-millimeter-bore ball bearings to be operated at 1200° F, completely dry. These bearings were operated at 5750 rpm under a 100-pound-thrust load at 1200° F. Successful operation was obtained for 44 hours. This is about eight times longer than any other bearing had been run successfully under these conditions. The bearings were then reassembled and run another 10 hours at 10,000 rpm and 1200° F without failure of the lubricating film. A photograph of the ball retainer is shown in figure 8–22 after the 44-hour run. The bearing retainer was in excellent condition, as proven by the subsequent reassembly and successful operation at a higher rotative speed.

FIGURE 8–22.—207 Ball bearing retainer with 0.001-inch lead oxide—silica coating run at 5750 rpm and 1200° F for 44 hours under 100-pound-thrust load. (From refs. 49 and 50.)

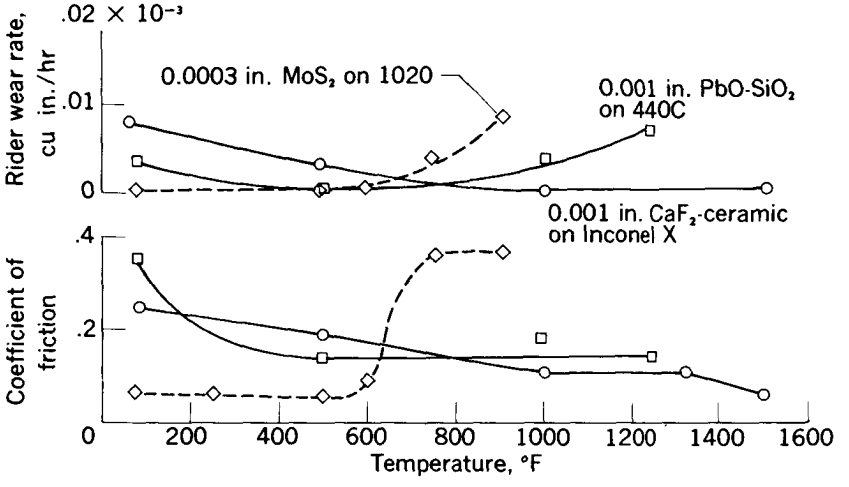

FIGURE 8–23.—Effect of temperature on wear and friction with lubricating solid films. Cast Inconel riders; sliding velocity, 430 feet per minute; load, 1000 grams. (From refs. 8, 43, and 49.)

CALCIUM FLUORIDE

As previously mentioned, the $PbO\text{-}SiO_2$ mixture is limited in usefulness to a temperature of about 1250° F because of softening of the coating at higher temperatures. In accordance, an analysis of some possible materials for operation at higher temperatures was made by Sliney (ref. 8). This analysis indicated that the compound calcium fluoride (CaF_2) should be considered for use at higher temperatures. An investigation was therefore made (ref. 8) with a coating of CaF_2 bonded with a ceramic binder (a mixture of CoO, B_2O_3, and BaO). The results of this investigation are shown in figure 8–23. Wear and friction coefficient are plotted against temperature for a ceramic-bonded CaF_2 film in comparison with a $PbO\text{-}SiO_2$ and a resin-bonded MoS_2 film. Both the MoS_2 and PbO coatings show an increase in wear at the higher temperatures. The CaF_2 wear curve is, however, quite flat over the temperature range from 800° to 1500° F. Also, the friction coefficient is quite low, particularly at 1500° F.

Films of MoS_2, PbO, and CaF_2 were subjected to an endurance test to determine the number of cycles to failure at a number of different temperatures. This test shows (fig. 8–24) that, at 75° F, MoS_2 is by far the best of the coatings. At 500° F, the PbO film is superior to MoS_2, and at 1250° F, the PbO film is slightly better than the CaF_2 film. At 1500° F, neither one of the other two films had any life at all, and the CaF_2 film was the only one which could be

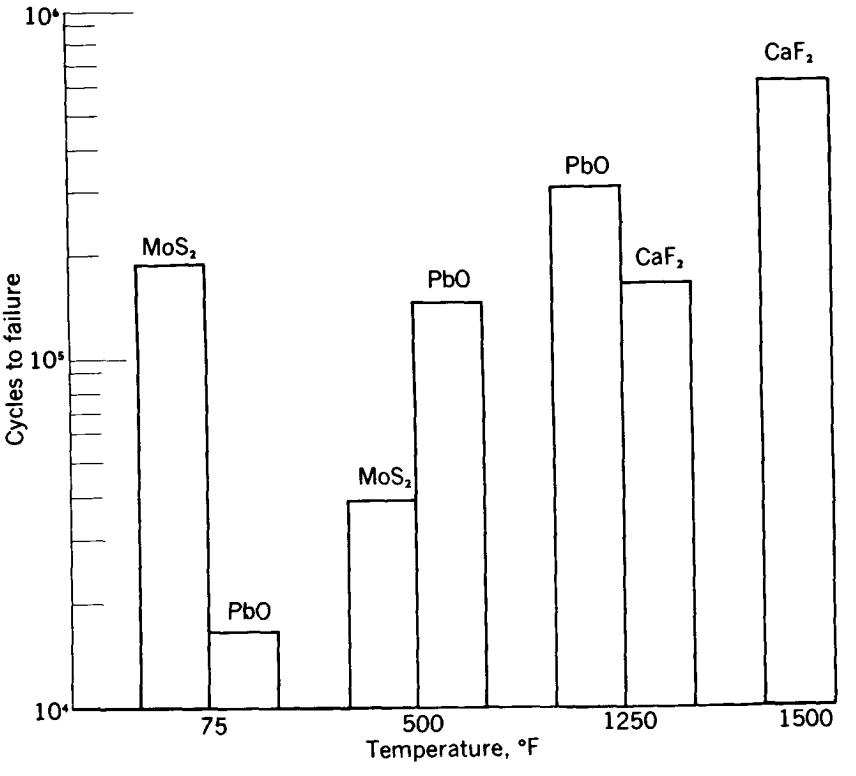

FIGURE 8–24.—Endurance of several dry film lubricants at various temperatures. Sliding velocity, 430 feet per minute; load, 2 kilograms. (From refs. 8, 43, and 49.)

utilized; at 1500° F, its life was even better than that for one of the best lubricants, MoS_2, at room temperature.

Recent experiments by Sliney at NASA (ref. 24) have shown that, with proper choice of base metals on which the CaF_2 film is bonded, such a film can lubricate effectively at temperatures as high as 1900° F.

In general, a rough estimate of the temperature ranges of usefulness (for long-term operation) of these materials is as follows:

Lubricant	Useful temperature range, °F
MoS_2-resin binder	To 600
PbO-SiO_2	500 to 1250
CaF_2-ceramic bonded	500 to >1900

OTHER SOLIDS

Boric Oxide

Some early experiments with boron nitride as a lubricant led to observations that this compound oxidizes at high temperatures and that the oxide acts as the lubricant. For example, Deacon and Goodman (ref. 25) indicate that the improvement in frictional properties of platinum on platinum lubricated with boron nitride at temperatures above 900° F is due to the formation of the oxide of boron. Similarly, Johnson, Swikert, and Buckley (ref. 26) suggest, in answer to a discussion of their paper, that reduction in friction using boron nitride as a solid lubricant at temperatures above 1350° F was probably due to oxidation of the boron nitride; in their experiments, physical evidence of oxidation was obtained.

Peterson, et al. (ref. 2) made some friction experiments with boric oxide (B_2O_3) as a lubricant at various temperatures. The results of this investigation are shown in figure 8–25. The friction coefficient

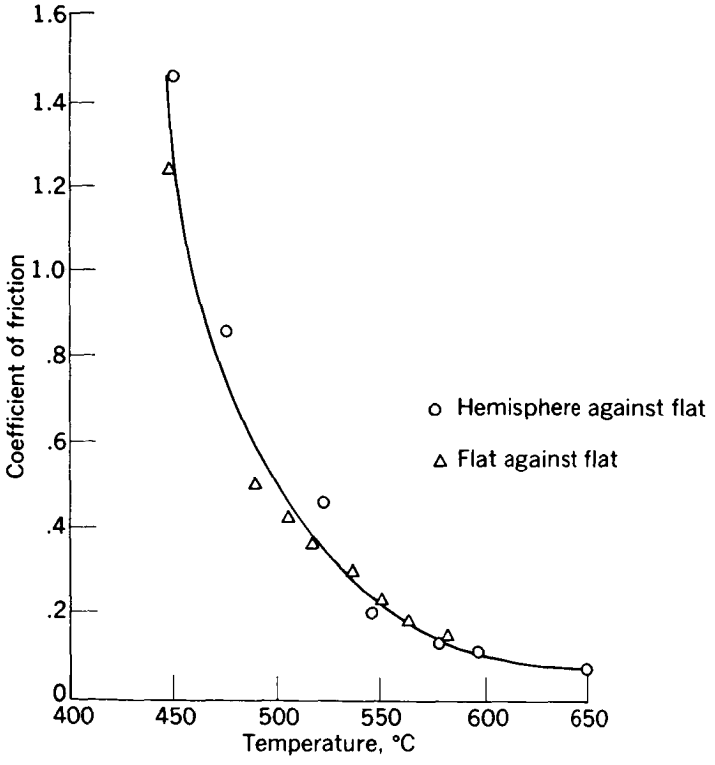

FIGURE 8–25.—Friction with boric oxide as lubricant at high temperatures. (From ref. 2.)

for B_2O_3 drops rapidly at temperatures greater than 450° C (840° F) and reaches a value of less than 0.10 at a temperature of 650° C (1200° F). As noted in the figure, two different combinations of specimens were used: (1) hemisphere on flat, and (2) flat on flat. The friction coefficients were independent of slider geometry. The viscosity of B_2O_3 at 600° C is 2400 poises (ref. 27). At temperatures below 600° C, the rise in friction coefficient is rapid. The viscosity of B_2O_3 at 450° C is approximately 1,000,000 poises.

Rabinowicz and Imai (ref. 28) conducted an investigation to show the beneficial effects of boric oxide as a high-temperature lubricant. They obtained results which showed, as did the results of Peterson, et al., that the friction coefficient peaked sharply (at approximately 800° F) as temperature was increased from 70° to approximately 2000° F (fig. 8–26). This friction peak is ascribed to softening within the

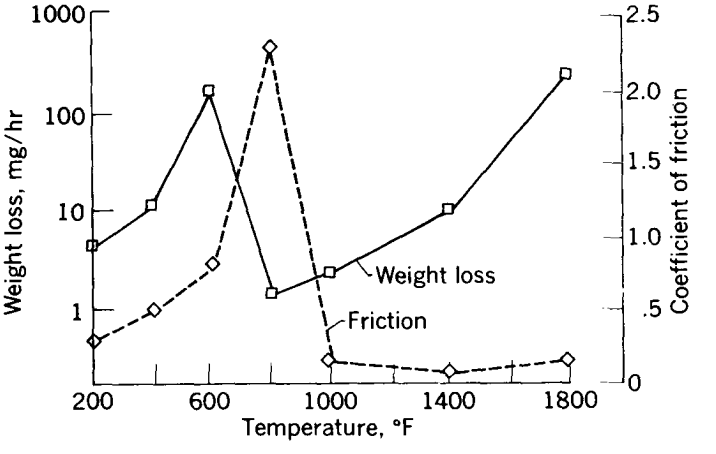

FIGURE 8–26.—Wear and friction with boric oxide as lubricant over a range of temperatures. (From ref. 28.)

film that permitted an increase in area of contact. At temperatures higher than that at which the peak friction coefficient is obtained, they believe hydrodynamic lubrication is obtained, because the B_2O_3 is forming a viscous film. If temperature is then increased sufficiently, boundary lubrication is obtained because of the marked decrease in viscosity with increase in temperature. Note that wear is very high at 1800° F even though friction coefficient is low. This high wear is undoubtedly the result of corrosion, since B_2O_3 is extremely corrosive at high temperatures.

Rabinowicz and Imai state,

> If boric oxide is to be used in practical high temperature sliding systems, the friction peak at intermediate temperatures may prove to be very unwelcome.

Klemgard (ref. [51]) has investigated various solids mixed with boric oxide, some of which seem to be very effective. We have ourselves, tried one such mixture, namely, a 50 percent mixture of graphite and boric oxide. This certainly lowers the height of the friction peak. . . . Clearly more work in this direction is called for. . . . We wish to call attention to boron-containing solids as potential bearing materials in the high temperature field. Boron carbide itself seems to show quite a degree of promise as it has quite a low oxidation rate to quite high temperatures and the boric oxide it forms has advantages over that provided by one-shot treatments in that it is renewed continuously to replace that lost by evaporation.

Johnson and Sliney (ref. 13) conducted experiments with both boric acid (H_3BO_3) and boric oxide (B_2O_3); their results are shown in figure 8–27. Their experiments were started at room temperature

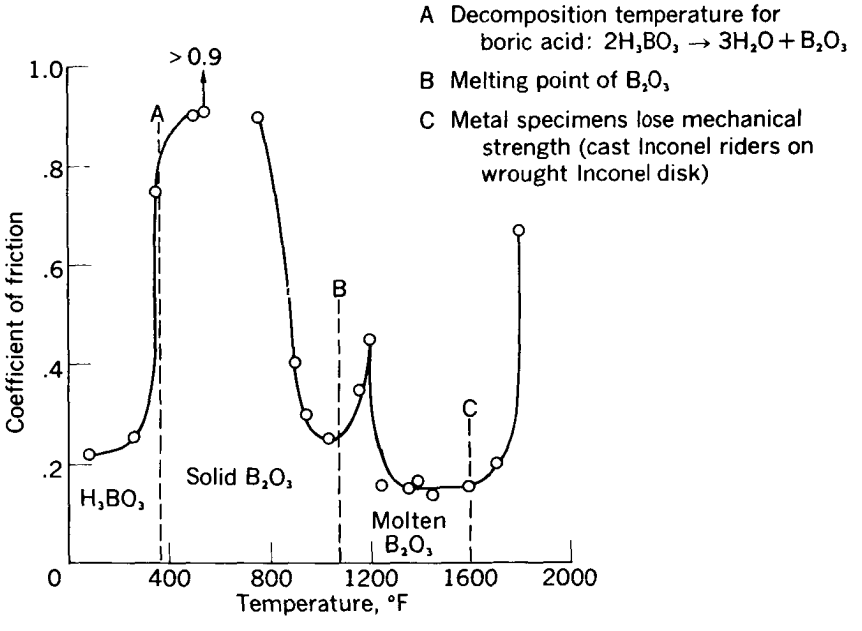

FIGURE 8–27.—Influence of physical and chemical changes on friction coefficients of boric acid and boric oxide. Sliding velocity, 6 feet per minute; load, 6 kilograms. (From ref. 13.)

with H_3BO_3; at a temperature close to the decomposition temperature (365° F) of H_3BO_3 to B_2O_3 and H_2O, the friction increased sharply. Above 700° F, the friction characteristics showed trends somewhat similar to those reported by Peterson, et al. and Rabinowicz and Imai. At the higher temperatures Johnson and Sliney (ref. 13) state that lubrication was by molten B_2O_3; severe corrosion occurred in these experiments.

Plastics

Plastics, such as Teflon, nylon, and some phenolics, have frequently been used as solid lubricants (refs. 6, 29, and 30). The nylon and phenolic materials are normally utilized to form solid bodies for use as dry bushings in applications where loads are light, speeds are limited, and it is preferable to exclude normal lubricants; under these conditions, low friction can be maintained. Phenolic laminate materials are also frequently utilized as the cage material for ball or roller bearings where temperatures are not too high, since the phenolic laminates are limited to temperatures of about 275° F. The phenolic laminate cages also show good performance at the low temperatures of cryogenic liquids; a detailed discussion of such performance is incorporated in chapters 10 and 11.

Teflon is used both in the form of solid bodies and as surface coatings. It is one of the better cage materials for rolling-element bearings operating in cryogenic liquids such as liquid hydrogen and liquid oxygen. It also shows good performance when applied as a thin coating at either low temperatures or at temperatures up to about 550° F. Teflon is very resistant to chemical attack since it is a fluorinated material and is, therefore, stable chemically. Some of the lowest friction coefficients observed have been obtained with Teflon. The chief disadvantages of Teflon are (1) it is a poor conductor of heat, and (2) it has a high value of linear expansion coefficient (47.5×10^{-6}/°F as compared with 7×10^{-6}/°F for ordinary steel). Both of these properties make using Teflon difficult either as a solid body or as a surface coating. In the case of coatings particularly, thickness of the coating must be limited in order to prevent spalling or separation of the coating from the base metal. The authors of reference 30 experimented with various binder compositions in order to achieve the combination of properties desired (good adherence, good friction and wear properties, as well as an expansion coefficient approaching that of the base metal to which the Teflon was bonded). The wear results achieved indicate that Teflon coatings can be tailored to a particular temperature range, as well as to specific metals.

The plastics have a very important place in applications where little or no lubrication is permitted; they are inherently self-lubricating provided that conditions of operation are not such as to result in excessive heat generation. They have, however, certain inherent limitations which, of necessity, must be respected.

SUMMARY

Solid lubricants have a very definite place in the lubrication of mechanisms at extreme temperatures. They can be used in one of three methods: (1) as loose powders, (2) as bonded films, or (3) as

constituents of a powdered-metal mix. Each of these methods has advantages and disadvantages, which must be given adequate consideration.

In general, a rough estimate of the temperature ranges of usefulness (for long term operation) of the various solid lubricants is as follows:

Lubricant	Approximate temperature range, °F
Bonded	
Molybdenum disulfide, resin bonded	−423 to 600
Molybdenum disulfide, silicate bonded	To 750
Lead oxide, silicate bonded	500 to 1250
Calcium fluoride, ceramic bonded	500 to >1900
Teflon	−423 to ≈500
Loose powder	
Molybdenum disulfide (oxidizing atmosphere)	To 700
Molybdenum disulfide (inert atmosphere)	To 900
Tungsten disulfide (oxidizing atmosphere)	To 1000
Tungsten disulfide (inert atmosphere)	To 1500[a]
Graphite (oxidizing atmosphere)	To 1200
Boric oxide	To 1000[a]

[a]Based on very limited data.

II. REACTIVE GASES

The increasing temperature level of most mechanisms required to operate in modern-day machines (subsonic and supersonic aircraft, missiles, spacecraft, etc.) has indicated a necessity for lubricants that have better thermal stability than do the ordinary liquid lubricants. As previously mentioned, there are a number of approaches to this problem, among them the use of

(1) More stable fluids, such as the polyphenyl ethers
(2) Solid lubricants, such as molybdenum disulfide, graphite, lead oxide, calcium fluoride, and boric oxide
(3) Air or inert gases as the working fluid in hydrostatic or externally pressurized gas bearings
(4) "Closed" lubrication systems to reduce contact of the liquid lubricants with air

This part of chapter 8 discusses another possibility, that of using nonconventional lubricants such as gases containing reactive atoms

in the molecule. The purpose of this part is therefore to explore the problem areas arising from use of reactive gases as lubricants and to indicate some of the proposed solutions to these problems. Some of the early research in this field was done by Murray, Johnson, and Swikert at the NACA (now NASA) laboratories (ref. 31). Extensive research in this area has been carried out by Buckley, Johnson, and others (refs. 32 to 39). Much of the discussion herein is taken from these references.

MECHANISM OF LUBRICATION WITH GASES CONTAINING REACTIVE ATOMS IN THE MOLECULE

The mechanism of lubrication with gases containing reactive atoms in the molecule is similar to that obtained by the use of the "extreme pressure" additives used in gear lubricants. The principle involves the availability of reactive atoms such as chlorine, bromine, phosphorous, or sulfur for reaction with the metal surface to form a low-shear-strength film, which can act as the lubricant. In the case of both "extreme pressure" additives and of "reactive gases," the molecules containing the reactive atoms are generally stable at the ambient temperature; these atoms are liberated only because of the high "flash temperatures" obtained when surface asperities slide over one another in the friction process. Because of the extremely high contact pressures involved at the contacting asperities, considerable heat is generated at these asperities, and since the area of contact is so small, the sudden liberation of energy results in extremely high temperature flashes. It has been shown by Blok, Holm, and by Bowden and Tabor that the temperatures at the asperities can approach the melting temperature of one of the sliding metals in spite of the fact that the bulk temperature of the metal immediately adjacent to the asperity is raised only a few degrees. These temperature flashes are such that molecules containing reactive atoms in the near vicinity can be decomposed, and active atoms thus liberated. These active atoms are then free to react with a metal surface to form compounds. If the combination of gases and metals has been chosen properly, a low-shear-strength film will be formed at the contacting asperities and effective lubrication will be obtained.

It should be emphasized that this process is one of "controlled corrosion"; hence, the choice of (1) gas, (2) metals to be lubricated, and (3) the ambient temperature is extremely important. The gases must of necessity be thermally stable at the ambient temperature, otherwise, mass corrosion is obtained.

Some of the halogenated methanes fall in the category of relatively stable gases. For example, tetrafluoromethane is a stable halocarbon as it does not show any measurable decomposition rate in glass below

2000° F (ref. 40); possibly the rate would be higher in metal at these same temperatures. Although partial substitution of chlorine for fluorine in this compound produces compounds having decomposition temperatures lower than the fully fluorinated material, the halogenated methanes so formed are still quite stable thermally and chemically. Murray, et al. (ref. 31) investigated halogenated methane and ethane gases in an attempt to determine lubricating effectiveness of such gases. Their early studies indicated that corrosion was an extremely important factor in the use of gases as lubricants.

FRICTION, WEAR, AND CORROSION

Fluorinated and Chlorinated Methanes and Ethanes

The early experiments of reference 31 were made with the experimental gaseous lubricants listed in table 8–IV; the results of these experiments are cited herein. The gases were commercial-grade materials having purities higher than 97 percent. The impurities were

TABLE 8–IV.—EXPERIMENTAL GASEOUS LUBRICANTS

Lubricant	Specific gravity of gas (air = 1)	Boiling point, ° F	Structure
Tetrafluoromethane, CF_4	3. 04	−198. 4	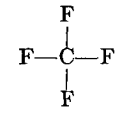
Trifluorochloromethane, CF_3Cl	3. 60	−114. 7	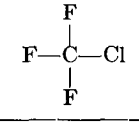
Difluorodichloromethane, CF_2Cl_2	4. 17	−21. 64	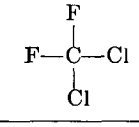
Fluorotrichloromethane, $CFCl_3$	4. 74	+74. 78	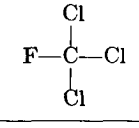
Tetrachloromethane (carbon tetrachloride), CCl_4	5. 31	+170	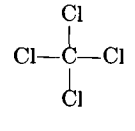

primarily noncondensable gases with less than 0.0025 percent water. An analysis of the atomosphere in the friction apparatus in runs using difluorodichloromethane and tetrafluorodichloroethane showed that the oxygen content was less than 0.5 percent after 5 minutes at the flow rate used in the test. (This flow rate and time period were equivalent to changing the atmosphere in the chamber 10 times.) Since this flow rate was maintained at all times during the test runs, contamination from the air was assumed to be negligible. Results of these experiments indicated that the halogenated methanes required at

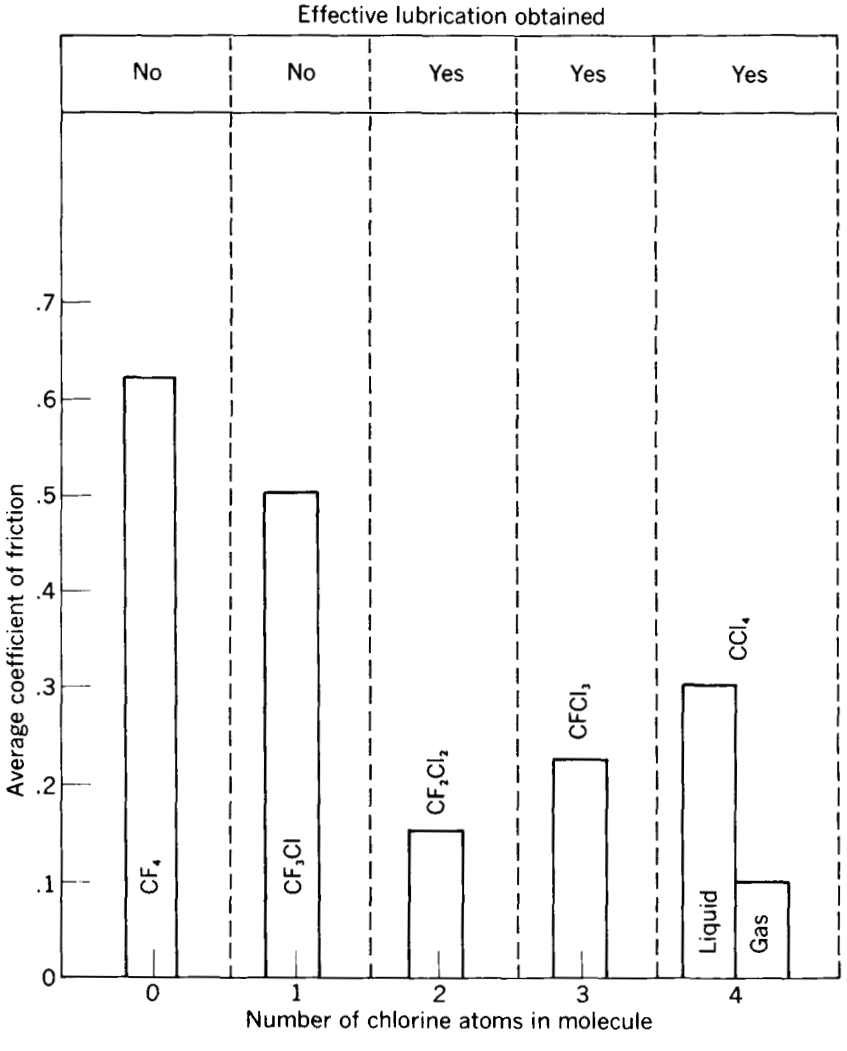

FIGURE 8–28.—Lubrication with gases containing chlorine. (From ref. 31.)

least two chlorine atoms in the molecule to provide effective lubrication for steel on steel. These results are indicated in bar graph form in figure 8–28. The friction coefficients for tetrafluoromethane (CF_4) and trifluorochloromethane (CF_3Cl) were quite high (greater than 0.5). On the other hand, with two or more chlorine atoms in the molecule, the friction coefficient was relatively low; for example, difluorodichloromethane (CF_2Cl_2) showed a friction coefficient of approximately 0.15. Visual observations of the sliding surfaces provided the information on effective lubrication included in the figure. As shown, effective lubrication (defined as operation of the specimens without severe surface damage and with low friction coefficient) was obtained with two or more chlorine atoms in the molecule. It should be noted that both liquid and gaseous tetrachloromethane (CCl_4) provided effective lubrication with respect to prevention of surface damage; the friction coefficient with the liquid was, however, appreciably greater than with the gas.

Figure 8–29 shows the rider wear areas after tests in air, CF_2Cl_2, and oil. These photomicrographs give ample evidence of the effectiveness of CF_2Cl_2 as compared with sliding of the specimens against one another in a dry, unlubricated condition. The wear spot for the rider run in air shows evidences of severe welding and tearing (fig. 8–29(a)); in contrast, the wear spot on the rider run with CF_2Cl_2 (fig. 8–29(b)) shows a relatively clean, smooth surface without evidences of welding

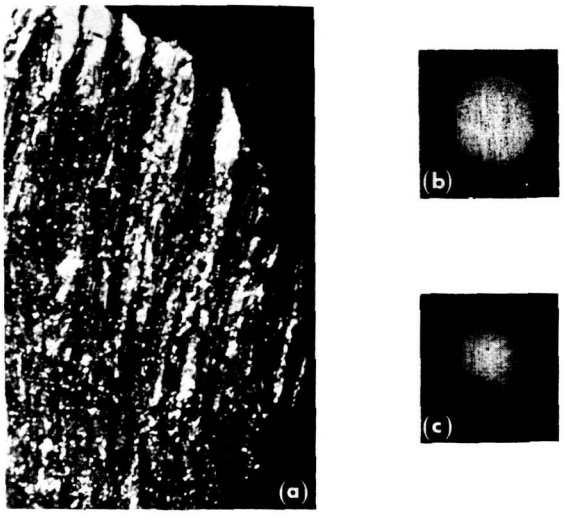

(a) Air. (b) CF_2Cl_2. (c) Oil.

FIGURE 8–29.—Rider wear areas after tests in air, difluorodichloromethane (CF_2Cl_2), and oil. (From ref. 31.)

or tearing. In fact, the marks which appear in this wear spot are abrasion marks rather than welding. The appearance of the wear spot for the rider run in CF_2Cl_2 is not unlike that for a wear spot run with an effective liquid lubricant as shown in figure 8–29(c).

The early experiments of reference 31 also included some tests at specimen temperatures of 480° F. These tests were made with CF_2Cl_2 lubricating steel on steel. The friction values observed during these high-temperature runs were higher than at room temperature (approximately 0.3 as compared with 0.15); the surfaces, however, appeared to be effectively lubricated and no surface failure or metal transfer was found. Later experiments (ref. 32) showed that corrosion could be an appreciable problem with the combination of iron-base alloys and halogenated methanes at temperatures up to 1200° F. In fact, corrosion of the bulk surface area of M–1 tool steel was objectionable at 1000° and 1200° F with all gases used in reference 32. These gases included CF_3Cl, CF_2Cl_2 and both of these gases with 1 percent sulfur hexafluoride (SF_6) added as a catalyst. Serious corrosion problems could exist with chlorine-substituted gases at temperatures as low as 600° F. It should be emphasized, however, that M–1 tool steel has been considered as a bearing steel, not because of its corrosion resistance, but primarily because of its good hot-hardness properties. M–1 is very susceptible to oxidation, corrosion, and other forms of chemical attack. In the experiments described in reference 32, attempts to obtain effective lubrication with less reactive gases were not successful with M–1 tool steel. Another approach to minimizing the corrosion problem is to utilize corrosion-resistant metals for slider surfaces; this approach will be discussed later.

A run-in procedure (gradually increased loads and speeds) was necessary in early research with these gases; this early research showed surface failures if no run-in was used. The surface failures were presumed to result from lack of sufficient time to form an effective reaction film.

Figure 8–30 shows the friction and wear of M–1 tool steel specimens lubricated with CF_2Cl_2 plus 1 percent SF_6 over the temperature range of 75° to 1200° F. At the low end of the temperature range, the data of figure 8–30 show that friction was relatively high and rather erratic; the low wear indicates that lubrication was quite effective. At the higher end of the temperature range, however, the friction coefficient was quite low although the corrosive wear was so severe as to make it impossible to measure the wear in this experiment. The wear-temperature curve shows an exponential shape typical of a reaction rate phenomenon. Chemical reaction over the entire surface is occurring under these conditions (i.e., the

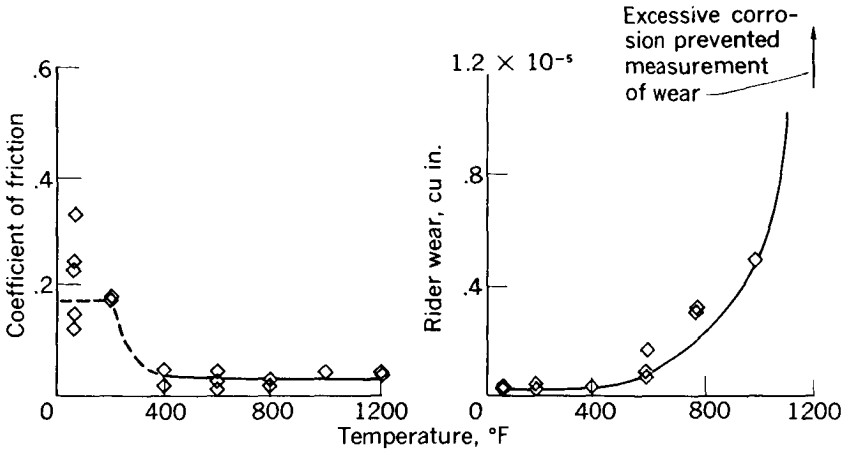

FIGURE 8–30.—Friction and wear of M–1 tool steel sliding on M–1 tool steel. Lubricant, difluorodichloromethane (CF_2Cl_2) with 1 percent sulfur hexafluoride (SF_6); sliding velocity, 120 feet per minute; load, 1200 grams; duration of run, 1 hour. (From ref. 32.)

gas is reacting directly with the bulk surface rather than selectively reacting only at the contacting asperities). Hence, the results show that this combination of materials and gas is not suitable at these elevated temperatures.

Since the results previously presented indicate that corrosion can become a limiting factor at elevated temperatures with certain material-gas combinations, it is necessary to consider carefully various combinations of materials and gases.

Corrosion-Resistant Materials

A corrosion study was made (ref. 33) of various materials with a mixture of CF_2Cl_2 plus 1 percent SF_6. On the basis of both friction and corrosion theories, the nickel-base alloys seem to have some promise for use with reactive gases at high temperatures. Friction theory would predict that the nickel-base alloys should react with chlorine or bromine from halogenated gases to form the nickel halides, which have been shown to have good frictional properties. Corrosion theory would also indicate that nickel should be more resistant to chemical reaction with the fluorine or bromine atoms at the ambient temperature than would iron from iron-base alloys. Corrosion can also be influenced strongly by alloy constituents, particularly chromium.

Table 8–V presents results of a corrosion study made with a mixture of CF_2Cl_2 plus 1 percent SF_6 and various materials. Of the materials

TABLE 8–V.—CORROSION STUDY DATA [a]

[Gas mixture: CF_2Cl_2 at 1.0 liter/min; SF_6 at 0.01 liter/min]

Material	Corrosion resistance at temperature, °F, of —		
	75	600	1200
M–1 Tool steel	Excellent [b]	Fair [c]	Poor [d]
440C Stainless steel		Fair	Poor
"L" Nickel		Good [e]	Fair
Cast Inconel		Good	Fair
Inconel S		Good	Fair
Inconel X		Excellent	Good
7½ percent silicon-nickel		Excellent	Good
"G" Nickel		Excellent	Good
Hastelloy C		Excellent	Good
Hastelloy R–235		Excellent	Good
Multimet		Good	Poor
Stellite 21		Good	Fair
Stellite 98M2		Excellent	Poor
Stellite Star J		Excellent	Poor
Molybdenum (arc cast)		Good	Poor
K–162 B Kentanium		Good	Fair
Titanium		Fair	Poor

[a] From ref. 33.
[b] No visible change.
[c] Tightly bonded layer.
[d] Profuse surface crystal growth.
[e] Surface coloration.

investigated in the corrosion study, the nickel-base alloys (particularly, 7½ percent silicon-nickel, Inconel X, and Hastelloy C) showed the least corrosion. These materials showed no evidence of corrosion at 75° and 600° F. At 1200° F, 7½ percent silicon-nickel and Inconel X showed the slight coloration of very thin chloride films; Hastelloy C showed some discoloration. The M–1 tool steel and 440C stainless steel were the poorest materials reported under these environmental conditions. They exhibited heavy deposits and showed marked weight changes.

On the basis of the corrosion studies, nickel- and cobalt-base alloys were chosen for test at elevated temperatures. Results of experiments with two gases, difluorodibromomethane (CF_2Br_2) and trifluorobromomethane (CF_3Br) plus 1 percent SF_6 are shown in figure 8–31. The CF_2Br_2 gas should be slightly less corrosive than the CF_2Cl_2 utilized in the corrosion experiments. From figure 8–31, however, the wear at 1200° F with CF_2Br_2 was rather high and the shape of the curve indicates the exponential corrosion function. Analysis of these data would make it appear that the concentration of

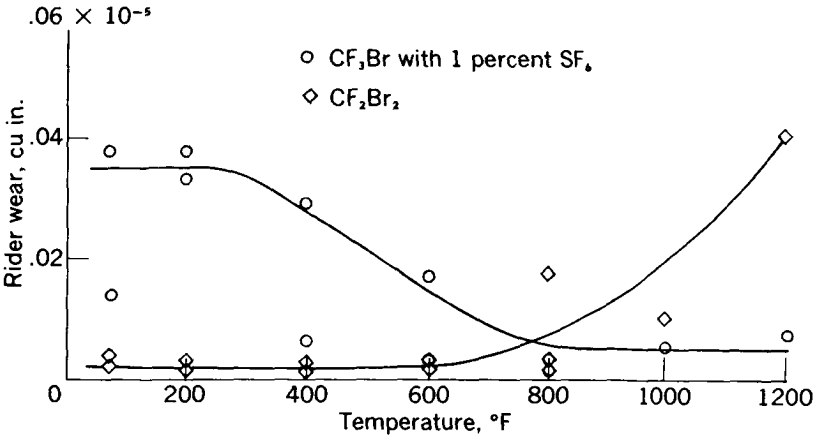

FIGURE 8–31.—Comparison of wear data for 98M2 Stellite rider sliding on Hastelloy C disk. Sliding velocity, 120 feet per minute; load, 1200 grams; duration of run, 1 hour. (From ref. 33.)

active atoms was too great; hence, experiments were conducted with the gas CF_3Br, which has only one active atom per molecule as compared with the two active atoms of CF_2Br_2. Results with CF_3Br plus 1 percent SF_6 (fig. 8–31) showed low wear at the elevated temperatures but indicated relatively high wear at the lower temperatures. The high wear at the low temperatures was the result of ineffective lubrication; in fact, the friction curve for this experiment showed relatively high friction coefficients (approximately 0.4) at temperatures below 400° F.

It was apparent from the results of these two experiments that the one compound (CF_2Br_2) was too reactive and the other compound (CF_3Br) was not sufficiently active over the entire temperature range. Hence, some experiments were conducted with a mixture of the two compounds. The mixture of gases, it was hoped, would provide a concentration of reactive atoms intermediate between that of either gas alone. Results of this investigation are presented in figure 8–32. This figure shows both wear and friction of a 1 to 1 mixture of CF_3Br and CF_2Br_2 along with the individual gases for comparison. The results show that the rate of wear for the 1 to 1 mixture of CF_3Br and CF_2Br_2 was very low over the entire operating temperature range. In explaining this result, Buckley and Johnson (ref. 36) state

> . . . the relative independence of wear with respect to varied temperatures may be explained in terms of the bromine available for surface reaction. At the lower ambient temperatures where a single bromine atom was inadequate, there was a 25 percent increase in bromine available from the blend [1 to 1 mixture] for surface reaction. At higher temperatures, however, the bromine content of the

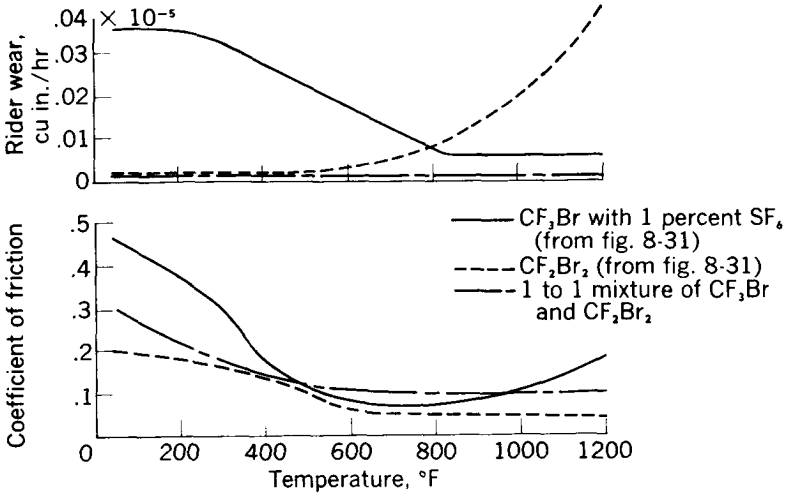

FIGURE 8–32.—Wear and friction of 98M2 Stellite sliding on Hastelloy C with gas lubricants. Sliding velocity, 120 feet per minute; load, 1200 grams; duration of run, 1 hour. (From ref. 36.)

blend was 25-percent less than that available with the dibrominated gas [CF_2Br_2] and, therefore, a reduction in corrosive wear was observed. Thus, an effective balance between adhesive and corrosive wear was achieved.

The friction data of figure 8–32 show that, as might be expected, friction coefficients for the mixture were approximately intermediate between those for the individual gases over the entire temperature range.

For even higher temperatures, another approach to the problem of reducing corrosive wear at high temperatures involves the use of nonreactive materials as one component of the sliding system. Based on the mechanism of gas lubrication, one of the sliding components must be a metal in order that metallic ions be present for the formation of the metal-halide lubricating film. High-temperature corrosion-resistant alloys with good hot hardness may be most effectively used. The other sliding component, however, may be a relatively nonreactive material such as a cermet or ceramic.

Data on friction and wear of aluminum oxide (Al_2O_3) sliding on a cobalt-base alloy with CF_2Cl_2 as the lubricant are presented as the circular points of figure 8–33. The corrosive effect of CF_2Cl_2 on the metal in this sliding combination was still rather dominant at the higher temperatures; however, the maximum temperature is 1500° F in contrast to the maximum temperature of 1200° F of figures 8–31 and 8–32. Friction coefficients were slightly high but were under 0.2 over the entire temperature range.

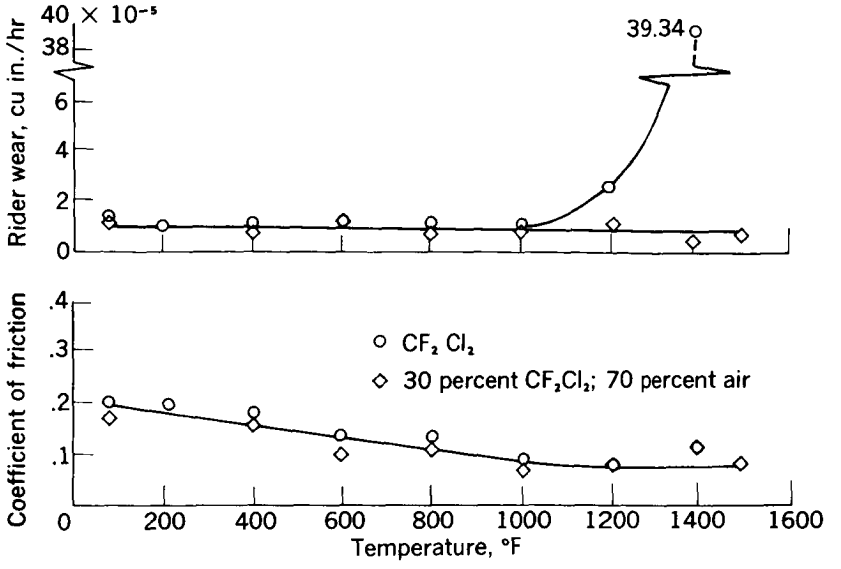

FIGURE 8–33.—Friction and wear of aluminum oxide sliding on a cobalt-base alloy with difluorodichloromethane and 30 percent difluorodichloromethane in 70 percent air. Sliding velocity, 3200 feet per minute; load, 1200 grams; duration of run, 1 hour. (From ref. 39.)

More Stable Gases

Another method of approaching the corrosion problem according to reference 37 is to use gas lubricants with extremely good thermal stability. It has been established in reference 32 that in gas molecules such as CF_2Cl_2 the carbon-to-fluorine bond is not ruptured upon initial molecular thermal degradation. The carbon-to-chlorine bond does cleave, however, and this separation liberates free chlorine and provides for the formation of the metallic halide that functions as the solid lubricant. Excessive liberation of free halogen can contribute to corrosion of the metallic components at extreme temperatures. Any molecular structure of the gas that would give greater stability to the carbon-to-chlorine bond would reduce corrosion at elevated temperatures. One such structure is the compound, 1,2-dichloro-1,1,2,2-tetrafluoroethane (CF_2Cl-CF_2Cl). This type of compound could conceivably reduce the tendency of corrosion to occur at extreme temperatures. Results obtained in studies using this gas (ref. 37) indicated some limited beneficial effect from using the more stable gas. This beneficial effect was not as great, however, as was the beneficial effect from using less reactive materials to be lubricated, such as Al_2O_3 sliding on a cobalt-base alloy. The use of a ceramic as one of the

two materials to be lubricated permitted operation at appreciably higher temperatures before the corrosion became so excessive as to prohibit operation at that temperature.

Corrosion Inhibitors

High-temperature corrosion can normally be reduced by employing corrosion inhibitors. This approach to control of corrosion involves a number of methods, three of which were considered by Buckley and Johnson (ref. 39). These three methods are as follows:

(1) Use of additive gases that can combine with excessive free halogen generated at the sliding interface to remove it in the combined form of a compound; these additive gases would be considered entrapping agents.

(2) Use of a diluent gas; an inert gas diluent reduces the concentration of reactants.

(3) Promotion of competitive reactions at the sliding interface. This may be achieved by adding inhibitor gases that react with a metal surface in competition with the halogen-containing gas. It is desired that the inhibitor form a dense, tenacious surface film in contrast to the porous nature of halide films.

Since the reaction would be competitive, both halide and inhibitor reaction products would be present in the surface film. With the halide in the film, it could still function as a lubricant under proper conditions.

As Buckley and Johnson report in reference 39, the use of gases as entrapping agents for the halogen-containing gases was unsuccessful. This lack of success was due primarily to the relative instability of the materials used at 1500° F. Some of the entrapping agents used were ethylene ($CH_2=CH_2$), acetylene ($CH\equiv CH$), ammonium hydroxide (NH_4OH), and monochlorotrifluoroethylene ($CF_2=CFCl$). The first two produced corrosive hydrogen chloride, the third was ineffective above 650° F and the fourth was totally ineffective.

These authors also indicated that the use of a diluent gas such as nitrogen to reduce the reactivity of a halogen-containing gas, CF_2Cl_2, at elevated temperatures was unsuccessful. The nitrogen diluent offered no beneficial influence; in fact, it was slightly detrimental.

The competitive reaction approach to the inhibitor concept was next considered by Buckley and Johnson. Examination of thermodynamic data indicated that the most likely potential inhibitor to react with metal surfaces in competition with chlorine would be oxygen. The oxides of nickel and cobalt are very tenacious and could conceivably form mixed films with the halides. In order to explore the possible influence oxygen could have on reducing halide volatility, experiments were conducted at 1500° F with mixtures of CF_2Cl_2

containing various percentages of air. The results showed a weight gain of the corrosion specimens with all air additions, including as little as 10 percent; this weight gain is in sharp contrast to the large weight losses in the 100 percent CF_2Cl_2 atmosphere. Since it has been previously established that nitrogen had an adverse influence, these beneficial results can be attributed to the oxygen of the air. X-ray diffraction patterns of surface films indicated the composition to be a mixture of a nickel oxide—chromic oxide spinel ($NiO{\cdot}Cr_2O_3$) and nickel chloride ($NiCl_2$). The same surface film identification was made for 10, 20, and 30 percent CF_2Cl_2 (with the remainder of the atmosphere air in all cases).

The desirable results obtained with the air-CF_2Cl_2 mixtures led to an investigation of the friction and wear properties of Al_2O_3 sliding on a cobalt-base alloy in a mixture of 70 percent air and 30 percent CF_2Cl_2 (fig. 8–33). The particular gas mixture was selected because it contains a sufficient number of active chlorine atoms to provide a good lubricating film and physical examination showed the surface film had good adherence to the substrate metal. The results show that at temperatures to 1000° F the mixed oxide-halide system gave friction and wear values nearly identical to those for the halide system alone (fig. 8–33). At temperatures from 1000° to 1500° F, however, the air addition definitely reduced the corrosive wear. It should be noted at this pont, however, that the wear that is plotted in figure 8–33 (and all figures of this part of the chapter) is rider wear only, that is, wear of the Al_2O_3. The disk specimen, which was the reactive metal in the combination, showed some evidences of wear at the higher temperatures.

It should again be emphasized that the choice of the gas, the material combination to be lubricated, and the operating temperature is extremely important. Great care must be taken to ensure that the reactivity is not so great as to result in corrosive wear, yet the reactivity must be great enough to provide effective lubrication.

An experiment was conducted at 1400° F with Al_2O_3 sliding on a cobalt-base alloy to determine the influence on friction coefficient of conversion of chloride to oxide in surface films. The results obtained are shown in figure 8–34. In the CF_2Cl_2 atmosphere, the friction coefficient was less than 0.1. On admission of air, the friction coefficient showed a continuous upward friction trend with increase in time (i.e., with decreasing concentration of chloride in the surface film). After an appreciable time in the air atmosphere, the friction coefficient reached a value approaching 0.5; at this time, the chloride film was believed to be totally converted to the oxide. The results indicate that the surface film has appreciable resistance to wear even though the halide film is not being reformed.

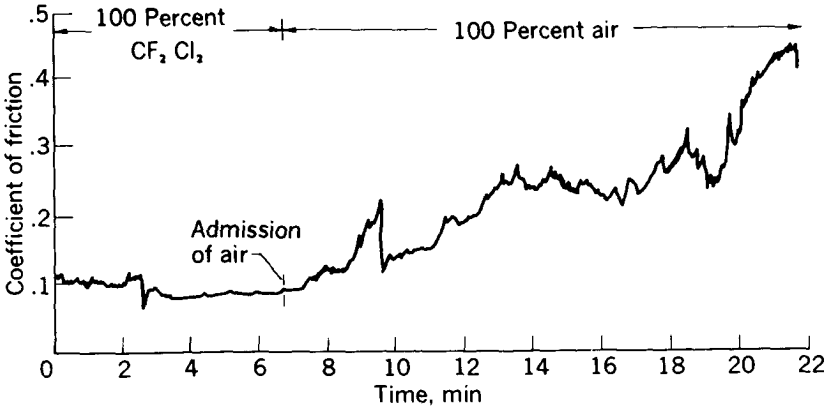

FIGURE 8-34.—Coefficient of friction of aluminum oxide sliding on a cobalt-base alloy at 1400° F. Atmospheres, difluorodichloromethane or air; sliding velocity, 3200 feet per minute; load, 1200 grams; duration of run, 1 hour. (From ref. 39.)

LUBRICATION OF FULL-SCALE BALL BEARINGS WITH REACTIVE GAS LUBRICANTS

It is of interest to note that Gray (ref. 41) reports some attempts to use gases containing reactive atoms as lubricants for full-scale rolling-element bearings. Gray concludes from his experiments that "operation of ball bearings over a temperature range of 110° to 1000° F on vapor Freon 12 (CF_2Cl_2) is shown not to be feasible under the circumstances described." The results of reference 41 were not unexpected in view of some difficulties experienced by the experimenters. At temperatures below 1000° F, bearings of 52100 and 440C steel with cages of bronze, monel, or silver were used. This choice of materials was unfortunate since the results of reference 31 show that silver and copper are not lubricated by CF_2Cl_2 at room temperature. Consequently, only the bearing with the monel cage had a chance of success *provided* that a run-in procedure had been used; reference 41 does not indicate that a run-in was provided. At 1000° F, the tests of reference 41 were performed with a tool-steel bearing; these also were reported as "unsuccessful." The results of reference 32 showed that the corrosion of M-1 tool steel by CF_2Cl_2 was very severe at elevated temperatures. In fact, figures 8 and 9 of reference 32 and the corrosion study results reported previously show that corrosive wear of M-1 becomes excessive above 600° F. Hence, unsuccessful operation under the conditions of reference 41 would not be unexpected.

A proper evaluation of reactive gases as lubricants for rolling element bearings has not, as yet, been conducted and thus their limitations as rolling-element-bearing lubricants cannot be assessed. Rolling-

element wear of any measurable magnitude cannot be tolerated; hence, the success of reactive gases would depend on their ability to provide lubricating films (at the cage rubbing surfaces and in the contact areas between the rolling elements and the races) without producing excessive wear.

SUMMARY

The mechanism of lubrication with reactive gases involves the following steps, in order: (1) generation of high temperatures at contacting asperities, (2) local decomposition of gas, which liberates active atoms, and (3) *local* reaction between metal and active atoms to form a low-shear-strength film at the precise location where protection (and lubrication) is required.

Reactive gas lubricants are promising for use in temperature ranges where conventional lubricants are completely ineffective or not permissible. Considerable research is required, however, on their utilization in practical mechanisms. Since they function on the basis of controlled corrosion, their use must be very judicious. The choice of the combination of gas, metals, and temperature is, therefore, most important.

REFERENCES

1. Peterson, Marshall B., and Johnson, Robert L.: Friction of Possible Solid Lubricants with Various Crystal Structures. NACA TN 3334, 1954.
2. Peterson, M. B., Florek, J. J., and Murray, S. F.: Consideration of Lubricants for Temperatures Above 1000° F. ASLE Trans., vol. 2, no. 2, May 1960, pp. 225–234.
3. Stillwell, Charles W.: Crystal Chemistry. McGraw-Hill Book Co., Inc., 1938.
4. Wyckoff, Ralph W. G.: The Structure of Crystals. Second ed., Chem. Catalog Co., Inc., 1931.
5. Helmholtz, Lindsay: The Crystal Structure of Anhydrous Cupric Bromide. Jour. Am. Chem. Soc., vol. 69, no. 4, Apr. 1947, pp. 886–889.
6. Bowden, F. P., and Tabor, D.: The Friction and Lubrication of Solids. Clarendon Press (Oxford), 1950.
7. Sejournet, J., and Delcroix, J.: Glass Lubricant in the Extrusion of Steel. Lubrication Eng., vol. 11, no. 6, Nov.–Dec. 1955, pp. 389–396.
8. Sliney, Harold E.: Lubricating Properties of Some Bonded Fluoride and Oxide Coatings for Temperatures to 1500° F. NASA TN D–478, 1960.
9. Ernst, Hans, and Merchant, M. Eugene: Surface Friction of Clean Metals. Proc. Conf. on Friction and Surface Finish, M.I.T., June 1940, pp. 76–101.
10. Godfrey, Douglas, and Bisson, Edmond E.: Bonding of Molybdenum Disulfide to Various Materials to Form a Solid Lubricating Film. I—The Bonding Mechanism. NACA TN 2628, 1952.
11. Devine, M. J., Lamson, E. R., and Bowen, J. H., Jr.: Inorganic Solid Film Lubricants. Jour. of Chem. and Eng. Data, vol. 6, no. 1, Jan. 1961, pp. 79–82.

12. Wilson, D. S., et al.: The Development of Lubricants for High-Speed Rolling Contact Bearings Operating Over the Range of Room Temperature to 1200° F. TR 60–732, WADD, Jan. 1961.
13. Johnson, R. L., and Sliney, H. E.: Ceramic Surface Films for Lubrication at Temperatures to 2000° F. Am. Ceramic Soc. Bull., vol. 41, no. 8, Aug. 1962, pp. 504–508.
14. Johnson, Robert L., Swikert, Max A., and Bisson, Edmond E.: Friction and Wear of Hot-Pressed Bearing Materials Containing Molybdenum Disulfide. NACA TN 2027, 1950.
15. Godfrey, Douglas, and Nelson, Erva C.: Oxidation Characteristics of Molybdenum Disulfide and Effect of Such Oxidation on Its Role as a Solid-Film Lubricant. NACA TN 1882, 1949.
16. Bisson, Edmond E., Johnson, Robert L., and Swikert, Max A.: Friction, Wear, and Surface Damage of Metals as Affected by Solid Surface Films: A Review of NACA Research. Proc. Conf. on Lubrication and Wear, Inst. Mech. Eng., 1957, pp. 384–391.
17. Bisson, Edmond E., Johnson, R. L., and Anderson, W. J.: Friction and Lubrication with Solid Lubricants at Temperatures to 1000° F with Particular Reference to Graphite. Proc. Conf. on Lubrication and Wear, Inst. Mech. Eng., 1957, pp. 348–354.
18. Peterson, M. B., and Johnson, R. L.: PbO and Other Metal Oxides as Solid Lubricants for Temperatures to 1000° F. Lubrication Eng., vol. 13, no. 4, Apr. 1957, pp. 203–207.
19. Smithells, Colin J.: Metals Reference Book. Second ed., Interscience Pub., Inc., 1955, pp. 575–616.
20. Mellor, J. W.: A Comprehensive Treatise on Inorganic and Theoretical Chemistry. Vol. VIII. Longmans, Green and Co., Ltd., 1940, p. 673.
21. Johnson, R. L., and Sliney, H. E.: High-Temperature Friction and Wear Properties of Bonded Solid Lubricant Films Containing Lead Monoxide. Lubrication Eng., vol. 15, no. 12, 1959, pp. 487–491; 496.
22. Coes, L., Jr.: Chemistry of Abrasive Action. Ind. and Eng. Chem., vol. 47, no. 12, Dec. 1955, pp. 2493–2494.
23. Herron, R. H.: Friction Materials—A New Field for Ceramics and Cermets. Am. Ceramic Soc. Bull., vol. 34, no. 12, Dec. 1955, pp. 395–398.
24. Sliney, Harold E.: Lubricating Properties of Ceramic-Bonded Calcium Fluoride Coatings on Nickel-Base Alloys from 75° to 1900° F. NASA TN D–1190, 1962.
25. Deacon, R. F., and Goodman, J. F.: Lubrication by Lamellar Solids. Proc. Roy. Soc. (London), ser. A, vol. 243, no. 1235, Feb. 1958, pp. 464–482.
26. Johnson, R. L., Swikert, M. A., and Buckley, D. H.: High Temperature Lubrication in Reactive Atmospheres. Corrosion, vol. 16, no. 8, Aug. 1960, pp. 101–104.
27. Kruh, R., and Stern, K. H.: The Effect of Solutes on the Properties and Structure of Liquid Boric Oxide. Jour. Am. Chem. Soc., vol. 78, no. 2, Jan. 1956, pp. 278–281.
28. Rabinowicz, E., and Imai, M.: Boric Oxide as a High Temperature Lubricant. Preprint 61–LUBS–17, ASME, 1961.
29. Milz, W. C., and Sargent, L. B., Jr.: Frictional Characteristics of Plastics. Lubrication Eng., vol. 11, no. 5, Sept.–Oct. 1955, pp. 313–318.
30. Wisander, D. W., and Johnson, R. L.: A Solid Film Lubricant Composition for Use at High Sliding Velocities in Liquid Nitrogen. ASLE Trans., vol. 3, no. 2, Oct. 1960, pp. 225–231.

31. MURRAY, S. F., JOHNSON, ROBERT L., and SWIKERT, MAX A.: Boundary Lubrication of Steel with Fluorine- and Chlorine-Substituted Methane and Ethane Gases. NACA TN 3402, 1955.
32. ALLEN, GORDON P., BUCKLEY, DONALD H., and JOHNSON, ROBERT L.: Friction and Wear with Reactive Gases at Temperatures up to 1200° F. NACA TN 4316, 1958.
33. BUCKLEY, DONALD H., and JOHNSON, ROBERT L.: Halogen-Containing Gases as Boundary Lubricants for Corrosion-Resistant Alloys at 1200° F. NASA MEMO 2-25-59E, 1959.
34. BUCKLEY, DONALD H., and JOHNSON, ROBERT L.: Halogenated Gases for High Temperature Lubrication of Metals. Ind. and Eng. Chem., vol. 51, no. 5, May 1959, pp. 699–700.
35. BUCKLEY, DONALD H., and JOHNSON, ROBERT L.: The Influence of Silicon Additions on Friction and Wear of Nickel Alloys at Temperatures to 1000° F. ASLE Trans., vol. 3, no. 1, Apr. 1960, pp. 93–99.
36. BUCKLEY, DONALD H., and JOHNSON, ROBERT L.: Lubrication of Corrosion Resistant Alloys by Mixtures of Halogen-Containing Gases at Temperatures to 1200° F. NASA TN D-197, 1959.
37. BUCKLEY, DONALD H., and JOHNSON, ROBERT L.: Use of Less Reactive Materials and More Stable Gases to Reduce Corrosive Wear When Lubricating with Halogenated Gases. NASA TN D-302, 1960.
38. JOHNSON, R. L., SWIKERT, M. A., and BUCKLEY, D. H.: High Temperature Lubrication in Reactive Atmospheres. Corrosion, vol. 16, no. 8, Aug. 1960, pp. 101–104.
39. BUCKLEY, DONALD H., and JOHNSON, ROBERT L.: Inhibiting Corrosive Wear in Lubrication with Halogenated Gases at 1500° F by Use of Competitive Reactions and Other Methods. ASLE Trans., vol. 4, no. 1, Apr. 1961, pp. 33–38.
40. SIMONS, J. H.: The Fluorocarbons. Chem. Eng., vol. 57, no. 7, July 1950, pp. 129–136.
41. GRAY, STANLEY: An Accessory Manufacturers Approach to Bearing and Seal Development. Paper 58-LUB-10, ASME, 1958. (Condensation pub. in Mech. Eng., vol. 81, no. 4, Apr. 1959, pp. 76–80.)
42. JOHNSON, ROBERT L., GODFREY, DOUGLAS, and BISSON, EDMOND E.: Friction of Solid Films on Steel at High Sliding Velocities. NACA TN 1578, 1948.
43. SLINEY, HAROLD E., and JOHNSON, ROBERT L.: Bonded Lead Monoxide Films as Solid Lubricants for Temperatures up to 1250° F. NACA RM E57B15, 1957.
44. NEMETH, Z. N., and ANDERSON, W. J.: Effect of Air and Nitrogen Atmospheres on the Temperature Limitations of Liquid and Solid Lubricants in Ball Bearings. Lubrication Eng., vol. 11, no. 4, July–Aug. 1955, pp. 267–273.
45. PETERSON, MARSHALL B., and JOHNSON, ROBERT L.: Friction and Wear Investigation of Molybdenum Disulfide. II—Effects of Contaminants and Method of Application. NACA TN 3111, 1954.
46. BISSON, EDMOND E., JOHNSON, ROBERT L., SWIKERT, MAX A., and GODFREY, DOUGLAS: Friction, Wear, and Surface Damage of Metals as Affected by Solid Surface Films. NACA TN 3444, 1955.
47. PETERSON, MARSHALL B., and JOHNSON, ROBERT L.: Friction Studies of Graphite and Mixtures of Graphite with Several Metallic Oxides and Salts at Temperatures to 1000° F. NACA TN 3657, 1956.

48. GELLER, R. F., CREAMER, A. S., and BUNTING, E. N.: The System: PbO-SiO_2. Jour. Res. Nat. Bur. Standards, vol. 13, no. 2, Aug. 1934, pp. 237–244.
49. BISSON, EDMOND E.: Étude du Frottement et de L'Usure À des Températures Élevées (jusqu'a 815° C) ou tres Basses (−250° C). (Study of Friction and Wear at Elevated Temperatures (to 815° C) or Very Low Temperatures (−250° C).) Rev. l'inst. Franc. pétrole, t. XVI, no. 4, Apr. 1961.
50. SLINEY, H. E.: Bearings Run at 1250° F with Solid Lubricant. Space Aero., vol. 35, no. 3, Mar. 1961, pp. 91–92; 94; 96; 98; 100.
51. KLEMGARD, E. N.: Fundamental Processes in Lubricating Metal Surfaces at 100° to 1700° F. Lubrication Eng., vol. 16, no. 10, Oct. 1960, pp. 468–476.

BIBLIOGRAPHY

BARWELL, F. T., and MILNE, A. A.: Use of Molybdenum Disulfide in Association with Phosphated Surfaces. Sci. Lubrication, vol. 3, no. 9, Sept. 1951, pp. 9–14.

BOWDEN, F. P., and ROWE, G. W.: Lubrication with Molybdenum Disulphide Formed from Gas Phase. Engineer, vol. 204, no. 5311, Nov. 1957, p. 667.

BOYD, JOHN, and ROBERTSON, B. P.: The Friction Properties of Various Lubricants at High Pressures. Trans. ASME, vol. 67, no. 1, Jan. 1945, pp. 51–56; discussion, pp. 56–59.

CAMPBELL, W. E.: Solid Lubricants. Lubrication Eng., vol. 9, no. 4, Aug. 1953, pp. 195–200.

DEACON, R. F., and GOODMAN, J. F.: Orientation and Frictional Behaviour of Lamellar Solids on Metals. Proc. of Conf. Lubrication and Wear, Inst. Mech. Eng., 1957, pp. 344–347.

DELCROIX, J.: Le Filage et ses Nouvelles Applications. Metallurgie et Construction Mecanique, t. 87, no. 6, Oct. 1955, pp. 793–795.

FENG, I-MING: Lubricating Properties of Molybdenum Disulfide. Lubrication Eng., vol. 8, no. 6, Dec. 1952, pp. 285–288; 306–308.

GODFREY, DOUGLAS, and BISSON, EDMOND E.: Bonding of Molybdenum Disulphide to Various Materials to Form a Solid Lubricating Film. II—Friction and Endurance Characteristics of Films Bonded by Practical Methods. NACA TN 2802, 1952.

GODFREY, DOUGLAS, and BISSON, EDMOND E.: Effectiveness of Molybdenum Disulfide as a Fretting-Corrosion Inhibitor. NACA TN 2180, 1950.

HODGMAN, CHARLES D., ed.: Handbook of Chemistry and Physics. Thirtieth ed., Chem. Rubber Pub. Co., 1947.

JOHNSON, ROBERT L., SWIKERT, MAX A., and BAILEY, JOHN M.: Wear of Typical Carbon-Base Sliding Seal Materials at Temperatures to 700° F. NACA TN 3595, 1956.

LAVIK, MELVIN T.: High Temperature Solid Dry Film Lubricants. TR 57–455, WADC, Feb. 1958.

LAVIK, MELVIN T.: High Temperature Solid Dry Film Lubricants. TR 57–455, pt. II, WADC, Oct. 1958.

LAVIK, MELVIN T.: High Temperature Solid Dry Film Lubricants. TR 57–455, pt. III, WADC, June 1959.

LAVIK, MELVIN T., and DANIEL, T. BRUCE: Development and Evaluation of High Temperature Solid Film Lubricants. Quarterly Prog. Rep. 1, Midwest Res. Inst., Jan.–Mar. 1959.

MACKS, E. F., NEMETH, Z. N., and ANDERSON, W. J.: Preliminary Investigation of Molybdenum Disulphide—Air-Mist Lubrication for Roller Bearings Oper-

ating at DN Values of 1×10^6 and Ball Bearings Operating to Temperatures of 1000° F. NACA RM E51G31, 1951.

MILNE, A. A.: Experiments on the Friction and Endurance of Various Surface Treatments Lubricated with Molybdenum Disulphide. Wear, vol. 1, no. 2, Oct. 1957, pp. 92–103.

MITCHELL, D. C.: The Wear of P.T.F.E. Impregnated Metal Bearing Materials. Proc. Conf. on Lubrication and Wear, Inst. Mech. Eng., 1957, pp. 396–404.

MITCHELL, D. C., and FULFORD, B. B.: Wear of Selected Molybdenum Disulphide Lubricated Solids and Surface Films. Proc. Conf. on Lubrication and Wear, Inst. Mech. Eng., 1957, pp. 376–391.

MITCHELL, D. C., and PRATT, G.: Friction, Wear, and Physical Properties of Some Filled P.T.F.E. Bearing Materials. Proc. Conf. on Lubrication and Wear, Inst. Mech. Eng., 1957, pp. 416–423.

MORDIKE, BARRY L.: Lubrication of Solids at High Temperatures. ASLE Trans., vol. 3, no. 1, Apr. 1960, pp. 110–115.

Page intentionally left blank

CHAPTER 9

Friction and Bearing Problems in the Vacuum and Radiation Environments of Space

By EDMOND E. BISSON

THE SPACE AGE HAS BROUGHT WITH IT a number of materials problems which have rarely been experienced in the past. These problems include exposure to certain peculiarities of space, which comprises such environmental conditions as (1) a very low ambient pressure, (2) a radiation environment, (3) the presence of meteoroids, (4) the absence of a gravitational field, and (5) the presence of different atomic species than those normally encountered. The various problems, their relative importance, and some indication of research in these various areas are discussed in considerable detail in references 1 to 6.

Friction and bearing problems are of particular importance in the coming space age. The various peculiarities of the environment of space all contribute to these friction and bearing problems. For example, the low-pressure environment contributes to rapid evaporation of the normal liquid or semisolid grease lubricants normally employed. Also, the presence of a radiation flux can theoretically influence the stability of some of these commonly employed lubricants. Other problems arise because of the lack of oxygen available. As previously mentioned, lubrication ordinarily takes place by means of contaminating films between the sliding or rolling surfaces. These contaminating films can be liquids, such as the common liquid lubricants, or solid films of low shear strength. The lubrication function is, with many metals, strongly influenced by the presence or absence of oxide films on these metals. The surface oxides frequently act as protective films and, in some cases, contribute to the final surface film through either chemical reaction or chemisorption.

One of the problems at altitudes greater than 55 miles involves the fact that air does not consist of the ordinary molecular species of

oxygen and nitrogen (ref. 7); both oxygen and nitrogen exist in the atomic species. The reaction rates between most metals and atomic oxygen are markedly different from those with molecular oxygen. The influence of this different reaction rate on the friction and lubrication process is unknown at the present time. Also, at altitudes greater than 800 miles, atomic hydrogen and helium are the principal species present.

Friction and bearing problems also become increasingly difficult in space travel as a result of the following factors (ref. 1): (1) length of mission, (2) duration and degree of high-temperature exposure, (3) duration and degree of exposure to radiation of various types, and (4) dangers of contamination by condensation. Clauss (ref. 2) indicates that shock and vibration loads occurring during launch, ascent, and reentry can also cause difficulties in mechanisms operating in a spacecraft. The authors of reference 1 indicate that missions lasting short periods of time (weeks or months) may be successful at 10^{-7} or 10^{-8} millimeter of mercury [1] with grease lubricated bearings under moderate temperature and radiation conditions. Fluids such as silicones, diesters, or polyethers are possibilities. For long-time missions, however, fluids will probably not be satisfactory as lubricants. Under these conditions, solid surface films having low vapor pressure will be necessary. Preformed solid surface films will, of necessity, have limited life. Hence, it is important that the mechanisms be so designed as to ensure that severe conditions of operation are not placed upon the preformed solid surface films. Other than preformed solid surface films, there are some materials which have inherent self-lubricating properties. These materials are of prime importance for this type of service.

Exact duplication of the various conditions existing in space is extremely difficult. For example, the combination of radiation flux, pressure level, and proper concentration of atoms of the various gases is difficult to achieve. Some of these conditions can be simulated, however, in such a manner that their relative effects can be measured or estimated.

This chapter discusses, in general, the friction and bearing problems that result from the exposure of mechanisms to the vacuum or radiation environments of space. While some of these problems can be eliminated by design techniques, such as the use of hermetically sealed systems, this solution is not always possible because of its complexity and weight disadvantages. Solutions involving self-lubricating materials or limited-life lubricants should be better and are discussed in this chapter.

---

[1] 1 mm Hg is essentially equal to 1 Torr.

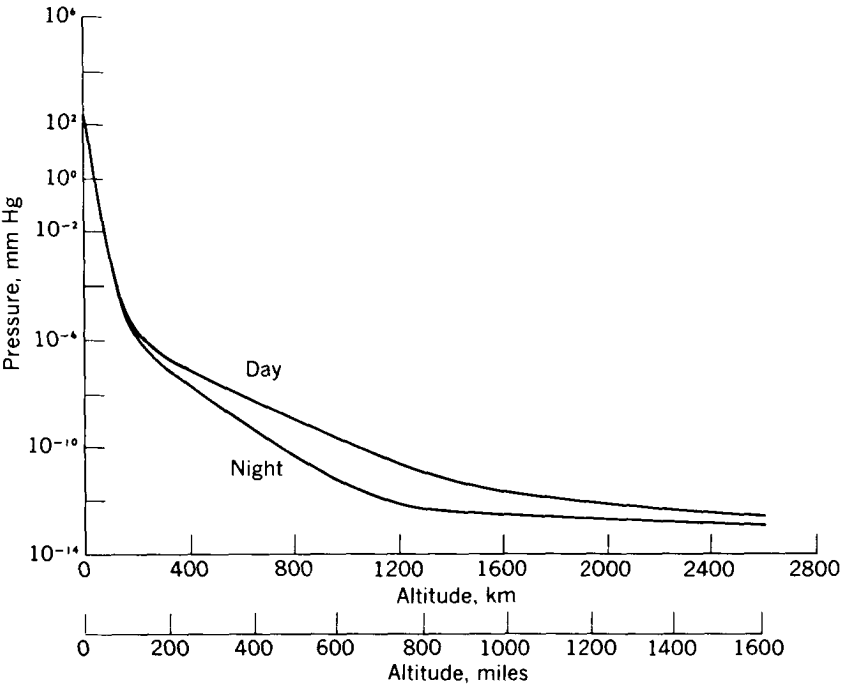

FIGURE 9–1.—Pressure as a function of altitude. (From ref. 25.)

VACUUM

Definition of Environment

The principal environmental change between space and the Earth's surface is that of pressure level. The absolute pressure outside the Earth's atmosphere is estimated at approximately 10^{-13} millimeter of mercury, while the absolute pressure in interstellar space is estimated at approximately 10^{-16} millimeter of mercury. Figure 9–1 shows the pressure as a function of altitude. Pressure drops rather sharply from normal atmospheric pressure down to 10^{-6} millimeter of mercury at 100 miles. Thereafter, the pressure drops more slowly and gradually approaches the value of 10^{-13} millimeter of mercury previously given. An important result of this very low pressure (and consequent lack of gaseous atmosphere) is that the temperature level will be dictated normally by radiation. Heat will be absorbed by radiation from any object that the mechanism "sees" and the mechanism will, in turn, reject heat to outer space by radiation. Various mechanisms will have different temperature levels depending upon these relative rates of heat gain and loss. It is important to note that evaporation from surfaces is an exponential function of temperature; in conse-

quence, the actual temperature of the mechanisms is important in this respect.

As previously mentioned, it is difficult to duplicate in a vacuum chamber the various conditions existing in space. Conduction of meaningful experiments in a vacuum chamber requires precise knowledge of the gaseous species present. Mass spectrometer data in a vacuum friction apparatus have been obtained (ref. 8) for some of the friction studies conducted at the NASA laboratories. Data representative of these studies are presented in figure 9–2. The

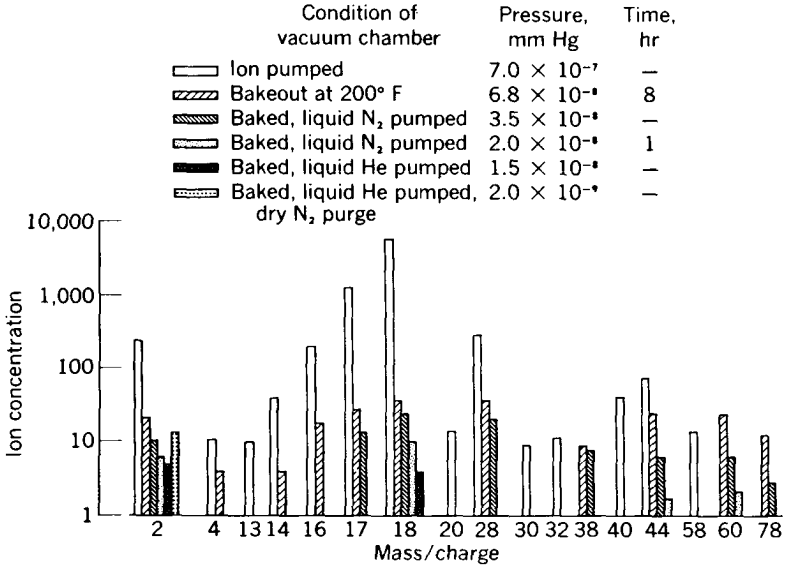

FIGURE 9–2.—Mass spectrometer data obtained in vacuum friction and wear apparatus. (From ref. 8.)

results show that many species are present with ion pumping, for example, hydrogen (2), nitrogen (14), oxygen (16), hydroxyl (17), water (18), carbon monoxide (28), nitrogen (28), and carbon dioxide (44). (The numbers in parentheses are the ratio of molecular weight to charge.) Figure 9–2 shows reduction of detectable gases by various techniques to the point where only hydrogen is present when liquid helium is used to cryopump the chamber after bakeout at 200° F and dry-nitrogen purge.

Evaporation Rates in Vacuum

The Langmuir equation for rate of evaporation is

$$G=\frac{P}{17.14}\sqrt{\frac{M}{T}} \tag{1}$$

where G is the rate of vaporization ((g)/(sq cm) (sec)), P is vapor pressure (mm Hg), M is molecular weight, and T is temperature (°K). The vapor-pressure equation can be written as follows:

$$P = Ce^{-L/RT} \tag{2}$$

where C is a constant, L is the heat of vaporization, and R is the gas constant. The Langmuir equation (1) is based on the assumption that all the atoms that evaporate from the surface are lost permanently: that is, none of the atoms are reflected back to the surface to permit possible recondensation. The Langmuir equation thus yields the maximum rate of loss.

If, on the other hand, the ambient pressure is sufficiently high, all the vaporizing atoms are not lost permanently because some of them are back reflected to the surface by collisions with other atoms or molecules in the gas phase. The net loss of material is thus lower than the maximum computed from equation (1). The pressure at which measurable deviation from equation (1) occurs is approximately that for which the mean free path is of the order of the dimensions of the evaporating surface. An example of the mean free path of a metal is that for silver:

Pressure, mm Hg	760	1	10^{-3}	10^{-6}	10^{-12}
Mean free path, cm	2×10^{-5}	1.5×10^{-2}	1.5×10^{1}	1.5×10^{4}	1.5×10^{10}

Vapor-pressure determinations at pressures of the order of 10^{-6} millimeter of mercury in which the evaporating material strikes a cryogenically cooled condensing surface do not generally suffer inaccuracy from the back-reflection phenomenon.

Experimentally determined vapor pressures are available for many pure metals (refs. 9 and 10). These vapor pressures were determined under conditions where back reflection was not a major factor. The rate of evaporation in space vacuum can thus be computed directly. Table 9–I lists vaporization losses, computed in terms of inches of thickness per year at two temperatures for a variety of metals.

Lad (ref. 3) indicates that evaporation rate of metals can be markedly influenced by oxide layers on the surface. Loss of metal from a surface covered with a dense oxide would depend on the rate of diffusion of metal atoms through the oxide layer rather than on the vapor pressure of the metal itself. At high temperatures, where the vapor pressure is high, metals generally form oxides that are porous, and thus no interference with measurements of vapor pressure is

TABLE 9–I.—MAXIMUM VAPORIZATION LOSSES COMPUTED FROM LANGMUIR EQUATION FOR VARIOUS METALS AT 50 AND 75 PERCENT ABSOLUTE MELTING POINT [a]

Metal	Melting point, °F	50 percent of absolute melting point		70 percent of absolute melting point	
		Temperature, °F	Loss, in./yr	Temperature, °F	Loss, in./yr
C	6700	3120	7.5×10^{-5}	4550	21.7
W	6170	2855	2.9×10^{-9}	4180	4.2×10^{-3}
Ta	5425	2480	3.6×10^{-11}	3660	3.3×10^{-4}
Mo	4760	2150	1.4×10^{-8}	3195	1.1×10^{-2}
Nb	4380	1960	4.6×10^{-15}	2930	1.5×10^{-6}
Cr	3272	1405	2.0×10^{-3}	2150	115
Pt	3224	1380	8.4×10^{-14}	2120	3.5×10^{-6}
Fe	2800	1170	7.7×10^{-9}	1820	1.4×10^{-2}
Co	2723	1130	8.1×10^{-12}	1770	8.7×10^{-5}
Ni	2650	1095	2.1×10^{-11}	1720	2.9×10^{-4}
Be	2340	940	1.6×10^{-9}	1550	6.6×10^{-3}
Al	1220	380	4.8×10^{-23}	715	2.6×10^{-12}
Mg	1200	370	1.0×10^{-3}	700	53

[a] From ref. 3.

obtained. Aluminum, however, appears to be an exception. The vapor-pressure data for aluminum are generally suspected to be low because the dense oxide forms very rapidly even at low temperatures and with little oxygen present. Table 9–I shows that the rates of evaporation of aluminum and magnesium at approximately the same temperature are different by a factor of 10^{20}. This difference is probably caused by the porosity of the oxide film since the oxide of aluminum is not porous while that of magnesium is porous.

It can be seen from table 9–I that choosing a material with a low evaporation rate cannot be based on melting point. It must be based on evaporation rate. A good example is that of chromium and platinum; the evaporation rates for these two materials are different by a factor of about 10^{10} in spite of the fact that their melting points are very nearly the same. The evaporation rates of alloys cannot be predicted solely on the basis of vapor pressure of the component elements of the alloys; in general, the measured rate is much lower (ref. 3).

It is also important to note that, since evaporation rates are strongly influenced by oxide films, the rate of formation of these oxides is very important. It has been reported (ref. 11) that, at 10^{-3} millimeter of mercury, copper oxidizes at almost the same rate as at atmospheric pressure. Also, at a vacuum of 10^{-6} millimeter of mercury, oxide

films can form in about 1 second. In consequence, presence of a relatively few oxygen atoms can markedly affect the evaporation rates from metals.

Oils and greases.—The evaporation rates for various oils and greases were determined under vacuum conditions (10^{-6} to 10^{-7} mm Hg) at various temperatures by Buckley, Swikert, and Johnson (ref. 5). These results are presented as figure 9–3. Mil–L–7808 is the synthetic lubricant in common use in aircraft turbine engines. This lubricant was reported (ref. 5) to have bubbled continuously while evaporating. The high-temperature mineral oils with the two viscosities shown in figure 9–3 showed evaporation rates somewhat lower than that for Mil–L–7808. The polyphenyl ether was a solid at 55° F and exhibited no detectable weight change in 60 hours at this temperature. At 200° F the ether was a liquid and the evaporation rate was relatively high. As would be suspected, the evaporation rate tests of the greases indicated that the base oil of each grease was evaporating first. The radiation-resistant grease showed a very low rate of evaporation at 55° F; however, it became rubbery at 200° F.

An arbitrary limit of 10^{-7} gram per square centimeter per second was set on the evaporation rate; values greater than this were considered excessive. While this choice is arbitrary, it is based on the fact that a boundary-lubricating film of liquid that is 20 molecular layers thick will evaporate in less than 1 minute. On this basis, none

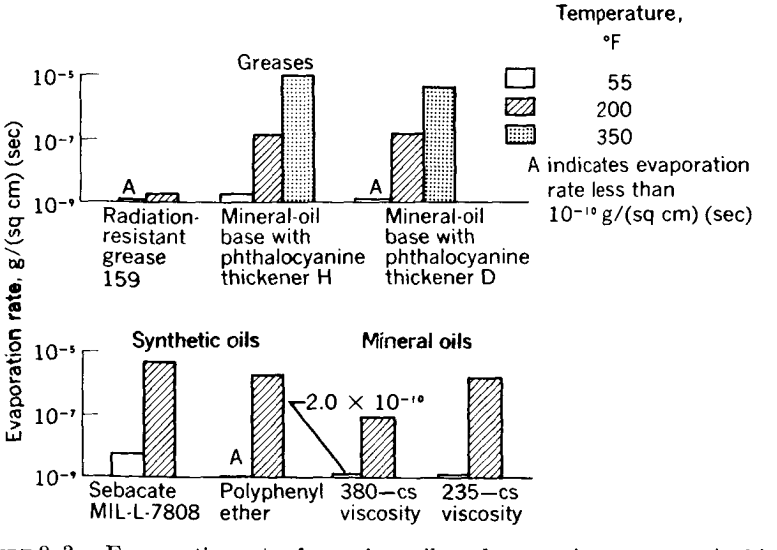

FIGURE 9–3.—Evaporation rates for various oils and greases in vacuum. Ambient pressure, 8.0×10^{-7} to 2.0×10^{-6} millimeter of mercury. (From ref. 5.)

of the materials of figure 9–3 are satisfactory at temperatures of 200° F or greater.

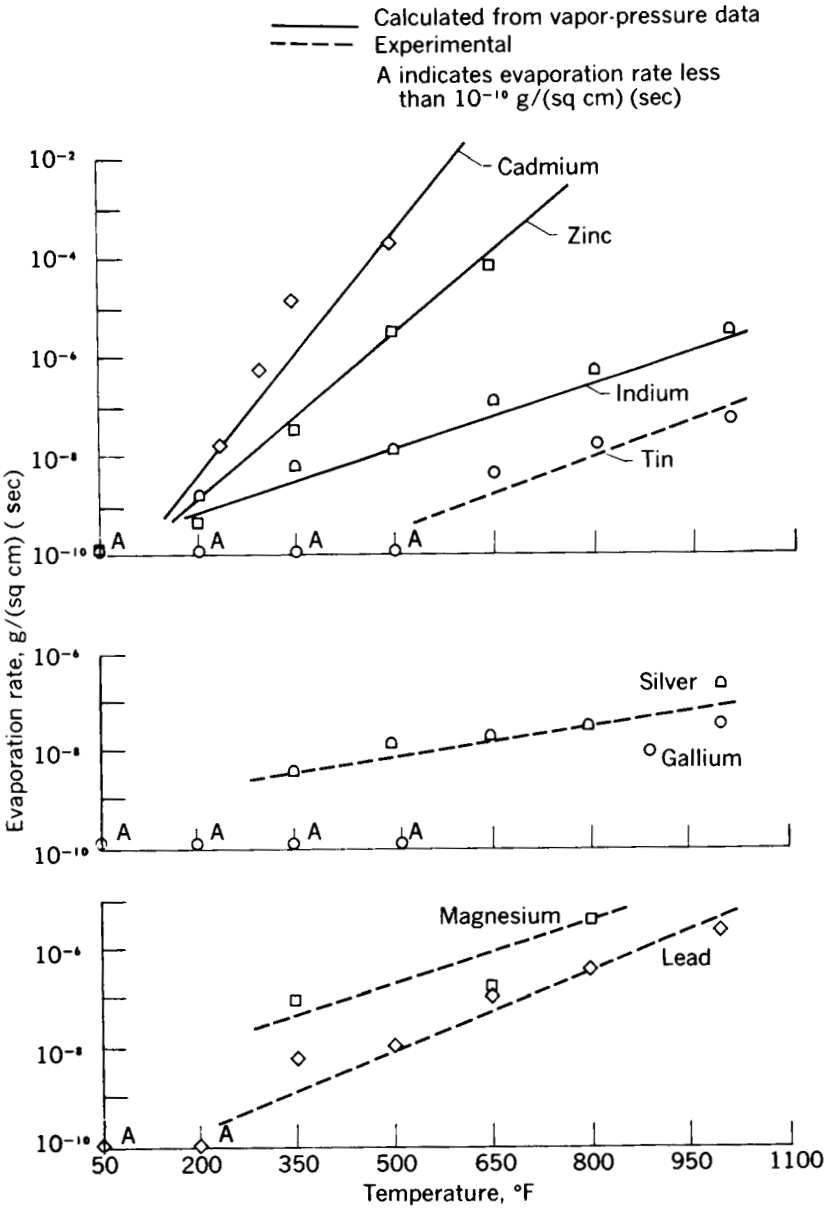

FIGURE 9–4.—Evaporation rates for various metals in vacuum. Ambient pressure, 8.0×10^{-7} to 2.0×10^{-6} millimeter of mercury. (From refs. 5 and 15.)

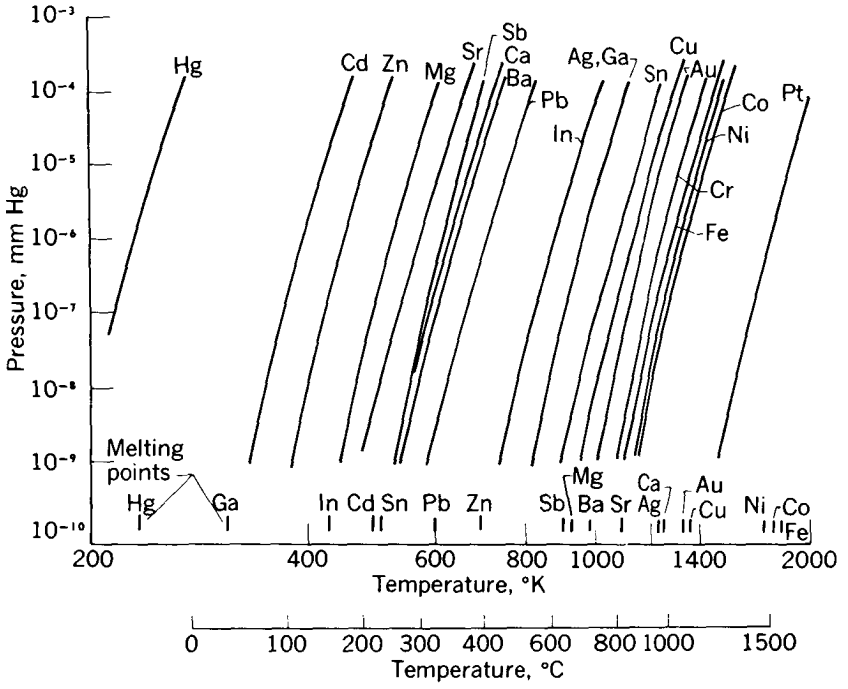

FIGURE 9–5.—Vapor pressure as a function of absolute temperature for soft and other selected metals. (From ref. 9.)

Metals.—Evaporation rates for various metals were determined in vacuum over the range of temperatures from 55° to 1000° F (ref. 5). The results of this investigation are presented in figure 9–4, which presents evaporation rate as a function of temperature for metals for which vapor pressure is known from the literature. The calculated evaporation rates based on measured vapor-pressure data are included in this figure as solid lines. The experimental data of the investigation of reference 5 are shown as the individual data points. In general, there is very good agreement between the calculated and measured evaporation-rate data.

Evaporation rates of the metals silver, gallium, magnesium, lead, and tin are shown in figure 9–4; lead, tin, and silver are seen to have the lowest rates of evaporation of the soft metals investigated. Gallium is a special case in that it showed very low evaporation rates at temperatures up to 1000° F (ref. 15). Gallium is discussed in more detail later in this chapter.

Figure 9–5 shows vapor-pressure data (from literature) for a variety of pure metals. It is from data such as these that the calculated curves of figure 9–4 were obtained.

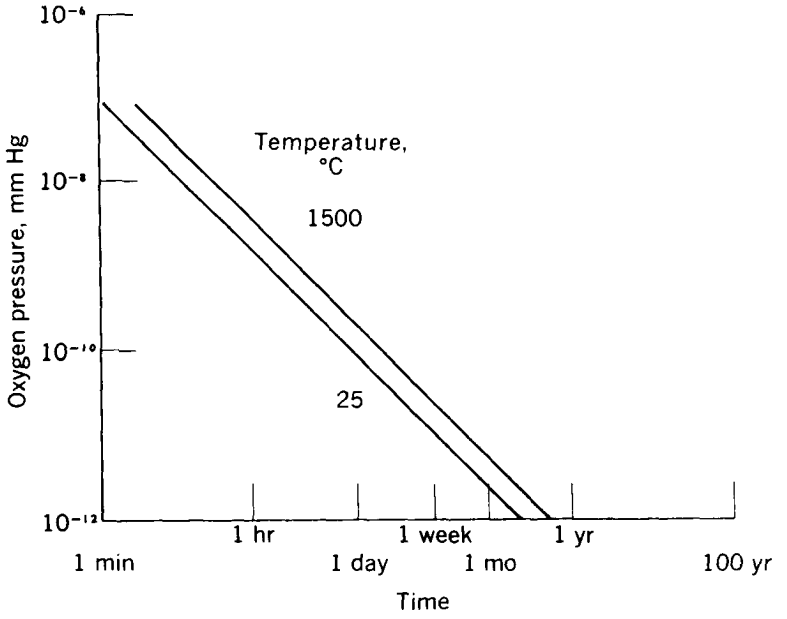

FIGURE 9-6.—Time required to form hypothetical 1-angstrom-thick film of FeO on iron. (From ref. 1.)

Since the principal gaseous species present in space (beyond 1200 km) are atomic hydrogen and helium, space simulation requires reduction of oxygen concentration to a negligible level. An additional reason for reducing the concentration of oxygen is the fact that it reacts with many metals to form oxides, which strongly influence the friction and wear mechanism.

Figure 9-6 is included to show the time required to form a hypothetical film of FeO on iron; this film is 1 angstrom thick. It will be noted that, at 25° C, a film of FeO forms on iron in 1 minute even at oxygen pressures as low as 10^{-7} millimeter of mercury. Hence, experimental data on friction in vacuum must be obtained at oxygen pressure levels lower than 10^{-7} millimeter of mercury; for example, conducting friction experiments at oxygen pressure levels of 10^{-9} or 10^{-10} millimeter of mercury is desirable since a 1-angstrom-thick film of FeO would require from 1 hour to 1 day to form under these conditions. Because these pressure levels of 10^{-9} to 10^{-10} millimeter of mercury are oxygen pressures, the total (or system) pressures need not be this low; however, it is important that the total pressure be low enough to ensure that oxygen concentration is negligible. Hence, it is believed that system pressure, for friction experiments, should be in the 10^{-9} millimeter of mercury range.

Coatings.—In order to interpret the evaporation rates of solid-film lubricant coatings, evaporation-rate data were obtained on the con-

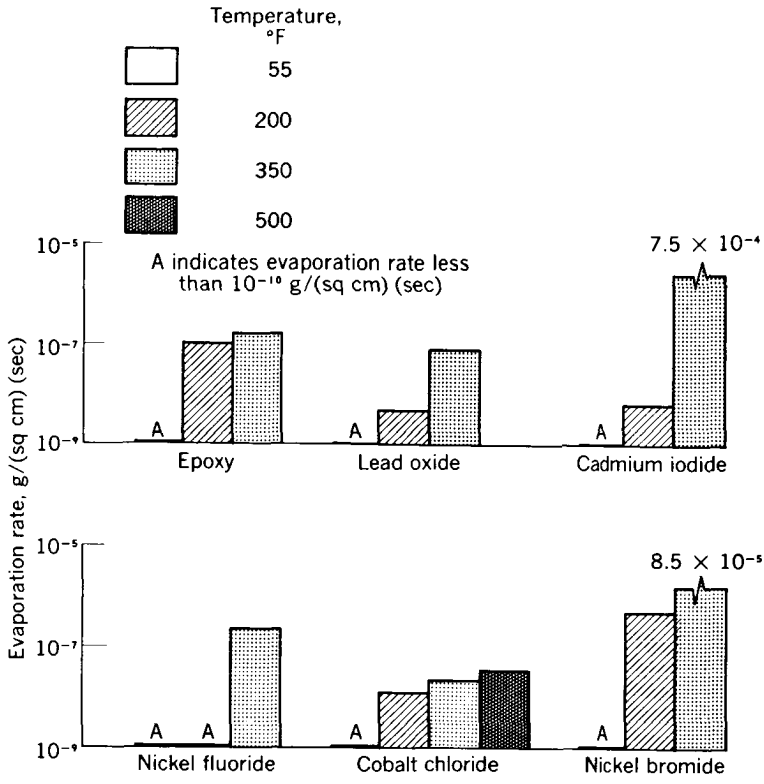

FIGURE 9–7.—Evaporation rates for constituents of solid-film-lubricant coatings in vacuum. Ambient pressure, 8.0×10^{-7} to 2.0×10^{-6} millimeter of mercury. (From ref. 5.)

stituents of the coating as well as the final coatings themselves. The data for compressed disks of various lubricant-coating constituents are presented in figure 9–7. Of these materials, the cobalt chloride had the lowest evaporation rate at the highest temperature (500° F). The nickel fluoride showed no evidence of evaporation at both of the lower temperatures; however, at 350° F, it dissociated to metallic nickel and fluorine. Lead oxide also dissociated at 350° F to metallic lead and oxygen. On the other hand, cobalt chloride, cadmium iodide, and nickel bromide evaporated and condensed on the condensing shield of the evaporation apparatus as cobalt chloride, cadmium iodide, and nickel bromide, respectively. The epoxy showed evidence of decomposition at the highest temperature tested (350° F).

The evaporation rates for molybdenum disulfide, tungsten disulfide, calcium fluoride, and barium fluoride at temperatures from 55° to 1000° F are shown in figure 9–8. The upper curve is for tungsten disulfide and the lower curve is a weighted average for the other three materials. In general, the evaporation rates of these materials in

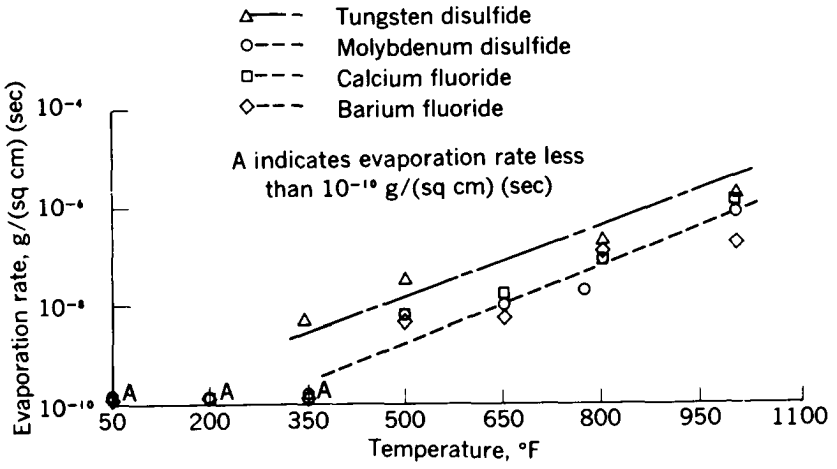

FIGURE 9–8.—Evaporation rates for various inorganic compounds in vacuum. Ambient pressure, 8.0×10^{-7} to 2.0×10^{-6} millimeter of mercury. (From ref. 5.)

vacuum were quite low even at elevated temperatures; these materials, therefore, appear to be the most stable of the inorganic substances tested (ref. 5).

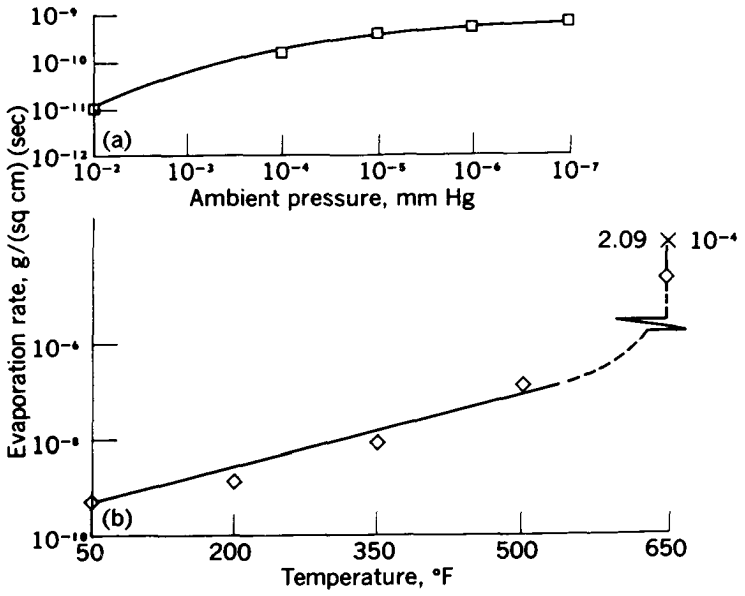

(a) Room temperature.
(b) Pressure, 8.0×10^{-7} to 2.0×10^{-6} millimeter of mercury.

FIGURE 9–9.—Evaporation rate of Teflon (polytetrafluorethylene) at various temperatures and pressures. (From ref. 5.)

The evaporation rates for Teflon (polytetrafluorethylene) as a pure polymer without plasticizer were determined for ranges of pressure (10^{-2} to 10^{-7} mm Hg) and of temperature (55° to 650° F). The results are presented in figure 9–9. In general, figure 9–9 shows relatively little change in evaporation rate with change in pressure. With change in temperature, however, the Teflon shows a marked increase in evaporation rate at the 650° F temperature. This result would be expected since decomposition of this material starts at about 550° F. Because Teflon is a polymer with a wide range of molecular weights, evaporation rates for different specimens will be different.

Because molybdenum disulfide coatings have been extremely effective lubricants at atmospheric pressures, the evaporation rates of a number of preformed bonded molybdenum disulfide coatings were determined. The coatings were as follows: ceramic bonded, metal matrix bonded, silicone resin bonded, and phenolic-epoxy bonded. The results of the evaporation-rate experiments are given in figure 9–10. These show that the evaporation rate for all coatings was relatively low. The evaporation-rate curve for each of the various

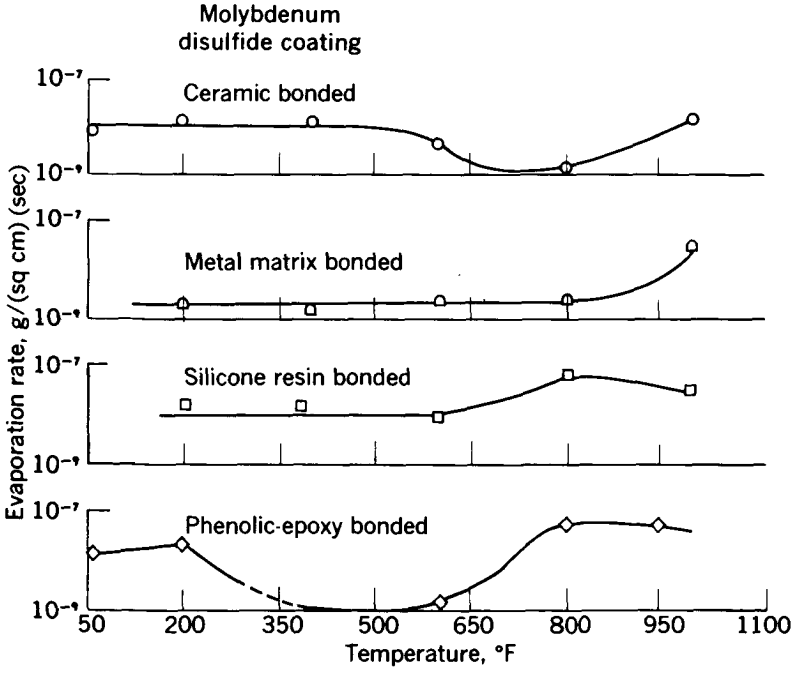

FIGURE 9–10.—Evaporation rate of various molybdenum disulfide coatings in vacuum. Ambient pressure, 1.0 to 2.0×10^{-6} millimeter of mercury; 0.001-inch coating on nickel-chromium alloy. (From ref. 5.)

coatings was broken; this result indicates a change in the evaporation rate. The change may be due to the difference in evaporation rate between that of the molybdenum disulfide and that of the binder.

Friction and Wear in Vacuum

With respect to friction, one of the most important adverse effects of the extremely low pressures in space is the possible removal of the surface films by evaporation. It is known from chapter 2 that, if the surfaces become sufficiently clean, the friction between these surfaces rises to a very high level; in fact, severe adhesion and welding can occur under these conditions. For example, Bowden and Tabor (ref. 11) showed that, with thorough outgassing of specimens in vacuum at relatively high temperatures (in the order of 800° to 900° C), friction coefficients increased by a factor of 10 or more. With specimens of nickel sliding on tungsten, initial friction coefficient before outgassing was of the order of 0.4; after outgassing, the friction coefficient was of the order of 6.0. Similarly, for specimens of copper on copper, the friction coefficient before outgassing was approximately 0.5; after outgassing, the value was approximately 4.5. Admission of a trace of oxygen into the chamber produced a marked reduction in friction coefficient of nearly the same order of magnitude as the original increase (see ch. 2).

In chapter 2, the importance of solid solubility to welding of metals was discussed. This effect is particularly of concern in the vacuum of space, since the metals have a tendency to rub together in their "virgin" states. It would appear that, to avoid this problem, the use of a dissimilar material combination should be attempted where possible. Examples of such dissimilar combinations include plastic-metal, plastic-ceramic, and ceramic-metal.

Metals.—In the studies of reference 5, friction and wear experiments were conducted in air and in vacuum with five alloy combinations in the unlubricated state. The results obtained in this investigation are shown in figure 9–11. The results for the iron-base alloy 52100 sliding on 52100 appear to contradict the results of reference 11, which showed that operation of metals in vacuum increased friction coefficient markedly. It should be noted that the specimens of reference 5 were not outgassed and, hence, had some oxide films on them. The reduction in friction coefficient under vacuum conditions for the 52100 specimens may possibly be the result of the formation of oxides of iron lower than the normal Fe_2O_3, that is, the formation of FeO or Fe_3O_4. These lower oxides have been shown (ref. 12) to be beneficial from the standpoint of friction and wear.

Figure 9–12 shows the friction of 52100 sliding on 52100 as a function of the ambient pressure in the chamber. This pressure was

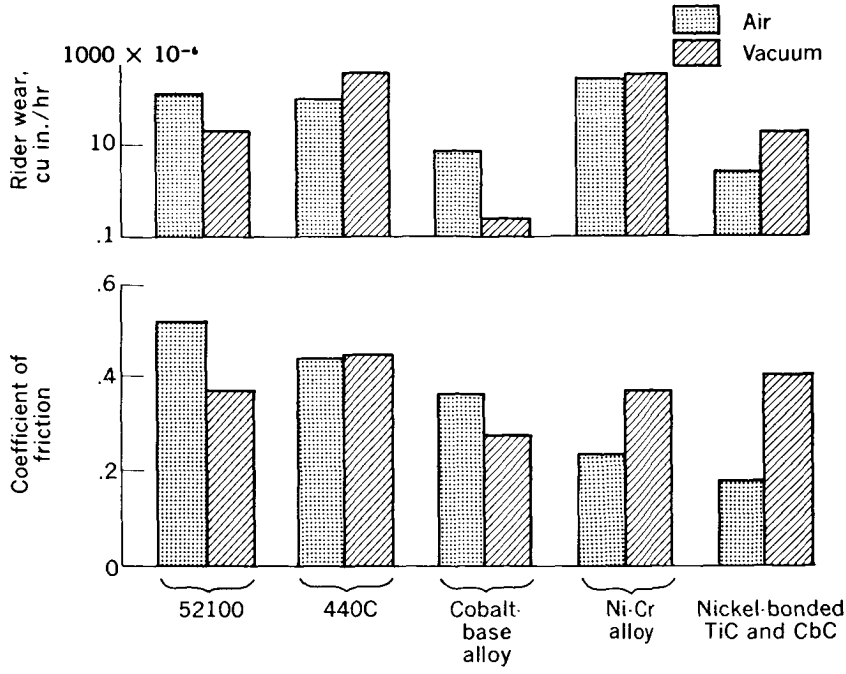

FIGURE 9–11.—Friction and wear of various alloys in air and in vacuum. Vacuum, 6.5×10^{-7} to 2.0×10^{-6} millimeter of mercury; sliding velocity, 390 feet per minute; load, 1000 grams; duration of run, 1 hour. (From ref. 5.)

varied from atmospheric down to 2×10^{-7} millimeter of mercury. The friction coefficient at atmospheric pressure is approximately 0.45 and decreases to a minimum of approximately 0.2 at 10^{-2} millimeter of mercury, after which it increases to about 0.38 at 2.0×10^{-7} millimeter of mercury. These results are presumed to be explained by the formation of the beneficial iron oxides FeO and Fe_3O_4 at the intermediate pressure levels. At the pressure levels of 10^{0} to 10^{-6} millimeter of mercury, the beneficial oxides would have a tendency to form because of the limited availability of oxygen atoms.

For some metals, the presence of extremely small quantities of oxygen has been found (ref. 13) sufficient to provide adequate surface protection of the metal by the oxide. For example, with 440C stainless steel sliding on 440C, 0.03 volume percent oxygen was sufficient to provide surface protection. Even at a pressure of 10^{-6} millimeter of mercury, the results of figure 9–12 show that sufficient oxygen is present to form the beneficial iron oxides. Hence, experiments were made with lower concentrations of oxygen.

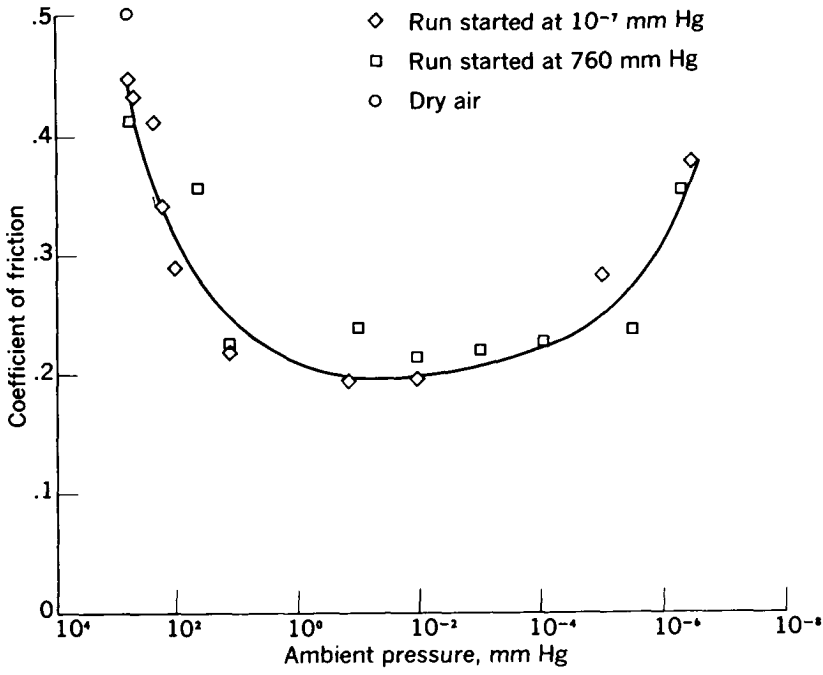

FIGURE 9–12.—Coefficient of friction for 52100 sliding on 52100 at various ambient pressures. Sliding velocity, 390 feet per minute; load, 1000 grams; temperature, 75° F. (From ref. 5.)

Figure 9–13 shows the results of experiments conducted on 52100 sliding against 52100 under a pressure of 10^{-6} to 10^{-7} millimeter of mercury obtained by cryopumping. In this case, a liquid-helium condensing coil was added inside the vacuum chamber in order to condense the condensable gases, such as nitrogen and oxygen. In this manner, the authors of reference 5 felt that the availability of oxygen atoms would be markedly reduced. Figure 9–13 confirms their belief. Friction coefficient as a function of time showed a slight increase from the initial value of 0.2 up to the value of about 1.0 at 30 minutes. After 30 minutes, the friction coefficient rose markedly to a value around 4, after which it continued rising until the specimens welded so firmly together that the drive motor of the mechanism was stalled. The initial low friction coefficient is believed to have been the result of the presence of the beneficial, lower oxides of iron. The time during which the friction coefficient remained relatively low (i.e., under 1.0), represents the time required to wear this beneficial oxide film from the surface. After the oxide film had been worn from the surface, it could not reform because of the limited availability of oxygen atoms. Hence, complete and total failure of the surfaces took place.

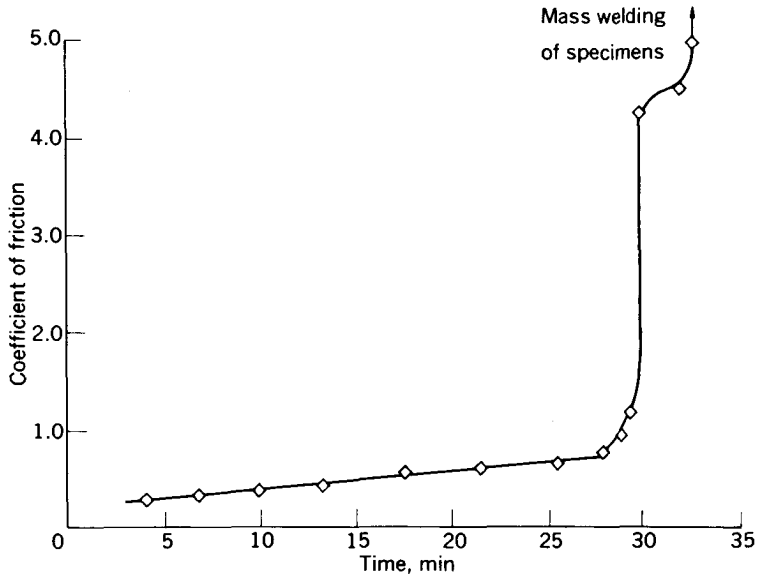

FIGURE 9–13.—Coefficient of friction for 52100 sliding on 52100 in vacuum with liquid-helium cryogenic pumping; pressure, 2.0×10^{-7} millimeter of mercury; sliding velocity, 390 feet per minute; load, 1000 grams. (From ref. 5.)

From the friction and wear results with the various alloys (fig. 9–11) the cobalt-base alloy apparently has the best friction and wear properties in vacuum. Examination of the rubbing surfaces yielded no evidence of mass metal transfer in vacuum. Other research (ref. 13) has indicated that this alloy has good friction and wear properties in inert and reducing atmospheres; the same results could, therefore, be expected in vacuum.

Coatings.—Friction and wear experiments were conducted (ref. 5) on a number of solid-film lubricant coatings. The friction and wear results for various molybdenum disulfide films in vacuum are presented in figure 9–14. These tests were conducted at a pressure of approximately 10^{-6} millimeter of mercury, with coatings of 0.0002- to 0.0003-inch thickness. From the results, it is obvious that the binder material plays some role in the friction and wear process. The best results were obtained with a silicone-resin-bonded and a phenolic-epoxy-bonded molybdenum disulfide film. The ceramic-bonded molybdenum disulfide film gave the poorest result; it should be pointed out, however, that these tests were at room temperature and a comparison of the ceramic-bonded and phenolic-epoxy coatings at elevated temperatures might produce vastly different results.

Figure 9–15 shows the results of experiments with other lubricant coatings. These other lubricant coatings include two coatings de-

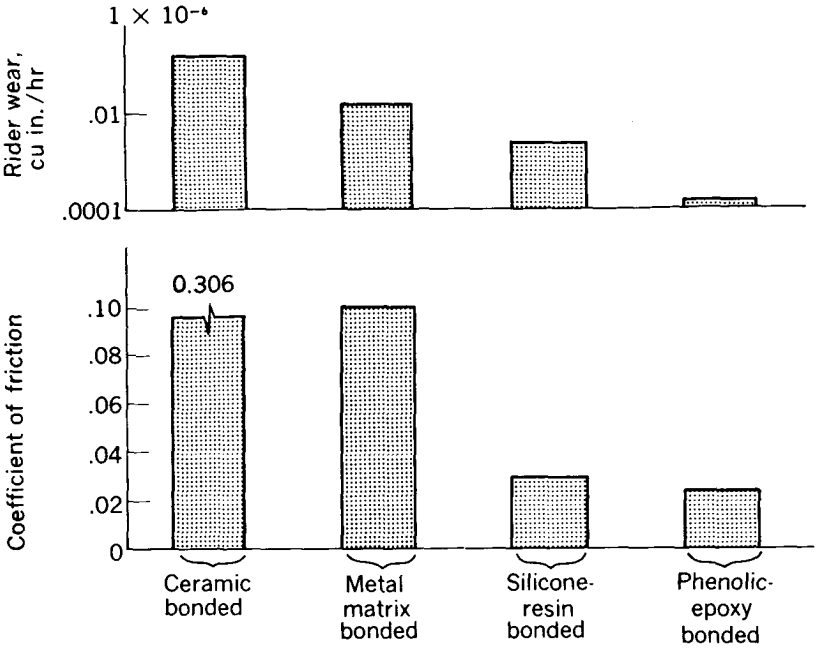

FIGURE 9–14.—Friction and wear of 440C on 440C with various molybdenum disulfide (0.0002- to 0.0003-in. thick) films. Ambient pressure, 8.0×10^{-7} to 2.0×10^{-6} millimeter of mercury; sliding velocity, 390 feet per minute; load, 1000 grams; duration of run, 1 hour. (From ref. 5.)

veloped particularly for high-temperature use in air (lead oxide—silicon dioxide ($PbO\text{-}SiO_2$) and calcium fluoride (CaF_2)). The coatings in figure 9–15 also encompass the soft metals: tin, gold, lead, and silver. The metal films have been used as lubricants under vacuum conditions in the past.

The results obtained with the $PbO\text{-}SiO_2$ coatings show reasonably low wear and lower friction coefficient than would normally be expected at room temperature in air. For example, in air at room temperature with this same sliding velocity, the $PbO\text{-}SiO_2$ coatings have shown friction coefficients of 0.3 (ref. 14). In vacuum, because of the loss of convective cooling, the surfaces became sufficiently heated without external heat addition to give a friction coefficient approximately similar to that normally obtained in air at 250° F (ref. 14).

The CaF_2 solid-lubricant coating gives results remarkably similar to those for the $PbO\text{-}SiO_2$ coatings. Both of these coatings were developed for high-temperature use. Again the friction coefficient

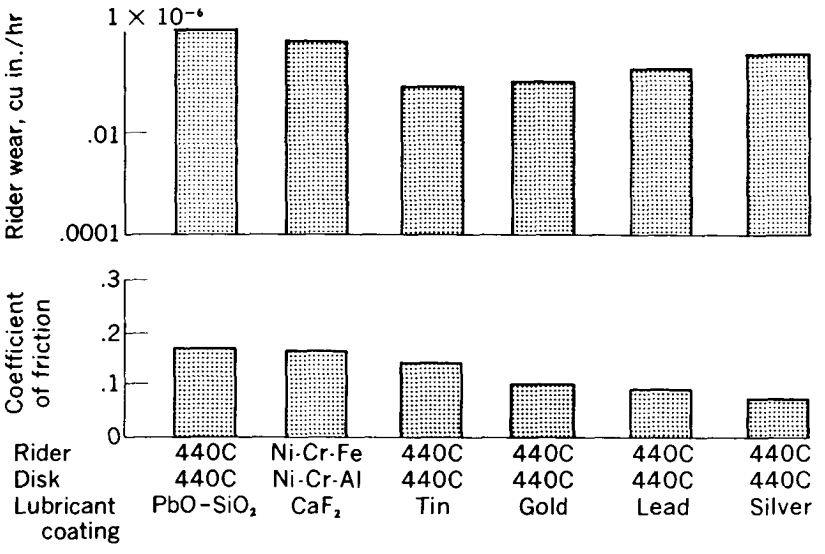

FIGURE 9–15.—Friction and wear of alloys with various 0.0004-inch-thick coatings in vacuum. Ambient pressure, 8.0×10^{-7} to 2.0×10^{-6} millimeter of mercury; sliding velocity, 390 feet per minute; load, 1000 grams; duration of run, 1 hour. (From ref. 5.)

obtained with this coating in vacuum was lower than that obtained in air at the same temperature.

The results for the thin metal coatings are also shown in figure 9–15. These results show that low wear and low friction coefficient were obtained with this type of coating. The results confirm those previously obtained in applications where mechanisms have operated in vacuum, such as rotating anodes of X-ray tubes.

Gallium films.—One of the materials of promise as a possible lubricant in the vacuum environment of space is gallium (ref. 15). For use as a space lubricant, a liquid lubricant should (1) have low vapor pressure in order that it may remain on the surfaces for long periods of time, (2) be liquid over a broad temperature range, and (3) have good wetting properties. Gallium possesses all these characteristics. It has very low vapor pressure to 1000° F (as shown in fig. 9–4), has a liquidus range of 86° to 3600° F, and will wet nearly all surfaces. One major problem associated with gallium as a lubricant is its extremely reactive nature toward other metals; it has a strong tendency to form alloys or solutions. Some materials, however, have resistance to corrosive attack by gallium (ref. 16).

Gallium is comparable to aluminum in its chemical properties (e.g., it is only superficially oxidized when heated in air or oxygen, it will

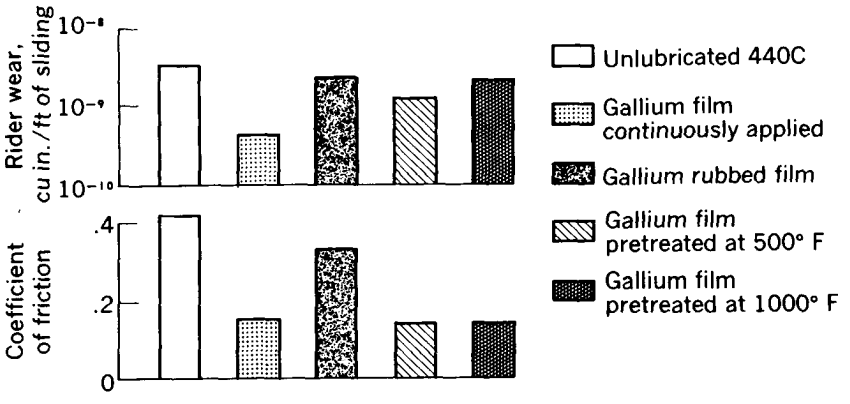

FIGURE 9–16.—Friction and wear of 440C sliding on 440C in air. Pressure, atmospheric; sliding velocity, 390 feet per minute; load, 1000 grams; duration of run, 1 hour; temperature, 75° F. (From ref. 15.)

dissolve in both acid and base, and it has extremely good wetting properties for metals, glass, and glazed ceramic surfaces). The refractory metals, such as tantalum, zirconium, and tungsten, appear to have good corrosion resistance when used with gallium. Graphite, carbon, ceramics, and glass are impervious to attack by gallium at low temperatures.

Gallium films can be applied to surfaces in a number of ways. In order to study effects of application techniques on friction and wear, the first experiments with gallium were conducted in air. The results of these experiments are shown in figure 9–16, which compares friction and wear of four different gallium films with each other and with an unlubricated specimen. Of these various films, the pretreated film appears most practical; the 500° F pretreatment was chosen because of its better results. All further experiments on pretreated gallium films will refer to the 500° F pretreatment.

Results of experiments in vacuum with various unlubricated material combinations and with the same combinations lubricated with a pretreated gallium surface film are presented in figure 9–17. These experiments were conducted in vacuum (10^{-8} mm Hg). The results show that, for all material combinations, wear and friction with the pretreated gallium surface film are much less than for the unlubricated combination. For example, with the combination 440C on 440C, wear with the gallium-lubricated specimens is only one-thousandth that of the unlubricated specimens.

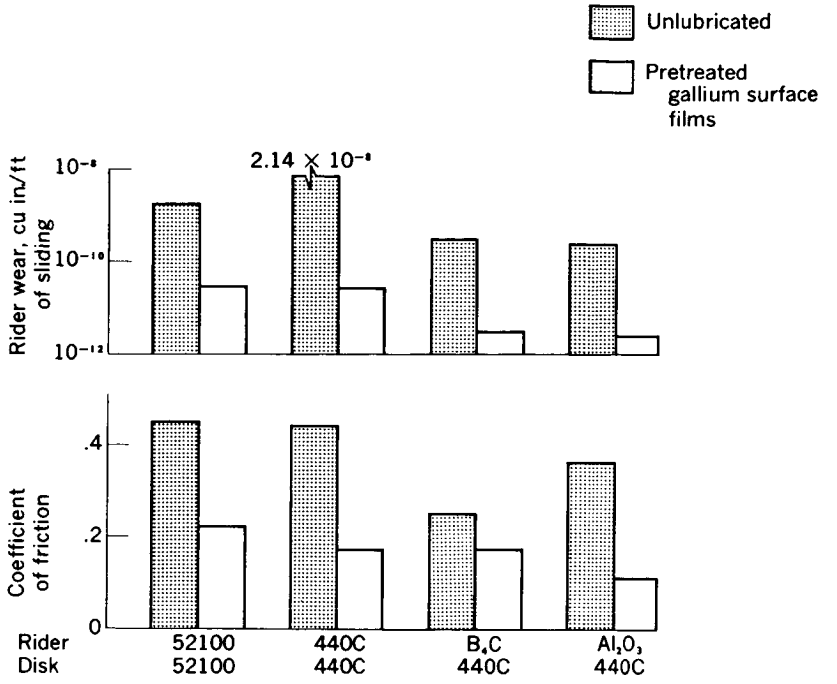

FIGURE 9–17.—Friction and wear of various materials in vacuum. Ambient pressure, 10^{-8} millimeter of mercury; sliding velocity, 390 feet per minute; load, 1000 grams; duration of run, 1 hour; liquid-nitrogen cryopumping. (From ref. 15.)

Bearing Operation in Vacuum

The rolling-element bearing appears particularly promising for use in space, where the problem of lubrication can be critical, because this type of bearing has very little sliding and therefore inherently requires very little lubricant. With this type of bearing, however, sliding as well as rolling occurs in the contact region between the rolling elements and the races. Therefore, lubrication must be supplied for adequate and reliable operation.

A survey of bearing and frictional problems is reported in reference 17. This survey covers various material combinations including metals, plastics, ceramics, and cermets. The friction characteristics of cermets are also discussed in reference 18.

As previously mentioned, relatively short space missions at pressure levels of 10^{-7} or possibly 10^{-8} millimeter of mercury may be satisfactorily carried out with rolling element bearings lubricated with liquids

or greases, provided that these lubricants have low vapor pressure. Adequate sealing such as by use of double-shielded bearings, should be of some help in this respect. Some bearing experiments at relatively low pressures have been reported (refs. 2, 6, 19, 20, 21, 22, and 23).

Tests described by Corridan in reference 21 were conducted at a pressure level of 10^{-6} millimeter of mercury, a temperature of 160° C, a speed of 11,500 rpm, and with R–3 bearings (3/16-in. bore). These were double-shielded bearings of 440C stainless steel, and the bearing loads ranged from 8 to 15 ounces. The DN value for the tests was 55,000. The bearings were lubricated with a number of different liquids or greases. The liquids included silicones and diesters, and the greases were primarily silicone greases with the exception of Apiezon T, which is a high-vacuum grease. Best results were obtained with the silicone fluids and silicone greases. Corridan (ref. 21) indicates that, for the silicone fluid, the failure was of a wear-out type. For the silicone grease, failure was not caused by wearout; in contrast, the metal surfaces remained in good shape, but the hardened residue from the grease prevented free movement of the bearing parts. Good results (long life) were surprisingly obtained with Apiezon T high-vacuum grease, which is not noted for its lubricating qualities but rather for its low vapor pressure.

Freundlich and Hannan (ref. 19) also conducted some tests on bearings of the R–2 size (1/8-in. bore) at 10^{-5} millimeter of mercury. In their tests, two bearings on each of 16 motors were lubricated with a particular oil or grease and operated continuously at 4000 rpm until 1000 hours or failure. The DN value for these tests was 13,000. These bearings were also double shielded, of 440C stainless steel, and, in this case, with paper-based phenolic retainers. The oils and greases tested in the bearings were selected on the basis of evaporation rates in preliminary tests of a number of candidate materials. In the case of oils, the bearings were vacuum impregnated with between 15 and 20 milligrams before tests. In the case of greases, the bearings were first impregnated with the base oil in order to prevent the retainer from drying out the grease, after which approximately 15 milligrams of grease were added to the bearing. Most of the motors operated for the full 1000-hour life test. Three bearing failures due to inadequate lubrication occurred. Again, the silicone oils and greases gave good performance. In both the tests of references 19 and 21, the lubricants giving the better performance results were a silicone oil (G.E. Versilube F–50) and a silicone grease (G–300).

Bearing tests were also conducted by Clauss (ref. 2). In these tests, the ball bearings were size R–3 (3/16-in. bore) with steel ribbon-type retainers and with machined phenolic composition (Synthane)

retainers. These bearings were also double shielded. Most of the bearing tests were at 8000 rpm, which gives a DN value of approximately 40,000, and the pressure range was of the order of 10^{-6} to 10^{-8} millimeter of mercury. When the bearings with machined phenolic-composition retainers were run, the retainers were vacuum impregnated with the oil under study. Periodically the power to each motor was cut off and the time required for coasting from 8000 rpm to full stop was measured. This coast time was considered an indication of the running torque of the bearings. Of the oils and greases tested, the longest life was achieved with ball bearings lubricated with a silicone oil (G.E. Versilube F–50); they operated for 4574 hours before failure. Even after 4000 hours of operation, the coast time for these bearings was 9 minutes, 55 seconds, which indicates a very low torque and good operation. Further tests with the F–50 silicone oils were made in an attempt to lengthen the life in vacuum; the F–50 oil was distilled to remove the more volatile fractions. While bearings employing steel ribbon-type retainers failed at shorter periods of time, results on bearings with Synthane retainers were reported to be more encouraging (ref. 2). In confirmation of some of the other results, bearings lubricated with a vacuum oil of low vapor pressure, Apiezon K, showed long life; these bearings had operated for 3353 hours (and were still operating) at the time that reference 2 was written. This oil, however, is much too viscous for use on cold parts and results in excessively high torque, as indicated by a coast time of only 20 seconds.

Several of the oils tested in reference 2 were high-temperature lubricants developed for use in turbojet engines. These oils had relatively low volatility for use in high-temperature operation. One of the oils showed relatively long life. The only grease tested in the investigation of reference 2 was G.E. Versilube G–300, which is the G.E. F–50 silicone oil in a lithium-base soap. These bearings had operated for 4363 hours and showed reasonably good coast times.

Experiments were conducted (ref. 22) on small ball bearings incorporating self-lubricating retainers made of various combinations of Teflon with glass fiber or with metals at pressure levels of approximately 10^{-7} millimeter of mercury. The results indicated that the self-lubricating retainers were promising for operation of about 100 hours.

Experiments in vacuum (10^{-7} mm Hg) on small ball bearings with various retainer materials and plated metallic film lubrication are reported in reference 23. Results of these experiments showed that thin metallic films are promising as lubricants and that gold plating with additives is more effective than pure gold plating. Bearing failures tended to be castastrophic in these studies (ref. 23).

Weinreb (ref. 6) discusses the successful operation of bearings in a mechanism for the TIROS II meteorological satellite. The mechanism that was operated successfully is a ". . . five-channel infrared radiometer . . . [this] system consists of five optical mirrors mounted on five gears and eight ball bearings driven by a low-power motor whose output torque is 0.03 inch-ounce. The shaft speed of all bearings is 2750 rpm." The radiometer operated successfully not only in vacuum-chamber testing but on the satellite, which had been in orbit (at the time of the writing of ref. 6) 2360 hours; no signs of deterioration had been observed at that time.

The requirements for the bearings in the radiometer were that alinement of optical elements must be preserved accurately; in consequence, bearing wear must be minimized. For this use, ". . . instrument ball bearings with conventional lubrication techniques were considered essential since low power drain, long life, and reliability in space vehicles must be obtained" (ref. 6).

The mechanisms described in reference 6 were designed for minimum loss of lubricant by evaporation. This design was based on the fact that, on a molecular scale, even smooth surfaces appear rough, and, according to Knudsen (ref. 24), the direction in which a molecule rebounds after a collision with the wall is statistically independent of the angle of incidence. For this reason, the molecular flow resistance of small orifices can be made relatively high. The vapor pressure inside the chamber can be maintained and vaporization of the lubricant can be minimized. The bearings in the mechanism of reference 6 were so designed as to employ lubricant reservoirs of oil-impregnated, sintered nylon (fig. 9–18). The lubricant employed was a Mil–L–

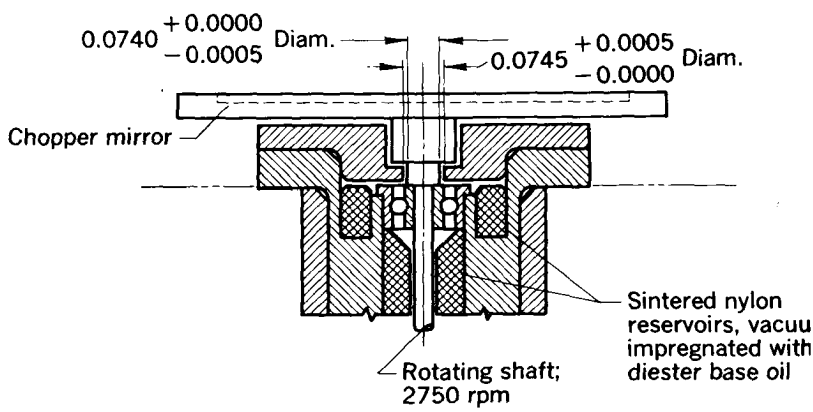

FIGURE 9–18.—Radiometer spindle assembly. (From ref. 6.)

6085A diester oil with a vapor pressure of approximately 10^{-4} millimeter of mercury. When the outside pressure reaches a value below 10^{-2} millimeter of mercury, molecular flow occurs around the shaft through the small clearance; the clearance was maintained at a nominal 0.0005 inch. Weinreb indicates that, with the aid of an equation derived by Knudsen and others, it is possible to calculate the escape rate of oil from the bearing assembly. This information can then be used to design a bearing for space application for the required life. The equation to which Weinreb refers is

$$Q=\frac{4}{3}\sqrt{2\pi}\left[\frac{(R_2^2-R_1^2)(R_2-R_1)}{L}\right]\frac{1}{\sqrt{\rho_1}}(p_1-p_2)$$

where

Q	volume flow rate of oil vapor
R_1,R_2	inside and outside radii of annulus
L	length of annulus
ρ_1	density of oil vapor at standard conditions
p_1	pressure in the housing
p_2	ambient pressure

RADIATION

"The radiation environment in [interplanetary] space is divided into four components: (1) cosmic radiation which is found universally in space, (2) ultraviolet radiation also found universally in space, (3) geo-magnetically trapped corpuscular radiation which is found in belts on either side of the equator up to altitudes of 40,000 kilometers above the center of the earth, and (4) auroral soft radiation which is found in the auroral regions of the earth" (ref. 1).

Vehicles in space will be exposed to cosmic radiation, which consists primarily of electrons and nuclei of various atomic numbers. The particle energies range from about 100 to 10^7 Mev. The ionization rate at these flux levels is about 24 milliroentgens per 24 hours; no detrimental effects are anticipated from cosmic rays on materials of any type (ref. 3). It might be pointed out, however, that the ionization rate at this flux level is near the maximum permissible rate for human beings (ref. 3).

The Van Allen radiation belts contain electrons of energy greater than 13 Mev and protons whose energy ranges to 700 Mev. The flux estimates by Van Allen on the basis of early experiments are in the range of 10 to 100 roentgens per hour, with more recent data indicating the possibility of 1000 roentgens per hour. By way of comparison, the fluxes in nuclear reactors are of the order of 10^5 to 10^6 greater than these.

The damage to plastics and elastomers caused by ultraviolet radiation results from ionization and excitation of electrons. These changes are (ref. 3) irreversible and include free-radical formation, polymerization, degradation (cleavage of carbon chains), and gas formation (oxygen, hydrogen, and low-molecular-weight hydrocarbon gases). These phenomena also occur with gamma-ray dosage and are thus also of concern in the application of plastics in other areas.

Clauss states (ref. 2) that, "based on present estimates of the amount of radiation experienced by spacecraft and on our knowledge of the radiation stability of oils and greases, it does not appear that [space] radiation will be a limiting factor in the use of oils and greases on spacecraft with lifetimes of several years." It should be pointed out, however, that since radiation levels from a nuclear reactor are so much higher than space radiation, this conclusion does not apply to nuclear powered spacecraft.

The general changes in lubricants caused by excessive radiation include the following: in oils the viscosity initially decreases and then increases with such fluids eventually becoming rubbery or solid; in greases some thickeners degrade rapidly and the greases become thin or soupy. Additional radiation causes the grease to become thicker and finally solid. In both oils and greases, volatility, as well as acidity and corrosiveness, generally increases. The oxidation resistance of oils and greases decreases with radiation. In general, the oils and greases showing the most resistance to radiation are also the oils and greases showing the greatest resistance to thermal instability. Very little information is available on radiation in vacuum, but that which does exist indicates that radiation effects observed in air may not be extrapolated to vacuum conditions.

As would be anticipated, most of the solid lubricant materials show improved radiation resistance over the liquids (oils and greases).

SUMMARY

The actual conditions of space are not precisely known; duplication of conditions is therefore difficult, but simulation is possible (pressure $\leq 10^{-9}$ mm Hg desirable). Evaporation rate of materials is very important since evaporation will remove the contaminating (lubricant) film from the surface, permit contact of virgin surfaces, and, hence, cause severe wear and friction problems. Low evaporation rates are obtained with metals (lead, silver, tin, and gallium) and some lubricating compounds (molybdenum disulfide, lead oxide-silicon dioxide, and calcium fluoride) as well as with Teflon. Friction and wear experiments of various lubricant coatings at 10^{-6} millimeter of mercury show that molybdenum disulfide and other films (various com-

pounds, plated metals, etc.) appear promising; of these, molybdenum disulfide showed the best results by far in these experiments.

Full-scale bearing experiments at 10^{-6} millimeter of mercury showed good results with silicones and silicone greases. Successful operation in space of a mechanism was obtained on an actual satellite (TIROS II). Lubrication was based on controlled loss of lubricant from a reservoir; this controlled loss was precalculated on the basis of a "molecular flow resistance" equation.

In general, natural radiation in space is no problem to oils and greases; the advent of nuclear reactors with much higher flux levels will change this, however.

REFERENCES

1. Atkins, J. H., Bisplinghoff, R. L., Ham, J. L., Jackson, E. G., and Simons, J. C., Jr.: Effects of Space Environment on Materials. Res. Proj. 40–1–041, Nat. Res. Corp., Aug. 15, 1960.
2. Clauss, F. J.: Lubricants and Self-Lubricating Materials for Spacecraft Mechanisms. LMSD–894812, Lockheed Aircraft Corp., Apr. 18, 1961.
3. Lad, Robert A.: Survey of Materials Problems Resulting from Low-Pressure and Radiation Environment in Space. NASA TN D–477, 1960.
4. van Vliet, R. M.: A Molecular Approach to Dry Film Lubrication in a Vacuum (Space) Environment. TR 59–127, WADC, July 1960.
5. Buckley, D. H., Swikert, M., and Johnson, R. L.: Friction, Wear, and Evaporation Rates of Various Materials in Vacuum to 10^{-7} mm Hg. ASLE Trans., vol. 5, no. 1, Apr. 1962, pp. 8–23.
6. Weinreb, Marius B.: Results of Tiros II Ball Bearing Operation in Space. Meteorology Branch, Goddard Space Flight Center, NASA, Wash. 25, D.C., Mar. 1961.
7. Anon.: Space Probe in an Observation Tube. Rensselaer Res., vol. 5, no. 1, 1960. (Pub. by Rensselaer Polytech. Inst.)
8. Buckley, Donald H., and Johnson, Robert L.: Influence of Microstructural Inclusions on Friction and Wear of Nickel and Iron in Vacuum to 10^{-9} Millimeter of Mercury. NASA TN D–1708, 1963.
9. Honig, R. E.: Vapor Pressure Data for the More Common Elements. RCA Rev., vol. XVIII, no. 2, June 1957, pp. 195–204.
10. Dushman, S., and Lafferty, J. M.: Scientific Foundations of Vacuum Technique. Second ed., John Wiley & Sons, Inc., 1962.
11. Bowden, F. P., and Tabor, D.: The Friction and Lubrication of Solids. Clarendon Press (Oxford), 1950.
12. Johnson, Robert L., Godfrey, Douglas, and Bisson, Edmond E.: Friction of Solid Films on Steel at High Sliding Velocities. NACA TN 1578, 1948.
13. Buckley, Donald H., and Johnson, Robert L.: Effect of Inert, Reducing and Oxidizing Atmospheres on Friction and Wear of Metals to 1000° F. NASA TN D–1103, 1961.
14. Johnson, R. L., and Sliney, H. E.: High-Temperature Friction and Wear Properties of Bonded Solid Lubricant Films Containing Lead Monoxide. Lubrication Eng., vol. 15, no. 12, 1959, pp. 487–491; 496.
15. Buckley, D. H., and Johnson, R. L.: Gallium Rich Films as Boundary Lubricants in Air and in Vacuum to 10^{-9} mm Hg. ASLE Trans., vol. 6, no. 1, Jan. 1963, pp. 1–11.

16. KELMAN, L. R., WILKINSON, W. D., and YAGGEE, F. L.: Resistance of Materials to Attack by Liquid Metals. ANL–4417, Argonne Nat. Lab., July 1950.
17. JOHNSON, JOHN H., and IRWIN, ARTHUR S.: Survey of Frictional Problems in Spacecraft. Final Rep., Marlin-Rockwell Corp., Feb. 16, 1962.
18. BROWN, R. D., BURTON, R. A., and KU, P. M.: Friction and Wear Characteristics of Cermets at High Temperature and High Vacuum. Preprint 61 LC–3, ASLE, 1961.
19. FREUNDLICH, M. M., and HANNAN, C. H.: Problems of Lubrication in Space. Lubrication Eng., vol. 17, no. 2, Feb. 1961, pp. 72–79.
20. FREUNDLICH, MARTIN M., and JAGODOWSKI, STANLEY S.: Lubricants for High-Vacuum Environment. TR 60–728, pt. I, WADD, Nov. 1960.
21. CORRIDAN, R. E.: Summary Report: Bearing and Lubrication Study. Advanced Tech. Lab. Div., Am. Standard Corp., June 30, 1959.
22. BOWEN, PAUL H.: Dry Lubricated Bearings for Operation in a Vacuum. ASLE Trans., vol. 5, no. 2, Nov. 1962, pp. 315–326.
23. EVANS, HAROLD E., and FLATLEY, THOMAS W.: Bearings for Vacuum Operation. Phase I. NASA TN D–1339, 1962.
24. KNUDSEN, M.: Kinetic Theory of Gases; Some Modern Aspects. Third ed., Methuen, London (England), 1950.
25. JASTROW, Robert.: Lunar and Terrestrial Atmospheres. Vol. 5 of Advances in Aero. Sci., Plenum Press, Inc., 1960, pp. 338–345.

BIBLIOGRAPHY

ALLAN, A. J. G.: Plastics as Solid Lubricants and Bearings. Lubrication Eng., vol. 14, no. 5, May 1958, pp. 211–215.

ANON.: Liquid-Metals Handbook. NAVEXOS P–733, Atomic Energy Commission and Bur. Ships, Dept. Navy, June 1952.

ANON.: Vacuum Bearings and Dry Film Lubricants. Tech. Bull. 463–6; CBS Labs., Stamford (Conn.).

APT, C. M., and WIEDERHORN, N. M.: Analysis of Problems of Oil Film Lubrication for Bearings Under Space Conditions. Paper Presented at SAE Nat. Aero. Meeting, New York, N.Y., Apr. 4–8, 1960.

ATLEE, Z. J., WILSON, J. T., and FILMER, J. C.: Lubrication in Vacuum by Vaporized Thin Metallic Films. Jour. Appl. Phys., vol. 11, no. 9, Sept. 1940, pp. 611–615.

BAMFORD, C. H., JENKINS, A. D., and JOHNSTON, R.: Studies in Polymerization. XI. Reactions Between Polymer Radicals and Ferric Chloride in Nonaqueous Media. Proc. Roy. Soc. (London), ser. A, vol. 239, no. 1217, Feb. 1957, pp. 214–229.

BELL, M. E., and FINDLAY, J. H.: Molybdenite as a New Lubricant. Phys. Rev., vol. 59, no. 11, June 1, 1941, p. 922.

BOWDEN, F. P., and YOUNG, J. E.: Friction of Clean Metals and the Influence of Adsorbed Films. Proc. Roy. Soc. (London), ser. A, vol. 208, no. 1094, Sept. 1951, pp. 311–325.

BOWERS, R. C., Clinton, W. C., and ZISMAN, W. A.: Frictional Behavior of Polyethylene, Polytetrafluorethylene, and Halogenated Derivatives. Lubrication Eng., vol. 9, no. 4, Aug. 1953, pp. 204–208.

BUECHE, A. M., and FLOM, D. G.: Surface Friction and Dynamic Mechanical Properties of Polymers. Wear, vol. 2, no. 3, Feb. 1959, pp. 168–182.

COFFIN, L. F., JR.: A Study of the Sliding of Metals, with Particular Reference to Atmosphere. Lubrication Eng., vol. 12, no. 1, Jan.–Feb. 1956, pp. 50–59.

COSGROVE, S. L.: The Effect of Nuclear Radiation on Lubricants and Hydraulic Fluids. REIC Rep. 4, Batelle Memorial Inst., Apr. 30, 1958.

DEVINE, M. J., LANSON, E. R., and BOWEN, J. H., JR.: Inorganic Solid Film Lubricants. Jour. Chem. and Eng. Data, vol. 6, no. 1, Jan. 1961, pp. 79–82.

HANSEN, SIEGFRIED: Research Program on High Vacuum Friction. Pub. 1023, Litton Industries, Inc., Mar. 30, 1959.

JAFFE, L. D.: Effects of Space Environment upon Plastics and Elastomers. TR 32–176, Jet Prop. Lab., C.I.T., Nov. 16, 1961.

JAFFE, L. D., and RITTENHOUSE, J. B.: Evaporation Effects on Materials in Space. TR 32–161, Jet Prop. Lab., C.I.T., Oct. 30, 1961.

JAFFE, L. D., and RITTENHOUSE, J. B.: Behavior of Materials in Space Environments. TR 32–150, Jet Prop. Lab., C.I.T., Nov. 1, 1961.

JELLINEK, H. H. G.: Degradation of Vinyl Polymers. Academic Press, Inc., 1955.

JOHNSON, VIRGIL R., and VAUGHN, GEORGE W.: Investigation of the Mechanism of MoS_2 Lubrication in Vacuum. Jour. Appl. Phys., vol. 27, no. 10, Oct. 1956, pp. 1173–1179.

JOHNSON, VIRGIL R., VAUGHN, GEORGE W., and LAVIK, MELVIN T.: Apparatus for Friction Studies at High Vacuum. Rev. Sci. Instr., vol. 27, no. 8, Aug. 1956, pp. 611–613.

LAVIK, M. T., GROSS, G. E., and VAUGHN, G. W.: Investigation of the Mechanism of Tungsten Disulfide Lubrication in Vacuum. Lubrication Eng., vol. 15, no. 6, June 1959, pp. 246–249.

MARGRAVE, J. L.: Physico Chemical Measurements at High Temperatures. Ch. 10. Academic Press, Inc., 1959.

MATACEK, GEORGE F.: Vacuum Volatility of Organic Coatings. Surface Affects on Spacecraft Materials, F. J. Clauss, ed., John Wiley & Sons, Inc., 1960.

RIEHL, W. A., LOONEY, W. C., and CARUSO, S. U.: Compatibility of Engineering Materials with Space Environment. Item 1, Pt. II, ARPA Order 92–59, Army Ord. Missile Command, Oct. 25, 1960.

SAVAGE, R. H.: Graphite Lubrication. Jour. Appl. Phys., vol. 19, no. 1, Jan. 1948, pp. 1–10.

SAVAGE, ROBERT H., and SCHAEFER, D. L.: Vapor Lubrication of Graphite Sliding Contacts. Jour. Appl. Phys., vol. 27, no. 2, Feb. 1956, pp. 136–138.

SHOFFNER, JAMES, P.: Effects of Radiation on "Teflon" Resins in Space. Jour. of Teflon, vol. 2, no. 1, Jan. 1961, pp. 6–8.

SIMON, I., MCMAHON, H. O., and BOWEN, R. J.: Dry Metallic Friction as a Function of Temperature Between 4.2° K and 600° K. Jour. Appl. Phys., vol. 22, no. 2, Feb. 1951, pp. 177–184.

WILLIAMS, HERBERT: Lubricants Limit Ball Bearings for Spacecraft. Space/Aero., vol. 37, no. 2, Feb. 1962, pp. 101–108.

WILLIAMSON, J.G.: Polarity Anchors New Space Lube Theory. Chem. and Eng. News, pt. 2, vol. 39, no. 5, Jan. 30, 1961, pp. 48–49.

Page intentionally left blank

CHAPTER 10

Friction of Metals, Lubricating Coatings, and Carbons in Liquid Nitrogen and Hydrogen

By EDMOND E. BISSON

IN HIGH-PERFORMANCE MISSILE APPLICATIONS, the use of high-energy propellants, such as liquid hydrogen, liquid oxygen, and other cryogenic liquids (liquefied gases) results in serious problems in the lubrication of seals, bearings, and other moving parts in the turbopumps, which of necessity pump these fluids. Since these high-energy propellants are for use in rocket engines, overall missile weight is extremely important. It is also extremely important that minimum complexity be obtained for any system which must operate with missiles. For minimum complexity and minimum weight, it is desirable that the bearings for the turbopump be lubricated by the fluid being pumped. In most cases, these fluids are very poor lubricants. They do, however, provide one function which is beneficial; that is, they serve as effective coolants (heat sinks).

Some of the properties of cryogenic liquids are shown in table 10–I. These properties include freezing point, boiling point, liquid density at the boiling point, and liquid viscosity at two temperatures. Reference to the viscosities at the boiling points indicates that all these liquids have extremely low viscosity at their boiling point. The range is from approximately 7 to 372×10^{-10} reyn at the boiling point. For comparative purposes, the viscosity of an ordinary SAE 30 oil at 100° F is approximately 10^{-5} reyn. Thus, the viscosity of these liquids ranges from one ten-thousandth to one two-hundredth that of an ordinary lubricant. (Also, it is of interest to note that the viscosity of liquid hydrogen at its boiling point is approximately equal to the viscosity of air at 80° F.) Since load-carrying capacity of hydrodynamic bearings is proportional to viscosity, the load-carrying ca-

TABLE 10–I.—PROPERTIES OF CRYOGENIC LIQUIDS

Liquid	Freezing point, °F	Boiling point, °F	Liquid density, lb/cu ft, at—	Liquid viscosity,[a] reyns, at—	
			Boiling point	Boiling point	−320° F
Helium	[b]−458	−452	7.6	7×10^{-10}	--------
Hydrogen	−434	−423	4.4	19	--------
Nitrogen	−346	−320	50.1	230	230×10^{-10}
Fluorine	−360	−306	94.0	372	489
Argon	−309	−303	87.4	--------	--------
Oxygen	−361	−297	71.2	274	333
Methane	−299	−258	25.8	--------	--------

[a] Viscosity of SAE 30 oil at 100° F is approximately 10^{-5} reyn.
[b] At pressure of 26 atm.

pacity of bearings utilizing any of these liquids as the lubricating fluid would be exceptionally small.

Liquid hydrogen is particularly poor as a lubricant for two reasons: (1) It has low viscosity, and (2) it has a chemical reducing effect on the normal surface films (such as oxides of metals), which help to provide lubrication to the bearings. Without the contaminating oxide films, metals will readily weld even at the temperatures of the cryogenic liquids.

Even though the bearings are submerged in the pumped fluid, it is necessary to have a rotating seal to prevent leakage of the fluid around the shaft driving the pump. It is extremely important that these seals have essentially zero leakage, since the fluids are combustible. Hence, the friction and wear properties of the materials for use in bearings and seals that operate in cryogenic liquids are important; in fact, these materials should be, as nearly as possible, self-lubricating.

Because of the low viscosity of cryogenic liquids (and, hence, low load-carrying capacity of hydrodynamic bearings employing cryogenic liquids as the working fluid), it would appear that hydrodynamic bearings are not particularly suited for operation in turbopumps for cryogenic liquids. The rolling-element bearings, such as ball or roller bearings, appear better suited to this type of service, since they require little lubrication at the rolling contacts. They do, however, require some lubrication at the surfaces in pure sliding, such as the contacts between the rolling elements and the cage (separator or retainer). The seals for shafts of turbopumps also have surfaces in pure sliding. Therefore, it appears that friction and wear data on various materials

in the presence of cryogenic liquids under pure sliding conditions are needed.

Early experiments (ref. 1) indicated that conventional bearings and seals could operate in liquid nitrogen and hydrogen. In reference 2, however, failures are reported for some miniature ball bearings operating in gaseous hydrogen at temperatures approaching those of liquid nitrogen and hydrogen. In this same investigation, bearings of type 440C stainless steel were operated successfully by using thick Micarta retainers. Simon, et al. (ref. 3) indicate that, for a number of metals, static friction did not change markedly with temperature over the range from 4.2° to 600° K.

Austenitic stainless steel is one of the materials most commonly employed at cryogenic temperatures primarily because of its good physical properties at these temperatures (e.g., see ref. 4). It is, however, widely known as an extremely poor material from the standpoint of friction, wear, and surface damage. The severe welding that occurs with austenitic stainless steel in sliding contact with other metals is explained (ref. 5, p. 81) by the fact that the completely homogeneous material does not provide any contaminating phase to inhibit surface welding and adhesion.

Early experiments on the friction and wear of various material combinations in liquid nitrogen and hydrogen were conducted at the NASA (formerly NACA) laboratories; these investigations are reported in references 6 through 11. Other investigations in this field are reported in references 12 and 13.

This chapter discusses data from friction and wear studies on various material combinations in liquid nitrogen and in liquid hydrogen.

FRICTION AND WEAR STUDIES

Metals

When clean metals are slid together in cryogenic liquids, severe surface welding takes place. This welding is a direct result of the lack of lubrication between the contacting surfaces. In an inert atmosphere such as nitrogen or a reducing atmosphere such as hydrogen, the formation of protective films which can help to reduce surface damage does not occur.

For comparison purposes (i.e., to establish a base line), friction and wear data were obtained with three common metals in liquid nitrogen. The initial experiments were conducted in liquid nitrogen because of the ease of working with and the safety of nitrogen, as compared with hydrogen. These data (fig. 10–1) show that, with the austenitic stainless steel 304 sliding on 304, the wear of the rider specimen is fairly high. With two other steels, a conventional bearing steel

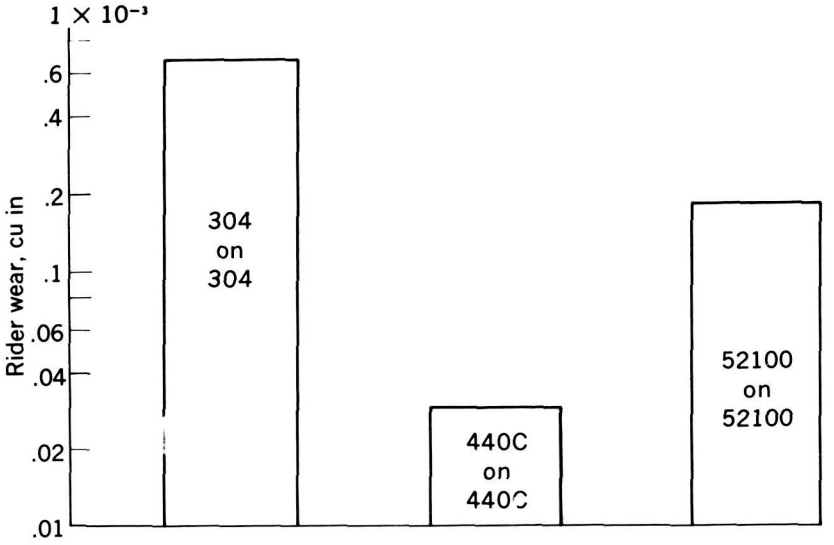

FIGURE 10–1.—Wear of reference metals in liquid nitrogen. Sliding velocity, 2300 feet per minute; load, 1000 grams; duration of run, 1 hour. (From ref. 7.)

52100 sliding on 52100 and type 440C stainless steel sliding on 440C, wear was lower than with 304 on 304.

It should be noted that the wear which is plotted in figure 10–1 is wear of the rider specimen only and that no indication is given in this figure of the wear of the disk specimen. Figure 10–2 shows the appearance of representative rider and disk specimens. Both specimens show welding and extreme surface damage. It is important to note that,

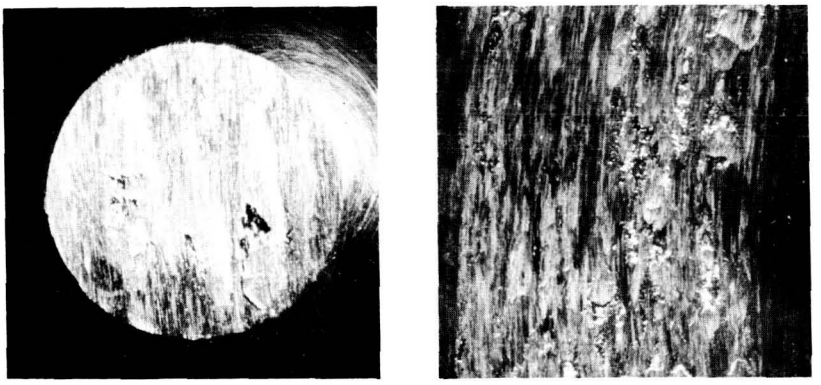

FIGURE 10–2.—Surfaces of reference metals after sliding in liquid nitrogen. Load, 1000 grams. (From ref. 7.)

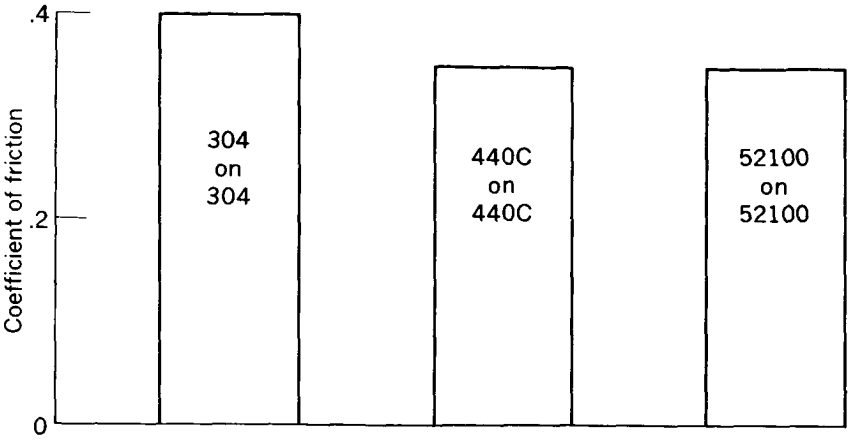

FIGURE 10–3.—Friction of reference metals in liquid nitrogen. Sliding velocity, 2300 feet per minute; load, 1000 grams. (From ref. 7.)

in many mechanisms, the surface damage which may occur is as significant as is friction or wear.

Figure 10–3 shows the friction coefficient data for the same three metals. Friction coefficient is quite high with all three metal combinations; therefore ineffective lubrication is indicated.

As was previously mentioned, the oxide films which are normally present on most metals contribute to their lubrication under conditions of operation in air or in an oxidizing atmosphere. In the presence of an inert atmosphere such as liquid nitrogen, the oxide films are quickly worn away and are not permitted to reform; hence, severe surface welding and metal transfer occurs with all metal-metal combinations of the type represented in figures 10–1 to 10–3.

When the surface oxides are worn away and thus contact of nascent metals is permitted, the mutual solubility of the contacting metals becomes of prime importance. Silver has little solubility in iron (refs. 14 and 15); hence, in the investigation of reference 6, studies were made of electrolytic silver sliding on type 304 stainless steel. Severe plastic flow of the silver was obtained. Welding in the usual sense did not occur, but a thin film of silver was transferred to the steel disk; therefore, the sliding was undoubtedly silver on silver.

After the poor results obtained with the combination of silver against 304, Wisander, et al. (ref. 6) conducted an investigation of a powdered metal composition containing 85 percent silver, 5 percent copper, and 10 percent molybdenum disulfide. This composition had previously (ref. 16) been shown to give good performance when operating dry against steel in air. The molybdenum disulfide in this composition was believed to act as a solid lubricant which interspersed

in the matrix of the metal would smear over the rubbing surfaces and, hence, provide lubrication and surface protection. The results obtained (ref. 6) with this composition showed that the wear was approximately the same as that for silver on 304 steel. The friction coefficient, however, was appreciably lower than for silver on 304 (0.3 as against 0.8). While the molybdenum disulfide did help to provide lower friction, the powdered metal composition was weaker than the solid silver rider and, hence, wear was not improved.

The data on metal combinations sliding in liquid nitrogen may be summarized as follows:

(1) Relatively high friction coefficients are obtained.

(2) Severe surface damage by welding and tearing is obtained under these conditions. In accordance, it would appear that self-lubricating materials are required for these conditions. Examples of self-lubricating materials would include (a) metals lubricated with various surface coatings, (b) plastics, (c) carbons, etc.

Surface Coatings

Wisander and Johnson (ref. 8) conducted an investigation of the friction and wear properties in liquid nitrogen of austenitic stainless

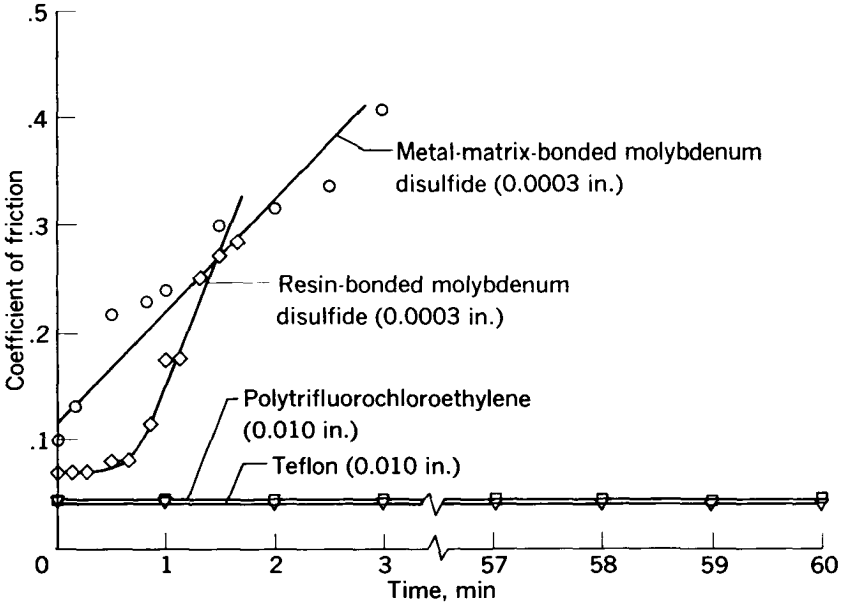

FIGURE 10-4.—Friction of stainless steel on solid lubricant coatings in liquid nitrogen. Sliding velocity, 2300 feet per minute; load, 1000 grams. (From ref. 8.)

steels with various surface coatings. The results of this investigation are reported in the following paragraphs. The surface treatments investigated included diffusion coatings with nitrogen, sulfur (ref. 17), and chromium, as well as chromium electroplating. Of these coatings, only that produced by sulfurizing gave any significant reduction in friction or wear when sliding against 304 steel riders.

Several lubricating surface coatings utilizing molybdenum disulfide (MoS_2), polytetrafluoroethylene (Teflon or PTFE), and polytrifluorochloroethylene (PTFCE) were studied. Some of these results are shown in figure 10–4. These curves are for coatings of a metal-matrix-bonded MoS_2, a resin-bonded MoS_2, PTFCE, and Teflon. As noted in the figure, only PTFCE and Teflon were effective at time periods up to 1 hour. The increased friction obtained with the two MoS_2 coatings after short times indicates film failure. Coating thickness is, however, of extreme importance. Later results obtained with MoS_2 coatings have shown that thicker coatings were effective over a considerably longer period of time than is shown in figure 10–4.

The coating thicknesses of the PTFCE and the Teflon of figure 10–4 were the most effective of several thicknesses. This is demonstrated for Teflon by the data of figure 10–5; for thin films, early film failure

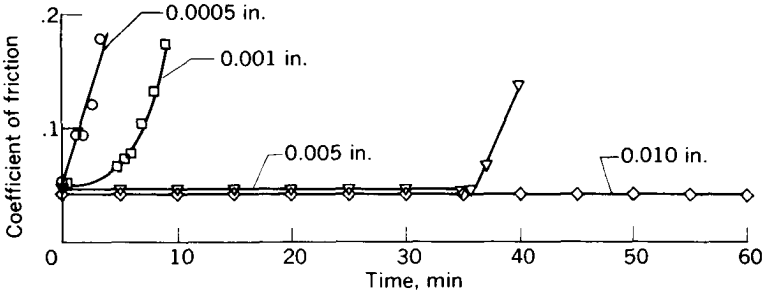

FIGURE 10–5.—Friction of stainless steel on Teflon coatings of various thicknesses in liquid nitrogen. Sliding velocity, 2300 feet per minute; load, 1000 grams. (From ref. 8.)

was experienced and only the thickest film (0.010 in.) gave effective lubrication throughout the 60 minutes of the run.

Figure 10–6 shows the wear of stainless-steel riders sliding against several types of Teflon coatings in liquid nitrogen. All coatings except the phenolic-bonded coating seemed to be quite effective.

One of the principal problems with Teflon is that it has an expansion coefficient markedly different from that of most metals to which a Teflon film could be bonded; hence, operation of a mechanism over a broad temperature range (such as from room temperature down to −320° F) can frequently result in spalling of the Teflon film from

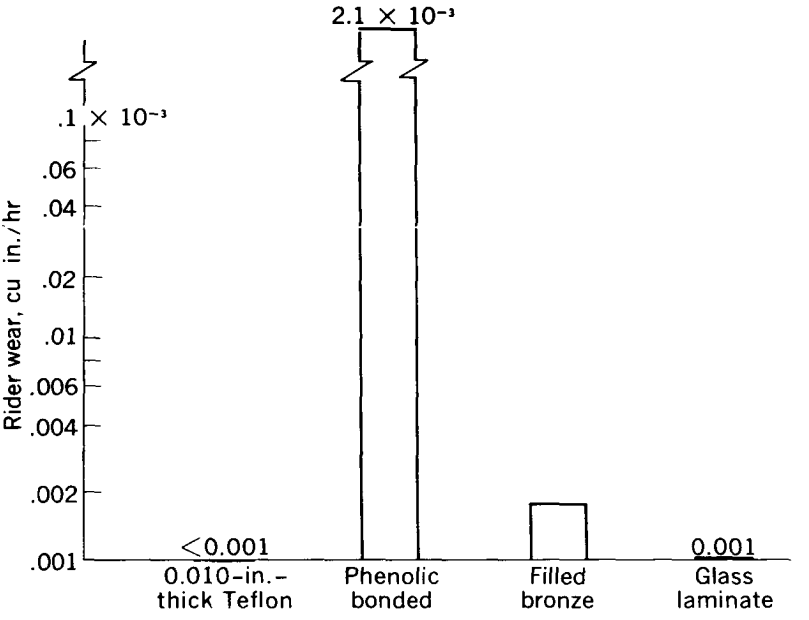

FIGURE 10–6.—Wear of stainless steel on special types of Teflon coatings in liquid nitrogen. Sliding velocity, 2300 feet per minute; load, 1000 grams. (From ref. 8.)

the surface. As might be expected, spalling was appreciably worse for thicker films. In order to combat the problem of differential expansion coefficient, Wisander and Johnson (ref. 18) prepared a lubricating film incorporating Teflon as the lubricant and two other components (a modified epoxy resin as a bonding agent and a lithium-alumina-silicate ceramic filler). The lithium-alumina-silicate was added to this composition because it has a negative expansion coefficient and the objective was to obtain a film which had an expansion coefficient more nearly equal to that of the base metal. The 304 stainless steel to which the lubricating film was applied has a calculated average expansion coefficient over the temperature range 70° to −320° F of 8.2×10^{-6} per degree Fahrenheit. For comparison, the Teflon has a calculated average expansion coefficient over this same temperature range of 48×10^{-6} per degree Fahrenheit. The experimental composition of reference 18 included 10 percent Teflon, 40 percent epoxy, and 50 percent lithium-alumina-silicate; this composition had a calculated coefficient of expansion of 19×10^{-6} per degree Fahrenheit. Thus, it is obvious that a much closer match of expansion coefficients was obtained with the experimental composition than with a straight Teflon film.

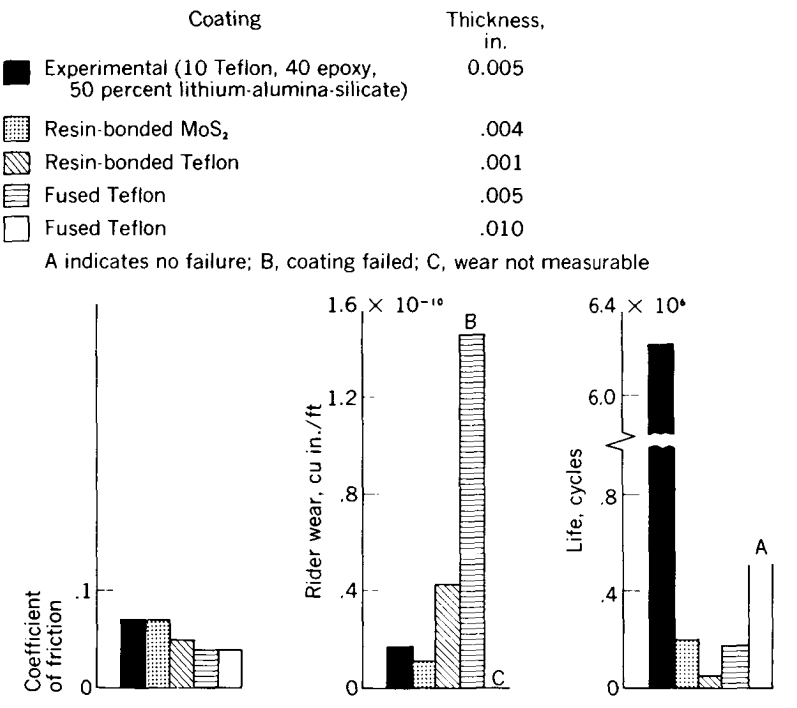

FIGURE 10–7.—Various solid lubricant coatings in liquid nitrogen. Sliding velocity, 2300 feet per minute; load, 1000 grams; 3/16-inch-radius rider sliding on coated disk of 304 stainless steel. (From ref. 18.)

The results of figure 10–7 show that the experimental composition has a friction coefficient on the same order of magnitude as the other films but has appreciably better wear and endurance properties. In fact, the life of the composition is superior to that of all other coatings except possibly the 0.010-inch-thick fused Teflon, which was not run to failure. These data, as well as previous data (ref. 8), show that relatively thick films are required for good endurance as a slider material. In order to avoid problems of spalling of the thick, fused Teflon films from the metal surface, these films were built up by repeated application of 0.0005-inch layers. While adherance of the fused Teflon coatings was satisfactory in liquid nitrogen, the high sintering temperature (700° F) required may limit its usefulness with certain metals or complicated shapes. Also, the coating procedure is time consuming.

Coating thickness is also of primary importance to endurance of the MoS_2 film. The 0.004-inch-thick film of figure 10–7 is appreciably

thicker than usual commercial MoS_2 films (0.0003 in.). Wisander and Johnson state (ref. 18),

> The results shown [in fig. 10–7], as well as unreported liquid nitrogen quenching experiments, show that contradictory requirements become evident for films. Best film adherence is obtained with coatings of least thickness, but best endurance in sliding is with coatings having greatest thickness. The advantage of the experimental composition is that it is not subject to film adherence failure. Therefore, coating thickness could be selected on the basis of either friction, wear and endurance properties or the most convenient thickness for processing. Where necessary, similar coating compositions can be formulated for use with other cryogenic liquids and base metals.

To summarize the results on surface coatings, it appears that Teflon is the most promising material under these conditions—although other solid lubricants (e.g., MoS_2) do have promise. Also, it would appear that solid bodies of self-lubricating materials should be promising under these conditions of operation. These solid bodies could include Teflon, nylon, carbon, etc. Studies of such solid bodies will be discussed in the following two sections: Plastics and Carbons.

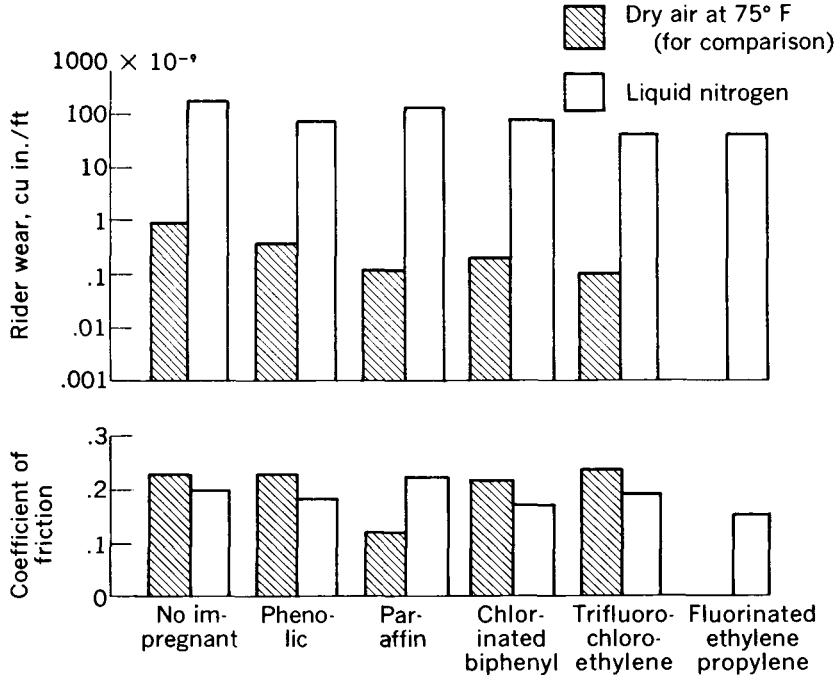

FIGURE 10–8.—Wear and friction of organic impregnated carbons in liquid nitrogen. Sliding velocity, 2300 feet per minute; load, 1000 grams; disk, 304 stainless steel. (From ref. 10.)

Plastics

References 6 and 7 report results of friction and wear investigations with solid bodies of various plastics. These plastics included Teflon, Kel-F (PTFCE), MoS_2 filled nylon, and Teflon with various fillers. (A filled nylon or Teflon is one in which filler material is added to the basic material. This filler material can be carbon, graphite, glass fiber, MoS_2, silver, copper, etc.) The friction and wear results as reported in references 6 and 7 generally show that the filler has relatively little effect on friction coefficient but does have an effect on wear. In many cases, a beneficial effect was obtained, although there were cases in which wear was increased by the addition of the filler. Many times the choice of filler is dictated by mechanical properties such as strength rather than by friction and wear.

Carbons

Wear and friction of impregnated carbons in liquid nitrogen and liquid hydrogen.—As previously mentioned, carbons had been con-

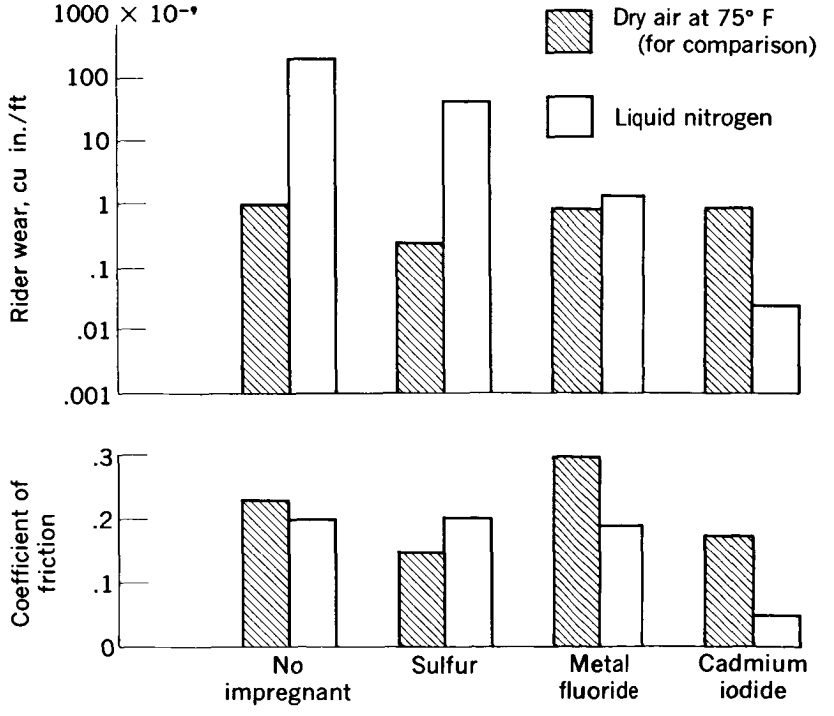

FIGURE 10–9.—Wear and friction of inorganic impregnated carbons in liquid nitrogen. Sliding velocity, 2300 feet per minute; load, 1000 grams; disk, 304 stainless steel. (From ref. 10.)

sidered as self-lubricating materials for use as sliding surfaces in the presence of cryogenic liquids. Standard, mechanical carbons, however, have high wear in an inert fluid such as liquid nitrogen or in a reducing medium such as liquid hydrogen. With carbons sliding against metals, earlier studies by many investigators (including those at the NASA laboratories) have shown that low wear is obtained *only* when a graphitic film is developed on the mating metal surface. These studies have also shown that development of such a film occurs in the presence of moisture or of oxygen. The latest studies show that the film is *not* developed in inert or reducing atmospheres. Prior researchers indicated that impregnants (addition agents or adjuncts) in the carbon would help in the development of the necessary mating film. The mechanism by which impregnants in carbon bodies promote graphite adherence to mating metal surfaces is not clearly understood; it is probable that, in individual cases, either or both physical and chemical factors may contribute to the mechanism of adherence.

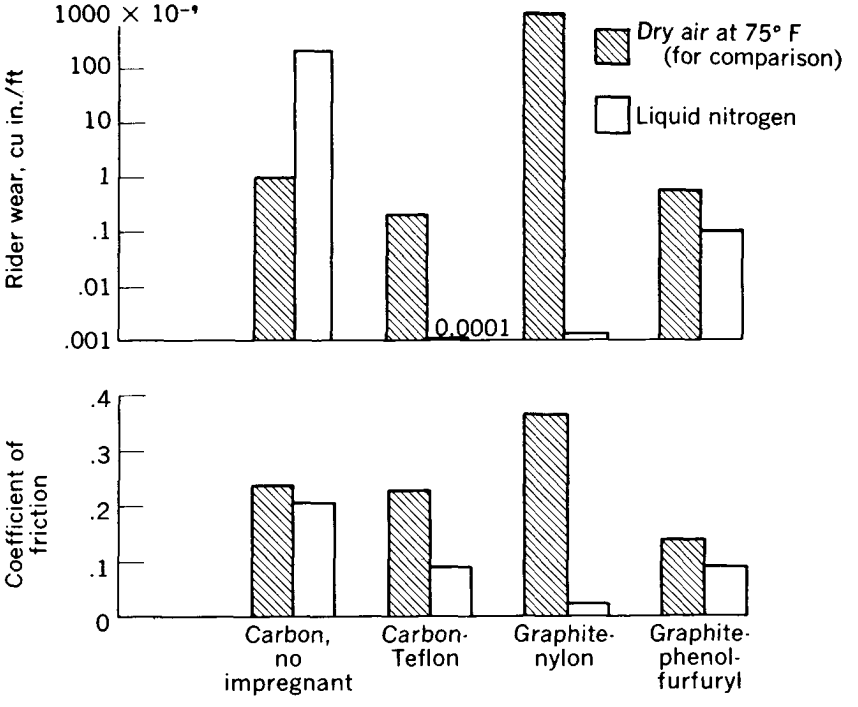

FIGURE 10–10.—Wear and friction of carbon-plastic compositions in liquid nitrogen. Sliding velocity, 2300 feet per minute; load, 1000 grams; disk, 304 stainless steel. (From ref. 10.)

Accordingly, the objective of a series of experiments conducted at NASA (ref. 10) was to explore the effectiveness of various impregnants. Studies were made of (1) organic impregnants, (2) inorganic impregnants, and (3) carbon-plastic compositions. The preliminary studies were conducted in liquid nitrogen, while the final studies were conducted in both liquid nitrogen and liquid hydrogen at various sliding velocities.

The results in liquid nitrogen with organic impregnants are shown in figure 10–8. These results show that no major improvement in either friction or wear of carbons sliding against the 304 stainless steel disk is obtained by use of the five organic impregnants including the chlorinated materials.

The results obtained with inorganic impregnants are presented as figure 10–9. These results show that inorganic impregnants, particularly the halides (such as metal fluoride or cadmium iodide), appreciably reduced wear when the tests were made in liquid nitrogen. For example, cadmium iodide (CdI_2) reduced wear in liquid nitrogen by a factor of 10,000 when compared with the unimpregnated carbon. Note that the inorganic impregnants show no apparent beneficial effect in air.

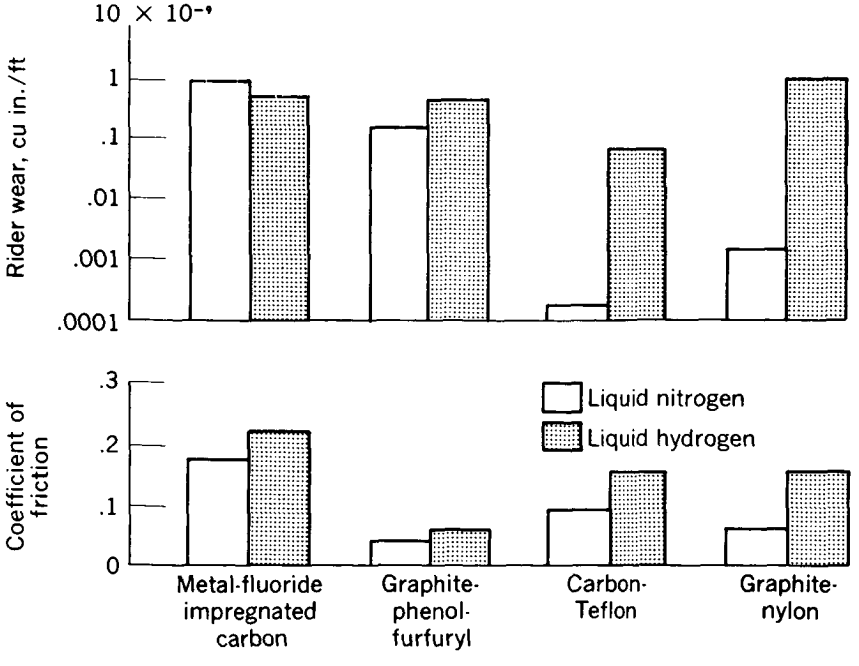

FIGURE 10–11.—Wear and friction of carbon-plastic compositions in liquid nitrogen and in liquid hydrogen. Sliding velocity, 2300 feet per minute; load, 1000 grams; disk, 304 stainless steel. (From ref. 10.)

Several carbon-plastic combinations show very marked reductions in wear for the tests in liquid nitrogen (fig. 10–10). In particular, the carbon-Teflon and graphite-nylon combinations showed extremely low wear in liquid nitrogen. These combinations consisted of approximately 15 percent carbon—85 percent Teflon and 5 percent graphite—95 percent nylon.

After results were obtained in liquid nitrogen, experiments were conducted in liquid hydrogen with the better materials from the liquid-nitrogen tests. These results are presented in figure 10–11. Unfortunately, those material combinations which showed *marked* differences in wear in liquid nitrogen showed *lesser* differences in wear in liquid hydrogen. For these particular combinations, therefore, results cannot be extrapolated from liquid nitrogen to liquid hydrogen.

The general conclusions obtained from these experiments are as follows:

(1) Inorganic impregnants can markedly reduce wear of carbons in nitrogen; these same impregnants also show some (but not great) reduction of wear in hydrogen.

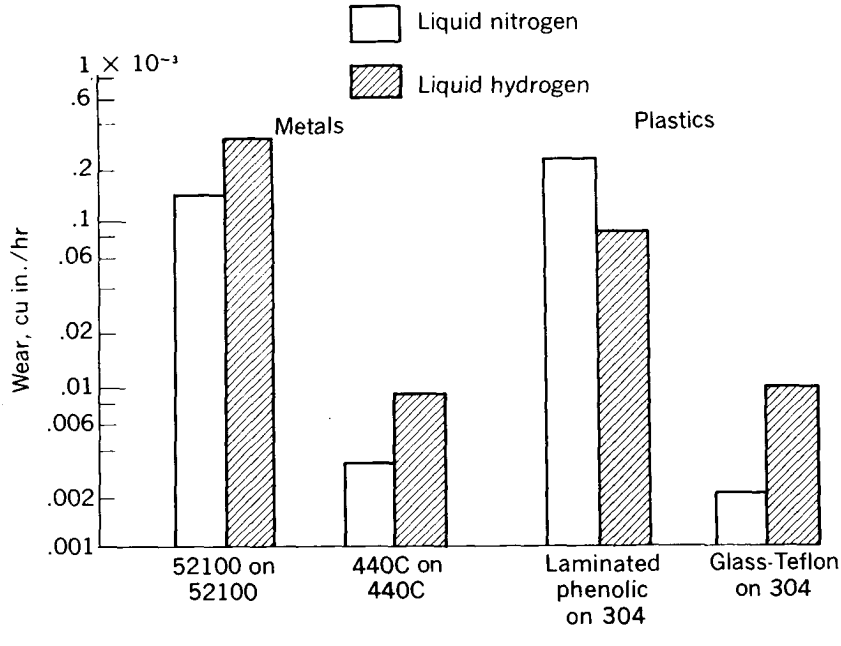

FIGURE 10–12.—Wear of various materials in liquid nitrogen and in liquid hydrogen. Sliding velocity, 2300 feet per minute; load, 1000 grams.

(2) A better correlation between nitrogen and hydrogen results was obtained with metal-metal combinations than with carbon-metal combinations (see fig. 10–12). Note that the combinations which showed marked differences of wear in nitrogen *also* showed marked differences in hydrogen.

The majority of the results of figures 10–8 to 10–12 are from reference 10.

Wear and friction of the combinations carbon-carbon and carbon—stainless steel in liquid nitrogen and liquid hydrogen.—The results presented in the previous section showed that even with impregnants which helped to form the mating film good performance is not always obtained in liquid hydrogen while sliding carbon against metals. It was, therefore, felt that the use of a carbon-carbon combination in cryogenic liquids might provide better performance than could a carbon-metal combination (ref. 11). In accordance, experiments were run with such combinations in order to study the wear and friction properties. The basic carbons used in these experiments were (1) a graphitic carbon of approximately 20 percent graphite content (labeled "Phenolic Impregnated Carbon" in figs. 10–13 to 10–15, and

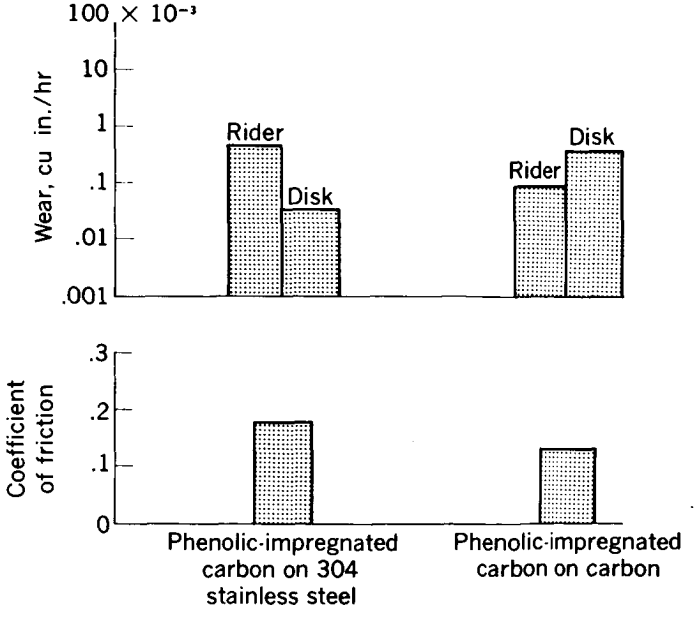

FIGURE 10–13.—Wear and friction of phenolic impregnated graphitic carbon in dry air with various disks. Sliding velocity, 2300 feet per minute; load, 1000 grams; temperature, 75° F. (From ref. 11.)

(2) a graphitic carbon of approximately 60 percent graphite content (labeled "Dense Graphitic Carbon" in figs. 10–14 and 10–15).

Figure 10–13 shows that sliding carbon against steel or carbon against carbon in dry air at 75° F yields approximately the same wear and friction results. Figure 10–14 shows that when run in liquid nitrogen the wear of a phenolic-impregnated carbon on carbon can be lower than that of the same carbon against a metal. Figure 10–15 shows that in liquid hydrogen the phenolic-impregnated carbon sliding against itself shows better rider wear properties than does the same carbon sliding against stainless steel. While the disk wear is higher in the case of the carbon disk, some disk wear is acceptable. In fact, reported and unreported experience shows that carbon-carbon seal surfaces have greater life than carbon—stainless steel seal surfaces in certain applications. In the presence of hydrogen, there is an appreciable reduction in friction coefficient with the carbon sliding against carbon as compared with the carbon sliding on stainless steel (fig. 10–15).

The better results with carbon on carbon in both liquid nitrogen and liquid hydrogen are due to the continued presence at the surface of graphite, which provides effective lubrication. On the other hand, for effective lubrication with carbon on steel, it is necessary to form

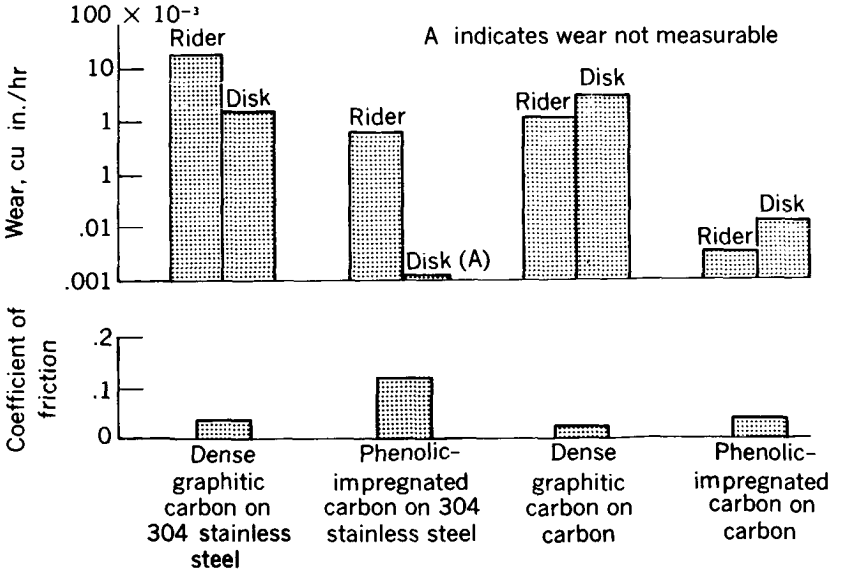

FIGURE 10–14.—Wear and friction of two graphitic mechanical carbons in liquid nitrogen. Sliding velocity, 2300 feet per minute; load, 1000 grams; temperature, −320° F. (From ref. 11.)

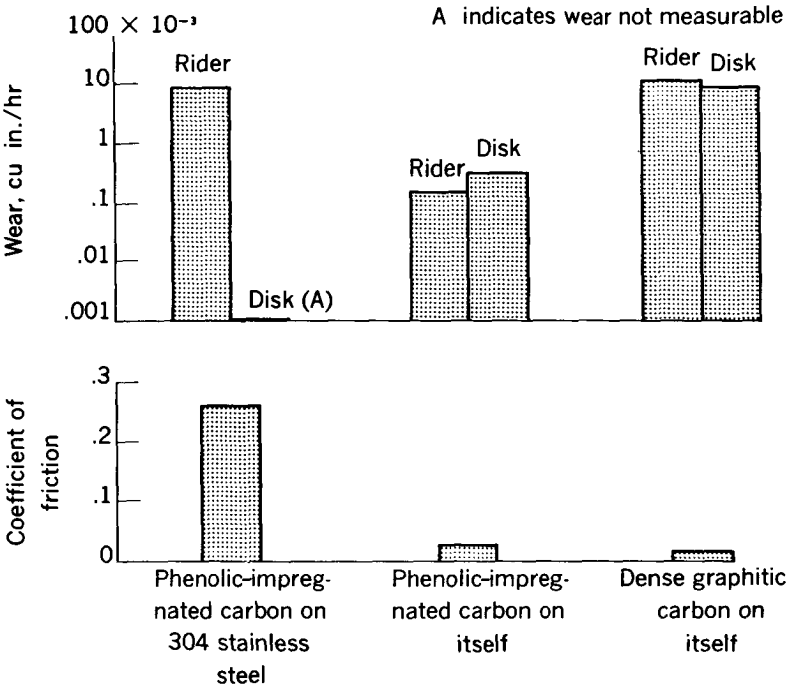

FIGURE 10–15.—Wear and friction of two graphitic mechanical carbons in liquid hydrogen. Sliding velocity, 2300 feet per minute; load, 1000 grams; temperature, −423° F. (From ref. 11.)

the mating carbon film on the metal disk; and this does not always occur, as has been demonstrated.

The general conclusions obtained from the investigation of the carbon-carbon combinations are as follows:

(1) Substantial reductions in carbon rider wear and lower friction can be obtained by using a carbon-carbon combination rather than a carbon-steel combination. Carbon-disk wear was greater than metal-disk wear, but some practical experience has been obtained that shows that carbon-carbon seal surfaces have greater life than carbon-steel seal surfaces in hydrogen.

(2) The results obtained support the view that a primary factor in lubrication with graphitic carbons is their ability to form an adherent film on the mating surface. The use of the carbon-carbon combinations makes it unnecessary for the carbon rider to form a mating film on the metal surface; effective lubrication is therefore obtained with the carbon-carbon combination even in an inert atmosphere such as liquid nitrogen or in a reducing atmosphere such as liquid hydrogen.

Rolling-Element Bearing Studies

Studies of rolling-element-bearing performance in liquid hydrogen and nitrogen at DN values as high as 1.6 million have been carried out (refs. 1, 2, 3, 19, 20, and 21). These studies are discussed in detail in chapter 11.

REFERENCES

1. JACOB, ROBERT B., MARTIN, KENNETH B., VAN WYLEN, GORDON J., and BIRMINGHAM, BASCOM W.: Pumping Cryogenic Liquids. Tech. Memo. 36, Rep. 3569, Cryogenic Eng. Lab., NBS, Feb. 24, 1956.
2. TANZA, G. F.: Development Program for a Non-Lubricated 10,000 rpm Bearing Operating over a Temperature Range from 40° R to 560° R. Vol. 2 of Advances in Cryogenic Eng., K. D. Timmerhaus, ed., Plenum Press, Inc., 1960, pp. 145–155.
3. SIMON, I., MCMAHON, H. O., and BOWEN, R. J.: Dry Metallic Friction as a Function of Temperature Between 4.2° K and 600° K. Jour. Appl. Phys., vol. 22, no. 2, Feb. 1951, pp. 177–184.
4. KRIVOBOK, V. N.: Properties of Austenitic Stainless Steels at Low Temperatures—Mechanical Properties at Low Temperatures. Cir. 520, NBS, May 7, 1952, pp. 112–134; discussion, pp. 134–136.
5. BOWDEN, F. P., and TABOR, D.: The Friction and Lubrication of Solids. Clarendon Press (Oxford), 1950.
6. WISANDER, D. W., HADY, W. F., and JOHNSON, R. L.: Friction Studies of Various Materials in Liquid Nitrogen. NACA TN 4211, 1958.
7. WISANDER, D. W., MALEY, C. E., and JOHNSON, R. L.: Wear and Friction of Filled Polytetrafluoroethylene Compositions in Liquid Nitrogen. ASLE Trans., vol. 2, no. 1, Apr. 1959, pp. 58–66.
8. WISANDER, D. W., and JOHNSON, R. L.: Wear and Friction in Liquid Nitrogen with Austenitic Stainless Steel Having Various Surface Coatings. Vol. 4 of Advances in Cryogenic Eng., K. D. Timmerhaus, ed., Plenum Press, Inc., 1960, pp. 71–83.
9. SLINEY, H. E., WISANDER, D. W., and JOHNSON, R. L.: NASA Studies of Solid Lubricants for Extreme Temperatures. TR 59–244, WADC, 1959.
10. WISANDER, D. W., and JOHNSON, R. L.: Wear and Friction of Impregnated Carbon Seal Materials in Liquid Nitrogen and Hydrogen. Vol. 6 of Advances in Cryogenic Eng., K. D. Timmerhaus, ed., Plenum Press, Inc., 1960, pp. 210–218.
11. WISANDER, D. W., and JOHNSON, R. L.: Wear and Friction in Liquid Nitrogen and Hydrogen of the Materials Combinations Carbon-Stainless Steel and Carbon-Carbon. Paper Presented at Air Force-Navy-Industry Prop. Systems Lubricants Conf., San Antonio (Texas), Nov. 15–17, 1960.
12. WILSON, W. A., MARTIN, K. B., BRENNAN, J. A., and BIRMINGHAM, B. W.: Evaluation of Ball Bearing Separator Materials Operating Submerged in Liquid Nitrogen. ASLE Trans., vol. 4, no. 1, Apr. 1961, pp. 50–58.
13. BURTON, R. A., LI, K. Y., LIU, T. S., and KU, P. M.: Research on Lubrication Behavior Under Extreme Low Temperatures. Southwest Res. Inst., TR 61–161, WADD, May 1961.
14. ROACH, A. E., GOODZEIT, C. L., and HUNNICUTT, R. P.: Scoring Characteristics of Thirty-eight Different Elemental Metals in High-Speed Sliding Contact with Steel. ASME Trans., vol. 78, no. 8, 1956, pp. 1659–1667.

15. GOODZEIT, C. L., HUNNICUTT, R. P., and ROACH, A. E.: Frictional Characteristics and Surface Damage of Thirty-nine Different Elemental Metals in Sliding Contact with Iron. ASME Trans., vol. 78, no. 8, Nov. 1956, pp. 1669–1674; discussion, pp. 1674–1676.
16. BISSON, EDMOND E., JOHNSON, ROBERT L., SWIKERT, MAX A., and GODFREY, DOUGLAS: Friction, Wear, and Surface Damage of Metals as Affected by Solid Surface Films. NACA Rep. 1254, 1956. (Supersedes NACA TN 3444.)
17. TROUP, GEORGE B.: Sulfurizing—A New Surface Treatment—Reduces Scoring and Seizing. Materials and Methods, vol. 44, no. 3, Sept. 1956, pp. 110–113.
18. WISANDER, D. W., and JOHNSON, R. L.: A Solid Film Lubricant Composition for Use at High Sliding Velocities in Liquid Nitrogen. ASLE Trans., vol. 3, no. 2, Oct. 1960, pp. 225–231.
19. SCIBBE, HERBERT W., and ANDERSON, WILLIAM J.: Evaluation of Ball-Bearing Performance in Liquid Hydrogen at DN Values to 1.6 Million. ASLE Trans., vol. 5, no. 1, Apr. 1962, pp. 220–232.
20. BUTNER, M. F., and ROSENBERG, J. C.: Lubrication of Bearings with Rocket Propellants. Lubrication Eng., vol. 18, no. 1, Jan. 1962, pp. 17–24.
21. BUTNER, MYLES F.: Propellant Lubrication Properties Investigation. TR 61–77, WADD, June 1961.

Page intentionally left blank

CHAPTER 11

Extreme-Temperature Bearings

By WILLIAM J. ANDERSON

EXTREME-TEMPERATURE BEARINGS ARE OF INTEREST (1) at temperatures from −65° F down to temperatures approximating those of liquid helium, a few degrees above absolute zero, and (2) at temperatures of 400° F and above, up to an absolute maximum of 3000° F.

For the low temperatures, one of the lubrication problems involves operating bearings in turbomachinery that pumps high-energy cryogenic propellants for chemical rockets. Lubrication with conventional oils in many of these applications may not be practicable because of the difficulty of raising the ambient temperature of the bearing to keep the oil hot enough so that it can be pumped. Even if heating is possible, the use of coventional lubrication systems may necessitate long overhung shafts to isolate the bearing from the cold region. These systems usually lead to various design and critical speed problems. Although not directly related to bearings, shaft seals are an additional problem. Many dynamic sealing problems can be alleviated or eliminated completely by operating the bearings in the working fluid. When reliable operation can be accomplished with bearings lubricated and cooled by the working fluid, shaft seals and bearing lubrication systems can be greatly simplified. This simplification results in an appreciable reduction of complexity, weight, and cost. Specific applications in the cryogenic region require bearings to operate at very high speeds with light to heavy loads for relatively short times as in turbopumps or at moderate speeds and loads as in cooling-system pumps.

At elevated temperatures, bearing applications include low rotative speed or oscillating conditions at very high loads, such as airframe control bearings for supersonic aircraft. Other applications at high temperatures involve high rotative speeds with loads ranging from

low to high. An example of this application would be small high-speed turbomachinery with bearings located close to hot turbines. Jet-engine rotor bearings for supersonic aircraft also operate hot at high DN values and loads. In these engines limited cooling capacity and high stagnation temperatures result in high ambient temperatures around the bearings.

The approaches to bearing operating problems in these two areas will be discussed separately. The results obtained by various investigators in this field will be examined. Problems in the cryogenic temperature region will be discussed first.

SYMBOLS

a	semimajor axis of contact ellipse, in.
b	semiminor axis of contact ellipse, in.
CF	centrifugal force on ball, lb
d	ball diameter, in.
E	bearing unit pitch diameter, in.
$E(k)$	complete elliptic integral of the second kind
f	race curvature
M_l	torque about bearing axis, in.-lb
M_s	ball spin moment, in.-lb
n	number of balls
P	normal ball load, lb
Q	oil flow, lb/min
Q_s	heat generated between balls and race due to ball spin, Btu/min
r	race-ball groove radius, in.
T	bearing thrust load, lb
V_B	linear velocity of inner-race ball contact, in./sec
W	thrust load, lb
$\alpha_1,\alpha_2,\gamma,\Delta,\theta$	angles, defined on figures, deg
β	contact angle under load, deg
β'	initial mounted no-load contact angle, deg
β_i	inner-race contact angle at load and speed, deg
β_o	outer-race contact angle at load and speed, deg
μ_s	coefficient of sliding friction
ω	angular velocity of a ball about its rolling axis, radian/sec

Subscripts:

i	inner race
o	outer race
R	rolling
s	spinning

LOW-TEMPERATURE BEARINGS

When bearings are operated in cryogenic fluids such as liquid nitrogen, liquid oxygen, or liquid hydrogen, ample cooling capacity is available. These fluids are poor boundary lubricants, however, so that the problem is one of preventing surface damage in sliding and in rolling contact. Before a rolling bearing can be operated successfully in an application where the lubrication is marginal, two principal problems must be overcome. First, the integrity of the surfaces in rolling and in sliding contact must be maintained. Therefore, the bearings should be made of materials that tend to exhibit minimum wear and maximum resistance to galling and to surface welding in sliding. Second, the heat generated within the bearing must be removed to maintain an equilibrium operating condition and to prevent a total loss of bearing operating clearance that could result in bearing seizure. The bearing material and design must be chosen to minimize heat generation within the bearing in order to provide a maximum assurance of success. There are two principal sources of heat generation within a ball bearing: (1) the sliding friction between the retainer and its locating race and the retainer and the balls, and (2) the friction due to ball spin in the ball-race contact area. Bearings must be designed to minimize both of these sources of heat generation to obtain maximum performance in cryogenic fluids. Therefore, retainer materials selected for test should be chosen from among those that exhibit low friction coefficients and good resistance to wear as determined by cryogenic friction and wear tests. These tests are much less expensive to conduct than full-scale bearing tests. A background of knowledge in friction and wear of candidate materials is necessary to conduct a bearing experimental program intelligently. To minimize heat generation due to ball spin losses requires an examination of various design parameters such as ball diameter and race curvatures to determine the amount of heat generation due to ball spinning.

Friction and Wear Experiments

References 1 and 2 present the results of friction and wear experiments in both liquid nitrogen and liquid hydrogen. These results indicate that filled Teflon compositions show promise for cryogenic applications. In reference 1, 25 percent glass-fiber-filled Teflon sliding against 304 stainless steel in liquid nitrogen showed low wear at sliding velocities to 6000 feet per minute. In this material, the Teflon provides the lubrication while the glass fibers are added to increase structural strength.

Early Bearing Experiments

Some of the early bearing experiments in cryogenic fluids are reported in reference 3. The authors started out with SAE 52100 steel bearings. These radial bearings had pressed steel separators and gave only limited service in liquid nitrogen and liquid hydrogen. In all these bearings, mechanical failures occurred in the separator. Further experiments with ½-inch and 15-millimeter-bore SAE 52100 steel angular-contact bearings equipped with cotton-cloth phenolic-laminated separators showed that successful operation could be obtained at speeds from 3300 to 8000 rpm. These experiments indicated, however, that 52100 steel, because of its lack of corrosion resistance, is not an ideal ball and race material for cryogenic applications where thermal cycling back to room temperature is apt to occur. When cycling does occur, condensation may form on the bearing surfaces, and since they are free from organic contaminants, corrosion may take place. Additional experiments were conducted with bearings that had races and balls made of 440C stainless steel, and satisfactory operation was obtained for 262 hours in liquid hydrogen at 12,000 rpm. Other bearings in these experiments were operated successfully at 3300 rpm for running times in excess of 4700 hours. Although the bearings in reference 3 were run at nominal speeds and light loads, the results indicated that with proper design and good choice of retainer materials bearing operation at very high DN values was a distinct possibility. A more systematic investigation of the operation of 10-millimeter-bore bearings at 3150 rpm under a thrust load of 144 pounds in liquid nitrogen was conducted in reference 4. In reference 4, bearings with cotton-cloth phenolic laminate, Teflon-coated steel, filled Teflon machined, Teflon-coated grade A phosphor bronze, grade A phosphor-bronze retainers, and full-complement bearings with alternate undersize 440C balls were investigated. Among the cotton-cloth phenolic laminates were inner-ring-riding retainers, outer-ring-riding retainers, and ball-riding retainers. With the exception of the machined retainers of filled Teflon material, all the other retainer configurations gave life results from 0.4 to 20 hours. The bearings with filled Teflon retainers operated without failure for 1000 hours. The criterion of failure used in these experiments was excessive torque.

High-Speed Bearing Experiments

In contrast to the work reported in references 3 and 4, which was aimed at the development of bearings with long lives at nominal running speeds, the work of reference 5 is directly related to bearings for high-speed turbomachinery with short-duration lives. The objective of the work reported in reference 5 was to study the performance as well as the operating limitations of ball bearings in liquid

hydrogen for running times of 1 hour at DN values to 1.5×10^6. In reference 5, both retainer material and bearing design were studied. The retainer material that performed best was again the filled Teflon material, which agrees with the results obtained in references 3 and 4. Among the bearing-design parameters investigated in reference 5 were the effects of diametral clearance, ball size, and bearing race curvatures on the limiting speed when bearings were submerged in liquid hydrogen and operated under thrust loads from 100 to 500 pounds. The majority of the work in reference 5 was conducted with 40-millimeter ball bearings, which were operated successfully at speeds to 42,000 rpm. A detailed discussion of the approach to the problem of heat generation in the ball-race contact is presented in reference 5. An approximate analysis was made of the effects of bearing design parameters on the amount of heat generation in the ball-race contact. This analysis showed that open-race curvatures reduce the amount of heat generation due to ball spin. Therefore, higher limiting speeds can be obtained with bearings designed for minimum heat generation. An additional important factor was shown to be ball diameter, which is discussed in reference 5.

Heat generation due to ball spin.—In a ball bearing that operates under any load condition other than radial, ball spinning, in addition to rolling, occurs at the ball-race contacts. If the bearing is operated at high speed, the centrifugal force on the balls creates an additional load at the outer-race contact. The effect of centrifugal force is to shift the contact points between the balls and the races from those at lower speeds. The result is an increase in the operating contact angle at the inner race. The normal ball load at the outer-race contact can be expressed by

$$P_o=CF\cos\beta_o+\frac{T\cos(\beta_i-\beta_o)}{n\sin\beta_i} \tag{11-1}$$

(ref. 6), whereas the ball load at the inner-race contact is

$$P_i=\frac{T}{n\sin\beta_i} \tag{11-2}$$

Usually the ball will have either outer-race or inner-race control, that is, rolling at one race contact without spin and spinning plus rolling at the other race contact. The frictional moment created by ball spin in the pressure ellipse at the ball-race contact can be expressed approximately as

$$M_s=\frac{3}{8}\mu_s PaE(k) \tag{11-2a}$$

(See ref. 7.) The ball will roll at the race contact where the value of the friction moment is the greater.

An approximate analysis to determine the heat generated in the ball-race contact of a thrust-loaded ball bearing is outlined in reference 8 for inner-race rotation where gyroscopic moments are neglected and the ball rolls on one race without spin. The following assumptions are made in this analysis:

(1) The effective ball rolling radius r at operating conditions is the unstressed radius $d/2$.

(2) In computing the spin moment M_s, the linear slip velocities in the direction of rolling that occur because of the curvature of the contact ellipse are small compared with the slip velocities due to ball spin.

(3) Gyroscopic moments are insufficient to cause ball slip.

(4) The rotating radial load that results from shaft unbalance at high speeds is neglected.

From figure 11–1(a) for inner-race control,

$$V_B=\omega_i\left(\frac{E}{2}-\frac{d}{2}\cos\beta_i\right) \tag{11–3}$$

$$\tan\alpha_1=\frac{\sin\beta_i}{\frac{E}{d}-\cos\beta_i} \tag{11–4}$$

$$\frac{1}{2}(\gamma+\alpha_2)=\frac{1}{2}(\pi-\theta) \tag{11–5}$$

$$\tan\frac{1}{2}(\gamma-\alpha_2)=\frac{\frac{E}{d}-\sin(\beta_i+\alpha_1)}{\frac{E}{d}+\sin(\beta_i+\alpha_1)}\tan\frac{1}{2}(\gamma+\alpha_2) \tag{11–6}$$

$$\alpha_2=\frac{1}{2}(\gamma+\alpha_2)-\frac{1}{2}(\gamma-\alpha_2) \tag{11–7}$$

$$\omega=\frac{\omega_i\sin\beta_i}{(\tan\alpha_1+\tan\alpha_2)\cos\alpha_1} \tag{11–8}$$

$$\omega_{s,o}=\omega\sin(\beta_i+\alpha_1-\beta_o) \tag{11–9}$$

$$Q_{s,o}=n\omega_{s,o}M_{s,o} \tag{11–10}$$

When equation (11–10) is converted to torque about the bearing axis,

$$M_{1,o}=\frac{Q_{s,o}}{\omega_i} \tag{11–11}$$

where, from reference 7

$$M_{s,o}=\frac{3}{8}\,\mu_s P_o a_o E(k_o) \tag{11-12}$$

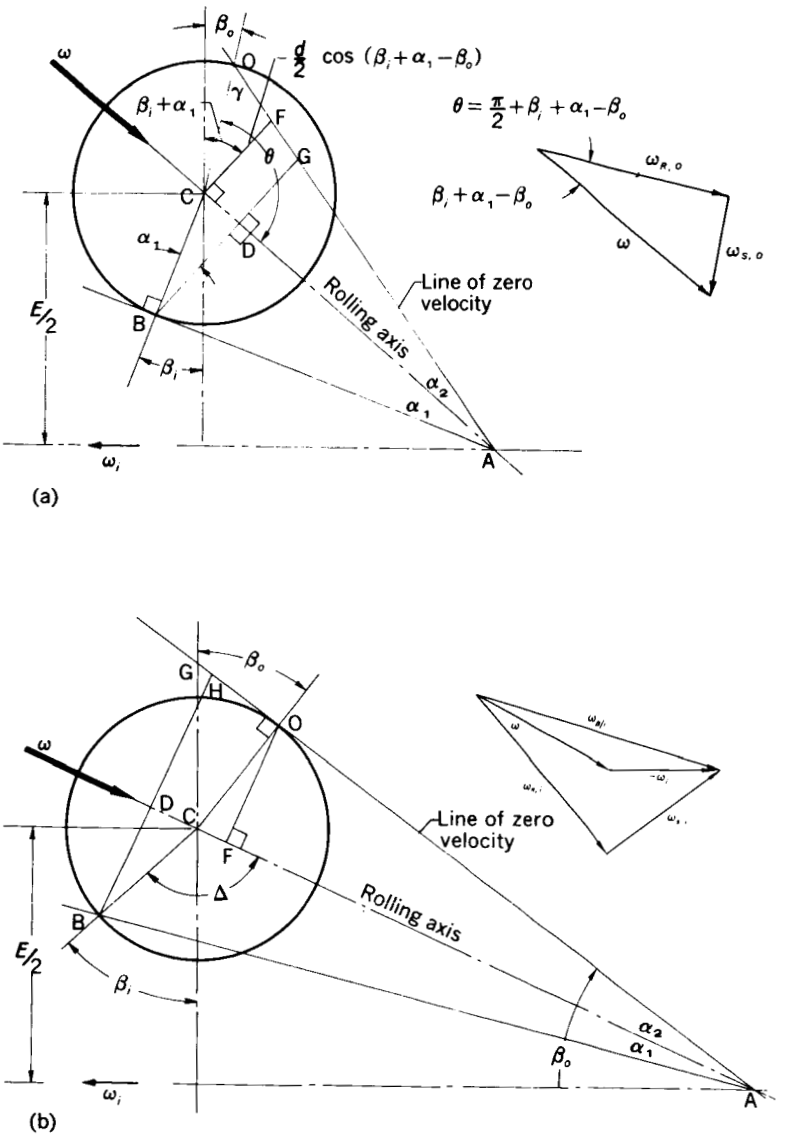

(a) Inner-race control.
(b) Outer-race control.

FIGURE 11–1.—Bearing geometric relations used to calculate heat generation due to ball spinning. (From ref. 5.)

From figure 11–1(b) for outer race control,

$$V_B=\omega_i\left(\frac{E}{2}-\frac{d}{2}\cos\beta_i\right) \tag{11–3}$$

$$\tan\alpha_2=\frac{\sin\beta_o}{\frac{E}{d}+\cos\beta_o} \tag{11–13}$$

$$\Delta=\frac{\pi}{2}+\beta_i-\beta_o+\alpha_2 \tag{11–14}$$

$$\sin\alpha_1=\frac{\sin\Delta}{\left\{1+\left[\frac{\frac{E}{d}}{\sin(\beta_o-\alpha_2)}\right]^2-2\left[\frac{\frac{E}{d}}{\sin(\beta_o-\alpha_2)}\right]\cos\Delta\right\}^{1/2}} \tag{11–15}$$

$$\omega=\frac{\omega_i\left(\frac{E}{d}-\cos\beta_i\right)\Big/(\sin\alpha_1+\tan\alpha_2\cos\alpha_1)}{\left\{1+\left[\frac{\frac{E}{d}}{\sin(\beta_o-\alpha_2)}\right]^2-2\left[\frac{\frac{E}{d}}{\sin(\beta_o-\alpha_2)}\right]\cos\Delta\right\}^{1/2}} \tag{11–16}$$

$$\omega_{s,\,i}=\omega\sin(\beta_i-\beta_o+\alpha_2)+\omega_i\sin\beta_i \tag{11–17}$$

$$Q_{s,\,i}=n\omega_{s,\,i}M_{s,\,i} \tag{11–18}$$

When equation (11–18) is converted to torque about the bearing axis,

$$M_{1,\,i}=\frac{Q_{s,\,i}}{\omega_i} \tag{11–19}$$

where, from reference 7

$$M_{s,\,i}=\frac{3}{8}\mu_s P_i a_i E(k_i) \tag{11–20}$$

Calculations were made on a digital computer for 40-millimeter-bore bearings of an extremely light series (1908 with 0.250-in.-diam. balls) and an extra light series (108 with 0.375-in.-diam. balls). Four race-curvature combinations were assumed, and calculations were made for thrust loads of 100, 200, and 300 pounds, initial contact angles of 5°, 10°, 15°, and 20°, and a rotative speed of 40,000 rpm (1.6 million DN). The results are shown in table (11–I).

A value of 0.56 was used for the sliding friction coefficient in calculating heat generation. This value was obtained in reference 2 for 440C sliding on 440C in liquid hydrogen. Since the heat-generation

TABLE 11–I.—TORQUE DEVELOPED ABOUT BEARING AXIS DUE TO BALL SPIN [a]

(a) 108-Series bearing: ball diameter, 0.375 in.; pitch diameter, 2.111 in.; coefficient of sliding friction, 0.56; angular velocity of inner race, 4190 radian/sec

Race curvature	$f_i=0.51, f_o=0.58$				$f_i=0.51, f_o=0.56$				$f_i=0.52, f_o=0.54$				$f_i=0.54, f_o=0.52$			
Initial mounted contact angle, β', deg	5	10	15	20	5	10	15	20	5	10	15	20	5	10	15	20
Inner-race contact angle at 300 lb, β_i, deg	18.8	24.0	32.7	44.5	20.1	24.8	32.5	42.7	19.1	22.3	27.4	34.0	16.5	18.8	22.5	27.0
Thrust load, T, lb	Torque about bearing axis, M_1, lb-in.															
100	2.143	2.095	2.132	2.314	2.143	2.099	2.106	2.214	1.698	1.653	1.620	1.612	1.356	1.319	1.285	1.259
200	4.830	4.755	4.755	4.978	4.941	4.755	4.755	4.904	3.752	3.693	3.789	3.648	2.931	2.894	2.853	2.831
300	7.579	7.504	7.467	7.616	7.579	7.504	7.467	7.579	5.870	5.795	5.758	5.758	4.569	4.532	4.495	4.458

(b) 1908-Series bearing: ball diameter, 0.250 in.; pitch diameter, 2.001 in.; coefficient of sliding friction, 0.56; angular velocity of inner race, 4190 radian/sec

Race curvature	$f_i=0.51, f_o=0.58$				$f_i=0.51, f_o=0.56$				$f_i=0.52, f_o=0.54$				$f_i=0.54, f_o=0.52$			
Initial mounted contact angle, β', deg	5	10	15	20	5	10	15	20	5	10	15	20	5	10	15	20
Inner-race contact angle at 300 lb, β_i, deg	[c] 13.2	[c] 15.1	[c] 17.9	31.7	[c] 14.1	21.1	25.7	32.0	18.6	21.0	24.8	29.8	17.2	19.2	22.4	26.4
Thrust load, T, lb	Torque about bearing axis, M_1, lb-in.															
100	1.839	1.831	1.850	1.939	1.835	1.831	1.846	1.910	1.419	1.412	1.412	1.423	1.096	1.092	1.092	1.092
200	3.789	3.789	3.789	3.864	3.789	3.789	3.789	3.884	2.916	2.912	2.920	2.946	2.259	2.255	2.251	2.262
300	2.964[b]	3.299[b]	3.864[b]	5.832	3.407[b]	5.795	5.795	5.832	4.458	4.458	4.458	4.458	3.462	3.448	3.433	3.440

[a] From ref. 5.
[b] Inner-race control, ball spinning at outer race.
[c] Outer-race contact angle β_o.

calculations are all relative and are used for comparative purposes only, the actual coefficient of friction is unimportant.

For the 108-series bearings, ball control was at the outer race for all combinations of race curvature and thrust load chosen. For the 1908-series bearings, ball control was at the outer race for all combinations except four. Ball control is at the inner race for a thrust load of 300 pounds and the following sets of curvatures and contact angles:

(1) $f_i=0.51$
$f_o=0.58$
$\beta=5°$, 10°, and 15°

(2) $f_i=0.51$
$f_o=0.56$
$\beta=5°$

Inner-race ball control is desirable because it results in relatively low friction torque due to ball spin.

At a specific thrust load, the values of M_1 do not change appreciably with initial mounted contact angle when control is at the outer race. The torque developed decreases with increasing race curvature at the spinning contact and is not affected by curvature at the rolling contact. This fact is apparent since close values of ball-race conformities (i.e., approaching 0.50) result in high rates of heat generation. The operating contact angle is given for a thrust load of 300 pounds. The operating contact angle and the angular velocity of ball spin increase with increasing initial mounted contact angle for all race-curvature combinations shown. Torque developed at the inner-race contact of the 108-series bearing with $f_i=0.52$ and $f_o=0.54$ at thrust loads of 100 and 200 pounds is greater than that developed in the 1908-series with the same race curvatures, which indicates the importance of ball diameter.

The importance of ball spin losses can be noted by comparing the results for the two series bearings shown on figure 11–2. The 1908-series bearings with inner- and outer-race curvatures of 0.54 operated to higher limiting DN values than did the 108-series bearings with inner- and outer-race curvatures of 0.52 and 0.54, respectively, over the entire range of thrust loads investigated. The results of these tests appear to indicate that ball-spin losses are important.

In addition to ball diameter and race curvatures, another bearing design parameter, which was found to be important in reference 5, was bearing diametral clearance. Limiting DN values increased with diametral clearance for 108-series bearings with two different retainer materials as shown in figure 11–3.

Bearing experiments in cryogenic and other propellants.—Reference 9 contains some data on the operation of rolling bearings in liquid hydrogen, liquid oxygen, nitrogen tetroxide, and RP–1, a kerosene base

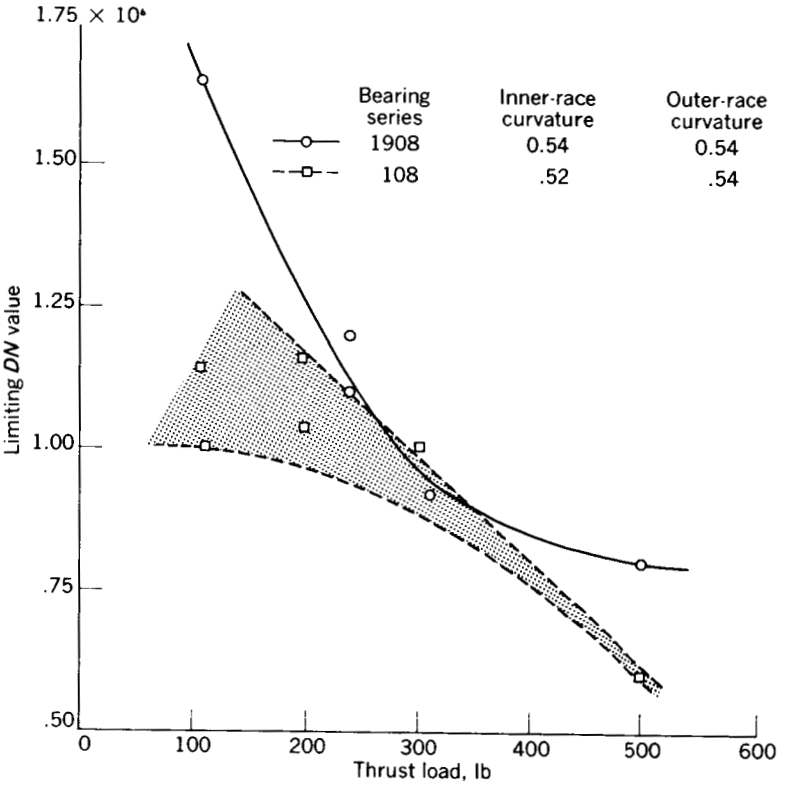

FIGURE 11–2.—Limiting DN value as function of thrust load for 108-series and 1908-series bearings with filled Teflon retainers. (From ref. 5.)

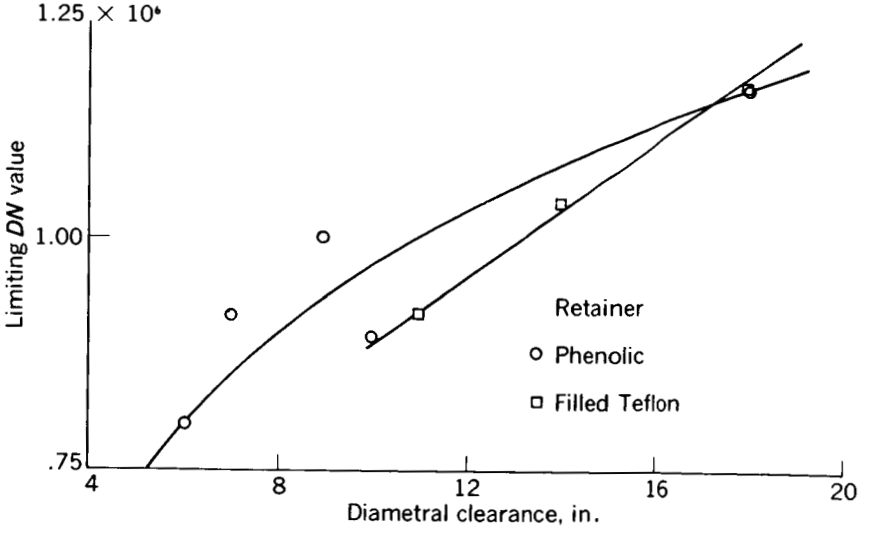

FIGURE 11–3.—Limiting DN value as function of diametral clearance for 108-series bearings with two different retainer materials. (From ref. 5.)

rocket fuel. As in references 4 and 5, the best results in the cryogenic propellants were obtained with bearings having glass-filled Teflon retainers and glass-supported Teflon retainers. The bearings used in this investigation were extra light (100 series) and light (200 series) with bore sizes from 35 to 45 millimeters. These bearings were run at speeds to 6400 rpm in liquid oxygen and nitrogen tetroxide and at 25,000 rpm in liquid hydrogen. These speeds correspond to the actual shaft speeds in a turbopump unit that pumps liquid oxygen and liquid hydrogen. In liquid hydrogen, bearings with several different types of metallic retainers all failed within a few minutes after starting. Likewise, in liquid oxygen and nitrogen tetroxide, bearings with metallic retainers had very short lives. Severe wear and galling caused failure.

Bearings with phenolic retainers were operated with some success in both liquid oxygen and liquid hydrogen. In liquid hydrogen, a speed of 20,000 rpm was successfully obtained. A tendency for the bearing to exhibit chatter at low shaft speeds existed, however, because of the high friction coefficient between the steel and the phenolic cage. Bearings with glass-supported Teflon retainers were operated successfully for almost 10 hours at 25,000 rpm in liquid hydrogen, 9 hours in liquid oxygen, and almost 5 hours in nitrogen tetroxide at 6400 rpm. In liquid oxygen successful operation was also obtained with a bearing that had a ribbon steel separator with a 0.010-inch coating of Teflon on the retainer parts. This bearing was run for 1 hour at 6400 rpm.

Some discrepancies existed in results obtained in various unpublished researches on the operation of rolling bearings in liquid oxygen. In some instances (ref. 9), no severe oxidation of the bearing, races, or balls was evident, and in unpublished tests, severe oxidation occurred. This discrepancy or anomaly in results has not been clarified, but there appears to be some evidence which indicates that the presence of moisture on the bearing is extremely critical. The presence of any moisture may cause severe corrosion in a highly reactive medium such as liquid oxygen. The problem of maintaining surface integrity is, of course, quite different in a reducing environment such as liquid hydrogen than it is in a highly oxidizing environment such as liquid oxygen. In liquid hydrogen, the temperature reached at the sliding asperities would be sufficient for the reactions between the hydrogen and any oxide films to ultimately produce clean nascent metals. Clean metals have characteristically poor friction and wear properties and gall readily. In a highly reactive oxidant, such as liquid oxygen, the opposite is true. Here the problem is one of controlling surface corrosion. Again the asperity temperatures would be sufficient to cause reaction between the oxygen and the metal at the asperities so that the maintenance of protective oxide films should not be a problem.

Discussion of Results

The general bearing design philosophy for bearings which are to be used in cryogenic applications is to design for minimum heat generation. The sources of heat generation are at the sliding surfaces between the retainer and the races, the retainer and the balls, and in the sliding contact between the balls and the races. Materials with good friction and wear properties such as filled Teflon should be used to reduce heat generation at the retainer sliding surfaces. For high-speed applications, reinforcement of retainers made of these materials with thin shrouds of either aluminum or stainless steel is necessary. For high-speed applications where loads are not too heavy and where heat generation is very critical, open-race curvatures and very liberal diametral clearances must be used. The open-race curvatures do reduce the load capacity of the bearing somewhat, but they also effect an appreciable reduction in the heat generation at these contacts; this extends the limiting speed at which the bearings can be successfully operated. Because centrifugal forces become predominant at extreme speeds and nominal loads, very light series bearings with small balls are found to have a higher load carrying capacity than heavier series bearings. This is in contrast to normal, conventionally lubricated bearing applications where the load capacity increases as the bearing series becomes heavier. A corrosion-resistant ball and race material, such as the ferritic tool steel 440C, is recommended rather than the standard bearing material SAE 52100 steel, which is subject to corrosion.

HIGH-TEMPERATURE BEARINGS

Applications and Problems

In the high-temperature region, applications include those at low rotative speeds or oscillating motion and very high load, such as airframe control bearings for supersonic aircraft, and applications at high rotative speeds with loads ranging from low to high. High rotative-speed applications include small high-speed turbomachinery with hot bearings located close to hot turbines and jet-engine rotor bearings for supersonic aircraft where limited cooling capacity and high stagnation temperatures result in high ambient temperatures.

The three major problems that are encountered in operating rolling-contact bearings at high temperatures are materials, lubricants, and bearing designs. These problems will be discussed in order.

Materials

Requirements.—The material problem involves obtaining materials that have adequate hot hardness, good oxidation resistance if the atmosphere is oxidizing, and good dimensional stability at high

temperatures. The loss of hardness at elevated temperatures of the standard bearing material SAE 52100 and MHT and M–50 steels are shown in figure 11–4, taken from reference 10. The loss of hardness results in lower load capacity or equivalently a lower fatigue life at constant load and in greater susceptibility to brinelling due to static or shock loads. The effect of hardness on fatigue life is discussed in chapter 12. Any brinelling of the races will result in rough operation and excessive vibration and make the bearing generally unsatisfactory. For many applications, a hardness of Rockwell C–55 is considered the minimum acceptable hardness at temperature. From figure 11–4, SAE 52100 steel is unacceptable at temperatures above 450° F.

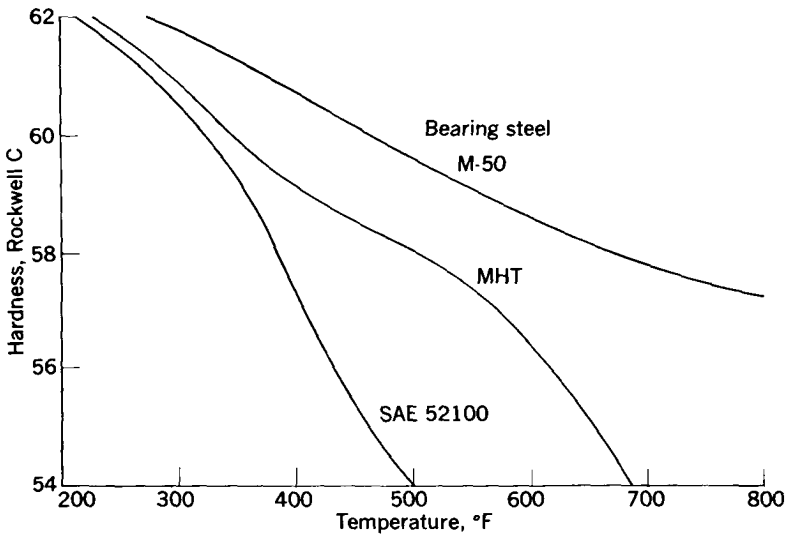

FIGURE 11–4.—Hardness as function of temperature for three bearing steels. (From ref. 10.)

Tool steels.—In a search for materials with better hot hardness, bearing manufacturers turned to several high alloy steels, which had been used in tools for a number of years. Compositions of some representative high-temperature bearing steels are given in table 11–II. Bearing steels for elevated temperatures may be divided into those suitable for mildly elevated temperatures from 400° to 600° F, those for higher temperatures from 600° to 1000° F, and the stainless steels. In the first category are MHT steel (which is SAE 52100 plus 1 percent aluminum), Halmo steel, and M–50 (or MV1) steel. Tool steels suitable for temperatures to approximately 1000° F are the molybdenum tool steels, such as M–1, M–2, and M–10. T–1 steel, sometimes known as 18–4–1, is also an acceptable material for this temperature range, although the high tungsten content

TABLE 11-II.—FERROUS ALLOYS FOR HIGH-TEMPERATURE BEARINGS [a]

Steel	Alloying element, percent by weight								
	C	Mn	Si	Ni	Cr	Mo	W	V	Al
MHT	0.95–1.10	0.25–0.45	0.25–0.55	------	1.30– 1.60	----------	----------	----------	0.75–1.25
M-50 (MV-1)	.80	.30	.30	------	4.00	4.25	----------	1.00	----------
HALMO	.58	.30	1.00	------	5.00	5.25	----------	.65	----------
M-1	.75– .85	.20– .40	.20– .40	------	3.75– 4.50	7.75–9.25	1.15– 1.85	.90–1.30	----------
M-2	.78– .88	.20– .40	.20– .40	------	3.75– 4.50	4.50–5.50	5.50– 6.75	1.60–2.20	----------
M-10	.85	.25	.25	------	4.00	8.00	----------	2.00	----------
T-1	.65– .75	.20– .40	.20– .40	------	3.75– 4.50	----------	17.25–18.75	.90–1.30	----------
440C	.95–1.20	1.00 Max.	1.00 Max.	------	16.00–18.00	.75 Max.	----------	----------	----------
Modified 440C	.95–1.20	1.00 Max.	1.00 Max.	------	14.00	4.00	----------	----------	----------
WB-49 [b]	1.09	.30	.30	0.04	4.24	3.70	6.72	1.91	----------

[a] From refs. 11 and 12.
[b] Contains in addition 5.18 percent cobalt.

makes it somewhat unattractive. Tool-steel bearings are generally considerably more expensive than those made of standard bearing materials because the initial cost of the materials is higher and also because of much higher machining costs.

In addition to adequate hardness at temperature, materials must have good corrosion resistance, if the atmosphere is oxidizing, and good dimensional stability. If a material is subjected to thermal cycling and does not retain its original dimensions, it cannot be used in a rolling-element bearing where a high degree of dimensional accuracy is a necessity. The research reported in reference 11 was undertaken to develop a ferrous alloy with these qualities, including a hot hardness of about Rockwell C–58 after 500 hours at 1000° F. The research of reference 11 was conducted generally to clarify the effects of alloying elements on secondary hardness, hardness retention at elevated temperatures, and other desirable properties for a high-temperature bearing steel; specifically, it was conducted to develop a high-temperature alloy. The alloy developed in reference 11 is designated as WB–49. Its composition is given in table 11–II. It has a hot hardness of Rockwell C–57 after 500 hours at 1000° F. It has hot hardness characteristics that are generally superior to those of the molybdenum base tool steels. To improve oxidation resistance, where oxidation is a factor, bearing manufacturers have turned to the use of martinsitic stainless steels. The conventional stainless steel material that has been used in roller bearings for a number of years is designated as 440C. The composition of this material is given in table 11–II. Its hot hardness, however, is deficient, and it cannot be used at temperatures much beyond those at which SAE 52100 is acceptable. A modified 440C material with 4 percent molybdenum added to the 440C composition has been found to have adequate hardness at 1000° F. The composition of this material is also given in table 11–II.

Super alloys.—When bearing temperatures exceed 1000 °F, ferrous-base alloys become unsatisfactory. In a temperature range above 1000° F, there are three classes of possible bearing materials. The first of these are the so-called super alloys with base compositions of cobalt, chromium, and molybdenum. These alloys may also contain significant percentages of nickel, tungsten, vanadium, and other alloying elements. A fairly large number of these super alloys exist, but many of the compositions are proprietary. In general super alloys with high carbon content are usually cast products that cannot be forged or machined. These alloys are cast to close dimensions and finish machined by grinding and lapping. Generally, bearings made of these cast products are quite expensive. Compositions of a number of representative super alloys are given in table 11–III (ref. 13).

TABLE 11-III.—NONFERROUS ALLOYS FOR HIGH-TEMPERATURE BEARINGS [a]

Material	Alloying elements, percent by weight											
	C	Cr	W	Ni	Fe	Co	V	Mo	Ti	Al	Mn	Si
Haynes 6B	1.1	30	4.5	3.0	3.0	Bal.						
Haynes 6K	1.6	31				Bal.						
Haynes-Stellite Star J	2.5	32	17	2.5	3.0	Bal.						
Haynes-Stellite 98M2	2.0	30	18.5	3.5	2.5	Bal.	4.0					
Haynes 25 (wrought)	.1	20	15	10	3.0 Max.	Bal.					1.5	1.0 Max.
René 41 (General Electric)	.09	19		Bal.		11		10	3.1	1.5		
M252 (General Electric)	.15	20		Bal.		10		10	3.0	1.0		
Haynes-Stellite 3	2.45	30.5	12.5	3.0	3.0 Max.	Bal.						

[a] From ref. 13.

These super alloys have been used in bearings for applications up to about 1500° F.

Cermets and ceramics.—At temperatures much above 1500° F, it is necessary to use cermet or ceramic materials for the bearing races and the rolling elements. Cermets are defined as any combination of ceramics and metals. Among the carbides used have been tungsten carbide, chromium carbide, and titanium carbide. Compositions of cermet materials that contain these carbides are shown in table 11–IV. Perhaps the most successful of these cermet compositions

TABLE 11–IV.—CERMET MATERIALS FOR HIGH-TEMPERATURE BEARINGS [a]

Material	Chemical composition, percent by weight
CA–3 Allegheny Ludlum	WC, 94; Co, 6. 0
779 General Electric	WC, 91; Co, 9.0
K 96 Kennametal	WC, 94; Co, 6.0
CA 815 Allegheny Ludlum	Cr_3C_2, 85; Ni, 15
608 General Electric	Cr_3C_2, 83; Ni, 15; WC, 2.0
CR 83 Metal Carbides	Cr_3C_2, 83; Ni, 15; WC, 2.0
K 162B Kennametal	TiC, 64; Ni, 25; CbC, 6; Mo, 5
K 175B Kennametal	TiC, 35; Mo, 15; Co, 4.5; Ni, 41; Al, 4; Ta, 0.3
K 196 Kennametal	TiC, 27; Cr, 5; Ni, 60; W, 7.5
K 175A Kennametal	TiC, 30; Al, 4.25; Ni, 40.5; CbC, 10; Mo, 15.25
K 163Al Kennametal	TiC, 50; Ni, 33.3; CbC, 10; Mo, 6.7

[a] From ref. 13.

used in high-temperature bearings has been titanium carbide. Tungsten carbide is unsuitable because of its extreme brittleness and because it oxidizes when exposed to air at very high temperature. Chromium carbide is sensitive to both thermal and physical shocks.

Ceramic materials are being considered for use in bearings at temperatures to about 3000° F. Among the ceramics being con-

sidered are aluminum oxide compacts, both hot and cold pressed, and zirconium oxide (table 11–V). Some experience has been obtained with ceramic and cermet materials in bearings (ref. 14), but further evaluations of them as bearing materials should be made. The results of reference 14 will be discussed later.

TABLE 11–V.—CERAMIC MATERIALS FOR HIGH-TEMPERATURE BEARINGS

Material	Composition, percent by weight
AD–99 Coors Porcelain	99 percent Al_2O_3
AP–100 Coors Porcelain	100 percent Al_2O_3
Zirconium oxide Zirconia Corporation	Zr_2O_3

Hardnesses at temperatures to 1600° F of the various classes of materials previously discussed are shown in figure 11–5. At tempera-

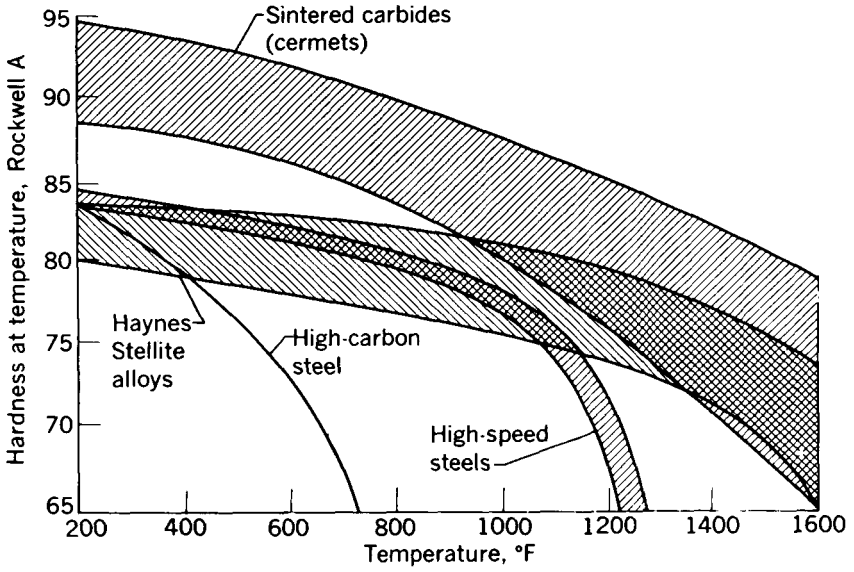

FIGURE 11–5.—Hardness as function of temperature for different classes of bearing materials.

tures above 1000° F, the super alloys have higher hardness than the high-speed tool steels. The cermets and ceramics have higher hot hardnesses than either the super alloys or the tool steels.

Retainer materials.—In addition to the race and the rolling-element-bearing material, careful consideration must be given to the choice of retainer material. In conventional rolling-element bearings, both metallic and nonmetallic retainers have found widespread use. Under normal temperatures, practically all the roller bearings in use and a large percentage of the ball bearings in use have been equipped with stamped retainers of low-carbon steel or with machined retainers of either iron-silicon-bronze or a leaded brass. Nonmetallic retainers have generally been cotton-cloth phenolic laminates, which are suitable for continuous use at temperatures to about 275° F. At higher temperatures, metallic retainers must be used. Precision bearings are usually equipped with machined retainers rather than stamped retainers, and these have been copper alloys of one form or another. In some applications, where marginal lubrication has been encountered during part of the operating cycle, silver plating on bronze has been used. An example of this is many of the rotor bearings used in present-day turbojet engines. Copper-base alloys are suitable up to a maximum of about 600° F. At this point, their strength begins to deteriorate rapidly so that they are unsuitable for use at higher temperatures. At temperatures above 600° F, some success has been obtained with low-carbon-steel or cast-iron retainers, but generally the most successful high-temperature retainers have been nickel-base alloys. Among the nickel-base alloys most widely used is monel. Both H monel and S monel have been used successfully for retainers in bearings operating at temperatures of 1000° F and above. Table 11–VI (ref. 12) illustrates the chemical compositions of the three most widely used retainer materials.

TABLE 11–VI.—COMPOSITIONS OF TYPICAL RETAINER MATERIALS [a]

Material	Alloying element, percent by weight					
	Cu	Ni	Si	Fe	Zn	Mn
Iron-silicon-bronze	90.00 Min.	--	3. 25	1. 50	2. 75	1. 00 Max.
H-monel	31	63	3. 00	2. 00	----	. 75
S-monel	30	63	4. 00	2. 00	----	. 75

[a] From ref. 12.

Liquid Lubricants for High-Speed Bearings

Limitations of liquid lubricants.—The oxidative and thermal stability of liquid lubricants limits the temperature range over which they can be used. Much work is presently being done to extend the temperature limits of liquid lubricants by developing lubricants with

better thermal and oxidative stability. A certain temperature limit exists, however, to which organic fluids can be used. Therefore, many researchers have explored the potentials of solid lubricants, such as graphite, molybdenum disulfide, metal-free phthalocyanine, and others, as lubricants for rolling-element bearings. Research results of the use of solid lubricants applied as powders in a stream of gas and as a solid film coating will be discussed. Much research has been devoted to developing techniques that utilize to the fullest extent the lubricating properties of liquid lubricants.

Most oil-lubricated bearings in high-speed machinery are lubricated by one or more oil nozzles that direct oil at the bearing face. The oil flows through and around the bearing, is scavenged either by gravity or by a scavenge pump, and is returned to a sump. Recirculation to the bearing follows. In such a system that is open to the atmosphere, the oil incurs a maximum exposure to oxidation and, if temperatures exceed the limit of thermal stability of the oil, the system eventually fails because of the accumulation of viscous products of oxidation and thermal degradation. The oil can be changed at intervals, but if system temperatures are high, the interval may be too short to be practical. Alternatives are to employ closed systems, to exclude oxygen from contact with the lubricant, or equivalently to provide a protective atmosphere for nonrecirculating systems in their various forms. These systems include oil-air-mist lubrication, vapor-phase lubrication, and nonrecirculating solid-oil systems.

In reference 15, an investigation of the temperature limitations of various lubricants was undertaken by use of a droplet feed nonrecirculating system. These tests were conducted with 20-millimeter ball bearings at 2500 rpm and 110-pound thrust load. Failure was indicated by excessive torque. Some of the results of reference 15 with liquid lubricants are shown in table 11–VII. For the conditions of these experiments, a bearing could be run successfully at temperatures to 538° F with grade 1010 light petroleum oil, to 697° F with jet-engine fuel grade JP–4, to 710° F with a diester, to 418° F with a phosphonate, to 548° F with a silicate ester, and to 875° F with a blend of silicone and a diester. In general the bearings were clean after test except for the bearing run with the phosphate, which showed heavy carbonaceous deposits. Photographs of all the bearings after test are included in reference 15. These tests were preliminary in nature, but they did indicate that successful bearing operation under nominal loads and speeds could be obtained at fairly high temperatures with synthetic and with petroleum lubricants.

The protective-atmosphere concept.—The use of protective atmospheres as a means for extending the useful temperature range of organic liquid lubricants has been the subject of several research programs.

TABLE 11–VII.—TEMPERATURE LIMITATIONS OF VARIOUS LIQUID LUBRICANTS [a]

[Speed, 2500 rpm; thrust load, 110 lb; bearing size, 204.]

Lubricant	Maximum successful outer-race operating temperature, °F	Remarks
Grade 1010 mineral oil	538	Bearing relatively clean
Grade JP–4 jet-engine fuel	400 and 697	Bearing torque high; bearing clean
Di(2-ethylhexyl)sebacate plus additives	710	Bearing clean but darkened
Dioctyl isooctene phosphonate	418	Heavy carbonaceous deposit on bearing
Tetrakis(2-ethylhexyl)silicate plus oxidation inhibitor	548	Slight deposit on bearing
Silicone-diester blend	875	Heavy salt-like silica deposit on bearing

[a] From ref. 15.

In reference 16 further experiments with 20-millimeter-bore ball bearings were conducted with a nitrogen atmosphere to determine the benefits to be obtained from an inert atmosphere. Some typical results are shown in figure 11–6. For both the grade 1010 mineral oil and the silicone-diester blend, successful lubrication could be obtained at a 150° F higher temperature in nitrogen than in air. Atlhough the silicone-diester blend was effective to 1000° F in nitrogen, heavy carbonaceous deposits were formed on the test bearing that prevented rotation of the bearing after cooling. Although oxidative breakdown of the lubricant was prevented by the inert atmosphere, thermal breakdown could not be prevented.

Further experiments to determine the effect of oxidation on the effectiveness of lubrication with oils were reported in reference 17. Studies were again made with 20-millimeter-bore ball bearings at 2500 rpm and at bearing temperatures to 850° F with grade 1010 mineral-oil lubrication. The ambient atmosphere consisted of air-nitrogen mixtures of various ratios. The results of this investigation are summarized in figure 11–7. Figure 11–7(a) shows the time to failure plotted against oil-oxygen ratio with a constant oil flow of 15 drops per minute and variable air-nitrogen ratio. The bearing temperature was held at 850° F. Increasingly effective lubrication is obtained in terms of longer time to failure, when the oil-oxygen

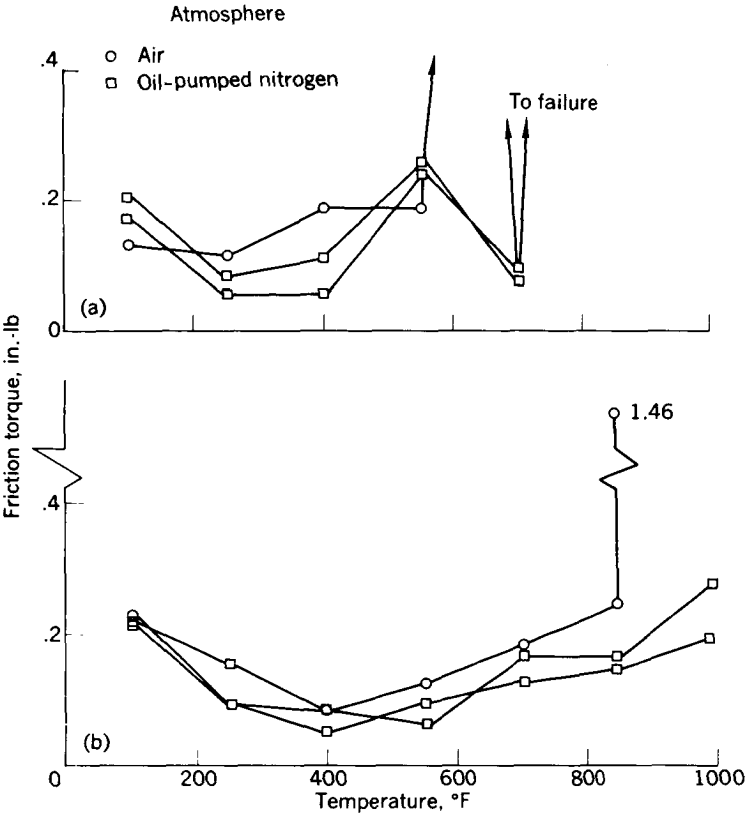

(a) Grade 1010 mineral oil.
(b) Silicone-diester blend.

FIGURE 11-6.—Effect of temperature on friction torque of bearings with liquid lubricants in atmospheres of oil-pumped nitrogen and of air. (From ref. 16.)

ratio reaches about twice the stoichiometric ratio. Figure 11-7(b) shows the time to failure plotted against oil-oxygen ratio with a constant atmosphere of 20 percent air and a variable oil flow from 15 to 52 drops per minute. Effective lubrication is obtained when the oil-oxygen ratio reaches about three times the stoichiometric ratio. These results show that a ball bearing will run at temperatures to 850° F with oil lubrication if the oil flow exceeds a critical amount, believed to be equal to that which is removed by evaporation, thermal decomposition, and oxidation. Oxidation of the oil was controlled by regulating the amounts of oxygen and nitrogen in the atmosphere that surrounds the test bearing.

In references 18 to 20, the concept of protective-atmosphere lubrication was thoroughly investigated, and the first results are reported in reference 18. Attempts were made to operate a deep-groove 206-size ball bearing with a steel cage at 10,000 rpm, at a radial load

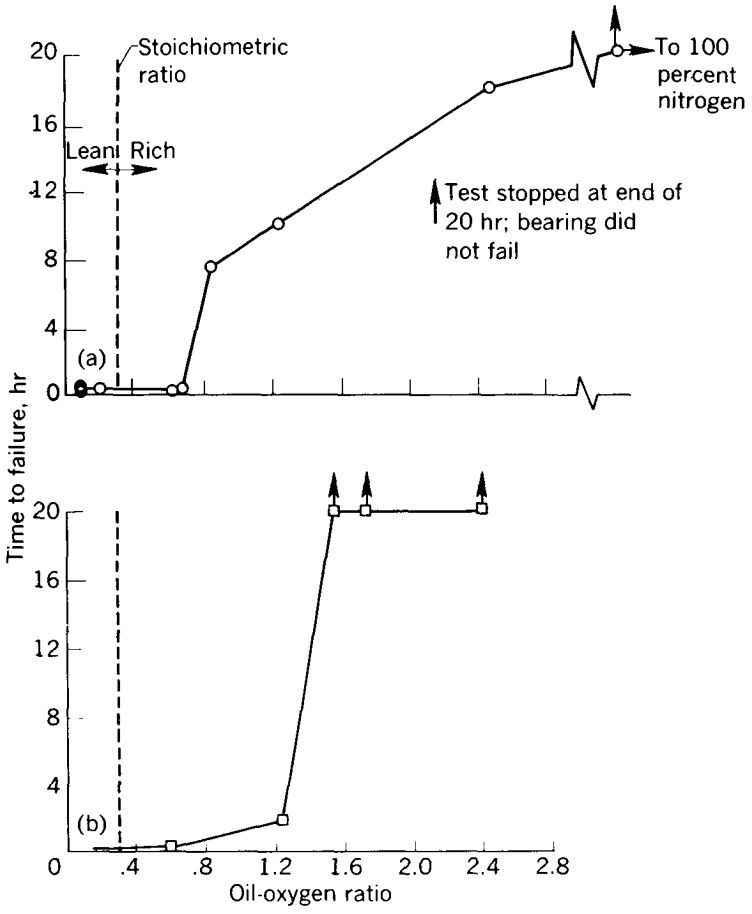

(a) Variable air-nitrogen ratio; constant oil flow, 15 drops per minute (0.0002 lb/min).

(b) Constant atmosphere, 20 percent air; variable oil flow, 15 to 52 drops per minute (0.0002 to 0.001 lb/min).

FIGURE 11-7.—Effect of oil-oxygen ratio on time to failure for 20-millimeter-bore ball bearings with grade 1010 mineral oil lubrication. Speed, 200 rpm; load, 110 pound thrust; bearing temperature, 850° F. (From ref. 17.)

of about 30 pounds, and at 600° F in the absence of any liquid lubricant. A 10-hour run was the goal in these initial experiments. First tests were run with a clean bearing, prelubricated with six drops of polyisobutylene. Operation in an atmosphere of air or commercial dry nitrogen resulted in bearing failures in 2 or 3 hours. Extreme abrasive wear was evident. The wear products contained oxides and finely divided metal. Substitution of carbon dioxide as a blanketing gas extended the operation to the full 10-hour cycle. Some oxidation of the bearing components, however, was still evident at a 600° F test temperature. A mixture of carbon dioxide and

hydrocarbon vapor consisting of JP–4 jet-engine fuel vaporized in the carbon dioxide line was used to blanket the bearing to provide a reducing atmosphere. Oxidation disappeared, but a considerable accumulation of soot was noted. This soot was believed to have been a cause of wear. Blanketing the bearing with an air-hydrocarbon mixture with sufficient oxygen to oxidize most of the carbon to carbon monoxide virtually eliminated the soot, and several 10-hour runs were completed with a blanketing gas that had an air-fuel ratio between 7 and 10. The conclusions reached from these experiments are as follows:

(1) When ball bearings are operated dry at high temperatures, metal oxidation and oxide-induced abrasion are the major causes of bearing wear.

(2) A blanket of reducing atmosphere will eliminate bearing oxidation and minimize abrasion. A mixture of air and hydrocarbon vapor provides a suitable reducing atmosphere.

(3) In the absence of bearing oxidation and oxide-induced abrasion, retainer scuffing becomes the limiting factor in the life of dry running bearings.

(4) Conventional extreme-pressure elements, such as sulfur, can increase the scuffing resistance of dry running bearings. These elements may be applied by bearing pretreatment or as a volatile compound in the reducing atmosphere blanket that surrounds the operating bearing. Use of a combination of pretreatment and operation with a small concentration of the extreme-pressure element in the reducing atmosphere is preferable.

Limitations of protective-atmosphere lubrication were studied in reference 19. Premixing the JP–4 and the air before they entered the bearing cavity was important in order to obtain good protective-atmosphere lubrication. Introduction of the JP–4 fuel and air into the bearing housing without prior mixing gave poor results. For further study of this phenomenon, experiments were conducted to mix the air and the JP–4 fuel at various preheat temperatures before they entered the bearing housing. When the preheat temperature was below the dewpoint temperature of the air—JP–4 mixture of about 450° F, protective-atmosphere operation was good. When the preheat temperature was above the dewpoint temperature, protective-atmosphere operation was not effective. In addition, the resin fraction of JP–4 fuel was found to be an important constituent of the protective-atmosphere mixture, which suggests that polymerization of these resins occurs to form at least a portion of the beneficial protective films. When the entrance line is too hot, the polymers formed may be deposited in the line rather than in the test bearing where they are needed. Further studies were made to define the upper temperature limit of successful protective-atmosphere lubrica-

tion. Good results could be obtained at temperatures up to about 800° F under the conditions of these tests. A 30-millimeter-bore bearing was run at 10,000 rpm under a light radial load.

Because of the importance of the resin component of JP–4 fuel to the success of this lubrication scheme, the resin in JP–4 fuel was studied further. The organic compounds, which make up these resins, can be classified into three general groups. The first group are nitrogen base compounds, such as *m*-toluidine, quinoline, and 2-, 4-, 6-collidine. The second group are oxygen compounds, mostly phenols, such as carboxylic acids and naphthenic acids. Adipic acid and paratertbutyl phenol were selected as typical compounds in the second group. The third general class of resins consists of neutral fractions, similar to the main hydrocarbon portion of the JP–4 fuel, except that it is rich in aromatic olefins. Indene and styrene were selected as typical aromatic olefins. These organic additives were compounded to the extent of 1 percent by weight with benzene to determine their effectiveness in producing protective films. All the organic compounds tested seemed to offer some benefit, and *m*-toluidine was outstanding. The effectiveness of these organic compounds suggests that surface films formed may be at least partly organic. An analysis of the films deposited on the test bearings with electron and X-ray diffraction and a spectrograph proved only that the films are partly organic and partly inorganic. The strongest band in the spectrum indicated the presence of a carbonyl.

Phase 2 of the work reported in reference 19 was to establish limiting loads and speeds for protective-atmosphere operation at high temperatures. Iron-silicon-bronze retainers were generally unsatisfactory for the establishment of protective films because of the low oxidation potential of the bronze. Much better performance could be obtained with a bearing of all ferrous metal construction. Tests carried on with 209-size, 45-millimeter-bore ball bearings indicated that considerable loads could be carried with protective-atmosphere lubrication at a speed of 7200 rpm and at a temperature of 700° F. Successful tests were obtained at radial loads up to 600 pounds. Operating times of these experiments varied up to 33 hours. In these experiments, the protective atmosphere consisted of air and JP–4 fuel plus 0.66 percent by weight of tri-isopropyl phosphite in a weight ratio of 8. The radial load of 600 pounds on the 209-size bearing is two-thirds of the catalog-rated load for this bearing. The bearing was in excellent condition at the end of the 33-hour test at 700° F.

The research of reference 20 was conducted to explore further the limitations of protective-atmosphere lubrication. No specific protective-atmosphere composition or bearing combination was exten-

sively explored. Rather, as limitations were encountered, the reasons for these limitations were examined and efforts made to remove them and permit operation under more severe conditions. Certain limitations were imposed by the bearing and others were due to limitations in performance of the protective atmosphere formulations. The first of these bearing limitations encountered was that of bearing materials. As previously discussed, SAE 52100 steel became dimensionally unstable at elevated temperatures. Bearings fabricated of the tool steels M–2, M–10, Halmo, and M–50 appeared to be satisfactory up to temperatures of about 800° F. Tool steel M–10 was used at temperatures up to 1000° F, but it began to show deformation under load at about 900° F.

Bearing retainers of iron-silicon-bronze became too weak for use at even moderate speeds above 800° F. Since the protective-atmosphere concept depends on a reaction between the lubricating component and the bearing metals, another limitation was imposed on this type of operation. Specifically, the reducing environment, which prevents the formation of destructive iron oxides, will also reduce lubricating films that are formed on metals of low oxidation potential. For example, a copper sulfide film on brass or bronze will be quickly reduced to leave only bare metal when it is exposed to a reducing atmosphere at high temperature. Thus, the use of copper alloys and silver plating will not work well with the protective-atmosphere system because the lubricating films that are formed on them are easily reduced. At the other extreme, as regards retainer materials, are those that are corrosion resistant by virtue of impervious and inert surface oxide films. Among those in this category are the stainless steels, monel, and Inconel. These materials will not work with a protective-atmosphere system of lubrication, because lubricating films are not formed. The previous two considerations show that a bearing of all-ferrous alloy construction will work best and that the race and the ball material must be a tool steel with adequate hot hardness and dimensional stability.

Two series of tests were run in reference 20. One utilized a 206-size ball bearing that ran under a radial load of 80 pounds and an axial load of 20 pounds at a normal test speed of 10,000 rpm or, in a few cases, a speed of 20,000 rpm. The second type of test used a 209-size bearing that operated at 7000 rpm and 600-pound radial load. In both types of tests, the results were evaluated after a 22-hour run. Lubrication was judged to be successful if the bearing still ran quitely, had no detectable roughness, was not excessively worn as indicated by radial-clearance measurements and visual inspection of parts, and displayed no other evidence of impending failure. A summary of the test results from reference 20 in table

11–VIII shows that successful performance was obtained at 20,000 rpm and 900° F under the light radial-load tests and at temperatures from 900° to 1000° F at the 7000-rpm test condition under a high radial load.

The authors of reference 20 point out that they did not investigate the ultimate bearing life with this type of lubrication under these test conditions. The data obtained, however, and the type of lubrication system employed would seem to indicate that bearing life would depend ultimately on wear. The types of films formed on which successful lubrication depends are all lost by attrition, which results in wear of the bearing surfaces. Some measurements of the buildup of lubricating films were made in the high radial-load tests. These measurements indicated that the film buildup was on the order of 0.0001 inch on ball and race surfaces and that this buildup took about 6 hours. Bearing clearances increased at a steady rate, which indicated an average chemical-wear rate of about 0.000025 inch per hour on all surfaces.

A summary of the results of the research reported in references 18 to 20 indicates that two principal mechanisms of failure were found to occur in bearings that operate under high-temperature, high-speed conditions:

(1) A rapid wear was caused by the formation of abrasive iron oxides; this wear occurred on the rubbing areas in the bearing and also in the areas of rolling contact.

(2) Scuffing wear resulted from contact welding of small areas of the contacting surfaces in the bearing. This type of failure normally occurred only between sliding surfaces, such as the rolling element and the retainer, and the retainer and its locating surface. This failure sometimes occurred between the rolling element and the races in bearings operating at high speeds, but this could be avoided by a break in run with oil lubrication. Methods of preventing the above failure mechanisms were sought without the use of oil lubrication. First, the abrasive oxide-induced wear was minimized with a reducing atmosphere around the bearing. Vapors of hydrocarbons and other organic compounds were satisfactory reducing agents if they were present in excess of the stoichiometric ratio with oxygen in the vicinity of the bearing. Scuffing wear was reduced by means of volatile film-forming agents, commonly known as extreme-pressure additives that contained active phosphorous, sulfur, or a halogen, which were added to the reducing atmosphere. Another type of lubricating film, which can serve the function of the extreme-pressure film or supplement it, was found to be a highly condensed organic film, such as that deposited at 600° to 800° F from gum in gasoline. These films result from vapors that contain traces of oxidized unstable

TABLE 11-VIII.—DEMONSTRATED PERFORMANCE OF BEARING COMBINATIONS IN SELECTED PROTECTIVE ATMOSPHERE [a]

Organic atmosphere component, air-fuel weight ratio = 8	Bearing			Maximum useful temperature, °F	Limiting criteria above maximum useful temperature
	Size	Speed, rpm	Metallurgy		
Light radial load tests [b]					
JP-4 fuel	206	10, 500	SAE 52100 steel	400–500	Dimensional instability of SAE 52100
JP-4 fuel	206	10, 500	M-2–M-10 steels	750	Objectionable deposits from JP-4 fuel heavy ends
n-Heptane plus 0.1 percent by weight P as tri-isopropyl phosphite	206	10, 500	M-2–M-10 steels	900	Strength of cage not sufficient [c]
JP-4 plus 0.1 percent by weight P as tri-isopropyl phosphite	206	20, 750	M-2–M-10 steels	750	Objectionable deposits from JP-4 fuel heavy ends
n-Heptane plus 0.1 percent by weight P as tri-isopropyl phosphite, 0.1 percent by weight S as dibenzyl disulfide	206	20, 750	M-2–M-10 steels	900	Strength of cage not sufficient [c]
High radial load tests [d]					
JP-4 fuel	209	7, 000	M-2 steel, 1010 cage	700	High cage wear, [e] tool-steel cage would be better
JP-4 plus 0.1 percent by weight P as tri-isopropyl phosphite	209	7, 000	M-2 steel, 1010 cage	750	Objectionable deposits from JP-4 fuel heavy ends
Ethylene-propylene oxide polymer	209	7, 000	M-2 steel, 1010 cage	700	High cage wear
Ethylene-propylene oxide polymer plus 0.1 percent by weight P as tri-isopropyl phosphite	209	7, 000	M-2 steel, 1010 cage	900–1000	Inner race shows signs of fatigue

[a] From ref. 20.

[b] All combinations have completed standard 22-hr test with no indication of impending bearing failure.

[c] Mechanical design of cage appeared to be contributing factor to limiting conditions.

[d] All combinations have completed standard 33-hr test with 600-lb radial load. No indications of pending failure were evident at end of test except as noted for temperatures of 900° to 1000° F.

[e] Softness of steel cage used in all size-209 bearing tests appeared to be limiting factor.

organic compounds. At higher temperatures similar organic films will be deposited from many organic compounds.

Minimum oil-flow systems.—There are bearing applications, such as in missiles and space vehicles, in which a nonrecirculating lubrication system, which operates with minimum possible oil flow, could be employed advantageously. Weight reduction of the system might be realized, especially if a pressurized-gas supply is available in the vehicle. To intelligently design a nonrecirculating lubrication system, however, the oil-flow requirements of the bearings must be known. In addition, this information is necessary to determine whether a nonrecirculating system has any advantage over a recirculating system. Some quantitative data on the actual oil-flow requirements of 75-millimeter-bore ball bearings at various speeds, loads, and temperatures are reported in reference 21. Tests were conducted at DN values of 0.6 to 1.2×10^6, thrust loads of 1000 and 3000 pounds, and temperatures to 500° F. A synthetic diester lubricant was supplied to the test bearings in the form of an air-oil mist. The authors of reference 21 found that the minimum oil-flow requirements for continuous bearing operation increased markedly with increasing DN and also with increasing bearing load. They found that bearings will operate satisfactorily at very low oil flows with an air-oil mist nonrecirculating system of lubrication. As an example, it was possible to run a 75-millimeter-bore ball bearing satisfactorily at 12,000 rpm (0.9×10^6 DN), 400° F, and a 1000-pound thrust load with oil flows as low as 0.003 pound per minute. An empirical relation between the oil flow Q, the thrust load W, and the DN value was developed and is given by the following equation:

$$Q=(1.51\times10^{-18})[W^{4.22}\times10^{1.18(S-8)}] \qquad (11\text{–}21)$$

In this equation, Q is in pounds per minute, W in pounds, and S is DN value$\times10^{-5}$. Oil flow Q is indeed a strong function of load and DN value. Further work is needed to define the exact oil-flow requirement of various size bearings that operate over wide ranges of speed, load, and temperature. The procurement of such data would make it possible to correlate these data into a generalized expression that involves load, speed, temperature, and bearing size.

High oil-flow systems.—In contrast to the work in references 16 to 21, the research reported in references 22 and 23 deals with the lubrication of ball bearings at high temperature with relatively high flow rates of liquid lubricant. These studies were conducted with bearings that were run at high speeds under an axial load to produce the most severe conditions of sliding between the balls and the races. Because of this sliding, or ball spin, appreciable energy may be released

at the ball-raceway contact, which causes contact temperatures to rise to damaging values unless the coefficient of friction is kept low by a lubricant that is performing adequately. Test bearings used in references 22 and 23 were 20- and 25-millimeter-bore deep-groove and angular-contact ball bearings. The various race and retainer material combinations and other characteristics of these bearings are shown in table 11–IX.

Two conditions of operation were chosen. The first was 40,000 rpm, 200-pound thrust load, and lubricant flow of 15 grams per minute. The second was 60,000 rpm, 300-pound thrust load, and lubricant flow of 70 grams per minute. The starting ambient temperature was 400° F, and temperature was increased in 100° F steps after temperature equilibrium had been reached. Since the test shaft was turbine driven, a large increase in bearing torque resulted in a drop in speed, and this was used as the criterion of failure. The inlet temperature of the oil was maintained equal to the temperature of the bearing outer race. The oil was discarded after one pass through the bearing. Various lubricants used in these experiments, together with some of their properties, are shown in table 11–X.

The test results at 40,000 rpm with various bearings lubricated with a mineral oil are shown in table 11–XI. The M–10 bearing with the S-monel retainer showed the highest friction-limited temperature, approximately 938° F. Although the 440C with the S-monel retainer showed a temperature limit about the same as that for the M–10 bearing, its friction was considerably higher and ball-retainer wear was also considerably higher than that for the M–10 bearing. Several bearing configurations were operated at 60,000 rpm with flow rates at 15 grams per minute and 70 grams per minute to investigate the effect of lubricant flow rate on the friction-limited temperature. These results are shown in table 11–XII. At the 15-gram per minute flow rate, the stainless-steel bearing failed at 500° F, and the very heavy retainer wear indicated inadequate retainer lubrication at this lubricant flow rate. At the flow rate of 70 grams per minute, the stainless-steel bearing ran to a friction-limited temperature of 720° F and the retainer wear was light. The superior strength properties of the S-monel as compared with the iron-silicon-bronze alloy allowed both the stainless-steel and the M–10 bearings to operate satisfactorily at considerably higher temperatures.

The effect of thrust load on bearing operation at two flow rates was investigated by use of stainless-steel bearings with bronze retainers and mineral-oil lubrication. These results are shown in table 11–XIII. At the low flow rate, increasing the bearing load from 200 to 300 pounds results in a considerable drop in the friction-limited temperature. At the high flow rate, however, increasing the bearing load

TABLE 11–IX.—GENERAL CHARACTERISTICS OF TEST BEARINGS [a]

Type	Bore size, mm	Ball and race material	Ball separator			Number of balls	Radial play, in.	Approximate maximum temperature limit, ° F
			Material	Construction	Control			
Angular contact	20 and 25	440C stainless steel	Bronze	One-piece machine	One-land outer race	11 13	0. 0009–0. 0014	600–800
Angular contact	25	440C stainless steel	S-monel	One-piece machine	One-land outer race	13	. 0009– . 0014	800
Deep groove	20	M–2 high-speed tool steel	Unhardened M–2 tool steel	One-piece machine	Two-land outer race	8	. 0008– . 0011	800–1000
Deep groove	20	M–10 high-speed tool steel	S-monel	Two-piece cast	Two-land outer race	8	. 0008– . 0012	800–1000

[a] From ref. 22.

TABLE 11-X.—CHARACTERISTICS OF VARIOUS LUBRICANTS [a]

Lubricant	Type	Viscosity, cs, at—						Flash point, °F
		100° F	210° F	300° F	400° F	500° F	600° F	
Mineral oil	Highly refined white oil	74. 8	8. 7	3. 48	1. 76	1. 09	0. 78	430
Mineral oil plus extreme pressure agent	Highly refined white oil plus phosphorus extreme pressure agent (5.9 percent by weight)	~74. 8	~8. 7	~3. 48	~1. 76	~1. 09	~. 78	430
MIL-L-7808C	Di-2-ethylhexyl sebacate ester	13. 9	3. 5	1. 86	1. 14	. 77	~. 56[b]	460
Experimental high-temperature lubricant	Pentaerythritol ester	29. 3	5. 3	2. 39	1. 29	. 83	~. 58	445
Meets British military specification	Polyester, similar to MIL-L-7808C but higher viscosity	37. 9	7. 8	3. 11	1. 79	1. 18	~. 85	490
Silicone DC 550	Methylphenyl silicone	80. 3	20. 0					575

[a] From ref. 22.
[b] Excessive loss of lubricant, result not positive.

TABLE 11–XI.—FRICTION-LIMITED TEMPERATURE OF VARIOUS BEARING MINERAL-OIL COMBINATIONS [a]

[Speed, 40,000 rpm; axial load, 200 lb; lubricant system, nonrecirculating continuous jet; lubricant quantity, 15 g/min; temperature, increased in 100° F increments starting at 400° F.]

Bearing material	Retainer material	Friction-limited temperature, ° F	Temperature at first friction rise, ° F	Ball-separator wear	Balls and raceways
440C	Bronze	760	675	Light to medium	Good
440C	S-monel	900 [b]	650	Heavy	Good
		935 [b] Operation marginal, failure not clear cut			
M–2	M–2	620 [b]	625	Very heavy	Outer race pitted
		868 [b]			
M–10	S-monel	938 No failure	640	Light to medium	Good

[a] From ref. 22.
[b] Duplicate tests.

TABLE 11-XII.—EFFECT OF LUBRICANT FLOW RATE ON HIGH-SPEED BEARING OPERATION [a]

[Speed, 60,000 rpm; lubricant, nonrecirculated mineral oil; axial load, 200 lb.]

Flow rate, g/min	Bearing	Retainer	Bearing temperature at first friction increase, ° F	Friction-limited temperature, ° F	Bearing damage
15	440C	Bronze	500	500	Very heavy separator wear, fractured
70	440C	Bronze	635	720	Separator fractured, light pocket wear
70	440C	S-monel	750	872 [b]	Heavy separator wear, no fracture
70	M-10	S-monel	850	905 [c]	Light to medium separator wear, minute pitting of inner raceway track

[a] From ref. 22.
[b] Incipient failure.
[c] No failure.

TABLE 11-XIII.—EFFECT OF LUBRICANT FLOW RATE ON HIGH LOAD OPERATION OF BEARINGS [a]

[Speed, 40,000 rpm; lubricant, nonrecirculating mineral oil; bearing, stainless steel with bronze retainer.]

Flow rate, g/min	Load, lb	Temperature at first friction increase, ° F	Temperature at failure, ° F	Damage
15	200	675	760	Light to medium separator wear
15	300	536	536	Very heavy separator wear
70	200	825	834	Light to medium separator wear
70	300	820	850	Medium to heavy separator wear

[a] From ref. 22.

does not seem to produce any appreciable effect in the friction-limited temperature. At the high flow rate, the retainer wear was considerably less than that at the low flow rate. It is apparent from the results shown in tables 11-XII and 11-XIII that, at the high speeds and high loads, the high flow rate is necessary to provide satisfactory lubrication. This is evidenced by the fact that high friction-limited temperatures are obtained and also by the fact that bearing wear is reduced considerably at the high flow rates.

Some preliminary experiments to determine the friction characteristics of various lubricants were conducted with 25-millimeter-bore angular-contact bearings at 40,000 rpm and 200 pounds thrust load. The silicone gave poor performance and was not satisfactory at even 360° F. The mineral oil gave low friction to about 650° F and the MIL–L–7808 oil, a synthetic diester, gave low friction at temperatures up to about 800° F. Preliminary experiments were also conducted with a recirculating system that used the mineral oil. The first results of these tests indicated that very heavy deposits formed on the bearing in a relatively short time and that the oil soon became extremely viscous.

An interesting side result of these experiments was the fact that fatigue failures were obtained in several of the M–10 bearings that were run at both 40,000 and 60,000 rpm over a wide range of varying temperature. These results are summarized in table 11–XIV. The extremely short running time of these bearings, together with the prevalence of fatigue failures, indicates that fatigue may be a critical problem and a life-limiting factor in the operation of ball bearings at high speeds and at high temperatures.

TABLE 11–XIV.—FATIGUE FAILURES OF THE M–10 BEARINGS WITH S-MONEL RETAINERS [a]

[Lubricant, mineral oil applied in nonrecirculating system at 70 g/min; axial load 200 lb; speed, as indicated.]

Test	Operation, hr	Speed, rpm	Bearing temperature, °F	Bearing component failed
1----	3 2. 5	40, 000 60, 000	400–600 500–905	Minute pitting of inner raceway track
2----	4. 5	60, 000	460–968	Minute pitting of inner raceway track
3----	1 1. 5 2	40, 000 60, 000 60, 000	426 570–960 994–1036	Severe spalling of one ball
4----	8 7	40, 000 60, 000	427–695 460–830	Outer raceway track pitted
5----	9. 8 5. 7	40, 000 60, 000	402–802 426–820	Good condition No failure

[a] From ref. 22.

The results of reference 22 showed that satisfactory operation with an M–10 tool-steel bearing equipped with an S-monel retainer and lubricated with a mineral oil in a nonrecirculating high-flow lubrication system can be obtained at 60,000 rpm, 200-pound axial load,

and at bearing temperatures approaching 1000° F. The limiting factor may be metal fatigue. The M–10 bearing equipped with an S-monel separator was superior in high-temperature performance to both M–2 bearings with annealed M–2 retainers and stainless-steel bearings with both iron-silicon-bronze and S-monel retainers. Critical flow rate depends on the operating conditions as shown by the fact that better performance, with regard to both temperature and wear, was obtained at high speeds and high loads by increasing the lubricant flow rate.

The work reported in reference 23 extends the work of reference 22 with similar test bearings and test conditions, except that recirculating rather than nonrecirculating systems were generally employed. Two types of tests were conducted in reference 23. The first was called a friction-limited temperature test, and was conducted with a nonrecirculating system at lubricant flow through the test bearing of 70 grams per minute. The lubricants evaluated in the friction-limited tests included the following: (1) a chlorophenyl silicone, (2) a highly refined mineral oil, (3) a MIL–L–7808C lubricant, (4) a MIL–L–9236A lubricant, and (5) a polyphenyl ether. The friction-limited temperatures of all these lubricants, with the exception of the MIL–L–9236A lubricant, were between 775° and 850° F. The MIL–L–9236A failed at 675° F.

The second type of test conducted was the lubricant-decomposition test, in which the lubricant was recirculated through the test bearing. The results of these tests are summarized in table 11–XV. The polyphenyl ether lubricant exhibited the best performance relative to high-temperature decomposition at a bearing temperature of 700° F and at 60,000 rpm. This lubricant operated satisfactorily for 110 passes through the hot zone. Bearing failure was due to excess deposit formation within the bearing, but lubricant deterioration as determined by increases in viscosity at 100° F and by acid number was slight. This life compares to 57 passes for the MIL–L–7808C, 19 passes for the mineral oil, 9 passes for the chlorophenyl silicone, and 11 passes for the MIL–L–9236A lubricant. Again, bearing fatigue appears to be a limiting factor at high temperatures. A summary of fatigue results with M–10 bearings is given in table 11–XVI. Fatigue becomes more critical at high temperatures, and the results indicate a dependence on the condition of the lubricants.

Oscillating and Accessory Bearings

As previously mentioned, in addition to the high-temperature, high-speed bearing problem, a very real need exists for bearings for high-temperature, low-speed or oscillating, and high-load applications. Airframe bearings for supersonic aircraft and spacecraft

TABLE 11–XV.—LUBRICANT DECOMPOSITION TESTS [a]

[Bearing speed, 60,000 rpm; bearing type, M–10 with monel retainer; axial load, 200 lb; recirculating lubricant flow rate, 70 g/min.]

Lubricant	Bearing ambient temperature, ° F	Bearing outside-diameter temperature, ° F	Oil in temperature, ° F	Number of passes to failure	Increase in viscosity at 100° F, percent	Increase in acidity, mg KOH/kg	Iron content of lubricant at end, ppm	Bearing deposits	Bearing condition	Bearing operation, hr
Mineral oil	400	450	450	[b] 71	200	4. 5	3. 6	Light	Good	[c] 130
MIL–L–7808	400	449	448	[d] 300	6. 3	1. 7	. 9	Light	Good, incipient pitting	102. 7
Mineral oil	700	677	677	19	50	. 56	1. 9	Medium to heavy	Good	10
MIL–L–7808C	700	667	660	57	290	1. 1	38. 2	Medium carbonaceous	Pitted	18. 6
MIL–L–9236A	700	705	704	11	15	3. 9	133. 0	Very heavy carbonaceous	Fair, medium to high wear	1. 5
Chlorinated silicone	700	760	790	9	1600	1. 7	6. 1	Heavy ceramic	Pitted	6
Mix–5P4E (polyphenylether)	700	755	746	110	10	nil	1. 1	Medium to heavy carbonaceous	Good	22

[a] From ref. 23.
[b] Continuous recirculation of given large batch of lubricant with no failure.
[c] Total accumulated bearing time to this point. Bearing was operated also with two previous batches of mineral oil for 67 hr.
[d] No failure, test terminated.

TABLE 11–XVI.—FATIGUE OF THE M–10 BEARING WITH S-MONEL RETAINER AS RELATED TO TEMPERATURE LEVEL AND DEGREE OF LUBRICANT DETERIORATION [a]

[Speed, 60,000 rpm; axial load, 200 lb; lubricant, highly refined mineral oil, 74.9 cs at 100° F, flow rate, 70 g/min.]

Ambient temperature, °F	Bearing outer-race temperature, °F	Method of lubrication	Test duration, hr	Lubricant passes through hot zone	Acidity, mg KOH/kg	Oxygen content, percent by weight	Iron content, ppm	Condition of bearing
400	450	Recirculating	165	35 41 71 40	4. 6	2. 51	3. 6	Good, no pitting
700	675	Recirculating	56	12, [b] 34 12, 6	1. 3 . 73	1. 38	4. 4	Pitted, ball and inner race
700	630	Nonrecirculating	165	1	. 17	. 16	. 2	Good, no ball pitting, slight race pitting
1000	1030	Nonrecirculating	2	1	. 28	. 19	1. 6	Spalled ball

[a] From ref. 23.
[b] Some fresh lubricant added because of evaporation.

must operate under extreme conditions of temperature and load during reentry conditions. Several research programs have been undertaken to study bearing designs and lubrication techniques for such applications.

Reference 24 describes the results of work done to develop ⅜-inch-bore roller bearings for use at 300° to 600° F under ±10° and ±35° oscillation amplitudes to carry up to a 10,000-pound load. Bearings were operated at oscillation frequencies of 250 cycles per minute and could be relubricated every 18 hours. Life results for bearings tested at 450° and 600° F are shown in figure 11–8. Modified 440C and

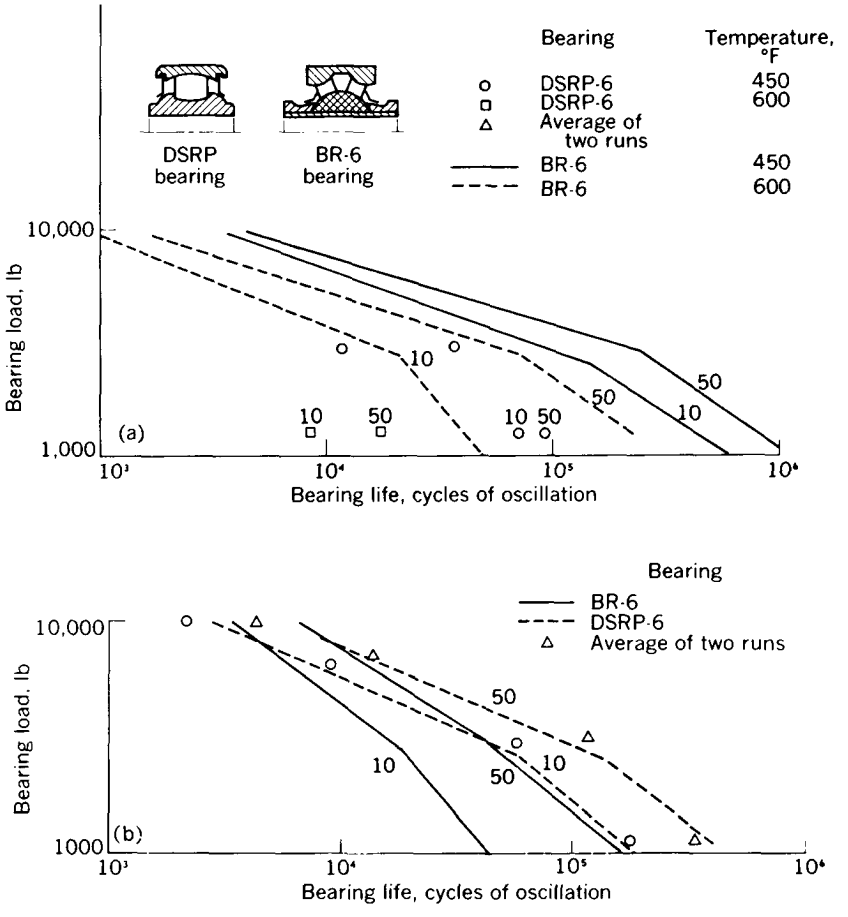

(a) With ±35° oscillation; operated at 450° and 600° F.
(b) With ±10° oscillations; operated at 600° F.

FIGURE 11–8.—Comparison of load-life characteristics of DSRP–6 and BR–6 bearings. Numbers beside curves and data points indicate percent life. (From ref. 24.)

M–2 materials were used. Bearings were equipped with Teflon-coated fiberglass shields and lubricated with several greases. Bearings failed by spalling and by plastic deformation.

At 600° F a silicone-base grease and a silicone-base grease modified by milling-in 50-percent metal-free phthalocyanine were evaluated. These results are shown in figure 11–9. Metal-free phthalocyanine

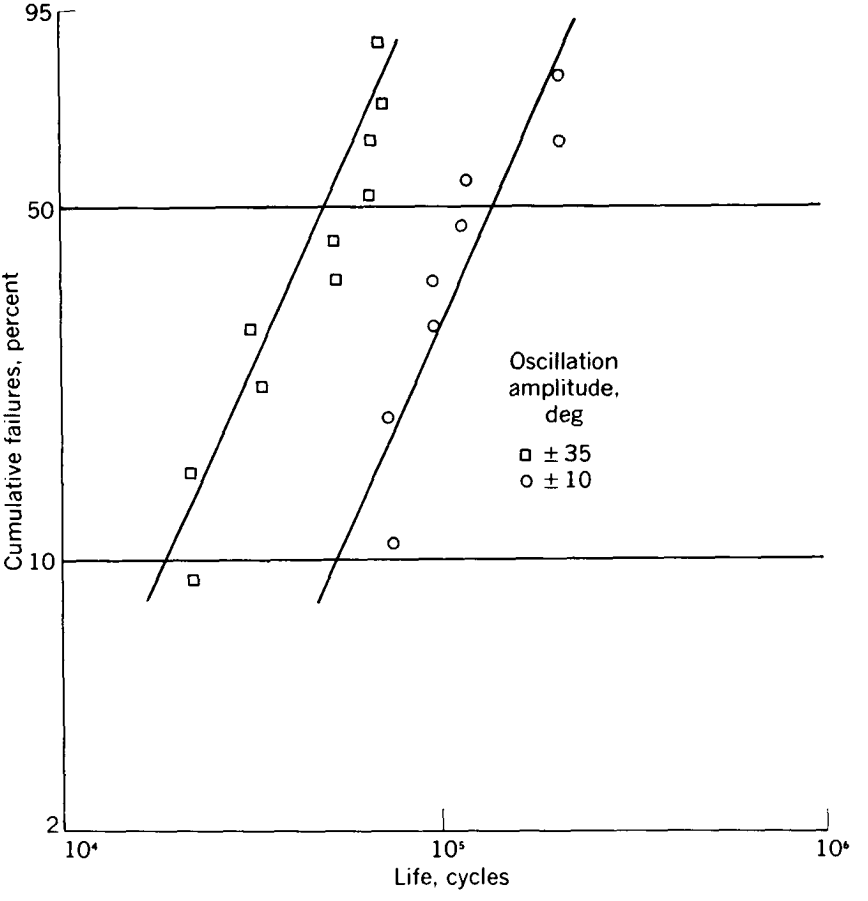

FIGURE 11–9.—Weibull plot of bearing-failure frequency for phthalocyanine-modified silicone-base grease. BR–6 bearings; material, 440C; temperature, 600° F; load, 3000 pounds. (From ref. 13.)

is an organic solid with a planar structure that reacts with heated metals to form metallated phthalocyanines. A brief description of the results of reference 24 is given in reference 13.

An extensive program to develop an airframe ball bearing for service from −65° to 1200° F is described in reference 25. The initial

phase of the experimental work involved evaluation of 54 different material combinations in a ball rolling between oscillating plates. Best results of the dry tests were modified 440C plates and K 161B balls at 600° F, M–2 plates and K 161B balls at 900° F, and CR–2 chromium carbide plates and Stellite Star J balls at 1200° F. These material combinations were used to evaluate 24 potential high-temperature lubricating aids. These aids included coatings, films, thickeners, and powders, but none of them produced any significant improvement in life at the loads of these experiments ($3300nd^2$, where n is the number of rollers and d the roller diam.). One-inch bore, full-complement deep-groove ball bearings with a loading groove were fabricated from the three most promising material combinations for testing at 600°, 900°, and 1200° F, radial loads of 1200 to 3500 pounds, oscillation frequencies of 106 cycles per minute, and an oscillation amplitude of $\pm 30°$. Change in radial play (wear) and torque increase were used as criteria of failure to obtain bearing-life data, as shown in figure 11–10. Although life was below the desired 40,000 cycles except at the lightest load at 900° F, the results justify further work on lubrication techniques and material evaluation for high-temperature airframe bearings.

In addition to airframe applications, bearings are required to operate at high temperatures in electrical accessories. It is estimated that bearings will operate at temperatures of 500° to 700° F in such devices. Reference 26 reports work done to develop a ball-bearing design, a suitable lubricant, and a self-contained lubrication system for use in aircraft electrical accessories that operate at this temperature range. General bearing design features thought to be desirable were loose clearances, open-race curvatures, and land-riding retainers. Grease packing and a modified nonrecirculating lubrication system showed the most promise. Fluids considered were silicones, silicate esters, silanes, mineral oils, polyphenyl ethers, flourinated organic compounds, esters, and polyolefins. Tests with grease fills (percentage of the total available volume that is filled with grease) of 30 to 90 percent revealed that life increased markedly with increased fill. A 90-percent fill showed the best life. Life was found to be an inverse logarithmic function of temperature over the range from 500° to 700° F. Four techniques for improving grease-lubricated life were evaluated. These included running-in at moderate temperature, blanketing with nitrogen, injecting grease periodically, and supplying auxiliary fluid through a porous medium adjacent to the bearing. Periodic addition of the fluid component of the grease to the system provided the longest extension of bearing life. Failure was found to occur primarily because of loss of fluid from the grease. Successful operation over the desired cycle was achieved by repacking with new

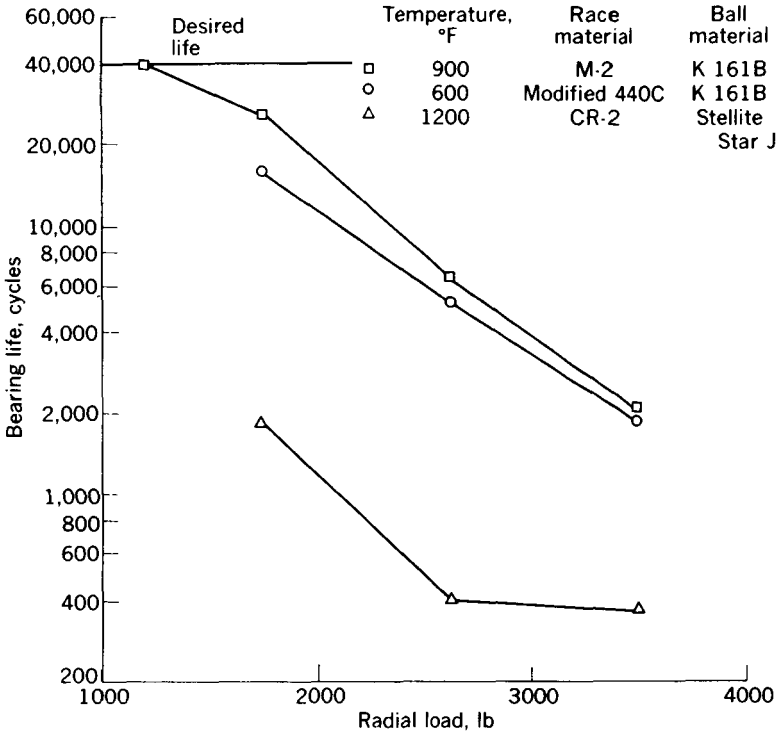

FIGURE 11-10.—Effect of load on bearing life at 600°, 900°, and 1200° F. Basic New Departure F-16 bearing used throughout; all operating conditions include ±30° oscillation frequency at 106 cycles per minute. (From ref. 25.)

grease and adding additional fluid periodically. Greases for use at 700° F are currently under development (ref. 27). Four classes of fluids are being considered: phenoxyphenyl ethers, chain-type polyphenyls, silphenylenes, and ferrocenes.

Solid Lubricants

Early experiments.—The feasibility of lubricating rolling-contact bearings with solid lubricants was established in references 28 and 29. Two types of experiments were conducted. In the first, 20-millimeter-bore ball bearings were operated at temperatures to 1000° F, and in the second, 75-millimeter-bore ball bearings were run with no heat addition to the bearings. The 20-millimeter-bore ball bearings were run at a constant speed of 2500 rpm, while the 75-millimeter-bore roller bearings were run at speeds up to 13,000 rpm (0.975×10^6 DN). In the high-speed tests, the effect of various lubricants and lubrication methods on the operating temperatures of these bearings and on the limiting DN values were investigated. Roller bearings with standard retainers and also cageless full-complement roller bearings were used

in these high-speed experiments. The molybdenum disulfide (MoS_2) lubricant was applied to the test bearing in the form of a coating on the retainer or in the form of an air-powder mist fed to the bearing itself. A cage-type bearing with a MoS_2 coating syrup-bonded to the retainer failed at a DN value of 0.3×10^6. A cageless bearing with a syrup-bonded MoS_2 coating could not be run at DN values higher than 0.375×10^6. Another 75-millimeter-bore roller bearing with a two-piece roller riding brass cage, which had a syrup-bonded MoS_2 coating, failed at a DN value of 0.375×10^6. Cage wear resulted in binding of the cage. From these early experiments, syrup-bonded coatings were shown to be of limited utility.

A cageless roller bearing precoated with a syrup-bonded MoS_2 coating and lubricated during test by the MoS_2 air-mist system was run successfully at a DN value of 0.975×10^6. Total running time at DN values up to the maximum was 11.8 hours. This bearing was sensitive to the amount of solid MoS_2 delivered to it per unit time. Difficulties in controlling the flow rate of MoS_2 powder caused wide variations in bearing temperature. No surface damage was evident in this bearing after test, and no measurable wear could be detected on any surfaces. A roller bearing with a one-piece inner-race-riding brass cage was operated to a DN value of 0.675×10^6 with the MoS_2 air-mist lubrication system. Operation was rather rough and operating temperature was unstable, but no failure occurred. The total running time of this test bearing was 8.4 hours. Further tests with this bearing were conducted with a modified type of feed system for the MoS_2 air mist. With the modified MoS_2 system (discussed in detail in ref. 28), operation to DN values of 0.9×10^6 was achieved and operating conditions were more stable, especially with respect to operating temperature. Temperatures obtained in these bearing tests are shown in figure 11–11. Despite the fact that there was no heat addition to the bearings in these tests, bearing temperatures reached 460° F.

For these high-speed tests with dry film and dry powder lubricants, the most satisfactory results were obtained with cageless bearings, as entry of the powder into the bearing is somewhat restricted by the presence of a retainer. The dry film lubricant, in order to lubricate the bearing, must reach the critical surfaces, and apparently this is more easily achieved in a cageless bearing than in one with a retainer.

The second group of experiments in reference 29 was conducted with 20-millimeter-bore tool-steel bearings, equipped with either silver-plated beryllium-copper cages or cast Inconel cages. These experiments were run over a temperature range from room temperature to 1000° F at a speed of 2500 rpm and a thrust load of 110 pounds. Bearing friction torque was measured and recorded throughout each test and was used as the criterion of successful operation. The results

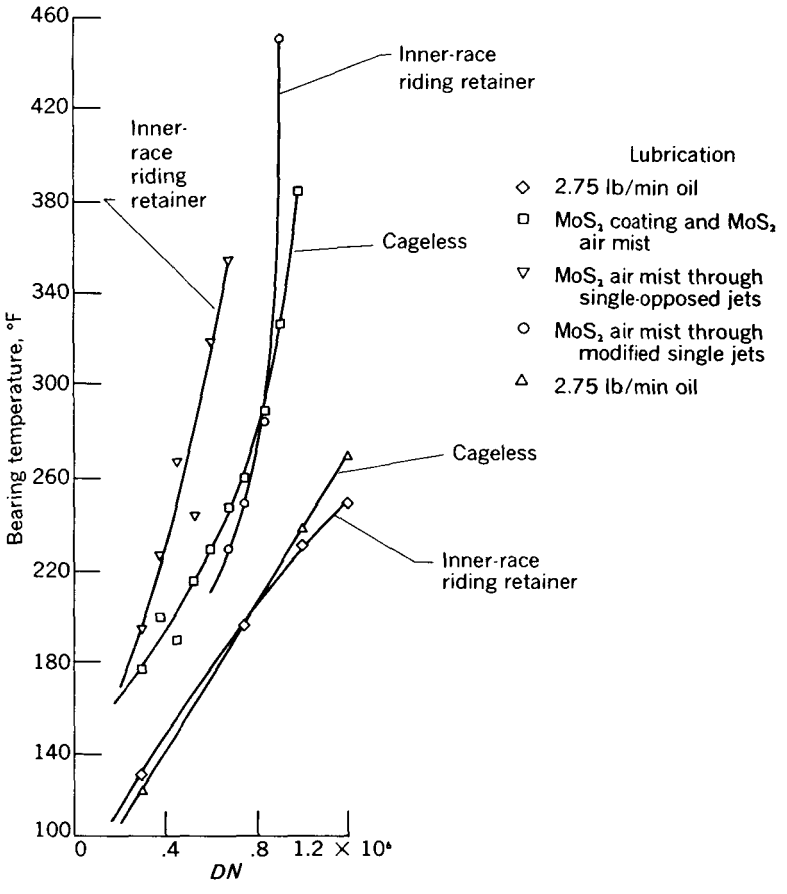

FIGURE 11–11.—Effect of DN on outer-race maximum temperature. DN, 0.3×10^6 to 1.2×10^6; load, 368 pounds. (From ref. 29.)

of the high-temperature experiments with solid air-mist lubricants are shown in figure 11–12. Bearings with both types of cages were lubricated satisfactorily over the entire temperature range to 1000° F with graphite air-mist lubricants. For reference purposes, the torque trace for a dry bearing run under this speed and load condition is shown on figure 11–12(a). The bearing failed almost immediately. Bearings with silver-plated beryllium-copper cages were run with moist graphite and with dry graphite over the entire temperature range. The dry graphite showed a slight torque peak in the region of 700° F, whereas the moist graphite lubricated with low torque over the entire temperature range to 1000° F. Reference 30 hypothesizes that graphite depends for its lubricating effectiveness on the presence of an adsorbate such as moisture or an oxide film. For the run with dry graphite, the lack of moisture, plus the fact that a surface oxide was not forming at a sufficient rate, probably caused the rise in torque

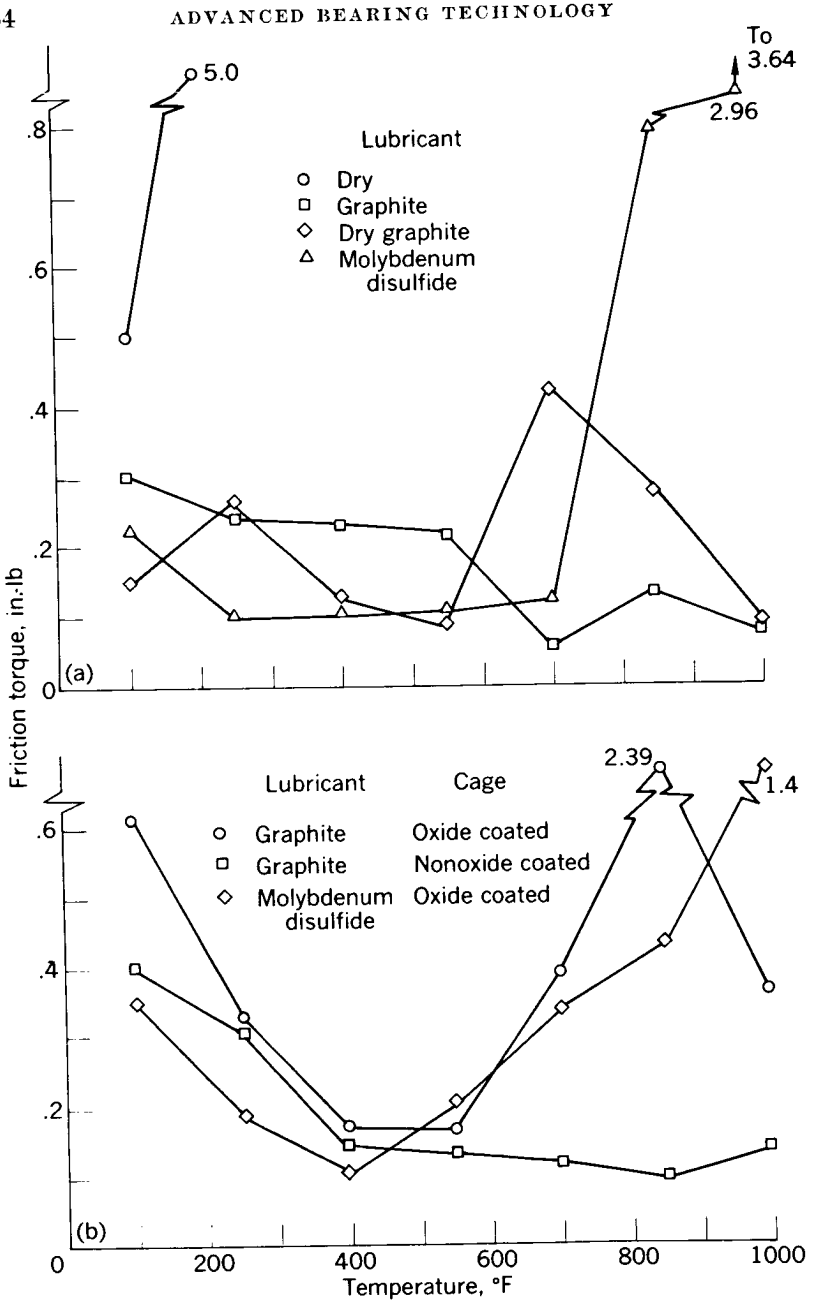

(a) Silver-plated beryllium-copper cages.
(b) Cast Inconel cages.

FIGURE 11–12.—Effect of temperature on friction torque of test bearings when lubricated with solid air-mist lubricants. (From ref. 29.)

in the region of 700° F. As the rate of oxide formation increased with the increasing temperatures, the effectiveness of the dry graphite as a lubricant increased until at 1000° F the torque difference between moist and dry graphite was negligible.

Some of the Inconel cages were treated with an oxide film. The set of curves in figure 11–12(b) shows that graphite with a nonoxide-coated Inconel cage was effective over the entire temperature range. Graphite was not effective, however, as a lubricant over a good portion of the temperature range of the experiment with an oxide-coated Inconel cage. Again, molybdenum disulfide with an oxide-coated cage was effective to only 850° F. At temperatures above 850° F, the torque rose considerably.

Collectively, the high-speed and then the high-temperature experiments of reference 29 indicate that dry film lubricants are feasible for use in rolling-contact bearings. The methods used for feeding the dry powders to the test bearings were quite crude; yet, in many of the experiments, surprisingly successful results were obtained. These experiments show that the useful temperature range of solid lubricants goes considerably beyond that of liquid lubricants, and, in fact, the present limitations may be due to the bearing materials and designs rather than to the lubricants themselves.

Similar experiments conducted with 20-millimeter-ball bearings in reference 16 indicated that the high-temperature effectiveness of molybdenum disulfide could be improved by the use of an inert nitrogen atmosphere in place of air. This atmosphere had the effect of nullifying the oxidation tendencies of molybdenum disulfide. The results of experiments with molybdenum disulfide mist lubrication and air-nitrogen atmospheres are shown in figure 11–13. In a nitrogen atmosphere, the molybdenum disulfide mist lubrication system was effective at 1000° F. In air, the limiting effectiveness was approximately 700° F. The effect of running time on bearing torque was also investigated in reference 16, with graphite mist lubrication at 1000° F. One experiment, in which lubricant flow was discontinued after 2 hours, resulted in a sharp increase in torque and a bearing failure at 2.6 hours (fig. 11–14). An endurance run of 20 hours with graphite mist lubrication at 1000° F was made in reference 16. Torque varied but slightly over the 20-hour period, and the bearing was in excellent condition at the conclusion of the run. No signs of wear or surface damage could be found on any of the bearing parts.

Under the conditions of the experiments conducted in references 16 and 29, solid lubricants were found to be the best high-temperature lubricants. Of all the lubricants tested, only graphite provided effective lubrication in an air atmosphere at 1000° F. All five bearings lubricated with graphite ran with low friction torque at 1000° F

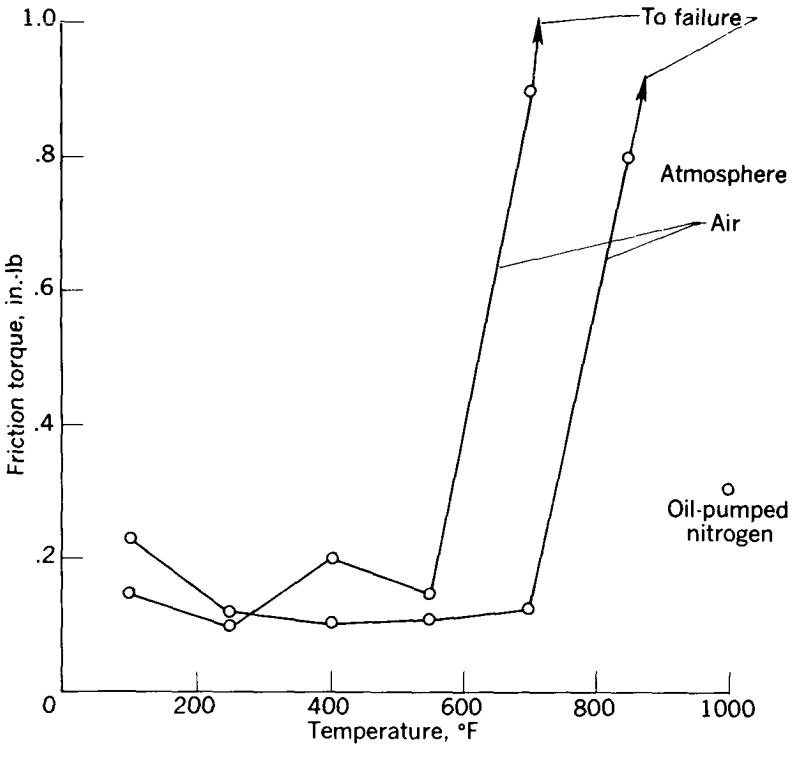

FIGURE 11–13.—Effect of temperature on friction torque of test bearings with beryllium-copper cage when lubricated with molybdenum disulfide. (From ref. 16.)

and were clean and free after test. Graphite was superior to MoS_2 in air, because its oxidation products are harmless, whereas those of MoS_2 are abrasive and corrosive. In a nitrogen atmosphere, MoS_2 showed none of the deleterious effects that occur in air at temperatures above 700° F and was an effective lubricant at 1000 °F. Bearings run with solid lubricants were generally clean and free after test, as opposed to carbonaceous deposits of various degrees obtained in the tests with liquid lubricants. With graphite and MoS_2 lubrication, only an extremely thin film of the solid lubricant was deposited on the bearing parts.

Further experiments to determine the mechanism of lubrication with graphite are reported in reference 30. Sliding friction tests in forming gas, dry air, and moist air are included as well as ball-bearing tests with graphite lubrication in moist air, dry air, dry purified nitrogen, and moist purified nitrogen. The results of the bearing experiments shown in figure 11–15 indicate that in both moist air and dry

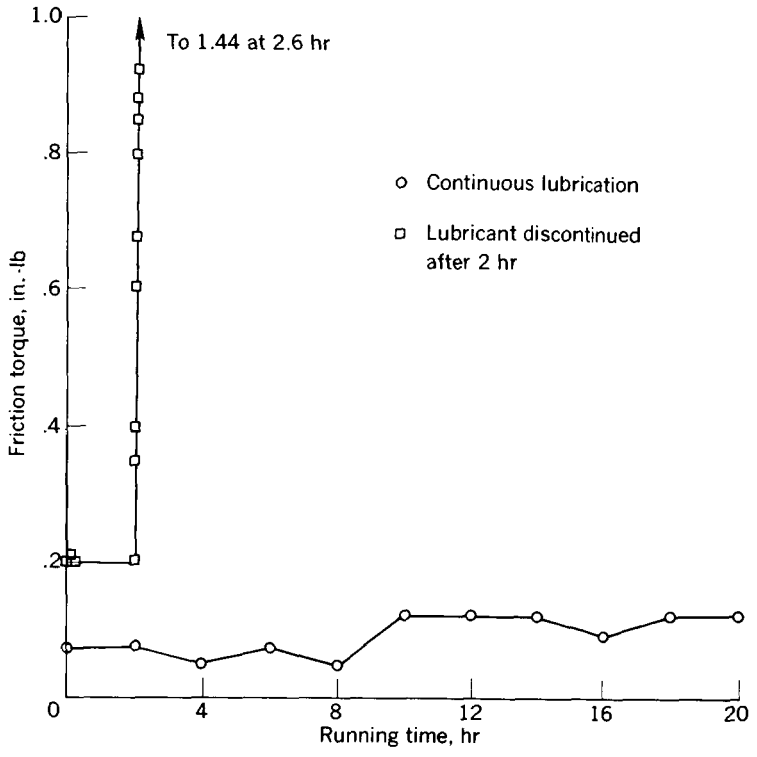

FIGURE 11-14.—Effect of running time on friction torque of test bearings when lubricated with graphite-air mist at 1000° F. (From ref. 16.)

air the bearing ran with low torque. In dry purified nitrogen, the bearing ran with high torque and failed after 5¼ hours at 1000° F. In moist purified nitrogen, the torque was still relatively high, compared with the torque in both moist and dry air, but the bearing was clean and free after 20 hours at 1000° F. Analysis of the friction and bearing experiments with graphite lubrication in various environments confirmed the hypothesis in regard to the mechanism of lubrication with graphite that was presented in chapter 8. A restatement of this hypothesis is that effective lubrication is possible with graphite, provided either of two conditions is met: (1) an adsorbed water or vapor film is present, or (2) an oxide film of the proper type is continuously present on one or both of the lubricated surfaces. This hypothesis presumes that graphite will lubricate effectively at all temperatures from 100° to 1000° F, provided that it can be maintained between the sliding surfaces. The oxide film is believed to influence the adherence of graphite to the surfaces.

Limitations of early experiments.—Early experiments with solid

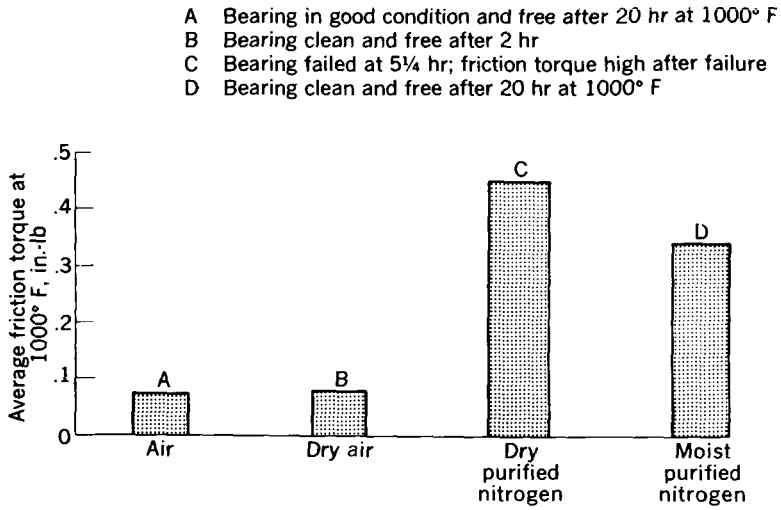

FIGURE 11–15.—Effect of air or inert atmosphere on lubrication of ball bearings with graphite. Temperature, 1000° F; speed, 2500 rpm; load, 110 pound thrust. (From ref. 30.)

lubricants in rolling-contact bearings reported in references 16 and 28 to 30 indicated that the degree of success obtained depended strongly on the effectiveness of getting the solid lubricant into the critical areas where surfaces were in sliding contact. The proper quantity of lubricant at a uniform flow rate must be supplied to the sliding surfaces for optimum performance. Speed and load limitations encountered in early work with solid lubricants were due largely to poor control of the lubricant feed rate and to the fact that test bearings were not designed specifically for use with solid lubricants. These bearings were designed for use with liquid lubricants; therefore they could not be construed as having optimum design for use with dry film or dry powder lubricants. Reference 28 reported that erratic flow rates of the solid lubricant caused sharp fluctuations in bearing temperature. Excessive flow rates into the bearing produced squeaking, which resulted from intermittent interference, as layers of the solid lubricant alternately built up in thickness to a maximum and then sloughed off.

Recent experience shows that the bearings used in earlier experiments were deficient in several respects. First, they had inadequate internal clearance or looseness. When lubricating with solids, little or no cooling of the bearing parts occurs, so that the temperature of internal bearing parts might be considerably higher than the temperature of the bearing housing. Almost all the heat generated in the

bearing must be removed by conduction from the rolling elements into the races and thence into the housing and the shaft. Little heat is removed by convection to the surrounding atmosphere and by radiation as contrasted to a bearing lubricated with a high flow rate of liquid where a significant portion of the heat generated is removed by the lubricant. Consequently, bearings with inadequate internal clearance were definitely speed limited. When the expansion of the rolling elements removed all the initial internal clearance, the speed limit was reached. Any further increase in speed would mean an increase in the rate of heat generation within the bearing and failure of the bearing because of internal lock-up.

Second, the bearings used in these experiments had retainers that were not properly designed for use with solid lubricants. The resistance that the retainer offers to lubricant flow into the bearing is not as critical with liquid lubricants as it is with solid lubricants. For good performance with solid lubricants, a retainer should offer minimum flow resistance of the lubricant into and out of the bearing. The dry powder must have both easy access to the critical areas that require lubrication and an easy exit from the bearing. The retainer must allow the dry powder to reach all areas of the bearing, and at the same time it must discourage accumulation of the powder within the bearing. Too much dry powder within the bearing may cause binding.

Experiments with retainer designs.—One of the life-limiting factors with preformed solid film lubrication is, of course, the life of the solid film itself. Since solid film lubricants can be applied only in thin coatings, these can be expected to wear through in a finite length of time. When these lubricants are worn through, effective lubrication can no longer be obtained and bearing failure will follow. Accordingly, the research reported in reference 31 was undertaken to devise means of extending bearing life with the bearing lubricated with a solid film lubricant. The solid film lubricant chosen for these experiments was an MoS_2 base coating with 71 percent by weight of MoS_2, 7 percent by weight of graphite, and 22 percent by weight of sodium silicate. Test bearings were 204-size 20-millimeter-bore bearings that were made of either T–1 tool steel or M–10 tool steel. The temperature range of these experiments was from 77° to 720° F. All tests were run at 10,000 rpm under a 5-pound thrust load and a 3-pound radial load. Since the bearing life is limited by the life of the dry film, attempts were made to extend bearing life by producing a number of depressions in each of the retainer ball pockets and by filling these depressions with the solid lubricant. An automatic punch was used that produced a cone-shaped recess in the retainer pockets. Then, a phosphate pretreatment was applied to the retainer surfaces, and the solid film lubricant was deposited in the reservoirs and on

the surfaces of the retainers and races. The results of a series of experiments with various configurations of reservoir at 350° F are shown in table 11–XVII. A plot of wear life as a function of reservoir diameter is shown in figure 11–16. The results of a similar series of experiments conducted at 750° F are shown in table 11–XVIII. These experiments were conducted at speeds of 3500 and 10,000 rpm. The

TABLE 11–XVII.—RESERVOIR EFFECT ON BEARING PERFORMANCE LIFE WITH HIGH-TEMPERATURE HIGH-SPEED BEARING PERFORMANCE APPARATUS[a]

[204-Size ball bearings; races and balls, Cr alloy (AISI–C52100); retainers, steel (AISI–1010); internal clearance 0.0003 to 0.0008 in.; load, 5 lb thrust, 3 lb radial; speed, 10,000 rpm; temperature, 350° F; continuous test; solid film composition, 71 percent MoS_2, 7 percent graphite, 22 percent sodium silicate.]

Reservoir diameter, in.	Reservoir depth, in.	Number of reservoirs per ball pocket	Total number of reservoirs	Pretreatment	Performance life, hr
				Phosphate	21, 29
0.025 (Max.)	0. 015	70	560	do	32, 33
.041	. 034	6	48	do	46, 58
.055	. 034	6	48	do	55
.063	. 034	6	48	do	65, 73
.067	. 034	6	48	do	89
.070	. 034	6	48	do	100, 95
.078	. 034	6	48	do	113, 107

[a] From ref. 31.

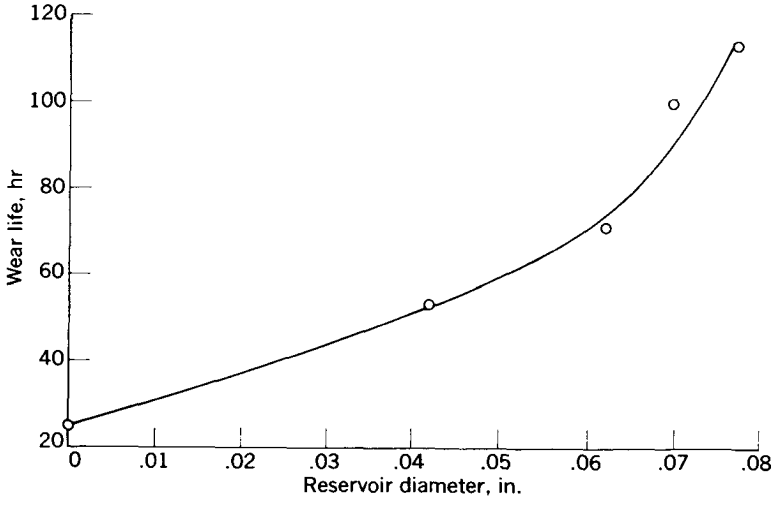

FIGURE 11–16.—Effect of reservoir diameter on wear life. (From ref. 31.)

TABLE 11–XVIII.—EFFECT OF RETAINER TYPE AND MODIFICATION ON PERFORMANCE LIFE WITH HIGH-TEMPERATURE HIGH-SPEED BEARING PERFORMANCE APPARATUS [a]

[204-Size ball bearing with internal clearance of 0.0008 in.; temperature, 750° F; continuous test; load, 5 lb thrust, 3 lb radial; solid film composition, 71 percent MoS_2, 7 percent graphite, 22 percent sodium silicate; ball-race material, T–1 tool steel.]

Retainer material	Retainer pocket				Retainer inner periphery				Speed, rpm	Performance life, hr
	Reservoir diameter, in.	Reservoir depth, in.	Site [b]	Number of reservoirs	Reservoir diameter, in.	Reservoir depth, in.	Site [b]	Number of reservoirs		
Cast iron	0. 093	0. 025	A	48	0. 113	0. 075	C	16	10, 000	20
		. 075	B							
		0. 037	A	48	0. 113	0. 075	C	16	10, 000	23
		. 075	B							
		0. 050	A	48	0. 113	0. 075	C	16	10, 000	27
		. 075	B							
		0. 073	A	48	0. 113	0. 075	C	16	10, 000	29
		. 075	B							
AISI 430	0. 093	0. 037	A	48	0. 113	0. 075	C	16	10, 000	20
		. 075	B							
		0. 050	A	48	0. 113	0. 075	C	16	10, 000	24
		. 075	B							
AISI 1010	0. 093	0. 050	A	48	0. 113	0. 075	C	16	10, 000	24
		. 075	B							
AISI 430	0. 093	0. 037	A	48	0. 113	0. 075	C	16	3, 500	96
		. 075	B							
Cast iron	0. 093	0. 037	A	48	0. 113	0. 075	C	16	3, 500	455
		. 075	B							
		0. 037	A	48	0. 113	0. 075	C	16	3, 500	333
		. 075	B							

[a] From ref. 31.
[b] Location of site shown in fig. 17.

experiments conducted at 750° F indicate that a performance life of several hundred hours can be obtained at 3500 rpm with a T–1 tool-steel bearing with a reservoir modified cast-iron retainer lubricated with the MoS_2, graphite, sodium silicate solid film. Locations of the reservoir sites A, B, and C in the retainer are shown in figure 11–17(a).

An analysis of the bearings run at 750° F indicated that a substantial increase in reservoir diameter or different reservoir geometry would be required to extend the running time. The modifications applied to machined retainers are shown in figure 11–17(b). The results of the experiments conducted with the modified retainers are shown in table 11–XIX. Rectangular-shaped reservoirs are effective for machined retainers lubricated with MoS_2, graphite, sodium silicate

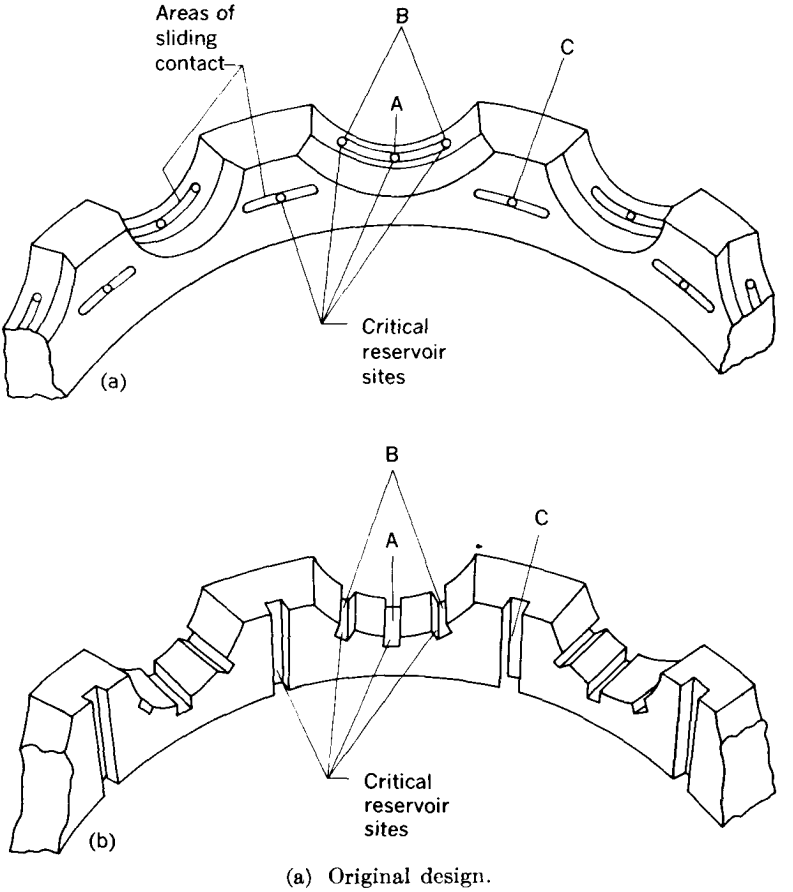

(a) Original design.
(b) Modified design.

FIGURE 11–17.—Section of machined bearing retainer. (From ref. 31.)

TABLE 11–XIX.—EFFECT OF RETAINER MODIFICATION ON PERFORMANCE WITH HIGH-TEMPERATURE HIGH-SPEED BEARING PERFORMANCE APPARATUS [a]

[204-Size ball bearing with internal clearance of 0.0008 in.; temperature, 750° F; speed, 10,000 rpm; load, 5 lb thrust, 3 lb radial; solid film composition, 71 percent MoS_2, 7 percent graphite, 22 percent sodium silicate; ball-race material, T–1 tool steel; reservoir dimensions: site A, 0.032×0.032×0.18 in.; site B, 0.032×0.050×0.18 in.; site C, 0.032×0.050×0.24 in.; locations of sites shown in fig. 11–17(b); continuous tests; running time for modified-cast-iron retainer for same test conditions without lubricant, 5 min.]

Retainer material	Retainer hardness, Rockwell	Performance life, hr
AISI 430	B–76	24
S-monel	C–36	31
AISI 1010	B–75	36
Cast iron	B–72	37
Iron-silicon-bronze	B–58	51
T-1 tool steel	B–98	53

[a] From ref. 31.

solid film, and retainer alloy is an important variable in ball-bearing performance life at 750° F and 10,000 rpm.

From the work reported in reference 31, the MoS_2, graphite, sodium silicate solid film is shown to provide ball-bearing lubrication for extended periods at temperatures from 77° to 750° F. Reservoirs produced in the retainers of ball bearings are effective in extending their performance life, and the geometry and the dimensions of the reservoir affect bearing life. Further work needs to be done on bearing and retainer geometry. In particular, the effect of bearing load on life and also the effect of bearing temperature at temperatures to and above 1000° F should be determined.

High-speed experiments with various dry powders.—Considerable success with two solid lubricants in the form of dry powders was obtained in reference 14 with 17-millimeter-bore ball bearings operating at speeds to 8000 rpm and temperatures to 1500° F. The bearing races were made of titanium carbide and the balls of either titanium carbide or aluminum oxide. Monel or M–1 tool steel were used for retainers operated at 1000° F, and a molybdenum alloy was used for retainers operated at 1500° F. Metal-free phthalocyanine was effective at 1000° F, and bearings were run successfully for 8 hours at 8000 rpm, 50-pound thrust load, and 1500° F with MoS_2 powder in an argon atmosphere. Flow rates of MoS_2 averaged about 0.16 gram per minute. The open-race curvatures used in these bearings resulted in outer-race contact stresses in excess of 300,000 psi at the outer race. This stress produced some pitting in the bearing when it was run at

1500° F. The bearing was otherwise in good condition after 8 hours at 1500° F.

Several solid lubricants in the form of dry powders were evaluated as lubricants for high-speed bearings in reference 32. The ultimate objective of this research was to obtain 10 hours of operation for a 20-millimeter-bore angular-contact bearing at 1200° F and 50,000 rpm under a combined 50-pound radial and 50-pound thrust load. Six different lubricants were chosen for evaluation based on the results of experiments at 1200° F in a rolling-disk machine: (1) molybdenum disulfide in a nitrogen environment, (2) metal-free phthalocyanine in a nitrogen environment, (3) lead monoxide in an air environment, (4) cadmium oxide plus graphite, 1 to 1 mixture by weight in an air environment, (5) proprietary organic polymer furnished by Batelle Memorial Institute, designated BMI–C, in a nitrogen environment, and (6) cerium sulfide in a nitrogen environment. The bearing materials shown in table 11–XX were chosen on the basis of strength,

TABLE 11–XX.—MATERIALS FOR BEARINGS TESTED AT 1200° F [a]

Code	Counter-bored race	Bearing material	Race material [b]	Ball material	Internal bearing play
A	Outer	Titanium carbide	Titanium carbide (K 175A)	Titanium carbide (K 163A1)	0.0010
B	Inner	Stellite Star J	Stellite 3	Stellite Star J	.0028
C	Outer	Titanium carbide	Titanium carbide (K 163A1)	Titanium carbide (K 163A1)	.0028
D	Outer	Titanium carbide	Titanium carbide (K 162B)	Titanium carbide (K 162B)	.0028
E	Outer	Wrought cobalt alloy	Wrought cobalt alloy	Cast cobalt alloy	.0028

[a] From ref. 32.
[b] Outer-race material, titanium carbide (K 163A1).

hot hardness, thermal stability, and resistance to oxidation at high temperatures. Machined one-piece, lightweight retainers, both inner- and outer-race located, were used. Grooves were cut in the retainer guide diameter to permit the flow of the lubricant through the bearing and to allow an exit port for wear debris. Retainer materials chosen were Haynes 25 wrought alloy, titanium carbide K 163A1, titanium carbide K 162B, Stellite 3, and Inconel X. A special variable-speed gear-feed lubricator was developed to provide a reliable lubricant-feed system with independent control of the lubricant-flow rate and the carrier gas-feed rate.

Results with the various lubricants are summarized in table 11–XXI and figure 11–18. The most successful bearing operation at 1200° F

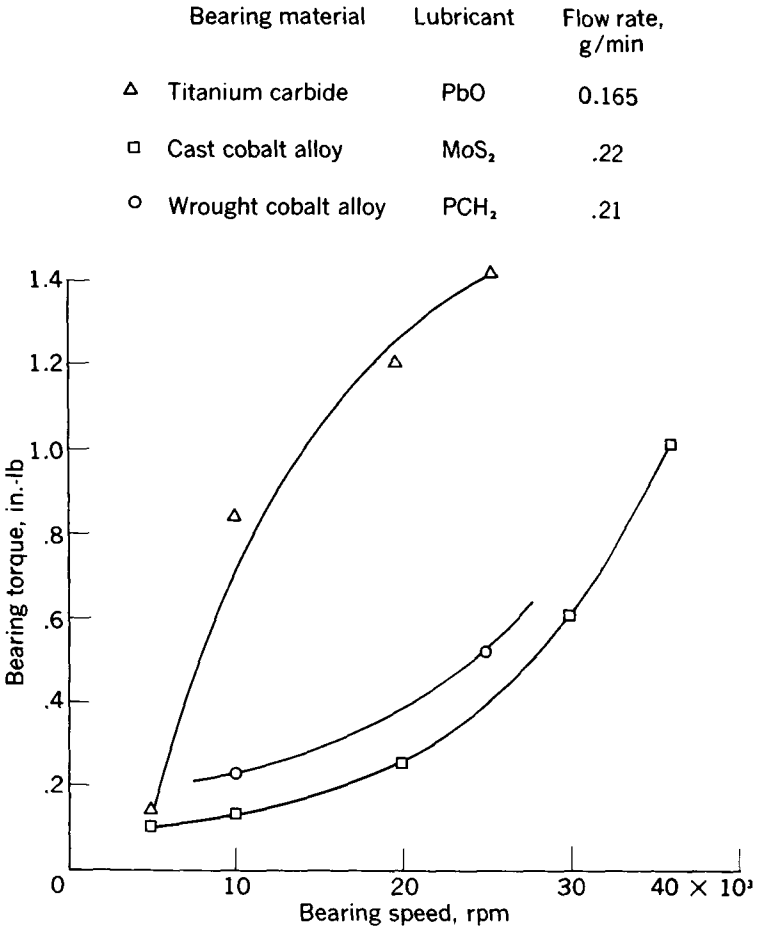

FIGURE 11–18.—Bearing-lubricant torque characteristics. Bearing tempareture, 1200° F. (From ref. 32.)

in terms of bearing wear and smoothness of operation was obtained with molybdenum disulfide. Wrought cobalt-alloy bearings were run for periods of 11.5 hours at speeds of 25,000 to 30,000 rpm under 50-pound thrust load. They have also been run for periods to 6 hours under the same conditions with combined radial and thrust loads of 50 pounds. The MoS_2 lubricant was run in both cast cobalt alloy and titanium carbide bearings for periods of 3 hours with equal success. The bearing-torque characteristics at 1200° F with molybdenum disulfide are shown in figure 11–18.

TABLE 11-XXI.—SUMMARY OF EVALUATIONS OF POWDERED LUBRICANTS USED IN 20-MILLIMETER ANGULAR-CONTACT BEARINGS[a]

[Thrust load, 52 lb except last 3 hr and 52 min of run 23, which was conducted with 53-lb radial and 52-lb thrust loads.]

Operating conditions										Results					
											Bearing wear				
											Weight loss, percent				
Run	Bearing code (b)	Lubricant (c)	Lubricant flow rate, g/min	Carrier gas, cu ft/min	Average outer-race temperature, °F	Bearing speed, rpm	Operating time at speed		Reason for termination of test	Change in internal clearance, in. (d)	Inner race (e)	Outer race (e)	Balls (e)	Retainer (e)	Remarks
							hr	min							
23	E-4S	MoS_2	1.5332	Nitrogen 0.77	1235	25,000 to 27,000	11	33	Bearing inspection	+0.0005	−0.846	−0.077	−0.573	−2.227	Bearing remained operable, heavy rough film in raceway
160	C-2S	MoS_2	.682	Nitrogen .70	1225	29,000	2	10	Bearing inspection	+.0003	−.0019	+.012	−.0094	+.014	Run started at 800° F, all contact surfaces dark polished, inner race pitted
13	A-1G	PCH$_2$[f]	.538	Nitrogen .40	1220	21,000	3	27	Lubricator failure	−.0043	−.008	−.223	−.885	−3.939	All surfaces dark polished, fine pitting and wear on contact surfaces, soft scale on fringes of track
26	E-4S	PCH$_2$[f]	.433 av.	Nitrogen .67	1260	25,000 to 30,000	3	05	Erratic operation	−.0035	−.122	−.078	−2.366	−1.524	Surfaces polished with spotty bluish areas, inner race unevenly
7	B-1R	PbO	.0367	Air 1.34	1250	23,800	1	03	Bearing inspection	−.0086	−.412	−.108	−1.624	+.250	Contact surfaces had smooth dark polish with thin pitted dark film evident
14	B-1G	Graphite +CdO	.0331	Air .84	1200	20,000	------	06	Erratic operation	+.0009	+.013	+.028	+.176	−.206	Contact surfaces had silver appearance, spotty adherent bluish buildup evident on all surfaces
25	E-1G	Ce_2S_3	.4484	Nitrogen .67	1282	25,000	------	22	Erratic operation	−.0070	−.225	−.198	−3.733	−.882	Heavy wear with pitted rough surfaces
24	E-1G	BM1-C	.2835	Nitrogen .67	1270	100 to 20,000	------	17	Erratic operation	+.0011	+.006	−.002	−.046	−.111	Hard crusty film buildup, rough surfaces

[a] From ref. 32.
[b] Bearing code defined in table 11-XX and as follows: S, solid; R, rimmed; G, grooved.
[c] Lubricant particle average size range, 10 to 25 microns.
[d] Plus (+) sign indicates loss in internal play or buildup of lubricant.
[e] Plus (+) sign indicates weight gain.
[f] Phthalocyanine radical is expressed as PC; thus metal-free phthalocyanine is expressed as PCH_2, and metal phthalocyanine is expressed as PCM.

Operation at speeds in excess of 30,000 rpm resulted in vibrations in the bearing because of a relatively rough film of lubricant in the running tracks of the raceways. Lubricant flows above 0.48 gram per minute resulted in a substantial film buildup during 3-hour periods of operation at speeds of 25,000 rpm. At flow rates below 0.20 gram per minute, wear was encountered. Smooth operation at speeds to 35,000 rpm is possible with submicron size (below 0.00008 in.) particles at a flow rate of 0.20 to 0.25 gram per minute. This operation is in contrast to the rough operation with the relatively coarse (0.00008 to 0.001 in.) powders used during the earlier runs.

Although phthalocyanine begins to decompose above 900° F, the rate is sufficiently low to permit the lubricant to perform its functions and to be replenished before complete decomposition occurs. This characteristic results in very clean operation of the bearing and tester with a negligible quantity of decomposed particles present after the completion of a run. The ability of the phthalocyanine to form a film on the bearing surfaces has been attributed in part to its chelating properties, that is, to the ability of the material to attach itself firmly to most metal atoms. The rate at which filming occurs on the cobalt-alloy and titanium carbide bearings at 1200° F has not proved rapid enough to prevent bearing wear. An average internal wear rate is approximately 0.001 inch per hour in both bearing types. Bearing operation was generally smooth with a minimum of vibration.

Only initial lubricant screening runs instead of endurance evaluations were conducted with lead oxide, graphite plus cadmium oxide, an organic polymer BMI–C, and cerium sulfide. Lead monoxide was characterized by smooth operation in a cobalt-base-alloy bearing. At the lowest flow rate attempted, 0.036 gram per minute, internal wear on the rolling-contact surfaces was high, although the wear on the retainer sliding surfaces was negligible. At an increased flow rate of 2.13 grams per minute, the lubricant tended to clog the bearing, which induced high bearing torques as shown in figure 11–18, and finally resulted in a sudden speed decrease after 25 minutes of operation. A film formed on all contact surfaces with no evidence of detectable wear. Additional evaluations were not conducted with this lubricant at intermediate flow rates, and, therefore, an optimum flow was not established.

The use of the graphite plus cadmium oxide mixture indicated very rapid buildup on the contact surfaces of a cobalt-base-alloy bearing during a period of only 6 minutes at a flow rate of 0.033 gram per minute. This material is believed to offer considerable merit as a lubricant at properly adjusted flow rates. More recent evaluations indicate that this lubricant will function well at bearing speeds of 30,000 rpm over the temperature range from 100° to 1200° F for

periods of 10 hours in an air environment. In contrast, the cerium sulfide appeared to offer no protection to the bearing surfaces.

The organic polymer (BMI–C) appeared to form films readily on both cobalt-base-alloy and titanium carbide bearings. The film formed, however, was hard and crusty, which caused rough operation that required the termination of testing.

These experiments indicated that the axial grooves in the retainer guide diameter tended to promote retainer wear by scraping off the buildup of lubricant film. The wrought cobalt alloy was found to be dimensionally unstable for long periods of time at 1200° F. The cast cobalt and titanium carbide materials were satisfactory in this respect.

Reference 33 reports data obtained in the continuation of the work reported in reference 32. In reference 33 all the tests were conducted at 100-pound thrust load and 10-pound radial load with 20-millimeter-bore angular-contact ball bearings. Bearings were fabricated from a cast cobalt-base alloy with wrought nickel-base-alloy retainers. In one series of tests at 30,000 rpm, the temperature was cycled between 150° and 1200° F. One hundred hours of successful operation was obtained with a lubricant consisting of 70 percent MoS_2 and 30 percent metal-free phthalocyanine. In another series of tests with the speed cycled between 5000 and 30,000 rpm and the temperature cycled between 150° and 1200° F, 75 hours of successful operation was achieved.

This research indicates the feasibility of utilizing solid lubricants in a continual injection-type system for lubricating rolling-contact bearings at temperatures to 1200° F for periods of at least 100 hours. The maximum bearing capabilities have not been explored fully, but operation at 25,000 to 30,000 rpm, equivalent to 0.5×10^6 DN, under light radial and thrust loads is possible. The degree of bearing wear and smoothness of operation are dependent upon the type and the characteristics of the lubricant film formed on the bearing contact surfaces. The formation of such a film is a function of both the lubricant and the bearing material; the degree of filming is dependent on the affinity of the metal for the lubricant.

REFERENCES

1. WISANDER, D. W., MALEY, C. E., and JOHNSON, R. L.: Wear and Friction of Filled Polytetrafluoroethylene Compositions in Liquid Nitrogen. ASLE Trans., vol. 2, no. 1, 1959, pp. 58–66.
2. WISANDER, D. W., and JOHNSON, R. L.: Wear and Friction of Impregnated Carbon Seal Materials in Liquid Nitrogen and Hydrogen. Vol. 6 of Advances in Cryogenic Eng., K. D. Timmerhaus, ed., Plenum Press, Inc., 1960, pp. 210–218.

3. MARTIN, K. B., and JACOBS, R. B.: Testing and Operation of Ball Bearings Submerged in Liquified Gases. ASLE Trans., vol. 2, no. 1, 1959, pp. 101–107.
4. WILSON, W. A., MARTIN, K. B., BRENNAN, J. A., and BIRMINGHAM, B. W.: Evaluation of Ball Bearing Separator Materials Operating Submerged in Liquid Nitrogen. ASLE Trans., vol. 4, no. 1, 1961, pp. 50–58.
5. SCIBBE, HERBERT W., and ANDERSON, WILLIAM J.: Evaluation of Ball-Bearing Performance in Liquid Hydrogen at DN Values to 1.6 Million. ASLE Trans., vol. 5, no. 1, Apr. 1962, pp. 220–232.
6. JONES, A. B.: The Life of High-Speed Ball Bearings. ASME Trans., vol. 74, no. 5, July 1952, pp. 695–699; discussion, pp. 699–703.
7. PORITSKY, H., HEWLETT, C. W., Jr., and COLEMAN, R. E., Jr.: Sliding Friction of Ball Bearings of the Pivot Type. Jour. Appl. Mech., vol. 14, no. 4, Dec. 1947, pp. 261–268.
8. JONES, A. B.: Ball Motion and Sliding Friction in Ball Bearings. Jour. Basic Eng. (ASME Trans.), ser. D, vol. 81, no. 1, Mar. 1959, pp. 1–12.
9. BUTNER, M. F., and ROSENBERG, J. C.: Lubrication of Bearings with Rocket Propellants. Lubrication Eng., vol. 18, no. 1, Jan. 1962, pp. 17–24.
10. IRWIN, A. S.: Effect of Bearing Temperature on Capacities of Bearings of Various Materials. Paper Presented at ASME Lubrication Symposium, New York (N.Y.), Mar. 14, 15, 1960.
11. PHILIP, T. V., NEHRENBERG, A. E., and STEVEN, G.: A Study of the Metallurgical Properties That are Necessary for Satisfactory Bearing Performance and the Development of Improved Bearing Alloys for Service up to 1000° F. TR 57–343, pt. II, WADC, Oct. 1958.
12. MCMULLAN, O. W.: High Temperature Materials and Their Heat Treatment for Anti-Friction Applications. Preprint 122A, SAE, 1960.
13. HANLON, P. C.: Recent Development in High Temperature Bearings and Lubricants. Preprint 176B, SAE, 1960.
14. TAYLOR, K. M., SIBLEY, L. B., and LAWRENCE, J. C.: Development of a Ceramic Rolling Contact Bearing for High Temperature Use. Paper 61 LUB–12, ASME, 1961.
15. NEMETH, Z. N., and ANDERSON, W. J.: Investigation of Temperature Limitations of Various Lubricants for High-Temperature 20-Millimeter-Bore Ball Bearings. NACA TN 3337, 1955.
16. NEMETH, Z. N., and ANDERSON, W. J.: Effect of Air and Nitrogen Atmospheres on the Temperature Limitations of Liquid and Solid Lubricants in Ball Bearings. Lubrication Eng., vol. 11, no. 4, July–Aug. 1955, pp. 267–273.
17. NEMETH, Z. N., and ANDERSON, W. J.: Effect of Oxygen Concentration in Atmosphere on Oil Lubrication of High-Temperature Ball Bearings. Lubrication Eng., vol. 12, no. 5, Sept.–Oct. 1956, pp. 327–330.
18. SOREM, S. S., and CATTANEO, A. G.: High-Temperature Bearing Operation in the Absence of Liquid Lubricants. Lubrication Eng., vol. 12, no. 4, July–Aug. 1956, pp. 258–260.
19. BAILEY, CHARLES H., and SOREM, STANLEY S.: Research in High Temperature Bearing Lubrication in the Absence of Liquid Lubricants. TR 56–370, pt. II, WADC, Mar. 1957.
20. COIT, R. A., SOREM, S. S., ARMSTRONG, R. L., and CONVERSE, C. A.: Research in High Temperature Bearing Lubrication in the Absence of Liquid Lubricants. TR 56–370, pt. III, WADC, Aug. 1958.
21. SCHULLER, F. T., and ANDERSON, W. J.: Operating Characteristics of 75-Millimeter Bore Ball Bearings at Minimum Oil Flow Rates Over a Tem-

perature Range to 500° F. Lubrication Eng., vol. 17, no. 6, June 1961, pp. 291–298.

22. ACCINELLI, J. B., and BEAUBIEN, S. J.: Fundamentals of High Temperature Bearing Lubrication. S–13773, Shell Dev. Co., 1958.
23. ACCINELLI, J. B., and BEAUBIEN, S. J.: Fundamentals of High Temperature Bearing Lubrication. S–13803, Shell Dev. Co., 1959.
24. GLAESER, WILLIAM A., ALLEN, C. MALCOLM, GRIESER, DANIEL R., and VAN DYKE, HERBERT A.: The Development of Oscillatory Rolling-Contact Bearings for Airframe Applications in the Temperature Range 300° F to 600° F. TR 59–145, WADC, Mar. 1959.
25. O'ROURKE, W. F.: Research on Developing Design Criteria for Anti-Friction Airframe Bearings for High Temperature Use. TR 60–46, WADD, Jan. 1960.
26. LEWIS, P., MURRAY, S. F., and SCHWARTZ, A. A.: Design Criteria for Bearings Systems for Use in High Temperature Aircraft Electrical Accessories. TR 59–563, WADC, Sept. 1959.
27. BORG, A. C., et al.: Development of Grease Lubricants for High Temperature Ball and Roller Bearings of Electrical Equipment. TR 60–557, pt. 2, WADD, Nov. 1961.
28. MACKS, E. F., NEMETH, Z. N., and ANDERSON, W. J.: Preliminary Investigation of Molybdenum Disulfide—Air-Mist Lubrication for Roller Bearings Operating to DN Values of 1×10^6 and Ball Bearings Operating to Temperatures of 1000° F. NACA RM E51G31, 1951.
29. NEMETH, ZOLTON N., and ANDERSON, WILLIAM J.: Temperature Limitations of Petroleum, Synthetic, and Other Lubricants in Rolling-Contact Bearings. SAE Trans., vol. 63, 1955, pp. 556–565; discussion, 565–566.
30. BISSON, EDMOND E., JOHNSON, R. L., and ANDERSON, W. J.: Friction and Lubrication with Solid Lubricants at Temperatures to 1000° F with Particular Reference to Graphite. Proc. Conf. on Lubrication and Wear, Inst. Mech. Eng., 1957, pp. 348–354.
31. DEVINE, M. J., LAMSON, E. R., and BOWEN, J. H., Jr.: The Lubrication of Ball Bearings with Solid Films. Paper 61–LUBS–11, ASME, 1961.
32. WILSON, D. S.: Evaluation of Unconventional Lubricants at 1200° F in High-Speed Rolling Contact Bearings. Paper 61–LUBS–9, ASME, 1961.
33. SCHLOSSER, A.: The Development of Lubricants for High-Speed Rolling Contact Bearings Operating Over the Range of Room Temperature to 1200 Degrees Fahrenheit. Prog. Rep. 5, Stratos Div., Fairchild Engine and Airplane Corp., Jan. 1962.

CHAPTER 12

Fatigue in Rolling-Element Bearings

By WILLIAM J. ANDERSON

SYMBOLS

A constant in Weibull equation, e ln A is vertical intercept on Weilbull plot when $L=1$
a half axis of pressure ellipse in direction normal to rolling direction, in.
C specific dynamic capacity
D rolling-element diameter, in.
d diameter, in.
E bearing-pitch diameter, in.
e slope of Weibull plot
F probability that a crack will occur
f_c coefficient dependent on material and bearing type
i number of rows of rolling elements
L life in millions of revolutions
l length of raceway contact, in.
l_a roller length, in.
N angular velocity, rpm
n millions of stress cycles
n load-life exponent
P bearing or system thrust load, lb
P_e bearing equivalent load, lb
p pressure, lb/sq in.
R rolling-element profile radius normal to direction of rolling
r race groove radius normal to direction of rolling
S probability of survival
T temperature
t time
V stressed volume

W bearing load, lb
y_E standardized excess life
y_T standardized theoretical life
z number of balls per row
z_o depth to maximum shear stress
α contact angle
β slope of pressure-viscosity curve
μ_o viscosity at atmospheric pressure, lb-sec/sq in.
μ_p viscosity at pressure p, lb-sec/sq in.
σ stress, psi
τ_o maximum shear stress, psi
ω_s angular spin velocity
Subscripts:
i inner
m pitch
o outer

SPECIFIC DYNAMIC CAPACITY

In chapter 6, the life dispersion, the load-life relations, and the meaning of specific dynamic capacity, or load rating, of rolling bearings were discussed. These three factors must be understood to predict the life of a given bearing in a specific application. Formulas for calculating the specific dynamic capacity must be available because large groups of bearings cannot be tested experimentally to determine the expected life for every application.

Lundberg-Palmgren Theory

Much of the analytical and the experimental work, which has resulted in specific-dynamic-capacity formulas, was done by Palmgren (ref. 1) and Lundberg and Palmgren (ref. 2). An empirical method for determining specific dynamic capacity is presented in reference 1, and a more refined method, based on statistics, is presented in reference 2.

The life formula developed in reference 2 is based on the known fact that, the more concentrated the stress is, the greater the endurance. Weibull's investigations (refs. 3 and 4) have resulted in a statistical theory of strength based on the theory of probability, where the dependence of strength on volume is explained by the dispersion in material strength. Therefore, the dependence on volume caused by the dispersion in material strength must be considered. Weibull's theory, however, assumes that the first crack that forms eventually leads to a break. Many bearing races were examined and were found to contain numerous subsurface cracks that never progressed to failure; thus Weibull's assumption is questionable. Therefore, the depth z_o, at which the maximum shear stress occurs, must also be

considered. According to Weibull's theory, the logarithm of the inverse of the probability of survival is proportional to the magnitude of the stressed volume. This relation results from the multiplicative law, which states that the probability of failure of the whole is equal to the product of the probabilities of failure of the parts. In equation form, the life formula is therefore

$$\ln \frac{1}{S} = F(\tau_o, \boldsymbol{n}, z_o)V \tag{12-1}$$

where

S probability of survival
F probability that a crack will occur
τ_o maximum shear stress
$\boldsymbol{n}$ number of stress cycles in millions
V stressed volume

The function F can be expressed as a power function:

$$F(\tau_o, \boldsymbol{n}, z_o) \sim \frac{\tau_o^c \boldsymbol{n}^e}{z_o^h} \tag{12-2}$$

where c, e, and h are exponents to be determined experimentally.

An arbitrary expression for V is

$$V = a z_o \boldsymbol{l} \tag{12-3}$$

where

a half axis of pressure ellipse in direction normal to rolling direction
$\boldsymbol{l}$ length of raceway

From equations (12–1) to (12–3)

$$\ln \frac{1}{S} \sim \frac{\tau_o^c \boldsymbol{n}^e a \boldsymbol{l}}{z_o^{h-1}} \tag{12-4}$$

The Lundberg-Palmgren dynamic capacity is developed from equation (12–4). The exponents in equation (12–4) are determined from the dispersion of bearing lives, the dependence of life on load, and the dependence of the specific dynamic capacity on bearing size. Lundberg and Palmgren extended the Hertz theory to calculate the shear-stress amplitude in a plane parallel to the direction of rolling and used this amplitude to determine the dependence of dynamic capacity on conformity between rolling elements and races. Their theory of fatigue strength is based on the assumption that the maximum shear stress in the plane parallel to the direction of rolling is the stress that causes failure. Other investigators believe that either the maximum orthogonal or the maximum octahedral shear stress is the stress that causes failure. Extensive studies in this area are needed.

The derivations of dynamic-capacity formulas in reference 2 are complex. Their principal value is that they improve the theoretical understanding of the relations between the statistical nature of bearing fatigue and bearing-load capacity. The empirical approach used by Palmgren in reference 1 is more direct and will be outlined herein. Weibull (ref. 5) postulated that the fatigue lives of a homogeneous group of rolling-element bearings are dispersed according to the following relation:

$$\ln \ln \frac{1}{S} = e \ln \frac{L}{A} \tag{12–5}$$

where L represents life in millions of revolutions and e is the dispersion exponent (slope of the Weibull plot) or a measure of the scatter in bearing lives. Experimental results confirm that bearing lives conform well to the Weibull distribution, at least at survival probabilities ranging from 0.5 to 0.9. Bearing-fatigue data will plot as a straight line with the coordinates given by equation (12–5), commonly known as Weibull coordinates.

The factors upon which the specific dynamic-load rating depends are the following:

(1) The size of the rolling elements
(2) The number of rolling elements per row
(3) The number of rows of rolling elements
(4) The conformity between the rolling elements and the races
(5) The contact angle under load
(6) The properties of the material
(7) The properties of the lubricant
(8) The operating temperature
(9) The operating speed

Factors 1 through 5 are considered in standard capacity formulas. The remaining factors will be discussed later.

According to the Hertz theory, the load-carrying capacity should be proportional to the square of the rolling-element diameter. From extensive experimental data, Palmgren (ref. 1) found that capacity varied as $D^{1.8}$ for balls up to about 25 millimeters in diameter and as $D^{1.4}$ for balls larger than 25 millimeters in diameter.

For a constant bearing load, the normal force between a rolling element and a race will be inversely proportional to the number of rolling elements. Therefore, for a constant number of stress cycles at a point, the capacity is proportional to the number of rolling elements. On the other hand, the number of stress cycles per revolution is also proportional to the number of rolling elements, so that for a constant rolling-element load the capacity for point contact is inversely proportional to the cube root of the number of rolling

elements. This comes from the inverse cubic relation between load and life for point contact. Then the capacity varies with

$$\frac{z}{z^{1/3}}=z^{2/3}$$

Multiple-row bearings with i rows of balls may be considered as a combination of i single-row bearings. From equation (12–5) and the theory of probability, the following relation between the life of a multirow bearing and the lives of the i individual rows is obtained:

$$\frac{1}{L^e}=\frac{1}{L_1^e}+\frac{1}{L_2^e}+\cdots+\frac{1}{L_i^e} \tag{12–6}$$

Then

$$\frac{1}{L^e}=\frac{i}{L_i^e} \tag{12–7}$$

If each row of the bearing is loaded with a load equal to the specific dynamic-load rating of one row C_i, then $L_i=1$ and, from equation (12–7),

$$L^e=\frac{1}{i} \tag{12–8}$$

or

$$L=\frac{1}{i^{1/e}} \tag{12–9}$$

The load on the entire bearing is iC_i. In chapter 6, the load-life relation was given as

$$L=\left(\frac{C}{P_e}\right)^n \tag{12–10}$$

where P_e is the equivalent bearing load. In this case,

$$P_e=iC_i \tag{12–11}$$

From equations (12–9) to (12–11),

$$\left(\frac{C}{iC_i}\right)^n=\frac{1}{i^{1/e}} \tag{12–12}$$

or

$$C=C_i\, i^{1-(1/en)} \tag{12–13}$$

For ball bearings, $n=3$ and e is approximately 1.1, so that the capacity of multirow bearings varies as $i^{0.7}$. For radial ball bearings, the normal force between a ball and a race varies as $1/\cos\alpha$, so that the capacity is proportional to $\cos\alpha$. The influence of the degree of conformity, bearing type, and internal dimensions is expressed by

$f_c/(\cos \alpha)^{0.3}$. Therefore the capacity of a radial ball bearing varies as $(i \cos \alpha)^{0.7}$.

For thrust ball bearings, the normal force between a ball and a race varies as $1/\sin \alpha$, so that the capacity is proportional to $\sin \alpha$ or to $\cos \alpha \tan \alpha$. When the influences of the degree of conformity, of bearing type, and of internal dimensions are included, the capacity of a thrust ball bearing varies as $(i \cos \alpha)^{0.7} \tan \alpha$.

For roller bearings with line contact, the exponent in the life equation is 4, so that the capacity varies as $z^{3/4}$. From equation (12–13) with $n=4$, the capacity of multirow-roller bearings is found to vary as $i^{0.78}$. Theoretically, the capacity of roller bearings should be proportional to $l_a D_a$. Experimental data indicate that capacity varies as $l_a^{0.78} D_a^{1.07}$.

The formulas for specific dynamic capacity as developed by Palmgren (ref. 1) and Lundberg and Palmgren (ref. 2) are as follows:

(1) For radial ball bearings with $D<25$ millimeters,

$$C=f_c(i \cos \alpha)^{0.7} z^{2/3} D^{1.8} \tag{12–14}$$

(2) For radial ball bearings with $D>25$ millimeters,

$$C=f_c(i \cos \alpha)^{0.7} z^{2/3} D^{1.4} \tag{12–15}$$

(3) For radial roller bearings,

$$C=f_c(i \cos \alpha)^{0.78} z^{3/4} D^{1.07} l_a^{0.78} \tag{12–16}$$

(4) For thrust ball bearings with $\alpha \neq 90°$,

$$C=f_c(i \cos \alpha)^{0.7} (\tan \alpha) z^{2/3} D^{1.8} \tag{12–17}$$

(5) For thrust roller bearings with $\alpha \neq 90°$,

$$C=f_c(i \cos \alpha)^{0.78} (\tan \alpha) z^{3/4} D^{1.07} l_a^{0.78} \tag{12–18}$$

(6) For thrust ball bearings with $\alpha=90°$,

$$C=f_c i^{0.7} z^{2/3} D^{1.8} \tag{12–19}$$

(7) For thrust roller bearings with $\alpha=90°$,

$$C=f_c i^{0.78} z^{3/4} D^{1.07} l_a^{0.78} \tag{12–20}$$

The coefficient f_c depends on the material and the bearing type. For ordinary bearing steels such as SAE 52100 with mineral-oil lubrication, f_c can be evaluated by using tables 12–I and 12–II.

Deviations From the Weibull Distribution

Until recently the analysis of bearing-fatigue data was based on the primary importance of two lives, the L_{10} and L_{50} (the lives at failure probabilities of 10 and 50 percent). As previously stated, the Weibull distribution (eq. (12–5)) predicts the life dispersion of bearings within the failure-probability range from 10 to 50 percent with satisfactory accuracy. Catalog ratings of bearings are based on the L_{10} and L_{50} lives.

Requirements for high-reliability mechanisms in space vehicles and other applications have made it necessary to investigate life dispersion at very low probabilities of failure. Bearing-fatigue data are, for the most part, taken from relatively small samples, so that the reliability cannot be determined accurately.

A true fit with the Weibull distribution would imply a zero minimum life, and knowing whether such a true fit exists over the entire range of failure probabilities from 0 to 100 percent is important.

Tallian (ref. 6) analyzed a composite sample of 2500 rolling-element bearings and concluded that a good fit was obtained in the failure probability region between 10 and 60 percent. Outside this region, experimental life is longer than the Weibull prediction. In the early failure region, bearings were found to behave as shown in figure 12–1.

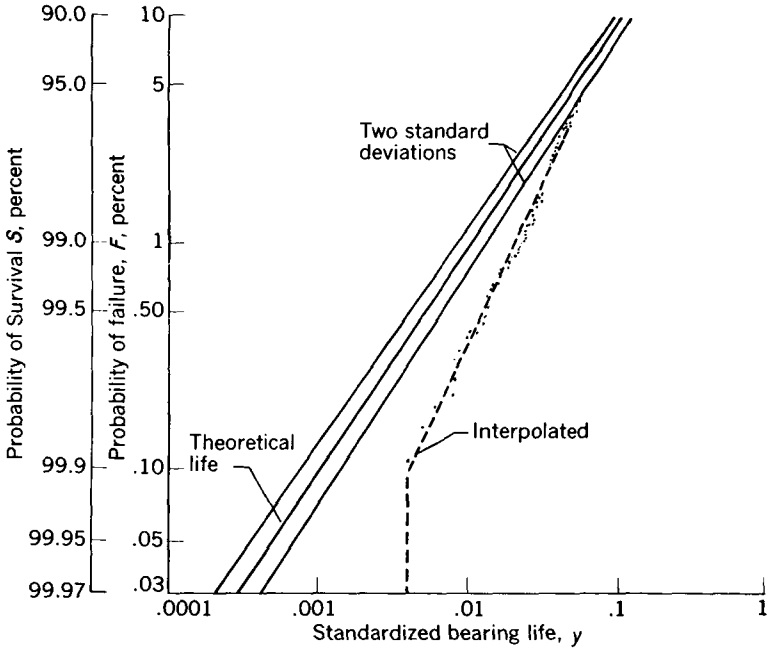

FIGURE 12–1.—Life distribution in early failure region. (From ref. 6.)

TABLE 12–I.—CONVENTIONAL BEARING TYPES [a]

[Units in kg and mm.]

Function	Point contact of ball bearings	Line contact of roller bearings
C	$f_c f_a i^{0.7} z^{2/3} D^{1.8}$	$f_c f_a i^{7/9} z^{3/4} D^{29/27} l_{a,i}^{7/9}$
f_c	$g_c f_1 f_2 \left(\frac{2r_i}{2r_i - D}\right)^{0.41}$	$g_c f_1 f_2$
g_c	$\left[1+\left(\frac{C_i}{C_o}\right)^{10/3}\right]^{-0.3}$	$\left[1+\left(\frac{C_i}{C_o}\right)^{9/2}\right]^{-2/9}$
C_i/C_o	$f_3 \left(\frac{r_i}{r_o}\frac{2r_o - D}{2r_i - D}\right)^{0.41}$	$f_3 \left(\frac{l_{a,i}}{l_{a,o}}\right)^{7/9}$

	Radial	Thrust		Radial	Thrust	
		$\alpha \neq 90°$	$\alpha = 90°$		$\alpha \neq 90°$	$\alpha = 90°$
γ	$\frac{D \cos \alpha}{d_m}$		$\frac{D}{d_m}$	$\frac{D \cos \alpha}{d_m}$		$\frac{D}{d_m}$
f_a	$(\cos \alpha)^{0.7}$	$(\cos \alpha)^{0.7} \tan \alpha$	1	$(\cos \alpha)^{7/9}$	$(\cos \alpha)^{7/9} \tan \alpha$	1
f_1	3. 7–4. 1	6–10		18–25	36–60	
f_2	$\frac{\gamma^{0.3}(1-\gamma)^{1.39}}{(1+\gamma)^{1/3}}$		$\gamma^{0.3}$	$\frac{\gamma^{2/9}(1-\gamma)^{29/27}}{(1+\gamma)^{1/3}}$		$\gamma^{2/9}$
f_3	$104 f_4$	f_4	1	$1.14 f_4$	f_4	1
f_4	$\left(\frac{1-\gamma}{1+\gamma}\right)^{1.72}$			$\left(\frac{1-\gamma}{1+\gamma}\right)^{38/37}$		

[a] From refs. 1 and 2.

TABLE 12–II.—POINT AND LINE CONTACT OF ROLLER BEARINGS [a]

$[C = C_i[1 + (C_i/C_o)^4]^{1/4}$; units in kg and mm.]

Function	Radial bearing	Thrust bearing		Radial bearing	Thrust bearing	
		$\alpha \neq 90°$	$\alpha = 90°$		$\alpha \neq 90°$	$\alpha = 90°$
	Inner race			Outer race		
γ	$\frac{D \cos \alpha}{d_m}$		$\frac{D}{d_m}$	$\frac{D \cos \alpha}{d_m}$		$\frac{D}{d_m}$
	Line contact C_i			Point contact C_o		
C_i or C_o	$f_1 f_2 f_a i^{7/9} z^{3/4} D^{29/27} l^{7/9}_{a.t}$			$f_1 f_2 f_a \left(\frac{2R}{D} \frac{r_o}{r_o - R}\right)^{0.41} i^{0.7} z^{2/3} D^{1.8}$		
f_a	$(\cos \alpha)^{7/9}$	$(\cos \alpha)^{7/9} \tan \alpha$	1	$(\cos \alpha)^{0.7}$	$(\cos \alpha)^{0.7} \tan \alpha$	1
f_1	18–25	36–60		3. 5–3. 9	6–10	
f_2	$\frac{\gamma^{2/9}(1-\gamma)^{29/27}}{(1+\gamma)^{1/3}}$		$\gamma^{2/9}$	$\frac{\gamma^{0.3}(1+\gamma)^{1.39}}{(1-\gamma)^{1/3}}$		$\gamma^{0.3}$

	Point contact C_i			Line contact C_o		
C_i or C_o	$f_1 f_2 f_a \left(\frac{2R}{D}\frac{r_i}{r_i-R}\right)^{0.41} i^{0.7} z^{2/3} D^{1.8}$			$f_1 f_2 f_a i^{7/9} z^{3/4} D^{29/27} l_{a,e}^{7/9}$		
f_a	$(\cos\alpha)^{0.7}$	$(\cos\alpha)^{0.7}\tan\alpha$	1	$(\cos\alpha)^{7/9}$	$(\cos\alpha)^{7/9}\tan\alpha$	1
f_1	3. 7–4. 1	6–10		15–22	36–60	
f_2	$\frac{\gamma^{0.3}(1-\gamma)^{1.39}}{(1+\gamma)^{1/3}}$		$\gamma^{0.3}$	$\frac{\gamma^{2/9}(1+\gamma)^{29/27}}{(1-\gamma)^{1/3}}$		$\gamma^{2/9}$

[a] From refs. 1 and 2.

The following table provides expressions for excess life in the early failure region:

Probability of survival, S, percent	Standardized theoretical life, y_T	Standardized life, y_T+y_E	Assumed behavior of points in figure 12–1
$S \geq 99.9$	$y_T \leq 0.001$	$y_T+y_E=0.004$	Points approach vertical asymptote
$99.9>S \geq 95$	$0.001<y_T<0.05$	$\ln (y_T+y_E) = 0.690 \ln 0.328y_T$	Points fit sloping interpolated straight line in Weibull plot
$95>S>40$	$0.05<y_T<0.9$	$y_E=0.013$	Points deviate from theoretical Weibull line by constant excess life

In the previous table, taken from reference 6, y_T represents the theoretical standardized life as obtained from reference 7, and y_E is the excess standardized life. The standardized life y is

$$y=\left(\frac{L}{A}\right)^e \tag{12–21}$$

In terms of the standardized life, equation (12–5) is written

$$S=\exp(-y) \tag{12–22}$$

When data are reduced, y is calculated from the following equation:

$$y=\left(\frac{L}{L_{50}}\right)^e \ln 2 \tag{12–23}$$

The expected life at very low probabilities of failure can be calculated with equation (12–23) to obtain y_T and the expressions given in the previous table for the sum of y_T and y_E. The sum of y_T and y_E at a specific survival probability gives the expected life.

OPERATING VARIABLES

Limitations of the Capacity Formulas

The capacity formulas for various types of bearings given by equations (12–14) to (12–20) are valid only for bearings of conventional steel lubricated with mineral oils when they are operated at nominal speeds. Since the development of the Lundberg-Palmgren capacity

formulas, many bearing applications exist in which rolling bearings are required to operate under extreme conditions of speed and temperature with a variety of lubricants and lubrication techniques. These operating conditions have made the development of new bearing materials necessary. In order to design bearing systems intelligently, the effects of bearing materials and lubricants, as well as speed and temperature, on fatigue life and load capacity have been investigated. The effects of various processing and operating variables will be discussed.

Among the processing variables that will be discussed are material composition, melting technique, hardness, fiber orientation, and contact angle. The operating variables to be discussed are load, speed, lubricant type (base stock), which includes dry-powder lubricants, lubricant viscosity, and temperature. Each of these processing and operating variables has an effect on fatigue. This effect must be known in order to design the best bearing-lubricant combination for a given set of operating conditions and to predict accurately its performance under fatigue conditions. Obtaining rolling fatigue data is expensive because many bearings must be tested so that the scatter in life can be treated statistically. The cost factor plus the urgent need for rolling-element-bearing fatigue data has stimulated the development of several bench-type fatigue testers. These testers obtain fatigue data quickly and economically with easily fabricated specimens such as balls or cylindrical rods. Many of the data reported herein were obtained on bench-type fatigue testers, which produce fatigue failures similar to those obtained in full-scale bearings at a reduction in time and cost.

Load

All experimental evidence obtained to date indicates that the inverse cubic relation between load and life, which was found to exist for point contact with conventional bearing materials with mineral-oil lubrication, is approximately true for other materials and lubricants and for bench-type fatigue testers used for studying the effects of different variables on rolling-element-bearing fatigue. Butler and Carter (ref. 8) report fatigue data obtained with 52100 steel balls in the fatigue spin rig. A description of this apparatus is given in reference 9. Balls of SAE 52100 steel were tested at maximum Hertz compressive stresses of 600,000, 675,000, and 750,000 psi in the fatigue spin rig. Weibull plots (given in ref. 8) were made for each of these three lots of ball specimens, and the results were plotted as the applied maximum Hertz stress against ball life at the 10-percent failure point (fig. 12–2). The slope of this line is 10.4. Normal full-scale bearing data produce a slope of approximately 9,

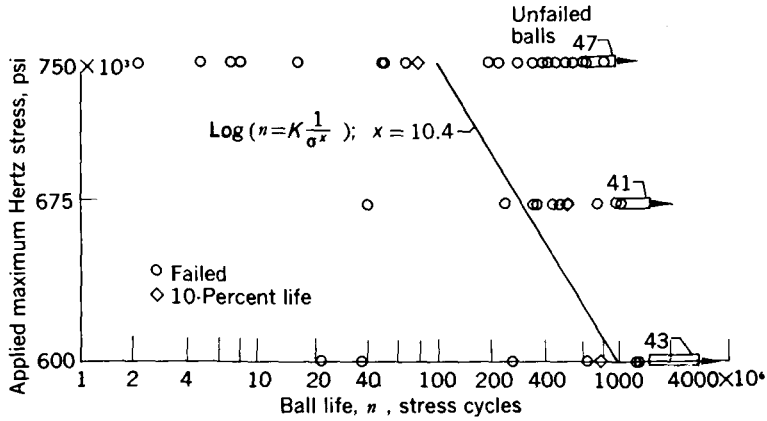

FIGURE 12–2.—Variation of ball life with applied stress for SAE 52100 balls. Room temperature; lubrication, SAE 10 mineral oil; fatigue spin rig. (From ref. 8.)

which corresponds to a load-life exponent of 3. These results indicate that the load- or stress-life relation in the fatigue spin rig approximates that which would be expected in full-scale bearings.

In reference 10 the relation of stress and life was investigated for two separate lots of crystallized glass ceramic balls using a five-ball fatigue tester. Crystallized glass ceramic balls taken from specimen lot A were run at maximum Hertz stresses of 265,000, 295,000, and 330,000 psi. Weibull plots (given in ref. 10) were made at each of these stress levels, and the 10- and 50-percent lives were determined from these Weibull plots. The plot of stress against life for specimen lot A is shown in figure 12–3(a). The stress-life exponent at the 10-percent level is 13.8 and at the 50-percent level is 11.6. For this particular material, the sensitivity of life to applied stress is slightly greater than that for steels. The results for specimen lot B, which were tested at maximum Hertz stresses of 265,000 and 330,000 psi, are shown in figure 12–3(b). Here the stress-life exponents are 10.6 at the 10-percent level and 10.5 at the 50-percent level. Again, these results indicate a slightly greater sensitivity of life to applied stress for this ceramic material than for steels.

For both the SAE 52100 steel and the ceramic material investigated, the load- or stress-life relation in two different types of bench fatigue testers approximate those for steels in full-scale bearing tests.

Barwell and Scott (ref. 11) used a four-ball fatigue tester to determine the load-life relation for five different lubricants. These lubricants were an aircraft mineral oil, a water glycol, a hydraulic petroleum oil, a chlorinated diphenyl, and a synthetic polyester.

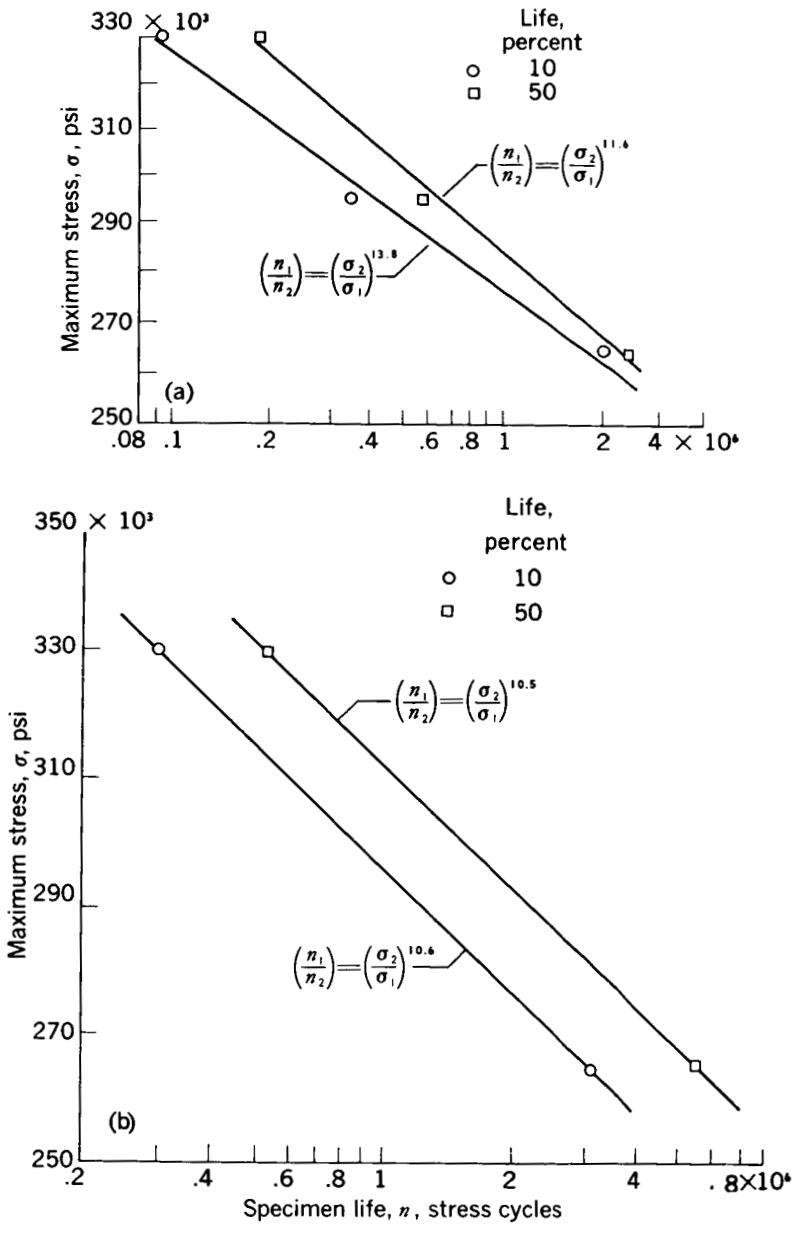

(a) Specimen lot A.

(b) Specimen lot B.

FIGURE 12-3.—Variation of ball life with applied stress for crystallized glass ceramic balls. Room temperature; synthetic diester lubricant; five-ball fatigue tester, contact angle, 40°. (From ref. 10)

The results of tests of standard ½-inch-diameter balls at maximum Hertz stresses of 660,000 to 950,000 psi are shown in figure 12–4. For all five lubricants, the inverse cubic load-life relation was found to be true. The life used in these tests was the average time to failure. Further load-life tests were conducted by Scott in reference 12 at 200° C (392° F) by use of a synthetic diester lubricant and T–1 tool-steel balls. These results are shown in table 12–III. Again, the inverse cubic relation was true.

Cordiano, Cochran, and Wolfe (ref. 13) report fatigue tests with 217-size angular-contact ball bearings that were flood lubricated with four oils. These oils included a mineral oil and three combustion-resistant hydraulic fluids: a phosphate ester, a phosphate ester base, and a water-glycol base. Bearings were run at thrust loads of 12,900 and 8600 pounds with the phosphate lubricants and at an additional load of 4300 pounds with the water-base glycol. The load-life relations obtained are plotted in figure 12–5. The exponents vary from 2.7 for the glycol to 4.2 for the phosphate ester.

Fatigue life varies inversely as the third to fourth power of the load for a variety of materials and lubricants (refs. 8 and 10 to 13). This relation apparently will exist for new bearing materials and lubricants.

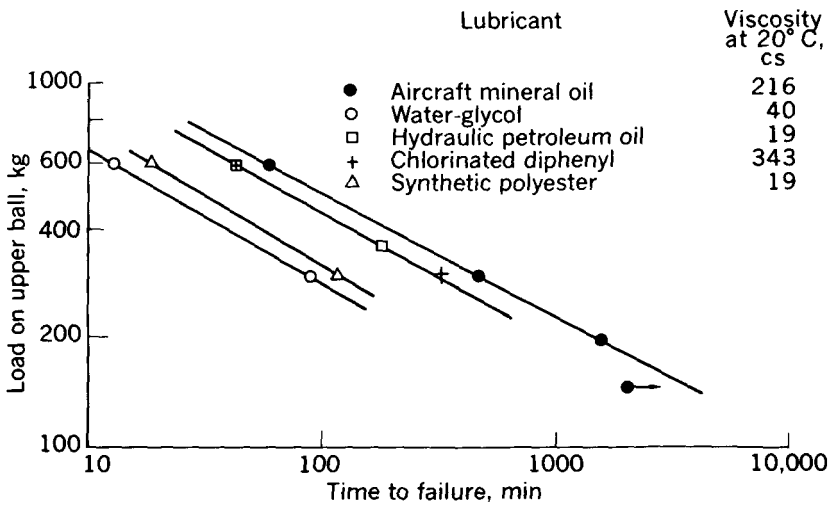

FIGURE 12–4.—Effect of load on time to failure for various lubricants. (From ref. 11.)

TABLE 12–III.—TEST RESULTS WITH DIESTER-TYPE SYNTHETIC LUBRICANT [a]

Test	Load on upper ball, kg	Temperature, ° C		Time to failure, min	Average time to failure, min	$t^{1/3}W$
		Start	Finish			
1	600	202	197	8	8.6	1229
2	600	202	202	7	8.6	1229
3	600	202	206	5	8.6	1229
4	600	201	200	8	8.6	1229
5	600	202	202	10	8.6	1229
6	600	198	195	11	8.6	1229
7	600	195	192	11	8.6	1229
8	500	203	202	13	14.3	1214
9	500	202	202	12	14.3	1214
10	500	202	203	13	14.3	1214
11	500	202	202	14	14.3	1214
12	500	201	197	17	14.3	1214
13	500	204	202	17	14.3	1214
14	400	202	201	32	31	1257
15	400	201	198	32	31	1257
16	400	203	202	24	31	1257
17	400	202	206	28	31	1257
18	400	201	201	24	31	1257
19	400	201	205	27	31	1257
20	400	205	198	36	31	1257
21	400	204	199	36	31	1257
22	400	202	202	40	31	1257

[a] From ref. 12.

Lubricant Base Stock

The need for lubricants with better oxidative and thermal stability has stimulated research on the synthesis of many synthetic compounds that offer promise as high-temperature lubricants. Rolling-element fatigue data are needed with these new lubricants, for new oils cannot be used with any confidence without some knowledge of their effect on the fatigue behavior of bearing steels.

In reference 11, fatigue tests with ½-inch-diameter balls were conducted with 26 different lubricants. The life results with five of these lubricants are shown in figure 12–4. Of these five oils, the aircraft mineral oil showed the best life and the water-based glycol showed the poorest life. Viscosity differences among these lubricants, however, make an unbiased comparison impossible since lubricant viscosity has a marked effect on fatigue life. The experiments of reference 11 were conducted at maximum Hertz stress levels up to 950,000 psi, where considerable plastic deformation occurs. This deformation makes the validity of extrapolating these data to lower stress levels questionable.

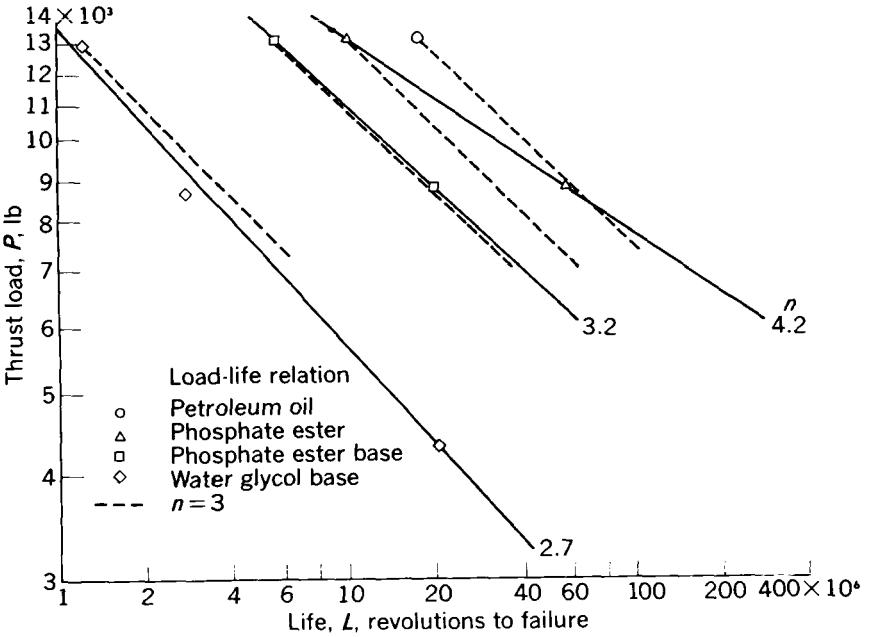

FIGURE 12–5.—Load-life relation of bearings operated in four hydraulic fluids; LP^n=constant. (From ref. 13.)

Table 12–IV shows data obtained with 13 of the lubricants tested in reference 11. Again, viscosity differences make unbiased comparisons

TABLE 12–IV.—VISCOSITY AND AVERAGE LIFE FOR DIFFERENT LUBRICANTS [a]

Type of lubricant	Viscosity at 20° C, cs	Average life, min
Aircraft mineral oil	216	59
Mineral-base hydraulic oil with additives	89	42
Hydraulic petroleum oil	19	40
Synthetic silicate ester	17	32
Nonflammable synthetic polyester	19	18
Phosphate ester	174	67. 5
Chlorinated diphenyl	343	40
Nonflammable water-base glycol	40	13
Polyalkalene glycol	16	11
Dimethyl siloxane	1. 6	58
Silicone	52	64
Tricresyl phosphate	97	48
Naphthenic-base oil	53	51

[a] From ref. 11.

difficult, but some general conclusions can be made. The mineral oils, which include the aircraft mineral oil, a hydraulic oil, and a naphthenic-base oil, appear to give good fatigue life. The nonflammable water glycol and the polyalkylene glycol appear to give the poorest fatigue results. Somewhat better are the synthetic polyester and the synthetic silicate. The (dimethyl) siloxane, despite its low viscosity, gave good life, and the silicone appeared to be one of the best lubricants. Closer control of viscosity among the various base stocks is necessary before more definitive conclusions can be drawn.

Fatigue lives of ½-inch-diameter test balls were determined at a maximum Hertz stress of 830,000 psi with two different greases in reference 12. These results are shown in table 12–V. The mineral-

TABLE 12–V.—AVERAGE TIME TO FAILURE FOR GREASES [a]

[Maximum Hertz stress, 830,000 psi; test temperature, 200° C.]

Lubricant	Average time to failure, min	Remarks
Lithium-base grease	93	Bearing surface and balls clean and bright
Experimental silicone grease containing chlorine	36	Balls dull with etched surface appearance

[a] From ref. 12.

oil lithium-base grease gave significantly better fatigue life than the experimental silicone grease that contained chlorines. These tests were conducted at 200° C (392° F).

Baughman (ref. 14) conducted fatigue tests using the rolling-contact fatigue tester. In this tester, the test specimen is a ½-inch-diameter cylindrical rod, which is stressed between two crowned cylinders, each 7.5 inches in diameter. Fatigue results with a synthetic diester (14.2 cs at 100° F), a mineral oil (10.2 cs at 100° F), and a methylphenyl silicone (10.8 cs at 100° F) are shown in figure 12–6. These results were obtained with M–1 tool steel at a maximum Hertz stress of 725,000 psi. Ten-percent fatigue lives for the silicone, mineral oil, and diester were 4.0, 2.2, and 1.1 million stress cycles, respectively. Figure 12–7 shows a plot of the log log of the 50-percent life plotted against the log of the viscosity at 80,000 psi for these three lubricants. Fatigue life appears to be related to the actual viscosity existing in the high-pressure region.

Experiments similar to those of reference 14 are reported in references 15 and 16. Five different base-stock lubricants, each with an atmospheric pressure viscosity of about 10 centistokes at 100° F were

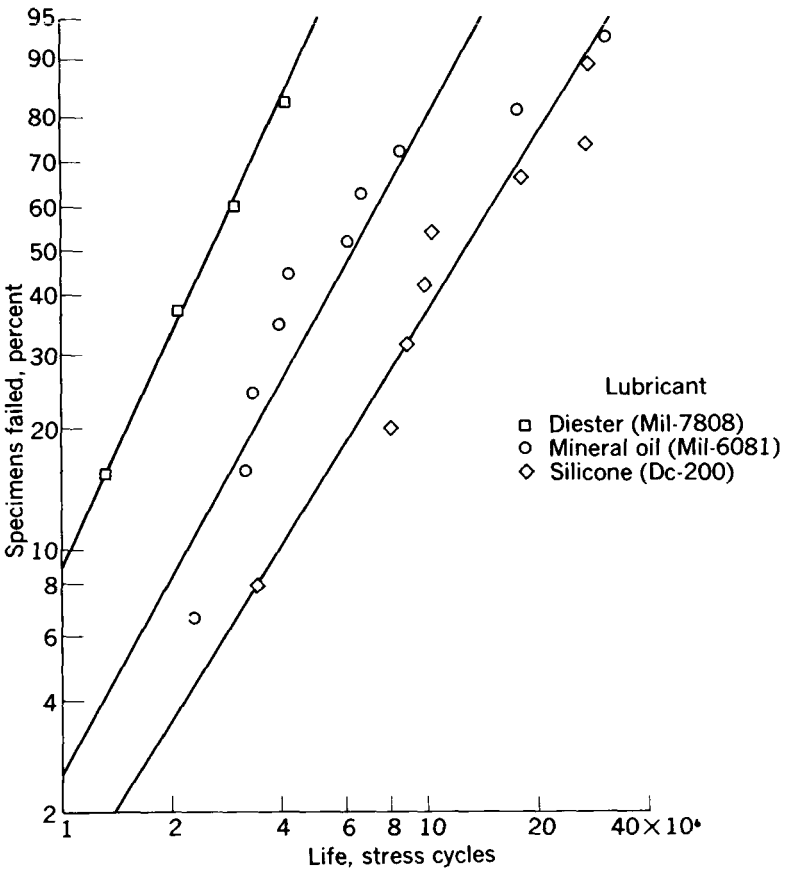

FIGURE 12–6.—Weibull plot of data from rolling-contact fatigue tester on M–1 tool steel when tested with three different lubricants. Maximum Hertz stress, 725,000 psi; room temperature. (From ref. 14.)

used in these experiments. AISI M–1 balls were tested at a maximum Hertz stress of 725,000 psi in the fatigue spin tester. Figure 12–8 shows the fatigue-life results. These data are summarized in table 12–VI. Again, as in reference 14, the silicone gave the best life, followed by the mineral oil, the polyalkylene glycol, the sebacate, and the dioctyl adipate.

Figure 12–9 shows the 10-percent-life data from figure 12–8 plotted against the pressure-viscosity coefficients for the five lubricants. The pressure-viscosity coefficient is defined as the slope of the curve of the log of absolute viscosity plotted against pressure. Since there is some curvature in each of these plots, the initial slope is used. The pressure viscosity is assumed to be given approximately by an equation of the following type:

$$\mu_p = \mu_o \times 10^{\beta p} \tag{12–24}$$

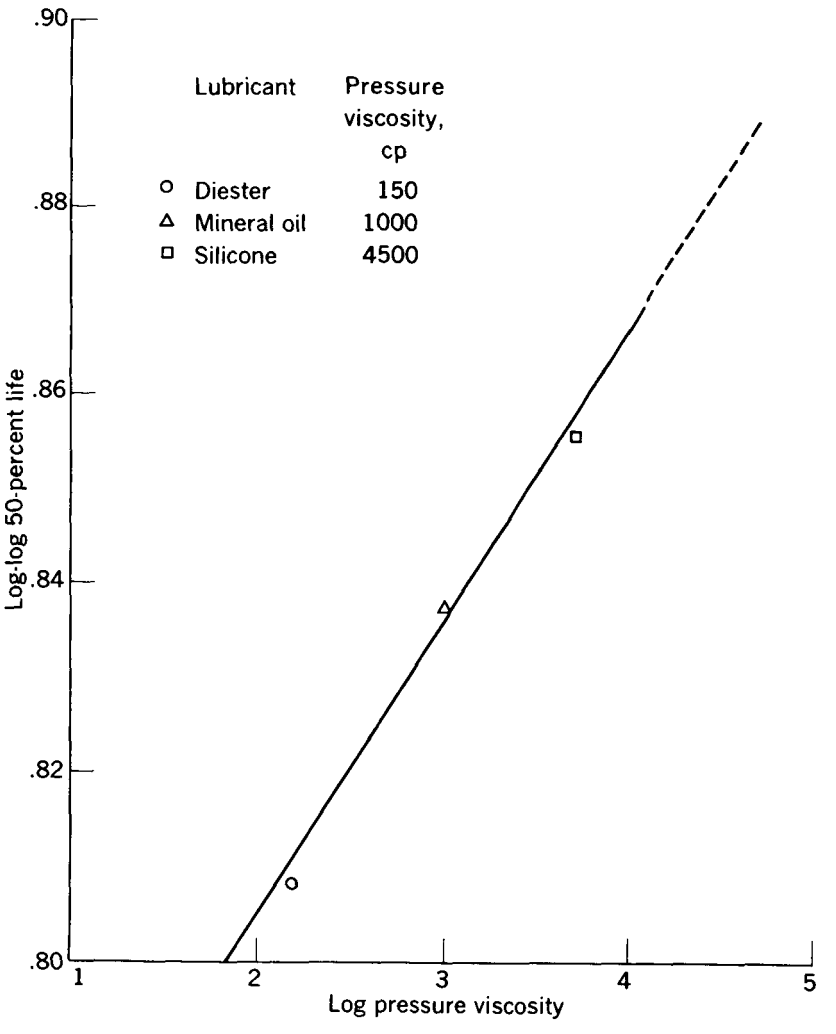

FIGURE 12–7.—Relation between lubricant viscosity at 80,000 psi and fatigue life of M–1 tool steel. Temperature, 210° F. (From ref. 14.)

Values of β shown in table 12–VI were obtained from reference 17 for all but the adipate oil. The curve of figure 12–9 indicates that fatigue life increases with increasing pressure-viscosity coefficient. Since the initial viscosities of these five lubricants were all approximately 10 centistokes, the actual viscosities under pressure would be expected to vary as the pressure-viscosity coefficient. The good correlation of figure 12–9 may indicate that actual viscosity is a variable of prime importance in determining fatigue life.

TABLE 12–VI.—FATIGUE LIVES OF ½-INCH AISI M–1 TOOL-STEEL BALLS LUBRICATED WITH VARIOUS BASE-STOCK FLUIDS [a]

[Test temperature, 100° F; maximum Hertz compressive stress, 725,000 psi.]

Lubricant	Pressure-viscosity coefficient, β, 1/psi	Specimens tested	Failures	Runouts	10-percent failure life, stress cycles	50-percent failure life, stress cycles
Methyl silicone	8.35×10^{-5}	26	5	21	106×10^{6}	$17,000\times10^{6}$ [b]
Paraffinic mineral oil	5.38	28	14	14	18	660
Glycol	3.28	16	11	5	7.6	167
Sebacate	2.52	22	15	7	5.2	200
Adipate	Unavailable	26	12	14	2.4	1,000

[a] From ref. 15.
[b] Extrapolated.

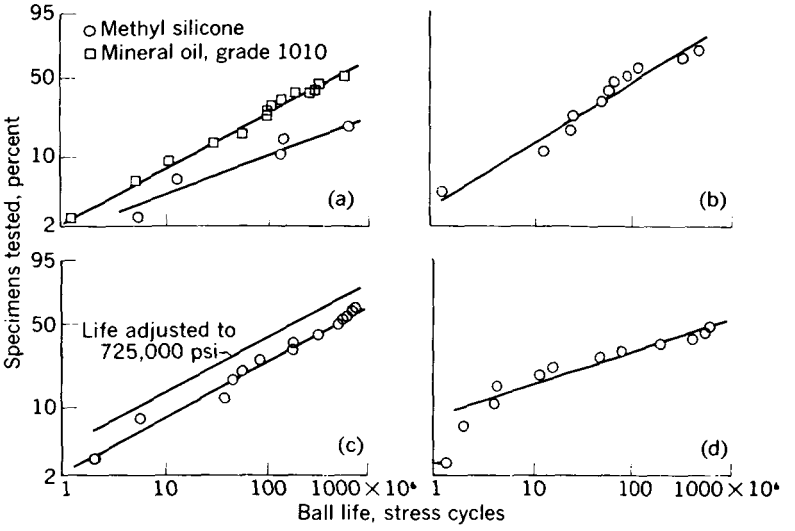

(a) Mineral oil and silicone.
(b) Polyalkylene glycol.
(c) Sebacate. Maximum Hertz stress, 650,000 psi.
(d) Adipate.

FIGURE 12–8.—Fatigue life of AISI M–1 tool-steel balls with various base stock lubricants. Test temperature, 100° F; maximum Hertz stress, 725,000 psi; fatigue spin tester. (From ref. 16.)

Fatigue tests with full-scale 217-size angular-contact ball bearings, lubricated with three combustion-resistant hydraulic fluids and a mineral oil, are reported in reference 18. These bearings were run at 2150 rpm, 12,900-pound thrust load, and flood lubricated with the oil outlet temperature adjusted to 150° to 160° F. Viscosities of the test oils are given in table 12–VII. The life results obtained are summarized in table 12–VIII. Comparison of modal lives with that of mineral oil shows that life with the phosphate ester is 58 percent,

TABLE 12–VII.—LUBRICANTS USED IN FATIGUE TESTS OF ANGULAR-CONTACT BALL BEARINGS [a]

Lubricant	Viscosity, Saybolts Seconds Universal at—	
	100° F	210° F
Petroleum oil	182	44. 3
Phosphate ester	214	42. 3
Phosphate ester base	231. 4	44. 2
Water-glycol base	280. 2	69. 5

[a] From ref. 18.

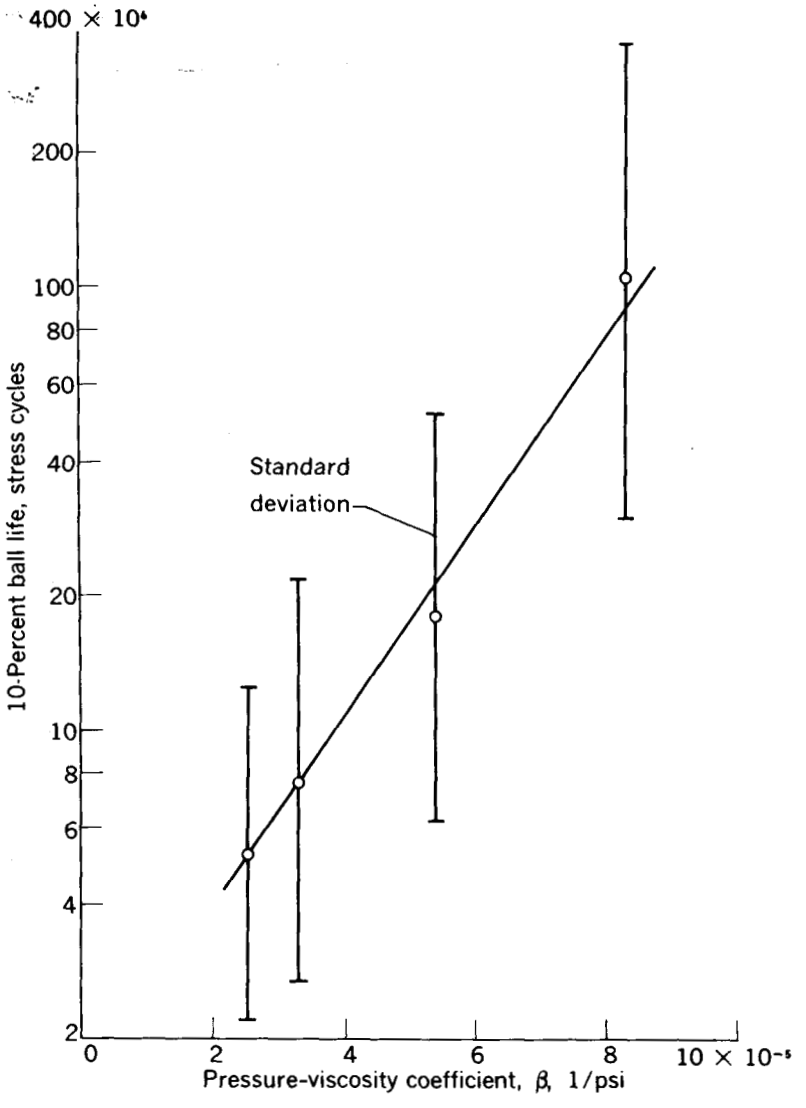

FIGURE 12-9.—Life of AISI M-1 tool-steel ball as function of pressure-viscosity coefficient. Test temperature, 100° F; maximum Hertz stress, 725,000 psi; fatigue spin tester. (From ref. 16.)

life with the phosphate ester base is 31 percent, and life with the water-glycol base is only 6 percent.

Reference 13 presents additional fatigue data obtained with the lubricants used in reference 18 at 200° F and at various loads. Fatigue life at 200° F was slightly lower than at 150° F for both the phosphate ester and the phosphate ester base lubricants. Attempts were made in reference 13 to determine the causes for the life differences

TABLE 12–VIII.—MODAL AND MEDIAN LIVES OF ANGULAR-CONTACT BALL BEARINGS OPERATED IN PETROLEUM OIL AND THREE COMBUSTION-RESISTANT FLUIDS[a]

Lubricant	Life, revolutions		Relative life	
	Modal	Median	Modal	Median
Petroleum oil	18.6×10^6	24.9×10^6	1.00	1.00
Phosphate ester	10.7	13.5	.58	.54
Phosphate ester base	5.8	6.8	.31	.27
Water-glycol base	1.2	1.3	.06	.05

[a] From ref. 18.

shown by the various fluids. Pressure-viscosity relations for the oils were determined at three temperatures and at pressures up to 50,000 psi by use of a rolling-ball viscometer to determine whether a correlalation existed between pressure viscosity and fatigue life. The results are shown in figure 12–10. The rise in viscosity with pressure for the phosphate ester base and phosphate ester fluids is similar to that for the petroleum oil but at a greater rate. In contrast, the relatively flat pressure-viscosity curves for the water-glycol-base fluid indicate that the relatively low viscosity of this fluid at high pressures may be a contributing factor to the poor fatigue life with this fluid. There is no correlation between pressure-viscosity coefficient and fatigue life, however, since the coefficients for the other three lubricants are in reverse to the fatigue lives. Thus, the data from bench tests in references 15 and 16 indicate that a correlation exists between pressure-viscosity coefficient and fatigue life, and the bearing data of reference 13 indicate that it does not. More work is necessary to establish the degree to which pressure-viscosity and other rheological properties affect fatigue life.

Rounds (ref. 19) has conducted an extensive investigation of the fatigue properties of many lubricants by use of a four-ball-type apparatus and ½-inch-diameter SAE 51100 test balls. Tests were conducted at a maximum Hertz stress of 1.2×10^6 psi, 1582 rpm, and 200° F. The extrapolation of these data to the lower stress levels that exist in bearings is questionable because of the extent of plastic deformation that occurs at Hertz stresses in the region of 10^6 psi. Some 60 base oils were selected from 11 different chemical classes that include mineral oils and most of the commonly used synthetic fluids. Figure 12–11 shows some fatigue-life data plotted against viscosity for mineral oils and several polyphenyl ethers. Figure 12–12 shows similar data obtained with a group of esters. Fatigue lives reported are relative to the life obtained with an Mil–L–7808C oil. All the ethers and all the esters with the exception of two high-viscosity diabasic acid

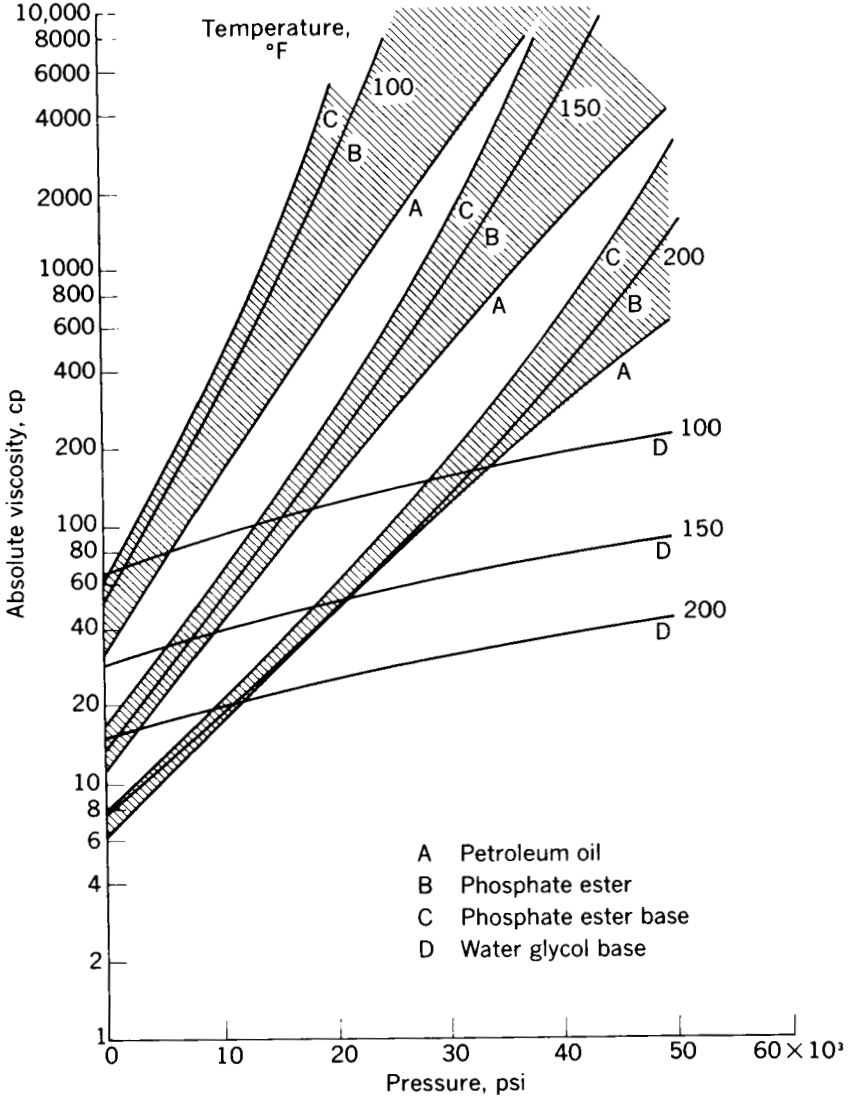

FIGURE 12–10.—Pressure-viscosity isotherms of four hydraulic fluids. (From ref. 13.)

esters showed better fatigue lives than the mineral oils when compared on the basis of similar viscosities.

Figure 12–13 shows fatigue data obtained with alcohols, polyglycols, and acids. The fatigue performance of the fatty acids is very poor, and the higher viscosity polyglycols show poor fatigue life. The fatigue performance of silicones is shown in figure 12–14. In

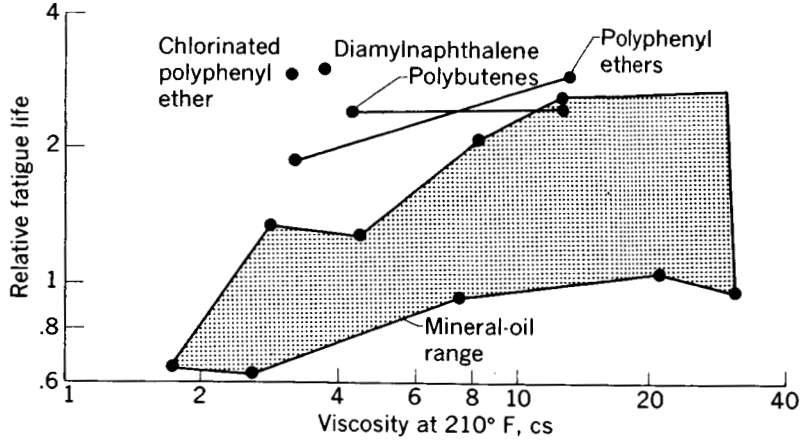

FIGURE 12–11.—Effect of polyphenyl ether and hydrocarbon lubricants on fatigue life. (From ref. 19.)

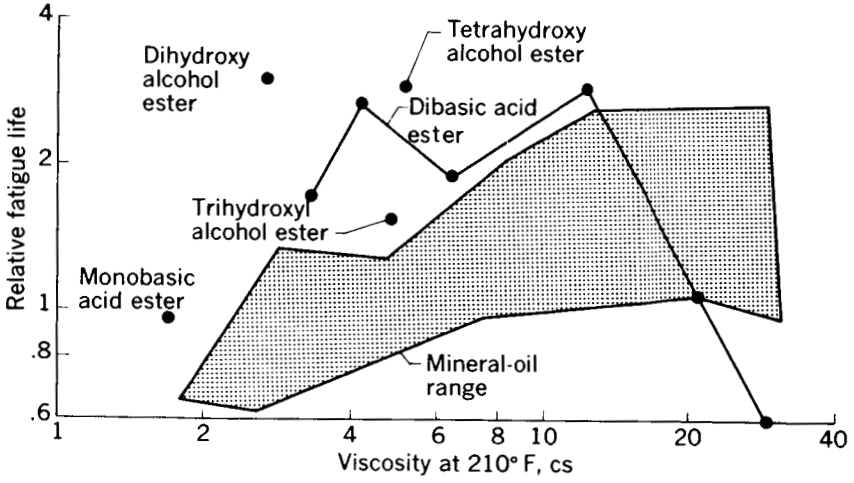

FIGURE 12–12.—Effect of ester lubricants on fatigue life. (From ref. 19.)

general, the performance of the silicones is good although the performance of the methylphenyl silicone with polyglycol chains is extremely poor. Most fatigue data obtained with silicone oils, such as those of references 11 and 15, indicate that silicones give superior fatigue performance.

Data obtained with phosphate esters and halogenated hydrocarbons are shown in figure 12–15. The phosphate esters gave good fatigue life but the other lubricants in this group gave poor fatigue life. Note the contrast in relative fatigue performance of the phos-

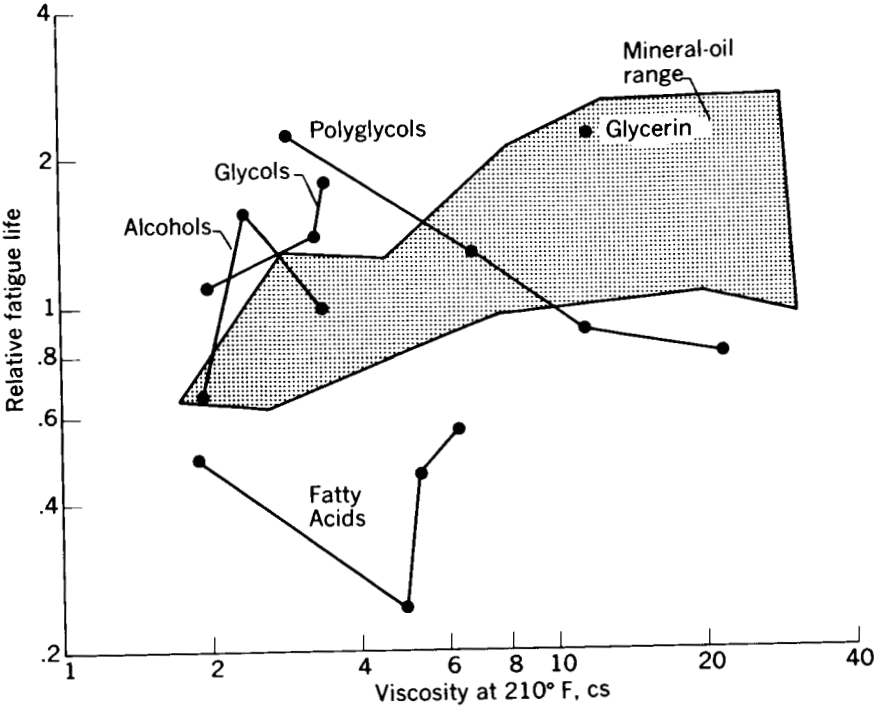

FIGURE 12–13.—Effect of alcohol, polyglycol, and acid lubricants on fatigue life. (From ref. 19.)

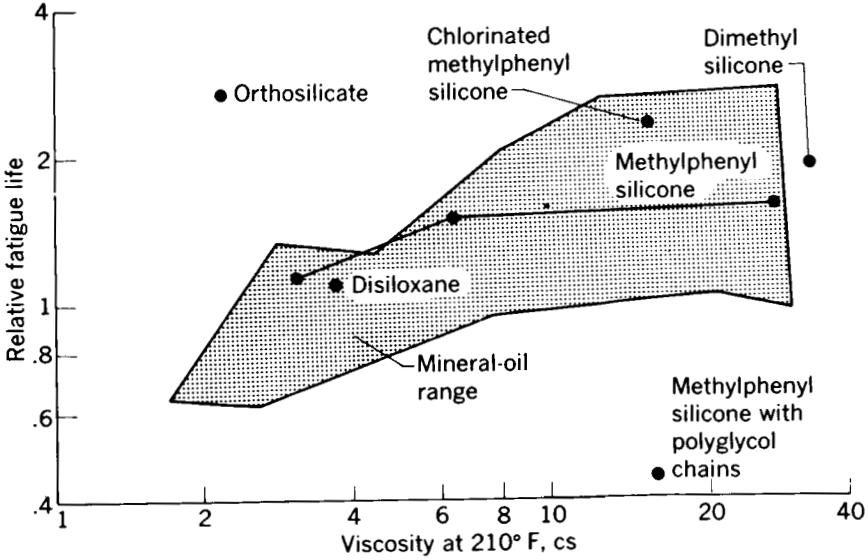

FIGURE 12–14.—Effect of silicone and related fluid lubricants on fatigue life (From ref. 19.)

phate ester in these tests and in the full-scale bearing tests of reference 13, where the phosphate ester gave poorer fatigue life than a mineral oil.

Among the mineral oils investigated in reference 19, the naphthenic oils showed consistently better fatigue life than paraffinic oils. These data are shown in figure 12–16.

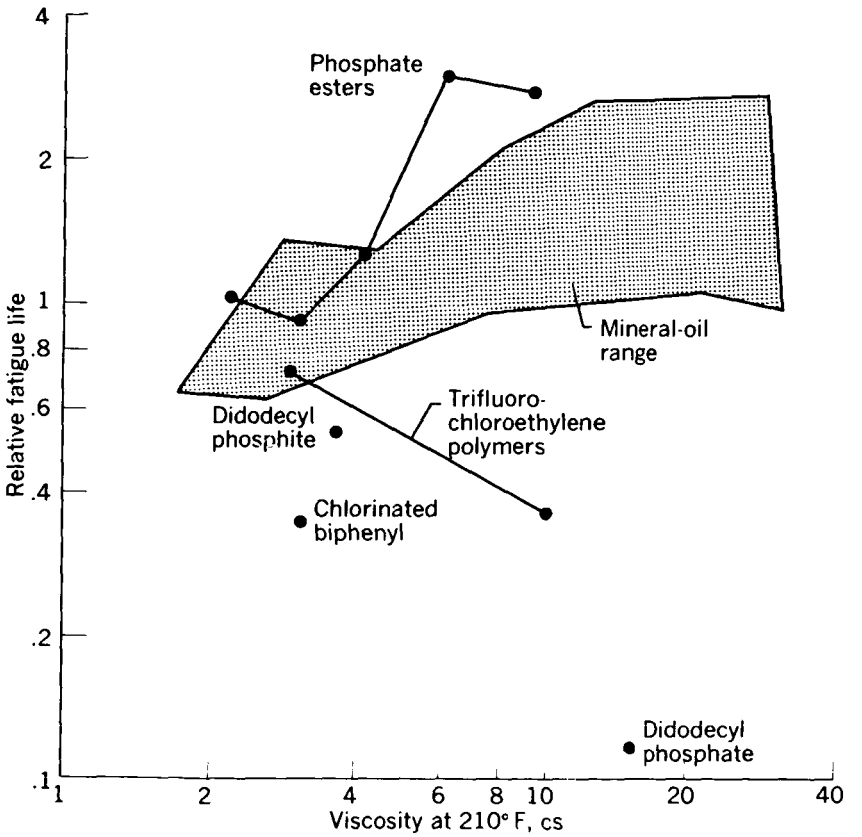

FIGURE 12–15.—Effect of phosphate ester and halogenated hydrocarbon lubricants on fatigue life. (From ref. 19.)

An analysis of the data of reference 19 showed that several factors significantly affect fatigue life. The effects of viscosity will be discussed more fully later. One factor of importance appears to be the physical shape of the average molecule in the lubricant. Fa-

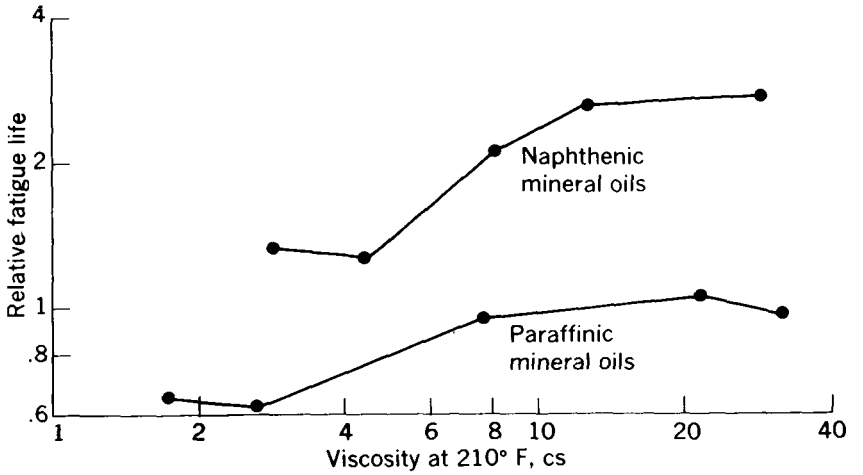

FIGURE 12–16.—Effect of mineral-oil lubricants on fatigue life. (From ref. 19.)

tigue life seems to be affected by the number of aromatic or naphthenic rings in the molecule as shown in the following table:

Base oil type	Average number of rings per molecule	Relative fatigue life at 6-cs viscosity
Fatty acids	0	0. 54
Paraffinic mineral oils	1–2	. 87
Naphthenic mineral oils	2–3	1. 62
Polyphenyl ethers	4–5	2. 32

The presence of ring structures in other classes of fluids is apparently beneficial to fatigue life. Phosphate esters with aryl groups gave better life than those with alkyl groups. The ring structure in phthalic acid may account for the better fatigue life with di(2-ethylhexyl)phthalate than with di(2-ethylhexyl)sebacate. In the alcohol series, the ring compound cyclohexane gave better life than the straight-chain alcohols. Except for the chlorinated biphenyl and a substituted silicone, all fluids containing ring structures gave longer lives than the paraffinic oils and many were superior to the naphthenic mineral oils. Ring structures tend to make the molecule more compact, which suggests that compactness of the molecule is beneficial to fatigue life.

Increasing the polarity or reactivity of the molecule appears to be detrimental to fatigue life. Changing the hydroxyl group in oleyl

alcohol to the more polar carboxyl group in oleic acid decreased the relative life from 1.01 to 0.23; with the phosphorous compounds, life decreased progressively in going from tri(2-ethylhexyl)phosphate to the strongly acid diodecyl phosphate. Esters, in which the polar carboxyl and hydroxyl groups of the reacted acid and alcohol have been effectively neutralized, generally gave longer lives than did either of the reactants used to make the ester. Examples include isodecyl pelargonate, which was superior to *n*-decyl alcohol and pelargonic acid, and dipropylene glycol dipelargonate, which was superior to dipropylene glycol and pelargonic acid.

An exception to this rule appears to be the chlorinated compounds. The addition of reactive chlorine compounds to mineral oil reduced life but chlorinating either the polyphenyl ether or the methylphenyl silicone increased life.

Scott (ref. 20) made a more extensive study of the effect of additives on lubricant fatigue life. A four-ball tester was used and tests were run at a maximum Hertz stress of 950,000 psi. A paraffinic mineral oil was used as a reference fluid, and several additives of the extreme-pressure type were added to the paraffin oil, first in normal percentages, and then in greater than normal percentages. Table 12–IX sum-

TABLE 12–IX.—BALL FATIGUE LIVES FOR PARAFFINIC MINERAL-OIL LUBRICANT AND VARIOUS ADDITIVES [a]

[With 600-kg load and normal additive concentrations.]

Lubricant	Additive	Average time to failure, min
Paraffinic mineral oil	None	41
	1 percent dibutyl phosphite	42
	1 percent tricresyl phosphate	40
	1 percent chlorinated wax	35
	0.36 percent elemental sulfur	58
	0.36 percent elemental sulfur +10 percent lead naphthenate	50
	1 percent graphite	109
	1 percent molybdenum disulfide	79

[a] From ref. 20.

marizes the results obtained with conventional amounts of additives. None of the five extreme-pressure additives reduced fatigue life any significant amount from that obtained with the base oil. The addition of 1 percent graphite or 1 percent molybdenum disulfide improved fatigue life. These results will be discussed fully in the section on solid lubricants.

The addition of greater than normal percentages of chlorinated wax and dibutyl phosphite produced a sharp reduction in fatigue life as shown in table 12–X. The addition of 10 percent tricresyl phosphate,

TABLE 12–X.—BALL FATIGUE LIVES WITH LUBRICANTS HAVING GREATER THAN NORMAL ADDITIVE CONCENTRATIONS[a]

Lubricant	Additive	Average time to failure, min
Paraffinic mineral oil	None	41
	5 percent chlorinated wax	14
	10 percent chlorinated wax	5½
	10 percent dibutyl phosphite	8
	10 percent tricresyl phosphate	43
100-percent tricresyl phosphate	None	48

[a] From ref. 20.

however, did not reduce fatigue life, and fatigue life with 100 percent tricresyl phosphate was comparable to that with the paraffin oil. Therefore, in lubrication systems where a single lubricant is used to lubricate both bearings and gears, tricresyl phosphate appears to be the most suitable extreme-pressure additive. It is effective as a gear additive and will not reduce bearing fatigue life.

Effect of Water in Lubricant

Some very interesting experiments to determine the effect of water content in the lubricant on rolling fatigue were conducted in reference 21. Tests were conducted in a four-ball-type apparatus at 1500 rpm using both standard 1.5-percent-chromium steel balls and also 12-percent-chromium stainless-steel balls. The maximum Hertz stress level was about 1×10^6 psi. Five lubricants, which are widely used in the lubrication of ball bearings, were chosen for testing. A description of the test oils is given in table 12–XI. The water content of each lubricant was varied over a wide range by a series of four treatments:

(1) Dry—The oil was dried over metallic sodium for 24 hours before test.

(2) As received.

(3) Saturated with water before test—A sample of the oil was thoroughly shaken with an equal volume of water and then allowed to settle 24 hours. The oil was carefully decanted for the test.

(4) Supersaturated with water during test—To ensure excess water

TABLE 12–XI.—LUBRICANTS USED IN BALL FATIGUE TESTS [a]

Lubricant	Type, composition, and description of lubricant	Viscosity at 20° C, cs
A	Compounded oil containing 94 percent mineral oil and 6 percent refined rape-seed oil	2200
B	Compounded oil containing 90 percent mineral oil and 10 percent blown rape-seed oil	600
C	Refined mineral oil containing 0.5 percent tricresyl phosphate as antiwear additive. Antioxidant, anticorrosive, and antifoam additives may be present	75
D	An oil containing extreme-pressure additives	90
E	Mineral oil formulated for use in aircraft engines	200

[a] From ref. 21.

during test, a small quantity (1 ml) of water was added to the lubricant bath immediately after the start of each test.

The moisture content of each oil in each condition is shown in table 12–XII. Moisture contents varied from essentially 0 to

TABLE 12–XII.—WATER CONTENT OF OILS AFTER VARIOUS TREATMENTS [a]

Lubricant	Water content, percent by weight			
	Lubricant condition			
	(1)	(2)	(3)	(4)
A	0.01	0.027	0.15	6.86
B	0	.022	.034	3.83
C	0	.052	.060	6.80
D	----	0	0	5.63
E	0	.033	-------	5.11

[a] From ref. 21.

almost 7 percent by weight. A summary of the fatigue lives of commercial EN 31 steel balls obtained with the various lubricants is presented in table 12–XIII. A considerable reduction in fatigue life occurs with all the oils with increasing water content as shown in figure 12–17. The fatigue results with the stainless-steel balls lubricated with three of the oils are summarized in table 12–XIV. The stainless-steel balls showed no reduction in fatigue life with increasing

TABLE 12–XIII.—FATIGUE LIFE WITH COMMERCIAL STEEL BALLS [a]

Lubricant	Mean fatigue life, min			
	Lubricant condition			
	(1)	(2)	(3)	(4)
A	157	124	123	61
B	123	110	102	54
C	82	62	54	36
D	-------	53	47	16
E	107	60	-------	34

[a] From ref. 21.

water content. The fatigue life of the stainless-steel balls, however, was no better than the fatigue life of the EN 31 balls with supersaturated oils. The fatigue life was, in fact, much shorter with lubricant A.

The reduction in fatigue life of the EN 31 balls with increasing lubricant-water content together with the lack of this effect with the stainless-steel balls suggests that corrosion fatigue may be an important factor in causing rolling fatigue. With oils A, B, and E, the track surface on EN 31 balls was bright and failure occurred as a single small pit, which was independent of the water content. Oils C and D, which contained reactive additives, produced stained or

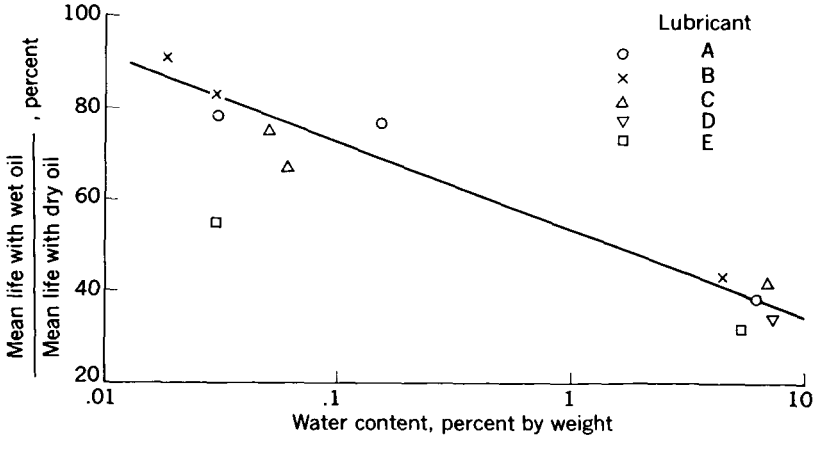

FIGURE 12–17.—Effect of water content of lubricant on mean life of balls. (See table 12–XI for definition of lubricant.) (From ref. 21.)

TABLE 12–XIV.—TESTS WITH STAINLESS-STEEL BALLS [a]

Lubricant	Lubricant condition	Mean life, min	Standard deviation, min	Coefficient of variation, percent	Number of tests
A	(1)	34	8	24	5
	(2)	35	10	29	10
	(3)	------	------	------	------
	(4)	31	7. 5	24	14
D	(1)	------	------	------	------
	(2)	16	4	25	8
	(3)	------	------	------	------
	(4)	16	5	31	5
E	(1)	33	14	42	7
	(2)	32	5. 5	17	12
	(3)	------	------	------	------
	(4)	33	1. 5	5	6

[a] From ref. 21.

dull tracks, and supersaturation of these oils produced roughening of the surface. Almost continuous pitting appeared under these conditions. The stainless-steel balls had generally bright surfaces and no differences were observed with oils with different water contents.

Effect of additives in lubricants containing water.—In an attempt to extend fatigue life of lubricants containing water, Grunberg and Scott (ref. 22) conducted ball fatigue tests with various additives added to the base oils. Two oils were chosen for these tests, which were conducted under the same conditions of speed and stress as those of reference 21. A description of these oils is given in table 12–XV. Five

TABLE 12–XV.—BASE LUBRICANTS USED IN BALL FATIGUE TESTS [a]

Code letter	Lubricant	Viscosity, cs		
		At 25° C	At 50° C	At 60° C
F	Blend of two high-viscosity index components from a Venezuelan source	636	134	82
G	Distillate from a Venezuelan source	14. 4	6. 5	5. 1

[a] From ref. 22.

different conditions of water content were used. Conditions (1), (2), and (3) were the same as those in reference 21. Condition (4) was supersaturated with ½ milliliter of water added before test, and condi-

tion (5) was the same as condition (4) *in reference* 21 (1 ml of water added before test). The fatigue lives obtained with the two lubricants in five conditions of saturation without additives are shown in table 12–XVI.

TABLE 12–XVI.—EFFECT OF WATER CONTENT ON FATIGUE LIFE [a]

Lubricant	Mean fatigue life, min				
	Lubricant condition				
	(1)	(2)	(3)	(4)	(5)
F	121	63	55	26	21
G	65	48	44	10	6

[a] From ref. 22.

The following additives were used:

(1) Isoamyl alcohol, 3 percent
(2) Oleic acid, 2 percent, a fatty acid
(3) Triethanolamine, 2 percent, an amine
(4) Imidazoline derivative, 2 percent, a dewatering agent
(5) Sarkosine derivative, 2 percent, a dewatering agent
(6) Phenoxy-acetic acid, 2 percent, a dewatering agent
(7) Sodium dodecane sulfonate, 0.5 percent, a typical detergent
(8) 0.5-Percent sodium nitrite plus 0.5-percent sodium benzoate, corrosion inhibitors

The fatigue results obtained with the base oils and the base oils with various additives are summarized in table 12–XVII. The addition of 3-percent isoamyl alcohol partially counteracted the deleterious effects of the presence of water in spite of the fact that the addition of the alcohol lowered the viscosity considerably.

Both oleic acid and triethanolamine lowered the fatigue life under conditions of water saturation (condition 3) and raised the fatigue life under conditions of high supersaturation. The data obtained with these two additives indicate that fatigue life is independent of water content. Of the three dewatering agents (imidazoline and sarkosine derivatives and phenoxy-acetic acid), only the imidazoline derivative was effective in improving fatigue life under all conditions tested. The sarkosine derivative and the phenoxy-acetic acid actually decreased fatigue life.

In reference 22, post-test examinations showed that the ball tracks were a brownish color under highly supersaturated conditions but were bright and polished when a surface active agent was added.

TABLE 12–XVII.—MEAN FATIGUE LIFE AS FUNCTION OF WATER CONTENT AND ADDITIVE CONTENT [a]

Lubricant	Additive	Mean fatigue life, min				
		Lubricant condition				
		(1)	(2)	(3)	(4)	(5)
Base oil F		121	63	55	26	21
	3 percent isoamyl alcohol	-----	----	93	33	---
	2 percent oleic acid	-----	----	33	----	32
	2 percent triethanolamine	-----	----	40	----	38
	2 percent imidazoline derivative	-----	----	70	----	37
	2 percent sarkosine derivative	-----	----	----	----	18
	2 percent phenoxyacetic acid	-----	----	----	----	17
	0.5 percent sodium benzoate and 0.5 percent sodium nitrite	-----	----	----	----	23
	0.5 percent sodium dodecane sulfonate	-----	----	----	----	20
Base oil G		65	48	44	10	6
	3 percent isoamyl alcohol	-----	----	50	34	----
	2 percent oleic acid	-----	----	27	----	23
	2 percent triethanolamine	-----	----	29	----	26
	2 percent imidazoline derivative	-----	----	50	----	17
	2 percent sarkosine derivative	-----	----	----	----	4
	2 percent phenoxyacetic acid	-----	----	----	----	8
	0.5 percent sodium benzoate and 0.5 percent sodium nitrite	-----	----	----	----	7
	0.5 percent sodium dodecane sulfonate	-----	----	----	----	4

[a] From ref. 22.

In the absence of additives under supersaturated conditions, electron photomicrographs revealed that the track surface was covered with fine pits and debris. This pitting is strong evidence of corrosion fatigue and of the likelihood that corrosion promoted fatigue pitting.

Lubricant Viscosity

The most important single property of a lubricant in its effect on

fatigue is viscosity. Fatigue data that treat the effects of viscosity will be dealt with as a separate operating variable. From the data obtained by Rounds (ref. 19), figure 12–16 shows the effect of viscosity on life for both paraffinic and naphthenic mineral oils over the range from 1.7 to 30 centistokes viscosity at 210° F. For both naphthenic and paraffinic base oils, the fatigue life doubles for a tenfold increase in viscosity at 210° F. Further gains in life, however, would not seem to result from increasing the viscosity above 30 centistokes. There do not appear to be sufficient data among some of the other classes of lubricants studied in reference 19 to evaluate the effects of viscosity. The dibasic acid esters (fig. 12–12) show an erratic and inconclusive trend. The polyglycols (fig. 12–13) show a decrease in fatigue life with an increase in viscosity. The methylphenyl silicones (fig. 12–14) show a fairly constant fatigue life with varying viscosity.

Scott (ref. 23) corroborated Rounds' data on the effects of viscosity on life for mineral oils and silicone oils (fig. 12–18). The mineral-oil results shown in figure 12–18, which were obtained in a four-ball fatigue tester, suggest that life increases at a rate approximately proportional to the 0.3 power of the viscosity. The silicone oils show no change in life with viscosity, which agrees with Rounds' data. The polyalkylene glycols, however, exhibit a small increase in life with viscosity, which contradicts the results obtained by Rounds.

Carter and Anderson (refs. 15 and 16) obtained data in the fatigue spin tester with M–1 tool-steel balls and four paraffinic mineral oils, which indicated that fatigue life varied approximately as the 0.2 power of viscosity. These oils varied in viscosity from 5.1 to 119.1 centistokes at 100° F. A more complex, but more versatile, equation was fitted to the results for life against viscosity in references 15 and 16 by consideration of extreme-value theory. Since each failure results from the weakest point on the running track, all other points

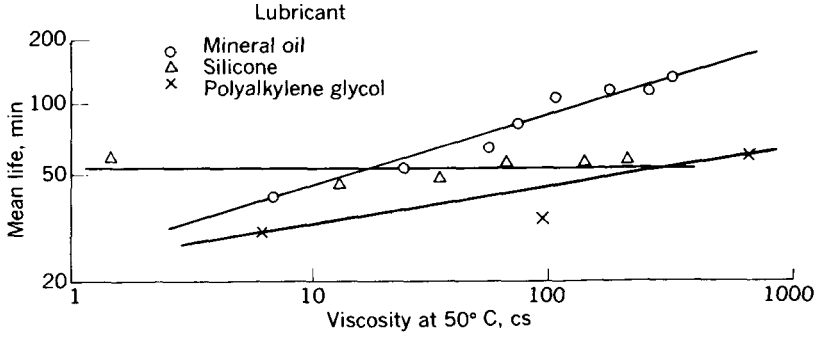

FIGURE 12–18.—Effect of lubricant viscosity on fatigue life with various types of lubricants. (From ref. 23.)

on the track are of necessity stronger; thus, the fatigue lives observed are a series of extreme values for all the infinitesimal areas of the running tracks. An extreme-value analysis results in an equation of the form

$$\ln \ln \frac{1}{S}=(0.625+0.007\sqrt{\mu_o}) \ln\left(\frac{L\times 10^{-8}}{5+0.42\sqrt{\mu_o}}\right) \tag{12–25}$$

where L is the life in millions of stress cycles. Equation (12–25) can be used to calculate the life as a function of viscosity at any level of survival, but calculations can be made more expedient by expressing equation (12–25) in the following exponential form:

$$S=\epsilon^{-\left(\frac{L\times 10^{-8}}{5+0.42\sqrt{\mu_o}}\right)^{(0.625+0.007\sqrt{\mu_o})}} \tag{12–26}$$

where ϵ is the Naperian base.

Equations (12–5) and (12–25) are similar in form. The constant e in equation (12–5) has been replaced by the function $0.625+0.007\sqrt{\mu_o}$ in equation (12–25) and the constant A by the function $\frac{10^{-8}}{5+0.42\sqrt{\mu_o}}$. The two constants e and A in the Weibull equation are obtained from experimental data for standard material bearings lubricated with a mineral oil. From equation (12–25), e and A are not constants but functions of viscosity. The function e represents the slope of the Weibull plot, and since

$$e=0.625+0.007\sqrt{\mu_o} \tag{12–27}$$

viscosity has a very small effect on the Weibull slope or scatter in life. The life at any survival level, however, is affected markedly by viscosity as shown by

$$A=\frac{10^{-8}}{5+0.42\sqrt{\mu_o}} \tag{12–28}$$

The 10- and 50-percent lives obtained in references 15 and 16 are plotted in figure 12–19 together with the simple exponential relations and the more versatile extreme-value relations. The exponential relations fit the data points well over the range of viscosities that were used, but they predict zero life at zero viscosity, which is unrealistic. The extreme-value relations also fit the data points well and are probably more correct for extrapolation because they predict a finite life at zero viscosity.

Barwell and Scott (ref. 11) in their four-ball investigation of several different types of lubricants found that life increased with increasing

viscosity with straight mineral oils, naphthenic base oils, and polyalkylene glycols, but not with silicone oils. The results for mineral

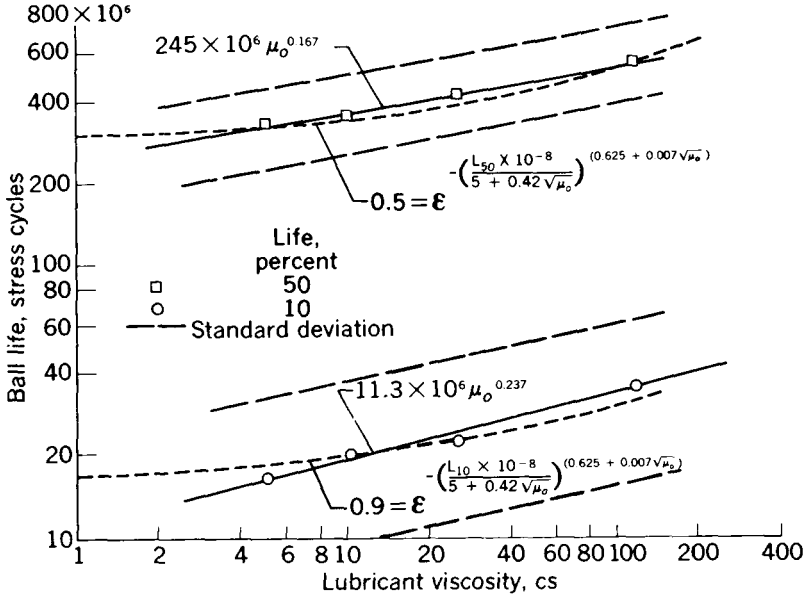

FIGURE 12–19.—Variation of fatigue life with lubricant viscosity. (From ref. 16.)

oils are shown in figure 12–20. These results are similar to those obtained in references 15, 16, 19, and 23.

Another approach to the study of the effect of lubricant viscosity on fatigue was taken by Baughman (ref. 14). He determined the actual viscosities of several test lubricants at 80,000 psi and found a correlation between this viscosity and fatigue life. These results, obtained in the rolling-contact tester, in which the test specimen is a cylindrical rod, are shown in figure 12–7. The log of life is a linear function of the log of viscosity.

Fatigue tests with full-scale roller bearings are reported by Otterbein in reference 24. Lubricants used were as follows:

(1) SAE 30 motor oil
(2) Five synthetic diesters (Mil–L–7808 oils)
(3) A polyester with a viscosity approximating that of SAE 30 motor oil
(4) SAE 10w motor oil
(5) A silicone oil

Figure 12–21 shows average life on a relative scale plotted against viscosity. A general trend exists toward longer life with higher viscos-

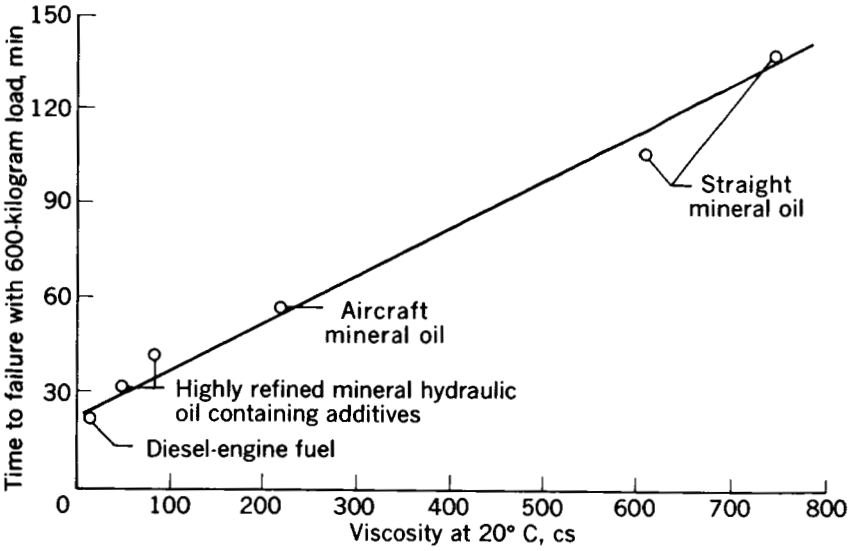

FIGURE 12–20.—Effect of viscosity on life of hydrocarbon lubricants. (From ref. 11.)

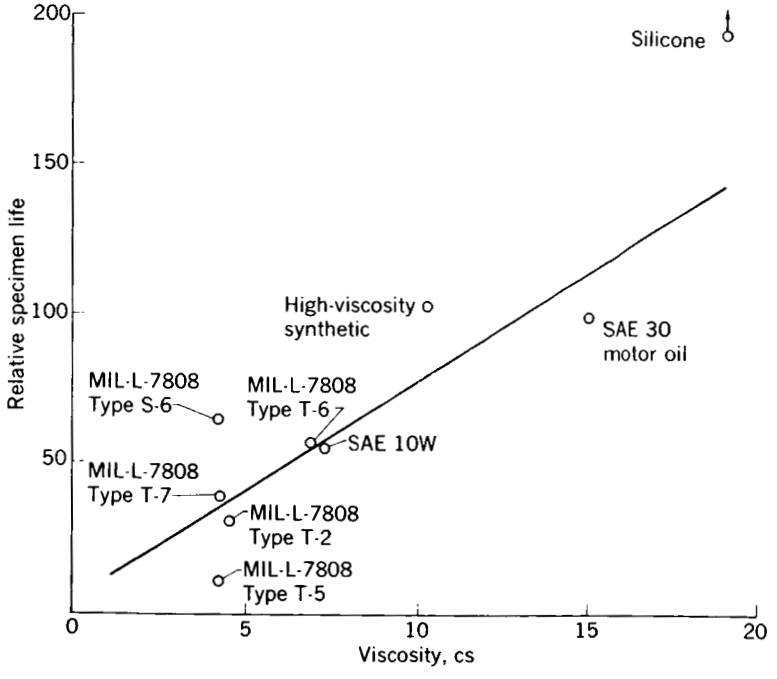

FIGURE 12–21.—Effect of viscosity on roller-bearing fatigue life. (From ref. 24.)

ity, although there is considerable scatter even among lubricants of the same type such as the diesters. Also, the silicone appears to have produced a much longer life than its viscosity would warrant.

Otterbein concluded that low-viscosity lubricants are detrimental to fatigue life and that additives such as viscosity improvers or thickeners are not effective in increasing the life with low-viscosity base oils. He also noted that some low-viscosity lubricants tend to produce shallow surface pitting that resembles corrosion fatigue. The cause of this shallow pitting was not determined.

Fatigue life in both bench tests and full-scale bearings appears to improve with viscosity for almost all the classes of fluids tested. The silicones appear to be an exception and exhibit approximately constant fatigue life over a range of viscosities. Life at the higher viscosities appears to level off in some instances, but more work with high-viscosity oils is needed to corroborate this. Life has been found to vary as the 0.2 to 0.3 power of viscosity for mineral oils over the range of viscosities investigated.

Discussion of Results With Lubricants

The reasons for the variation in life with viscosity and with base stock are not known. In addition to its function as a lubricant for sliding surfaces and as a coolant, the lubricant may influence the stress distribution and thus influence the maximum stress that occurs in the contact zone between a ball and a race. Since fatigue life for point contact varies inversely as the maximum stress raised to the ninth or tenth power, small reductions in the maximum contact stress would produce significant increases in life.

Way (ref. 25) proposed that increasing viscosity results in longer fatigue life because forcing a more viscous lubricant into an incipient fatigue crack is difficult. In fatigue tests of steel rollers, Way found that (1) a lubricant must be present if pitting is to take place, and (2) pitting can be prevented if the lubricant is of a viscosity above a certain critical value, which depends on the load.

Way's theory that the lubricant acts as a wedge offers a plausible explanation for those applications in which fatigue cracks originate at the surface. As discussed in chapter 6, however, the maximum shear stress occurs, in most applications, below the surface. Since the maximum shear stress is the stress considered most damaging, many fatigue cracks may originate in the subsurface. Evidence in the literature shows that this is true. Subsurface structural changes due to cyclical stresses were observed by both Jones (ref. 26) and Carter (ref. 15). The change in structure resulted from additional tempering of the martensite and is believed to be caused by a combination of thermal and strain energy. Carter (ref. 15) observed that many fine

cracks developed in the areas of structural change and that these cracks generally became enlarged and elongated with longer running times. Many instances of fatigue failures that originate at inclusions or other material defects in the subsurface region of high shear stress have been observed; thus fatigue failures may originate either in the subsurface or on the surface. Therefore, Way's theory does not completely explain the role of the lubricant in fatigue.

Viscosity of lubricants varies with pressure, and various lubricants have different pressure-viscosity characteristics. The actual viscosity under pressure is a function of the initial viscosity and of the pressure-viscosity coefficient. The pressure-viscosity coefficient has a greater effect on the actual viscosity under pressure than does the atmospheric pressure viscosity. Therefore, for lubricants in the normal viscosity range, the pressure-viscosity coefficient is of prime importance in determining the actual viscosity under pressure.

Several attempts have been made to treat analytically the problem of lubricated nonconforming bodies in contact under high pressure. This is the so-called elastohydrodynamic problem, which requires the simultaneous solution of energy, elasticity, hydrodynamic, and viscosity equations for an exact solution. Simplifying assumptions must be made to make a numerical solution feasible on a digital computer.

Dörr (ref. 27) obtained a solution for the pressure distribution between an infinitely long roller and a race. His results predict a decrease in maximum contact pressure with an increase in viscosity, but his assumption of constant viscosity may affect the validity of the results. Other notable contributors to the solution of the elastohydrodynamic problem are Grubin (ref. 28), Petrusevich (ref. 29), Poritsky (ref. 30), and Weber and Saafeld (ref. 31); however, none of the solutions in these references is completely satisfactory.

A numerical solution to the two-dimensional problem of elastic cylinders is presented by Dowson and Higgenson in reference 32. Their findings indicate that the maximum contact pressure when a lubricant is present is about the same as the Hertzian pressure. The only significant variations in the pressure distribution from the Hertzian when a lubricant is present occur at the inlet and the exit of the load zone where the pressures are low. Dowson and Higgenson assumed that the viscosity varied exponentially with pressure and simultaneously solved the Reynolds and the elasticity equations.

Sternlicht, Lewis, and Flynn (ref. 33) present a number of solutions to the two-dimensional problem of rollers in contact. These solutions contain varying degrees of simplifying assumptions. For specific minimum film thickness, rolling velocity, viscosity, and variation of viscosity with temperature and pressure, the following load capacities were obtained:

Viscosity	Load capacity, lb/in.	
	Rigid surfaces	Elastic surfaces
Constant	140	450
$f(p)$	320	12, 000
$f(p,T)$	232	9, 780

From this comparison, the influence of pressure on viscosity and on surface deformation increases the load-carrying capacity significantly, while temperature decreases the load-carrying capacity.

The results of reference 33 agree with those of reference 32 in that the elastohydrodynamic pressure distribution was found to be similar to the Hertzian pressure distribution. The results of reference 33 are based on a simultaneous solution of the Reynolds, the energy, and the elasticity equations with the assumption that viscosity varies with both pressure and temperature. While the stresses were found not to vary with various lubricant viscosity-pressure-temperature functions, the temperature distributions did vary. Reference 33 hypothesizes that temperature gradients produce thermal stresses that must be considered in conjunction with normal pressures in order to determine maximum shear stress. Thus, the lubricant that produces lower thermal gradients within the contact zone will yield longer fatigue life in rolling contact.

Full-scale bearing-fatigue tests with two lubricants were conducted in reference 33, which confirmed the analysis. The oil that produced the lower temperature gave longer fatigue life.

Lubricants do not appear to affect fatigue life because of direct influences on the pressure distribution. Thermal effects may be important as may other lubricant properties such as chemical stability, chemical activity, or bulk modulus. In the experiments of references 15 and 16, the best fatigue life was obtained with the least reactive lubricants (silicone and mineral oil), and the poorest fatigue life was obtained with the most reactive lubricants (adipate and sebacate). Further experimental fatigue work with lubricants is necessary to define the important lubricant properties.

Temperature

Temperature and its effect on fatigue life are of extreme interest because of the many high-temperature applications in which bearings are expected to perform satisfactorily over extended periods of time. The effects of temperature are reflected on both the lubricant and on

the material. Decreasing viscosity will, in most instances, result in decreased fatigue life. Since the viscosity of lubricants decreases with rising temperature, an increase in temperature would be expected to be detrimental to fatigue life. The hardness of bearing materials is reduced as temperatures rise, and this is detrimental to fatigue life, as shown in the discussion of PROCESSING VARIABLES.

Carter (ref. 15) reports fatigue data obtained with M–1 steel balls and a sebacate lubricant at 100°, 250°, and 450° F in the fatigue spin tester. Weibull plots of these data are shown in figure 12–22. These results show a reduction in early failure lives with an increase in test temperature. On the basis of the relation between life and lubricant viscosity given in reference 15, $L_1/L_2=(\mu_{o,1}/\mu_{o,2})^{0.2}$, some reduction in life could be anticipated because of the change in viscosity. Table 12–XVIII shows the theoretical reduction in ball life due to viscosity reduction alone. The observed lives were less than those expected if viscosity of the lubricant were the only variable that affected fatigue life. The difference between the observed and the theoretical lives is probably caused by the amplification at the high test temperatures of other factors that affect fatigue life. No significant changes in the appearance of the test tracks with temperature were noted. In particular, there was no evidence of chemical corrosion present on any of the specimens.

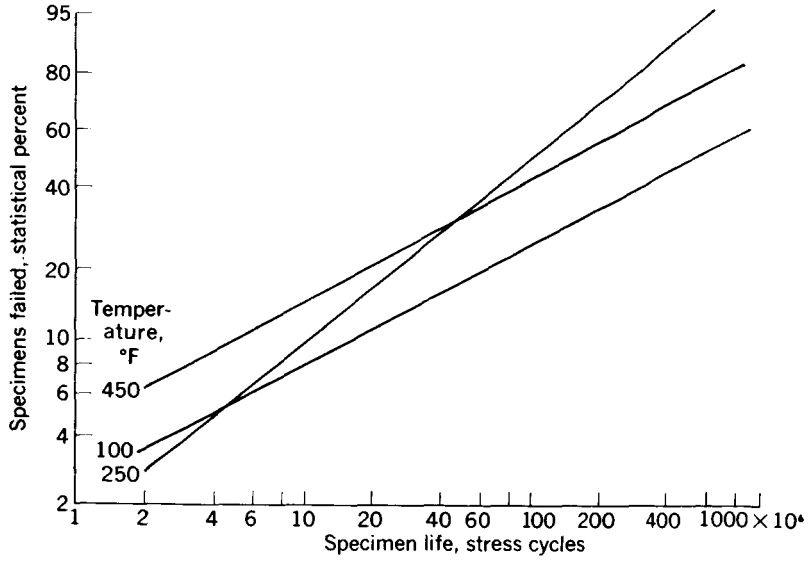

FIGURE 12–22.—Fatigue life for ½-inch-diameter AISI M–1 tool-steel balls at various test temperatures. Lubricant, di(2-ethylhexyl)sebacate; maximum Hertz compressive stress, 650,000 psi. (From ref. 15.)

TABLE 12–XVIII.—FATIGUE LIFE FOR ½-INCH AISI M–1 BALLS AT VARIOUS TEMPERATURES [a]

[Lubricant, di(2-ethylhexyl)sebacate; maximum Hertz compressive stress, 650,000 psi.]

Temperature, °F	Lubricant viscosity, cs	Observed 10 percent life, stress cycles	Theoretical 10 percent life, stress cycles
100	13. 5	15.7×10^6	[a] 15.7×10^6
250	3. 8	10. 2	[b] 12. 2
450	1. 66	4. 75	[b] 10. 3

Temperature, °F	Life ratio, $\frac{\text{observed}}{\text{theoretical}}$	Observed 50 percent life, stress cycles	Theoretical 50 percent life, stress cycles	Life ratio, $\frac{\text{observed}}{\text{theoretical}}$
100	1	580×10^6	[b] 580×10^6	1
250	. 84	109	[c] 450	. 24
450	. 46	160	[c] 382	. 42

[a] From ref. 15.
[b] Assumed the same as observed life.
[c] Based on relation $L_1/L_2=(\mu_{o,1}/\mu_{o,2})^{0.2}$, where L is life in stress cycles and μ_o is lubricant viscosity.

Post-test sectioning of the test specimens of reference 15 revealed a metallurgical transformation in the subsurface shear zone. This transformation increased with increase in number of test cycles and in temperature. Jones (ref. 26) reported a deterioration of metallurgical structure in the subsurface zone of maximum shear for SAE 52100 steel bearings. This transformation consisted of a further tempering of the martensite and resulted from the accumulation of hysteresis energy in the zone of high shear stress. The structure of the transformed M–1 steel that was reported by Carter in reference 15 has not been definitely identified. The deterioration of structure in the subsurface shear zone may be one of the factors that contributed to the loss in fatigue life at higher test temperatures.

Fatigue tests of crystallized glass ceramic (Pyroceram) balls are reported in reference 34. These tests were conducted at test temperatures of 80° and 700° F in the five-ball fatigue tester at 330,000 psi maximum Hertz stress with a highly refined paraffinic mineral oil. The fatigue life at 700° F was approximately one-fourth that at 80° F (fig. 12–23). The viscosity of the test oil was 107 centistokes at 100° F and 1.1 centistokes at 700° F. If the life-viscosity relation of reference 15 is used, this difference in viscosity would produce a reduction in life of about 3⅓ to 1. Thus, the observed loss in fatigue life at the higher temperature could be accounted for by changes in

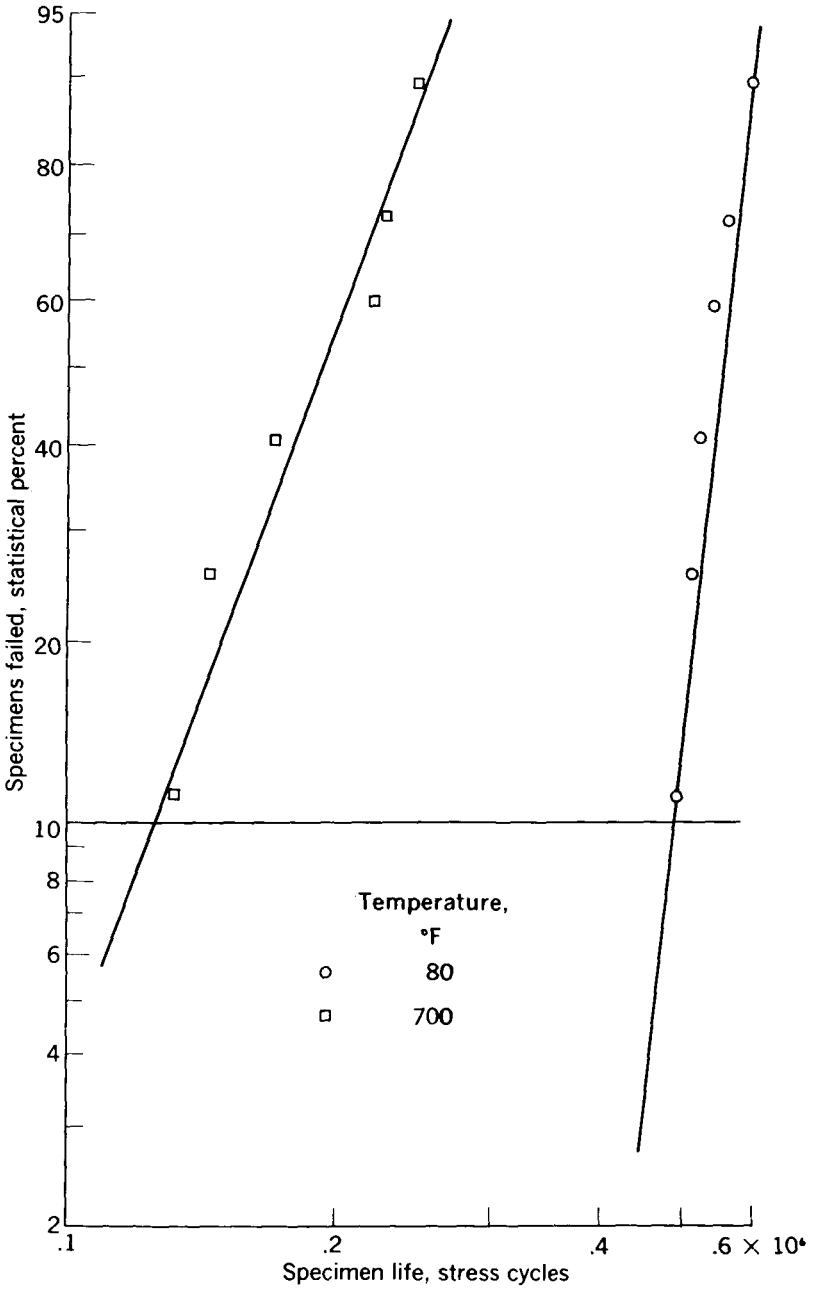

FIGURE 12–23.—Rolling-element-contact fatigue life of crystallized glass ceramic balls as function of temperature. Contact angle, 40°; lubricant, mineral oil; maximum Hertz stress, 330,000 psi. (From ref. 34.)

lubricant properties, so that a deterioration of the Pyroceram material did not necessarily occur.

Otterbein (ref. 24) found that roller-bearing fatigue life decreased steadily with an increase in temperature over the temperature range from 120° to 300° F when a single diester oil was used as the lubricant. The relative life was a linear function of viscosity, as shown in figure 12–24. These data show a stronger relation between life and viscosity than do the data of Scott (ref. 23) or Carter (ref. 15) because two variables, viscosity and temperature, are present in figure 12–24. Decreasing viscosity and increasing temperature both contribute to a loss in fatigue life. An increase in temperature from 120° to 250° F results in a drop in relative life from 70 to 20, which is a decrease of about 70 percent. The significant effect that operating temperature has on fatigue life is thus apparent.

Further data on the effects of temperature on full-scale ball-bearing fatigue life are shown in table 12–XIX. These data are from reference 37, which reports the results of a comprehensive investigation of the effects of melting practice and other variables on ball-bearing fatigue life. This work includes some of the early investigations into the fatigue properties of tool steels. Data were obtained with 45-millimeter-bore ball bearings under a radial load, and results are expressed in terms of the basic AFBMA load capacity for conventionally lubricated SAE 52100 steel bearings. Bearings of three tool steels, M–10,

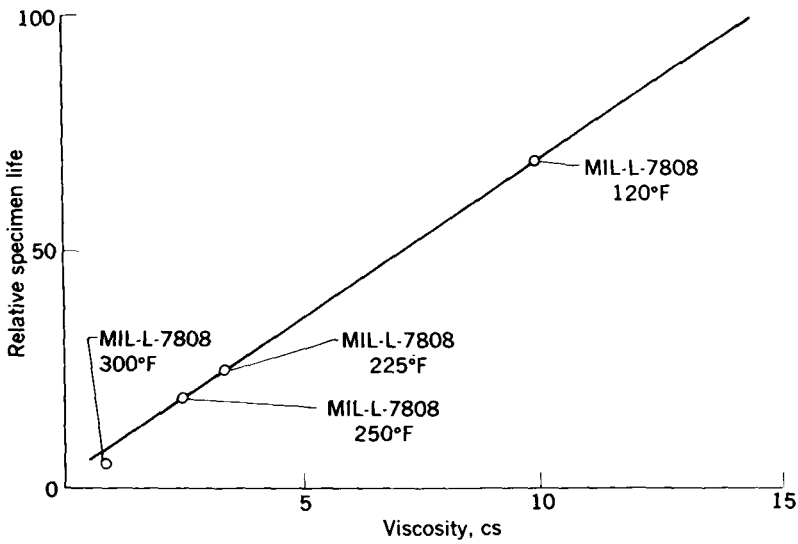

FIGURE 12–24.—Effect of viscosity on ball-bearing life. (From ref. 24.)

TABLE 12–XIX.—BEARING LOAD RATINGS FOR TOOL STEELS [a]

Melting practice	Tool steel	Temperature, °F	Rating as percent AFBMA basic load rating, based on	
			10-percent life	50-percent life
Basic arc	M–10	Room	77	70
	M–10	450	64	64
	M–1	Room	83	91
	M–1	Room	76	78
	M–1	450	60	54
Induction vacuum	M–1	Room	132	122
Induction vacuum	M–1	450	64	77
Consumable vacuum	M–50	Room	144	126
Consumable vacuum	M–50	450	93	100

[a] From ref. 37.

M–1, and M–50, were tested at room temperature and at 450° F. The reduction in load ratings from room temperature to 450° F are believed to be caused principally by the lubricant; the bearings at room temperature were lubricated by a mineral-based grease and those at 450° F by a synthetic diester. A discussion of the effects of melting practice will be given in the section PROCESSING VARIABLES.

Solid Lubricants

Because of the requirement that rolling-element bearings operate at temperatures above the range in which organic liquid lubricants are usable, solid lubricants such as graphite and molybdenum disulfide (MoS_2) have been considered as lubricants for rolling-element bearings. The effectiveness of solid lubricants in preventing failures other than those due to fatigue is discussed in chapter 11. Some data on the influence of solid lubricants on rolling fatigue are contained in references 12, 15, and 20. In reference 15, fatigue tests of ½-inch-diameter M–1 steel balls were conducted in the fatigue spin tester with the following lubricants:

(1) Polyalkylene glycol at 100° F
(2) Synthetic sebacate at 450° F
(3) Polyalkylene glycol plus 0.2 percent molybdenum disulfide at 100° F
(4) Polyalkylene glycol plus 0.2 percent molybdenum disulfide at 450° F
(5) Dry graphite at 450° F

The fatigue results for these five lubricants are given as Weibull plots

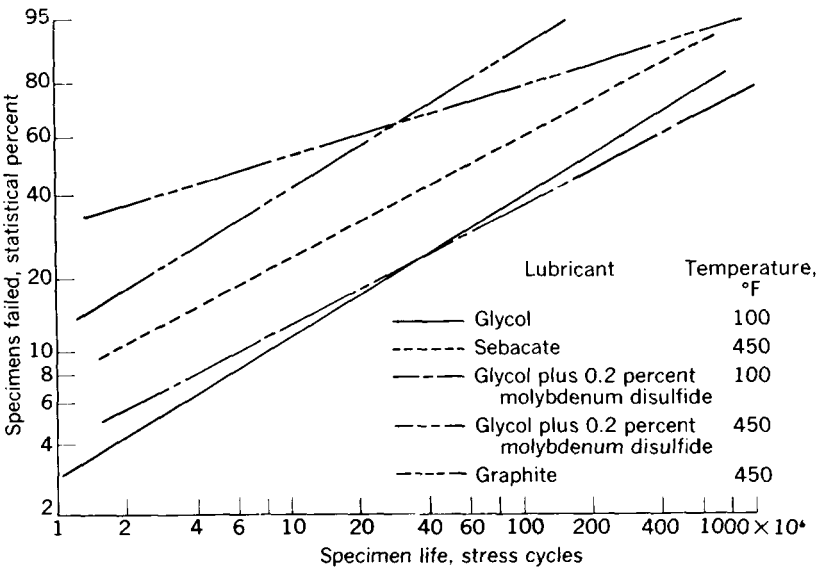

FIGURE 12–25.—Fatigue life for ½-inch-diameter AISI M–1 tool-steel balls with various lubricants. Maximum Hertz compressive stress, 725,000 psi. (From ref. 15.)

in figure 12–25. Fatigue lives obtained with the glycol and the suspension of glycol and MoS_2 at 100° F are almost identical, which indicates no effect from the presence of the MoS_2. The suspension of glycol and MoS_2 produced a poorer fatigue life at 450° F. The glycol was chosen as a carrier for the MoS_2 because it evaporates at 350° F and leaves no residue. Thus, at 450° F, the lubricant present was essentially dry MoS_2 powder. Fatigue tests with dry graphite and air dust produced even poorer fatigue life as shown in figure 12–25. The results with a synthetic sebacate at 450° F are shown for comparison with the graphite and the MoS_2 results. Fatigue life with the synthetic sebacate was better than with the dry-powder lubricants by a factor of at least five.

Either physical or chemical factors could have been responsible for the poor fatigue life with the dry-powder lubricants. Since graphite is quite different from MoS_2 chemically but similar physically, different results would be expected if chemical activity were a major factor. The similar life results with graphite and MoS_2 seem to preclude chemical effects. Post-test examination of the test balls run with dry-powder lubricants revealed two annular bands of small spalls located at the rolling bands rather than the usual single track-centered spall obtained in tests with liquid lubricants. Examination of the dry powders revealed a maximum particle size of about 25 microns.

This size is believed to be sufficiently large for the particles to act as stress raisers in the regions where they were not sheared. The appearance of the spalls in the rolling bands apparently confirms this, since the relative motion of the two surfaces is perpendicular to the plane of the surfaces in the rolling bands. The stress on the lubricant particles would be purely compressive in these regions and, because of the quasi-hydrostatic loading, the particles could carry compressive stresses higher than their yield strength.

The theory that the dry-lubricant particles produce high, localized compressive stresses in the bands of pure rolling is a hypothetical one, but one that is supported by substantial evidence which indicates that some localized stress raiser that is not present in fluid lubricants is present with dry lubricants. The unique appearance of the spalling, the intense localized incipient matrix damage confined to the region of the unique spalling, and the short lives support this theory. The stress-raising effects that were noted in these tests may not be present to such an extent in full-scale rolling-element bearings because better conformity exists between balls and races and because relative sliding of the surfaces is greater.

Scott (ref. 12), in four-ball tests conducted at 200° C (392° F) and at a maximum Hertz stress of 830,000 psi, reported improvements in fatigue life with MoS_2 and graphite suspensions in oils. The average time to failure with two silicone oils was 36 and 23 minutes (table 12–XX). A suspension of MoS_2 in a soap-thickened silicone fluid, 2- and 10-percent suspensions of graphite in mineral oil, and a MoS_2 paste in a mineral-oil carrier generally extended fatigue life. Dry MoS_2 was beneficial to fatigue life, but dry graphite and a mixture of dry graphite and lead oxide produced fatigue lives equal to or less than those with the liquid lubricants. With the dry MoS_2, failure was caused by a progressive surface roughening rather than by the appearance of a surface pit. The particle size of the dry powders used in reference 12 was not given, but possibly they were smaller than those used in reference 15.

Further tests of solid lubricants by Scott are reported in reference 20. The results of these tests, which were conducted at a maximum Hertz stress of 10^6 psi, are shown in table 12–XXI. These tests were conducted with solid lubricants in the form of dry powders and dispersed in various media; however, the particle size of the dry powders was not given. The results with MoS_2 were considerably better than those with graphite, which agree with reference 12. Better results were achieved when MoS_2 was suspended in a mineral-oil carrier than when it was suspended in water. Dilution of the paste-like suspension of MoS_2 in water resulted in severe reduction of life.

TABLE 12–XX.—FATIGUE LIFE RESULTS WITH VARIOUS LUBRICANTS [a]

[Maximum Hertz stress, 830,000 psi; test temperature, 200° C.]

Lubricant	Average time to failure, min	Remarks
Typical conventional silicone	36	Considerable amount of wear on upper ball; bottom balls dull
Experimental silicone intended for use at −50° C and above; contains chlorine	23	Normal pitting failure; single small pit
Suspension of molybdenum disulfide in soap-thickened silicone fluid; lubricant formulated to combine thermal and physical properties of silicone with lubricating potentialities of molybdenum disulfide	50	Considerable amount of wear on upper ball; bottom balls dull
Experimental lubricant: 2 percent graphite in special mineral oil	55	Normal pitting failure
10 percent graphite in thin mineral-oil base	41	Normal pitting failure
Dry graphite power	26	Considerable wear and damage, bottom balls black
Dry graphite powder with graphite-coated balls	20	Bottom ball from previous test used
Mixture of dry graphite and lead oxide in ratio 1:2	36	Considerable wear and severe damage; bottom balls black
Dry molybdenum disulfide	98	Considerable wear
Molybdenum disulfide in paste form with mineral-oil carrier	135	Normal pitting failure

[a] From ref. 12.

The results of the experiments conducted in references 12, 15, and 20 indicate that solid lubricants can be beneficial to fatigue and that MoS_2 appears to be better than graphite. Suspensions of solids in conventional lubricants give better results than dry powders or aqueous suspensions. Particle size appears to be critical with submicron size particles that are necessary for good fatigue results.

Speed

Conventional calculations of bearing life are based on the fatigue of the components due to the externally applied loads. At high

TABLE 12–XXI.—EFFECT OF SOLID LUBRICANTS ON BALL FATIGUE LIFE [a]
[Maximum Hertz stress, 10^6 psi.]

Description of lubricant	Duration of test, min	Remarks
N, suspension of larger particle variety of molybdenum disulfide in water; soft cream consistency	105 115 80 110	Test to failure
N, diluted 1:2 with water	120 120 80	Test to failure
N, diluted 1:5 with water	12 8 9 6 5	Test to failure; two test balls fractured
N, diluted 1:9 with water	4 4 3	Test to failure
Molybdenum disulfide in paste form in mineral-oil carrier	120 150 285	No failure
Suspension of molybdenum disulfide in soap-thickened silicone fluid	50 60 120 160	No failure by normal pitting; considerable wear in every instance; bearing track had abraded appearance
2 percent by weight conventional graphite in mineral oil	124 130 131 75 105	Test to failure
10 percent by weight colloidal graphite in petroleum base	75 63 65 100	Test to failure
Dry molybdenum disulfide	145 210 240	No failure
Dry graphite	13 15 10	Test to failure; considerable damage to upper ball; lower balls black color
Dry graphite	17 15	Test to failure; lower balls from above test apparently covered with graphite layer used as upper ball
Dry graphite lead oxide mixture, 1:2	18 15 20	Test to failure; considerable wear and damage to upper ball
Graphite suspension in alcohol	55 32 35	Test to failure; considerable damage to upper ball; alcohol evaporated and test ran almost dry

[a] From ref. 20.

speed, the centrifugal force on the balls increases the load at the outer-race contact. In addition, bearing temperature may rise with increasing speed and may produce an effect on fatigue life.

Jones (ref. 35) analyzed the effects of high speed on both radial-loaded and thrust-loaded bearings. In radial ball bearings under radial load, the effect of speed is to reduce life because the centrifugal force on the balls increases the probability of failure of the outer race. These results are shown in figure 12–26 for a 209-size bearing operating under a 400-pound radial load. The divergence between the calculated static load life and the high-speed life increases with increasing speed.

In angular-contact bearings, which operate under thrust load,

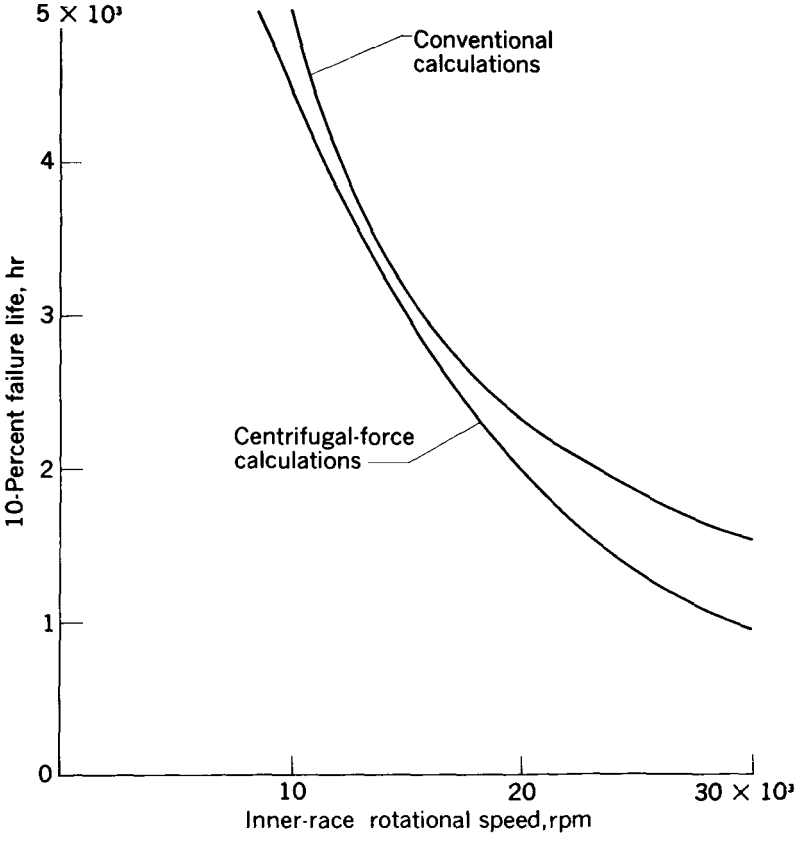

FIGURE 12–26.—Ten-percent failure life as function of speed as calculated by conventional means and with consideration of centrifugal force for 209-size bearing with nine balls of ½-inch diameter; race curvatures: inner, 51 percent; outer, 52 percent; 400-pound radial load. (From ref. 35.)

centrifugal loading of the balls increases the inner-race contact angle and reduces the stress at the inner-race contacts. Thus, the relative probabilities of outer- and inner-race failure are different from those calculated from static load conditions, and bearing life is accordingly different. Calculations made for a 214-size bearing that operates at 10,200 rpm with an initial contact angle of about 20° are shown in figure 12–27. The ratio of life for load at high speed to that for static load is plotted against thrust load. At zero external load, the life ratio is effectively zero because the total load originates from centrifugal forces. The life ratio increases with increasing thrust load and is greater than 1 at thrust loads above about 500 pounds. Thus, the changes in contact angle produced by the high speed theoretically increase the bearing fatigue life. Experimental results are needed to confirm these analyses.

The load capacity of a bearing increases as the rolling-element diameter (or the bearing series) is increased. This theory is true only in the nominal speed range. At extreme speeds, higher loads may be carried with a lighter series bearing because of the predominance of centrifugal forces on the rolling elements; an example is discussed in chapter 11. The Marlin-Rockwell Corporation has developed the following criterion for establishing the limiting speed of thrust-loaded ball bearings:

$$\frac{EN^3D^3}{\cos^3\alpha} < 31\times10^8 \qquad (12\text{–}29)$$

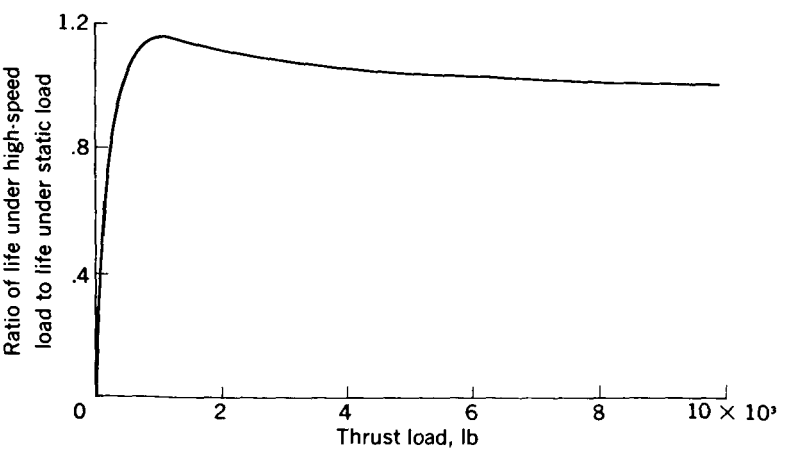

FIGURE 12–27.—Ten-percent failure life for load at high speed relative to life for static load as function of thrust load for 214-size bearing with 16 balls of $^{11}/_{16}$-inch diameter; contact angle α, 19.64°; race curvatures: inner, 51 percent; outer, 52 percent; inner race rotating at 10,200 rpm. (From ref. 35.)

The term D^3, which is proportional to the mass of a rolling element, appears in the inequality. The expression in the numerator is akin to a centrifugal force multiplied by an angular velocity since it contains terms equivalent to a radius, an angular velocity cubed, and a mass.

Zaretsky, Anderson, and Parker (ref. 36) ran fatigue tests of ½-inch M–1 balls in the five-ball fatigue tester at 5000 and 10,000 rpm at a contact angle of 30°. In a series of fatigue tests at 10,000 rpm at various contact angles (ref. 36), life decreased with increasing contact angle at a constant normal load. The significance of these results will be discussed later, but of importance here is the fact that, as contact temperature increased, fatigue life decreased. Contact temperature at 5000 rpm was lower than at 10,000 rpm so that, on the basis of temperature, a longer fatigue life would be expected at the lower speed. A 5000-rpm life was predicted from the 10,000 rpm data and measured contact temperatures. As shown in figure 12–28, the predicted life is almost identical to the actual life at 5000 rpm. These experiments were conducted under conditions where centrifugal loads were not present, and the appearance of the specimens after test indicated that hydrodynamic lubrication may not have existed. Contact tempera

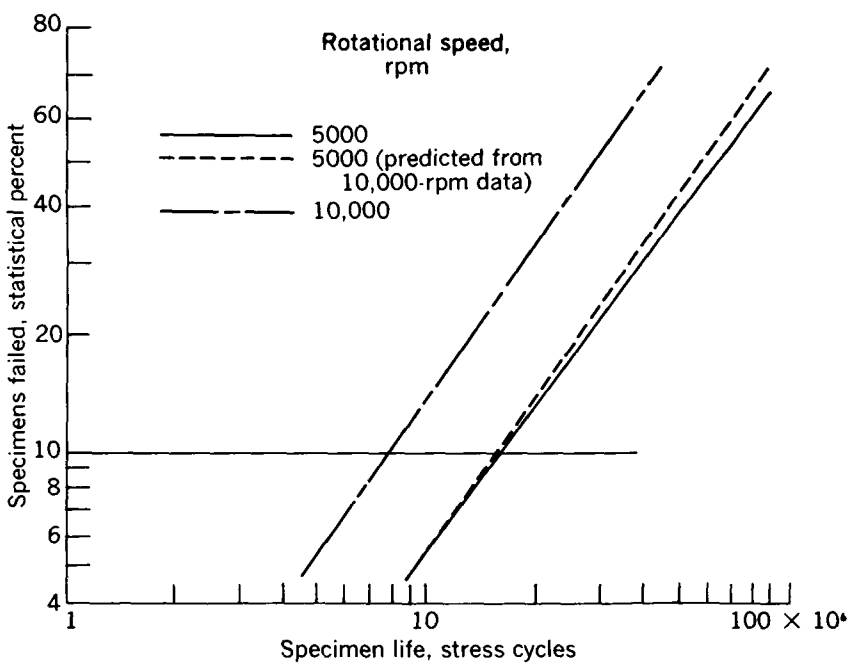

FIGURE 12–28.—Rolling-element-contact fatigue life at 5000 and 10,000 rpm of AISI M–1 tool-steel balls for contact angle of 40°. Initial maximum Hertz stress, 800,000 psi; race temperature, 120° F. (From ref. 36.)

ture appears to be an important variable that is influenced by speed, but further experimental data are needed to confirm this hypothesis.

PROCESSING VARIABLES

In addition to the environmental or operating variables, processing variables such as material and melting technique, material hardness, material fiber orientation, and contact angle also affect fatigue.

Material and Melting Technique

Morrison, Walp, and Remorenko (ref. 37) thoroughly investigated the effects of melting practice with vacuum-melted 52100 steel and with both air and vacuum melts of several tool steels. For reference, the nominal analyses of a number of bearing materials are given in table 12–XXII. Table 12–XXIII, from reference 37, shows some data obtained with induction and consumable-electrode vacuum-melted 52100 steel. Load ratings are given in terms of the AFBMA basic load rating. Specimens were inner rings of 6309-size bearings or outer rings of 1309-size self-alining bearings. These data show, generally, that consumable-electrode melting produces material with better fatigue properties than induction vacuum melting. Unpublished results obtained by other investigators generally confirm that consumable-electrode vacuum-melting produces the most consistent high-quality bearing material. A partial explanation may be that a refractory crucible is used in the induction-melting process with the result that refractory particles sometimes get into the melt. In the consumable-electrode-melting process, the ingot is used as one terminal of the arc, and the process is completely clean.

Results with tool steels, obtained in reference 37, are shown in table 12–XIX. In addition to the two vacuum-melting techniques, several heats of material were basic-arc air melted. The air-melted M–10 and M–1 materials were deficient in load-carrying capacity. At room temperature, load capacities based on the 50-percent life ranged from 70 to 91 percent. At 450° F with synthetic diester lubrication, the load capacities were even poorer. The induction-vacuum-melted M–1 was superior to the standard AFBMA rating at room temperature, but quite poor at 450° F. Only the consumable-vacuum-melted M–50 was comparable to or better than the standard at both room temperature and at 450° F.

The authors of reference 37 state that little correlation was found with cleanliness as determined by inclusion ratings obtained from the Jernkontoret chart in that the improvement in life was not commensurate with improvements in cleanliness. This conclusion was generally confirmed by Carter (ref. 15), who conducted ball-fatigue tests of 10 different materials in the fatigue spin rig. The life results of these tests are shown in a bar graph in figure 12–29. All these materials

TABLE 12-XXII.—NOMINAL ANALYSIS OF BEARING MATERIALS

Steel	Analysis, percent by weight										
	C	P (max)	S (max)	Mn	Si	Cr	V	W	Mo	Al	Co
SAE 52100	1.00	0.025	0.025	0.35	0.30	1.45	----	----	----	----	----
AISI M-1	.80	.030	.030	.30	.30	4.00	1.00	1.50	8.00	----	----
AISI M-50	.80	.030	.030	.30	.25	4.00	1.00	----	4.25	----	----
AISI M-2	.83	.030	.030	.30	.30	3.85	1.90	6.15	5.00	----	----
AISI M-10	.85	.030	.030	.25	.30	4.00	2.00	----	8.00	----	----
AISI T-1	.70	.030	.030	.30	.25	4.00	1.00	18.00	----	----	----
AISI MV-1	.80	.030	.030	.30	.25	4.10	1.10	----	4.25	----	----
Al steel (MHT)	1.03	.025	.025	.35	.35	1.50	----	----	----	1.36	----
L.A.T.S. (Halmo)	.65	.030	.030	.27	1.20	4.6	.55	----	5.2	----	----
TMT	1.00	.025	.025	.50	1.00	1.45	----	----	.30	.08	----
440C	1.03	.018	.014	.48	.41	17.3	.14	----	.50	----	----
WB49	1.07	.006	.007	.30	.02	4.4	2.0	6.8	3.9	----	5.2

TABLE 12–XXIII.—TEST RESULTS FOR VACUUM-MELTED SAE 52100 STEEL [a]

Approximate ingot size, in.	Melting practice	Rating, percent AFBMA basic load rating	
		10-percent life	50-percent life
5½-in. diam	Induction vacuum	95	90
5½-in. diam	Induction vacuum	108	112
6 in. sq	Induction vacuum	71	83
	Induction vacuum	100	97
	Induction vacuum	95	93
	Induction vacuum	91	94
	Induction vacuum	80	90
9⅝ in. sq	Induction vacuum	103	103
9⅝ in. sq	Induction vacuum	126	123
16-in. diam	Consumable electrode	124	116
16-in. diam	Consumable electrode	106	112

[a] From ref. 37.

had inclusion ratings of 1 in the A and D categories of the Jernkontoret rating system, but within that group each material was given a rating of excellent, good, fair, or poor based on the metallographer's judgment. The air-melted materials tested by Carter included SAE 52100, M–1, MHT, TMT, M–10, T–1, MV–1, and M–50. Among these materials, no particular correlation between cleanliness and fatigue life was noted. Two heats of M–1 steel, one air melt, and one vacuum melt were tested with a glycol lubricant. The vacuum melt M–1 produced significantly better fatigue life. The two modified SAE 52100 base alloys (MHT with 1-percent aluminum and TMT with 1-percent silicon) showed an improvement over standard SAE 52100. With the addition of these deoxidizers, fewer short-lived failures were obtained, and the scatter in life was reduced.

Balls of several materials were fatigue tested by Jackson (ref. 38) in a modified one-ball fatigue tester. These data are shown in figure 12–30. Metallurigical data obtained with balls with the lowest and highest life from each series are shown in table 12–XXIV. Good cleanliness does not ensure good fatigue life although the M–50, which was quite clean, had the best fatigue life. The MHT, which was quite dirty, had good fatigue life, whereas the Halmo, which was fairly clean, had poor life. Jackson found that life can vary appreciably for several apparently similar heats of the same material, which agrees with the findings of the authors of reference 37 (table 12–XXIII). Note, for example, on table 12–XXIII, the load-capacity data for bearing groups 5 and 6. These are two groups of bearings made from the same heat poured to the same ingot size, and yet bearing group 6 had a 15 percent greater capacity than did group 5

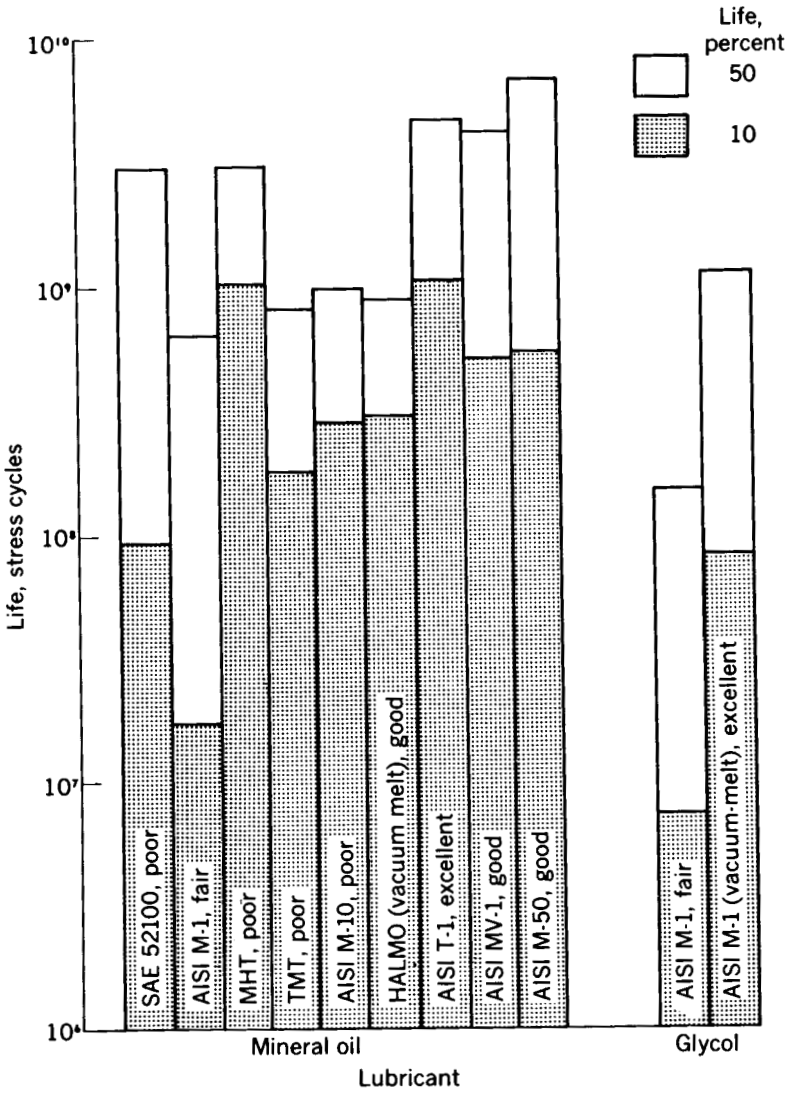

FIGURE 12–29.—Summary of fatigue-life data giving material and cleanliness ranking within A–1 and D–1 Jernkontoret ratings. (From ref. 15.)

based on the 50-percent life. A 15-percent difference in capacity corresponds to a 50-percent difference in life.

The important conclusions regarding the effects of material and melting technique on fatigue from the data of references 15, 37, and 38 are as follows:

(1) The standard Jernkontoret cleanliness measurements are not sufficient to establish relative quality.

TABLE 12-XXIV.—METALLURGICAL OBSERVATIONS OF FATIGUE SPECIMENS[a]

[Lowest- and highest-life balls from each series.]

Steel	Lot	Series [b]	Jernkontoret cleanliness rating [c]	ASTM grain size [d]	Carbide distribution	Polarity, deg [e]	Life, stress cycles
SAE 52100	19A	16	2D thin	20	None	60	0.1×10^6
	19A	16	2D thin	20	None	60	35
Al steel (MHT)	21A	17	3D thick	20	Light	45	42
	21A	17	3D thick	20	Light	90	45
440C	18	11	2D thin	13	Light	0	1.3
	18	11	2D thin	13	Light	0	47
L.A.T.S. (Halmo)	3	10	1D thin	8	Heavy	30	11
	3	10	1D thin	7	Heavy	75	41
AISI M-50	23	20 A and B	Very clean	10	Heavy	30	26
	23	20 A and B	Very clean	10	Medium	45	103
	25	22	Very clean	10	Light	60	33
	25	22	Very clean	10	Light	45	176
	25A	19	1C thin	10	Heavy	30	6
	25A	19	1C thin	10	Heavy	75	53
	4	6, 8	Very clean	13	Light	15	17
	4	6, 8	Very clean	15	Light	0	116
	26	18	Very clean	13	Light	45	35
	26	18	Very clean	13	Medium	0	80
	26	21	Very clean	13	Light	0	15
	26	21	Very clean	13	Light	30	37

[a] From ref. 38.
[b] Lowest-life ball in each series is listed first.
[c] By comparison with ASTM E45-51 charts.
[d] Intercept method.
[e] Degrees between failure pit and pole as determined by deep etch.

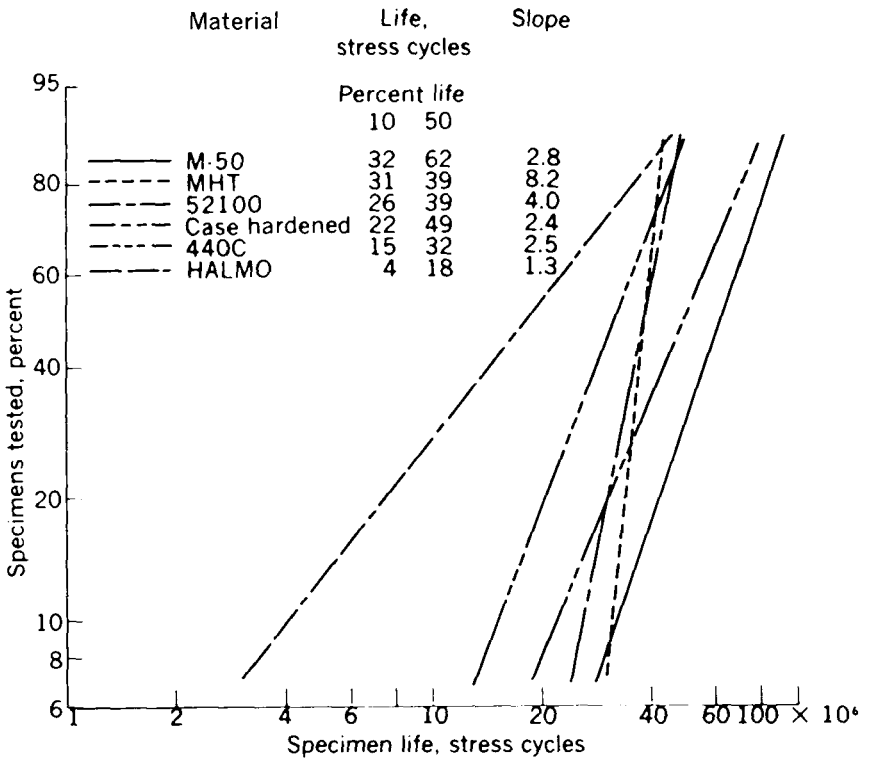

FIGURE 12–30.—Best results obtained with each of six materials tested. (From ref. 38.)

(2) Vacuum melting appears to improve fatigue life but not in proportion to the improvement in cleanliness, and consumable-electrode vacuum melting produces the most consistently good material.

(3) Vacuum melting does not reduce the number of early failures, since the scatter in life is about the same with vacuum-melted materials as with air-melted materials.

(4) The material M–50, especially vacuum-melted M–50, appears to have good fatigue life (refs. 37 and 38).

Hardness

Material hardness is of prime importance because a minimum hardness is required to prevent brinelling and plastic flow in the race grooves. In addition, hardness varies with temperature. Knowing how fatigue life varies with hardness is necessary so that the secondary effects of temperature can be assessed. Hardness is intimately associated with heat treatment and structure and therefore is of general interest in studying rolling-element fatigue.

Early work on the effect of hardness on bearing life was reported by Irwin (ref. 39). Four groups of SAE 52100 207-size bearings were fatigue tested and produced the results shown in figure 12–31. A continuous improvement in fatigue life was noted over the hardness range from Rockwell C–59 to C–63. The life data shown in figure 12–31 were replotted in terms of relative capacity as a function of hardness and are shown in figure 12–32. Also shown in figure 12–32 are plots of hardness and temperature for SAE 52100, MHT, and M–50. When the hardness and relative-capacity curve is assumed the same for all three materials, the relative capacity can be calculated for each material at any temperature over the range for which hardnesses are given. At 400° F, for example, the Rockwell hardnesses of 52100, MHT, and M–50 are C–57.4, C–59.1, and C–60.8, respectively; these hardnesses produce relative capacities of 65, 86, and 95 percent, respectively. The importance of maintaining high hardness is thus evident.

Jackson (ref. 38) conducted fatigue tests of three groups of M–50 balls in a modified one-ball fatigue tester. These data, which are

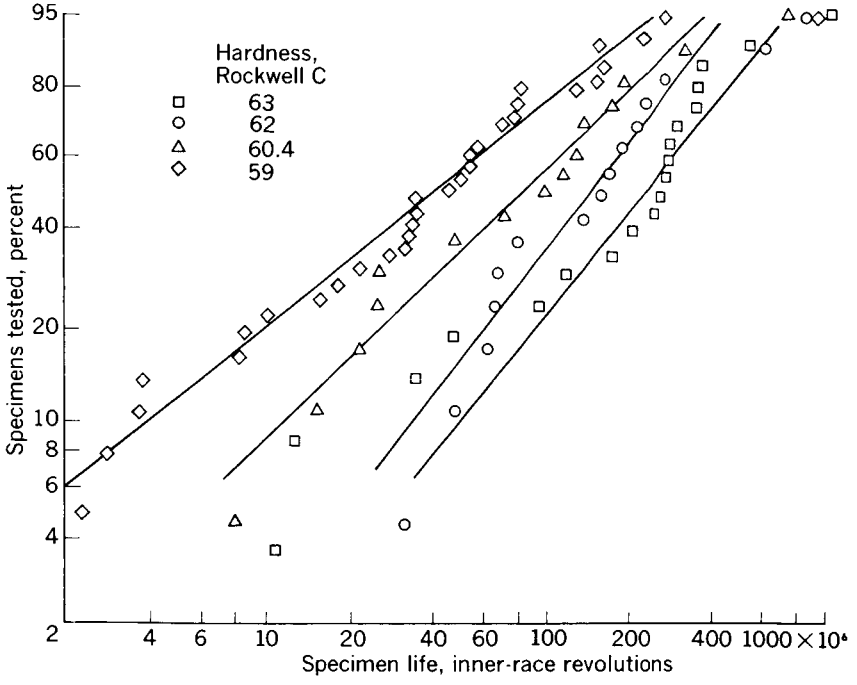

FIGURE 12–31.—Ball-bearing fatigue life at four hardness levels. (From ref. 39.)

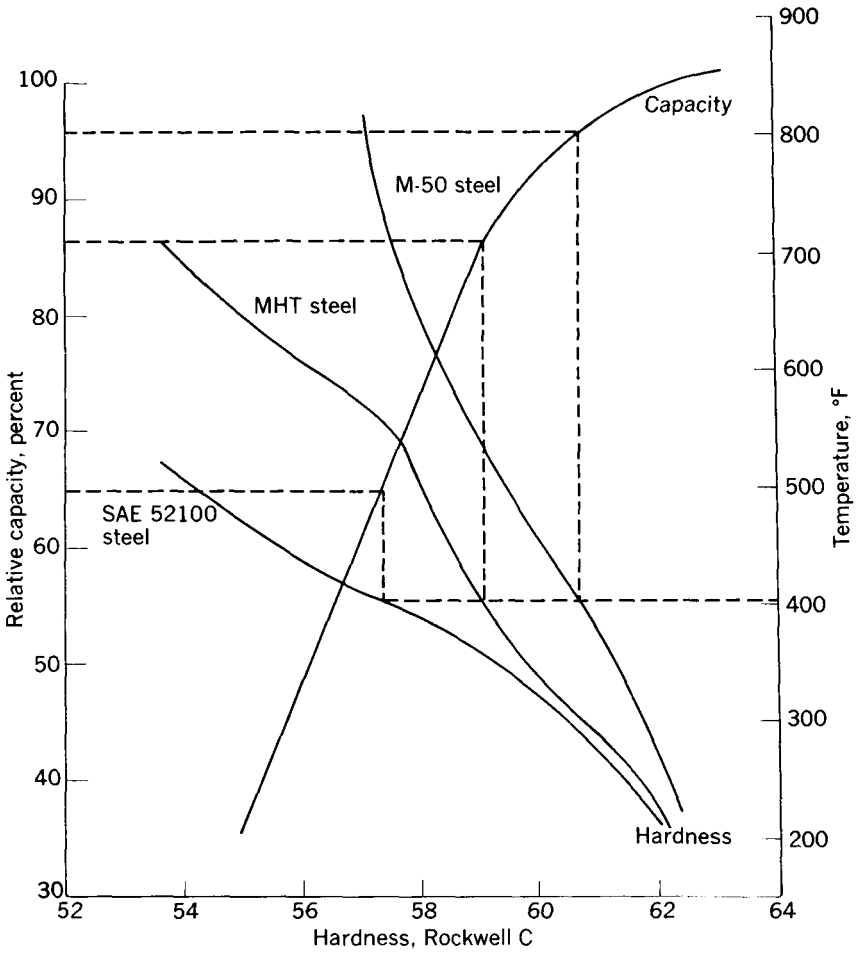

FIGURE 12–32.—Relation between temperature, hardness, and bearing load capacity for three materials. (From ref. 39.)

shown in figure 12–33, indicate a continuous increase in fatigue life with increasing hardness over the hardness range from Rockwell C–60 to C–63.5. The improvement in life over this hardness range is greater than one order of magnitude. Similar data were obtained by Zaretsky and Anderson (ref. 40) for M–1, M–50, and Halmo steel balls in the fatigue spin tester and for WB–49 steel balls in the five-ball fatigue tester. These data are summarized in figure 12–34. Fatigue life for each of these materials increased continuously with increasing hardness over the ranges of hardness investigated. For these four materials, the 10-percent fatigue life at the highest hardness was 3 to 15 times the life at the lowest hardness. These data

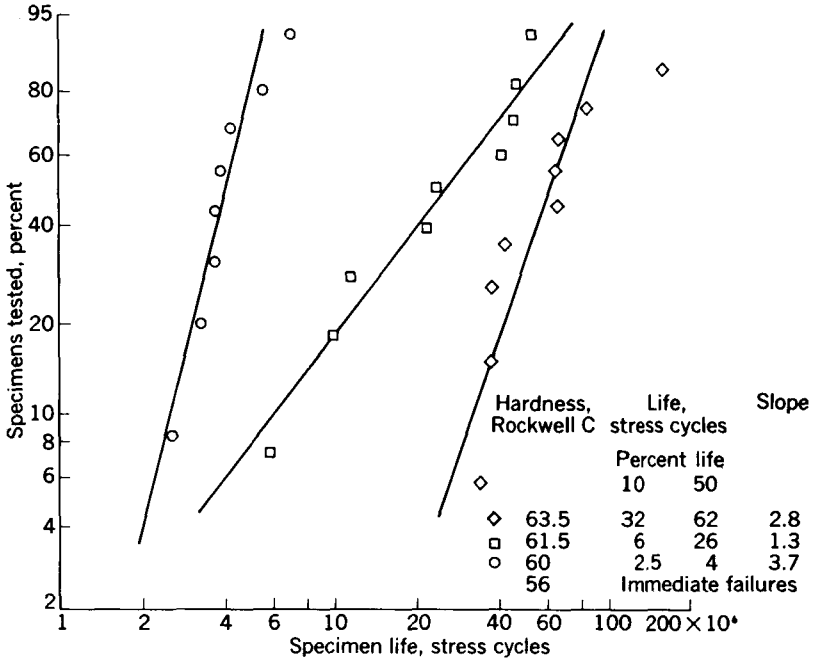

FIGURE 12–33.—Effect of hardness on fatigue life. One lot of M–50 retempered Lubricant, fresh Mil–L–7808C. (From ref. 38.)

from reference 41 are plotted in terms of relative capacity in figure 12–35. The capacity of the softest of each of the materials varied from 70 to 40 percent of the capacity of the hardest material of each alloy. Thus, a few points of hardness can easily double the load capacity of a given material.

Baughman (ref. 42) conducted fatigue tests on M–50 specimens in the rolling-contact tester to determine the effects of hardness, surface finish, and grain size on fatigue life. Four tests were conducted at each combination of grain size, hardness, surface finish, and stress level. This number of tests for each combination of variables is a bare minimum; justification is based on previously published reproducibility studies (ref. 14). A statistical analysis was used to determine the influence of each variable on the 10-percent life. Because of the small number of data points obtained in reference 14, the validity of the conclusions is questionable.

The effect of grain size at various hardness levels and values of surface finish is shown in figure 12–36. Large grains (indicated by a small grain-size number) are beneficial, especially in the high hardness range. The sensitivity of the 10-percent life to grain size diminishes as the hardness is lowered. Life appears to improve with surface

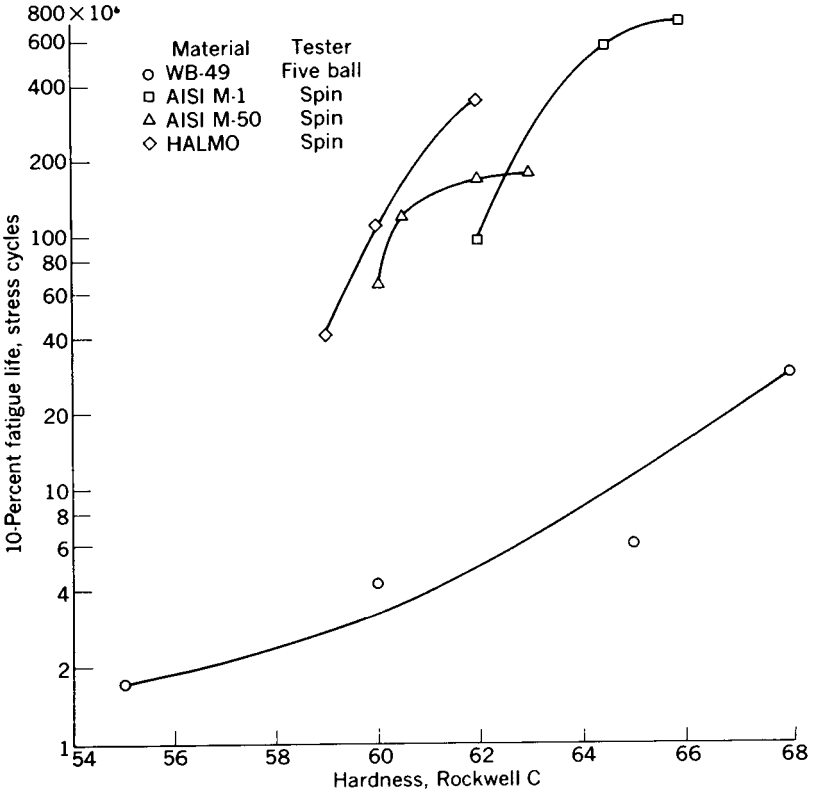

FIGURE 12–34.—Ten-percent fatigue failure life as function of hardness for four tool steels. (From ref. 40.)

finish since the upper bound on life is formed by the 2 rms surface finish (fig. 12–37). As the surface is roughened, life decreases. As with grain size, the sensitivity of 10-percent life to surface finish diminishes as the hardness is lowered. The effect of hardness on the 10-percent life at various values of grain size is shown in figure 12–38. At the larger grain sizes, a continuous improvement in 10-percent life with increasing hardness is indicated over the entire range of hardness investigated. As the grain size decreases, the 10-percent life peaks at an intermediate hardness. For example, at a grain size of 10 and a surface finish of 2 rms, the maximum life occurs at a hardness of Rockwell C–62. The sensitivity of 10-percent life to hardness decreases with decreasing grain size.

Figure 12–39 (ref. 42) shows the effect of hardness on 10-percent life at various values of surface finish. The sensitivity of 10-percent life to hardness is greatest at the finest surface finish and diminishes as

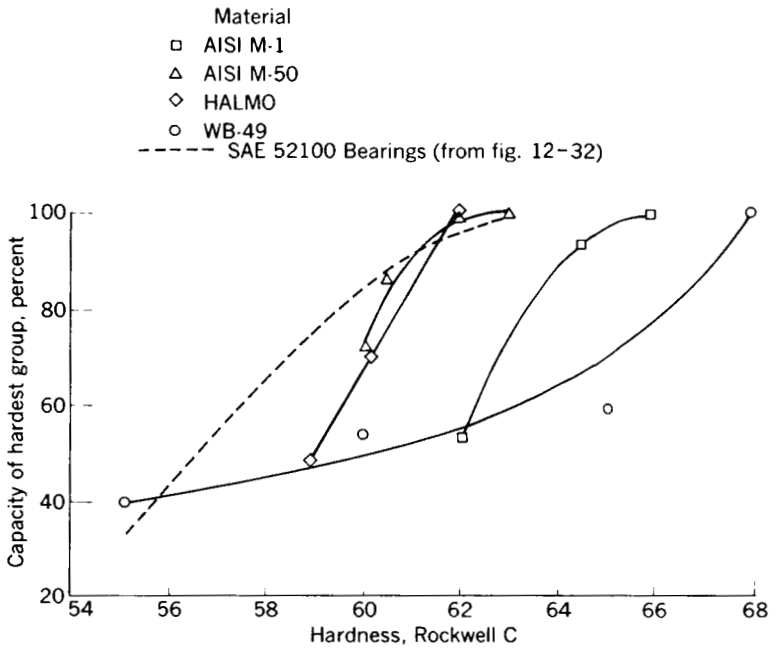

FIGURE 12–35.—Relative load-carrying capacity of bearing steel balls tempered to different hardness levels. (From ref. 41.)

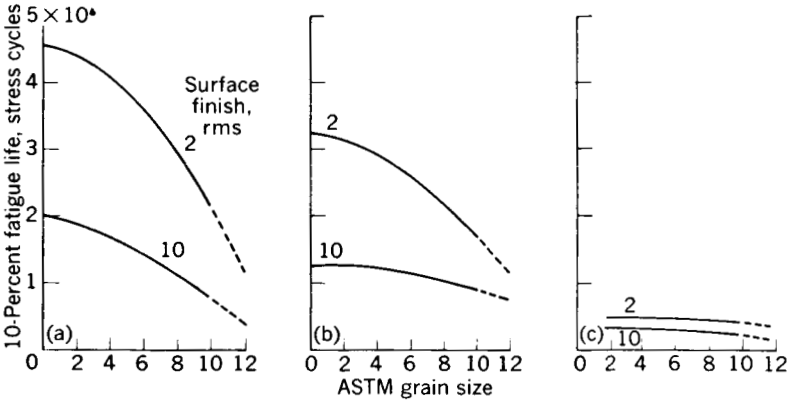

(a) Hardness, Rockwell C–62¼. (b) Hardness, Rockwell C–58. (c) Hardness, Rockwell C–54.

FIGURE 12–36.—Effect of grain size on 10-percent fatigue life for various hardnesses and surface finishes. (From ref. 42.)

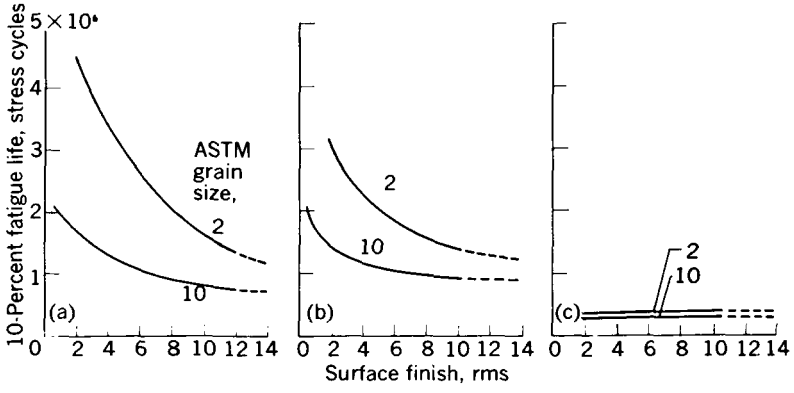

(a) Hardness, Rockwell C–62¼. (b) Hardness, Rockwell C–58. (c) Hardness, Rockwell C–54.

FIGURE 12–37.—Effect of finish on 10-percent fatigue life for various hardnesses and grain sizes. (From ref. 42.)

the surface becomes rougher. Life appears to improve continuously over the entire range of hardnesses at the finer values of surface finish and to peak at an intermediate hardness level at the coarsest surface finish. For example, at a surface finish of 10 rms and a grain size of 2, the maximum 10-percent life occurs at a hardness of Rockwell C–62. From the results of reference 42, maximum 10-percent life for M–50 steel is obtained at maximum hardness (Rockwell C–64 in this investigation), the finest surface finish, and the largest grain size.

From the mass of fatigue data accumulated with materials of various hardnesses, maximum fatigue life is obtained with the highest hardness material. Highest hardness means the maximum hardness obtainable with reasonable heat-treatment procedures. This conclusion appears to be true for the various iron-base alloys, which are candidates for bearing materials for service at temperatures up to 1000° F. In most instances, the rate of increase of fatigue life (or load capacity) with increasing hardness diminished at higher hardness values, which indicates that further increases in hardness would produce little benefit in extended life.

Fiber Orientation

The races and rolling elements of most rolling-element bearings are formed by forging. Any metallic object formed by forging generally possesses a fiber flow pattern that reflects the flow of metal during the forming operation. Nonmetallic inclusions are progressively elongated during each forming operation from the ingot to the final bearing-element shape, and although the desired metallic crystalline

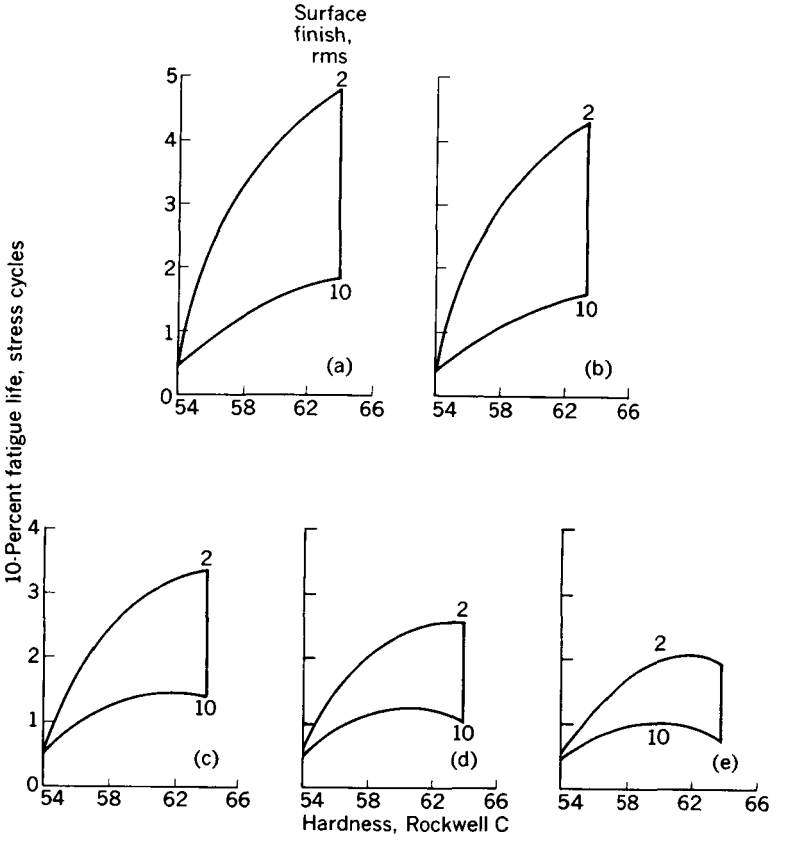

(a) ASTM grain size, 2. (b) ASTM grain size, 4.

(c) ASTM grain size, 6. (d) ASTM grain size, 8. (e) ASTM grain size, 10.

FIGURE 12–38.—Effect of hardness on 10-percent fatigue life for various grain sizes and surface finishes. (From ref. 42.)

structure is obtained by heat treatment, the inclusions retain their accumulated elongation pattern. This pattern is best described as fibrous in appearance; hence the term fiber flow lines. The type of forging used to produce rolling-element bearing components determines the fiber pattern that exists in these bearing parts. The effect on fatigue of the orientation of fibers with respect to the surface being tested is reported in references 15 and 41.

In particular, steel balls are usually fabricated by upsetting between hemispherical dies. This fabrication technique produces a fiber flow pattern with two diametrically opposed areas having fibers oriented approximately perpendicular to the surface. These areas are commonly known as the poles. The excess metal extruded from between

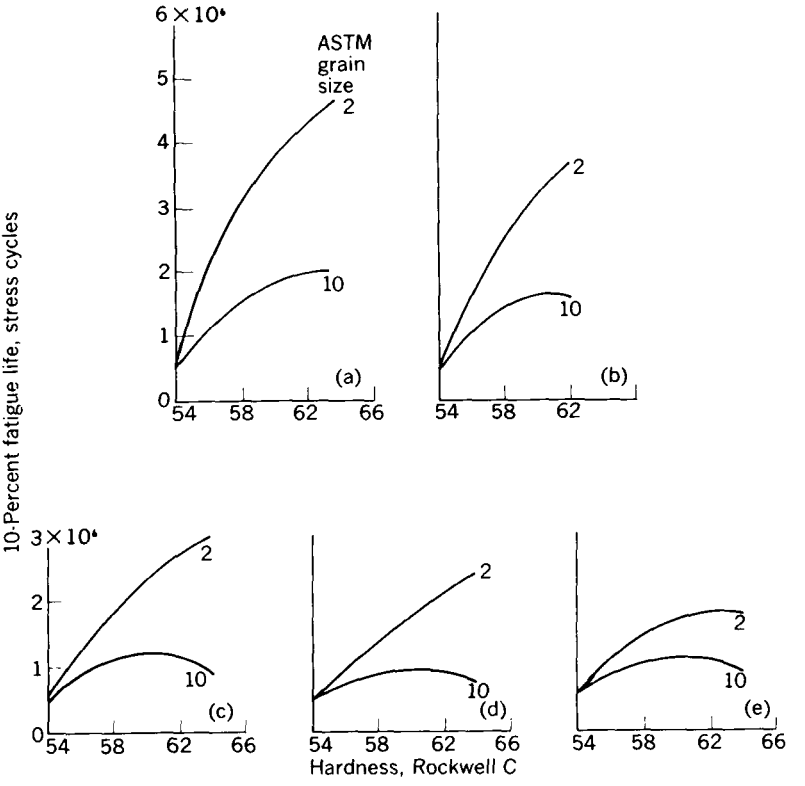

(a) Surface finish, 2 rms. (b) Surface finish, 4 rms.

(c) Surface finish, 6 rms. (d) Surface finish, 8 rms. (e) Surface finish, 10 rms.

FIGURE 12–39.—Effect of hardness on 10-percent fatigue life for various grain sizes and surface finishes. (From ref. 42.)

the two dies produces a thin band of perpendicularly oriented fiber when the flashing at the die parting line is removed. This line, when present, is commonly termed the equator. Thus, a typical ball has several surface areas with varying fiber orientation.

The initial effect of fiber orientation on fatigue life (ref. 15) was carried out in the spin tester using two lots of SAE 52100 balls. Each of these two lots of balls was modified during manufacture by a 0.050-inch hole drilled diametrically through it. This predetermined the axis of rotation and enabled one lot to be run over the poles and the other on the equator. The results obtained from these tests are shown in figure 12–40. The results are shown as a bar graph, because most of the balls run on the equator did not fail after 10^9 stress cycles. The 10-percent life obtained from the balls run over the poles was of the order of 17×10^6 stress cycles. These results indicate a significant

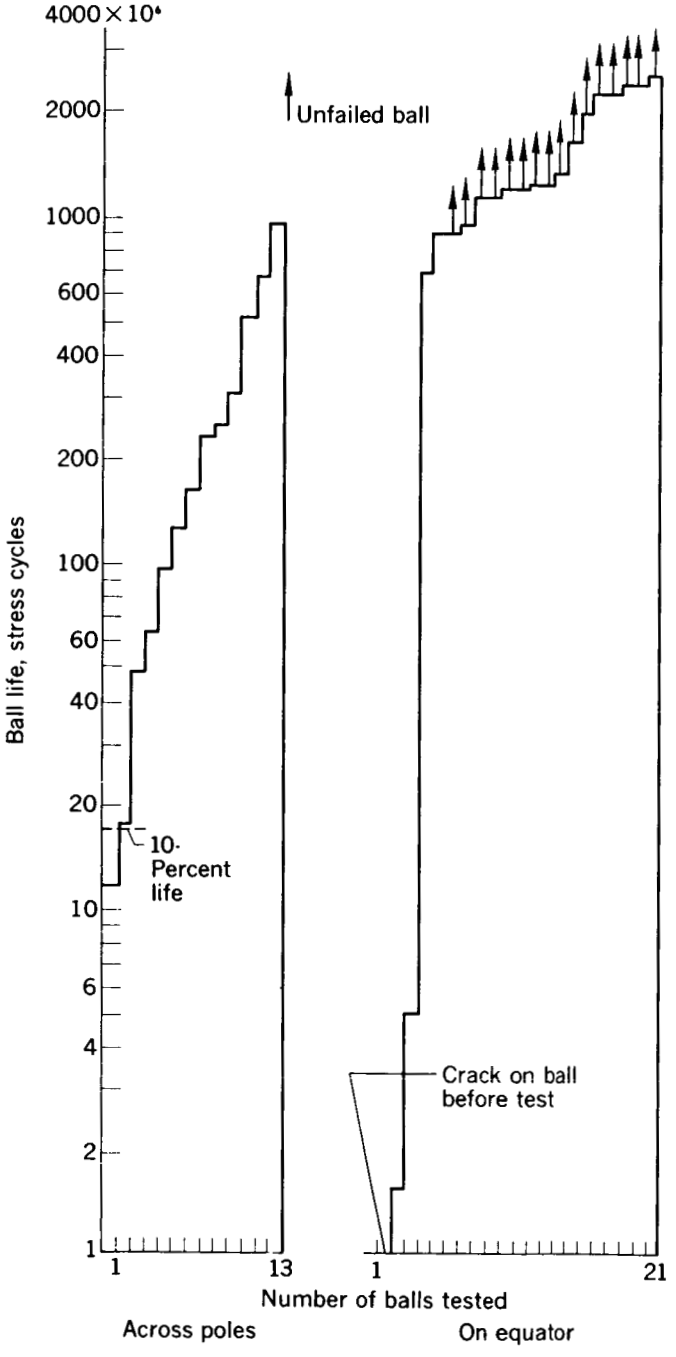

FIGURE 12–40.—Comparison of tests in which SAE 52100 balls ran on equator and across poles. Room temperature; synthetic diester lubricant; maximum Hertz compressive stress, 714,000 psi. (From ref. 41.)

improvement in fatigue life when the test track did not pass through the poles.

Fatigue data obtained with 10 different ball materials (ref. 15) were then examined with respect to the location of specific spalls on the ball test specimens. Each of the ball specimens was destructively etched after testing to indicate the location of the failure relative to the pole areas. From these data, a plot of failure density against ball latitude starting at 0° at the equator and going 90° to the center of each pole was made. These data (fig. 12–41) indicate that a small increase in

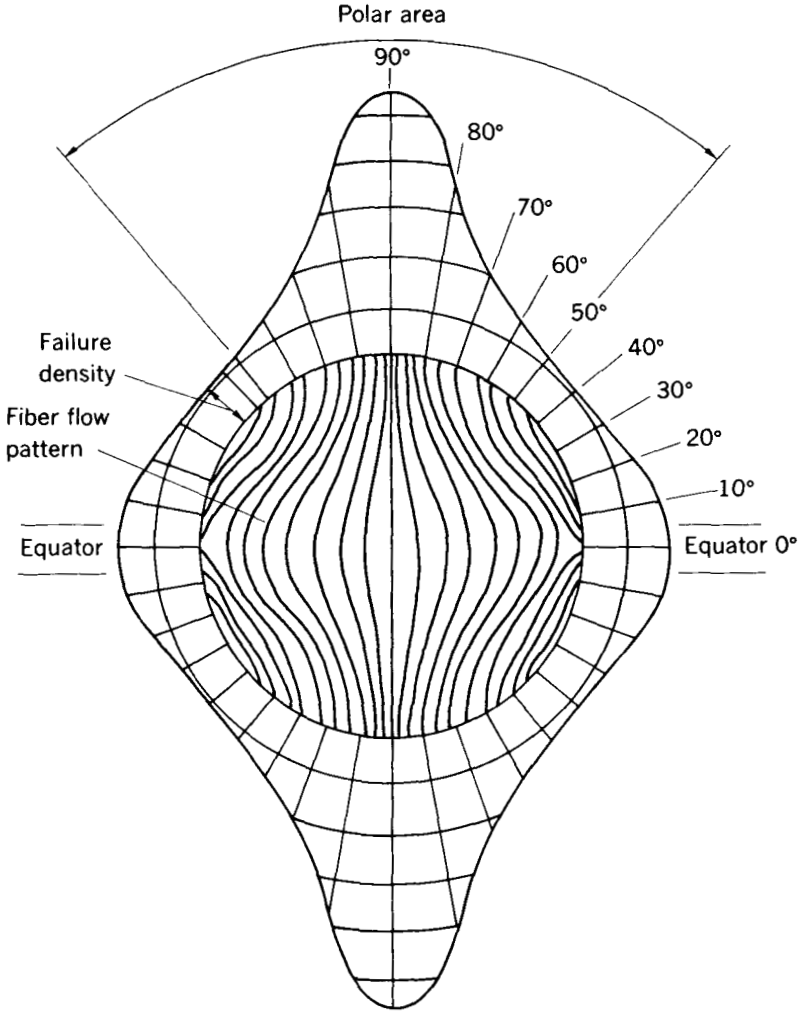

FIGURE 12–41.—Failure density as function of ball latitude (for 211 failures and 10 materials). (From ref. 41.)

failure density occurs at the equator where the thin band of perpendicular fiber exists, and a very significant increase in failure density occurs in the polar areas or regions where fiber is essentially perpendicular to the test surface.

Specimens with controlled fiber flow were obtained by machining race cylinders from a billet of AISI T–1 steel at various angles to the direction of forging to obtain better control of fiber orientation than is available in ordinary test balls. As shown in figure 12–42, three cylinders were machined with axes parallel to, at 45° to, and perpendicular to the direction of fiber flow. The first cylinder had fiber flow parallel to the test surface (0° cylinder), the second had fiber orientation that ranged continuously from parallel to 45° to the test surface (0° to 45° cylinder), and the third had fiber orientation that ranged continuously from parallel to perpendicular to the test surface (0° to 90° cylinder). For each of these three test cylinders, approximately 60 failures were obtained. The fatigue-life results for the three special test cylinders are given in figure 12–43. The 0° cylinder had the best life, while the 0° to 45° and 0° to 90° cylinders had approximately equal lives. The difference in 10-percent lives represents about two standard deviations. These data indicate that there is a significant difference in life between the 0° cylinder and the other two cylinders.

In addition to the fatigue-life data obtained from these cylinders, further evidences of the effect of fiber orientation on fatigue were obtained by examining failure density as a function of fiber-orientation angle. In both the 0° to 45° and 0° to 90° cylinders, there are four similar 90° quadrants so that the data could be condensed into one equivalent quadrant. The equivalent quadrant was then divided into four zones for the 0° to 45° cylinder and five zones for the 0° to 90° cylinder, and the number of failures in each zone were counted. The resulting histograms are shown in figure 12–44. This figure shows

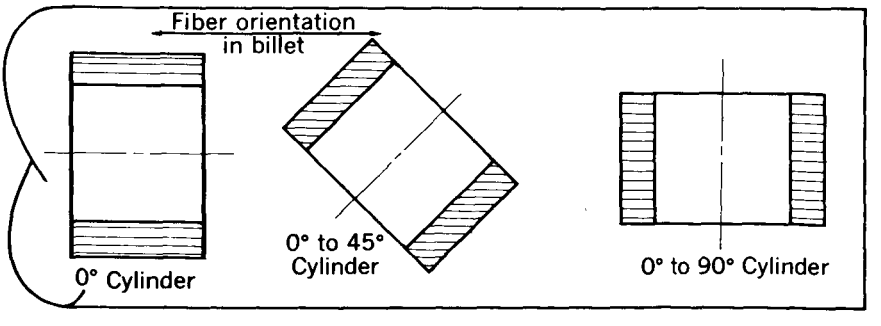

FIGURE 12–42.—T–1 tool-steel-cylinder orientation in billet stock. (From ref. 41.)

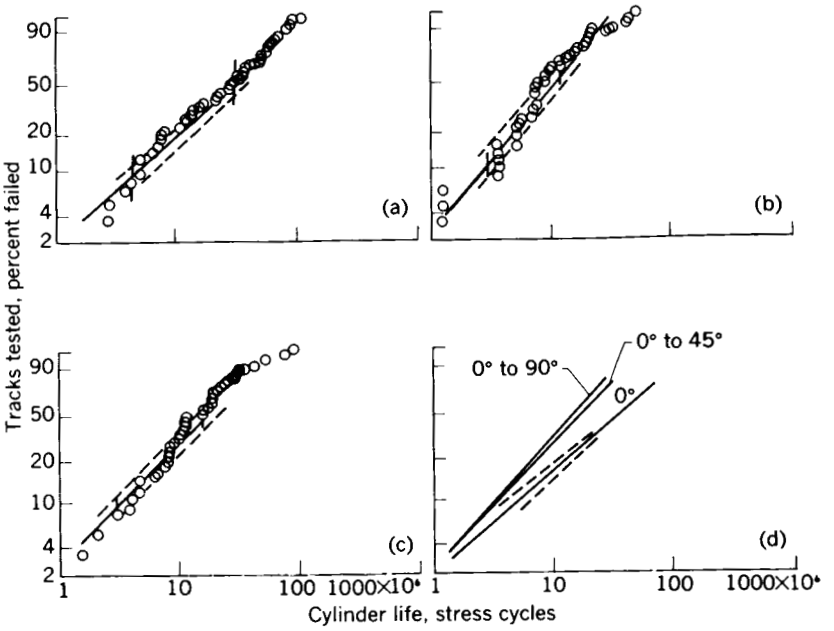

(a) 0° cylinder.

(b) 0° to 45° cylinder.

(c) 0° to 90° cylinder.

(d) Comparison of three cylinders.

FIGURE 12–43.—Fatigue life data for specially oriented T–1 tool-steel cylinders. Dashed line indicates standard deviation. Room temperature; lubricant, SAE 10 mineral oil; maximum Hertz compressive stress, 750,000 psi. (From ref. 41.)

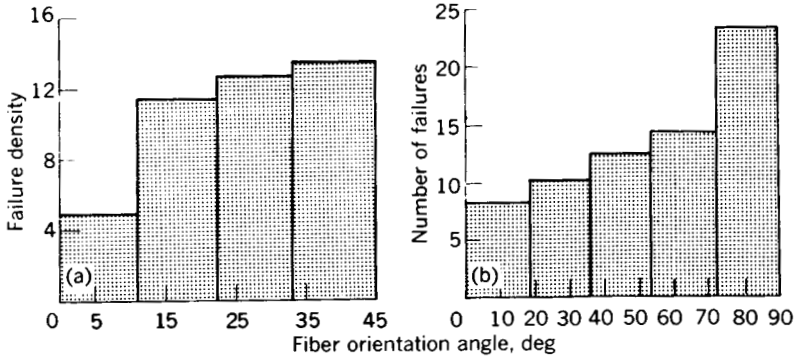

(a) 0° to 45° cylinder.

(b) 0° to 90° cylinder.

FIGURE 12–44.—Variation in failure density with fiber-orientation angle in the 0° to 45° and 0° to 90° T–1 tool steel cylinders. (From ref. 41.)

that for both cylinders, the failure density is significantly higher in the regions of greater fiber-orientation angles than in the regions where

the fibers are oriented almost parallel to the test surface. Thus both life and failure-density data indicate that large fiber-orientation angles are detrimental to rolling-contact fatigue.

Jackson (ref. 38) also found that a greater than expected failure incidence occurred in the polar areas of ball specimens. These data are shown in table 12–XXIV.

To summarize the fiber orientation results obtained in references 15, 38, and 41 with ball and cylinder specimens, it would appear that better life could be obtained with rolling-element bearings if forging processes are used, which result in parts having fiber flow parallel or nearly so to the test surface.

Contact Angle

Palmgren (ref. 1) and Lundberg and Palmgren (ref. 2) suggest that the load-carrying capacity of a thrust bearing increases as a function of increasing contact angle. As contact angle is increased for a constant bearing thrust load, the normal ball load is decreased. Since the Lundberg-Palmgren theory predicts constant life with constant normal ball load, fatigue life should increase. Unpublished ball-fatigue data obtained from Pratt & Whitney Aircraft for specimens in the one-ball tester indicate that at contact angles of 30° to 55°, fatigue life decreases with increasing contact angle at constant normal ball load. These data, therefore, imply a quantitative discrepancy between the theory and the experimental results. Further experiments to determine the effect of contact angle on fatigue are reported in reference 36. The five-ball fatigue tester was used in these experiments with tests conducted at contact angles of 10°, 20°, 30°, and 40°. The Pratt & Whitney tests, in the one-ball tester, were conducted using V-grooved rollers with the V-groove angle changed to vary the contact angle. The fatigue-life results obtained by Pratt & Whitney and in reference 36 are summarized in figure 12–45. A smooth curve results when the data from both testers are plotted against contact angle, with life at constant contact stress that shows a continuous decrease with increasing contact angle. These life data were converted to thrust-load capacity and compared with the predicted thrust-load capacity as shown in figure 12–46. Again, the data for the two testers plot as a smooth curve. The experimental capacity agrees well with the predicted capacity at contact angles up to 30°. At contact angles above 30°, the experimental capacity is less than the predicted capacity, and the deviation increases as contact angle is increased.

The discrepancy between thrust capacity as predicted by the Lundberg-Palmgren theory and experimental results may be due to one or more of several factors. As contact angle is increased, the ball

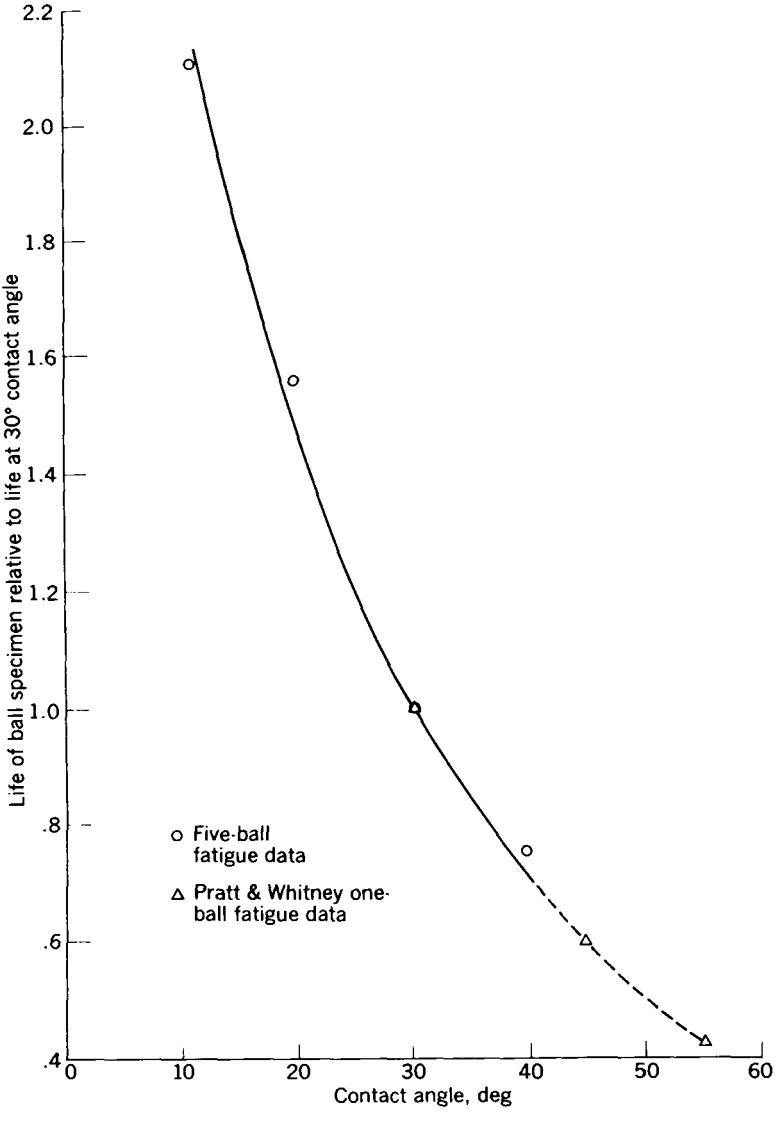

FIGURE 12–45.—Effect of contact angle at constant stress and stress volume on life of ball specimen relative to life at 30° contact angle. (From ref. 36.)

spin velocity (and, therefore, the relative sliding between ball and race) is increased. The variation of life with relative angular spin velocity is shown in figure 12–47. As contact angle, and thus spin velocity, are increased, the rate of heat generation rises. An increase in contact temperature, which has already been shown to be detrimental to fatigue life, results. Increased friction and heat generation

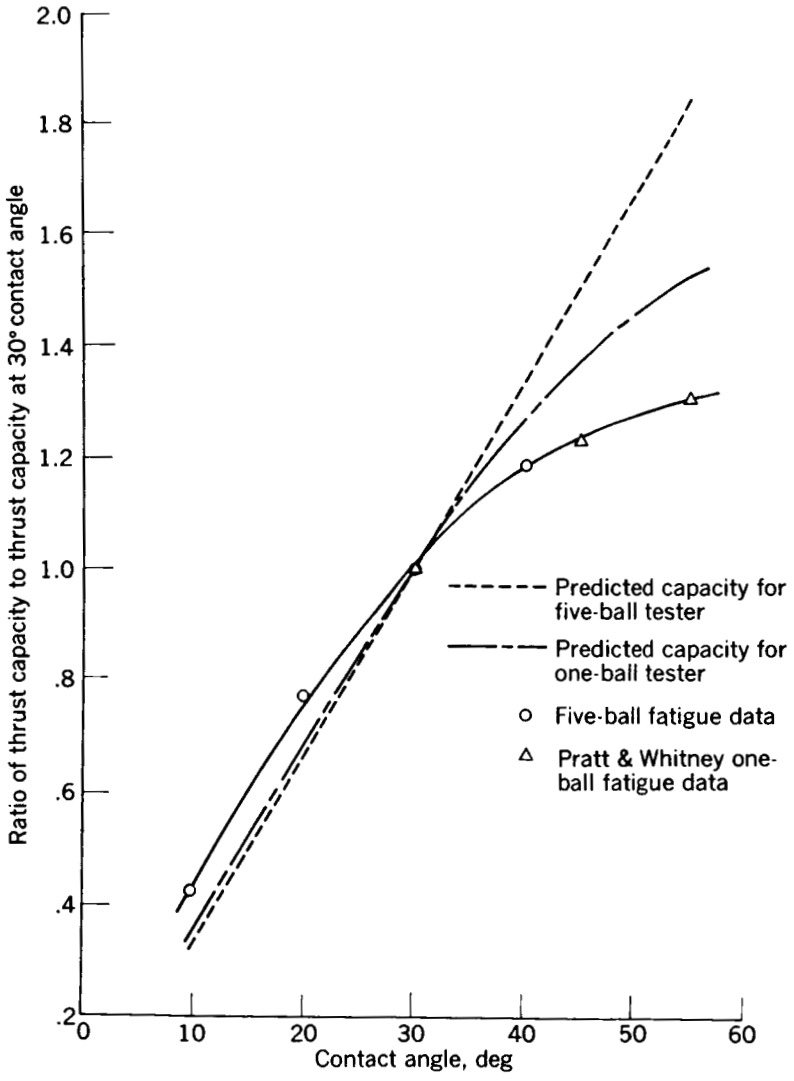

FIGURE 12–46.—Increase in thrust capacity relative to thrust capacity at 30° measured experimentally and as predicted by the Lundberg-Palmgren equation. (From ref. 36.)

can also increase the shearing stresses for two bodies in contact. The effects of friction coefficient on shearing stresses are treated theoretically by Smith and Liu (ref. 43) and those of heat generation by Melan (ref. 44). The authors of reference 33 discuss possible effects of thermal stresses.

Another factor, which may be relevant, is the effect of sliding on viscosity and other rheological properties of the lubricant film. Sibley

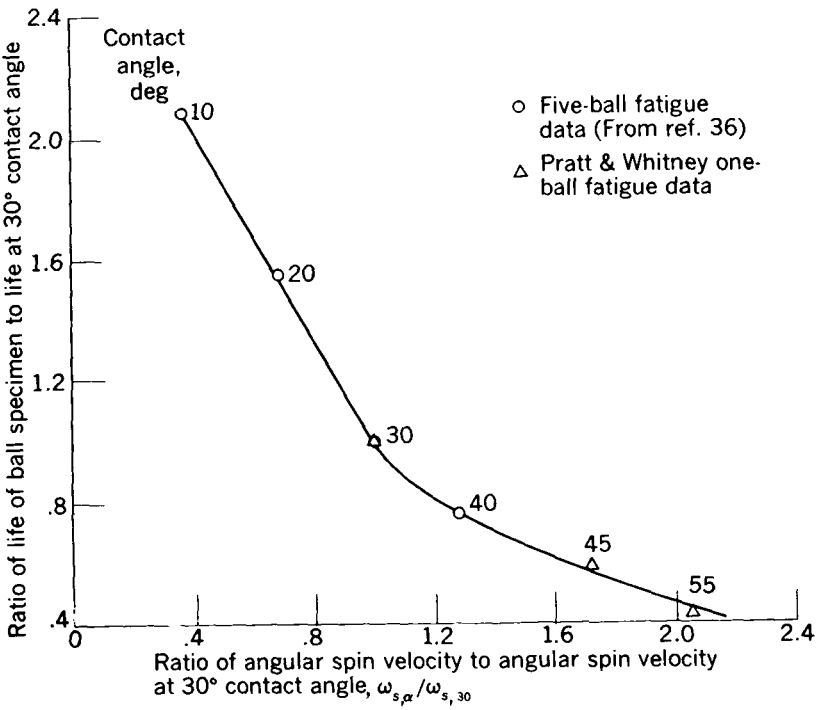

FIGURE 12–47.—Life of ball specimen relative to life at 30° contact angle against angular spin velocity relative to angular spin velocity at 30° contact angle at constant stress and stress volume.

and Orcutt (ref. 45) show experimentally that the geometry of the contact area of two rolling surfaces changes with lubricant shear rate and temperature. Further investigations with carefully controlled variables are necessary to define the importance of rheological properties on fatigue life.

REFERENCES

1. PALMGREN, A.: Ball and Roller Bearing Engineering. Third ed., SKF Industries, Inc., 1959.
2. LUNDBERG, G., and PALMGREN, A.: Dynamic Capacity of Rolling Bearings. Acta Polytech., Mech. Eng. Ser., vol. 1, no. 3, 1947.
3. WEIBULL, W.: A Statistical Theory of the Strength of Materials. Proc. Roy. Swedish Academy Eng. Sci., no. 151, 1939.
4. WEIBULL, W.: The Phenomenon of Rupture in Solids. Proc. Roy. Swedish Academy Eng. Sci., no. 153, 1939.
5. WEIBULL, W.: A Statistical Representation of Fatigue Failures in Solids. Trans. Roy. Inst. Tech., no. 27, Stockholm (Sweden), 1949.
6. TALLIAN, T.: Weibull Distribution of Rolling Contact Fatigue Life and Deviations Therefrom. Trans. ASLE, vol. 5, no. 1, Apr. 1962, pp. 183–196.

7. LIEBLEIN, J., and ZELEN, M.: Statistical Investigation of the Fatigue Life of Deep-Groove Ball Bearings. Jour. Res. Nat. Bur. Standards, vol. 57, no. 5, Nov. 1956, pp. 273–316.
8. BUTLER, ROBERT H., and CARTER, THOMAS L.: Stress-Life Relation of the Rolling-Contact Fatigue Spin Rig. NACA TN 3930, 1957.
9. MACKS, E. F.: The Fatigue Spin Rig—A New Apparatus for Rapidly Evaluating Materials and Lubricants for Rolling Contact. Lubrication Eng., vol. 9, no. 5, Oct. 1953, pp. 254–258.
10. CARTER, THOMAS L., and ZARETSKY, ERWIN V.: Rolling-Contact Fatigue Life of a Crystallized Glass Ceramic. NASA TN D-259, 1960.
11. BARWELL, F. T., and SCOTT, D.: Effect of Lubricant on Pitting Failure of Ball Bearings. Engineering, vol. 182, no. 4713, July 6, 1956, pp. 9–12.
12. SCOTT, D.: Lubricants at Higher Temperatures: Assessing the Effects on Ball Bearing Failures. Engineering, vol. 185, no. 4811, May 23, 1958, pp. 660–662.
13. CORDIANO, H. V., COCHRAN, E. P., JR., and WOLFE, R. J.: A Study of Combustion Resistant Hydraulic Fluids as Ball Bearing Lubricants. Lubrication Eng., vol. 12, no. 4, July–Aug. 1956, pp. 261–266.
14. BAUGHMAN, R. A.: Experimental Laboratory Studies of Bearing Fatigue. Paper 58–A–235, ASME, 1958.
15. CARTER, THOMAS L.: A Study of Some Factors Affecting Rolling-Contact Fatigue Life. NASA TR R–60, 1960.
16. ANDERSON, W. J., and CARTER, T. L.: Effect of Lubricant Viscosity and Type on Ball Fatigue Life. Trans. ASLE, vol. 1, no. 2, Oct. 1958, pp. 266–272.
17. Anon.: Viscosity and Density of Over 40 Lubricating Fluids of Known Composition at Pressures to 150,000 PSI and Temperatures to 425° F. Vol. II. ASME, 1953.
18. CORDIANO, H. V., COCHRAN, E. P., JR., and WOLFE, R. J.: Effect of Combustion Resistant Hydraulic Fluids on Ball Bearing Fatigue Life. Preprint 55–LUB–21, ASME, 1955.
19. ROUNDS, F. G.: Effects of Base Oil Viscosity and Type on Bearing Ball Fatigue. Preprint 61 LC–13, ASLE, 1961.
20. SCOTT, D.: Study of the Effect of Lubricant on Pitting Failure of Balls. Proc. of Conf. on Lubrication and Wear, Inst. Mech. Eng., 1957, pp. 463–468.
21. GRUNBERG, L., and SCOTT, D.: The Acceleration of Pitting Failure by Water in the Lubricant. Jour. Inst. Petroleum, vol. 44, no. 419, Nov. 1958, pp. 406–410.
22. GRUNBERG, L., and SCOTT, D.: The Effect of Additives on the Water-Induced Pitting of Ball Bearings. Jour. Inst. Petroleum, vol. 46, no. 440, Aug. 1960, pp. 259–266.
23. SCOTT, D.: The Effect of Lubricant Viscosity on Ball Bearing Fatigue Life. Rep. LDR 44/60, Dept. of Sci. and Ind. Res., Nat. Eng. Lab., Dec. 1960.
24. OTTERBEIN, MARK E.: The Effect of Aircraft Gas Turbine Oils on Roller Bearing Fatigue Life. Trans. ASLE, vol. 1, no. 1, Apr. 1958, pp. 33–40.
25. WAY, STEWART: Pitting Due to Rolling Contact. Jour. Appl. Mech., vol. 2, no. 1, June 1935, pp. A49–A58; discussion, pp. A110–A114.
26. JONES, A. B.: Metallographic Observations of Ball Bearing Fatigue Phenomena. Symposium on Testing of Bearings, ASTM, 1947, pp. 35–48; discussion, pp. 49–52.
27. DÖRR, J.: Schmiermitteldruck und Randverformungen des Rollenlagers Ing. Archiv, bd. XXII, 1954, pp. 171–193.

28. GRUBIN, A. N., and VINOGRADOVA, I. E., eds.: Investigation of the Contact of Machine Components. CTS-235, Dept. Sci. and Ind. Res. (British), 1949. (Trans. of Russian book.)
29. PETRUSEVICH, A. E. (I. C. Lecompte, trans.): Basic Conclusions from the Contact-Hydrodynamic Theory of Lubrication Greases. Reps. Acad. Sci. USSR, Dept. Tech. Sci., no. 2, Feb. 1951, pp. 209–223. (Bur. Ships Trans. 480.)
30. PORITSKY, H.: Lubrication of Gear Teeth, Including the Effect of Elastic Displacement. Paper Presented at ASLE Nat. Symposium on Fundamentals of Friction and Lubrication in Eng., 1952.
31. WEBER, C., and SAAFELD, K.: Schmierfilm bei Walzen mit Verformung. Zs. angew. Math. Mech., bd. 34, 1954, p. 54.
32. DOWSON, D., and HIGGINSON, G. R.: A Numerical Solution to the Elasto-Hydrodynamic Problem. Jour. Mech. Eng. Sci., vol. 1, no. 1, 1959, pp. 6–15.
33. STERNLICHT, B., LEWIS, P., and FLYNN, P.: Theory of Lubrication and Failure of Rolling Contacts. Jour. Basic Eng. (Trans. ASME), ser. A, vol. 83, no. 2, June 1961, pp. 213–226.
34. ZARETSKY, ERWIN V., and ANDERSON, WILLIAM J.: Rolling-Contact Fatigue Studies with Four Tool Steels and a Crystallized Glass Ceramic. Jour. Basic Eng. (Trans. ASME), ser. D, vol. 83, no. 4, Dec. 1961, pp. 603–612.
35. JONES, A. B.: The Life of High-Speed Ball Bearings. Trans. ASME, vol. 74, no. 5, July 1952, pp. 695–703.
36. ZARETSKY, E. V., ANDERSON, W. J., and PARKER, R. J.: The Effect of Contact Angle on Rolling-Contact Fatigue and Bearing Load Capacity Trans. ASLE, vol. 5, no. 1, Apr. 1962, pp. 210–219.
37. MORRISON, T. W., WALP, H. O., and REMORENKO, R. P.: Materials in Rolling-Element Bearings for Normal and Elevated (450° F) Temperatures. Trans. ASLE, vol. 2, no. 1, Apr. 1959, pp. 129–146.
38. JACKSON, E. G.: Rolling Contact Fatigue Evaluation of Bearing Materials and Lubricants. Trans. ASLE, vol. 2, no. 1, 1959, pp. 121–128.
39. IRWIN, ARTHUR S.: Effect of Bearing Temperature on Capacities of Bearings of Various Materials. Paper Presented at ASME Lubrication Symposium, New York (N.Y.), Mar. 14–15, 1960.
40. ZARETSKY, E. V., and ANDERSON, W. J.: Relation between Rolling-Contact FatigueLife and Mechanical Properties for Several Aircraft Bearing Steels. Trans. ASTM, vol. 60, 1960, pp. 627–649.
41. BIDWELL, J. B.: Rolling Contact Phenomena. Elsevier Pub. Co., 1962, pp. 317–345.
42. BAUGHMAN, R. A.: Effect of Hardness, Surface Finish, and Grain Size on Rolling-Contact Fatigue Life of M-50 Bearing Steel. Jour. Basic Eng. (ASME Trans.), ser. D, vol. 82, no. 2, June 1960, pp. 287–294.
43. SMITH, J. O., and LIU, C. K.: Stresses Due to Tangential and Normal Loads on an Elastic Solid with Application to Some Contact Stress Problems. Jour. Appl. Mech., vol. 20, no. 2, June 1953, pp. 157–166.
44. MELAN, E.: Wärmespannungen in einer Scheibe infolge einer Wandernden Wärmequelle. Ingenieur-Archiv, bd. 20, 1952, pp. 46–48.
45. SIBLEY, L. B., and ORCUTT, F. K.: Elasto-Hydrodynamic Lubrication of Rolling-Contact Surfaces. ASLE Trans., vol. 4, no. 2, Nov. 1961, pp. 234–249.

CHAPTER 13

Liquid Metals as Working Fluids for Power-Generation Systems to be Used in Space

By EDMOND E. BISSON

SPACE EXPLORATION REQUIRES THE DEVELOPMENT of power-generation systems suitable both as auxiliary-power and as main-power sources for space vehicles. These space vehicles may be satellites or man-carrying vehicles; in either case, long periods of continuous, reliable operation of the power-generation system will be necessary. Requirements for these power systems are light weight, high reliability, and minimum complexity. Attainment of these goals depends on a number of factors, each of which has a strong influence on the success or failure of a particular system.

This chapter therefore reviews and discusses the following items:

(1) The required power for various missions
(2) The various systems to produce these powers
(3) The turbine generator system for both low and high power levels
(4) Working fluids (includes a discussion of physical properties and corrosion)

While the discussion will chiefly concern space power-generation systems, some of the features discussed also apply to stationary Earth-based power stations.

REQUIRED POWER AND COMPARISON OF VARIOUS SYSTEMS

Electric power is required in space for communications, propulsion, and other miscellaneous tasks. Slone and Lieblein (ref. 1) indicate that

> . . . for the next 5 to 8 years it is anticipated that, for unmanned scientific satellite and [space] probes, power requirements of up to about 5 kilowatts will be adequate in most cases. An average power of about 260 watts and a peak power not to exceed 1000 watts will be required for the first manned flight planned by the NASA. This mission, called Project Mercury, will send one man into a low-altitude orbit for about 4 hours. Following Project Mercury, early manned flight may require up to about 2 kilowatts per man depending on the duration of the flight.

Slone and Lieblein also indicate that primary electric propulsion systems for unmanned (space) probes will be in the power level range from 30 to about 20,000 kilowatts for the next decade. On the basis of their studies, they plotted the data of figure 13–1, which presents

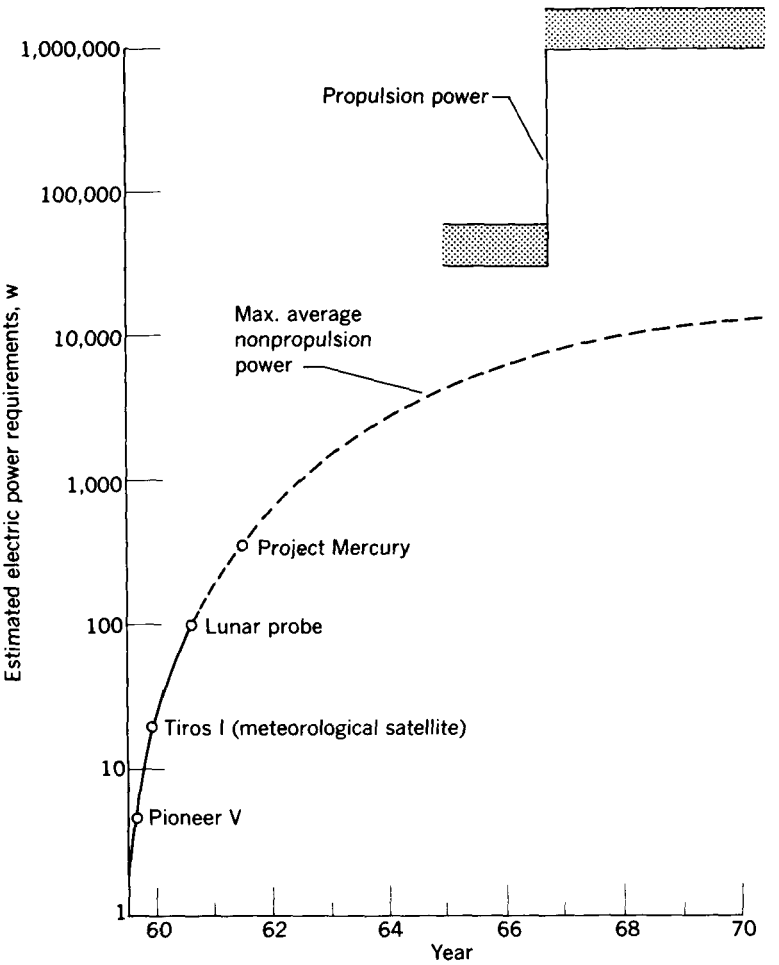

FIGURE 13–1.—Space power requirements. (From ref. 1.)

a curve of the maximum average nonpropulsion power in the period from 1959 through 1970. This figure also shows the propulsion power anticipated in the period from 1965 through 1970. This power level is something in the order of 30,000 watts at first and reaches into the million-watt range later. In accordance with figure 13–1, therefore, it is obvious that power requirements ranging from several hundred watts up to millions of watts will be required.

Slone and Lieblein also made a comparison of the various energy systems on the basis of the four major factors, reliability, weight, lifetime, and power level. Their conclusions were that systems based on chemical-energy sources (the battery, the fuel cell, and the chemical turbogenerator) have high specific weights except for short-time applications. They also concluded that conversion devices based on solar energy will probably be restricted to low (less than 1 kw) or moderate (about 1 to 100 kw) power levels; nuclear energy sources should be more practical for the high power levels (100 kw and up). They felt that limitations on inventory size as well as on specific weight would restrict radioisotope systems to power levels below about 1 kilowatt. Of the many possible conversion devices that can be used with solar and nuclear energy sources for these requirements, the turbogenerator system and the thermionic emitter system have low specific weights.

Figure 13–2 is a plot of specific weight as a function of electric power of a number of power-generation systems. The specific points in figure 13–2 represent actual systems in the development stage such as Snap 1, Snap 2, Snap 8, Snap 10, and Sunflower 1. In the power range from 1 to 10 kilowatts, the turbogenerator and the reactor

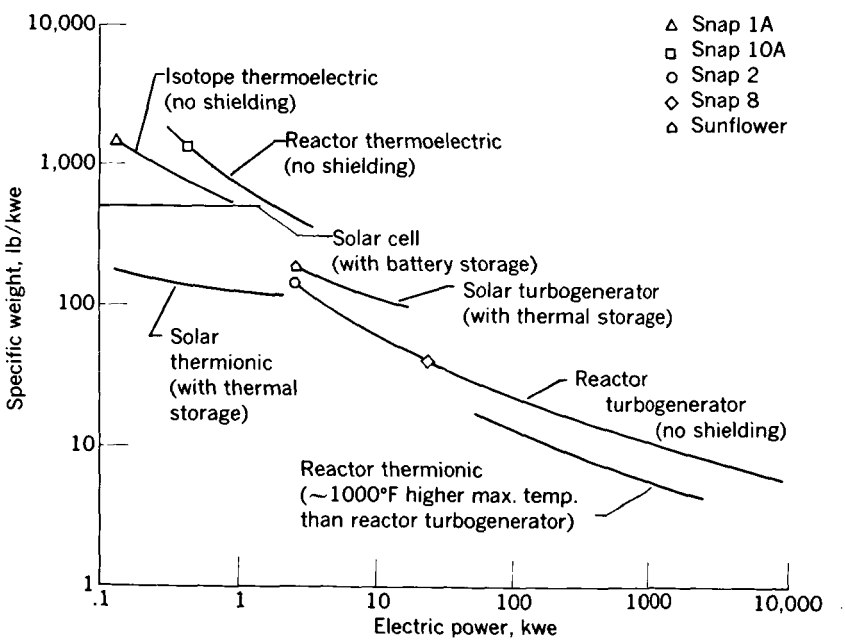

FIGURE 13–2.—Estimated specific weights of power-generation systems. (From ref. 7.)

thermionic systems are promising. In this power range, these systems are approximately competitive. For proplusion power (powers greater than 10 kw), the reactor turbogenerator and the reactor thermionic systems are the only systems with apparent promise. As power level increases, the specific weight of these systems decreases because of the general reduction in reactor specific weight and improved component efficiencies.

From the studies just discussed, it appears that both turbogenerator and thermionic systems are promising at high power levels. Both of these systems of necessity will operate at high temperature for low weight. The turbogenerator system may, as shown later, utilize a liquid metal as the system working fluid. It is also possible that a liquid metal may be used as the coolant for the anode of the thermionic converter. In any event, liquid metals apparently will be employed, and wherever they are used pumps must be used to circulate and increase the pressure of the fluid. These pumps will contain bearings, which will, in all probability, be lubricated and cooled by the working fluid, that is, by a liquid metal. There will be a serious bearing problem under these conditions because of (1) the corrosive nature of the fluid; (2) the reducing nature of the fluid on metal surfaces; (3) the low viscosity of the fluid; (4) bearing erosion, since the fluid may be close to its boiling point and, hence, subject to cavitation; and (5) possible bearing instability problems due to light loads in a poorly damped system. Background information relative to problems 1, 2, and 3 are discussed in this chapter, and detailed discussion of all problems is included in chapter 14.

TURBOGENERATOR SYSTEMS

Cycle Selection

A typical heat-transfer cycle for a turbogenerator using a reactor as the heat source would transfer heat from the reactor to a working fluid, expand the working fluid through a turbine, reject heat, and finally complete the cycle by raising the pressure of the working fluid to its initial pressure level. For space applications, waste heat is rejected by thermal radiation. The Carnot cycle illustrated in figure 13–3(a) is an idealized thermodynamic cycle. The Carnot cycle gives the maximum amount of work obtainable for a heat engine operating between two given temperature limits. The fluid undergoes isentropic compression between points 4 and 1, heat is then added to the fluid isothermally between points 1 and 2, the fluid is expanded isentropically between points 2 and 3, and heat is rejected from the fluid isothermally between points 3 and 4. The Carnot cycle efficiency is equal to $1 - (T_3/T_2)$ (where T is absolute temperature).

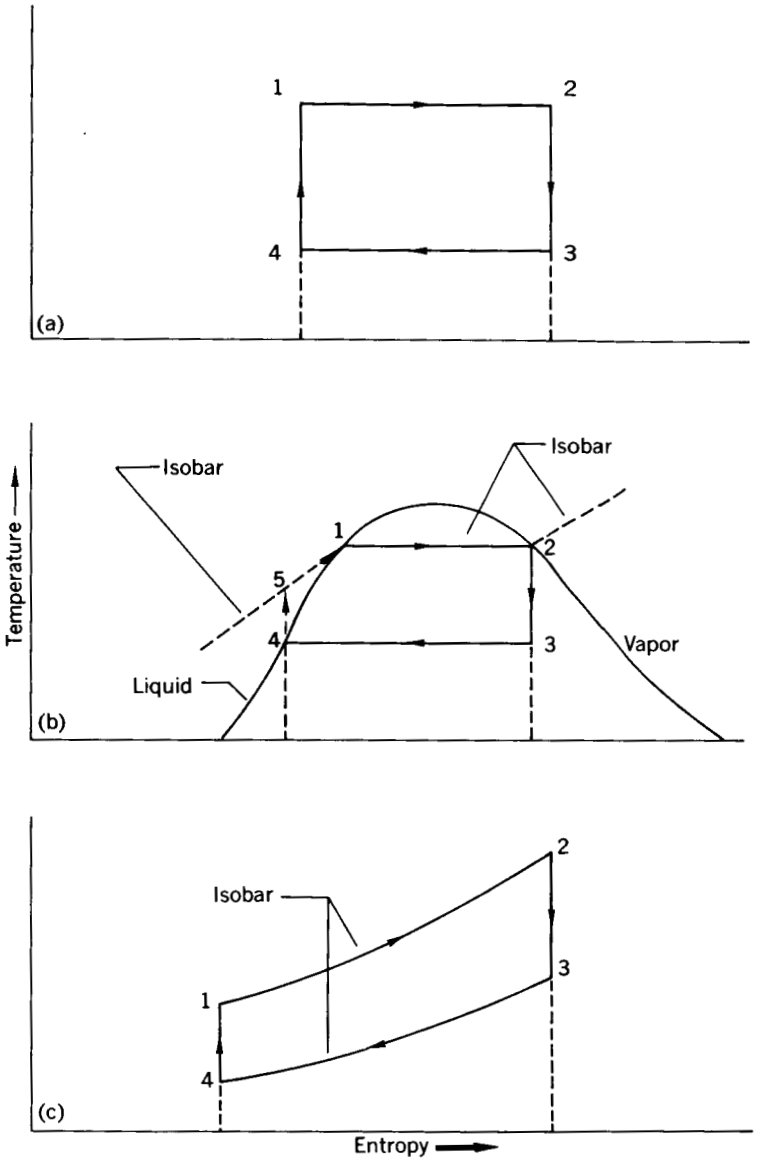

(a) Carnot cycle.
(b) Saturated vapor-liquid cycle.
(c) Brayton gas cycle.

FIGURE 13-3.—Basic (idealized) thermodynamic work cycles. (From ref. 4.)

The Rankine cycle approaches the Carnot cycle in principle, as shown in figure 13-3(b). The liquid is pumped from point 4 to a pressure corresponding to the constant pressure line, point 5 (which

corresponds to the saturation pressure at points 1 and 2). The fluid is then heated at constant pressure to the saturation temperature, point 1; it is vaporized isothermally to reach point 2 and the resulting vapor at point 2 is expanded isentropically in the turbine to the lower temperature at point 3. This fluid is condensed isothermally to point 4 while rejecting heat to the radiator, and the cycle is then repeated. The efficiency of the Rankine cycle is less than that of the corresponding Carnot cycle because the path between points 4 and 1 is not isentropic.

Most actual vapor-liquid cycles differ from the Rankine cycle to the extent that the various portions of the cycle do not correspond exactly to those assumed in the ideal cycle. For example, the flow processes involve pressure losses caused by fluid friction and changes in fluid momentum during phase changes; also the actual pumping and expansion processes are accompanied by entropy increases. Hence, the efficiency is less than that indicated by the ideal Rankine cycle.

The Brayton cycle illustrated in figure 13–3(c) is a gas cycle in that superheated vapor is used throughout the process. As indicated in the figure, the gas is compressed isentropically from points 4 to 1 and is heated at constant pressure to a temperature corresponding to point 2. The fluid is then expanded isentropically in the heat engine to point 3 and this fluid is brought back to point 4 by the rejection of heat to the heat sink. The Brayton cycle is less efficient than a Carnot cycle operating between the same overall temperature limits.

English, Slone, Bernatowicz, Davison, and Lieblein (ref. 2) state that

> preliminary studies show that the radiator is a significant component (weight-wise) at low power levels and becomes the dominant component as the power level is increased. One method for reducing radiator size is to increase the radiator operating temperature. . . . The minimum radiator area occurs at a relatively fixed value of the ratio of radiator-inlet to turbine-inlet temperature. Therefore, in order to minimize radiator area, increasing the turbine-inlet temperature permits an increase in the temperature of the radiator.

Figure 13–4 shows the variation of radiator area required for each kilowatt of power generated for the Rankine cycle. This curve shows that, as vaporization temperature increases, the specific radiator area decreases appreciably. Also, for a given vaporization temperature, the radiator size can be minimized; this minimum is found to be a constant ratio of condensing temperature to vaporization temperature and is approximately 0.75.

Slone and Lieblein (ref. 1) made a comparison of two general types of thermodynamic cycles for nuclear or solar turbogenerator systems. These were the Brayton gas cycle employing helium as the working fluid and the Rankine cycle employing a liquid metal as the working

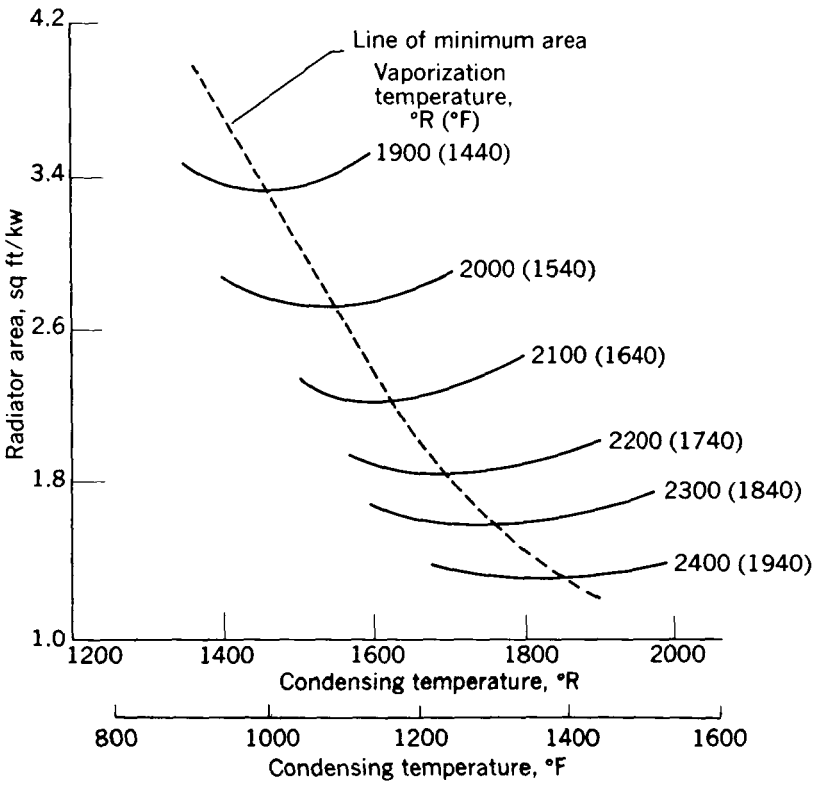

FIGURE 13–4.—Radiator area as a function of temperature. (From ref. 6.)

fluid. For the Brayton cycle, a large gas compressor is required, while for the Rankine cycle only a liquid pump is required. As pointed out in references 1, 2, and 3, component efficiencies can have a large influence on the required specific radiator area. This point is illustrated in figure 13–5. As previously mentioned, the Brayton cycle is less efficient than the Carnot or Rankine cycles; also, the Brayton cycle requirement of a large compressor results in low cycle efficiencies. Therefore, the specific radiator areas required for the helium gas cycle shown in figure 13–5 are considerably higher than those for the vapor cycles utilizing either mercury or sodium vapors. For a turbine-inlet temperature of 2500° R (2040° F), the minimum radiator area for the gas cycle is about six times that of the corresponding vapor cycles. Even if turbine-inlet temperatures as high as 3500° R (3040° F) were permitted, the specific radiator area for the gas cycle would be almost twice that of the vapor cycles. As a consequence, the liquid-vapor cycle is considered most promising.

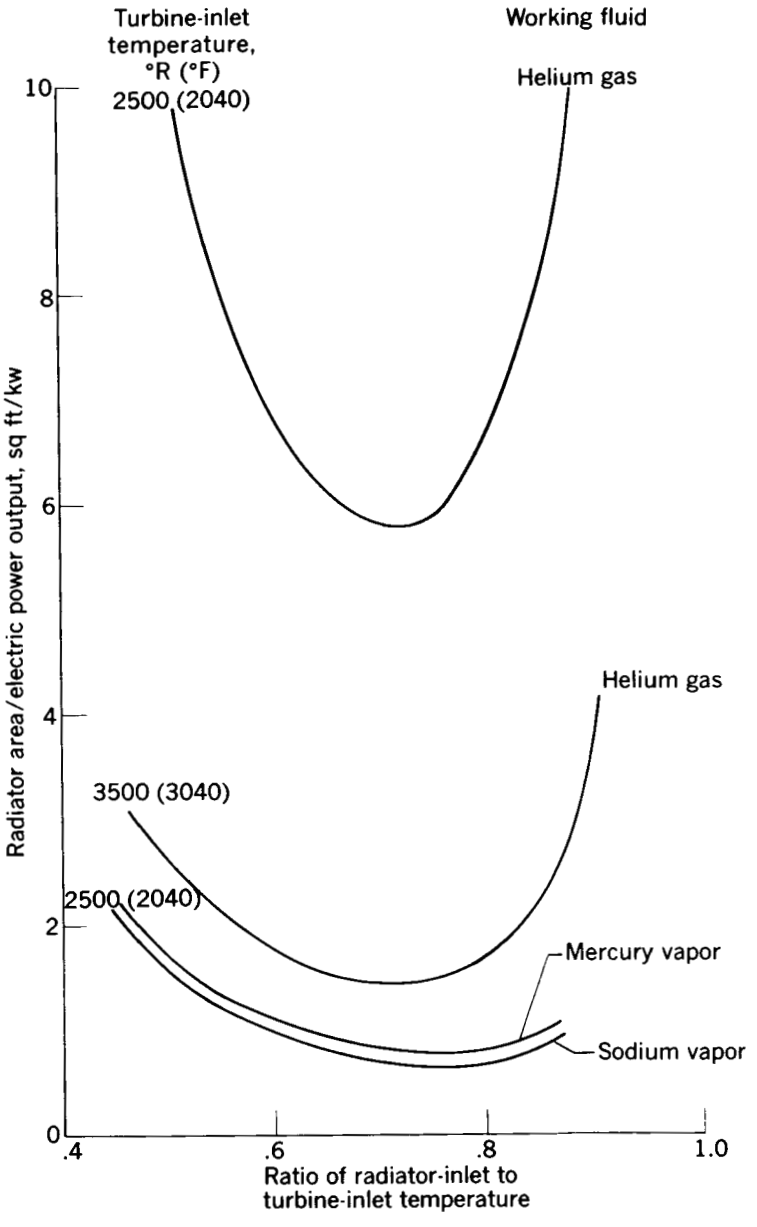

FIGURE 13–5.—Radiator area per kilowatt for turbogenerator systems. (From ref. 1.)

Low-Power System

A schematic diagram of a typical low-power system using a Rankine mercury-vapor cycle and a nuclear-reactor heat source is shown in

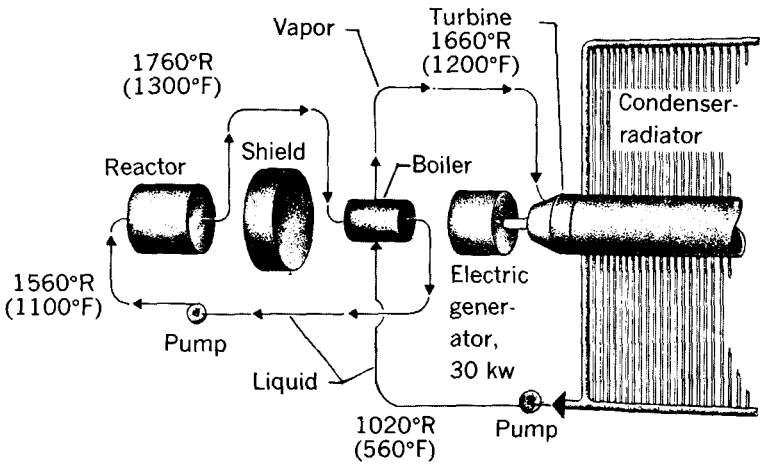

FIGURE 13–6.—Schematic arrangement of typical, low-power nuclear turbogenerator system. (From ref. 1.)

figure 13–6. In this system NaK (sodium-potassium alloy) is heated by the reactor in the primary loop to a temperature of 1760° R (1300° F). The NaK is used to vaporize mercury in the secondary loop. The mercury vapor at 1660° R (1200° F) is then expanded to a temperature of 1020° R (560° F). The vapor from the turbine is condensed in the radiator where the waste heat is rejected by thermal radiation to space. The liquid mercury is then pumped back through the boiler to complete the cycle. This is a two-loop system, which is typical of many of those now under consideration. In this case, a two-loop system was employed for two reasons: (1) to prevent activation of the working fluid (mercury) in the reactor and subsequent contamination of the remainder of the system, and (2) to avoid problems of boiling in the reactor core. As noted, a massive shield is maintained between the reactor and the rest of the system.

Turbogenerator systems may be two-loop systems, as shown in figure 13–6, or one-loop or three-loop systems. Where the working fluid does not become radioactive in the reactor, it may be circulated through the reactor to pick up heat, passed through a "flash boiler," subsequently expanded through a turbine, and returned to the reactor by a condensate pump. In the three-loop system, a third loop may by utilized if the vapor from the turbine is condensed in a separate condenser and the heat is rejected to a coolant in a separate loop between condenser and radiator.

The principle of operation of solar turbogenerator systems is similar to that for the reactor systems with the exception that the

heat source becomes a solar collector, which provides heat to the boiler.

As previously noted, in order to reduce radiator area, it is necessary to maintain (1) high turbine-inlet temperatures, (2) ratio of radiator to turbine-inlet temperature close to its optimum value, and (3) high component efficiencies. It should be recognized that the limitation on turbine-inlet temperatures will be set by corrosion, erosion, and turbine-material strength properties.

High-Power System

English, Slone, Bernatowicz, Davison, and Lieblein (ref. 2) discuss a 20,000-kilowatt turbogenerator system. A schematic arrangement of their system is shown in figure 13–7. As indicated, the arrange-

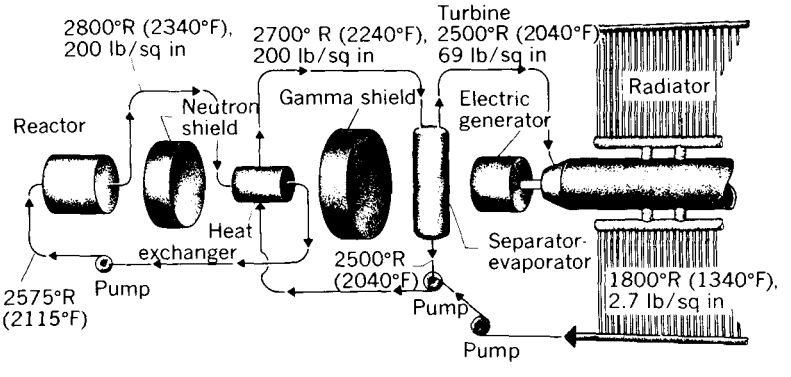

FIGURE 13–7.—Schematic arrangement of high-power nuclear turbogenerator system. (From ref. 2.)

ment is somewhat similar to that for the low-power system previously discussed. In this case, they chose sodium as the working fluid for both loops. This arrangement has sometimes been called a 2½-loop system, since it has sodium flowing through the separator-evaporator, where flash vaporization occurs, as well as through the turbine. In essence, however, this system can be considered a two-loop system. Again, a fluid is circulated through the reactor to be heated, in this case, to 2800° R (2340° F). This sodium is then utilized to heat sodium in the heat exchanger to a temperature of 2700° R (2240° F) at the same pressure of 200 pounds per square inch. The fluid in the primary loop is cooled in this process to 2575° R (2115° F) and is returned to the reactor by a pump. The secondary fluid from the intermediate heat exchanger enters the separator-evaporator and is expanded to 69 pounds per square inch and a high velocity. At this point, the high-velocity fluid (which is about 4 percent vapor)

is centrifuged so as to separate vapor and liquid. The vapor then enters the turbine at a temperature of 2500° R (2040° F) and a pressure of 69 pounds per square inch while the liquid from the separator-evaporator is mixed with the radiator condensate and returned to the heat exchanger. The vapor is expanded in the turbine to 2.7 pounds per square inch (saturation temperature, 1800° R (1340° F); exit quality, 79 percent) to produce work in the turbine. The work fluid is then condensed in the radiator, its pressure is raised in the condensate pumps, and it is returned to the heat exchanger. English, et al. have assumed that the overall cycle efficiency is approximately 20 percent.

A general concept of the reactor area of the powerplant of figure 13–7 is shown in figure 13–8. As noted, the primary fluid passes

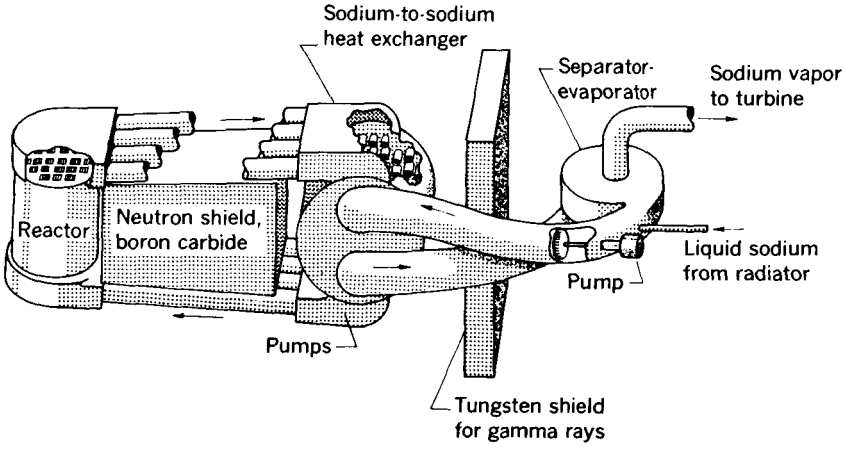

FIGURE 13–8.—Reactor area of powerplant of figure 13–7. (From ref. 2.)

through the reactor and the sodium-to-sodium heat exchanger and is returned to the reactor by pumps. A neutron shield of boron carbide is included; boron carbide has good neutron slowing and absorption properties in addition to its high melting point (ref. 2). Tungsten was chosen as the gamma-shield material for this application because it has a high density and a high melting point.

English, et al. conceived of a space vehicle having a configuration approximately that of figure 13–9. The reactor and its shield were placed at one end of the vehicle and the crew compartment at the other end. The structure joining the reactor and crew compartments is assumed to be so rigid as to maintain the proper orientation of crew compartment and reactor in order that the shadow shield will be effective. The length of the vehicle is rather long in order that advantage may be taken of distance to attenuate the radiation

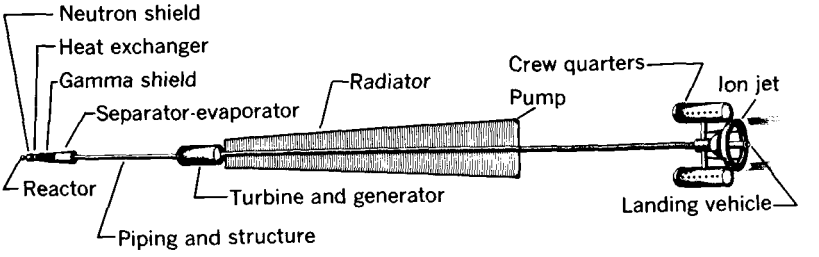

FIGURE 13–9.—Space-vehicle configuration. (From ref. 2.)

received by the crew. The crew dose rate allowed per week was 100 mrem (milliroentgen equivalent man).

Two vehicle lengths were considered: 624 and 286 feet. Shield weights were calculated for these two separation distances. The 624-foot distance was finally chosen because the overall vehicle weight was 8000 pounds less than that for the 286-foot distance.

Working Fluids

Physical properties.—The materials of interest as working fluids for turbogenerator systems are mercury, cesium, rubidium, potassium, NaK, sodium, lithium, bismuth, lead, and sulfur (ref. 4). The properties of interest include vapor pressure, density, viscosity, surface tension, electrical resistivity, thermal conductivity, specific heat, latent heat, enthalpy-entropy relation, melting point, critical properties, dielectric constant, ionization potential, magnetic susceptibility, thermal neutron cross section, and corrosion. Many of these properties are discussed in considerable detail in references 4 and 5.

Table 13–I lists some of the important physical properties of six of the liquid metals. These metals include mercury, rubidium,

TABLE 13–I.—PROPERTIES OF LIQUID METALS

Metal	Melting point, °F	Boiling point, °F	Liquid density, lb/cu ft, at—		Liquid viscosity,[a] reyns, at —		Vapor pressure at 2200° R, lb/sq in. abs
			Boiling point	1200° F	Boiling point	1200° F	
Mercury	−38	674	794	752	13×10^{-8}	[b] 10×10^{-8}	3044
Rubidium	102	1295	81.9	82.7	2.2	2.2	91
Potassium	146	1395	41.4	43	1.9	2.0	64
Sodium	208	1630	46.3	49.3	2.2	2.9	25
Lithium	357	2430	26.2	29.2	[b] 2.0	[b] 2.7	0.5
NaK-78	12	1456	42.6	44.7	2.0	2.2	51

[a] Viscosity of SAE 30 oil at 100° F is 10^{-5} reyn.
[b] Extrapolated.

potassium, sodium, lithium, and NaK. The table shows that the melting point ranges from −38° to 357° F; boiling point ranges from 674° to 2430° F. Viscosities are generally low at the boiling point, being in the order of 10^{-8} reyn for the alkali metals. Mercury, on the other hand, has a viscosity at its boiling point of 13×10^{-8} reyn.

Selection of liquid metals for vapor-liquid cycles is usually made on the basis of vapor pressure, liquid physical properties, and corrosion characteristics in addition to the usual thermodynamic properties (which are important to the thermodynamic cycle utilized). The vapor-pressure data of figure 13–10 illustrate the range of operating pressures that can be encountered at various temperatures with the alkali metals and mercury in vapor-liquid cycles. The shaded band of figure 13–10 indicates the ranges of pressure and

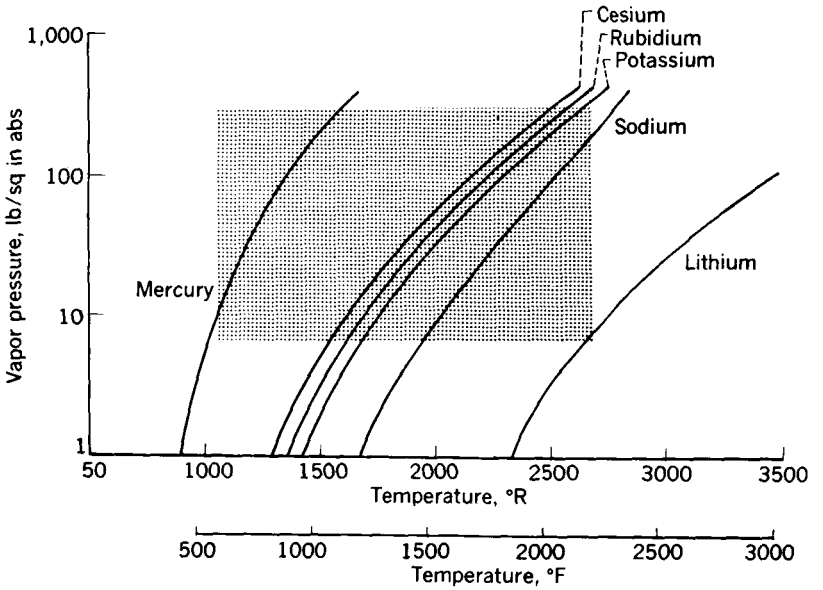

FIGURE 13–10.—Vapor pressure of mercury and alkali metals. Shaded band indicates ranges of pressure and temperature of interest.

temperature of interest (e.g., 5 to 200 lb/sq in. abs and 1000° to 2600° R (540° to 2140° F)). From figure 13–10 it is seen that, as the temperature of the cycle increases, we move progressively from materials like mercury (at the lower temperatures) to cesium, rubidium, potassium, and sodium. (Lithium is being considered primarily as a heat-transfer fluid within the reactor loop.) The range of temperatures and pressures is defined by other requirements. For example, the upper boundary of pressure is set by weight limitations and the lower pressure is related to pump cavitation; the high tem-

perature limit is defined by corrosion and the lower limit by radiator heat transfer (ref. 6).

Each range of operating temperature under consideration for a liquid-vapor cycle has a fluid which fits the required conditions best, particularly with reference to vapor pressure. For example, the vapor pressure of mercury is so high (5800 lb/sq in.) at 2500° R (2040° F) that it cannot be used without a very serious weight penalty resulting. On the other hand, at the lower turbine-inlet temperatures (such as 2000° R (1540° F)) the vapor pressure of sodium is so low that it is difficult to consider it for use as a cycle working fluid. In general, on the basis of vapor pressure alone, mercury appears best suited at turbine-inlet temperatures of approximately 1600° R (1140° F), rubidium at approximately 1900° R (1440° F), potassium at about 2200° R (1740° F), and sodium at about 2500° R (2040° F) (ref. 1).

Corrosion.—The corrosion resistance of materials which are used to contain a liquid-metal working fluid are extremely important since long-term, maintenance-free operation of system components is required in space applications. The authors of reference 4 have divided the corrosion problem areas for liquid-metal working fluids into five distinct (but arbitrary) operating-temperature ranges. These temperature ranges, the most suitable type of alloy for each, and the appropriate fluids for each are summarized in table 13–II. As noted, mild-steel alloys are suitable for temperatures less than 1060° R (600° F)

TABLE 13–II.—CORROSION PROBLEM AREAS [a]

Temperature range		Appropriate fluids	Type of alloy required
° R	° F		
<1060	<600	Hg	Mild-steel alloys
1060–1660	600–1200	Hg, Cs, Rb, NaK, K, Na	Iron-base superalloys
1660–2260	1200–1800	Cs, Rb, NaK, K, Na, Li	Iron-, cobalt-, nickel-, and chromium-base alloys
2260–2860	1800–2400	Cs, Rb, NaK, K, Na, Li, Bi, Pb	Refractory-metal alloys
>2860	>2400	Li, Bi, Pb	Refractory-metal alloys, ceramics, or cermets

[a] From ref. 4.

when mercury is used. Iron-base superalloys are suitable for the temperature range 1060° to 1660° R (600° to 1200° F) with mercury and the alkali metals (cesium, rubidium, sodium-potassium alloy, potassium, and sodium). Iron-, cobalt-, nickel-, and chromium-base

superalloys appear to be suitable for the temperature range 1660° to 2260° R (1200° to 1800° F) with the alkali metals previously listed, as well as with lithium. The refractory metals (columbium, molybdenum, tantalum, tungsten, etc.) and their alloys appear to be suitable in the temperature range 2260° to 2860° R (1800° to 2400° F) with the alkali metals previously listed plus bismuth and lead. Finally, refractory metal alloys, ceramics, or cermets appear satisfactory in the temperature range greater than 2860° R (2400° F) for lithium, bismuth, and lead.

Figure 13–11 shows the relative ratio of strength to weight for a

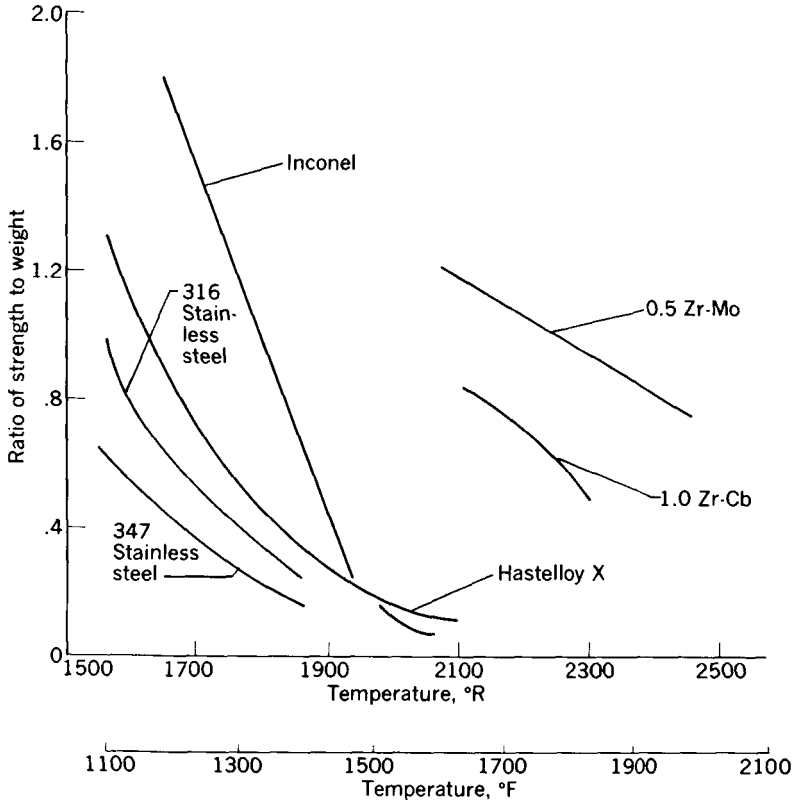

FIGURE 13–11.—Ratio of strength to weight of various high-temperature materials (10,000-hr life). (From ref. 6.)

number of materials as a function of temperature. The stainless-steel alloys are limited to temperatures of about 1960° R (1500° F); the refractory metal alloys, on the other hand, appear promising in the high-temperature range. Promising refractory metal alloys, other

than the two shown in figure 13–11, include Ta–10W and W–2ThO_2. Very little data are available, however, on the mechanical properties of the refractory metal alloys as a class; hence, considerable research is required in this area.

Corrosion by liquid metals and their vapors may result from several causes and the various types of corrosion may lead to different effects. Several representative causes and effects are briefly summarized in table 13–III. The table shows difficulties with (1) solution of the con-

TABLE 13–III.—CORROSION CAUSES AND EFFECTS [a]

Cause	Typical mechanism	Effect on—		
		Corroded part	System	Fluid
Thermal gradient	Dissolution, chemical reaction	Weight loss	Mass transfer	Contaminated
Dissimilar metals	Dissolution, chemical reaction	Weight loss	Mass transfer	Contaminated
Reactive fluid	Chemical reaction	Weight loss (or gain), scaling, subsurface voids, penetration	Sludge	Contaminated
Fluid flow	Fluid boundary layer effects	Accelerated (or altered) corrosion mechanisms	----------	----------

[a] From ref. 4.

tainment material in the working fluid, (2) chemical reaction with the working fluid or with contaminants in the working fluid, (3) abrasion by a contaminated fluid, or (4) fluid boundary-layer effects of the working fluid. These mechanisms can result in weight losses or weight gains. Mass transfer can be a serious problem where there is an appreciable thermal gradient (as is the case with most thermodynamic cycles). In its elementary form, mass transfer occurs because of the difference in solubility of the containment metal in the working fluid at two different temperatures. Hence, some of the containment material goes "into solution" in the hot zone and comes "out of solution" in the cold zone, and thus effectively transfers material from the hot zone to the cold zone. This mass transfer can block passages and thus result in loss of the system. Chemical reaction can achieve the same effect of transferring material from one zone to another because of the difference in chemical reactivity at various temperatures. Chemical reaction can also result in sludge, which can cause adverse effects at practically any point in the system.

The authors of reference 4 indicate it is possible that mass transfer of a pure metal phase from a hot zone to a cold zone may proceed by way of the formation of an intermediate chemical compound in the dissolution step. For example, it is believed that sodium oxide dissolved in liquid sodium may react with iron in a hot zone to form a compound containing iron, sodium, and oxygen; this compound may then revert to sodium oxide and free iron in the cold zone and thereby cause a net transport of metallic iron.

The presence in most alkali metals of dissolved oxygen or oxides (dissolved nitrogen or nitrides in the case of lithium) results in a more corrosive fluid. This increase in corrosivity may result from compound formations just discussed or it may be the result of the surface-fluxing ability of dissolved oxides. It is well to eliminate this problem in practice by using cold traps to remove oxide contaminants. These cold traps reduce the temperature of the molten metal to near its freezing point and precipitate the contaminants.

CONCLUDING REMARKS

From the results of work cited in the references, it appears obvious that the turbogenerator system is very promising for generation of large amounts of power for space applications. The most effective cycle for such a turbogenerator system would appear to be one employing a liquid metal as the working fluid in a liquid-vapor cycle. On the basis of vapor pressure alone, the following liquid metals appear most promising at the approximate maximum temperatures listed:

Liquid metal	Maximum temperature	
	°R	°F
Mercury	1600	1140
Rubidium	1900	1440
Potassium	2200	1740
Sodium	2500	2040

Each of these working fluids has appreciable problems of one kind or other. Among these, the most important problem is that of corrosion of the containment material. Corrosion will also be extremely important to the bearings employing liquid metals as the coolant-lubricant.

REFERENCES

1. SLONE, HENRY O., and LIEBLEIN, SEYMOUR: Electric Power Generation Systems for Use in Space. Paper presented at Second Int. Cong., Int. Council of Aero. Sci., Zurich (Switzerland), Sept. 12–16, 1960.
2. ENGLISH, ROBERT E., SLONE, HENRY O., BERNATOWICZ, DANIEL T., DAVISON, ELMER H., and LIEBLEIN, SEYMOUR: A 20,000-Kilowatt Nuclear Turboelectric Power Supply for Manned Space Vehicles. NASA MEMO 2–20–59E, 1959.
3. MOFFITT, THOMAS P., and KLAG, FREDERICK W.: Analytical Investigation of Cycle Characteristics for Advanced Turboelectric Space Power Systems. NASA TN D–472, 1960.
4. WEATHERFORD, W. D., JR., TYLER, JOHN C., and KU, P. M.: Properties of Inorganic Energy-Conversion and Heat-Transfer Fluids for Space Applications. TR 61–96, WADD, Nov. 1961.
5. JACKSON, CAREY B.: Liquid Metals Handbook—Sodium (NaK) Supplement. TID 5277, AEC, July 1, 1955.
6. ZIPKIN, M. A., BROOKS, R. D., and NICHOLS, H. E.: Materials and Stress Problems in Nuclear Turbogenerators for Space Power. General Electric Co., 1961.
7. ROSENBLUM, LOUIS: The Application of Liquid Metals in Space Power Systems. Paper Presented at AIME Meeting, New York (N.Y.), Feb. 22, 1962.

CHAPTER 14

Lubrication of Bearings With Liquid Metals

By WILLIAM J. ANDERSON

BECAUSE OF THE HIGH TEMPERATURE INVOLVED, closed-cycle space power systems will employ liquid metals and possibly other inorganic fluids as the cycle working fluid. One of the primary problems in space power systems is the rejection of heat. Since heat must be dissipated by thermal radiation, the surface area required to dissipate a given quantity of heat is inversely proportional to the fourth power of the radiating surface temperature. In order to keep the radiator area within reasonable limits, heat rejection temperatures must be kept high. Present theory is that this temperature will vary from about 400° to 1500° F. This temperature becomes the minimum cycle temperature unless auxiliary cooling, which is undesirable because of weight and complexity, is employed. Therefore, *minimum* bearing temperatures of 400° to 1500° F can be expected. Bearing temperatures will probably be somewhat higher than this, since the liquid leaving the radiator must be pumped to a high pressure and may be forced to flow through lines passing through hot areas. The use of organic fluids as lubricants at these temperature levels is not feasible.

In addition to avoiding problems of thermal degradation through the use of inorganic fluids as lubricants, using the cycle working fluid as the lubricant is highly advantageous because of several other reasons. These include

(1) Reduced complexity
(2) Ease of sealing problems
(3) Fewer mechanical design problems because of the elimination of overhung shafts, etc.

Fluids primarily considered for use as cycle working fluids are mercury and the alkali metals—rubidium, potassium, sodium, and

lithium. The properties of liquid metals which can affect the performance of bearings are their low viscosity and their corrosivity. The alkali metals will reduce most metal oxides, and the high mass density of mercury tends to promote erosion because of high particle inertia.

Because of the high chemical activity of the alkali metals, especially at elevated temperatures, materials compatibility is expected to be a severe problem. Materials can certainly be found which have good compatibility with the alkali metals; however, a good bearing material must also possess other characteristics.

SYMBOLS

C	clearance, in.
C_d	diametral clearance, in.
D	diameter, in.
f	coefficient of friction
L	length, in.
N	speed, rps
P	load pressure, W/LD, lb/sq in.
Re	Reynolds number, $\rho UC/\mu$
S	Sommerfeld number, $\left(\frac{D}{C_d}\right)^2 \frac{\mu N}{P}$
U	velocity, in./sec
W	load, lb
η	eccentricity ratio
μ	viscosity, (lb) (sec)/sq in.
ρ	mass density, (lb) $(sec^2)/in.^4$

TYPES OF BEARINGS

In evaluating the possible merits of various types of bearings for liquid-metal applications, it is necessary to consider the characteristics of each type of bearing in relation to the fluid properties. Rolling-element bearings, hydrodynamic bearings, and hydrostatic bearings will be considered separately.

Rolling-Element Bearings

In order for the rolling-element bearing to function properly, especially in high-speed applications, there must be no wear or surface degradation of the rolling elements or races. A high-speed rolling-element bearing is a precise machine component and must retain its precision during operation. Surface damage of any kind results in high-amplitude vibrations and rough operation, which further accel-

erate wear and quickly lead to complete failure. This is not true of the cage or separator, which can tolerate considerable wear. The combination of high pressures which exist in the contacts between the rolling elements and the races (even under light load conditions) plus the poor conformity of these contacting surfaces discourages the formation of a hydrodynamic film, which would prevent intimate contact of the surfaces. The success of any bearing in a liquid-metal environment will depend partly on preventing intimate contact of the surfaces. The liquid metal will either reduce the thin oxide coatings which exist on the bearing parts or prevent the reformation of the coating after it has worn off.

The use of surface coatings or contaminating films to reduce friction and wear is well known. In addition to low shear strength coatings that are used as lubricants, simple surface films, such as oxides, are valuable because they help to prevent clean surfaces from coming into intimate contact. In this way they are effective in preventing (or minimizing) surface welding. In the Earth's atmosphere, contaminating films of one type or another are present on all surfaces.

In a rolling bearing the net result of poor conformity is that clean metal surfaces come into intimate contact. This contact produces surface welding, which may result in material transfer or catastrophic wear, either or which constitutes bearing failure.

A further requirement of rolling-element bearings is an absolute compatibility of the race and the rolling-element materials with the environmental fluid for the same reason as the complete absence of wear. In other words, any corrosive surface damage that occurs on the rolling elements or races would have the same end effect as wear or surface damage arising from effects other than corrosion. This requirement for absolute material compatibility with the environmental fluid results in a low probability of success for rolling bearings in applications involving liquid metals where a long life with high reliability is required.

It is quite true that successful operation of rolling-element bearings has been achieved in other applications, such as in liquid hydrogen, where the lubricating ability of the environmental fluid is at best marginal. The temperature levels of liquid-metal applications plus the corrosivity of the fluids, however, would generally prevent the use of the self-lubricating retainer materials of the type which have been successful in cryogenic applications (e.g., Teflon). In addition, success in cryogenic applications has been achieved only because of the short life requirements. Bearings for chemical-rocket turbopumps, for instance, need have a life of no more than several hours. Bearings for auxiliary electric power systems for space vehicles will, in contrast, be required to operate reliably for 10,000 hours.

Hydrodynamic Bearings

A second type of bearing under consideration for liquid-metal applications is the hydrodynamic (fluid film) bearing. In this type of bearing, a continuous film maintains separation of the surfaces in relative sliding, and the pressure required to support the load is generated within the bearing itself. In a hydrodynamic bearing, the only external pressure required is that sufficient to feed only enough lubricant into the bearing to maintain a full fluid film. Hydrodynamic bearings offer several advantages when compared with rolling-element bearings in applications such as these. The first advantage is that of tolerating some wear and still maintaining their function. They can tolerate some corrosion and surface damage so that the requirements for material compatibility are not as severe as those for rolling-element bearings. The materials problem for hydrodynamic bearings is also less stringent because high hardness is not a requirement, whereas it is for rolling-element bearings. This requirement of high material hardness for rolling-element bearings eliminates a number of materials which might have excellent compatibility, but which are otherwise deficient with regard to hardness. The maintenance in hydrodynamic bearings of a fluid film (which keeps the surfaces in relative motion apart) tends to minimize the importance of the reduction of surface oxides and the resulting production of clean, nascent metals. As long as these materials are kept apart and prevented from coming into intimate contact, the possibilities of surface welding, material transfer, and high rates of wear occurring are minimized.

The principal disadvantage of hydrodynamic bearings lies in their tendency to exhibit instability under the light or zero load conditions that will exist in machinery in orbit. The term instability in hydrodynamic bearings refers to the tendency of the journal or shaft center to rotate in some orbit rather than to remain fixed in one spot within the bearing. If the amplitude of this journal center motion becomes large enough, touching of the shaft and the bearing occurs with, in most cases, a disastrous failure. This tendency toward instabilities in hydrodynamic bearings arises because the radial fluid film force is generally not colinear with the load vector. This produces a component of force, which tends to propel the journal in a whirling motion; hence, if the whirl is truly unstable, failure of the bearing follows. Whether or not the whirl is unstable depends upon the radial fluid-film stiffness. When the whirl frequency or the frequency of rotation of the journal center is equal to one-half that of the journal about its own center, the load-carrying capacity, or the radial-film stiffness, of a hydrodynamic bearing is essentially zero. Because of this relation, instability frequencies are most often equal to one-half

the frequency of rotation of the shaft. This type of self-excited whirl is commonly called half-frequency whirl. If a rotor is run at twice its first critical speed, a type of instability known as resonant whip develops. The whirl frequency is equal to one-half the rotational frequency (the resonant frequency of the rotor). Excessive amplitudes of vibration, which can lead to destruction of the bearings, develop.

Hydrostatic Bearings

The third type of bearing which might possibly be used in liquid-metal applications is the hydrostatic bearing. This is a fluid-film bearing in which complete separation of the surfaces in relative motion is maintained by a continuous fluid film. In contrast with a hydrodynamic bearing, however, the load-supporting pressures in a hydrostatic bearing are supplied from an external pressure source. The pressures that support the load are not generated within the bearing but are supplied through a flow restrictor of some type from an external source. The hydrostatic bearing offers the advantages of high load capacity at no rotation or at low rotative speeds and a load capacity which is independent of the fluid viscosity. The load capacity of a hydrodynamic bearing, in contrast, is proportional to the viscosity of the fluid; since the viscosities of liquid metals are quite low, the load capacities of hydrodynamic bearings using liquid metals are likewise quite low.

The hydrostatic bearing also has several disadvantages. The first of these is a dependence on an external pressure source. This dependence requires that a relatively high pressure source of the liquid metal be available at all times. The flow through a hydrostatic bearing, because of the high inlet pressure, is generally considerably higher than that of a hydrodynamic bearing. This makes the power loss (associated with the pump capacity required to supply the bearings) somewhat higher than that of a hydrodynamic bearing. To function properly, a hydrostatic bearing also requires a flow resistance of some type in the feed line between the high-pressure source and the inlet to the bearing. The restrictor may be a capillary tube or an orifice. Flow restrictors are generally sensitive to dirt and may be sensitive to erosion over a long period of time, especially a sharp-edge orifice in the case of a high-density fluid such as mercury. On the other hand, the hydrostatic bearing offers relative freedom from instabilities such as half-frequency whirl present in hydrodynamic bearings. Because it deflects under load in the direction of the load, the radial-fluid-film force, which opposes the load, is generally colinear with the load vector. There is, therefore, no tendency to promote a whirling or orbital motion of the journal or shaft center.

BEARING EXPERIMENTS

Rolling-Element Bearings

As mentioned previously, the materials-compatibility problem with rolling-element bearings will be severe, at best, and perhaps even insurmountable because of the requirements of this type of bearing. Reference 1 contains the results of experiments conducted with ball bearings operating in sodium-potassium alloy or sodium at a temperature of 250° F. Bearings of 50- to 140-millimeter bore size were run at 850 to 3600 rpm at thrust loads of 400 to 4300 pounds. Seven different metal alloys and a cotton-cloth-laminated phenolic material were evaluated as retainers. With all the metallic retainers, failure was due to severe wear of the retainer and metal transfer from the retainer to the balls and races. The phenolic showed better wear characteristics than the metallics, but such materials are not suitable for the temperature levels to which bearings in space power systems will be subjected.

Some work was done in reference 1 on the effect of speed on bearing life with 7320 size (100 mm bore) bearings with malleable iron retainers (fig. 14–1). An increase in speed from 850 to 3600 rpm resulted in a 90 percent decrease in life. The results of reference 1 indicate that the future for rolling bearings in liquid metals at extreme temperatures is not promising and that major development efforts in this area should be concentrated on fluid-film bearings.

Fluid-Film Bearings

The major portion of bearing work with liquid metals has been done with fluid-film bearings. The performance of tungsten carbide journal bearings in both NaK and sodium is described in reference 2. Test bearings were 2⅜ inches in diameter and in length. Experiments were conducted at temperatures from 100° to 600° F in NaK and 250° to 450° F in sodium at speeds of 1200 to 1700 rpm. These test conditions correspond to a maximum sliding velocity of approximately 18 feet per second.

In the experiments of reference 2, the bearings were wetted by exposing them to the liquid metal at 450° F for at least 8 hours before being tested. Runs were made with increasing load until a sharp increase in motor power, which indicated a rupture of the lubricant film, was observed. The liquid-metal-lubricated journal bearings operated with full film hydrodynamic lubrication. This was determined from the measurements of bearing torque, which agreed fairly well with existing theory. Figure 14–2(a) is a plot of friction variable as a function of Sommerfeld number for NaK lubricated bearings. These data show increasing friction with increasing temperature at high values of Sommerfeld number with the various curves con-

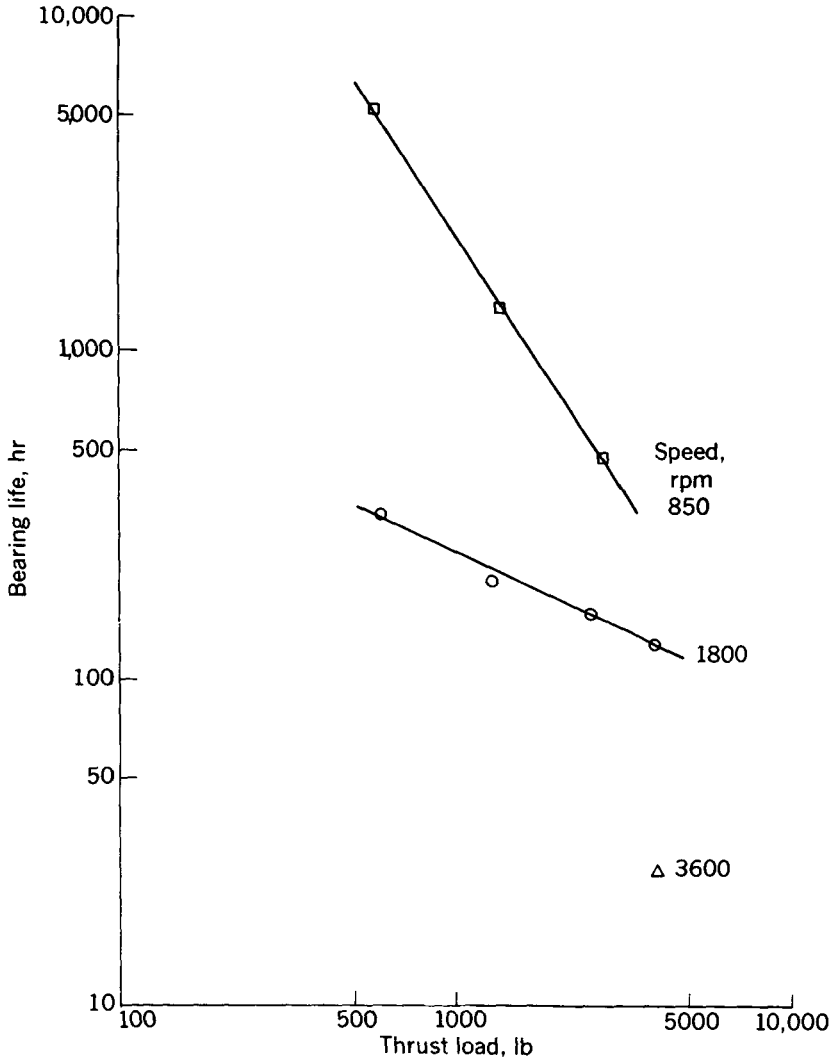

FIGURE 14–1.—Life of 7320 bearings at various speeds in sodium-potassium alloy at 250° F. Malleable iron ball guided retainers. (From ref. 1.)

verging to a single value of friction coefficient at a Sommerfeld number of 0.025. The curves of figure 14–2(a) were plotted by using the calculated bearing clearance at temperature based on known expansion coefficients of the bearing and journal materials. Any restraint on the bearing, however, may result in bearing operating clearances somewhat smaller than those predicted by using expansion coefficients and an initial clearance. This would shift the higher

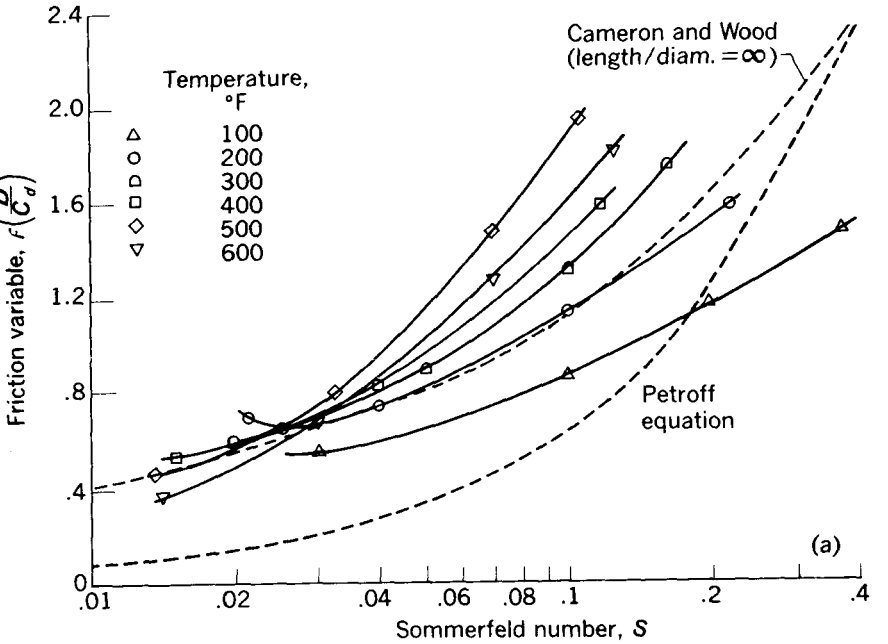

(a) In sodium-potassium alloy at temperatures from 100° to 600° F.

FIGURE 14–2.—Frictional characteristics of tungsten carbide journal bearings Test bearing, Carboloy 55A; test journal, Carboloy 779, bearing length-diameter ratio, 1; diameter, 2⅜ inches. (From ref. 2.)

temperature curves to the right and bring the curves into closer coincidence.

The author of reference 2 points out that higher temperatures may have produced misalinement of one of the bearings. Several of the high-temperature runs were discontinued because of roughening of the guide bearing surfaces due to boundary lubrication. Since the lubricant film thicknesses of the guide bearings should have been greater than those of the test bearings, it was concluded that misalinement of the guide bearings occurred at the higher temperatures.

Typical results obtained with sodium in reference 2 are shown in figure 14–2(b). The agreement between the data obtained at various temperatures is much better than in NaK, but the temperature range in sodium was narrower than in NaK. Examination of figure 14–2 shows that the frictional characteristics of bearings running in NaK and sodium can be predicted with fair accuracy using the Cameron and Wood analysis for an infinite bearing.

The test bearings used in reference 2 were Carboloy 55A (tungsten carbide plus 13 percent cobalt) and the test journals were Carboloy

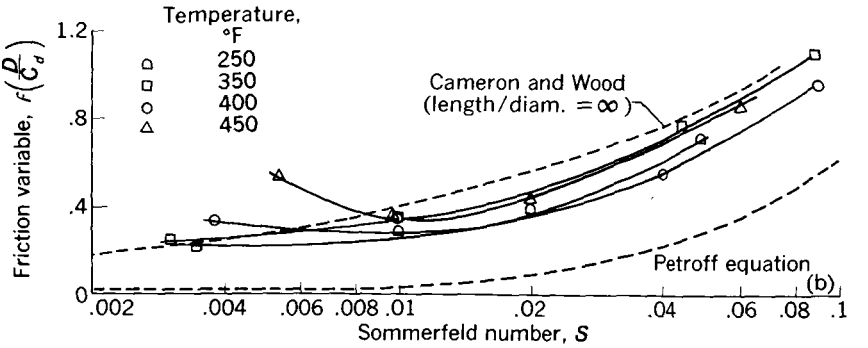

(b) In sodium at temperatures from 250° to 450° F.

FIGURE 14–2—Concluded.—Frictional characteristics of tungsten carbide journal bearings. Test bearing, Carboloy 55A; test journal, Carboloy 779; bearing length-diameter ratio, 1; diameter, 2⅜ inches. (From ref. 2.)

779 (tungsten carbide plus 9 percent cobalt). Guide bearings were made of 18–4–1 tool steel or an aluminum alloy. The tungsten carbide cermets resisted seizure to a greater extent than did the other bearing materials, but some roughening of the bearing surfaces occurred for the particular ceramals used in the tests of reference 2.

Further discussions of the misalinement problem are given in reference 3, in which both thrust-bearing and journal-bearing tests are reported. These tests were conducted in NaK at temperatures from 75° to 760° F. Thrust bearing loads as high as 2000 pounds and journal bearing loads as high as 1800 pounds were carried. The journal bearings were tested at speeds from 900 to 1750 rpm and at loads in the region of 375 pounds per square inch. Boundary conditions occurred at high loads, and under conditions of film rupture tungsten carbide bearings showed better score resistance than tool-steel bearings. In addition to the materials used in reference 2, bearings were fabricated from Stellite Star J, Stellite 1, and Hastelloy B.

In reference 3, failure of the bearings to operate under boundary-lubrication conditions was attributed primarily to incompatibility of the bearing materials and the liquid metal. Many of the experiments reported in reference 3 are the same as those reported in reference 2.

Experiments with aluminum-alloy (percent composition: 4.4 copper, 0.8 silicon, 0.8 manganese, 0.8 magnesium, balance aluminum) thrust and journal bearings operating in NaK at temperatures of 80° to 400° F are reported in reference 4. Thrust bearings were 2¾ inches in outside diameter by 1¾ inches in inside diameter and were operated under a 75-pound load (21 lb/sq in.). They showed little deterioration

after 11,000 hours of exposure and intermittent operation in contaminated NaK. In contrast to the satisfactory performance of the thrust bearings, the 1-inch-diameter, 1-inch-long journal bearings failed under a 20-pound load (20 lb/sq in.). The initial journal-bearing diametral clearance was 0.002 inch, which was rebored to 0.006 inch because of the seizures.

The data of reference 4 indicate that the performance of aluminum-alloy bearings may be satisfactory in NaK at nominal temperatures if properly designed. For higher temperature use, the aluminum alloys may not be suitable for use in liquid metals because of poor compatibility.

Other data on the operation of fluid-film bearings at nominal speeds are given in references 5 and 6. It is apparent that the data reported in the literature on liquid-metal-lubricated bearings have been obtained at nominal temperatures and speeds. The anticipated bearing operating conditions in space powerplants range far beyond the experimental data available, both temperaturewise and speedwise. Therefore, the data discussed here can be used only as a guide to designing bearings for operation at more extreme conditions.

Some work on alkali-liquid-metal-lubricated fluid-film bearings operating at high speeds has recently been initiated. Experimental results for both water- and liquid-potassium-lubricated aluminum-bronze bearings are reported in reference 7. Journal bearings 1 inch in diameter were operated at speeds to 20,000 rpm in potassium at 450° F. Hydrodynamic operating conditions were achieved, and at the higher speeds significant increases in bearing torques, which indicate the presence of turbulent flow, were noted. This occurrence will be discussed in the section on turbulent flow.

The experimental results of reference 7 are quite promising. They indicate that operation of fluid-film bearings at the speeds required by space powerplants is feasible. Further work on bearing designs and materials is required to improve bearing reliability.

PROPERTIES OF BEARING MATERIALS

Compatibility

Certain conclusions can be drawn regarding material compatibility with NaK at 850° F. The results of corrosion tests conducted on several classes of materials are shown in table 14–I. From these tests the following conclusions were drawn:

(1) Porous tungsten carbide cermets gave excellent results and appear to be suitable for oscillating bearing applications.

(2) Combinations of titanium carbide and tungsten carbide cermets exhibit good compatibility and low coefficients of friction.

TABLE 14-I.—RESULTS OF FRICTION AND WEAR TESTS IN NaK AT 850° F [a]

[I, negligible wear; no material transfer; polish both specimens; II, smooth wear; fixed specimen; no material transfer; polish rotating specimen; III, smooth wear; both specimens; minor material transfer; IV, excessive wear; surface roughening; material transfer, or friction; V, test not completed because of excesses in IV.]

Specimen 1		Specimen 2													
Material	Composition	Carboloy 44A	Carboloy 779	Sintercast WF87	Carboloy X3040D	Carboloy 190	Carboloy 78	Carboloy 907	Carboloy 77B	Kentanium 138	Kentanium 138A	Firthite HT77	Colmonoy 6	Stellite 98M2	416 SS Chrome plated
Carboloy 44A	WC; Co binder	I	-----	I	-----	-----	-----	-----	-----	III	-----	III	-----	-----	-----
Carboloy X3040D		I	-----	-----	I	-----	-----	-----	-----	-----	-----	III	-----	-----	-----
Kentanium K-12		-----	-----	V	-----	-----	-----	-----	I	-----	-----	-----	III	-----	-----
Carboloy 55A		-----	-----	IV	-----	-----	-----	-----	-----	II	III	III	-----	-----	-----
Carboloy 190		-----	-----	-----	-----	III	-----	-----	-----	-----	-----	-----	-----	-----	-----
Carboloy 78		-----	-----	III	-----	-----	V	-----	-----	-----	-----	III	-----	-----	-----
Carboloy 907	WC; TiC, TaC; Co binder	-----	-----	I	-----	-----	-----	I	-----	-----	-----	III	-----	-----	-----
Carboloy 77B		-----	-----	-----	-----	-----	-----	-----	-----	-----	-----	III	-----	-----	-----
Carboloy 831		-----	-----	V	-----	-----	-----	-----	-----	-----	-----	I	-----	-----	-----
Kentanium 138	TiC; Co binder	-----	I	-----	I	-----	-----	-----	-----	III	III	-----	-----	-----	-----
Kentanium 138A		-----	I	-----	-----	-----	-----	-----	-----	V	III	-----	-----	IV	-----
Kentanium 151		-----	I	-----	-----	-----	-----	-----	-----	III	-----	I	-----	IV	-----
Kentanium 152B	TiC; Ni binder	-----	III	-----	-----	-----	-----	-----	-----	-----	I	-----	-----	-----	-----
Firthite HT77		-----	-----	-----	-----	-----	-----	-----	-----	-----	-----	III	-----	-----	-----
Kentanium	TiC; Fe binder	-----	I	-----	-----	-----	-----	-----	-----	-----	III	-----	-----	-----	V
Carboloy X3345	Cr_3C_2; Co binder	-----	-----	-----	-----	-----	III	-----	-----	-----	-----	-----	-----	-----	-----
Colomony 6		-----	IV	-----	-----	-----	-----	-----	-----	-----	-----	III	III	-----	-----
Stellite 98M2		-----	-----	-----	-----	-----	-----	-----	-----	-----	-----	-----	-----	IV	-----
Copper	Noncarbides	-----	-----	IV	-----	-----	-----	-----	-----	II	-----	-----	-----	-----	-----
Beryllium-copper		-----	-----	-----	-----	-----	-----	-----	-----	-----	-----	-----	-----	-----	II
Aluminum-bronze		-----	-----	-----	-----	-----	-----	-----	-----	-----	-----	-----	-----	III	-----

[a] From ref. 8.

(3) The lower the percentage of cobalt binder in tungsten carbide cermets, the less the tendency for superficial surface damage under boundary conditions. (This may be due either to the increased hardness or to the finer grain structure.)

(4) Titanium carbides not containing a solid-solution type of carbide exhibited less surface damage than did those containing solid-solution carbides.

(5) Titanium carbide cermets tested with similar cermets exhibited good compatibility at temperatures below 850° F.

(6) The compatibility of nickel-bonded cermets compares favorably with the compatibility of cobalt-bonded cermets.

(7) Copper and some copper alloys are most compatible with chromium or cermets at temperatures up to 600° F.

(8) Nickel and nickel alloys did not exhibit good compatibility at high temperatures.

(9) Chromium—tungsten-cobalt alloys have poor compatibility at temperatures above 600° F.

(10) Chromium carbide cermets are unsatisfactory bearing materials.

(11) Iron alloys are unsatisfactory at temperatures above 600° F.

More recent compatibility data have been compiled from a number of sources and are reported in reference 9. Compatibility ratings are based on a 10,000-hour exposure. These data are summarized in figure 14–3(a) for mercury, figure 14–3(b) for rubidium, figure 14–3(c) for sodium and potassium, and figure 14–3(d) for lithium. All these data were obtained in static tests with satisfactory compatibility based on an absence of corrosive attack.

Figure 14–3(a) indicates that the ferritic stainless steels and the low-carbon silicon steels have excellent compatibility with liquid mercury; they are satisfactory for use in dynamic systems to 1300° and 1500° F, respectively. The use of chromium, molybdenum, and silicon as alloying agents appears to be beneficial. It is advantageous in bearings to use a wetting agent. Magnesium offers promise in this area. It is to be noted from figure 14–3(a) that the materials discussed have better compatibility with liquid mercury than do the more expensive refractory metals and ceramics.

Figure 14–3(b) shows the compatibility of various classes of materials with liquid rubidium. The refractory metals—molybdenum, columbium, tantalum, and tungsten—are all compatible with rubidium to the maximum temperature of the investigation, 2000° F. The broken bars do not indicate the limit of compatibility but rather that no information is available on behavior at higher temperatures. Of the more conventional ferrous alloys, the ferritic stainless steels and the austenitic stainless steels are compatible to a temperature

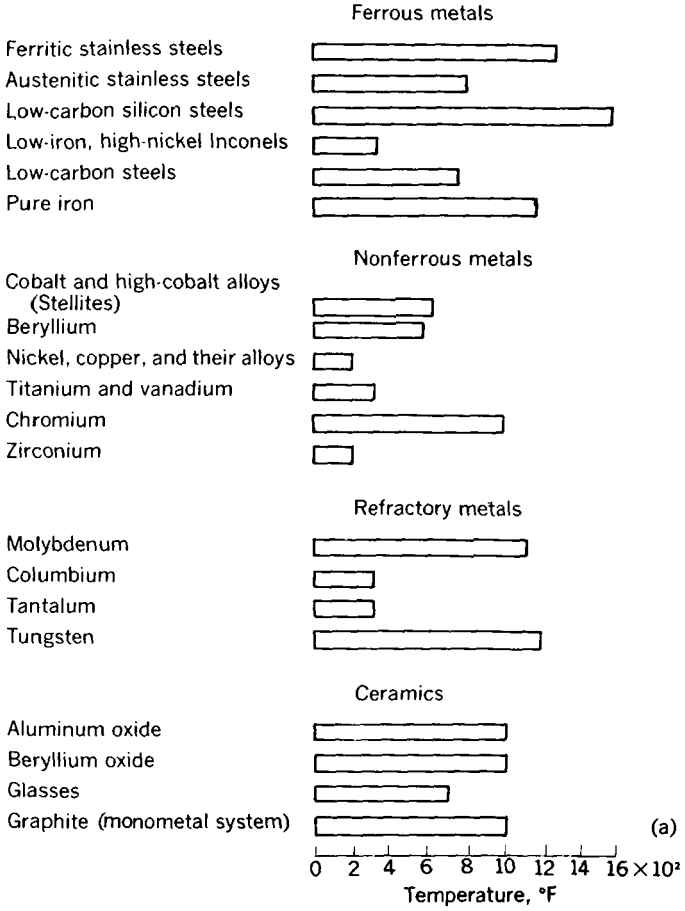

(a) Mercury.

FIGURE 14–3.—Compatibility of various materials with several liquid metals. Exposure, 10,000 hours. (From ref. 9.)

of at least 1600° F. The high-nickel alloys such as Inconel also exhibit good compatibility. Several of the 18–8 type austenitic stainless steels such as 310, 316, and 347 are suitable to the region of 1500° F. At higher temperatures the refractory metals are recommended.

The compatibility of various materials with liquid sodium and potassium is shown in figure 14–3(c). In general, the behavior of the various classes of materials with sodium and potassium is similar to that with rubidium. Both the austenitic stainless steels and the ferritic stainless as well as nickel alloys such as Inconel are satisfactory for use at temperatures to the region of 1500° F. As with rubidium,

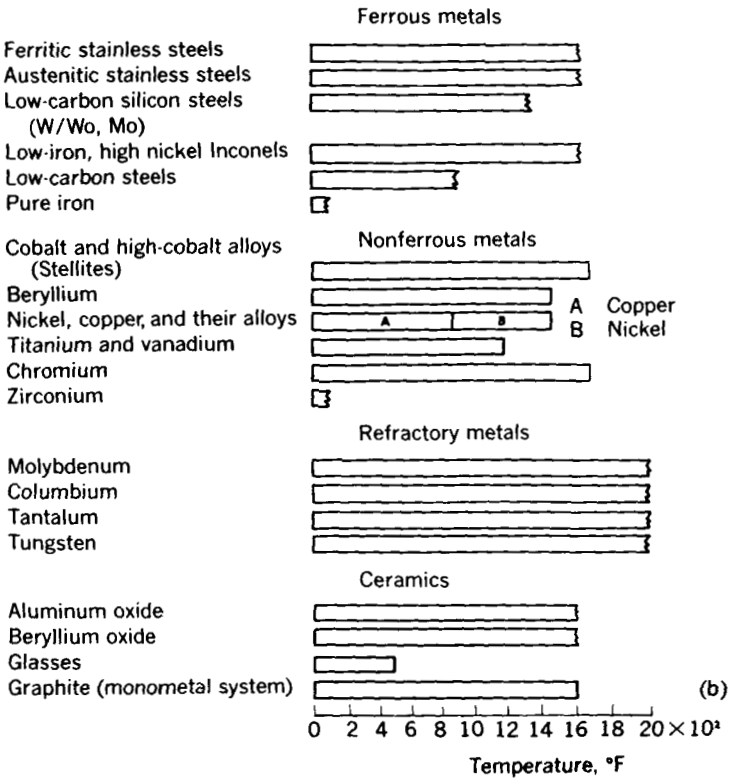

(b) Rubidium.

FIGURE 14–3—Continued.—Compatibility of various materials with several liquid metals. Exposure, 10,000 hours. (From ref. 9.)

the refractory metals are recommended for use at temperatures above 1500° F.

The most difficult of the alkali metals, from a materials viewpoint, is lithium. Conventional ferrous alloys and a variety of nonferrous alloys have satisfactory compatibility at temperatures from 600° to 1000° F. In particular, ferritic stainless steels and austenitic stainless steels may be used in dynamic systems at temperatures to 1000° F. At temperatures above 1000° F, the refractory metals must be used.

Static corrosion resistances of some alloys and elements in sodium at 1832° F (ref. 10) are shown in table 14–II. An alloy of 80 percent nickel and 20 percent chromium and pure nickel were the only materials unattacked after 400 hours of exposure.

Reference 11 contains data on the corrosion resistance of various ceramics and cermets to sodium and lithium. The data of reference 11 are based on a 100-hour exposure at 1500° F unless otherwise indicated.

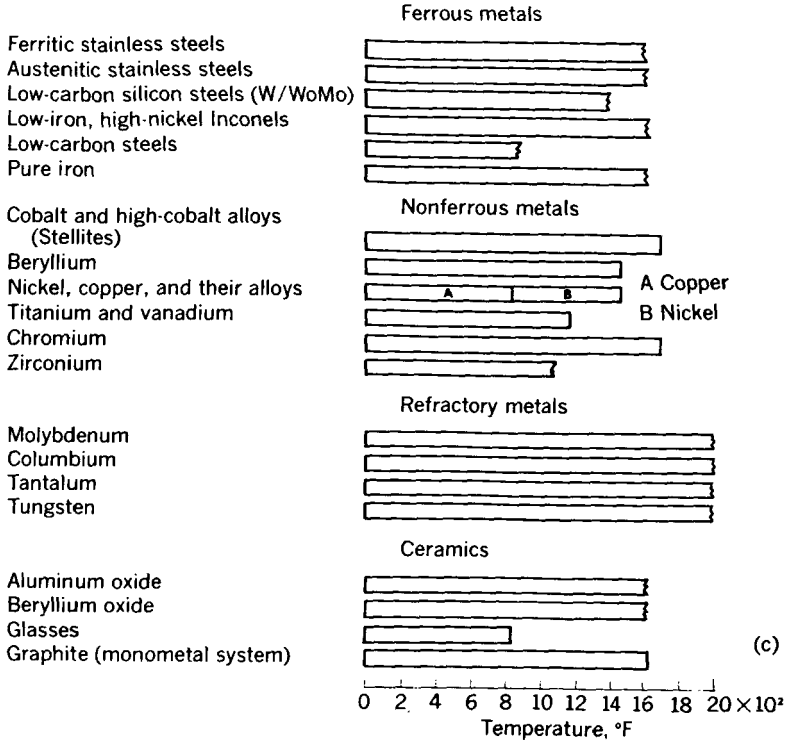

(c) Sodium and potassium.

FIGURE 14–3—Continued.—Compatibility of various materials with several liquid metals. Exposure, 10,000 hours. (From ref. 9.)

The data for ceramics in sodium and lithium are shown in table 14–III and the data for cermets in sodium in table 14–IV. As shown in table 14–III, a number of ceramics have good corrosion resistance in sodium. These include carbides, oxides, and borides. In the test of reference 11, good compatibility is defined as a depth of attack of 0.001 inch or less. As one would expect, the choice of materials for lithium is considerably narrower than for sodium. The carbides of titanium, zirconium, and chromium have good compatibility with lithium at 1500° F.

Among the cermet materials tested in reference 11, several of the Carboloys and Kentanium materials had good compatibility with sodium. None of these were tested in lithium.

The resistance to corrosion in liquid sodium and in lithium of the various ceramics tested in reference 11 generally agreed with the results that would be predicted for these media and ceramic materials from their free energies of formation. The author of reference 11, however, states that thermodynamic data are not available for many

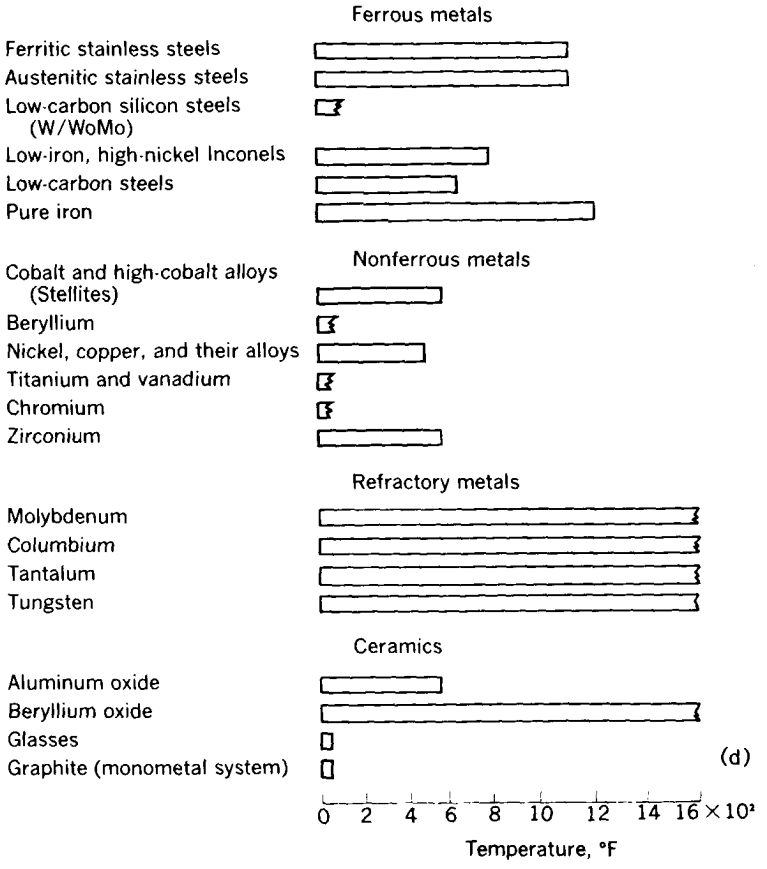

(d) Lithium.

FIGURE 14–3—Concluded.—Compatibility of various materials with several liquid metals. Exposure, 10,000 hours. (From ref. 9.)

of the materials. The limited results obtained on single-crystal specimens tended to parallel predicted corrosion resistance trends, while the results obtained on polycrystalline sintered specimens did not. The author of reference 11 concludes that thermodynamic data can be useful as qualitative guides for planning tests and for selecting materials to be tested, but corrosion tests are required to secure the quantitative data.

As discussed in chapter 13, material incompatibility may manifest itself as mass transfer. Material is transferred from a high-temperature zone to a low-temperature zone because of differences in solubility in the alkali metal. This phenomenon is more likely to occur in a system containing several materials, and therefore it would be advantageous to design a monometallic system. This system, however,

TABLE 14–II.—STATIC CORROSION RESISTANCE OF ELEMENTS AND ALLOYS IN SODIUM [a]

[Temperature, 1832° F; 400 hr.]

	Unattacked	Very good	Good	Fair
Alloys	80 percent Ni; 20 percent Cr	446 SS [b] 316 SS Inconel Stellite 25 Vitallium 310 SS	410 SS 430 SS [b] 446 SS [c] 304 SS 347 SS	405 SS
Elements	Nickel	Titanium Chromium Cobalt Molybdenum Tantalum	Beryllium	Vanadium

[a] From ref. 10.
[b] 0.08 percent C.
[c] 0.006 percent C.

TABLE 14–III.—CERAMIC MATERIALS HAVING GOOD CORROSION RESISTANCE IN SODIUM AND LITHIUM AT 1500° F [a]

[100-hr test unless otherwise indicated.]

Sodium	Lithium
ZrB_2 TiC ZrC Cr_3C_2 BeO MgO (single crystal) Al_2O_3 (single crystal) Sm_2O_3 (1000-hr test) Rare-earth oxides body (45 to 49.5 percent Sm_2O_3 plus 22.5 to 27 percent Gd_2O_3; balance primarily other rare-earth oxides). $MgAl_2O_4$ (single crystal)	TiC ZrC Cr_3C_2

[a] From ref. 11.

may not be feasible because materials with desirable structural properties may not have the properties desired in a bearing material. A material may be chosen for system piping, etc., because it possesses good compatibility and is easily machined and welded.

Wear and Seizure Resistance

In addition to compatibility, which (in the case of bearing materials for liquid metals) implies a resistance to corrosion, fluid-film bearing materials should possess other characteristics. First in importance after compatibility is wear and seizure resistance. This cannot be considered a property of either the bearing or the journal material,

TABLE 14–IV.—CERMET MATERIALS HAVING GOOD CORROSION RESISTANCE IN SODIUM [a]

[100-hr test.]

Material	Test conditions
Carboloy 779 (91 percent WC—9 percent Co) Carboloy 55A (87 percent WC—13 percent Co) Carboloy 907 (74 percent WC—20 percent TaC—6 percent Co) Carboloy 608 (83 percent Cr_3C_2—2 percent WC—15 percent Ni)	Static at 1500° F
Kentanium 150A (80 percent TiC—10 percent $NbTaTiC_3$—10 percent Ni) Kentanium K151A (70 percent TiC—10 percent $NbTaTiC_3$—20 percent Ni)	Seesaw test: Hot zone, 1500° F Cold zone, 1150° F

[a] From ref. 11.

but one of both the bearing and the journal materials in combination with the particular liquid metal used. The necessity for good wear resistance is self-evident since the wear that a bearing can tolerate and function properly is limited. Of somewhat less importance than wear resistance is low friction. High resistance to wear and low friction do not, in many instances, occur simultaneously. If a fluid-film bearing is operating in the hydrodynamic region, the bearing friction is a function of the viscosity of the lubricant rather than of the coefficient of sliding friction between the bearing and the journal materials.

Embeddability

At the extreme condition of temperature under which liquid-metal-lubricated bearings will operate, some wear and surface degradation can be expected. Wear particles will therefore be present in the bearing. In addition, other solids such as oxides coming out of solution may be flowing through the bearing. These situations emphasize the need for bearing materials with good embeddability, which is the ability to absorb foreign particles and thus minimize scoring and wear. The experimental evidence obtained to date indicates that hard materials such as tungsten carbide perform best in liquid metals. The fact that this class of materials has poor embeddability emphasizes the need for extremely good wear resistance.

Conformability

Conformability, the ability to compensate for misalinement and geometric inaccuracies, is another important property of bearing materials. The problem of misalinement will most certainly be present

in liquid-metals systems because of the extreme temperatures. Good conformability generally results from low hardness and low modulus of elasticity. Unfortunately, the classes of materials which exhibit good compatibility with liquid metals generally have high hardness and high modulus of elasticity. The necessity for maintaining extreme cleanliness and accuracy in liquid-metal systems is apparent because of the probable poor embeddability and conformability of bearing materials. The necessity for research on different classes of materials with low hardness and low modulus of elasticity is also indicated.

Low-Shear-Strength Surface Films

The importance of contaminating films in reducing friction and wear was discussed thoroughly in chapter 2. In liquid-metals systems, such films may be of greater importance than in oil-lubricated systems because of the inherently poor lubricating qualities of the liquid metals and the poor friction and wear characteristics of materials compatible with the liquid metals. The formation of one such film, sodium molybdate, on molybdenum in sodium was investigated in references 12 and 13. The experiments conducted in references 12 and 13 were low-speed friction tests at sliding speeds of about ½ inch per minute, a Hertz contact stress of about 100,000 psi, and temperatures of 80° to 1300° F. With tungsten carbide (20 percent cobalt binder) in sodium (ref. 12), kinetic friction remained high and essentially constant up to 1000° F and increased above 1000° F. Molybdenum, however, showed considerably lower friction in the presence of sodium at higher temperatures. Moreover, marked changes in friction occurred when the molybdenum specimens were conditioned by exposure to various temperatures for extended periods in vacuum or in inert-gas atmospheres. These results were attributed to the formation of the oxide molybdenum trioxide (MoO_3), which was formed when molybdenum was heated in air, and to molybdenum dioxide (MoO_2), which was formed after heating in vacuum. The coefficient of friction for the MoO_2 was less than for the MoO_3, but surface damage was comparable and relatively severe. When sodium was added to the MoO_2 filmed specimens, the friction was somewhat lower up to 1000° F and surface damage was essentially nonexistent. In this case, the surface-film composition was sodium molybdate (Na_2MoO_4). The results of friction tests of filmed molybdenum specimens run dry and in sodium are shown in figure 14–4.

From the experiments of reference 12, it is evident that the formation of sodium molybdate films is highly beneficial because of their low friction and good resistance to wear and surface damage at high unit loads. Some oxygen must be present to form this film in a practical sodium system. As stated by the authors of reference 12,

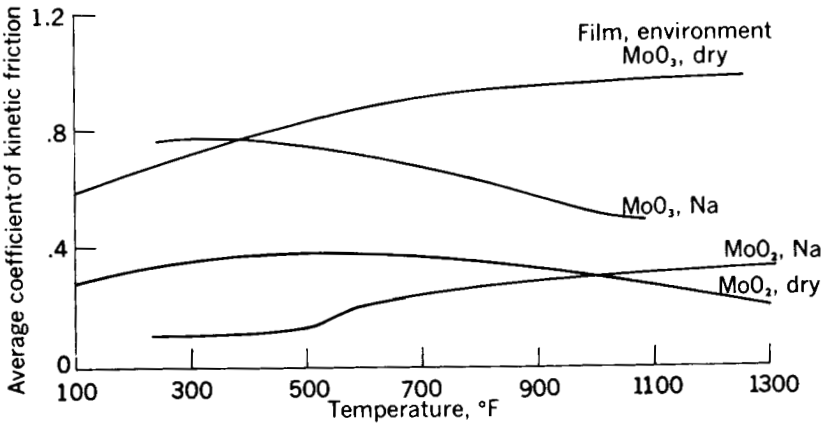

FIGURE 14–4.—Summary of molybdenum friction studies with respect to different surface films found on test surfaces. (From ref. 12.)

the oxygen may be initially available as sodium oxide (Na_2O), but this may be removed by filters. The use of preformed films on sliding bearing surfaces may be necessary.

Since tungsten behaves chemically like molybdenum, the authors of reference 13 investigated the possibility of the formation of sodium tungstate films (Na_2WO_4) on sodium-lubricated tungsten specimens. The coefficients of friction for dry and sodium-lubricated tungsten are shown in figure 14–5. As with molybdenum, friction when the specimen was run in sodium was lower than when it was run dry. The initial high friction at temperatures below 600° F suggests that

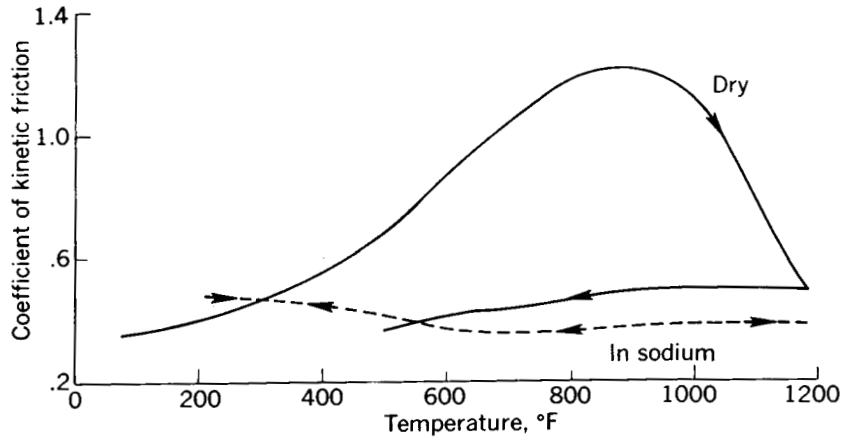

FIGURE 14–5.—Friction-temperature behavior for tungsten-tungsten system. (From ref. 13.)

the sodium tungstate film may not have formed until subsequent exposure at higher temperatures. The presence of a sodium tungstate film was verified by electron-diffraction techniques on a specimen exposed to sodium vapor at 1200° F. Both molybdate and tungstate films afforded protection to their respective substrate materials equally well under the test conditions of references 12 and 13.

The frictional behavior of a titanium carbide—niobium carbide—cobalt (TiC—NbC—Co) cermet was also investigated dry and in sodium (ref. 13). The behavior of the titanium carbide cermet was quite different from that of molybdenum and tungsten in that the cermet exhibited lower friction when run dry than when run in sodium. These results are shown in figure 14–6(a). The relatively low kinetic

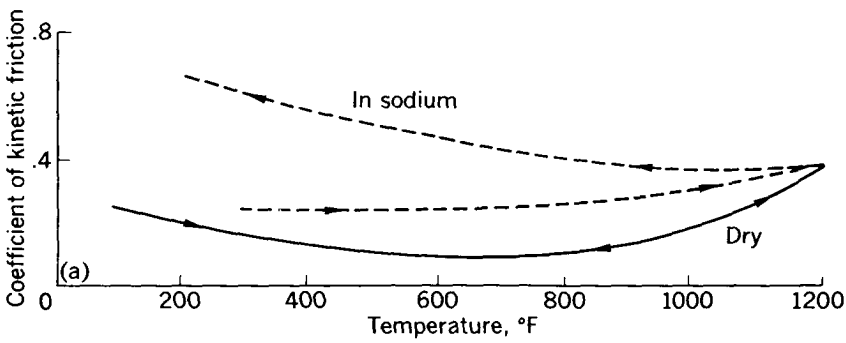

(a) Titanium carbide—titanium carbide system.

FIGURE 14–6.—Friction-temperature behavior of two systems. (From ref. 13.)

friction under dry conditions is believed to be due to the presence of a preformed film of titanium dioxide. In sodium it was postulated that a sodium titanate film was formed, although residual sodium on the surface prevented positive identification.

In reference 13 the frictional behavior of a tungsten carbide—cobalt (WC—Co) cermet was found to be similar to that of the TiC—NbC—Co cermet. These results are shown in figure 14–6(b). The addition of sodium stabilized the frictional level for both ascending and descending temperatures but did not produce significantly lower values of friction. Films similar to those postulated for tungsten may have been formed on the WC, but the differences in frictional behavior may be associated with the hardness of the substrate.

The overall results obtained in references 12 and 13 indicate that the presence of surface films on substrates can provide effective protection against gross surface damage. Caution must be used in extrapolating these results to high-velocity systems because the experiments were conducted in a stick-slip apparatus at a very low sliding

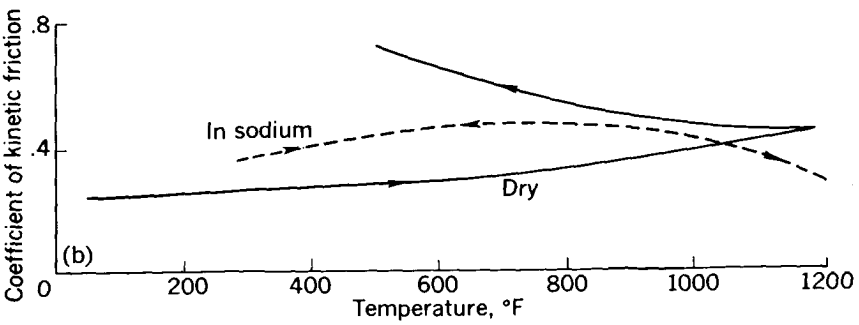

(b) Tungsten carbide—tungsten carbide system.

FIGURE 14–6—Concluded.—Friction-temperature behavior of two systems. (From ref. 13.)

velocity. It must also be kept in mind that the formation of such films in practical systems may be very difficult.

PROPERTIES OF LIQUID METALS

The most important property of a lubricant in fluid-film bearings is viscosity. The load-carrying capacity of hydrodynamic bearings is directly proportional to the lubricant viscosity, while the flow from the bearing (the flow required to maintain a film) is inversely proportional to viscosity. Thus the low viscosities of the liquid metals result in low load capacity and high flow requirements. On the other hand, bearing power loss is proportional to viscosity so that the power loss in liquid-metal bearings should not be of concern unless turbulent flow occurs. One of the problems concerned with the use of liquid metals will, therefore, be that of low load capacity, while the advantage gained in reducing power loss is not expected to be significant. Viscosities of four alkali metals and mercury are shown in figure 14–7. Values are given at temperatures up to the boiling point for all the fluids except lithium. At approximately 200° F the viscosities of the alkali metals are on the order of 10^{-7} reyn. At this temperature an SAE 30 oil has a viscosity of about 20×10^{-7} reyn. Thus, relative to a medium viscosity mineral oil, reductions in load capacity greater than an order of magnitude can be expected with the alkali liquid metals.

Other properties of interest, including melting and boiling points, thermal conductivity, specific heat, density, and viscosity of liquid and vapor phases, are given in table 14–V. Relative to conventional oils, the liquid metals have lower specific heats and higher thermal conductivities. A lower specific heat will result in a higher temperature rise for a given amount of shear work done on the fluid. On

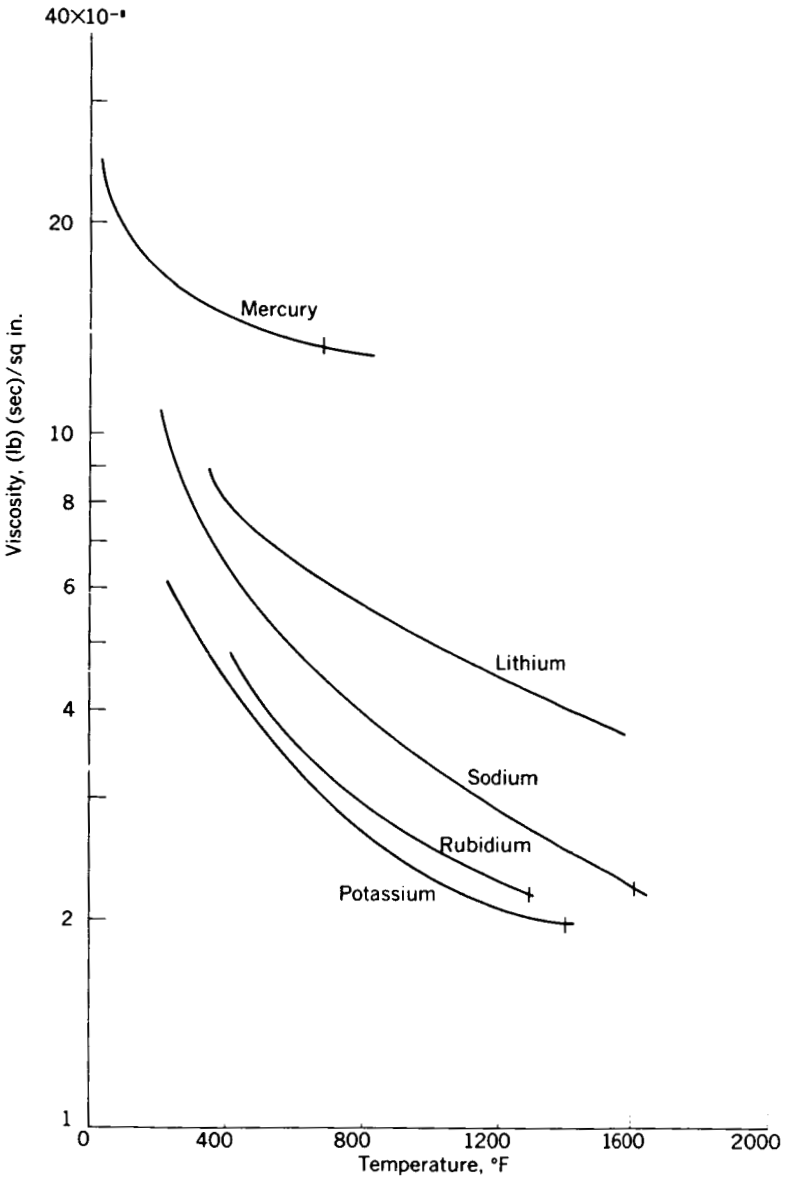

FIGURE 14–7.—Viscosity of mercury and four alkali liquid metals. (From ref. 9.)

the other hand, a higher thermal conductivity will result in lower temperature gradients within the fluid for a given quantity of heat transferred. The net result will be that liquid-metal-lubricated bearings will experience a different thermal growth from convention-

TABLE 14-V.—PROPERTIES OF INORGANIC FLUIDS FOR SPACE APPLICATIONS [a]

	Metal				
	Mercury	Rubidium	Potassium	Sodium	Lithium
Melting point, ° F	−38	102	145.	208	357
Boiling point, ° F	674	1270	1400	1618	2437
Density of liquid at boiling point, lb/cu ft	794	82. 15	41. 4	46. 3	26. 2
Density of vapor at boiling point, lb/cu ft	0. 26	0. 060	0. 0305	0. 0165	----------
Viscosity of liquid at boiling point, (lb)(sec)/sq in.	1.34×10^{-7}	2.17×10^{-8}	1.94×10^{-8}	2.21×10^{-8}	8.98×10^{-8} [b]
Viscosity of vapor at boiling point, (lb)(sec)/sq in.	8.85×10^{-9}	2.43×10^{-9}	1.41×10^{-9}	1.87×10^{-9}	----------
Surface tension, lb/ft, at ° F	0. 0318 at 68	0. 0034 at 102	0. 0059 at 145. 8	0. 01306 at 212	0. 027 at 357
Vapor pressure at 2200° R, lb/sq in. abs	3000 (extrapolated)	112	65	26. 5	5
Thermal conductivity of liquid, Btu/(hr)(ft)(° F)	8. 1 [c]	11. 8 [c]	18. 0 [c]	30. 1 [c]	27. 2 [b]
Thermal conductivity of vapor, Btu/(hr)(ft)(° F)	0. 0055 [c]	0. 00354 [c]	0. 0045 [c]	0. 0083 [c]	----------
Specific heat of liquid, Btu/(lb)(° F)	0. 0323 [c]	0. 0877	0. 1868 [c]	0. 305 [c]	0. 98 [c]
Specific heat of vapor, Btu/(lb)(° F)	0. 0248 [c]	0. 0579 [c]	0. 1267 [c]	0. 214 [c]	0. 716

[a] From ref. 9.
[b] At melting point.
[c] At boiling point.

ally lubricated bearings. This factor must be considered in setting bearing clearances.

The specific heat of the fluid will determine its ability to carry away heat since the product of specific heat, temperature rise, and flow equals the rate of heat dissipation. The low specific heat of the liquid metals may determine the minimum allowable flow. The probable high operating temperature of liquid-metal-lubricated bearings will tend to minimize this problem, however.

Liquid-metal-lubricated bearings operating in the region of the fluid boiling point may be subject to cavitation. If the pressure at any point in the bearing falls below the vapor pressure of the lubricant, vaporization can occur with a resultant discontinuity in the fluid film. Cavitation forces can promote erosion of the bearing material.

OPERATING PROBLEMS

Space powerplants will be called upon to operate unattended for long periods of time at high rotative speeds in a weightless environment. The low viscosity of the working fluid will result in low bearing load capacity, and the combination of low viscosity and high speed will help to promote turbulent flow. Bearing power consumption under turbulent flow conditions is significantly higher than with laminar flow. The weightless environment intensifies problems related to bearing instability. Material problems such as compatibility and dimensional stability are aggravated by the extreme temperatures to which the bearings will be subjected. All these problems with the exception of those arising from bearing instability and turbulence have been discussed previously. These two problems will now be discussed in detail.

The origin of half-frequency whirl has been discussed previously in chapter 3. In space powerplants, the occurrence of this type of whirl would be encouraged by the high speeds, low viscosity, and absence of gravity forces. In systems where whirl is a problem, it may be necessary to resort to the use of nonstandard journal-bearing configurations. Several types of bearings with good anti-whirl characteristics have been designed into rotating machinery. These are, in approximate order of increasing ability to prevent whirl,

(1) Elliptical bearings
(2) Pressure bearings
(3) Longitudinal groove bearings
(4) Three-lobe bearings
(5) Pivoted-shoe bearings
(6) Nutcracker-type bearings

All these bearings suppress whirl by generating an artificial load within the bearing. This artificial load is created by generating

wedge films, by dragging fluid into a pressure pool with restricted flow paths, or by tapping fluid from the high-pressure region and feeding it back into the bearing on the unloaded side. Determination of the operating characteristics of and design procedures for antiwhirl bearing shapes is at best difficult and sometimes impossible unless many simplifying assumptions are made. Solutions must often be obtained by trial and error because of the interaction of the various regions of the bearing. For example, in a three-lobe bearing, the operating characteristics of each lobe can be computed by considering each lobe to be a 120°-arc journal bearing. The forces generated in each lobe, however, are interdependent so that the solution must be sought by trial-and-error methods until the summation of all the oil film forces is equal and opposite to the external bearing load. Procedures for determining the characteristics of several bearing types are given in reference 14.

Turbulence

Most fluid-film-bearing analyses are based on the assumption of laminar flow. These analyses are valid so long as the speed at which turbulent flow begins is not exceeded. The transition to turbulent flow begins when the Reynolds number is given by the following equation (ref. 14, p. 231):

$$\frac{\pi\rho NDC_d}{2\mu}=41.1\sqrt{\frac{D}{C_d}} \qquad (14\text{–}1)$$

When turbulent flow exists, bearing power loss rises and the oil flow decreases. Figure 8–13, on page 231 of reference 14 is a chart for computing the power loss under turbulent flow conditions. The experiments of reference 6 showed that the transition from laminar to turbulent flow occurred at higher speeds than predicted by Taylor's criterion (eq. (14–1)).

An investigation of the load-carrying capacity of journal bearings with turbulent flow was carried out by Tao (ref. 15). Tao assumed that the short-bearing-theory assumption (that the pressure flow in the circumferential direction is small compared with the velocity flow) is valid and that the pressure flow in the z-, or axial, direction can be derived from the Blasius one-seventh power law of velocity profile.

The results of Tao's analysis, plotted as eccentricity ratio against dimensionless numbers, are shown in figures 14–8 and 14–9. Figure 14–9 shows that the load capacity of a bearing operating with turbulent flow is greater than that of a bearing operating with laminar flow. Thus, turbulent flow results in increased load capacity and friction and decreased flow. In reference 7, recorded bearing torques in the turbulent region were 4 to 40 times as great as predicted by laminar theory.

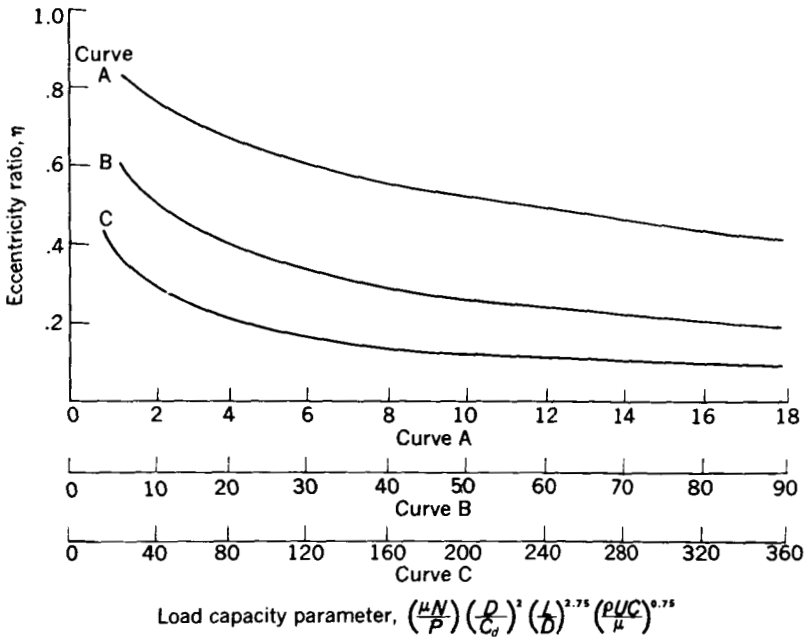

FIGURE 14–8.—Eccentricity ratio as function of load-capacity parameter for fully developed turbulent flow. (From ref. 15.)

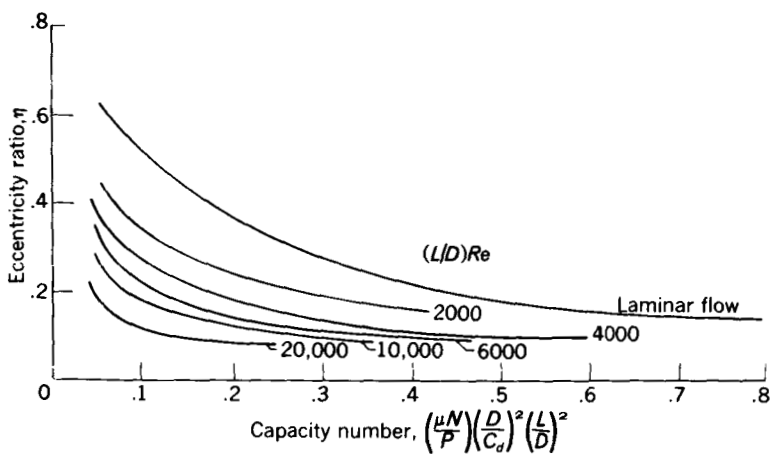

FIGURE 14–9.—Eccentricity ratio as function of capacity number for laminar flow and turbulent flow at various Reynolds numbers. (From ref. 15.)

REFERENCES

1. Markert, W., Jr., and Ferguson, K. M.: Use of Rolling Contact Bearings in Low Viscosity Liquid Metal Lubricants. Lubrication Eng., vol. 13, no. 5, May 1957, pp. 285–290.
2. Vail, D. B.: The Performance of Tungsten Carbide Journal Bearings Operating in Liquid Metals. KAPL–1079, Knolls Atomic Power Lab., Jan. 25, 1954.
3. Apkarian, H.: Investigation of Liquid Metal Lubricated Bearings. Rep. 50GL 231, General Electric Co., Nov. 27, 1950.
4. Greenert, W. J., and Gross, M. R.: Basic Information on the Bearing Properties of Various Materials in Liquid Metals. Rep. 090014B, U.S. Naval Eng. Exp. Station, July 1954.
5. Vail, D. B.: Summary of Journal Bearing Tests with Copper Bearings and Tungsten Carbide Journals Operating in Sodium-Potassium Alloy. KAPL–877, Knolls Atomic Power Lab., Feb. 1953.
6. Robinson, J. E., Jr., Vail, D. B., and Bedford, A. W., Jr.: Control Cylinders Guide Bearing Test. KAPL–M–EDL–10, Knolls Atomic Power Lab., Jan. 5, 1953.
7. Stahlhuth, Paul H., and Trippet, Richard: Liquid Metal Bearing Performance in Laminar and Turbulent Regimes. Trans. ASLE, vol. 5, no. 2, Nov. 1962, pp. 427–436.
8. Blackmer, Richard K.: Research on Liquid Metals as Power Transmission Fluids. TR 57–294, WADC, Feb. 1958.
9. Weatherford, W. D., Jr., Tyler, John C., and Ku, P. M.: Properties of Inorganic Working Fluids and Coolants for Space Applications. TR 59–598, WADC, 1959.
10. Amateau, M. F.: The Effect of Molten Alkali Metals on Containment Metals and Alloys at High Temperatures. Rep. 169, DMIC, May 1962.
11. Cook, W. H.: Corrosion Resistance of Various Ceramics and Cermets to Liquid Metals. Rep. ORNL–2391, Oak Ridge Nat. Lab., June 15, 1960.
12. Kissel, J. W., Glaeser, W. A., and Allen, C. M.: Sliding Contact Frictional Behavior in Sodium Environments. Trans. ASLE, vol. 5, no. 1, Apr. 1962, pp. 39–44.
13. Kissel, J. W., Glaeser, W. A., and Allen, C. M.: Frictional Behavior of Sodium-Lubricated Materials in a Controlled High-Temperature Environment. Paper 61–LUBS–16, ASME, 1961.
14. Wilcock, Donald F., and Booser, E. Richard: Bearing Design and Application. McGraw-Hill Book Co., Inc., 1957, pp. 256–280.
15. Tao, L. N.: A Theory of Lubrication in Short Journal Bearings with Turbulent Flow. Trans. ASME, vol. 80, no. 8, Nov. 1958, pp. 1734–1740.

AUTHOR INDEX

Names of those who collaborated with the authors are in italics.

Page intentionally left blank

SUBJECT INDEX

☆ U.S. GOVERNMENT PRINTING OFFICE: 1972 O—460-844